

Metamorphic evolution of ultrahigh-temperature granulite
facies and upper amphibolite facies rocks of the Epupa
Complex, NW Namibia

Dissertation zur Erlangung des
naturwissenschaftlichen Doktorgrades
der Bayerischen Julius-Maximilians-Universität Würzburg

vorgelegt von

Sönke Brandt

aus Kiel

Würzburg 2003

Eingereicht am:

Gutachter:

Gutachter:

der Dissertation

Prüfer:

Prüfer:

der mündlichen Prüfung

Tag der mündlichen Prüfung:

Doktorurkunde ausgehändigt am:

TABLE OF CONTENTS

ZUSAMMENFASSUNG.....	5
ABSTRACT	7
ACKNOWLEDGEMENTS.....	9
1 INTRODUCTION	11
1.1 LOCATION OF THE STUDY AREA	11
1.2 GEOLOGICAL FRAMEWORK.....	12
1.2.1 <i>The Palaeo- to Mesoproterozoic Epupa Complex.....</i>	<i>15</i>
1.2.2 <i>The Mesoproterozoic Kunene Intrusive Complex.....</i>	<i>19</i>
1.2.3 <i>Mesoproterozoic granitoids.....</i>	<i>20</i>
1.2.4 <i>Syenites and nepheline-syenites and mafic-ultramafic intrusions.....</i>	<i>21</i>
1.2.5 <i>Neoproterozoic sediments of the Damara Supergroup.....</i>	<i>21</i>
1.3 PREVIOUS INVESTIGATIONS	22
1.4 AIM OF THE STUDY.....	24
2 GEOLOGY OF THE STUDY AREA.....	25
2.1 UPPER AMPHIBOLITE FACIES ROCKS OF THE ORUE UNIT.....	25
2.1.1 <i>Volcano-sedimentary sequence</i>	<i>26</i>
2.1.1.1 <i>Metavolcanics.....</i>	<i>28</i>
2.1.1.2 <i>Paragneisses</i>	<i>29</i>
2.1.2 <i>Metagranitoids.....</i>	<i>32</i>
2.1.3 <i>Mafic dykes metamorphosed under amphibolite facies conditions</i>	<i>34</i>
2.1.4 <i>Contact metamorphic phenomena</i>	<i>34</i>
2.2 UHT GRANULITES OF THE EPEMBE UNIT	35
2.2.1 <i>Volcano-sedimentary sequence</i>	<i>37</i>
2.2.2.1 <i>Metavolcanics.....</i>	<i>37</i>
2.2.2.2 <i>Paragneisses</i>	<i>39</i>
2.2.2 <i>Metagranitoids.....</i>	<i>43</i>
2.2.3 <i>Mafic dykes metamorphosed under granulite facies conditions.....</i>	<i>45</i>
2.3 TECTONICS	46
2.3.1 <i>Structure of the Orue Unit.....</i>	<i>46</i>
2.3.2 <i>Structure of the Epembe Unit</i>	<i>47</i>
2.3.3 <i>Ductile shear zones.....</i>	<i>49</i>
2.3.4 <i>Ductile-brittle shear zones.....</i>	<i>49</i>
2.3.5 <i>Brittle faults</i>	<i>50</i>

3 GEOCHEMISTRY.....	53
3.1 CHARACTERIZATION OF THE PROTOLITHS	56
3.1.1 <i>Orthogneisses</i>	56
3.1.1.1 Mafic metavolcanites.....	56
3.1.1.2 Felsic metavolcanites.....	63
3.1.1.3 Metagranitoids.....	65
3.1.2 <i>Paragneisses</i>	66
3.2 TECTONIC ENVIRONMENT DURING PROTOLITH FORMATION.....	71
3.2.1 <i>Mafic metavolcanites</i>	71
3.2.2 <i>Felsic metavolcanites and metagranitoids</i>	71
3.2.3 <i>Paragneisses</i>	73
3.3 CHEMICAL VARIATIONS RELATED TO METAMORPHISM	74
3.4 CONCLUSION	75
4 METAMORPHIC EVOLUTION OF THE UPPER AMPHIBOLITE FACIES ROCKS OF THE ORUE UNIT.....	77
4.1 PETROGRAPHY.....	78
4.1.1 <i>Mafic rocks</i>	78
4.1.1.1 Amphibolites	80
4.1.1.2 Garnet-hornblende schists and (garnet-bearing) hornblendites.....	83
4.1.2 <i>Felsic gneisses and Hbl-Bt metagranitoids</i>	84
4.1.2.1 Felsic Hbl-Bt-bearing gneisses.....	85
4.1.2.2 Hbl-Bt metagranitoids	86
4.1.3 <i>Paragneisses</i>	87
4.1.3.1 Metagreywackes	87
4.1.3.2 Metapelites	90
4.2 MINERAL CHEMISTRY	97
4.2.1 <i>Garnet</i>	98
4.2.2 <i>Biotite</i>	102
4.2.3 <i>Cordierite</i>	104
4.2.4 <i>Staurolite</i>	104
4.2.5 <i>Clinopyroxene</i>	105
4.2.6 <i>Amphibole</i>	106
4.2.7 <i>Ilmenite</i>	106
4.2.8 <i>Rutile</i>	107
4.2.9 <i>Magnetite</i>	107
4.2.10 <i>Sillimanite</i>	107
4.2.11 <i>Plagioclase</i>	107

4.2.12 Alkalifeldspar.....	108
4.3 MINERAL REACTION HISTORY	109
4.3.1 Mafic and felsic orthogneisses.....	109
4.3.2 Metapelites and metagreywackes	110
4.3.3 Contact metamorphic Grt-Sil-Crd rocks	112
4.4 PHASE RELATIONSHIPS	114
4.5 P-T CONDITIONS	115
4.5.1 Metapelites and metagreywackes	115
4.5.2 Amphibolite.....	119
4.6 DISCUSSION AND CONCLUSION	121
4.6.1 P-T path reconstruction.....	121
4.6.2 Geodynamic model	123
5 METAMORPHIC EVOLUTION OF THE UHT GRANULITES OF THE EPEMBE UNIT	127
5.1 PETROGRAPHY	128
5.1.1 Mafic granulites.....	129
5.1.1.1 (Garnet-bearing) two-pyroxene granulites	131
5.1.1.2 Grt-Cpx granulites.....	134
5.1.1.3 (Grt-bearing) Opx-Pl-Qtz granulites	136
5.1.2 Felsic granulites and Grt-Opx metagranitoids.....	137
5.1.2.1 Felsic pyroxene-bearing granulites	138
5.1.2.2 Grt-Opx metagranitoids.....	139
5.1.3 Paragneisses.....	141
5.1.3.1 Fe-rich Grt-Opx gneisses.....	141
5.1.3.2 Qtz-rich Grt-Opx rocks and Mg-rich Grt-Opx gneisses.....	144
5.1.3.3 Grt gneisses and Grt-Sil gneisses	152
5.1.3.4 Sapphirine-bearing Opx-Sil gneisses and Opx-Grt rocks	160
5.1.3.5 Mineral assemblages in the light of the whole-rock geochemical data.....	170
5.2 MINERAL CHEMISTRY	172
5.2.1 Garnet.....	173
5.2.2 Biotite.....	180
5.2.3 Cordierite.....	182
5.2.4 Clinopyroxene.....	184
5.2.5 Orthopyroxene	184
5.2.6 Amphibole.....	190
5.2.7 Sapphirine.....	192
5.2.8 Spinel	193
5.2.9 Ilmenite	194

5.2.10 Rutile.....	195
5.2.11 Sillimanite.....	195
5.2.12 Plagioclase.....	195
5.2.13 Alkalifeldspar.....	198
5.3 MINERAL REACTION HISTORY	199
5.3.1 Mafic granulites.....	199
5.3.2 Felsic granulites and Grt-Opx metagranitoids.....	203
5.3.3 Paragneisses.....	204
5.3.3.1 Fe-rich and Mg-rich Grt-Opx gneisses and Qtz-rich Grt-Opx rocks.....	204
5.3.3.2 Grt-Sil gneisses and Grt gneisses	212
5.3.3.3 Sapphirine-bearing Opx-Sil gneisses and Opx-Grt rocks.....	219
5.3.4 Summary and conclusions	228
5.4 P-T CONDITIONS.....	231
5.4.1 Mafic granulites.....	235
5.4.2 Grt-Opx metagranitoids.....	237
5.4.3 Paragneisses	238
5.4.3.1 Fe-rich and Mg-rich Grt-Opx gneisses and Qtz-rich Grt-Opx rocks.....	238
5.4.3.2 Grt-Sil gneisses and Grt gneisses	242
5.4.3.3 Sapphirine-bearing Opx-Sil gneisses and Opx-Grt rocks.....	244
5.4.4 Summary and conclusions	247
5.5 P-T PSEUDOSECTIONS.....	250
5.5.1 Comparison with previously published FMASH grids	251
5.5.2 Sapphirine-bearing Opx-Sil gneisses.....	251
5.5.3 Grt-Sil gneisses.....	256
5.5.4 Discussion.....	259
5.6 DISCUSSION AND CONCLUSIONS	260
5.6.1 P-T path reconstruction.....	260
5.6.2 Evidence for UHT metamorphism in the granulites of the Epembe Unit	263
5.6.3 The preservation of UHT conditions in the granulites of the Epembe Unit.....	264
5.6.4 Geodynamic model	265
5.6.5 Other UHT occurrences of southern Africa.....	267
6 COMPARISON BETWEEN THE ORUE UNIT AND THE EPEMBE UNIT	269
7 A GEODYNAMIC MODEL FOR THE EPUPA COMPLEX.....	273
8 REFERENCES	275

ZUSAMMENFASSUNG

Der hochgradig metamorphe Epupa Komplex (EK) ist in Nordwest Namibia aufgeschlossen und bildet den südwestlichen Rand des archaischen bis proterozoischen Kongo Kratons. Der nordöstliche Teil des EK wurde geochemisch und petrologisch untersucht, um seine tektono-metamorphe Entwicklung zu rekonstruieren. Hierbei wurden zwei unterschiedliche metamorphe Einheiten erkannt: (1) Gesteine der oberen Amphibolitfazies (Orue Einheit) und (2) Ultrahochtemperatur (UHT)-granulitfazielle Gesteine (Epembe Einheit). In dem untersuchten Gebiet sind die Gesteine der oberen Amphibolitfazies der vorherrschende Gesteinstyp, während die Ultrahochtemperatur-Granulite in einem begrenzten Gebiet auftreten, das von den umgebenden amphibolitfaziellen Gesteinen durch steil einfallende, duktile Scherzonen getrennt ist. Die Gesteine des EK werden von einem gewaltigen Anorthosit-Massiv, dem Kunene-Intrusiv-Komplex (KIK), durchschlagen.

Die Orue Einheit und die Epembe Einheit wurden von zwei unterschiedlichen mesoproterozoischen Metamorphosen erfaßt, wie Unterschiede im Metamorphosegrad, in den rekonstruierten P-T Pfaden und den Altern der Metamorphose-Höhepunkte belegen:

(1) Die Orue Einheit setzt sich aus einer paläoproterozoischen vulkano-sedimentären Abfolge zusammen, die von großen Mengen an I-Typ Granitoiden und von Basaltgängen intrudiert wurde. Während des Mesoproterozoikums (1390-1318 Ma) wurde die Orue Einheit unter Bedingungen der oberen Amphibolitfazies metamorph überprägt. Die vulkano-sedimentäre Abfolge wird von einer Wechsellagerung von basaltischen (Grt-)Amphiboliten und rhyolitischen Hbl-Bt-führenden felsischen Gneisen aufgebaut, in die migmatitische Grt-Bt Gneise (Metagrauwacken), Grt-Hbl Schiefer, Hornblendite, migmatitische Metapelite, Metaquartzite, Metaarkosen und Kalksilikate eingeschaltet sind. Die Granitoide wurden im Zuge der amphibolitfaziellen Metamorphose zu migmatitischen Hbl-Bt Metagranitoiden überprägt während die Basaltgänge zu Amphiboliten umgewandelt wurden.

Anhand der beobachteten Mineralparagenesen und der berechneten P-T Bedingungen wird die Orue Einheit in drei Regionen untergliedert (nördlicher Teil, südwestlicher Teil, südöstlicher Teil), die unterschiedliche Krustenbereiche repräsentieren. Für die Gesteine der drei Regionen der Orue Einheit wurden ähnliche Aufheizungs-Abkühlungs-Pfade unter vermutlich annähernd konstanten Druckbedingungen rekonstruiert: Prograde Aufheizung führte zur partiellen oder vollständigen Verdrängung von Amphibol, Biotit und Muskovit durch Dehydratations-Schmelz-Reaktionen. Für die drei Regionen der Orue Einheit wurden unterschiedliche höchstgradige P-T Bedingungen berechnet: (a) südöstlicher Teil: $\sim 700^{\circ}\text{C}$, $\sim 6.5 \pm 1.0$ kbar; (b) südwestlicher Teil: $\sim 820^{\circ}\text{C}$, $\sim 8 \pm 0.5$ kbar und (c) nördlicher Teil: $\sim 800^{\circ}\text{C}$, $\sim 6.0 \pm 1.0$ kbar. Diese P-T Bedingungen stimmen mit den jeweiligen Mineralparagenesen der Metapelite überein; es handelt sich hierbei um Grt-Bt-Sil-Gneise und -Schiefer in der südöstlichen und -westlichen Region während im nördlichen Teil des EK (Grt-)Crd-Bt-Gneise auftreten. Hinsichtlich der Hauptdeformationsphase D_1 erfolgte die Bildung dieser höchstgradigen Paragenesen syn- bis post-tektonisch. Auf den Metamorphose-Höhepunkt folgte eine Phase der retrograden Abkühlung zu Bedingungen der mittleren Amphibolitfazies (ca. 600°C).

Ein Aufheizungs-Abkühlungs-Pfad unter annähernd konstanten Drucken konnte auch für undeformierte metapelitische Grt-Sil-Crd Gesteine rekonstruiert werden, die im direkten Kontakt zum KIK auftreten: Prograde Aufheizung von Bedingungen der mittleren Amphibolitfazies führte zur Bildung der höchstgradigen Grt-Sil-Crd Paragenese unter Bedingungen der oberen Amphibolitfazies von $\sim 750^{\circ}\text{C}$ und ~ 6.5 kbar. Anschließend erfolgte die Abkühlung der Gesteine unter Bedingungen der mittleren Amphibolitfazies.

(2) Die Epembe Einheit besteht aus einer paläoproterozoischen vulkano-sedimentären Abfolge, die von kleinen Körpern an S-Typ Granitoiden und von Andesitgängen intrudiert wurde. Die Gesteine wurde im frühen Mesoproterozoikum (1520-1447 Ma) von einer UHT granulitfaziellen Metamorphose erfaßt. Die vulkano-sedimentäre Abfolge wird durch basaltische Zwei-Pyroxen Granulite, selten Granat-führend,

wechsellagernd mit Pyroxen-führenden Granuliten rhyolitischer-dacitischer Zusammensetzung dominiert. Migmatitische metapelitische Grt-Sil Gneise, Qtz-reiche Grt-Opx Gesteine und migmatitische grauwackenartige Grt-Opx Gneise und Grt Gneise sind in die Metavulkanite eingeschaltet. MgAl-reiche, Sapphirin-führende Opx-Sil Gneise und Mg-reiche Opx-Grt Gesteine treten als restititische Schlieren in den migmatitischen Grt-Opx Gneisen auf. Die Granitoide wurden im Zuge der UHT-Metamorphose zu Grt-Opx Metagranitoiden überprägt, während die Andesitgängen zu mafischen Grt-Opx-Pl-Qtz Granuliten umgewandelt wurden.

Für die UHT-Granulite der Epembe Einheit wurden detaillierte P-T Pfade rekonstruiert, die entgegen des Uhrzeigersinnes verlaufen und die in mehrere Stufen untergliedert sind: Während annähernd isobarer Aufheizung zu UHT-Bedingungen unter moderaten Drucken von ~ 7 kbar wurden Biotit- oder Hornblende-führende Mineralparagenesen weitgehend oder vollständig im Zuge von Dehydratations-Schmelzreaktionen durch trockene Mineralparagenesen verdrängt. In den Grt-Sil Gneisen entstanden während der prograden Aufheizung Spl-Qtz Paragenesen. Im Zuge eines anschließenden Druck-Anstieges um 2-3 kbar wurden die höchstgradigen Mineralparagenesen unter UHT Bedingungen gebildet. Dabei handelt es sich um (i) Grt-Opx und (Grt-)Opx-Cpx in den Orthogneisen und (ii) Grt-Opx, Grt-Sil und (Grt-)(Spr-)Opx-Sil-Qtz in den Paragneisen. Im Gegensatz zu den meisten der bislang weltweit bekannten UHT-Vorkommen sind in den Granuliten der Epembe Einheit höchstgradige Mineralzusammensetzungen erhalten. Daher konnten für diese Gesteine anhand von konventioneller Geothermobarometrie ultrahohe Temperaturen von $970 \pm 70^\circ\text{C}$ bei Drucken von 9.5 ± 2.5 kbar berechnet werden. UHT-Bedingungen werden zudem durch den sehr hohen Al-Gehalt von höchstgradigem Orthopyroxen (bis zu 11.9 Gew.% Al_2O_3) in zahlreichen Paragneisen belegt. Des weiteren ist das Auftreten der Paragenese Opx-Sil-Qtz in den Sapphirin-führenden Opx-Sil Gneisen charakteristisch für UHT-Granulite. Extreme Temperaturen von $1030\text{-}1100^\circ\text{C}$, berechnet für einen Opx-Grt Restit, lassen vermuten, dass in der Epembe Einheit noch höhere Temperaturen von $\sim 1050^\circ\text{C}$ erreicht wurden, die mit dem Auftreten von Spr-Qtz Paragenesen in den Opx-Sil Gneisen konsistent sind. Während der spätesten Phase der höchstgradigen Metamorphose wurden die Granulite von der Hauptdeformation D_1 erfaßt. Eine anschließende Dekompression ist durch Mineralzonierungsmuster und zahlreiche Korona- und Symplektit-Gefüge belegt, die sich auf Kosten der höchstgradigen Mineralphasen gebildet haben: Initiale Dekompression um ~ 2 kbar erfolgte noch unter UHT-Bedingungen ($940 \pm 60^\circ\text{C}$; 8 ± 2 kbar), hauptsächlich belegt durch Sapphirin-führende Symplektite in den Opx-Sil Gneise und Opx-Pl Koronen um Granat. Anhaltende Dekompression erfolgte anschließend unter Hochtemperatur-Bedingungen ($800 \pm 60^\circ\text{C}$; 6 ± 2 kbar) und führte zur Bildung von Crd-Opx-Spl, Crd-Opx und Spl-Crd Symplektiten in den Paragneisen. Der Aufstieg der Granulite aus der Unterkruste (~ 29 km) in die mittlere Kruste (~ 18 km) erfolgte vermutlich entlang der subvertikalen Scherzonen, die Epembe Einheit umgeben. Anschließend annähernd isobare Abkühlung zu Bedingungen der oberen Amphibolitfazies ($660 \pm 30^\circ\text{C}$; 5 ± 1.5 kbar) führte zum Wiederwachstum von Biotit, Hornblende, Sillimanit und Granat, gebildet durch Reaktionen zwischen den Symplektit-Phasen oder reliktschen höchstgradigen Phasen mit kristallisierenden anatektischen Schmelzen. Während anhaltender Dekompression wurde in zahlreichen Paragneisen Orthopyroxen mit niedrigem Al-Gehalt und Cordierit auf Kosten von retrogradem Biotit gebildet.

Basierend auf diesen Daten wird ein geodynamisches Model für den EK entwickelt, das die zeitliche und räumlichen Zusammenhänge zwischen der metamorphen Entwicklung der UHT-Granulite der Epembe Einheit, die der amphibolitfaziellen Gesteine der Orue Einheit und mesoproterozoischen anorogenem Magmatismus in NW Namibia diskutiert. Dieses bringt die UHT-Metamorphose mit der Bildung einer Magmenkammer an der Kruste-Mantel-Grenze in Zusammenhang, welche zugleich die Magmenquelle für die Anorthosite des KIK darstellt. Die amphibolitfazielle Metamorphose der Orue-Einheit wird dagegen mit einer regionalen Kontaktmetamorphose während der Platznahme der anorthositischen Magmen in Verbindung gebracht.

ABSTRACT

The high-grade metamorphic Epupa Complex (EC) is exposed in north-western Namibia and constitutes the south-western margin of the Archean to Proterozoic Congo Craton. The north-eastern portion of the EC has been geochemically and petrologically investigated in order to reconstruct its tectono-metamorphic evolution. Two distinct metamorphic units have been recognized: (1) Upper amphibolite facies rocks (Orue Unit) and (2) ultrahigh-temperature (UHT) granulite facies rocks (Epembe Unit). The upper amphibolite facies rocks are the dominant rock type in the study area; the UHT granulites are exposed in a limited terrane, separated from the surrounding Orue Unit rocks by steeply-dipping ductile shear zones. The rocks of the EC are transected by a large anorthosite massif, the Kunene Intrusive Complex (KIC).

The Orue Unit and the Epembe Unit were affected by two distinct Mesoproterozoic metamorphic events, as is evident from differences in their metamorphic grade, in the constructed P-T paths and in the age of peak-metamorphism:

(1) The Orue Unit consists of a Palaeoproterozoic volcano-sedimentary sequence, which was intruded by large masses of I-type granitoids and by rare mafic dykes. During the Mesoproterozoic (1390-1318 Ma) the Orue Unit rocks underwent upper amphibolite facies metamorphism. The volcano-sedimentary sequence is constituted by interlayered basaltic (Grt-) amphibolites and rhyolitic Hbl-Bt-bearing felsic gneisses, with intercalations of greywacke-type migmatitic Grt-Bt gneisses (metagreywackes), Grt-Hbl schists, hornblendites, migmatitic metapelites, metaquartzites, metaarkoses and rare calc-silicate rocks. The granitoids were metamorphosed to migmatitic Hbl-Bt metagranitoids and the mafic dykes to amphibolites.

Based on the observed mineral assemblages and the calculated P-T conditions, the Orue Unit is subdivided into three parts (northern part, south-western part, south-eastern part), which represent individual crustal levels. Similar heating-cooling paths with probably minor pressure variations are constructed for the rocks of the three parts of the Orue Unit:

Prograde heating led to the partial or complete replacement of amphibole, biotite and muscovite through dehydration melting reactions. Systematic variations of the peak-metamorphic P-T conditions are calculated for the three parts of the Orue Unit: (a) South-eastern part: $\sim 700^{\circ}\text{C}$, $\sim 6.5 \pm 1.0$ kbar; (b) south-western part: $\sim 820^{\circ}\text{C}$, $\sim 8 \pm 0.5$ kbar and (c) northern part: $\sim 800^{\circ}\text{C}$, $\sim 6.0 \pm 1.0$ kbar. The calculated P-T conditions correlate well with regional variations of the mineral assemblage in the metapelites, i.e. Grt-Bt-Sil gneisses and schist in the south-eastern and south-western region and (Grt-)Crd-Bt gneisses in the northern part. The formation of the peak-metamorphic mineral assemblages occurred syn- to post-tectonically with respect to the main deformation phase D₁. Peak-metamorphism was followed by retrograde cooling to middle amphibolite facies conditions of $\sim 600^{\circ}\text{C}$.

A heating-cooling P-T path at near-isobaric conditions is also recorded by massive metapelitic Grt-Sil-Crd rocks, sampled in direct contact to the KIC: Prograde heating from middle to upper amphibolite facies conditions of $\sim 750^{\circ}\text{C}$ at ~ 6.5 kbar led to the formation of a peak-metamorphic Grt-Sil-Crd assemblage and was followed by retrograde cooling to middle amphibolite facies conditions.

(2) The Epembe Unit consists of a Palaeoproterozoic volcano-sedimentary succession, which was intruded by small bodies of S-type granitoids and by andesitic dykes. All these rocks underwent UHT granulite facies metamorphism during the early Mesoproterozoic (1520-1447 Ma). The volcano-sedimentary succession is dominated by interlayered basaltic two-pyroxene granulites, rarely containing garnet, and pyroxene-bearing granulites of rhyolitic to dacitic composition. Migmatitic metapelitic Grt-Sil gneisses, Qtz-rich Grt-Opx rocks and migmatitic greywacke-type Grt-Opx gneisses and Grt gneisses are intercalated in the metavolcanites. MgAl-rich sapphirine-bearing Opx-Sil gneisses and Mg-rich Opx-Grt

rocks occur as restitic schlieren in the migmatitic Grt-Opx gneisses. The granitoids were metamorphosed to Grt-Opx metagranitoids and the intermediate dykes to mafic Grt-Opx-Pl-Qtz granulites.

Detailed anti-clockwise P-T paths are constructed for the UHT granulites of the Epembe Unit, which are subdivided into several distinct stages: During prograde near-isobaric heating to UHT conditions at moderate pressures of ~ 7 kbar biotite- or hornblende-bearing mineral assemblages were almost completely replaced by anhydrous mineral assemblages through various dehydration melting reactions. In the Grt-Sil gneisses Spl-Qtz assemblages were formed. During a subsequent pressure increase of 2-3 kbar the peak-metamorphic mineral assemblages, i.e. (i): Grt-Opx and (Grt-)Opx-Cpx in the orthogneisses and (ii): Grt-Opx, Grt-Sil and (Grt-)(Spr-)Opx-Sil-Qtz in the paragneisses, were formed at UHT conditions. In contrast to most of the few worldwide known UHT occurrences, ultrahigh temperatures of $970 \pm 70^\circ\text{C}$ at 9.5 ± 2.5 kbar are calculated from conventional geothermobarometry for the UHT granulites of the Epembe Unit, due to the partial preservation of the highest-grade mineral composition. UHT conditions are supported by the very high Al content of peak-metamorphic orthopyroxene (up to 11.9 wt.% Al_2O_3) in many paragneisses and by the presence of Opx-Sil-Qtz assemblages in the sapphirine-bearing Opx-Sil gneisses. Extreme temperatures calculated for a restitic Opx-Grt rock ($1030\text{-}1100^\circ\text{C}$) suggest that even higher temperatures of $> 1050^\circ\text{C}$ were attained in the Epembe Unit, which are consistent with the postulated presence of Spr-Qtz assemblages in the Opx-Sil gneisses. During the latest stage of peak-metamorphism the mineral assemblages were affected by the main deformation phase D_1 . Post-peak decompression is recorded by several corona and symplectite textures, formed at the expense of the peak-metamorphic phases, and is supported by garnet zonation patterns: Initial UHT decompression of about ~ 2 kbar to $940 \pm 60^\circ\text{C}$ at 8 ± 2 kbar is mainly evident from the formation of sapphirine-bearing symplectites in the Opx-Sil gneisses and from Opx-Pl coronas around garnet. Subsequent high-temperature decompression to 6 ± 2 kbar at $800 \pm 60^\circ\text{C}$ resulted in the formation of Crd-Opx-Spl, Crd-Opx and Spl-Crd symplectites in the paragneisses. Uplift from initial lower crustal depths (~ 29 km) into mid-crustal levels (~ 18 km) probably proceeded along subvertical shear zones, which surround the UHT granulites. Subsequent near-isobaric cooling to upper amphibolite conditions of $660 \pm 30^\circ\text{C}$ at 5 ± 1.5 kbar led to the re-growth of biotite, hornblende, sillimanite and garnet, formed at the expense of the symplectitic phases or of relic peak-metamorphic phases by interaction with crystallizing melts. During continued decompression low-alumina orthopyroxene and cordierite were formed at the expense of retrograde biotite in several paragneisses.

Based on these data, an geodynamic model is developed for the EC, which discusses the temporal and spatial relationship between the metamorphic evolution of the UHT granulites of the Epembe Unit, that of the upper amphibolite facies rocks of the Orue Unit and Mesoproterozoic anorogenic magmatism in NW Namibia. UHT metamorphism of the Epembe Unit is correlated with the formation of a large magma chamber at the mantle-crust boundary, which forms the source for the anorthosites of the KIC. In contrast, amphibolite facies metamorphism of the Orue Unit is ascribed to a regional contact metamorphic event, caused by the emplacement of the anorthositic crystal mushes in the middle crust.

ACKNOWLEDGEMENTS

Special thanks are due to my supervisor Professor Dr. R. Klemd. His unrestricted support and willingness for discussions greatly improved this study. I am greatly indebted to Professor Dr. M. Okrusch who initiated this project. His encouragement and readiness for debates contributed to the success of this study.

I am grateful to PD Dr. Thomas Will for the calculation of the petrogenetic FMAS(H) grid for the high-grade metamorphic metapelites and for the introduction to the calculations of P-T pseudosections. I also wish to thank PD Dr. U. Schüssler for his help and advice with the EMP work and PD Dr. A. Zeh for stimulating discussions concerning all kinds of petrological questions.

Dr. Kirsten Drüppel is thanked for fruitful discussions regarding the relationships between metamorphism and magmatism in the study area.

I am grateful to Mrs. R. Baur for her friendly advice with the RFA work, to Mr. P. Späthe for his excellent preparation of the thin sections, to Mr. K.-P. Kelber for the introduction to the digital photography and to Mrs. A. Kirchner for her always friendly administrative help.

Dr. U. Hünken (KFA Jülich, Außenstelle Potsdam) is thanked for his assistance during the first field campaign in 1998 and Professor Dr. L. Ratschbacher (University of Freiberg) for his help and advice concerning the structural investigations during the second field campaign in 1999. Thanks go to Professor Dr. Jay Barton (Rands University, Johannesburg) for the great field trip to the Limpopo Belt in 2000.

Dipl.-Min. S. Littmann (GeoForschungsZentrum Potsdam) is acknowledged for providing sample material of 1997 and Professor Dr. S. Harley (University of Edinburgh) for sending me an excel spreadsheet of a modified version of the Aranovich & Berman (1997) Grt-Opx Al-thermometer formulation.

The project benefited from the logistical support of the Geological Survey of Namibia. I appreciate financial support from the Postgraduate Research Program 'Interdisciplinary Geoscience Research in Africa' at the University of Würzburg supported by the Deutsche Forschungsgemeinschaft (grant: GRK 144/3).

My special thanks go to my parents for their financial support and to Kirsten Drüppel for her unrestricted encouragement throughout the completion of this study and for her critical reading of the manuscript.

1 INTRODUCTION

The Epupa Complex (EC) is a high-grade metamorphic gneiss terrane, which is exposed in north-western Namibia (Fig. 1.1). The EC forms part of the Palaeoproterozoic basement of north-western Namibia and south-western Angola, that was mainly formed during the Eburnian Orogeny between 2250 and 1600 Ma (e.g. Tegtmeier & Kröner, 1985; Carvalho et al. 2000).

Due to the remoteness and inaccessibility of the studied area detailed petrological, structural and geochemically investigations were lacking for the EC, so far.

1.1 LOCATION OF THE STUDY AREA

The study area is situated between longitudes E 12°57' and E 13°50' and latitudes S 16°58' and 17°37' (Fig. 1.1). It is composed of upper amphibolite facies and ultrahigh-temperature granulite facies rocks of the EC, which were intruded by a large Mesoproterozoic anorthosite massif, the Kunene Intrusive Complex (KIC). Towards the north and east, the study area is bounded by the Kunene River, that forms the natural border between Namibia and Angola, whereas the EC rocks are overlain by Neoproterozoic sediments of the Damara Supergroup towards the south and west (Fig. 1.1).

1.2 GEOLOGICAL FRAMEWORK

According to Trompette (1994), the EC is situated at the south-western margin of the Archean to Proterozoic Congo Craton of central Africa, which is limited towards the east by the Mesoproterozoic (~ 1250 Ma) Kibaria fold belt (Trompette, 1994; see inset on Fig. 1.1). Towards the north, west and south, the Congo Craton is bordered by a system of mobile belts, that was developed during the Pan-African orogeny in the late Proterozoic to early Palaeozoic (e.g. Trompette, 1994). The mobile belts include the Oubanguide Belt in the north, the West-Congo Belt in the west, the Damara Belt in the south and the Kaoko Belt in the south-west.

Archean to Palaeoproterozoic rocks are mainly exposed in the marginal zones of the Congo Craton and are subdivided into four blocks (Trompette, 1994; see inset on Fig. 1.1): (1) the Cameroon-Gabon block in the north-west, (2) the NE-Zaire block in the north-east, (3) the Kasai block in the central eastern part, and (4) the Angolan block in the south-west. Following this subdivision the EC forms part of the Angolan block. Structural relationships between individual blocks, however, remain uncertain, as the central part of the Congo Craton is largely covered by Cenozoic to Quaternary sediments of the Congo basin. Following Alkmim & Marshak (1998) and Carvalho et al. (2000) the Cameroon-Gabon block was connected with the São Francisco Craton of proto-South America during the Palaeoproterozoic, whereas for the Angolan block a correlation with Palaeoproterozoic rocks of South America is lacking, so far.

The Angolan block is predominantly exposed in south-western Angola and extends into north-western Namibia. The metamorphic basement of Angola was mainly formed during the Eburnian Orogeny (2250-1600 Ma, Carvalho et al., 2000). The crustal evolution of Angola is mainly constrained by Rb-Sr whole rock ages, combined with field relationships (e.g. Carvalho et al., 2000): Late Archean to early Palaeoproterozoic gneisses ('Pre-Eburnian gneisses') were partly migmatized during the Eburnian orogeny ('Eburnian gneisses', 2250-1800 Ma) and intruded by large volumes of syn-tectonic granitoids ('Eburnian granitoids'; Carvalho et al., 1979; Torquato et al., 1979). During the final stages of the Eburnian orogenic cycle (1800-1600 Ma) post-tectonic granitoids were emplaced ('Late Eburnian granitoids'; e.g. Torquato & Olivera, 1977; Carvalho et al., 1979; Torquato & Carvalho, 1992).

In northern Namibia Proterozoic basement rocks of the Angolan block are mainly exposed in three inliers, that constitute the basement for Neoproterozoic rocks of the Damara Supergroup (e.g. South African Committee for Stratigraphy (SACS), 1980; Fig. 1.1): (1) the Kamanjab Inlier, (2) the Abbabis Inlier of the central Damara belt and (3) the Epupa Complex.

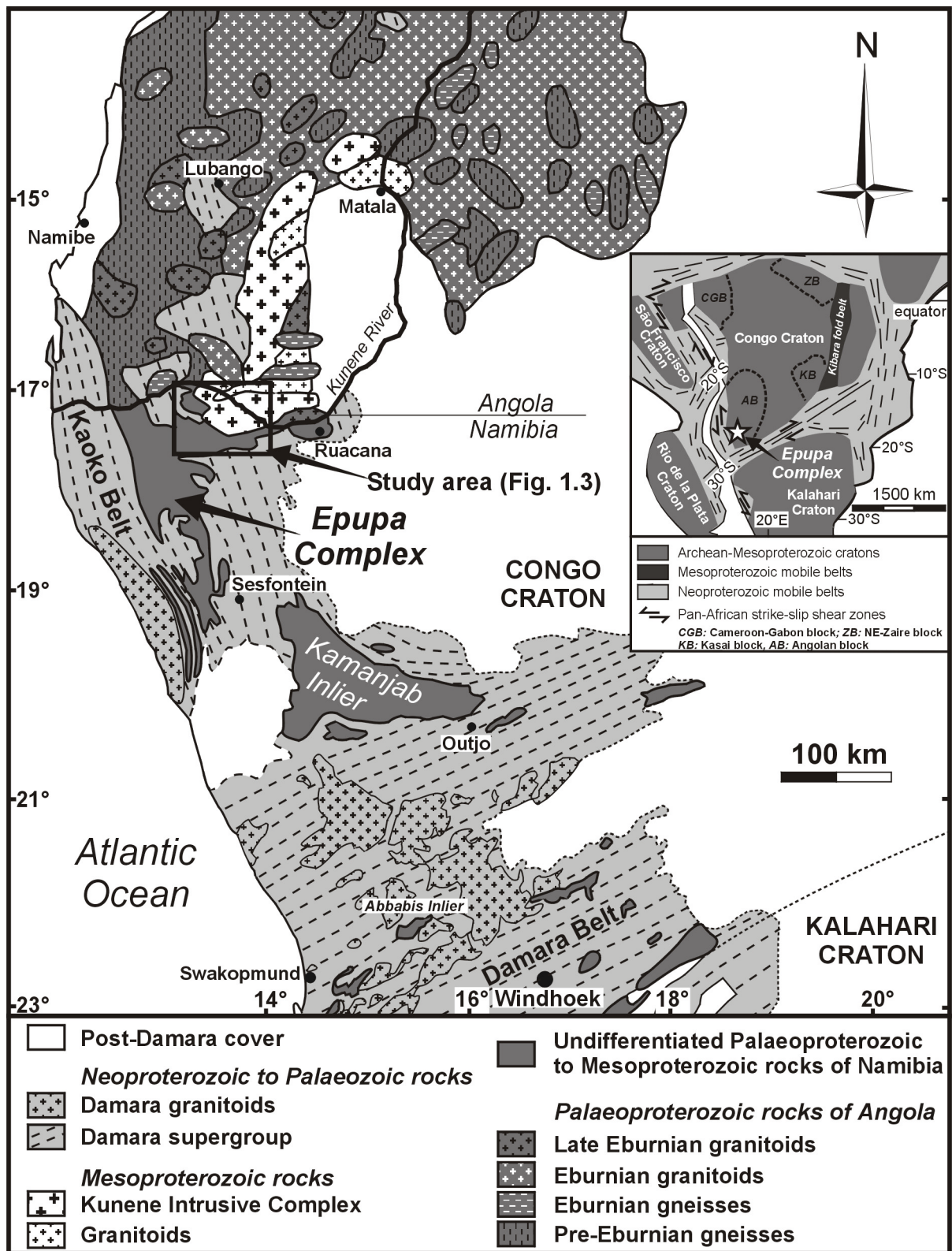


Fig. 1.1: Simplified geological map of northern Namibia and southern Angola, indicating the distribution of pre-Pan-African basement rocks (modified after Miller et al., 1983 (Namibian part) and Carvalho et al., 2000 (Angolan part)) and the location of the study area. The inset map illustrates the palaeogeographic position of the Epupa Complex at the south-western margin of the Congo Craton.

	Unit	Lithology	Age (Ma)
Mesoproterozoic			
Namibia	Granite	granite	1374 ± 6 (U-Pb zircon; B. Seth, pers. com.)
	Kunene Intrusive Complex	leucogabbro	1385 ± 25 (U-Pb zircon; Drüppel et al., 2000b)
	Orue Unit of the EC	upper amphibolite facies	1367-1318 (U-Pb zircon; B. Seth, pers. com.)
		ortho- and paragneisses	1390-1330 (Pb-Pb garnet; B. Seth, pers. com.)
	Epembe Unit of the EC	UHT granulite facies	1520-1450 (U-Pb zircon; Seth et al., 2003)
		ortho- and paragneisses	1490-1447 (Pb-Pb garnet; Seth et al., 2003)
	EC (undifferentiated)	granitic gneiss	~ 1470 (U-Pb zircon; Burger, in Menge, 1996)
	EC (undifferentiated)	amphibolite	~ 1394 (U-Pb zircon; Burger, in Menge, 1996)
Angola	Red Granite	granite	~ 1400–1300 (Rb-Sr, w.r.i.; Carvalho et al., 1979)
	Kunene Intrusive Complex	mangerite	1370 ± 4 (U-Pb zircon; Mayer et al., 2000)
Palaeoproterozoic			
Namibia	Ruacana augengneiss of the EC	granitic Augengneiss	~ 1795 (U-Pb zircon; Tegtmeier & Kröner, 1985)
	Fransfontein Granitoid Suite	granitoids	1838 ± 30 & 1662 ± 30 (U-Pb zircon; Burger et al., 1976)
	Khoabendus Group	acid lava	1765 ± 40 (U-Pb zircon; Burger & Coertze, 1975)
	Huab Complex	quartzofeldspathic gneiss	~ 1811 (U-Pb zircon; Tegtmeier & Kröner, 1985)
	Granitoids of the EC	granitic augengneiss	1971 ± 7 (U-Pb zircon; Seth et al., 1998)
	Protholiths of the Epembe Unit	ortho- and paragneisses	~1810-1635 (U-Pb zircon; Seth et al., 2003)
	Protholiths of the Orue Unit	ortho- and paragneisses	~1997-1640 (U-Pb zircon; B. Seth, pers. com.)
Angola	Bibala granitoid	porphyritic granitoid	1596 ± 86 (Rb-Sr, 4 w.r.i.; Torquato & Olivera, 1977)
	Caraculo granitoid	porphyritic granitoid	1686 ± 69 (Rb-Sr, w.r.i.; Torquato & Carvalho, 1992)
	Leucocratic granite	equigranular granite	1763 ± 21 (Rb-Sr, 8 w.r.i.; Carvalho et al., 1979)
	Eburnian gneisses	porphyroblastic gneiss	1790 ± 21 (Rb-Sr, 6 w.r.i.; Carvalho et al., 2000)
	Schist, Quartzite & Amphibolite Complex	basic migmatites	1826 ± 48 (Rb-Sr, 6 w.r.i.; Carvalho et al., 1979)
	Regional granite	granite, granodiorite	2191 ± 60 (Rb-Sr, 4 w.r.i.; Torquato et al., 1979)
	Granite, Gneiss & Migmatite Complex	migmatites	2206 ± 197 (Rb-Sr, w.r.i.; Torquato et al., 1979)
	Quibala granite	granite, granodiorite	2243 ± 43 (Rb-Sr, 4 w.r.i.; Carvalho et al., 1979)
Archean			
Namibia	Archean gneisses of the EC	augengneiss	2590 ± 14 (U-Pb zircon; Franz et al., 1999)
	Archean gneisses of the EC	granitoid gneiss	2645 ± 6 (U-Pb zircon; Seth et al., 1998)
Angola	Pre-Eburnian gneisses	granitoids gneisses	2520 ± 36 (Rb-Sr, 6 w.r.i.; Carvalho, 1984)

Table 1.1: Correlation of the pre-Pan-African rocks of southern Angola, of the Kamanjab Inlier of northern Namibia and of the study area of the Epupa Complex (EC); w.r.i.: whole-rock isochron.

(1) The Kamanjab Inlier is constituted by the amphibolite facies, partly migmatitic volcano-sedimentary Huab Complex and the low-grade metamorphic volcano-sedimentary Khoabendus Group (Frets, 1969). A Palaeoproterozoic U/Pb zircon upper intercept age of $1811 \pm 38/-35$ Ma for a quartzofeldspathic gneiss of the Huab Complex (Tegtmeier & Kröner, 1985) correlates well with $^{207}\text{Pb}/^{206}\text{Pb}$ zircon minimum ages of 1765 ± 40 and 1860 ± 40 Ma for metavolcanites of the Khoabendus Group (Burger & Coertze, 1975). Both the Huab Complex and the Khoabendus Group were intruded by syn- to post-tectonic granitoids of the Fransfontein Granitoid Suite (Frets, 1969). The granitoids yielded U/Pb zircon ages between 1838 ± 30 Ma and 1662 ± 30 Ma (Burger et al, 1976; recalculated by Cahen et al, 1984).

(2) Granitic gneisses of the Abbabis Inlier yielded a slightly higher Palaeoproterozoic U-Pb zircon age of 1935 ± 150 Ma (Jacob et al, 1978, recalculated by Cahen et al, 1984).

The data indicate that the Kamanjab Inlier and Abbabis Inlier of northern Namibia were affected by an Eburnian metamorphic event between 1900 and 1800 Ma (Tegtmeier & Kröner, 1985), which correlates well with Eburnian high-grade metamorphism at ~ 1800 Ma in south-western Angola. Syn- to post-tectonic granitoid emplacement of the Fransfontein Granitoid Suite, like that of the Angolan granitoids, occurred down to at least 1660 Ma. Following these arguments, the Palaeoproterozoic evolution of at least the Kamanjab and the Abbabis inliers of north-western Namibia correlates well with that of basement rocks of south-western Angola (Table 1.1), indicating that these basement complexes formed part of the Congo Craton during the Palaeoproterozoic. In the following, a detailed description of the third Palaeoproterozoic basement complex of NW Namibia, the Epupa Complex, will be given.

1.2.1 The Palaeo- to Mesoproterozoic Epupa Complex

The EC is the largest of the three pre-Pan-African basement complexes of northern Namibia and extends from Sesfontein in the south up to the Angolan-Namibian border in the north (Fig. 1.1). It is named after the type locality at the Epupa Falls of the Kunene River (South African Committee for Stratigraphy (SACS), 1980), Fig. 1.2). To the west the EC is bordered by the Pan-African Kaoko Belt (Fig. 1.1), which was formed by the collision between the Congo Craton and the São Francisco Craton of proto-South America (e.g. Hartnady et al. 1985; Dingeldey et al., 1994; Franz et al., 1999). While the western part of the EC was strongly affected by the Pan-African event and was partly incorporated into the Pan-African mobile belt (e.g. Dingeldey et al., 1994; Dingeldey, 1997; Fig. 1.1), the north-eastern portion of the EC, comprising the study area, remained a stable part of the Congo Craton during Pan-African times and therefore records the

original pre-Pan-African crustal evolution. According to Carvalho & Alves (1990, 1993), the EC extends into southern Angola, where it is designated as Schist, Quartzite and Amphibolite Complex (SQAC). The SQAC belongs to the pre-Eburnian (> 2200 Ma) rocks of Angola and is described as a low-grade metamorphic volcano-sedimentary sequence by Carvalho & Alves (1990, 1993).



Fig. 1.2: The Epupa Falls of the Kunene River, NW Namibia / SW Angola.

Regarding its Archean to Palaeoproterozoic crustal evolution the EC is remarkably similar to the other basement complexes of northern Namibia and the pre-Pan-African basement of southwestern Angola (Table 1.1): Late Archean granitoid gneisses with SHRIMP U-Pb zircon intrusion ages of 2645-2585 Ma (Seth et al., 1998; Franz et al., 1999) are exposed towards the west of Sesfontein (Fig. 1.1), in a region, which probably represents the southernmost extension of the EC. As in south-western Angola, these Archean rocks were intruded by Palaeoproterozoic granitoids with SHRIMP zircon ages of 1985-1960 Ma (Seth et al., 1998) during the Eburnian Orogeny. Syn-tectonic granitic augengneisses of Ruacana, situated at the easternmost margin of the EC (Fig. 1.1), yielded an U-Pb single zircon age of $1795 \pm 33/-29$ Ma (Tegtmeier & Kröner, 1985), which demonstrates that the EC was affected by an Eburnian metamorphic event and syn-tectonic granitoid magmatism at ~ 1800 Ma, also recorded from the Kamanjab Inlier (Fransfontein Granitoid Suite) and SW Angola (Late Eburnian granitoids). It has to be mentioned, however, that the rocks of the EC exposed in the study area exhibit remarkable differences in both their metamorphic grade and their Mesoproterozoic metamorphic evolution

when compared to the adjacent parts of the EC and to all other basement lithologies of the Congo Craton. It can thus be concluded, that the part of the EC, investigated in this study, experienced an unique crustal evolution in the Mesoproterozoic.

Based on field relationships and petrological investigations the EC of the studied area is subdivided into two distinct metamorphic units (Brandt et al, 1999, 2003; Fig. 1.3):

(1) As recognized by previous workers (Martin, 1965; Köstlin, 1967; 1974; SACS, 1980), this part of the EC predominantly consists of a widely migmatized volcano-sedimentary sequence, which was intruded by large masses of metagranitoids. Due to their uniform upper amphibolite facies metamorphic grade and structural similarities, the volcano-sedimentary sequence and the metagranitoids are grouped together as ‘Orue Unit’ by Brandt et al. (2003).

(2) In the southern part of the study area a limited, but well-defined terrane of ultrahigh-temperature (UHT) granulite facies ortho- and paragneisses has been recognized and termed ‘Epembe Unit’ by Brandt et al. (2000; 2003). This broadly E-W trending unit is approximately 50 km in length and up to 10 km in width and is constituted by a volcano-sedimentary sequence, which is transected by rare metagranitoids and by metamorphosed mafic dykes.

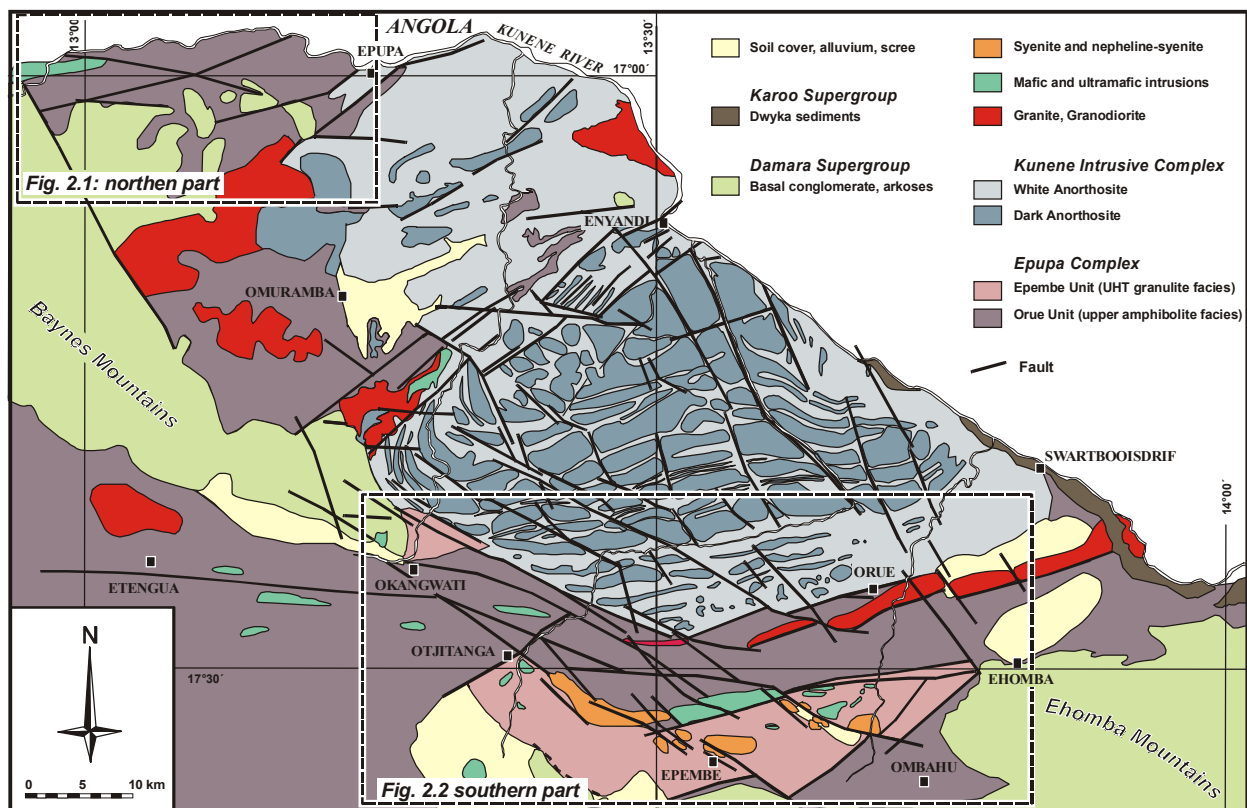


Fig. 1.3: Geology of the study area (modified after Köstlin, 1967; Menge, 1996; Drüppel et al., 2001; Brandt et al. 2003). Insets mark the locations of the mapped areas presented in Fig. 2.1 and Fig. 2.2.

The high metamorphic grades of the Orue and the Epembe Unit of the EC, when compared to the low-grade metamorphic SQAC of southern Angola, suggest an unique, post-Palaeoproterozoic metamorphic event in NW Namibia, which, however, did not affect the basement of SW Angola. Indeed, the two rock units are exceptional from all other basement rocks of the Congo Craton in preserving Mesoproterozoic ages of high-grade metamorphism. Mesoproterozoic ages have first been reported for the EC rocks of the study area by A. J. Burger (unpubl. data, in Allsopp, unpubl. data, 1975; cited in Menge, 1996; Carvalho et al., 2000): A granitic gneiss, sampled ~ 4.5 km to the south of the KIC near Orue (Fig. 1.3), and an amphibolite sample from Epembe (Fig. 1.3), yielded U-Pb single zircon ages of 1470 Ma and 1394 Ma, respectively. Although sample descriptions are not available, the sample locations suggest that the granitic gneiss belongs to the Orue Unit whereas the amphibolite might be a retrogressed mafic granulite of the Epembe Unit. Recently, however, age relationships of the UHT granulites of the Epembe Unit and the upper amphibolite facies rocks of the Orue Unit were investigated in more detail by Seth et al (2001, 2003) and B. Seth (pers. com.) using the SHRIMP ion microprobe and the Pb-Pb stepwise leaching technique: For zircon cores of the UHT granulites of the Epembe Unit Palaeoproterozoic U-Pb ages of 1810-1635 Ma were obtained, whereas zircon rims yielded Mesoproterozoic U-Pb ages of 1520-1510 Ma. Pb-Pb garnet ages range between 1490-1447 Ma and are interpreted to date UHT granulite facies metamorphism. U-Pb zircon dating on the upper amphibolite facies Orue Unit yielded Palaeoproterozoic U-Pb ages between 2115-1637 Ma for zircon cores and Mesoproterozoic U-Pb ages of 1367-1318 Ma for zircon rims. Pb-Pb garnet ages range between 1390-1330 Ma. The Palaeoproterozoic protolith ages of the EC rocks of the study area correlate well with those obtained for (1) the EC rocks exposed at Ruacana, (2) the Kamanjab Inlier and (3) the basement of southern Angola and hence demonstrate that all these basement complexes underwent a similar Palaeoproterozoic evolution. In contrast, high-grade metamorphic rocks of Mesoproterozoic age were unknown from the Congo Craton, so far. In the remaining pre-Pan-African basement domains of Namibia and south-western Angola magmatic or metamorphic activity of comparable age is restricted to the emplacement of a granitic dyke with a SHRIMP U-Pb upper intercept age of 1507 ± 16 Ma into presumably Palaeoproterozoic or late Archean rocks from the south-western part of the EC (Seth et al., 1998) and to the emplacement of a granitic augengneiss from the same region with a mean age of 1530-1500 Ma, obtained by Kröner et al. (2002) using the Pb-Pb zircon evaporation method and the conventional U-Pb zircon method. Metamorphism of the Kibarian fold belt, bordering the Congo Craton to the east (see inset of Fig. 1.1), is younger (1290-1200 Ma) than in the study area and of low-metamorphic grade (Trompette, 1994). Following these arguments, it can be concluded, that the EC underwent a unique Mesoproterozoic metamorphic evolution.

1.2.2 The Mesoproterozoic Kunene Intrusive Complex

The EC rocks exposed in the studied area are intruded by Mesoproterozoic anorthositic rocks of the Kunene Intrusive Complex (KIC; Drüppel, 1999, 2003; Drüppel et al, 2001; Fig. 1.1 & 1.3), which forms the largest massif-type anorthosite complex of the world (e.g. Ashwal, 1993, Drüppel et al, 2001). Although the contacts between the EC and the KIC are largely covered by soil, obliterated by late faults or intruded by syenite or dolerite dykes, xenoliths of EC rocks, such as amphibolites, in the anorthosites (Fig. 1.4a) demonstrate the intrusive character of the KIC (e.g. Beetz, 1933; Menge, 1996; Drüppel, 1999, 2003). Furthermore, the lack of a metamorphic overprint of the massive anorthosites (Drüppel, 1999, 2003; Drüppel et al., 2000a; 2001) proves that the emplacement of the KIC post-dates high-grade metamorphism of the EC.

The KIC is subdivided into two major units (Morais et al., 1998; Drüppel et al., 2001), that are separated by an E-W trending belt of granitoids (Fig. 1.1): (1) The majority of the Angolan

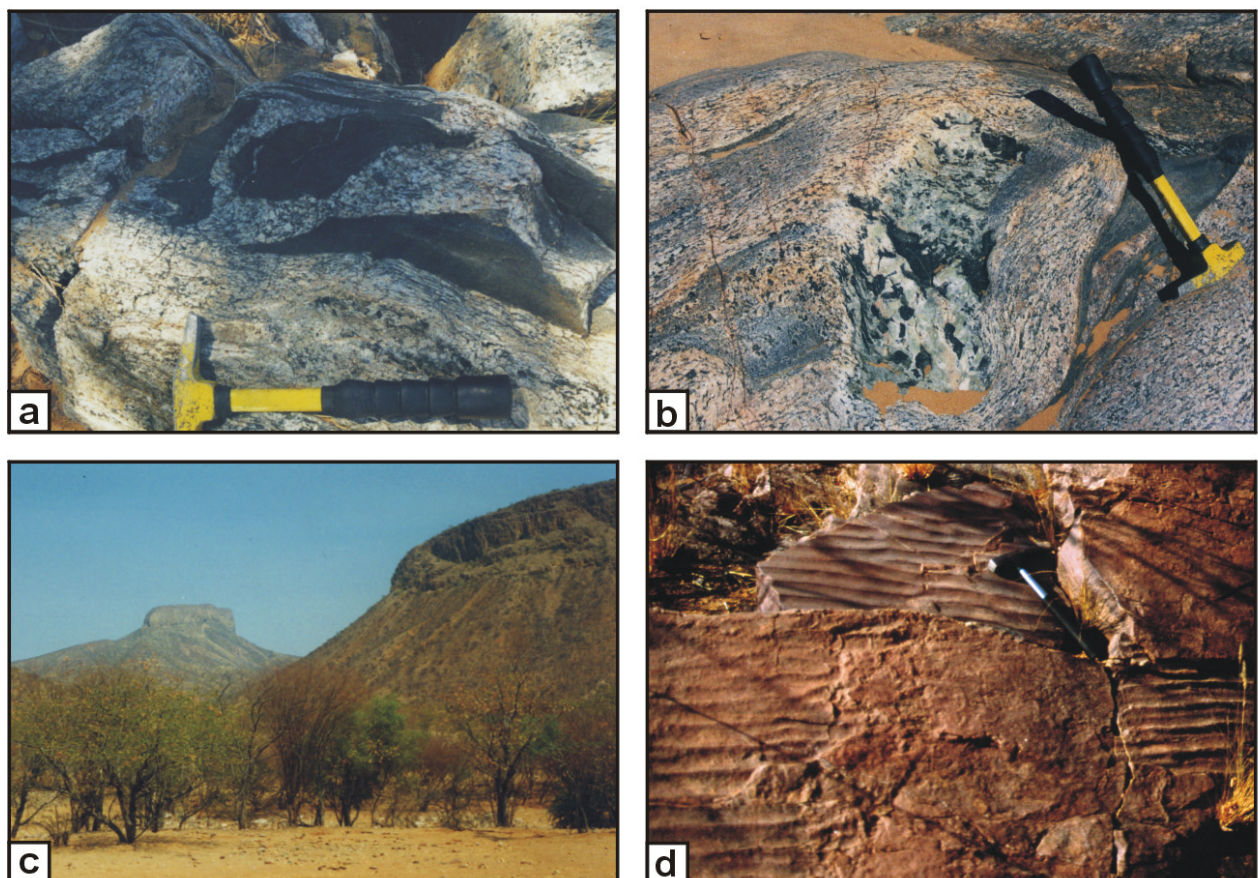


Fig. 1.4: Regional geology of the study area. **a)** Angular xenoliths of EC amphibolites in Mesoproterozoic anorthosites of the KIC. **b)** Xenolith of a leucogabbro of the KIC in foliated Mesoproterozoic granite. **c)** Horizontally bedded Neoproterozoic sediments of the Damara Supergroup, unconformably overlying the rocks of the Epupa Complex. **d)** Ripple marks on bedding planes of Neoproterozoic sandstone of the Damara Supergroup.

part of the KIC shows a N-S elongation. (2) In contrast, the southernmost part of the KIC, which is mainly exposed in Namibia and intruded the EC rocks of the study area, has a pronounced E-W elongation (Fig. 1.3). Two distinct suites of anorthositic rocks are distinguished in NW Namibia (Drüppel, 1999, 2003; Drüppel et al, 2001; Fig. 1.3): (i) whitish, heavily altered anorthosites and leucogabbros ('white anorthosites'; Drüppel et al, 2001) where intruded by (ii) younger, dark coloured and weakly altered anorthosites, leucotroctolites, leucogabbros and leuconorites, grouped together as 'dark anorthosites' (Drüppel, 1999; Drüppel et al, 2001).

Recent radiogenic age determinations indicate a Mesoproterozoic emplacement age for the KIC. An almost concordant U-Pb single zircon age of 1370 ± 4 Ma was obtained for a cogenetic mangerite vein from the Angolan part of the KIC (Mayer et al. 2000), consistent with an almost concordant U-Pb single zircon age of 1385 ± 25 Ma for a pegmatitic dark anorthosite sample from the Namibian part of the KIC (Drüppel et al., 2000b). The age of the white anorthosites is unknown, so far, but the ~ 1380 Ma age of the intrusive dark anorthosites may be interpreted as a minimum age.

1.2.3 Mesoproterozoic granitoids

Mesoproterozoic anorogenic granitoids, termed 'Red Granites' (Carvalho & Alves, 1990) intruded the anorthosites of the KIC in Angola (Fig. 1.1). Rb-Sr whole rock ages of 1400-1300 (Carvalho et al., 1979; Carvalho et al., 1987) indicate that granitoid emplacement is coeval with the intrusion of the KIC.

In the study area homogeneous and generally massive granites intruded the upper amphibolite facies rocks of the Orue Unit in the vicinity of the southern margin of the KIC (Fig. 1.3). The medium-grained, hornblende-bearing granites, previously misinterpreted as metaquartzites (Menge, 1996), form a prominent WSW-ENE elongated body of ~ 40 km in length, that is separated by late dextral strike-slip faults into several individual parts (Fig. 1.3). The reddish granites are strongly deformed at their margins with steeply inclined, E-W trending foliation planes. However, evidence for a high-grade metamorphic overprint is not observed in the rocks, that generally preserve their magmatic textures. Therefore, their emplacement is interpreted to post-date upper amphibolite facies metamorphism in the surrounding Orue Unit rocks. East of Orue, foliated granites occur in direct contact with the anorthosites of the KIC (Fig. 1.3). Xenoliths of anorthosites in the granites (Fig. 1.4b) demonstrate that the emplacement of the granites post-dates the emplacement of the KIC. For the granites, a Mesoproterozoic U-Pb zircon age of 1373.8 ± 5.6 has been obtained by B. Seth (pers. com.) using the SHRIMP ion

microprobe, suggesting that the emplacement of the NW Namibia granites is related to the widespread granite magmatism in southern Angola.

1.2.4 Syenites and nepheline-syenites and mafic-ultramafic intrusions

In the southern part of the study area several syenite and nepheline-syenite bodies with U-Pb single zircon ages of 1216 ± 2.4 and 1213 ± 2.5 Ma (Littmann et al., 2000), locally associated with carbonatites, intruded the rocks of the EC along NNW-SSE trending faults (Fig. 1.3).

Predominantly in the southern part of the study area mafic and ultramafic intrusions of yet unknown age intruded the EC (Köstlin, 1967; Menge, 1996, 1998; Fig. 1.3). The intrusions generally form E-W-elongated bodies up to 10 km in length, that were emplaced along major faults transecting the EC.

While contact thermal effects in the basement rocks of the EC bordering the mafic and ultramafic intrusions are not observed, the emplacement of the syenites and nepheline-syenites and carbonatites was locally associated with fenitisation of the surrounding EC rocks in a zone up to 1 km in width (Ferguson et al., 1975).

1.2.5 Neoproterozoic sediments of the Damara Supergroup

Siliciclastic Neoproterozoic sediments of the Nosib Group, the lowest member of the Damara Supergroup (SACS, 1980), rest unconformably on the metamorphic rocks of the EC in the study area (Fig. 1.3 & 1.4c). A minimum age for the Nosib Group is provided by an U-Pb single zircon age of 756 ± 2 Ma for an intrusive syenite (Hoffmann et al., 1996). The sediments of the Nosib Group extend into southern Angola (Fig. 1.1), where they are correlated with the Chela Group (Cahen et al, 1984).

In the studied area a basis conglomerate of the Nosib Group is developed on top of the basement rocks of the EC, which are incorporated as clasts into the conglomerates. The conglomerate is followed by a horizontally bedded, probably several hundred meters thick sequence of red arkoses and feldspathic sandstones. Rounded to subrounded quartz grains, lacking recrystallisation textures, demonstrate the lack of a Pan-African metamorphic event. This interpretation is confirmed by well-preserved sedimentary structures, such as ripple marks on bedding planes (Fig. 1.4d) and cross-bedding structures. Therefore, the study area is interpreted to have been a stable part of the Congo Craton during the Pan-African Orogeny.

1.3 PREVIOUS INVESTIGATIONS

The rocks of the Epupa Complex (EC) were firstly investigated by Beetz (1933), who described a widely migmatized succession of metavolcanic and metasedimentary rocks, which was intruded by large masses of granitic gneisses, occurring at the Kunene River in the vicinity of the Epupa Falls.

Martin (1965) introduced to term 'Epupa Formation' for the volcano-sedimentary succession, which is correlated with the Huab Complex of the Kamanjab Inlier by the author. Based on this correlation an age of > 1700 Ma was postulated for the Epupa Formation, which is the age of the Fransfontein Granitoid Suite intrusive into the Huab Complex.

According to Köstlin (1967; 1974) the western portion of the studied part of the EC consists of a succession of interlayered granitic and amphibolitic gneisses, termed 'Mixed Gneisses'. Following the author, hornblende-bearing granitic gneisses are the dominant rock type in the central and the southern part of this region while amphibolitic hornblende-plagioclase gneisses prevail in the north-western and south-eastern parts of the western portion of the EC. Köstlin (1967, 1974) observed rare siliciclastic metasediments, with hornblende-epidote or muscovite-biotite assemblages. Higher-grade metamorphic minerals, such as garnet and sillimanite, were not described by this author. According to Köstlin (1967, 1974), the low-grade metamorphic mineral assemblages of the amphibolitic rocks mainly correspond to the albite-epidote-amphibolite facies, whereas the granitic rocks might exhibit a higher metamorphic grade. Köstlin (1967, 1974) mentioned the possibility that pre-existing higher-grade mineral assemblage were completely replaced due to retrogression.

Ferguson et al. (1975) investigated the metasomatic effects in the rocks of the EC related to the emplacement of carbonatites and nepheline-syenites at Epembe.

The term 'Epupa Complex', used in the present study, was introduced by the South African Committee for Stratigraphy (SACS, 1980) for the volcano-sedimentary succession and the intrusive metagranitoids.

Tegtmeier & Kröner (1985) investigated syn-tectonic granitic augengneisses of Ruacana and obtained an U/Pb zircon age of 1795 +33/-29 Ma for their emplacement.

A combined field and petrographical study of the southern part of the study area, including the Epembe Unit and part of the Orue Unit, has been performed by Menge (1996; 1998). The results of this study together with those of Köstlin (1967, 1974) were compiled by Menge (1996) in a geological map on a 1:100000 scale, which formed the basis for the present investigations. The metamorphic rocks of the southern part of the study area have been termed 'Okatjite Metamorphic Suite' by Menge (1996), subdivided into two major rock units: The granulite facies

rocks of the Epembe Unit are described as amphibolitic gneisses, bearing rare orthopyroxene relics. These rocks have been ascribed to a facies transitional between the amphibolite and granulite facies by Menge (1996). The upper amphibolite facies rocks of the Orue Unit are suggested by Menge to represent amphibolite facies granitic gneisses with rare intercalated metasediments. Based on lithological constraints, the Okatjite Metamorphic Suite was correlated with the Khoabendus Group of the Kamanjab Inlier by Menge (1996; 1998).

1.4 AIM OF THE STUDY

The study is aimed at the reconstruction of the metamorphic evolution of the amphibolite facies Orue Unit and the granulite facies Epembe Unit of the Proterozoic Epupa Complex (EC), by interpreting geochemical data and constructing pressure-temperature paths (P-T paths). By these studies, the following problems will be solved:

- Detailed field studies will place constraints on the regional extent and the lithology of the Epembe Unit and the Orue Unit and their contact relationships. This study is aimed at answering the question whether the amphibolite facies rocks of the Orue Unit retrogressed equivalents of the Epembe Unit rocks or if the two metamorphic units represent independent rock suites, formed in distinct crustal levels. Structural investigations will constrain the relationships between metamorphism and deformation.
- Geochemical investigations were performed in order to characterize the protoliths of the high-grade metamorphic gneisses of the Orue Unit and the Epembe Unit, to discriminate the tectonic setting during the formation of their protoliths and to recognize possible chemical variations related to the high-grade metamorphism.
- Detailed petrographical and mineral chemical investigations will outline the prograde, peak-metamorphic and retrograde mineral assemblages and reaction textures of the various lithologies of the Orue Unit and the Epembe Unit and to answer the question as to whether the variations of the mineral assemblages are related to changes of the respective bulk-rock compositions.
- Based on the petrographical observations and by using mineral chemical data for geothermometer and -barometer calibrations, the P-T conditions will be constrained for both the observed stages of the metamorphic evolution and the individual metamorphic units.

Moreover, a detailed phase petrological investigation of selected granulite samples, using phase diagrams drawn for a specific bulk rock composition (i.e. P-T pseudosections) in the system FMAS, will be performed in order to:

- reconstruct detailed P-T paths by investigating all relevant mineral assemblages and reaction textures in the context of changing P and T, which is generally not possible with conventional geothermobarometry and
- investigate the influence of the bulk rock composition on the stability of the respective mineral assemblages.

The resulting P-T paths will be used to construct a geodynamic model, by taking into consideration both the regional geological context and the available geochronological data.

2 GEOLOGY OF THE STUDY AREA

The Epupa Complex (EC) rocks of the study area are subdivided into two main zones, a western and a southern zone (Fig. 1.3): The EC rocks of the western zone are limited by the anorthositic rocks of the Kunene Intrusive Complex (KIC) towards the east whereas, towards the west and south, they are unconformably overlain by Neoproterozoic sediments of the Damara Supergroup, forming the Baynes Mountains. In the southern zone the EC rocks occur in a broadly E-W trending strip of up to 20 km in width, that is bordered by the anorthositic rocks of the KIC towards the north and covered by Neoproterozoic sediments of the Damara Supergroup to the south, building the Ehomba Mountains.

The rocks of the EC are subdivided into two metamorphic rock units on the basis of the metamorphic grade (Brandt et al., 2003): (1) Upper amphibolite facies rocks of the Orue Unit and (2) ultrahigh-temperature (UHT) granulite facies rocks of the Epembe Unit, separated by steeply dipping ductile shear zones (Fig. 1.3). In order to investigate the composition and structure of and field relationships between the two metamorphic units, two parts of the study area have been investigated in some detail with their regional extent given in Fig. 1.3:

- In the western zone, field work concentrated on an E-W trending strip, ~ 30 km in length, consisting of upper amphibolite facies rocks of the Orue Unit exposed along the Kunene River ('northern part'; Fig. 2.1).
- In the southern zone, investigations were mainly performed in the central part, including the UHT granulites of the Epembe Unit and the surrounding lithologies of the Orue Unit ('southern part'; Fig. 2.2).

The geological maps given in Figs. 2.1 and 2.2 are based on the geological map of Köstlin (1967) and Menge (1996) and were modified by incorporating the results of field work combined with both landsat satellite images and aerial photographs interpretation. Since large parts of the basement are covered by soil, the scattered outcrops are generally small and isolated. Larger outcrops of solid basement rocks are generally restricted to river beds.

2.1 UPPER AMPHIBOLITE FACIES ROCKS OF THE ORUE UNIT

The rocks of the Orue Unit have been previously described as high-grade metamorphic granitic gneisses of the Okatjite Metamorphic Suite (Menge, 1996; 1998) in the southern zone and as low-grade metamorphic Mixed Gneisses (Köstlin, 1967; 1974) in the western zone of the study area. However, field work indicates striking lithological similarities and a comparable upper amphibolite facies metamorphic grade for rocks of both zones. Therefore, the rocks of both

zones were grouped together as Orue Unit by Brandt et al. (2003). Based on field relationships three subunits are recognized in the Orue Unit: In both zones (1) a succession of mafic and felsic metavolcanites interlayered with paragneisses is exposed (Fig. 2.1 & 2.2), that is interpreted as a high-grade metamorphic volcano-sedimentary sequence. Most paragneisses and part of the mafic metavolcanites comprise characteristic migmatitic textures (Fig. 2.3d; Fig. 2.4a, b & c), that indicate similar, at least upper amphibolite facies peak-metamorphic conditions. The upper thermal limit is given by the lack of orthopyroxene in the mafic and felsic metavolcanites, suggesting that granulite facies conditions were not attained. The volcano-sedimentary sequence was intruded by large volumes of (2) migmatitic metagranitoids (Fig. 2.5a & b), which, in turn, are locally transected by (3) metamorphosed mafic dykes.

Evidence for a regionally limited contact metamorphic overprint, induced by the emplacement of the anorthosites of the KIC, is recorded by massive metapelitic rocks (Fig. 2.5d), exposed at the contact to the southern margin of the KIC.

2.1.1 Volcano-sedimentary sequence

The volcano-sedimentary sequences of the Orue Unit were subdivided into a succession, which is dominated by interlayered mafic and felsic metavolcanics with or without rare intercalations

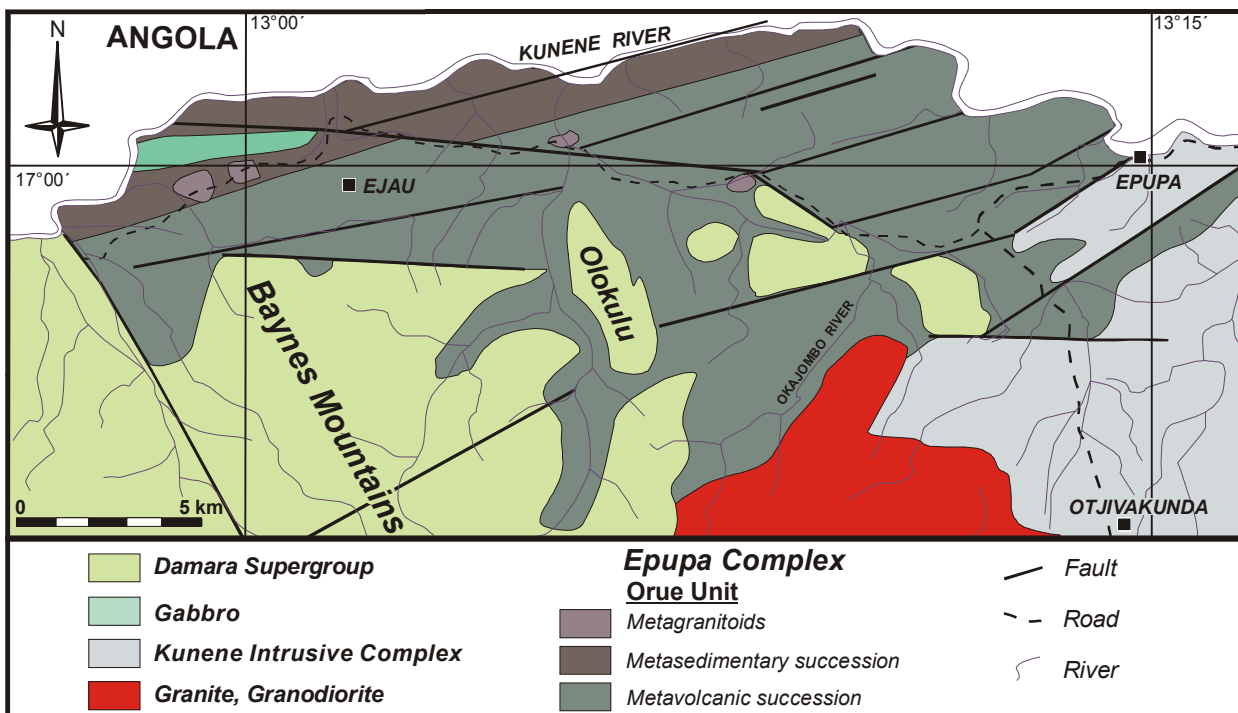


Fig. 2.1: Geological map of the northern part of the study area (modified after Köstlin, 1967).

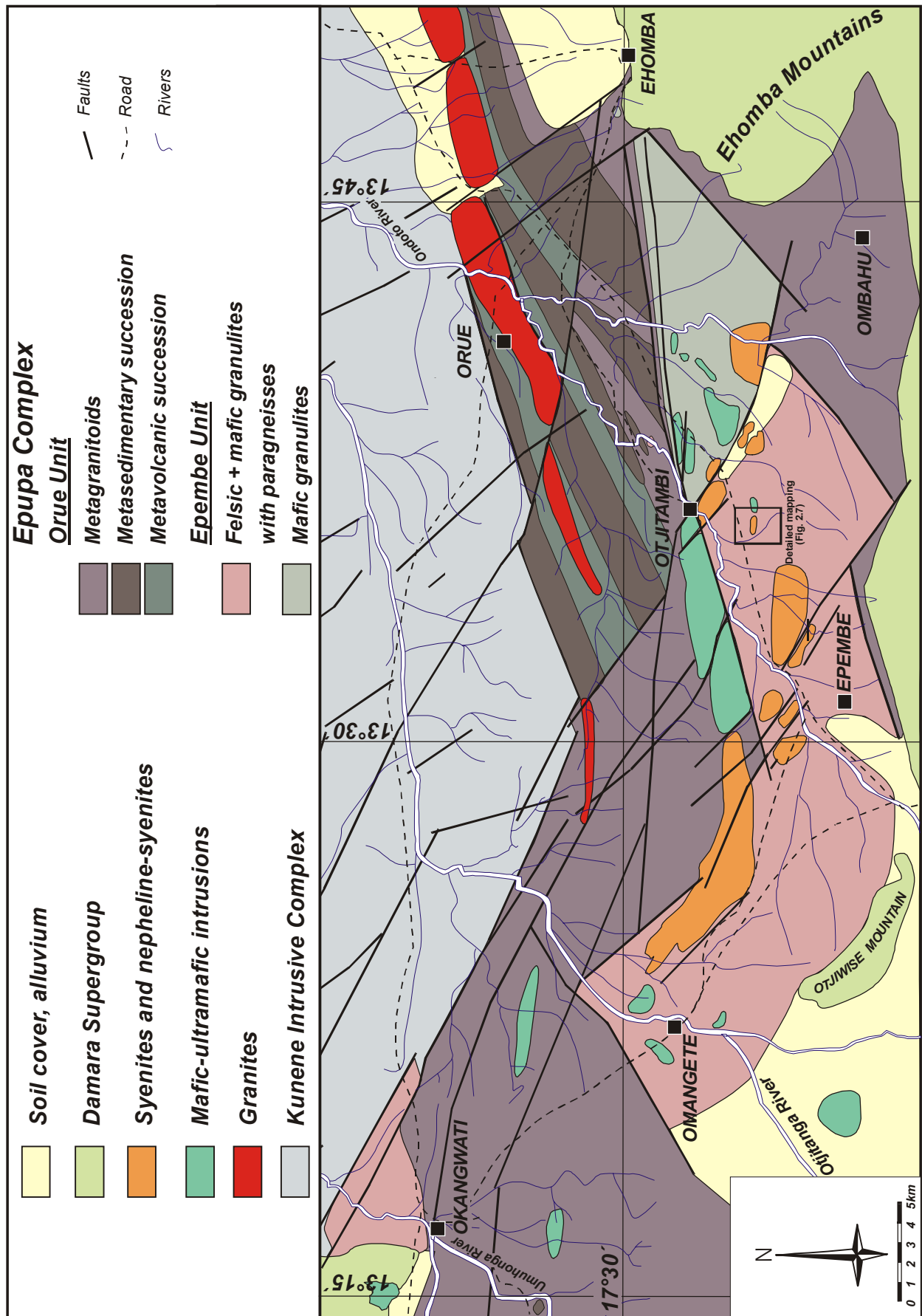


Fig. 2.2: Geological map of the southern part of the study area (modified after Menge, 1996).

of paragneisses ('metavolcanic succession'; Fig. 2.1, 2.2, 2.3a & b) and a succession, which is dominated by paragneisses with rare mafic and felsic metavolcanites ('metasedimentary succession'; Fig. 2.1, 2.2, 2.3c; 2.4). The metavolcanic succession is interpreted to have originated from bimodal volcanism. The metasedimentary succession is dominated by migmatitic metagreywackes, that comprise intercalations of mafic metavolcanites, migmatitic metapelites, metaarkoses, metaquartzites and rare calc-silicate rocks (Fig. 2.3c; 2.4d), the protoliths of which were presumably deposited contemporaneously with the volcanic activity.

The northern part of the EC (Fig. 2.1) is dominated by interlayered felsic and mafic metavolcanites with paragneisses becoming more abundant to the north. Rare metagranitoids occur as small bodies, which intruded the volcano-sedimentary sequence. The sequence is transected by several mylonitic, WNW-ESW trending faults and by a major mylonitic, broadly E-W trending subvertical dextral strike-slip fault, which displaces the former faults.

In the southern part of the study area the metamorphosed volcano-sedimentary sequence constitutes an E-W-trending strip of ~ 8 km in width, which is exposed in the eastern region of the mapped area ('south-eastern region'), situated between the KIC and the granulites of the Epembe Unit (Fig. 2.2). In this region, interlayered metavolcanites and metasediments form WSW-ENE-trending layers of several hundred meters thickness. Towards the west the volcano-sedimentary sequence is limited by WNW-ESE trending strike-slip faults. In the western region of the southern part ('south-western region') paragneisses are generally rare and only recognized in an isolated outcrop surrounded by metagranitoids at the Umuhonga River (Fig. 2.2). This outcrop (Loc. 246) comprises a ~ 400 m thick sequence of migmatitic metagreywackes, that contain intercalated schlieren and layers of migmatitic metapelites (of up to 30 m in width) and lenses of Grt-Hbl schists. However, as the south-western region of the Orue Unit is largely covered by soil, a more widespread occurrence of paragneisses is possible.

2.1.1.1 Metavolcanics

Felsic and mafic metavolcanites constitute the major rock types of the metavolcanic succession. Metavolcanic mafic rocks furthermore occur in the paragneiss succession.

The reddish to light grey felsic metavolcanites are quartzofeldspathic rocks (Fig. 2.3b), which contain rare hornblende and biotite and are termed *Hbl-Bt-bearing felsic gneisses*. The fine-grained rocks constitute homogeneous layers of a few centimeters up to several meters in width, interlayered with homogeneous, black bands of similar size composed of fine- to medium-grained garnet-free *amphibolites* (Fig. 2.3b). The amphibolite layers are generally persistent over several meters; in rare cases they are boudinaged into elongated lenses, which are wrapped by

the less competent felsic gneisses (Fig. 2.3b). The well-developed foliation of the amphibolites parallels both the compositional layering of the succession and the foliation of the felsic gneisses. Migmatitic textures are commonly developed in amphibolites, indicating partial melting during amphibolite facies metamorphism (Fig. 2.3d). Whitish, quartzofeldspathic leucosomes of several centimeters in width are developed as concordant bands parallel to the foliation planes ('stromatic leucosomes'). Locally, the coarse-grained leucosomes are isoclinally folded on a centimeter- to decimeter scale with the axial planes of the isoclinal folds oriented subparallel to the main foliation (Fig. 2.3d), indicating that the anatexis temperatures were attained prior to, or synchronous with, deformation.

In the metasedimentary succession medium-grained *amphibolites* and *garnet-amphibolites* form persistent and homogeneous black layers of up to 3 m in width (Fig. 2.3e). Remarkably, Grt-amphibolites are restricted to the metasedimentary successions of the southern part of the Orue Unit; comparable lithologies of the northern part are garnet-free.

Garnet-hornblende schists and *garnet-hornblendites* occur as layers of up to 3 m in width (Fig. 2.3c, f) or as partly boudinaged, lenticular lenses of up to one meter in width, which are elongated parallel to the main foliation (Fig. 2.3f), in the paragneisses. Sharp contacts between the garnet-hornblende schists and the adjacent paragneisses (Fig. 2.3f) suggest that the mafic metavolcanites occurring within the metasedimentary succession represent former basaltic dykes or sills. The (Grt)-amphibolites and the Grt-Hbl schists comprise a well-developed foliation, which parallels the foliation of the adjacent paragneisses, indicating their contemporaneous deformation.

2.1.1.2 Paragneisses

The paragneiss succession is dominated by migmatitic metagreywackes. The garnet- and biotite-bearing rock (*Grt-Bt gneisses*) exhibit a compositional banding, which is accentuated by dark-grey, biotite-rich layers alternating with light-grey biotite-poor layers (Fig. 2.3e). A well-developed foliation of the Grt-Bt gneisses parallels the compositional banding. The Grt-Bt gneisses comprise migmatitic textures with a separation into fine-grained, biotite-rich palaeosomes alternating with biotite-free, coarse-grained leucosomes, that are generally developed as light grey or whitish concordant bands and lenses parallel to the foliation ('stromatic leucosomes') of the palaeosomes (Fig. 2.4a), indicating pre- to syn-tectonic partial melting. Garnet occurs as distinct porphyroblasts up to 5 cm in diameter in the palaeosome as well as in the leucosome domains (Fig. 2.4a). Based on the migmatitic textures and the presence of garnet, the metagreywackes are distinguished from the texturally similar, but garnet-free and

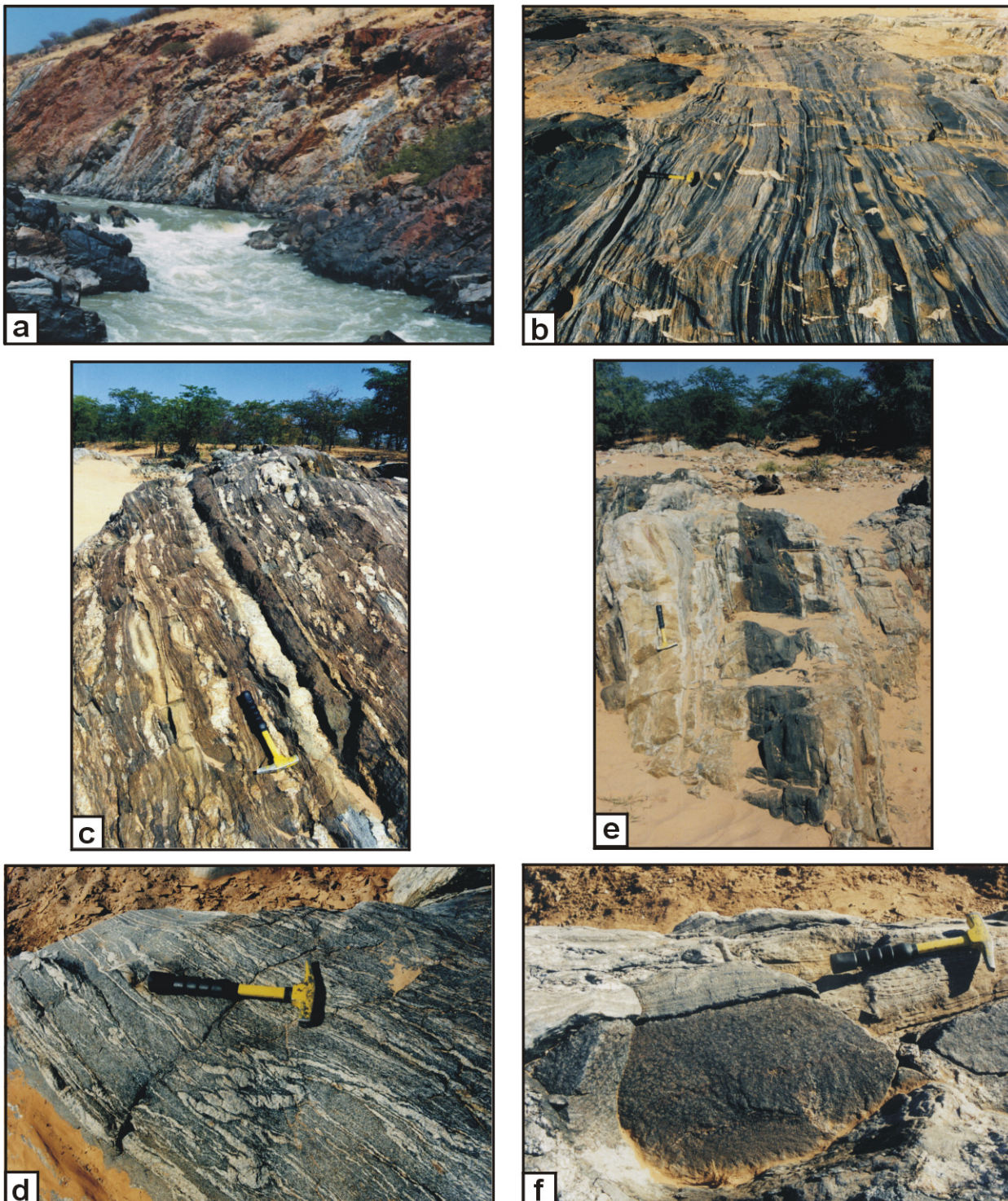


Fig. 2.3: Field relationships of the volcano-sedimentary sequence of the Orue Unit. **a)** Sequence of mafic (black) and felsic (red) metavolcanites with intercalations of paragneisses (grey) exposed at the Kunene River (Loc. 167). **b)** Interlayered amphibolites and felsic gneisses of the metavolcanic succession (Loc. 410). **c)** Metasedimentary succession with migmatitic metapelites (dark grey) with intercalated black layer of mafic garnet-hornblende schist and greenish lenses of calc-silicate rocks (Loc. 342). **d)** Migmatitic amphibolite of the metavolcanic succession with concordant and isoclinally folded leucosomes (Loc. 446). **e)** Layer of garnet-amphibolite with sharp contacts against adjacent metagreywackes (Loc. 401). **f)** Boudinaged lens of garnet-rich hornblende-schist with sharp contacts against adjacent metagreywackes (Loc. 588).

homogeneous metavolcanic felsic gneisses.

Metapelites form rare layers of up to 10 m in width intercalated in the metagreywackes. Remarkable lithological differences are recognized between metapelites of the southern and the northern part: Metapelites of the southern part are ***Grt-Bt-Sil gneisses and schists*** whereas metapelites of the northern part are generally garnet-free ***Crd-Bt gneisses***. The metapelitic Grt-Bt-Sil schists and gneisses of the southern part comprise migmatitic textures with a well-developed separation into dark grey or black, biotite-sillimanite-rich palaeosomes and white, biotite-free quartzofeldspathic leucosomes, that form pods, streaks and bands concordant to the foliation of the palaeosomes (Fig. 2.4b & c), indicating pre- to syn-tectonic partial melting. The foliation of the palaeosomes is defined by aligned biotite and sillimanite (Fig. 2.4c). Garnet occurs as porphyroblasts of up to 2 cm in diameter in the palaeosomes (Fig. 2.4c) and in the coarse-grained leucosomes. Due to the generally higher modal amount of biotite and the presence of macroscopically visible sillimanite, the metapelites can be distinguished from the texturally similar metagreywackes.

Like the metapelites of the southern part, the generally fine- to medium-grained garnet-free ***Crd-Bt gneisses*** of the northern part are characterized by migmatitic textures, indicating at least upper amphibolite facies temperatures. Dark grey, biotite-bearing palaeosomes alternate with light grey, biotite-poor or -free quartzofeldspathic leucosomes, that form streaks or bands concordant to the foliation of the fine-grained palaeosomes. Sillimanite is not observed on the macroscopic scale. Isoclinal folding of the leucosomes indicates pre- to syn-tectonic partial melting. At one locality, situated at the westernmost part of the northern field area, a garnet-bearing Crd-Bt gneiss (***Grt-Crd-Bt gneiss***) has been recognized. The fine-grained rock exhibits a cm-scaled banding into felsic leucosomes alternating with cordierite-rich palaeosomes. Fine-grained (< 1 mm) garnet occurs in both, the leucosomes and the palaeosomes.

Fine-grained, reddish biotite-bearing ***metaarkoses*** and grey ***metaquartzites*** constitute concordant and homogeneous layers of up to 20 m in width within the metasedimentary succession. ***Calc-silicate rocks*** generally occur as rare greenish lenses up to 1 meter in length, that are elongated parallel to the regional foliation of the surrounding paragneisses (Fig. 2.3c & 2.4d). In one outcrop (Loc. 181) folded calc-silicate rocks form a distinct layer of several meters in width. The calc-silicate rocks are fine- to medium grained, inhomogeneous with a granoblastic texture. Calc-silicate lenses locally display a compositional zoning, with the brownish cores being extremely Grt-rich whereas the outer zones are mainly composed of greenish amphibole (Fig. 2.4d).

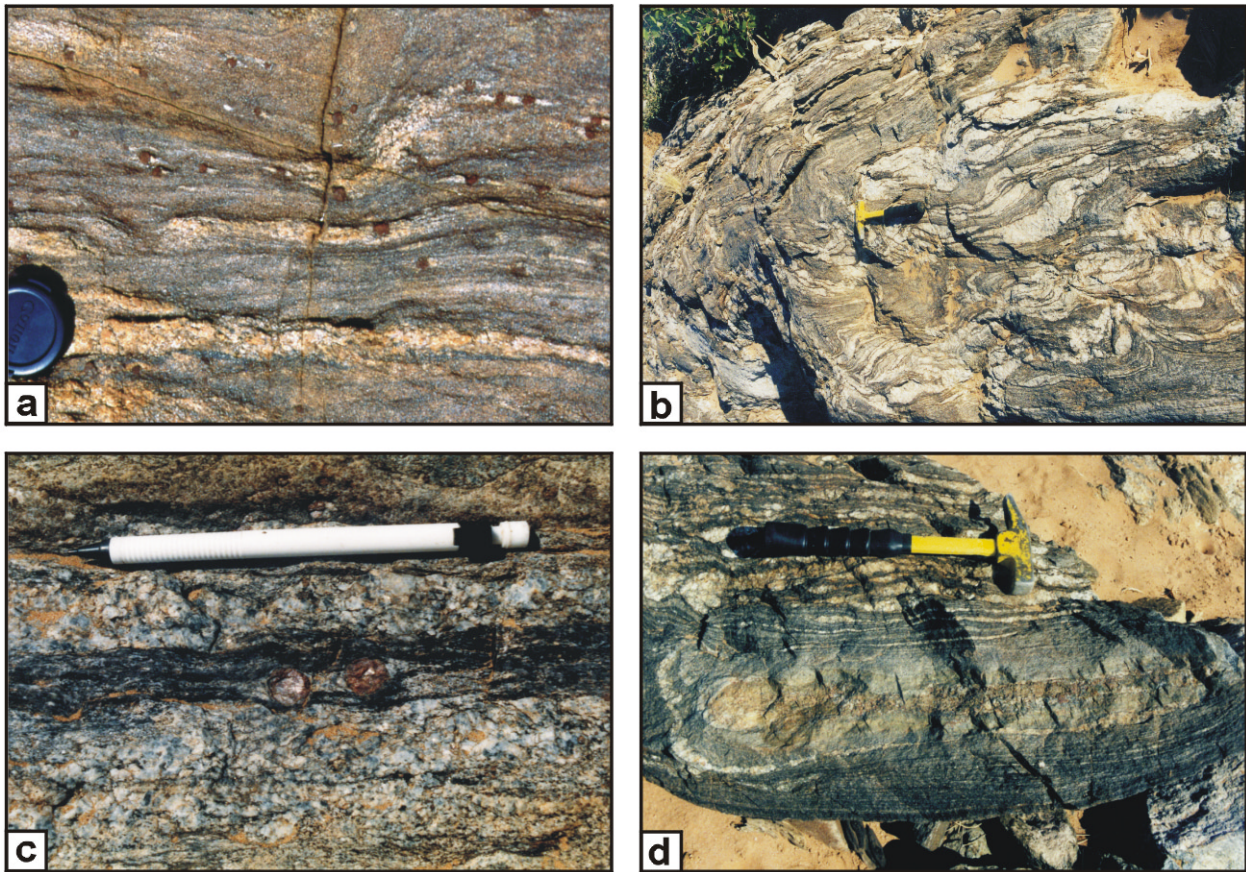


Fig. 2.4: Field relationships of the paragneisses of the Orue Unit. **a)** Migmatitic metagreywacke-type Grt-Bt gneiss with stromatic leucosomes and asymmetric pressure shadows around garnet (Loc. 177). **b)** Folded layer of migmatitic metapelitic Grt-Bt-Sil schist of the southern part. Abundant leucosomes occur as schlieren and bands concordant to the foliation of the palaeosomes (Loc. 588). **c)** Rotated garnet in a Bt-Sil-rich palaeosome of a Grt-Bt-Sil gneiss of the southern part (Loc. 401). **d)** Elongated lens of calc-silicate rock in a metapelite layer displaying a compositional zoning with Grt-rich cores and Hbl-rich rims (Loc. 342).

2.1.2 Metagranitoids

Large parts of the southern part of the Orue Unit are occupied by hornblende and biotite-bearing metagranitoids (*Hbl-Bt metagranitoids*; Fig. 2.2), whereas they are just rarely observed in the northern part of the study area (Fig. 2.1).

The Hbl-Bt metagranitoids exhibit characteristic migmatitic textures (Fig. 2.5a). Due to a separation into palaeosomes and concordant leucosomes, that preferentially crystallized along pre-existing foliation planes, a striking, centimeter to decimeter scaled banding is developed (Fig. 2.5a). Dark, relatively hornblende- and biotite-rich palaeosomes alternate with pale red or grey, quartzofeldspathic leucosomes, which rarely contain coarse hornblende. The fine-grained palaeosomes display a foliation defined by aligned biotite. Locally, the medium- to coarse-

grained leucosomes are folded on a decimeter scale (Fig. 2.5a), indicating that melting of the Hbl-Bt metagranitoids occurred pre- to syn-tectonically. Primary intrusive contacts against the para- and orthogneisses of the volcano-sedimentary sequences were not observed, since the contacts are generally overprinted by late faults. However, as the metagranitoids contain isolated, meter-scaled angular xenoliths of amphibolites (Fig. 2.5b) and paragneisses, which partly preserve an early, discordant foliation, they are interpreted to be intrusive into the volcano-sedimentary sequence.

In the south-western part of the Orue Unit metagranitoids were affected by ductile deformation giving the rocks an augengneiss structure (Fig. 2.5c). Partly elongated K-feldspar porphyroblasts of up to 15 cm in diameter are wrapped by a fine-grained mylonitic foliation.



Fig. 2.5: Field relationships of the metagranitoids and the contact metamorphic rocks of the Orue Unit. **a)** Migmatitic metagranitoid with concordant hornblende-bearing quartzofeldspathic leucosomes (Loc. 401). **b)** Isolated xenolith of amphibolite in a metagranitoid (Loc. 401). **c)** Granitic gneiss with a typical augengneiss texture defined by K-feldspar porphyroblasts wrapped by a mylonitic matrix (Loc. 241). **d)** Streaks of contact-metamorphic massive metapelitic Grt-Sil-Crd rock in a quartzofeldspathic matrix, exposed in the southern part of the Orue Unit close to the contact to the KIC (Loc. 302).

2.1.3 Mafic dykes metamorphosed under amphibolite facies conditions

The metagranitoids were locally intruded by persistent and homogeneous *mafic dykes* of up to 2 m in width, which were metamorphosed to black, medium-grained amphibolites. Sharp contacts against the metagranitoids testify to the intrusive character of the mafic rocks. The well-developed foliation of the garnet-free amphibolites parallels the foliation of the surrounding metagranitoids, indicating contemporaneous deformation.

2.1.4 Contact metamorphic phenomena

A contact thermal effect probably induced by the emplacement of the anorthosites of the KIC is restricted to a narrow reaction zone, that parallels the southern margin of the KIC, and is recorded by massive metapelitic *Grt-Sil-Crd rocks* (Brandt et al. 2003). As the contact region between the EC and the KIC is largely covered by soil a more accurate determination of the regional extent of the contact phenomena is impossible.

The Grt-Sil-Crd rocks occur as centimeter- to decimeter-sized streaks in a grey, fine- to medium-grained quartzitic host rock (Fig. 2.5d). They are dominated by cm-sized sillimanite, coexisting with rare cm-sized garnet, which are set in a fine-grained hornfels-like cordierite-rich matrix. In clear contrast to the well-developed foliation of the southward following Grt-Bt-Sil gneisses and schists, the Grt-Sil-Crd rocks exhibit a massive texture. Their close spatial association with the anorthosites as well as their massive texture suggest that the formation of the Grt-Sil-Crd rocks is related to a contact thermal effect induced by the emplacement of the KIC.

2.2 UHT GRANULITES OF THE EPEMBE UNIT

The Epembe Unit is an orthogneiss-dominated granulites facies terrane, which is exposed at the southern margin of the KIC (Fig. 2.2). Major parts of the Epembe Unit were previously misinterpreted as amphibolitic gneisses (Menge, 1996). Nonetheless, the widespread occurrence of orthopyroxene in the mafic and felsic gneisses and in part of the paragneisses provides a first-order indication of granulite facies conditions during peak-metamorphism. Along the surrounding shear zones the granulites of the Epembe Unit are partly or completely retrogressed to fine-grained, mylonitic amphibolite facies rocks.

Based on field observations three lithostratigraphic subunits are recognized in the Epembe Unit: The Epembe Unit is essentially (1) a succession of interlayered mafic and felsic metavolcanites with intercalated layers of metapelites, metagreywackes and Qtz-rich Grt-Opx rocks (Fig. 2.6a), that is interpreted as a granulite facies volcano-sedimentary sequence compositionally similar to the volcano-sedimentary sequence of the Orue Unit. Conspicuous sapphirine-bearing Opx-Sil gneisses and Opx-Grt rocks occur as rare schlieren in part of the metagreywacke layers (Brandt et al., 2003). The volcano-sedimentary sequence of the Epembe Unit was locally intruded by (2) Grt-Opx metagranitoids and by (3) mafic dykes, both metamorphosed under granulite facies conditions together with their country rocks.

Besides this large continuous terrane, granulite facies rocks are exposed in three more occurrences, all of them situated in or near late faults hence suggesting that these granulite-facies rocks represent tectonic slabs, which were sheared off in the lower crust and uplifted by the hosting fault:

(a) The largest occurrence (~ 7 km in length) is exposed north of Okangwati and occurs in a major shear zone, which separates the anorthositic rocks of the KIC from the Orue Unit (Fig. 2.2). The contact to the adjacent anorthosites of the KIC is marked by a steeply dipping major shear zone whereas the contact to the Orue Unit is covered by soil. The granulites are predominantly garnet-free felsic granulites, which are interlayered with mafic granulites and are rare layers of garnet-rich metaquartzites and of garnet-bearing metagreywackes.

(b) A lens of granulite facies rocks is situated east of Otjitambi in the Ondoto riverbed (Fig. 2.2). This lens is ~ 10 m in width and is mainly composed of garnet-rich metapelitic granulites, that are concordantly interlayered with felsic and mafic granulites (Fig. 2.6b). This succession resembles the granulite succession of the central part of the Epembe Unit and is therefore attributed to the Epembe Unit. Contacts to the surrounding metagranitoids of the Orue Unit are covered by soil.

(c) A small lens of granulite facies rocks (2 m in width) is exposed to the west of Ehomba (Fig. 2.2) within a NNE-SSW trending subvertical shear zone, which is composed of strongly foliated granitic gneisses. This shear zone is interpreted as the east-ward continuation of the shear zone, that separates the eastern part of the Epembe Unit from the Orue Unit (Fig. 2.2). Sharp and discordant contacts against the surrounding granitic gneisses indicate that the lens is of tectonic nature. (Fig. 2.6c). It is constituted by black bands of mafic Grt-Cpx granulites of up to 30 cm in width, that are concordantly interlayered with greenish, plagioclase-rich bands, containing only rare garnet (Fig. 2.6c).

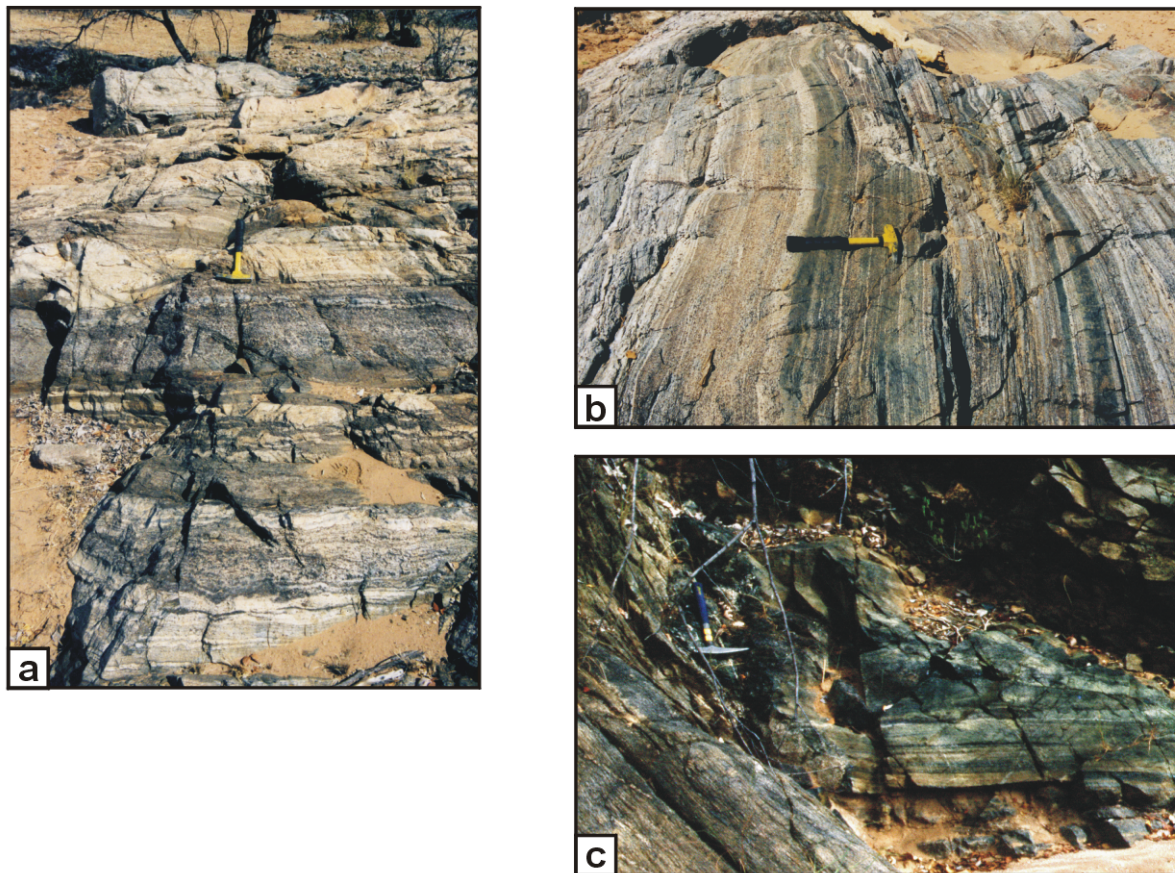


Fig. 2.6: Field relationships of the Epembe Unit. **a)** Volcano-sedimentary sequence of the Epembe Unit consisting of metavolcanic felsic granulites (white bands), metavolcanic mafic granulites (black bands) and garnet-rich metapelites (grey layer in the center of the photo) of the Epembe Unit (Loc. 551). **b)** Lens of granulite facies rocks in the Ondoto River, consisting of interlayered mafic granulites (black bands), felsic granulites (white bands) and garnet-rich metapelitic granulites (Loc. 509). **c)** Tectonic lens of banded mafic Grt-Cpx granulites (right) within a shear zone composed of strongly foliated granitic gneisses (left): Note sharp and discordant contacts of the granulites against the granitic gneisses (Loc. 311).

2.2.1 Volcano-sedimentary sequence

The lithology of the volcano-sedimentary sequence exhibits some minor regional variations (Fig. 2.2): In the central part of the Epembe Unit abundant paragneisses are intercalated with the felsic and mafic metavolcanites, while they are rare in an eastern portion.

In order to constrain the composition and the structure of the Epembe Unit in some more detail a subarea of the central part (shown in Fig. 2.2), which comprises the best rock exposures, has been mapped in detail (Fig. 2.7a): This central part of the Epembe Unit is dominated by garnet-free metavolcanic felsic granulites, which are concordantly interlayered with metavolcanic mafic granulites on a decimeter to several hundred meter scale. Layers of metapelites, Qtz-rich Grt-Opx rocks and metagreywackes, the latter containing schlieren of sapphirine-bearing Opx-Sil gneisses and of orthopyroxene-garnet rocks, are concordantly intercalated in the metavolcanites. In contrast to the Orue Unit, calc-silicate rocks are absent in the Epembe Unit. In the northern part of the mapped area the granulites comprise a WNW-ESE trending banding, which is steeply inclined towards SSW (Fig. 2.7a & b). In the central and southern part, the granulites show an E-W trending banding, which is steeply inclined to either N or S. The sequence is transected by several subvertical, E-W trending cataclastic faults, which were intruded by late syenites and gabbros. The orientation of the banding of the granulites changes between these shear zones, and thus the individual granulite blocks were probably weakly contorted during the formation of the shear zones.

In the following the field relationships of the various granulite facies lithologies of the Epembe Unit will be described in order to resolve the temporal sequence of magmatic and metamorphic events. The granulite facies rocks of the volcano-sedimentary sequence of the Epembe Unit are broadly subdivided into (1) metavolcanites including mafic granulites and felsic granulites, and (2) paragneisses with metapelites, Qtz-rich Grt-Opx rocks and metagreywackes with schlieren of sapphirine-bearing Opx-Sil gneisses and sapphirine-free Opx-Grt rocks.

2.2.2.1 *Metavolcanics*

Garnet-free felsic granulites are the most abundant rock type of the Epembe Unit and constitute homogeneous layers of up to several 10 meters in width (Fig. 2.7a). The white or light grey rocks contain rare brown orthopyroxene, which occurs as weakly aligned, cm-sized porphyroblasts in a fine-grained, quartzofeldspathic matrix (Fig. 2.8a), and are therefore termed as *pyroxene-bearing granulites*.

Mafic granulites form abundant, homogenous layers of a few centimeters up to several 10

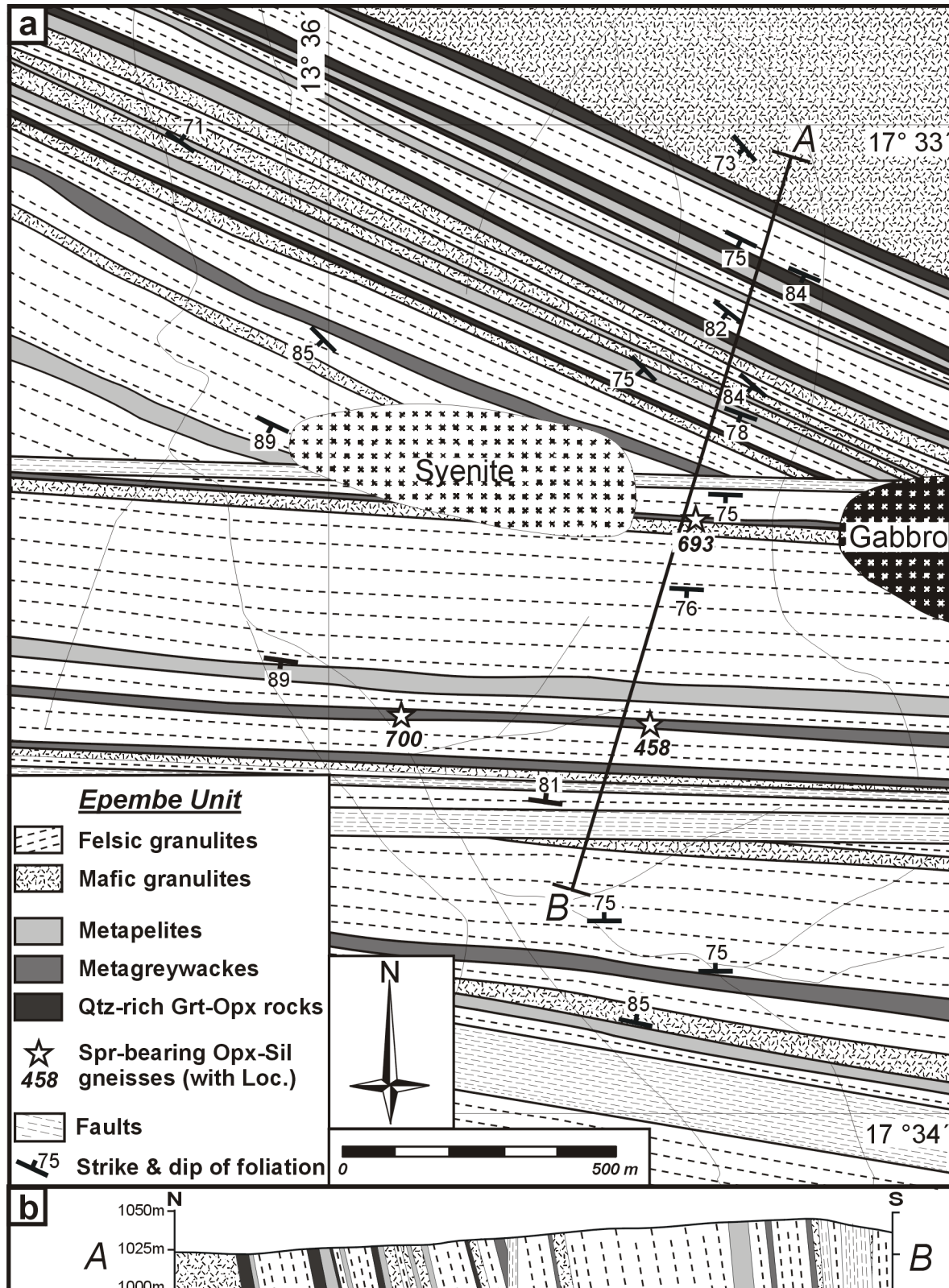


Fig. 2.7: **a)** Detailed mapping of the central part of the Epembe Unit (see Fig. 2.2 for the location of the area mapped) with the occurrence of sapphirine-bearing Opx-Sil gneisses in the metagreywacke-type Grt-Opx gneisses. **b)** Cross section through the central part of the Epembe Unit (see Fig. 2.7a for the location of profile).

meters thickness, which are concordantly interlayered with the felsic pyroxene-bearing granulites (Fig. 2.8a). The fine- to medium-grained mafic granulites are generally massive to weakly foliated, homogenous *two-pyroxene granulites* with a brownish alteration rind; fresh samples are black (Fig. 2.8b). In places, small- scaled isoclinal folding, accentuated by thin layers enriched in plagioclase, is observed (Fig. 2.8b). *Garnet-bearing two-pyroxene granulites* are rare. Garnet occurs as cm-sized porphyroblasts (< 5 cm in diameter) in the fine-grained two-pyroxene matrix (Fig. 2.8c). Undeformed, cm-sized plagioclase-rich corona textures around garnet indicate post-tectonic retrograde garnet replacement. In places, former garnet is pseudomorphosed by fine-grained plagioclase and orthopyroxene (Fig. 2.8d). Locally developed migmatitic textures with garnet-free and plagioclase-rich, coarse-grained leucosomes indicate that the mafic granulites were affected by partial melting. (Fig. 2.8e). Retrogressed two-pyroxene granulites exposed in shear zones are transformed into fine-to medium grained amphibolites, displaying hornblende-coronas around the pyroxenes and a secondary foliation (Fig. 2.8f).

Mafic garnet- and clinopyroxene-bearing granulites (*Grt-Cpx granulites*) exclusively occur in the tectonic lens exposed to the west of Ehomba in a shear zone (Fig. 2.2; Fig. 2.6c). The coarse-grained massive rocks contain abundant garnet, which forms porphyroblasts of up to 5 cm in diameter and is set in a black matrix mainly composed of cm-sized clinopyroxene and hornblende. In contrast to the two-pyroxene granulites, the Grt-Cpx granulites are almost devoid of plagioclase.

2.2.2.2 Paragneisses

Garnet- and sillimanite-bearing metapelites (*Grt-Sil gneisses*) constitute homogeneous layers of up to 40 m in width, that are concordantly interlayered with the metavolcanic felsic and mafic granulites (Fig. 2.7a). In contrast to the biotite-rich metapelites of the Orue Unit, the metapelitic Grt-Sil gneisses of the Epembe Unit are essentially biotite-free. The Grt-Sil gneisses were affected by extensive partial melting. Two structural types of leucosomes were distinguished (Fig. 2.9a-c): (1) A distinct cm-scaled banding of the Grt-Sil gneisses is defined by white bands of concordant coarse-grained quartzofeldspathic leucosomes ('stromatic leucosomes'), that alternate with black layers of sillimanite-rich palaeosomes (Fig. 2.9a-c), indicating pre- to syn-tectonic partial melting. The stromatic leucosomes generally parallel the well-developed foliation of the palaeosomes. Abundant garnet occurs as porphyroblasts of up to 4 cm in diameter in both the palaeosomes and the leucosomes (Fig. 2.9b). (2) The second type of leucosomes crystallized as homogeneous and weakly deformed quartzofeldspathic streaks and masses, which cross-cut the banding of the Grt-Sil gneisses ('agmatic leucosomes'; Fig. 2.9c). Locally, partial melting was extensive and restitic Grt-Sil gneisses occur as schollen and rafts in the garnet-bearing,

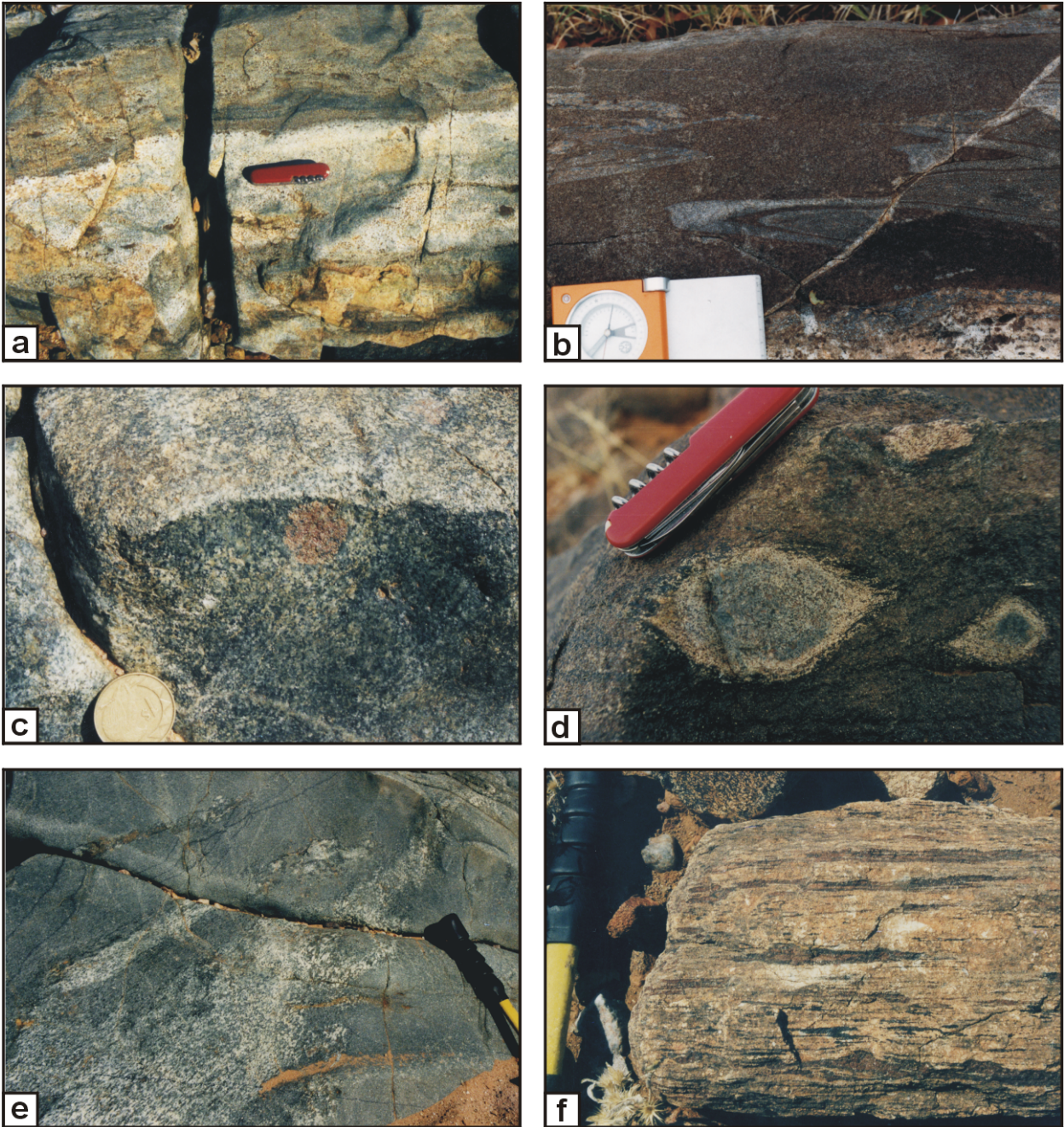


Fig. 2.8: Field relationships of the felsic and mafic granulites of the Epembe Unit. **a)** White, garnet-free felsic granulite with porphyroblasts of orthopyroxene (brown patches) interlayered with dark mafic granulite (Loc. 580). **b)** Brownish, garnet-free mafic two-pyroxene granulite with small scaled isoclinal folds, transsected by a late fissure (Loc. 634). **c)** Massive, mafic two-pyroxene granulite with porphyroblastic garnet (Loc. 326). **d)** Fine-grained mafic two-pyroxene granulite with pseudomorphs of orthopyroxene and plagioclase after deformed porphyroblasts of garnet (Loc. 493). **e)** Migmatitic mafic two-pyroxene granulite with coarse-grained plagioclase-rich leucosome (Loc. 326). **f)** Strongly deformed plagioclase-rich mafic two-pyroxene granulite with corona textures of black hornblende around brownish pyroxene (Loc. 528).

coarse-grained leucosomes (Fig. 2.9c).

Qtz-rich Grt-Opx rocks occur as distinct layers of up to 20 m in width within the volcano-sedimentary sequence of the Epembe Unit (Fig. 2.7a, 2.9d). Due to their high modal amounts of quartz, these layers are exceptionally resistant to weathering; therefore they can be traced over several 10's of meters in the field (Fig. 2.9d). The layers are oriented parallel to the regional banding; gradual contacts towards adjacent metapelite layers suggest their derivation from sedimentary protoliths. The Qtz-rich Grt-Opx rocks display a massive or banded texture with abundant porphyroblastic garnet (up to 5 cm in diameter) and minor amounts of orthopyroxene, which are homogeneously distributed in a grey, fine- to medium-grained quartzitic matrix (Fig. 2.9e). Brown, orthopyroxene-bearing corona textures around garnet are already visible on a macroscopic scale (Fig. 2.9e). The rocks contain distinct dark lenses, which are almost completely composed of coarse-grained garnet of up to 7 cm in diameter and possibly represent restitic domains.

The granulite facies metagreywackes are subdivided into two units: (1) Garnet-bearing metagreywackes (**Grt gneisses**) constitute layers of up to several meters in width. These rocks commonly display a characteristic banding, which results from partial melting and is defined by fine- to medium-grained, black palaeosomes with abundant garnet and minor biotite. These palaeosomes alternate with concordant light grey and coarse-grained quartzofeldspathic stromatic leucosomes, which also contain garnet but are essentially biotite-free (Fig. 2.10a). Furthermore, Grt gneisses occur as weakly foliated, homogeneous rocks, which contain abundant garnet and are devoid of biotite. (2) Garnet-and orthopyroxene bearing migmatitic metagreywackes, termed **Grt-Opx gneisses**, occur as layers up to 8 m in width within the volcano-sedimentary sequence and are oriented parallel to the regional banding. Gradual contacts towards adjacent metapelite layers suggest a derivation from sedimentary protoliths. As recognized for the metapelites, two structural types of leucosomes are observed in the Grt-Opx gneisses, i.e.: (1) Due to the formation of concordant, stromatic leucosomes, developed during initial pre- to syn-tectonic partial melting, the Grt-Opx gneisses exhibit a distinct small-scaled banded texture, which is defined by black, medium- to coarse-grained melanosomes of restitic, orthopyroxene-rich composition, alternating with light grey and medium-grained quartzofeldspathic leucosomes, that only contain subordinate orthopyroxene (Fig. 2.10b). Garnet occurs as rare cm-sized porphyroblasts in the leucosomes and in the palaeosomes (Fig. 2.10b). (2) Locally, the banded migmatitic texture of the Grt-Opx gneisses is modified by the extensive formation of a second generation of leucosomes (Fig. 2.10c), which crystallized as discordant,

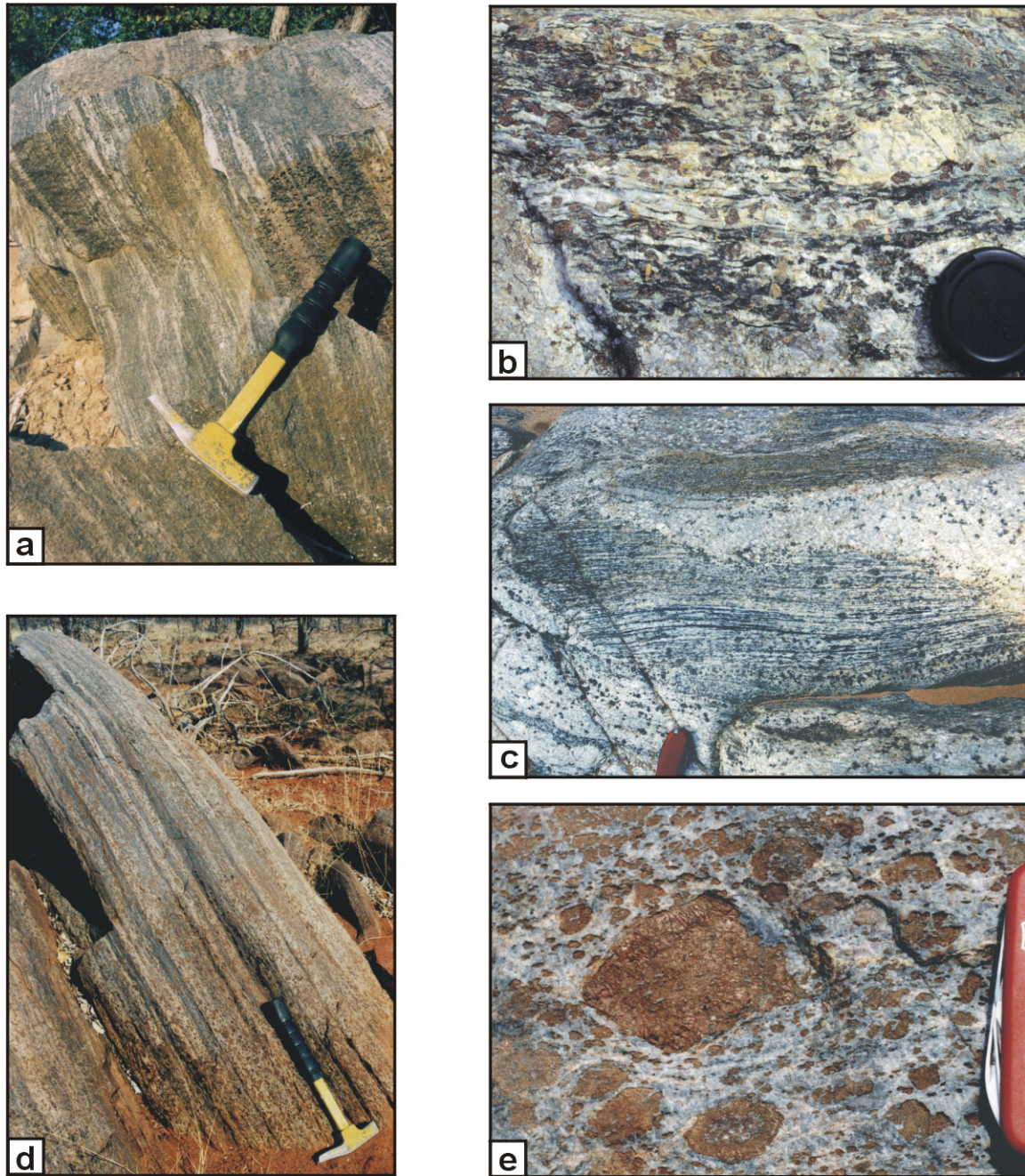


Fig. 2.9: Photomicrographs illustrating field relationships of the metapelite Grt-Sil gneisses and the Qtz-rich Grt-Opx rocks of the Epembe Unit. **a)** Layer of migmatitic metapelite Grt-Sil gneiss with characteristic banding, which is defined by white concordant leucosomes alternating with black palaeosomes (Loc. 545). **b)** Migmatitic metapelite Grt-Sil gneiss with abundant garnet in the palaeosomes and in the leucosomes (Loc. 212). **c)** Schollen of banded, metapelite Grt-Sil gneiss with early, concordant garnet-bearing leucosomes, transected by late, discordant garnet-bearing leucosomes (Loc. 465). **d)** Layer of banded Qtz-rich Grt-Opx rocks. Note the high modal abundance of garnet (Loc. 614). **e)** Porphyroblastic garnet in a quartzitic matrix of a Qtz-rich Grt-Opx rock; smaller garnet is surrounded by a brown orthopyroxene-bearing corona of (Loc. 614).

agmatic quartzofeldspathic streaks. The coarse-grained discordant leucosomes contain garnet and, in contrast to the orthopyroxene-bearing concordant leucosomes, cm-sized biotite.

Sapphirine-bearing Opx-Sil gneisses and *Opx-Grt rocks* have been recognized in three localities, shown in Fig. 2.7a. In these localities the rocks occur as black schlieren of up to 1m in diameter within the metagreywacke-type migmatitic Grt-Opx gneisses (Fig. 2.10d & e) and are aligned parallel to the regional banding. The Opx-Sil gneisses contain abundant coarse-grained orthopyroxene of up to 1 cm in length and rare cm-sized prismatic sillimanite, which is rimmed by a blue-greenish corona (Fig. 2.10d); microscopic investigations indicate that this corona is mainly composed of sapphirine (see Chapter 5.1.3.4). The weak foliation of the Opx-Sil gneisses parallels the foliation of the hosting Grt-Opx gneisses and the regional foliation, suggesting contemporaneous deformation. In contrast, the sapphirine- and sillimanite-free Opx-Grt rocks are massive and dominated by coarse-grained orthopyroxene and garnet (Fig. 2.10e). The restitic mineralogy of both the sapphirine-bearing Opx-Sil gneisses and the Opx-Grt rocks and their restricted occurrence within the migmatitic metagreywacke-type Grt-Opx gneisses suggest that both rock units represent restitic material, derived during partial melting of the hosting metagreywacke-type migmatitic Grt-Opx gneisses.

2.2.2 Metagranitoids

The volcano-sedimentary sequence of the Epembe Unit was intruded by granitoid bodies, which were subsequently metamorphosed to *Grt-Opx metagranitoids*. In contrast to the Orue Unit, however, metagranitoids are but rarely observed in the Epembe Unit, constituting small, isolated bodies. The rocks contain abundant angular xenoliths of mafic granulites of the volcano-sedimentary sequence (Fig. 2.11a), which partly exhibit a discordant internal foliation (Fig. 2.11b).

The medium- to coarse-grained metagranitoids contain sporadic cm-sized garnet and orthopyroxene, which are set in white or light grey, granoblastic quartzofeldspathic matrix. The presence of orthopyroxene indicates that the metagranitoids were affected by a comparable granulite facies metamorphic event like the intruded volcano-sedimentary sequence. Due to the lack of migmatitic textures, the Grt-Opx metagranitoids can be distinguished from the metagreywacke-type Grt-Opx gneisses. The generally weak foliation of the metagranitoids parallels the regional foliation of the intruded gneisses of the volcano-sedimentary sequence, suggesting their contemporaneous deformation.

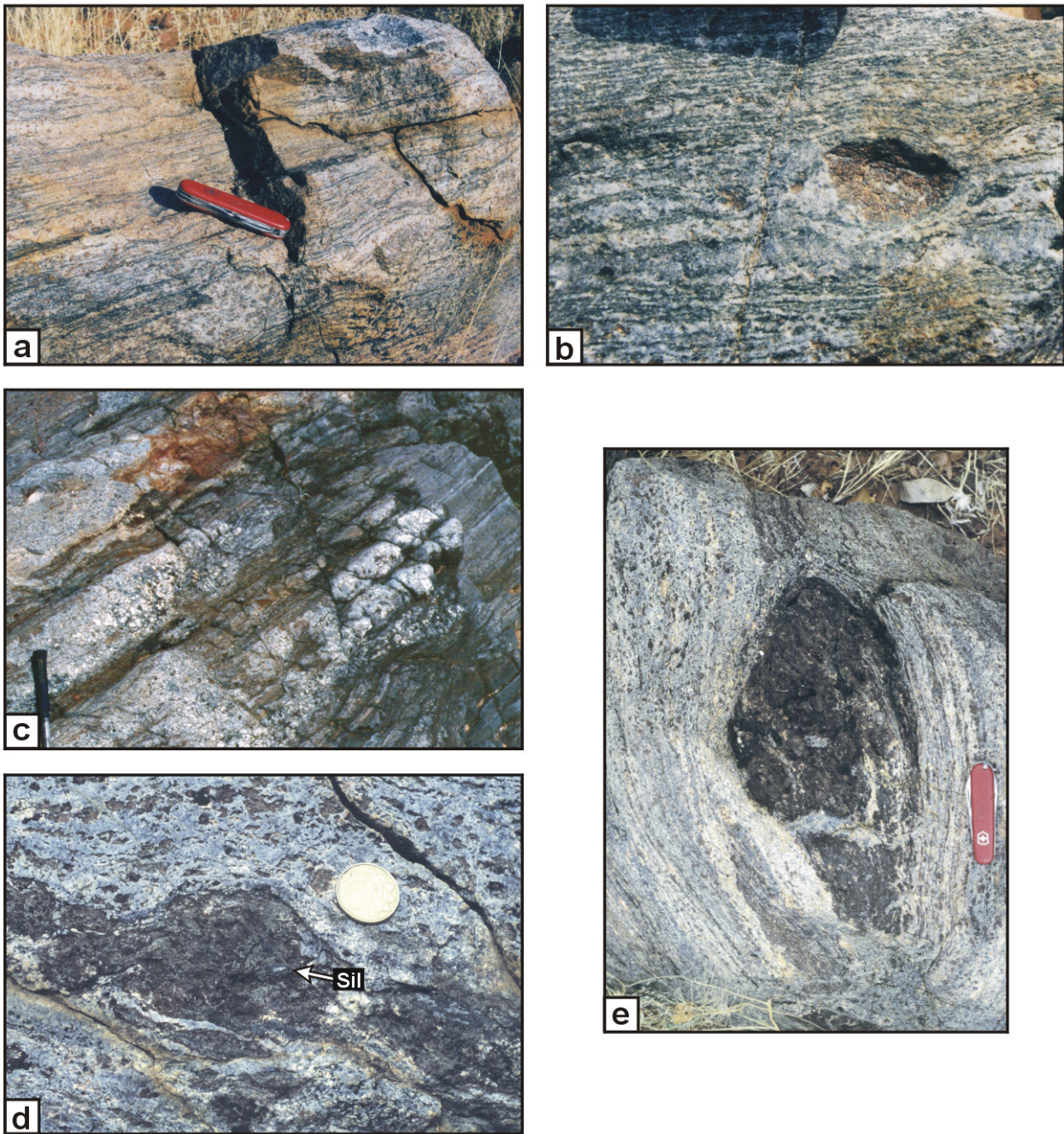


Fig. 2.10: Field relationships of the metagreywacke-type Grt gneisses and Grt-Opx gneisses and of the sapphirine-bearing Opx-Sil gneisses and Opx-Grt rocks of the Epembe Unit. **a)** Migmatitic metagreywacke-type Grt gneiss displaying concordant leucosomes (Loc. 574). **b)** Garnet porphyroblast of a migmatitic metagreywacke-type Grt-Opx gneiss, consisting of concordant quartzofeldspathic leucosomes and black orthopyroxene-rich palaeosomes (Loc. 486). **c)** Migmatitic metagreywacke-type Grt-Opx gneiss with discordant leucosomes (Loc. 690). **d).** Schlieren of sapphirine-bearing Opx-Sil granulite in a migmatitic metagreywacke-type Grt-Opx gneiss (Loc. 458). Arrow marks sillimanite (Sil), rimmed by a blue-green sapphirine-bearing corona. **e)** Boudinaged lens of Opx-Grt rock in a migmatitic metagreywacke-type Grt-Opx gneiss (Loc. 700).

2.2.3 Mafic dykes metamorphosed under granulite facies conditions

The volcano-sedimentary sequence was furthermore intruded by discordant black or dark grey veins and dykes mafic dykes of up to 50 cm in width (Fig. 2.11c), which crosscut the compositional banding of the volcano-sedimentary sequence under a low angle. These dykes were metamorphosed under granulite facies conditions to fine-grained mafic granulites, i.e. (***Grt-bearing***) ***Opx-Pl-Qtz granulites***, suggesting that they were affected by the same granulite facies metamorphic event like their country rocks. Dark contact zones, developed between mafic dykes and the surrounding migmatitic paragneisses, point to an interaction between the anatectic melts of the paragneisses and the dykes. Lenses and schlieren of mafic granulites observed in the paragneisses are interpreted as boudinaged mafic dykes.



Fig. 2.11: Field relationships of the metagranitoids and the metamorphosed mafic dykes of the Epembe Unit. **a)** Weakly foliated granulate facies Grt-Opx metagranitoid with abundant xenoliths of mafic granulites (black). The metagranitoid is transsected by a late aplite dyke (Loc. 661). **b)** Grt-Opx metagranitoid with angular xenolith of mafic granulite, which preserves an internal foliation (Loc. 661). **c)** Discordant granulate facies mafic dyke, which crosscuts the banding of a Qtz-rich Grt-Opx rock under a low angle (Loc. 614).

2.3 TECTONICS

To constrain the temporal relationship between metamorphism and deformation, the orientation of gneisses of both the Orue Unit and the Epembe Unit have been investigated in some detail.

2.3.1 Structure of the Orue Unit

Xenoliths of amphibolite and paragneiss of the volcano-sedimentary sequence, incorporated by metagranitoids, display an internal foliation which is oriented discordant to the regional foliation of their host rock, hence providing evidence for an early but yet unspecified deformation event (Fig. 2.5b).

During the main, ductile deformation event D_1 a strong foliation was developed in both the ortho- and paragneisses of the volcano-sequence succession and in the intrusive Hbl-Bt metagranitoids, indicating that both subunits were affected by the same tectonic event, which post-dates the emplacement of the metagranitoids. The orientation of the S_1 foliation is uniform throughout the Orue Unit: In the northern part the steeply inclined S_1 foliation planes broadly dip to SE and NW with two maxima at 153/84 and 320/68 (Fig. 2.12). Both the S_1 foliation and the leucosomes of migmatitic gneisses are isoclinally folded, suggesting that melting pre-dates deformation D_1 . Rare mineral stretching lineations L_1 on S_1 foliation planes generally plunge

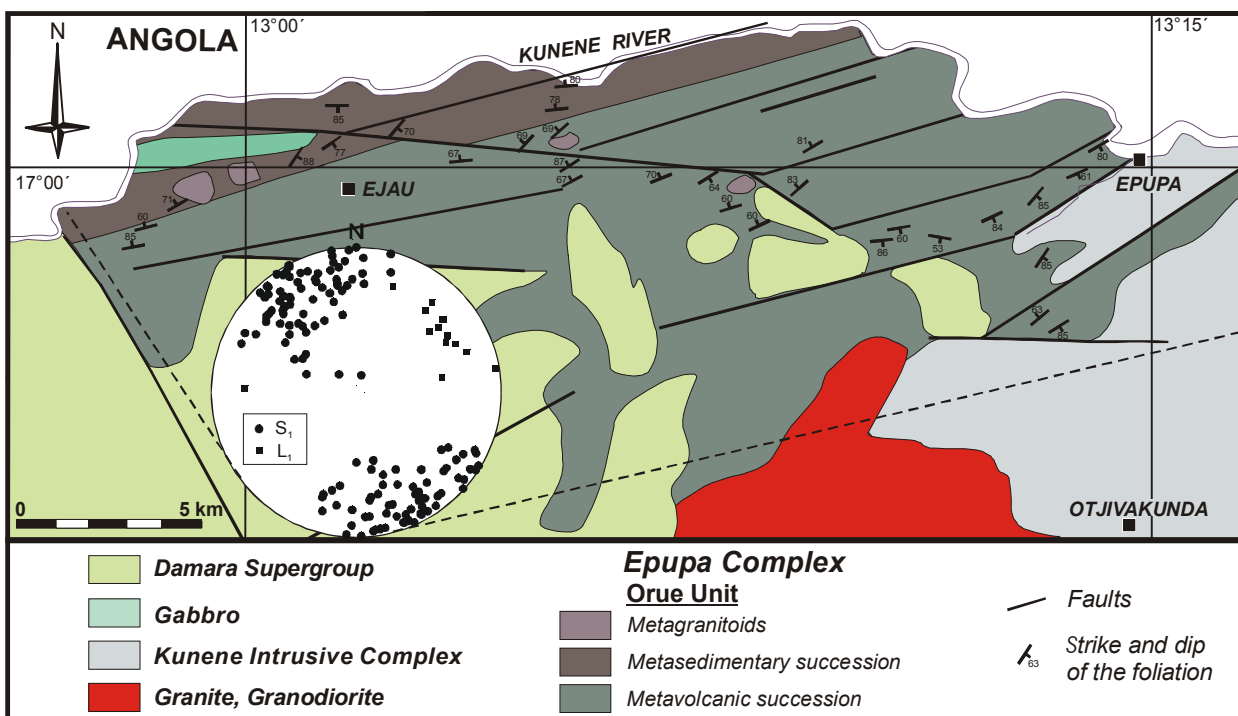


Fig. 2.12: Geological map of the northern part of the study area with equal area (lower hemisphere) stereographic projection of D_1 fabrics: S_1 : poles of foliation planes, L_1 : plunge of mineral stretching lineations.

with $\sim 25^\circ$ to ENE. In the eastern portion of the southern part (south-eastern region) the subvertical S_1 foliation planes show a similar orientation, generally dipping to NNW and SSE with maxima of 151/86 and 331/81 (Fig. 2.13). As in the northern part, the S_1 foliation and leucosomes of the migmatitic gneisses are folded to E-vergent isoclinal folds. The axes of the F_1 folds plunge with 15° to WSW. They are orientated subparallel to the mineral stretching lineations L_1 , which plunge moderately to the SW-WSW. These structural relationship points to a syn-metamorphic deformation. Asymmetric pressure shadows around garnet porphyroblasts (Fig. 2.4c), that are oriented parallel to the L_1 lineations, boudinage structures, small-scaled shear zones and deformed leucosomes demonstrate that D_1 was associated by shearing. The weakly exposed south-western region is structurally similar to the south-eastern region, but the foliation planes are less steeply inclined (Fig. 2.13).

Structural similarities indicate that all parts of the Orue Unit developed under the same tectonic regime. The orientation of the S_1 foliation planes points to a compression from SSE or NNW during D_1 .

2.3.2 Structure of the Epembe Unit

The earliest visible deformational structures are observed in xenoliths of mafic granulites, which are incorporated by the intruded Grt-Opx metagranitoids (Fig. 2.11a & b). The xenoliths preserve an early, internal foliation, which is oriented perpendicular to the external, regional foliation S_1 of the intrusive suite, hence indicating an early but yet unspecified tectonic event, that predates the main deformation event D_1 .

Fabrics of the main deformation phases D_1 developed under ductile rock behavior. The foliation planes S_1 of the central and the eastern part of the Epembe Unit exhibit a similar orientation, which is defined by aligned pyroxene and/or sillimanite. In the central part of the Epembe Unit the S_1 foliation planes are generally steeply inclined, dipping NNE to NNW and SSW to SSE with a distinct maximum of 012/86 (Fig. 2.13). The relatively large scatter in the orientation of the foliation planes is probably related to the occurrence of abundant shear zones in the Epembe Unit along which the granulites are moderately rotated. Due to the generally granoblastic textures of the granulites, mineral stretching lineations L_1 on S_1 foliation planes are generally rare and plunge WNW with a variable but shallow dip of $4-42^\circ$. Due to the predominance of massive to weakly foliated mafic granulites, structural data for the eastern part of the Epembe Unit is limited. However, a few measurable and steeply inclined S_1 foliation planes, like those of the central part, dip to the NNE and SSW (Fig. 2.13). In contrast, the steeply

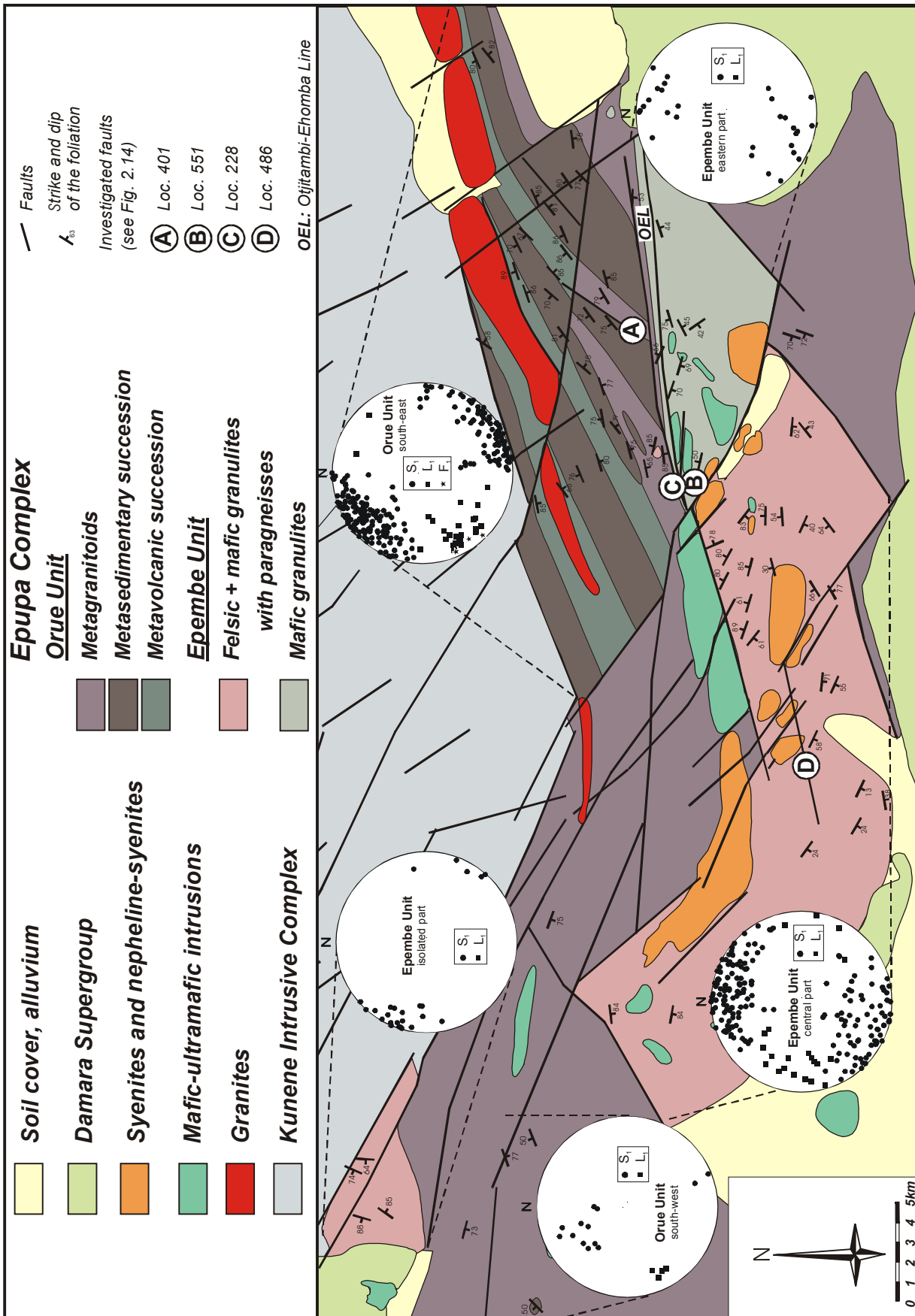


Fig. 2.13: Geological map of the southern part of the study area with equal area (lower hemisphere) stereographic projection of D₁ fabrics: S₁: poles of foliation planes, L₁: plunge of mineral stretching lineations, F₁: plunge of fold axes.

inclined S_1 foliation of granulites exposed in the isolated granulite occurrence situated in the NNW-SSE trending shear zone north of Okangwati dips to the ENE and WSW (Fig. 2.13), thus suggesting that the granulites were rotated during shearing.

The S_1 foliation of the Epembe Unit granulites is generally straight; in contrast to the Orue Unit folding is rare. Rare asymmetric pressure shadows surround feldspar and rotated garnet porphyroclasts, defining δ and σ structures; boudinage structures are common. The orientation of the S_1 foliation planes in the central and eastern part of the Epembe Unit points to broadly N or S directed compression during D_1 .

2.3.3 Ductile shear zones

Both, the Epembe and the Orue Unit, are transected by rare ductile shear zones. One subvertical ductile shear zone transecting the Orue Unit trends NE-SW (Fig. 2.13). At locality 401 (marked as A in Fig. 2.13) this shear zone is predominantly composed of ultramylonitic metagranitoids, separating metapelitic gneisses of the volcano-sedimentary sequence from metagranitoids (Fig. 2.13). Mineral lineations on the subvertical to SW inclined mylonitic foliation planes plunge subvertically to NE (Fig. 2.14a), indicating that the shear zone represents a normal fault with a subordinate sinistral strike-slip component.

In contrast, ductile shear zones are mostly absent in the Epembe Unit. At locality 551, close to Otjitambi (marked as B in Fig. 2.13), a ductile sinistral shear zone, intruded by weakly deformed granitic dykes, transects a sequence of felsic and mafic granulites. The S_1 foliation of the granulites sigmoidally curves into the ENE-WSW trending shear zone, indicating that the shear zone developed under ductile rock behaviour. The shear zone was not affected by late retrogression and consists of blastomylonites and ultramylonites derived from the surrounding mafic and felsic granulites. Mineral stretching lineations on the mylonitic foliation planes plunge with variable angles of 18-54° to the E-SE, defining a sinistral shear sense (Fig. 2.14b). Based on these data the shear zone is interpreted as a normal fault with a significant sinistral strike-slip component.

Following these data, ductile normal faulting of both the Orue and the Epembe Unit occurred under the same tectonic regime like the structures formed during the main deformation event D_1 .

2.3.4 Ductile-brittle shear zones

During the emplacement of the anorthosites of the KIC (~ 1380 Ma) the tectonic regime

drastically changed. The orientation of the ENE-WSW trending dark anorthosite ridges, which intruded the white anorthosites (Drüppel, 1999, 2003) is consistent with the orientation of the ENE-WSW elongated and marginally foliated granite body exposed near the southern margin of the KIC (see Fig. 2.13). This granite intruded the Orue Unit broadly along the strike of the S_1 foliation. Following Drüppel (2003), the orientation of these intrusions demonstrates a broadly NNW directed extension, that presumably occurred in response to doming of the anorthosite massif. This direction, however, runs parallel to the former compressional direction that prevailed during the main deformation and hence indicates that D_1 pre-dated the emplacement of the KIC.

A major, E-W to ENE-WSW trending subvertical shear zone up to ~ 800 m in width, termed as Otjitambi-Ehomba Line (OEL), separates the Epembe Unit and the Orue Unit and parallels the orientation of the granite and the dark anorthosite ridges (Fig. 2.13). The OEL is a major shear zone of up to 700 m in width, that is composed of tectonized metagranitoids at the contact to the Orue Unit and of tectonized mafic granulites at the contact to the Epembe Unit. The western continuation of the OEL was intruded by an E-W trending gabbroic body, that separates the central part of the Epembe Unit from the rocks of the Orue Unit. At Loc. 228 (see Fig. 2.13) the OEL is composed of S-C tectonites, which define a sinistral shear sense (Fig. 2.14c). The S-foliation dips to the SSW and NNE is crosscut by a set of shear bands (C-foliation), that dip to the N, subparallel to the boundaries of the shear zone. Mineral lineations plunge moderately (14-45°) to E-NE. Based on these data the OEL is interpreted as a sinistral strike-slip fault with a reverse fault component. Similar faults composed of SC-tectonites transect the Epembe Unit (Fig. 2.13). At Loc. 486 (see Fig. 2.13) the steeply inclined S-foliation planes dip to SW and are cross-cut by C-shear bands, that dip to SSE resulting in typical SC-textures with sinistral shear sense (Fig. 2.14d). Lineations plunge with a low angle to WSW, indicating that the shear zone is a strike-slip fault with a minor reverse fault component. Judging from its orientation the formation of this shear zone presumably occurred contemporaneously with the anorthosite and granite emplacement.

2.3.5 Brittle faults

Following the emplacement of the KIC, both the metamorphic rocks of the EC and the anorthosites of the KIC were subjected to extensive dextral strike-slip faulting (Drüppel, 2003). Faults transecting the EC generally trend WNW-ESE. These faults are up to 5.5 km in width with the dextral displacement reaching up to 2 km (Fig. 2.13).

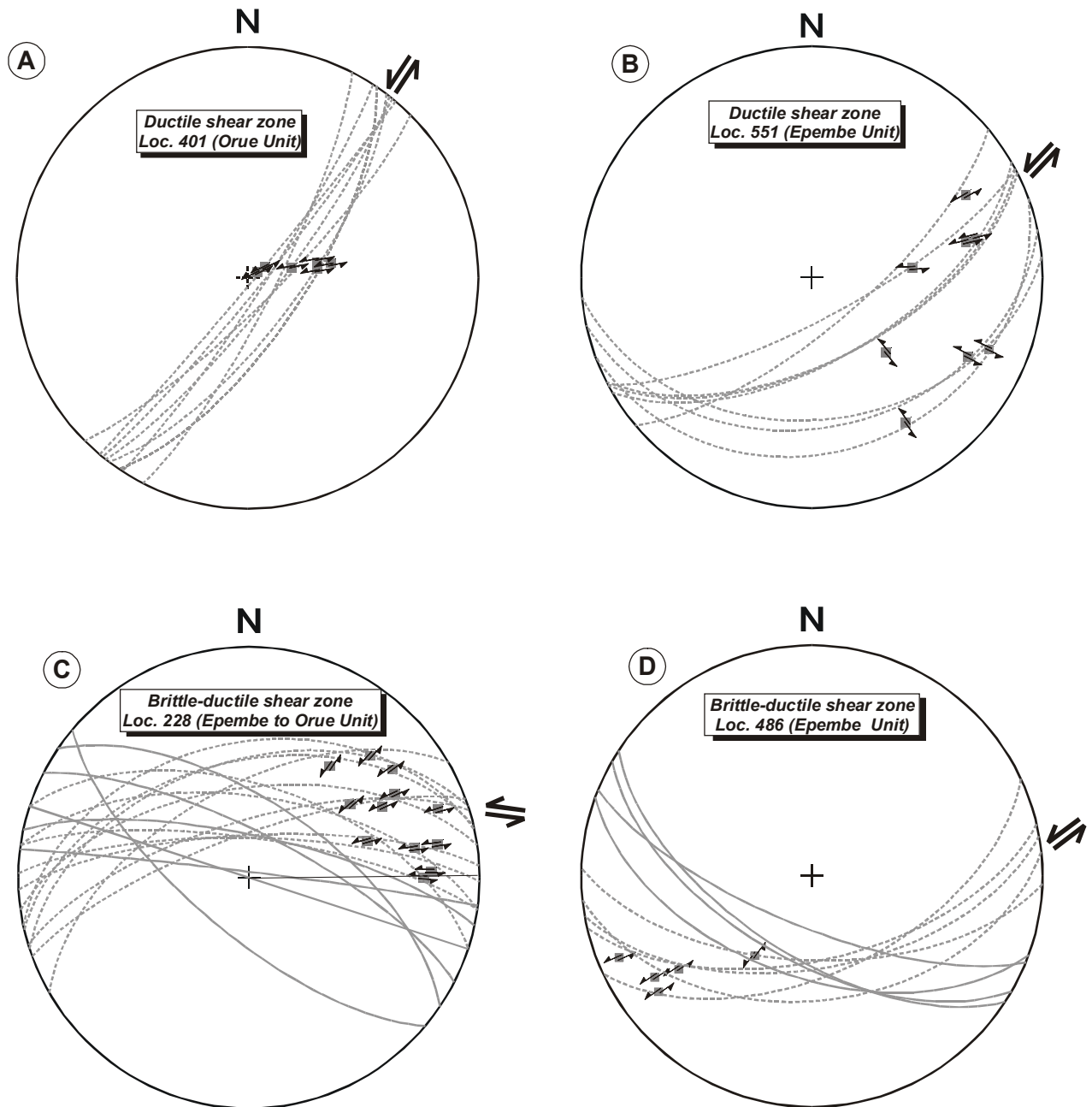


Fig. 2.14: Faults of the Epupa Complex, indicated by (A)-(D) in Fig. 2.13. Sample locations are listed in Table A.2.1 in the Appendix. **a)** Ductile shear zone of the Orue Unit; **b)** ductile shear zone of the Epembe Unit; **c)** brittle-ductile Otjitambi-Ehomba line. Separating the Orue Unit from the Epembe Unit; **d)** brittle-ductile shear zone in the Epembe Unit. For the location of the localities see Fig. 2.13.

3 GEOCHEMISTRY

Major and trace element geochemical data were obtained for 29 rock samples of the Orue Unit, 49 rock samples of the Epembe Unit and two Mesoproterozoic granites (see Chapter A.3.1 in the Appendix for analytical procedure). Results are given in Tables A.6.1.1 and A.6.1.2 in the Appendix. The investigations were performed with the following aims:

- Geochemical characterization of the protoliths of the high-grade metamorphic gneisses of the Orue Unit and the Epembe Unit.
- Discrimination of the tectonic setting during the formation of the protoliths.
- Recognition of possible chemical variations related to high-grade metamorphism.

The only previous study on the bulk-rock geochemistry of the Epupa Complex (EC) rocks of the studied area concentrated on metasomatic effects related to the emplacement of carbonatites and nepheline-syenites at Epembe (Ferguson et al., 1975).

By using geochemical data for the characterization of high-grade metamorphic rocks it has to be taken into account that even under low-grade metamorphic conditions Fe, Mg, Na and K may behave mobile whereas under amphibolite facies conditions in addition Si and Ca behave mobile (Rollinson, 1983). It should be kept in mind that under granulite facies condition, as realized in the Epembe Unit, the relatively immobile elements, such as Ti, Zr, Nb, Y, V, Cr and Ni, used in many classification and discrimination diagrams, may become mobile, due to the presence of CO₂-rich fluids (Janardhan et al., 1982). However, in several studies granulite facies rocks have been successfully discriminated and classified by major and trace element geochemical data (e.g. Talarico et al., 1995; Biswal et al., 1998; Raith et al., 1999).

Based on field relationships the high-grade metamorphic rocks of the Orue Unit and of the Epembe Unit are subdivided into, 1) orthogneisses (including felsic and mafic metavolcanites of the volcano-sedimentary sequences, metagranitoids and metamorphosed mafic dykes) and 2) paragneisses (see Chapter 2.1 & 2.2). The investigated samples comprise representative samples of the major lithological subunits:

Orthogneisses

Mafic metavolcanites

Orue Unit

- Amphibolites B-177-B-98, B-305-2-99, B-446-99

- Grt-amphibolites B-191-B-98, B-405-1-99

Epembe Unit

- Mafic two-pyroxene granulites B-230-B-98, B-423-99, B-447-1-99, B-545-3-99, B-573-99
- Mafic Grt-bearing two-pyroxene granulites B-326-99, B-434-2-99, B-469-99, B-512-99
- Mafic Grt-Cpx granulites B-311-1-99, B-311-3-00
- Mafic Grt-Opx-Pl-Qtz granulite of a dyke B-692-00

Felsic metavolcanites and metagranitoids

Orue Unit

- Felsic Hbl-Bt-bearing gneisses B-174-A-98, B-410-99, B-702-00
- Hbl-Bt metagranitoids B-190-1-98, B-202-A-98, B-401-1-99, B-406-2-99, B-644-1-00, Ku-97-46, Ku-97-47

Epembe Unit

- Felsic Px-bearing granulites B-434-1-99, B-614-2-99
- Grt-Opx metagranitoids B-206-B1-98, B-329-1-99, B-661-2-00, B-646-1-00

Paragneisses

Orue Unit

Metapelites

- Grt-Bt-Sil gneisses and schists B-246-A-98, B-342-3-99, B-401-2-99, B-679-1-00, B-703-00 A, with leucosomes B-219-98, B-342-5-00
- Crd-Bt-(Grt) gneisses B-103-A-98, B-148-A-98
- Contact metamorphic Grt-Sil-Crd rocks B-302-2-A-99, B-302-2-B-99

Metagreywackes

- Grt-Bt gneisses B-137-C-98 B-171-A-98, B-191-A-98

Epembe Unit**Metapelites**

- Grt-Sil gneisses B-212-A-98, B-230-F-98, B-457-99, B-615-5-99, B-699-00

Metagreywackes

- Grt gneisses B-230-A-98, B-230-E-98, B-358-2-99
- Fe-rich Grt-Opx gneisses B-461-1-99, B-486-5-99, B-509-3-99, B-556-1-99, B-572-1-99, B-572-3-99, B-615-3-99, B-690-1-00, B-690-2-00
- Mg-rich Grt-Opx gneisses B-458-1-99, B-540-1-99, B-634-00

Qtz-rich Grt-Opx rocks

B-587-4-99, B-614-1-A-99, B-614-1-B-99, B-614-10-00

Restitic domains

- Spr-bearing Opx-Sil gneisses B-458-4-A-99, B-458-4-B-99, B-458-5-00, B-458-9-00, B-693-00, B-700-2-00
- Opx-Grt rock B-700-1-00

In addition, two samples of Mesoproterozoic granites (samples B-170-A-98, B-180-1-99) have been investigated, in order to enlighten the tectonic setting at the south-western margin of the Congo Craton during the Mesoproterozoic.

3.1 CHARACTERIZATION OF THE PROTOLITHS

Based on field relationships major parts of both the Orue Unit and the Epembe Unit are interpreted as metamorphosed volcano-sedimentary sequences, which were intruded by metagranitoids. Furthermore, metamorphosed late mafic dykes intruded the volcano-sedimentary sequences.

An unambiguous identification of the protolith nature of the high-grade metamorphic gneisses is essential for the reliable reconstruction of the crustal evolution of the EC. However, due to the pronounced structural and compositional modifications, which occurred during deformation and partial melting, primary sedimentary or magmatic textures are generally obliterated and, as a result, field relationships yield not always straightforward information. Therefore, chemical characteristics are combined with field aspects in order to identify the protolith nature in terms of magmatic or sedimentary origin. Based on this clarification it is possible to classify and characterize the protoliths of the high-grade metamorphic rocks of the EC.

3.1.1 Orthogneisses

The orthogneisses include the mafic metavolcanites and the felsic metavolcanites of the volcano-sedimentary sequences of the Orue Unit and Epembe Unit and the metagranitoids of the both units.

3.1.1.1 Mafic metavolcanites

The metavolcanic amphibolites and Grt-amphibolites of the volcano-sedimentary sequence of the Orue Unit and the metavolcanic mafic granulites (Grt-Cpx granulites and (Grt-bearing) two-pyroxene granulites) of the volcano-sedimentary sequence of the Epembe Unit exhibit remarkable geochemical similarities, that testify to a cogenetic evolution of the both metamorphic units and will be described in some detail in the following.

Major and trace element data support the field observation of a magmatic origin for the protoliths of the metabasites of the Orue Unit and the Epembe Unit (Fig. 3.1): Following the discrimination diagrams of Walker et al. (1960) and of Leyreloup et al. (1977), the metabasites of both volcano-sedimentary sequences are orthogneisses, which plot in the field of basalts (Figs. 3.1a & 3.1b). The Grt-Opx-Pl-Qtz granulite of the metamorphosed late dyke of the Epembe Unit falls outside the basalt field, but is discriminated as orthogneiss, which is in agreement with its dyke-like occurrence. Furthermore, the low Zr/Ti versus Ni ratios of all mafic rocks of the EC are typical of igneous-derived metabasites (Fig. 3.1c).

Following the TAS (total alkali versus silica) diagram of Le Maitre (1989) the basic to intermediate amphibolites and the less siliceous, basic Grt-amphibolites of the Orue Unit compositionally correspond to basalts and subordinately to basaltic andesites (Fig. 3.2a). CIPW normative compositions range from olivine tholeiite to quartz tholeiite (Fig. 3.2b).

The mafic (Grt-bearing) two-pyroxene granulites of the Epembe Unit are compositionally similar to the (Grt-)amphibolites of the Orue Unit and predominantly exhibit basic and less abundantly intermediate compositions (Fig. 3.2a). With one exception, garnet-bearing two-pyroxene granulites have lower Si than garnet-free samples. As the (Grt-)amphibolites, the (Grt-bearing) two-pyroxene granulites can be classified as basalts and subordinately as basaltic andesites (Fig. 3.2a). CIPW normative compositions testify to olivine tholeiitic and subordinate quartz tholeiitic protoliths (Fig. 3.2b). The Grt-Cpx granulites of the Epembe Unit are exceptional in their ultrabasic compositions, which correspond to picritic basalts (Fig. 3.2a). CIPW normative compositions plot on both sides of the olivine tholeiite / alkali-olivine basalt boundary (Fig. 3.2b). The Grt-Opx-Pl-Qtz granulite of the metamorphosed late dyke of the Epembe Unit has an intermediate, basaltic andesite composition, which is characterized by a diopside-free quartz tholeiite CIPW normative composition (Fig. 3.2a & b).

The generally sub-alkaline (tholeiitic) trend of all metabasites of the EC, indicated by the CIPW normative compositions, is furthermore supported by low Zr/Ti and Nb/Y ratios and low P_2O_5/Zr ratios (Fig. 3.2c & d). The Grt-Opx-Pl-Qtz granulite of the metamorphosed late dyke of the Epembe Unit exhibits exceptional high Zr contents but also belongs to the sub-alkaline series. By subdividing the sub-alkaline series into tholeiitic and calc-alkaline basalts all but one metabasites of the EC show an affinity to the tholeiitic series, due to their high FeO^{tot} contents and moderate to high FeO^{tot}/MgO ratios (Fig. 3.2e & f).

When plotted in selected Harker diagrams systematic variations of the compositions of the metabasites with Si are rare (Fig. 3.3). The amphibolites of the Orue Unit display a negative correlation of Mg, Ca, Al and Sr with Si, probably related to magmatic fractionation processes. The Grt-amphibolites are less magnesian than the garnet-free amphibolites (bulk-rock X_{Mg} : 0.38-0.39 and 0.41-0.53, respectively) and have higher Fe^{tot} and Ti than the latter (Fig. 3.3). Further systematic chemical differences between the two types of amphibolites are not observed.

Garnet-free and garnet-bearing two-pyroxene granulites of the Epembe Unit display no systematic differences of the bulk-rock X_{Mg} (0.48-0.61 and 0.46-0.62, respectively). With exception of a weak negative correlation of Ca with Si, systematic variations are not observed in Harker diagrams (Fig. 3.3). With exception of Si, major and trace element contents and the bulk-rock X_{Mg} (0.53-0.55) of the Grt-Cpx granulites are generally similar to those of the (Grt-bearing)

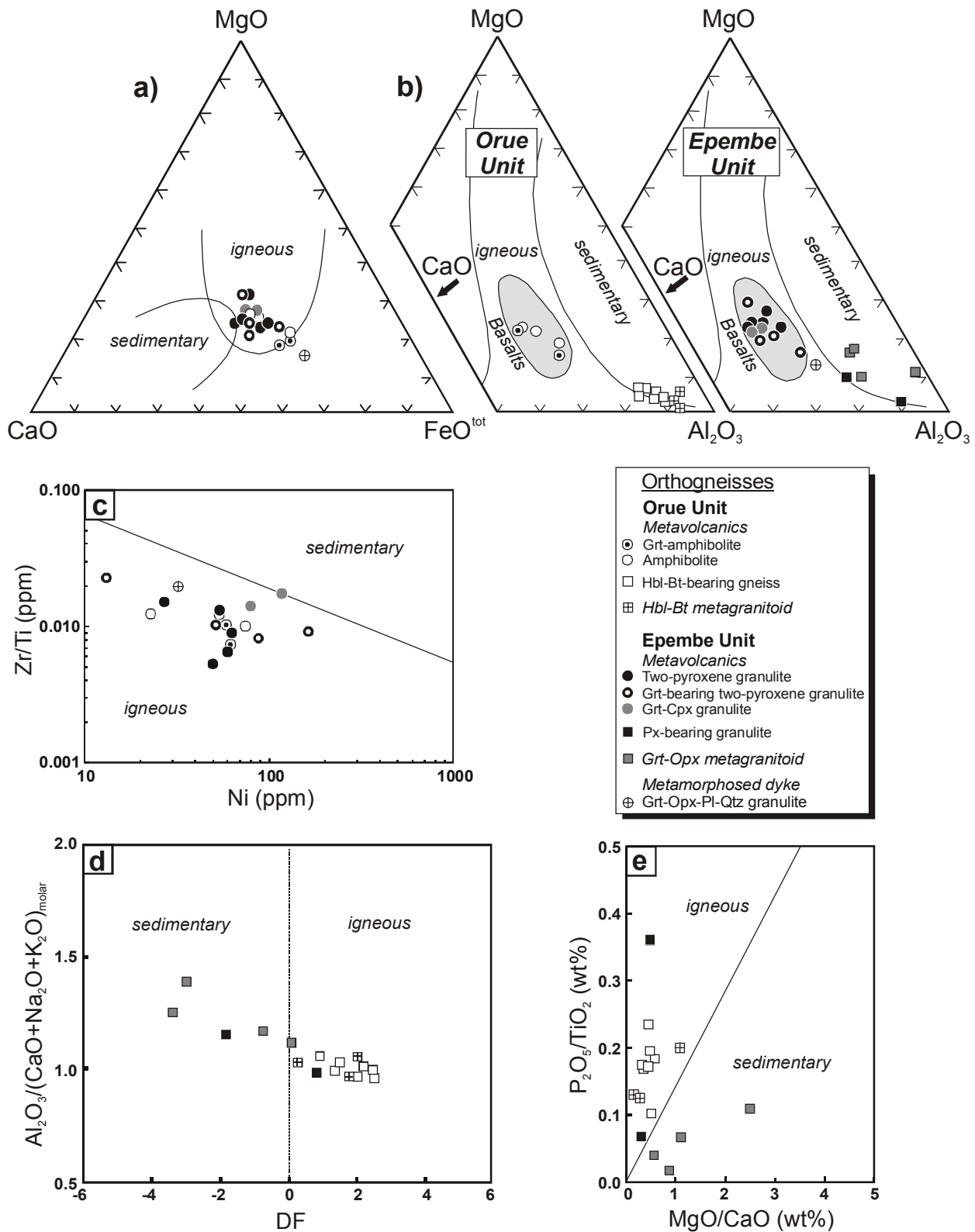


Fig. 3.1: Geochemical discrimination between sedimentary and igneous derived protoliths for the mafic (Fig. 3.1a-c) and the felsic (Fig. 3.1d & e) orthogneisses of the EC. **a)** MgO-CaO-FeO^{tot} diagram after Walker et al. (1960). **b)** MgO-CaO-Al₂O₃ diagram after Leyreloup et al. (1977). **c)** Zr/Ti vs. Ni diagram after Winchester et al. (1980). **d)** Al₂O₃/(CaO+Na₂O+K₂O)_{molar} vs. DF diagram after Raith et al. (1999); DF: =10.44 - 0.21 SiO₂ - 0.32 Fe₂O₃^{tot} - 0.98 MgO + 0.55 CaO + 1.46 Na₂O + 0.54 K₂O. **e)** P₂O₅/TiO₂ vs. MgO/CaO diagram after Werner (1987).

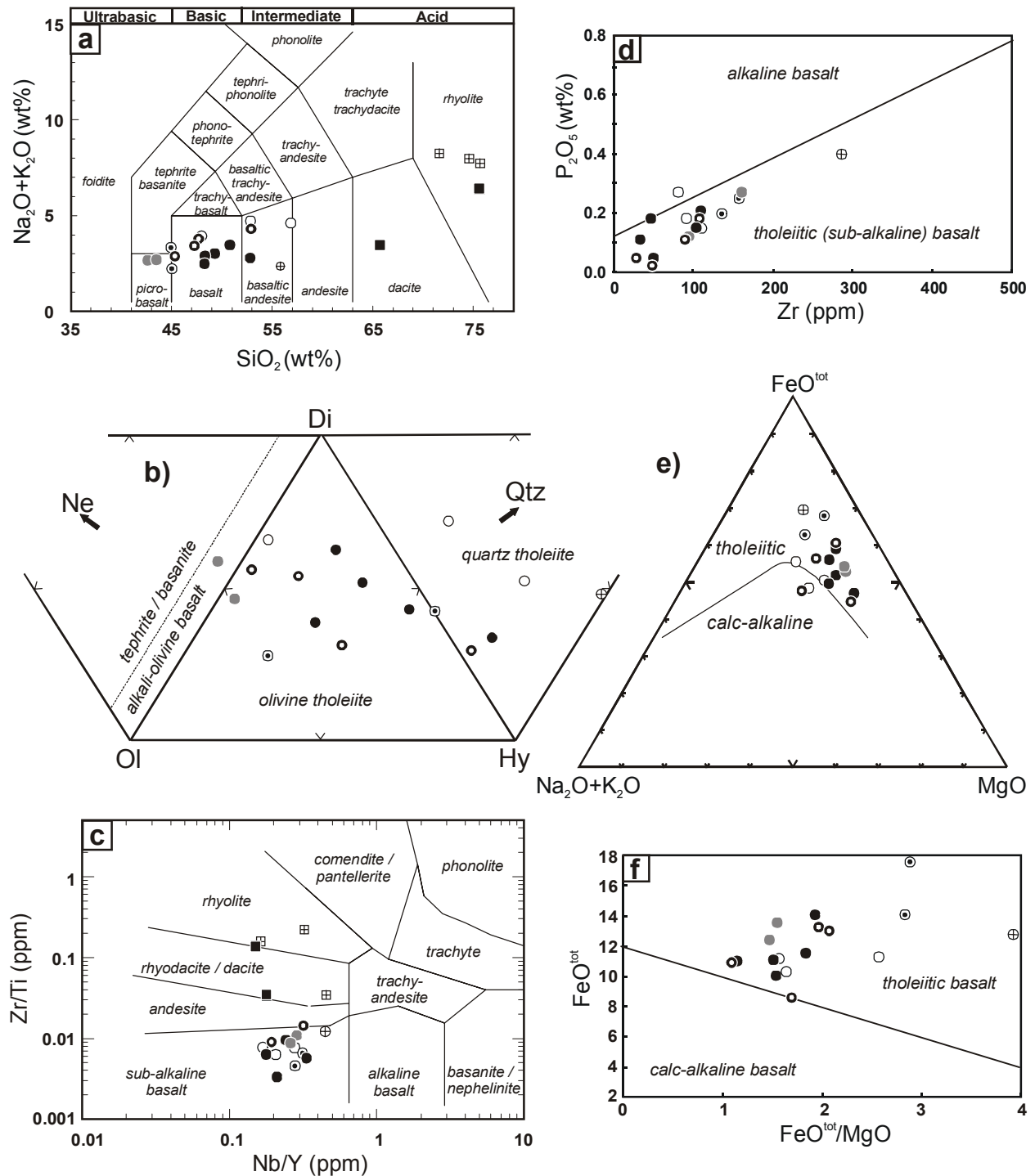


Fig. 3.2: Geochemical classification and characterization of the felsic and mafic metavolcanites of the EC. **a)** Classification of volcanic rocks in the total alkali vs. silica (TAS) diagram after Le Maitre (1989). **b)** Classification of basalts on the basis of the molecular normative Ne-Di-Ol-Hy-Qtz content after Thompson (1984). **c)** Diagram Zr/Ti vs. Nb/Y after Winchester & Floyd (1977); note that analyses with Nb content below the detection limit were excluded. **d)** Diagram P₂O₅ vs. Zr after Winchester & Floyd (1976). **e)** Ternary diagram (Na₂O+K₂O)-MgO-FeO^{tot} after Irvine & Baragar (1971). **f)** Diagram FeO^{tot} vs. FeO^{tot}/MgO after Miyashiro (1974). Symbols as in Fig. 3.1.

two-pyroxene granulites, suggesting a cogenetic evolution of their respective protoliths. The only striking difference is the higher Rb content of the Grt-Cpx granulites when compared to the (Grt-bearing) two-pyroxene granulites (Rb: 150-156 ppm and 9-91 ppm, respectively).

The intermediate Grt-Opx-Pl-Qtz granulite of the metamorphosed late dyke of the Epembe Unit has lower Mg, Ca and Cr and higher Ti, Y and Zr than the metabasites of the volcano-sedimentary sequence (Fig. 3.3). Furthermore, the rock is significantly less magnesian (bulk-rock X_{Mg} : 0.31) than the other metabasites. These chemical differences suggest that the formation of the dyke is genetically unrelated to the formation of the volcano-sedimentary sequence of the Epembe Unit.

A cogenetic evolution of the metabasites of the Orue Unit and of the Epembe Unit is strengthened by the application of normalized multi-element plots (Fig. 3.4). Average N-type mid-ocean-ridge basalt (N-MORB)-normalized spider diagrams, using the normalization factors of Pearce (1982), show a steep slope for the metabasites of the EC with a marked enrichment of the incompatible LIL elements Sr, K, Rb and Ba whereas the compatible HFS elements are not significantly modified with respect to the N-MORB composition. Ni is enriched whereas Cr is depleted when compared to N-MORB composition. A P_2O_5 -trough of the (Grt-bearing) two-pyroxene granulites is defined by only one sample and is not a systematic characteristic of the (Grt-bearing) two-pyroxene granulites. Remarkably, the patterns of the (Grt-)amphibolites of the Orue Unit and of the (Grt-bearing) two-pyroxene granulites and Grt-Cpx granulites of the Epembe Unit are quite similar, thus suggesting a cogenetic formation of their basaltic protoliths. The Grt-Opx-Pl-Qtz granulite of the metamorphosed late dyke generally exhibits a comparable slope, but is slightly enriched in the incompatible elements. Assuming that the enrichment of the mobile elements is a primary feature and not related to secondary processes, the steep slope of all mafic rocks is typical of enriched MORBs (P-type), of island arc basalts (IAB) and of back-arc basalts (BAB; e.g. Wilson, 1989). Ni and Cr are immobile during regional metamorphism (e.g. Kataria et al., 1988) and therefore record the original pre-metamorphic concentrations. Among the common rock-forming minerals of basic igneous rocks clinopyroxene and olivine are the most important carriers of Cr and Ni, respectively. Consequently, depletion of Cr and enrichment of Ni suggests fractionation of clinopyroxene whereas olivine fractionation presumably did not occur in the parental melt.

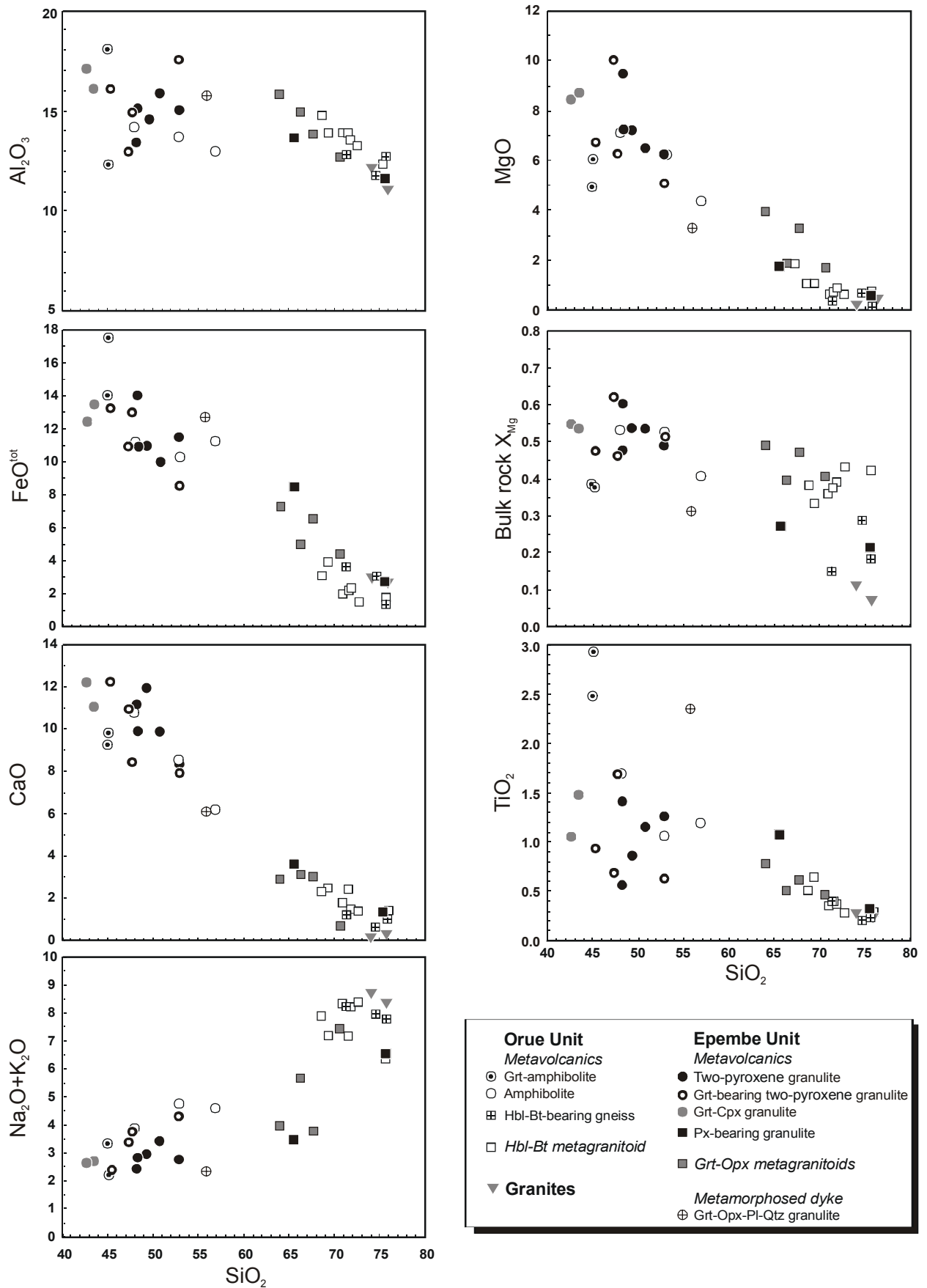


Fig. 3.3: Harker variation diagrams (major element oxides (in wt.%) and bulk-rock X_{Mg} vs. SiO_2) for the orthogneisses of the EC and the Mesoproterozoic granites.

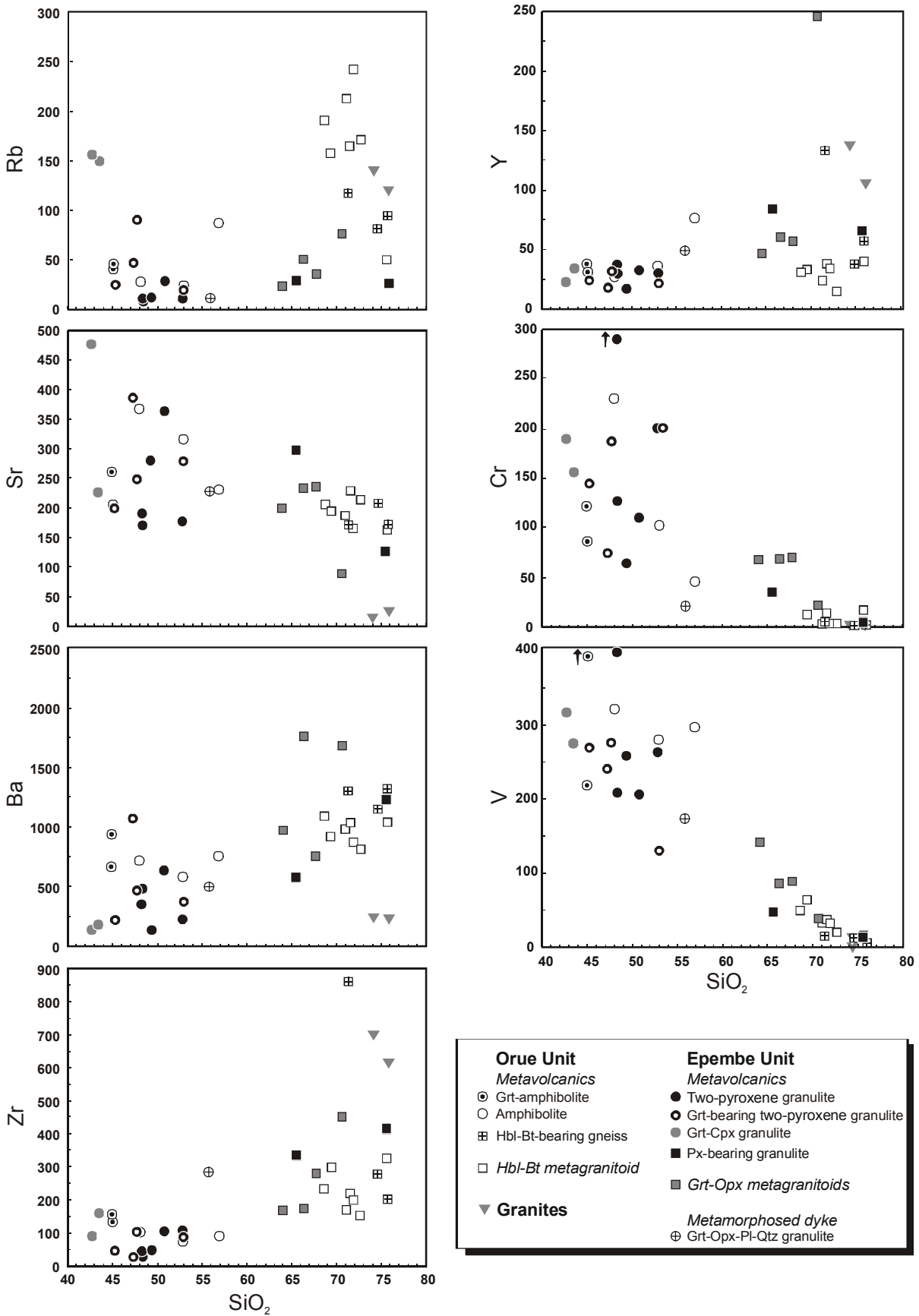


Fig. 3.3 (continued): Harker variation diagrams (trace elements (in ppm) vs. SiO₂) for the orthogneisses of the EC and the Mesoproterozoic granites.

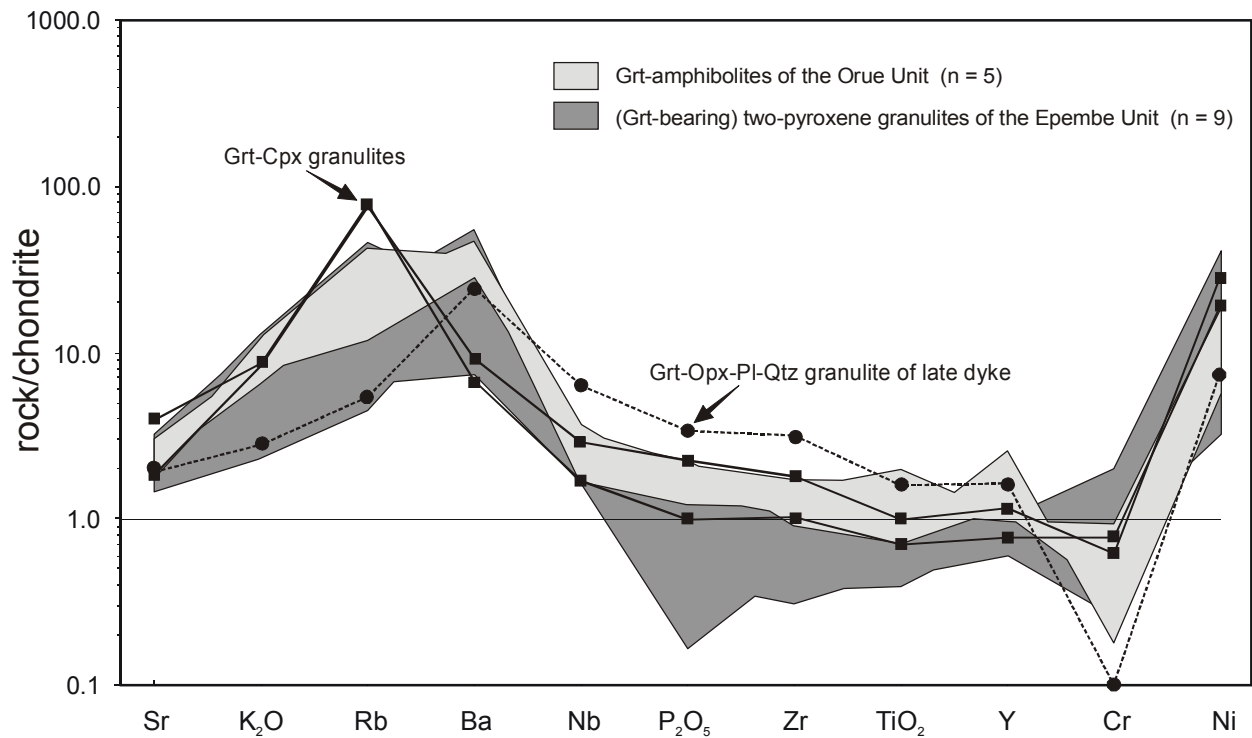


Fig. 3.4: MORB-normalized multi-element variation plot for the mafic rocks of the EC, using the normalization factors of Pearce (1982).

3.1.1.2 Felsic metavolcanites

In the discrimination diagram of Leyreloup et al. (1977) the felsic rocks of the EC plot on the boundary between the sedimentary and igneous field (Fig. 3.1b). Therefore, the discrimination diagram of Werner (1987) and the discrimination function $DF = 10.44 - 0.21 \text{ SiO}_2 - 0.32 \text{ Fe}_2\text{O}_3$ (total Fe) - $0.98 \text{ MgO} + 0.55 \text{ CaO} + 1.46 \text{ Na}_2\text{O} + 0.54 \text{ K}_2\text{O}$ of Shaw (1972) were used to distinguish between igneous and sedimentary protoliths for the felsic rocks of the EC (Fig. 3.1d & e). In general, positive DF values point to an igneous parentage whereas negative DF values indicate a sedimentary origin. In addition, high $\text{Al}_2\text{O}_3/(\text{Na}_2\text{O}+\text{K}_2\text{O}+\text{CaO})_{\text{molar}}$ ratios are typical of sedimentary rocks.

The felsic Hbl-Bt-bearing gneisses and the felsic Px-bearing granulites of the volcano-sedimentary sequences of the Orue Unit and the Epembe Unit, respectively, generally exhibit positive DF values, low $\text{Al}_2\text{O}_3/(\text{Na}_2\text{O}+\text{K}_2\text{O}+\text{CaO})_{\text{molar}}$ ratios and high $\text{P}_2\text{O}_5/\text{TiO}_2$ versus MgO/CaO ratios, indicating igneous protoliths (Fig. 3.1d & e) and thus supporting the field interpretation of their volcanic origin.

As observed for the mafic metavolcanites, remarkable chemical similarities are also observed for the felsic metavolcanites of the Orue Unit and of the Epembe Unit:

The major and trace element composition of the acid Hbl-Bt-bearing gneisses and of the acid Px-bearing granulites corresponds to rhyolites and subordinate to dacites of the sub-alkaline series (Fig. 3.2a & c) with generally low amounts of normative corundum (0.0-0.4 % in the Hbl-Bt-bearing gneisses and 0.0-2.7 % in the Px-bearing granulites). Due to high $\text{FeO}^{\text{tot}}/\text{MgO}$ ratios of the Hbl-Bt-bearing gneisses and the Px-bearing granulites (bulk-rock X_{Mg} 0.15-0.29 and 0.22-0.27, respectively) and partly high contents of HFS elements, the peraluminous acid metavolcanites (Fig. 3.5a) of both metamorphic units plot in the fields of fractionated granites and A (anorogenic)-type granitoids (Fig. 3.5b).

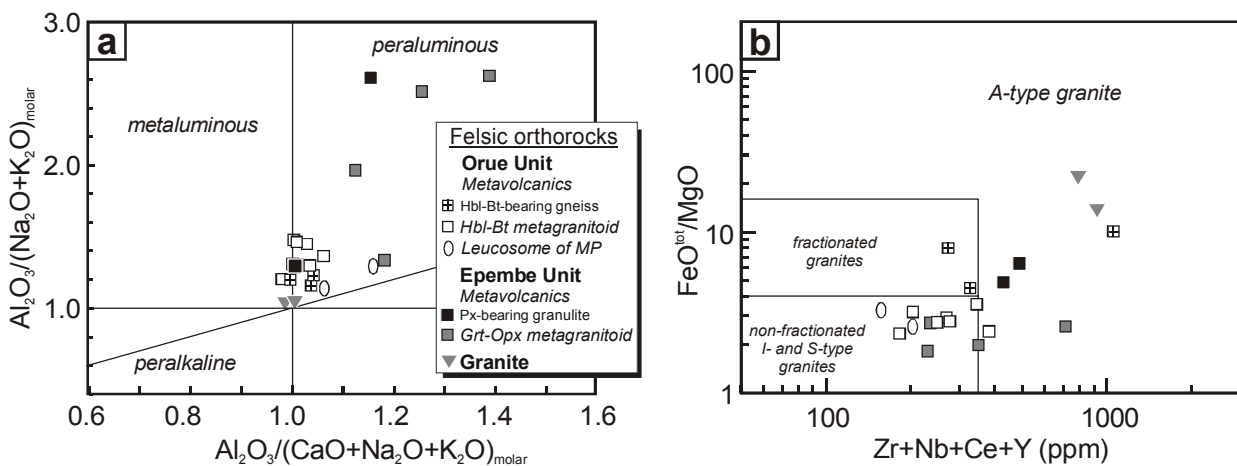


Fig. 3.5: Geochemical characterization of the felsic orthogneisses of the EC, of the leucosomes of metapelites (MP) of the Orue Unit and of the Mesoproterozoic granites. **a)** Shand's alkalinity index (plot of $\text{Al}_2\text{O}_3/(\text{Na}_2\text{O}+\text{K}_2\text{O})_{\text{molar}}$ vs. $\text{Al}_2\text{O}_3/(\text{Na}_2\text{O}+\text{K}_2\text{O}+\text{CaO})_{\text{molar}}$). **b)** Discrimination between A, S and I type granitoids in the $\text{FeO}^{\text{tot}}/\text{MgO}$ vs. $\text{Zr}+\text{Nb}+\text{Ce}+\text{Y}$ diagram after Whalen et al. (1987).

In selected Harker diagrams the felsic metavolcanites of both units show a linear correlation with the mafic metavolcanites for some elements (Fig. 3.3). Compared to the metabasites, the felsic metavolcanites are strongly depleted in Ca, suggesting fractionation of either plagioclase or clinopyroxene in the parental magma. As Al and Sr show no systematic depletion, fractionation of plagioclase seems rather unlikely and clinopyroxene is interpreted to be the dominant Ca fractionating phase. This interpretation also explains linear decrease of Mg, Fe^{tot} and bulk-rock X_{Mg} towards the felsic metavolcanites. The linear decrease in V is probably related to crystallization of magnetite in the parental magma. Enrichment of Na+K and Ba probably reflects fractionation of alkali feldspar into the acid volcanics. These linear relationships support the interpretation, that the interlayered mafic and felsic metavolcanites of the Orue Unit and the Epembe Unit represent part of a bimodal volcanic sequence. This model is strengthened by the striking gap in the magma series, which is defined by the very restricted occurrence of

intermediate metavolcanites.

3.1.1.3 *Metagranitoids*

The metagranitoids of the Orue Unit and the Epembe Unit exhibit minor but systematic chemical variations when compared to the acid metavolcanites.

Positive DF values, low to moderate $\text{Al}_2\text{O}_3/(\text{Na}_2\text{O}+\text{K}_2\text{O}+\text{CaO})_{\text{molar}}$ ratios, low MgO/CaO ratios and moderate to high $\text{P}_2\text{O}_5/\text{TiO}_2$ ratios testify to igneous protoliths for the Hbl-Bt metagranitoids of the Orue Unit (Fig. 3.1d & e), consistent with the intrusive character of the rocks whereas the geochemical data for the Grt-Opx metagranitoids of the Epembe Unit contrasts the field relationships: Although the Grt-Opx metagranitoids obviously intruded into the volcano-sedimentary sequence, they are discriminated as paragneisses (Fig. 3.1d & e).

In terms of major element composition and molecular normative feldspar composition the acid Hbl-Bt metagranitoids of the Orue Unit mostly fall into the field of granites and subordinately in that of adamellites and trondhjemites of the sub-alkaline series whereas the acid Grt-Opx metagranitoids of the Epembe Unit plot in the fields of tonalite, granodiorite and granite of the sub-alkaline series (Fig. 3.6a & b).

In selected Harker diagrams the metagranitoids of the Orue Unit and of the Epembe Unit (bulk-rock X_{Mg} : 0.33-0.43 and X_{Mg} : 0.40-0.47, respectively) are distinguished from the acid metavolcanites of both units by their Mg-rich composition (Fig. 3.3). Furthermore, they are generally more calcic than the latter. Negative linear correlations of Al, Mg, Fe^{tot} , Ca, Ti and V with Si are observed.

The metagranitoids of Orue Unit are metaluminous to peraluminous whereas those of the Epembe Unit are peraluminous (Fig. 3.5a). Due to the low $\text{FeO}^{\text{tot}}/\text{MgO}$ ratios and generally low to moderate contents of HFS elements, the metagranitoids mainly plot in the field of non-fractionated I and S-type granites (Fig. 3.5b), and thus contrast the more fractionated geochemical character of the acid metavolcanites. The Hbl-Bt metagranitoids of the Orue Unit predominantly exhibit characteristics of I-type granites, such as a low $\text{Al}_2\text{O}_3/(\text{Na}_2\text{O}+\text{K}_2\text{O}+\text{CaO})_{\text{molar}}$ ratio (Fig. 3.6c), low contents of normative corundum (0.0-0.7 %) and high CaO contents, which indicate their derivation by melting of an igneous source. In contrast, the Grt-Opx metagranitoids of the Epembe Unit are S-type granitoids, as is mainly evident from their high contents of normative corundum (1.5-4.4 %) and high $\text{Al}_2\text{O}_3/(\text{Na}_2\text{O}+\text{K}_2\text{O}+\text{CaO})_{\text{molar}}$ ratios (Fig. 3.6c). The S-type character of the rocks might explain the discrimination as paragneisses.

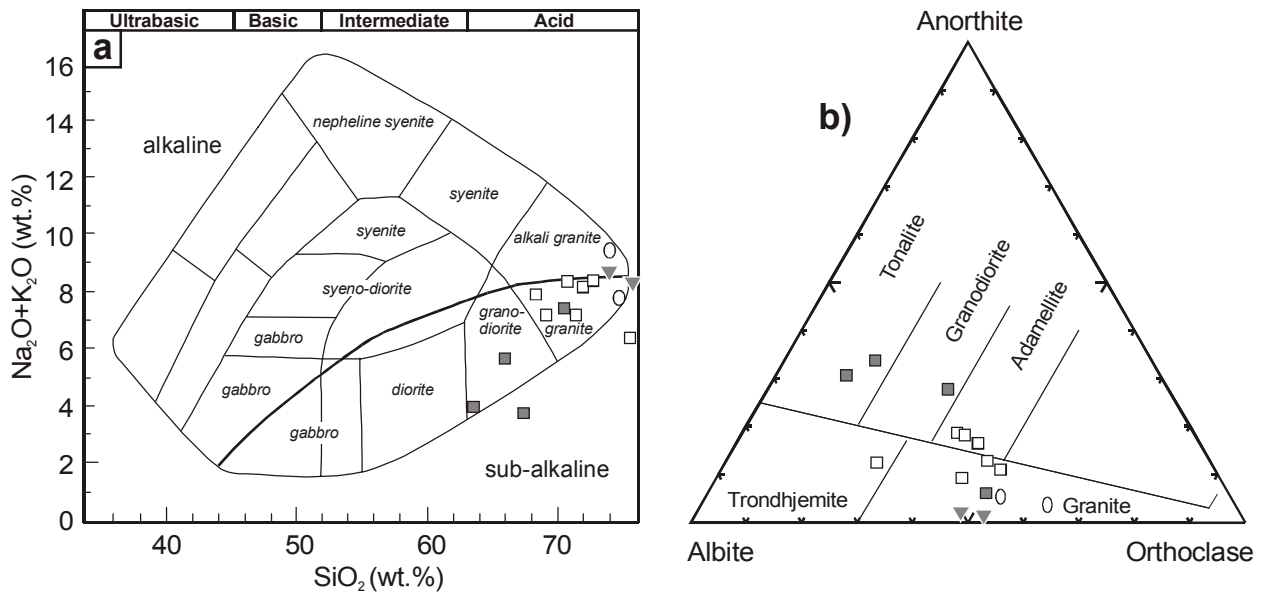


Fig. 3.6: Geochemical classification of the metagranitoids of the EC and the Mesoproterozoic granites. **a)** Classification of plutonic rocks in the total alkali vs. silica (TAS) diagram after Wilson (1989), with the dividing line between alkaline and sub-alkaline magma series after Miyashiro (1978). **b)** Classification of felsic plutonic rocks on the basis of the molecular normative An-Ab-Or content after Barker (1979). **c)** Discrimination between S and I-type granitoids in the $\text{Al}_2\text{O}_3 / (\text{Na}_2\text{O} + \text{K}_2\text{O} + \text{CaO})_{\text{molar}}$ vs. FeO^{tot} (wt.%) diagram. Symbols as in Fig. 3.5.

The composition of the Mesoproterozoic granites differs significantly from all felsic rocks of the EC by lower contents of Ca, Sr, Ba and lower bulk-rock X_{Mg} (0.07-0.11) and higher Zr and Y. Their major element and CIPW normative composition corresponds to alkali granites and granites (Fig. 3.6a & b). The granites are metaluminous to peraluminous (Fig. 3.5a). Due to the high $\text{FeO}^{\text{tot}}/\text{MgO}$ ratios and high contents of HFS elements, the rocks fall into the field of A-type granites in Fig. 3.5b. Furthermore, the $\text{Al}_2\text{O}_3 / (\text{Na}_2\text{O} + \text{K}_2\text{O} + \text{CaO})_{\text{molar}}$ ratio and the content of normative corundum (0.1 %) are lower as in the metagranitoids.

3.1.2 Paragneisses

Based on field relationships and modal compositions the paragneisses of the EC are broadly

subdivided into sillimanite- or cordierite-bearing metapelites and sillimanite-free metagreywackes. Furthermore, Qtz-rich Grt-Opx rocks, sapphirine-bearing Opx-Sil gneisses and Opx-Grt rocks of the Epembe Unit were investigated.

The low CaO contents, generally negative DF values and generally high $\text{Al}_2\text{O}_3/(\text{Na}_2\text{O}+\text{K}_2\text{O}+\text{CaO})_{\text{molar}}$ ratios displayed by the metapelites of both metamorphic units are typical of sedimentary rocks (Fig. 3.7a & b). A sedimentary origin is further supported by high amounts of normative corundum (4.5-15.8 %).

The metagreywackes of both units generally have slightly higher CaO contents but still fall into the field of sedimentary protoliths (Fig. 3.7a). Furthermore, the generally negative DF values, the moderate to high $\text{Al}_2\text{O}_3/(\text{Na}_2\text{O}+\text{K}_2\text{O}+\text{CaO})_{\text{molar}}$ ratios (Fig. 3.7b), the low $\text{P}_2\text{O}_5/\text{TiO}_2$ and high MgO/CaO ratios (Fig. 3.7c) and the presence of normative corundum (0.5-5.0 %) support their sedimentary origin.

The Qtz-rich Grt-Opx rocks, the sapphirine-bearing Opx-Sil gneisses and the Opx-Grt rock of the Epembe Unit exhibit very high DF values of < -10 and commonly $\text{Al}_2\text{O}_3/(\text{Na}_2\text{O}+\text{K}_2\text{O}+\text{CaO})_{\text{molar}}$ ratios > 3 , thus clearly indicating a sedimentary origin. However, due to these very high values, they are not shown in Fig. 3.7b.

Orue Unit

The metapelitic Grt-Bt-Sil gneisses and schists (bulk-rock X_{Mg} : 0.33-0.44) of the southern part of the Orue Unit and the Crd-Bt-(Grt) gneisses (bulk-rock X_{Mg} : 0.28-0.36) of the northern part of the Orue Unit have comparable compositions with highly variable SiO_2 (53.1-70.2 wt.%), high Al_2O_3 (14.8-24.2 wt.%) and K_2O (3.7-6.9 wt.%), moderate Na_2O (0.8-2.7 wt.%) and low CaO (0.4-1.2 wt.%). Due to the high $\text{K}_2\text{O}/\text{Na}_2\text{O}$ and low $\text{SiO}_2/\text{Al}_2\text{O}_3$ ratios, they can be classified as pelites and subordinately as arkoses using the classification diagram of Wimmenauer (1984; Fig. 3.7d). Leucosomes of the Grt-Bt-Sil gneisses (bulk-rock X_{Mg} : 0.36-0.41) have a granitic to alkali granitic composition (Fig. 3.6a & b) and are peraluminous (Fig. 3.5a). Low $\text{FeO}^{\text{tot}}/\text{MgO}$ ratios and low contents of HFS elements are typical of non-fractionated I- and S-type granites (Fig. 3.5b). However, moderate to high $\text{Al}_2\text{O}_3/(\text{Na}_2\text{O}+\text{K}_2\text{O}+\text{CaO})_{\text{molar}}$ ratios (Fig. 3.6c) and high amount of normative corundum (0.7-1.7 %) demonstrate their formation by partial melting of a sedimentary protolith, consistent with the field observation.

The contact metamorphic metapelitic Grt-Sil-Crd rocks (bulk-rock X_{Mg} : 0.40-0.41) are generally chemically similar to the other metapelites with variable SiO_2 (53.7-60.3 wt.%), high Al_2O_3 (22.4-25.2 wt.%) and moderate Na_2O (2.1-2.6 wt.%) but exhibit lower K_2O (1.6-2.0 wt.%) and higher CaO (1.3-1.7 wt.%). Due to the lower $\text{K}_2\text{O}/\text{Na}_2\text{O}$ ratio, the Grt-Sil-Crd rocks are

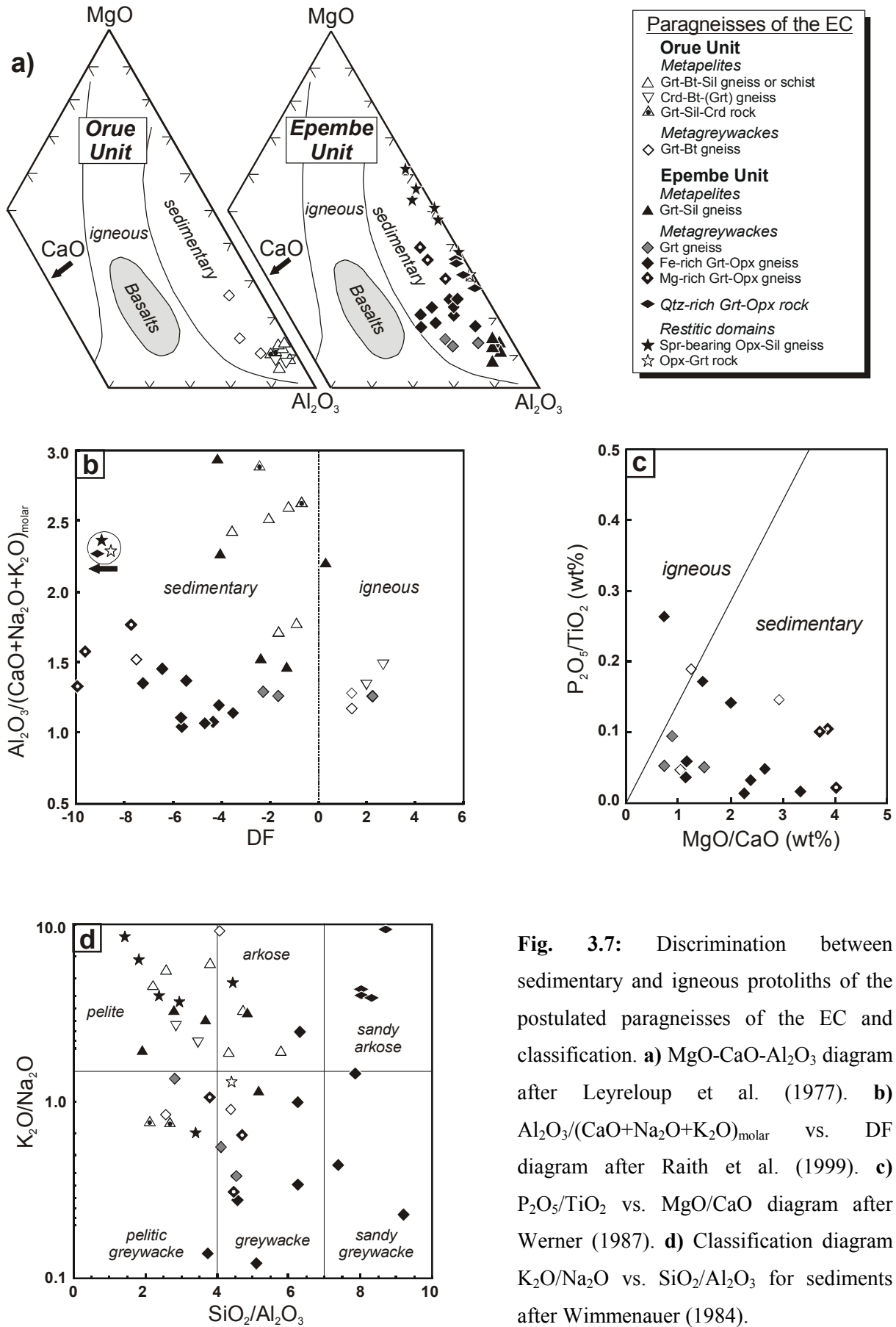


Fig. 3.7: Discrimination between sedimentary and igneous protoliths of the postulated paragneisses of the EC and classification. **a)** MgO-CaO-Al₂O₃ diagram after Leyreloup et al. (1977). **b)** Al₂O₃/(CaO+Na₂O+K₂O)_{molar} vs. DF diagram after Raith et al. (1999). **c)** P₂O₅/TiO₂ vs. MgO/CaO diagram after Werner (1987). **d)** Classification diagram K₂O/Na₂O vs. SiO₂/Al₂O₃ for sediments after Wimmenauer (1984).

classified as pelitic greywackes (Fig. 3.7d).

The metagreywacke-type Grt-Bt-gneisses of the Orue Unit (SiO_2 : 51.1-67.2 wt.%; bulk-rock X_{Mg} : 0.35-0.46) differ from the metapelites by slightly lower Al_2O_3 (12.9-19.9 wt.%) and mostly slightly higher CaO (1.6-3.1 wt.%) and Na_2O (0.5-3.9 wt.%). The rocks display compositional variations as they have arkose, greywacke and pelitic greywacke composition (Fig. 3.7d).

Epembe Unit

The metapelitic Grt-Sil gneisses of the Epembe Unit (SiO_2 : 49.1-73.0 wt.%; bulk-rock X_{Mg} : 0.39-0.47) are chemically similar to the metapelites of the Orue Unit and predominantly have typical pelite compositions with high Al_2O_3 (14.1-25.5 wt.%), K_2O (2.9-4.9 wt.%), moderate Na_2O (1.0-2.5 wt.%) and low CaO (0.9-1.4 wt.%).

The metagreywackes of the Epembe Unit are generally less aluminous when compared to the metapelites (Fig. 3.7a & b):

The metagreywacke-type Grt gneisses (SiO_2 : 55.0-66.4 wt.%; bulk-rock X_{Mg} : 0.39-0.44) generally exhibit similar geochemical characteristics like the Grt-Sil gneisses but have slightly lower Al_2O_3 (14.6-19.4 wt.%) and K_2O (1.1-5.1 wt.%) but higher CaO (2.1-3.5 wt.%) and Na_2O (2.5-3.7 wt.%) than the latter and can therefore be classified as pelitic greywackes and greywackes (Fig. 3.7d).

The metagreywacke-type Grt-Opx gneisses generally have lower Al_2O_3 (8.5-15.2 wt.%) than the Grt gneisses whereas SiO_2 (52.9-77.7 wt.%), CaO (1.0-4.8 wt.%), Na_2O (1.7-3.3 wt.%) and K_2O (0.4-4.2 wt.%) contents are similar. Based on the bulk-rock X_{Mg} the Grt-Opx gneisses are subdivided into two types:

- Fe-rich Grt-Opx gneisses (bulk-rock X_{Mg} : 0.37-0.46)
- Mg-rich Grt-Opx gneisses (bulk-rock X_{Mg} : 0.59-0.62)

The high bulk-rock X_{Mg} of the Mg-rich Grt-Opx gneisses is related to their exceptional high MgO contents (6.4-10.6 wt.%; Fig. 3.7a) whereas FeO^{tot} (7.9-12.5 wt.%) is in the range of the Fe-rich Grt-Opx gneisses (MgO: 2.3-4.7 wt.%; FeO : 5.4-12.5 wt.%). Furthermore, the Mg-rich Grt-Opx gneisses generally have slightly higher $\text{Al}_2\text{O}_3/(\text{Na}_2\text{O}+\text{K}_2\text{O}+\text{CaO})_{\text{molar}}$ ratios than the Fe-rich Grt-Opx gneisses (Fig. 3.7b). Due to the slightly more aluminous composition, the Mg-rich Grt-Opx gneisses are classified as greywackes and pelitic greywackes whereas the Fe-rich Grt-Opx gneisses predominantly have greywacke to sandy greywacke compositions (Fig. 3.7d).

The Qtz-rich Grt-Opx rocks are characterized by a high Si content (74.0-78.7 wt.% SiO_2) and

a high bulk-rock X_{Mg} of 0.52 to 0.56, only slightly lower than in the Mg-rich Grt-Opx gneisses. Low Al_2O_3 (9.1-9.3 wt.%), CaO (0.2-0.4 wt.%), Na_2O (0.1-0.2 wt.%) and K_2O (0.7-1.3 wt.%) explain the feldspar-poor composition of the rocks, that are classified as sandy arkoses (Fig. 3.7d).

The sapphirine-bearing Opx-Sil gneisses exclusively occur in the migmatitic metagreywacke-type Mg-rich Grt-Opx gneisses. The composition of the Opx-Sil gneisses is characterized by high MgO (11.0-17.7 wt.%) and generally high Al_2O_3 (14.5-27.7 wt.%) contents, whereas SiO_2 (36.9-49.2 wt.%), Na_2O (0.4-1.4 wt.%), K_2O (1.5-3.8 wt.%), CaO (0.2-1.4 wt.%), Sr and V are low. These compositional characteristics, combined with the occurrence of the Opx-Sil gneisses as schlieren in the migmatitic Mg-rich Grt-Opx gneisses, suggests that their formation is related to the extraction of a Fe-rich granitoid melt, now probably occurring as the leucosomes in the Mg-rich Grt-Opx gneiss host rock. This is supported by the more magnesian composition of the Opx-Sil gneisses (bulk-rock X_{Mg} : 0.64-0.78) when compared to the Grt-Opx gneisses (bulk-rock X_{Mg} : 0.59-0.62). These relationships suggest that the Opx-Sil gneisses are melanosomes, which were derived from partial melting of a Mg-rich metagreywacke-type palaeosome. The origin of compositionally similar sapphirine granulites, such as those of the Gruf Complex (Italy) or the Eastern Ghats belt (India), was interpreted in the same way by Droop & Bucher-Nurminen (1984) and Bhattacharya & Kar (2002), respectively.

The Opx-Grt rocks have a comparably Si-poor and highly magnesian bulk-rock composition (49.6 wt.% SiO_2 ; bulk-rock X_{Mg} : 0.67) with respect to the sapphirine-bearing Opx-Sil gneisses but are less aluminous (Al_2O_3 : 11.2 wt.%; Fig. 3.7a), which explains the sillimanite-free Opx-Grt assemblage. The rocks can be classified as metagreywackes (Fig. 3.7d).

3.2 TECTONIC ENVIRONMENT DURING PROTOLITH FORMATION

Based on the chemical characterization of the protoliths of the high-grade metamorphic gneisses of the EC it is possible to reconstruct the tectonic environment, which prevailed during the emplacement and the sedimentation of the precursor rocks.

3.2.1 Mafic metavolcanites

The geochemical data demonstrated that the protoliths of the mafic metavolcanites of the EC are subalkaline tholeiitic basalts. Following Pearce & Gale (1977), the basaltic protoliths of the studied metabasites were emplaced at a plate margin (Fig. 3.8a). According to Pearce (1982), the moderate Ti vs. Zr of the metabasites ratios are typical of mid-ocean ridge basalts (MORBs) and island arc tholeiites (IATs; Fig. 3.8b). An affinity to MORB and IAT is furthermore evident from the application of the ternary discrimination diagrams of Pearce & Cann (1973) and Mullen (1983; Fig. 3.8c & d). In the discrimination diagrams of Pearce & Gale (1977) and Shervais (1982) the majority of the mafic rocks of the EC shows an affinity to ocean floor basalts (OFB), emplaced at mid-ocean ridges or at back-arc spreading centres (Fig. 3.8e & f). This interpretation is consistent with the slopes of the normalized spider diagrams, which correspond to either IAT, back-arc basin basalts or enriched P-type MORBs.

For the mafic Grt-Opx-Pl-Qtz granulite of the metamorphosed dyke of the Epembe Unit an attribution to a specific tectonic setting is impossible as the studied sample plots in different fields in the used discrimination diagrams (Fig. 3.8a-f).

3.2.2 Felsic metavolcanites and metagranitoids

For the felsic metavolcanites of the volcano-sedimentary sequences of the EC, an attribution to a specific tectonic setting during their emplacement is not straightforward as the samples plot in different fields in the discrimination diagrams of Pearce et al. (1984; Fig. 3.9a & b). This may be a consequence of a possible mobilisation of Nb and/or Rb during high-grade metamorphism. The same holds true for the S-type Grt-Opx metagranitoids of the Epembe Unit. The I-type Hbl-Bt metagranitoids of the Orue Unit are characterized by low Nb and Y contents and therefore fall into the field of volcanic arc granites and syn-collision granites (Fig. 3.9a). However, their low Rb contents indicate an emplacement at a volcanic arc. Following Pearce (1996), the composition of the Hbl-Bt metagranitoids is typical of post-collision granites (Fig. 3.9b). These relationships suggest that the emplacement of the Hbl-Bt metagranitoids of the Orue Unit may be related to widespread post-tectonic granitoid emplacement between 1800 and 1600 Ma in southwestern Angola and northern Namibia (see chapter 1.2).

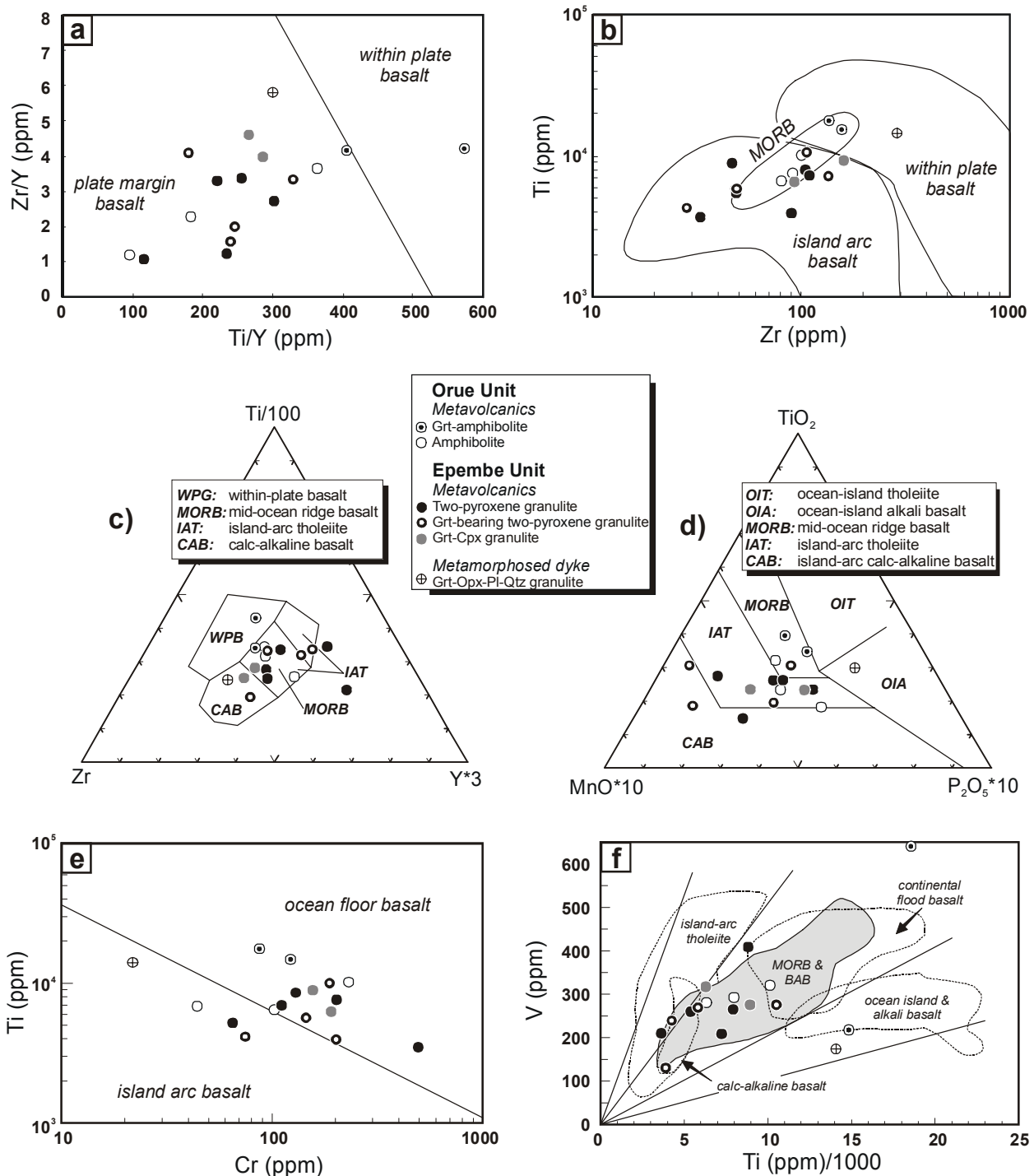


Fig. 3.8: Discrimination of the tectonic setting of basalts. **a)** Zr/Y vs. Ti/Y diagram of Pearce & Gale (1977). **b)** Ti vs. Zr diagram of Pearce (1982). **c)** Ti/100-Zr-Y*3 diagram of Pearce & Cann (1973). **d)** MnO-TiO₂-P₂O₅ diagram of Mullen (1983). **e)** Ti vs. Cr diagram of Pearce & Gale (1977). **f)** V vs. Ti/1000 diagram of Shervais (1982).

In contrast to the felsic rocks of the EC, the Mesoproterozoic granites are discriminated as within-plate granites (Fig. 3.9a & b), in good accordance with a coeval granite-anorthosite emplacement at about 1380 Ma.

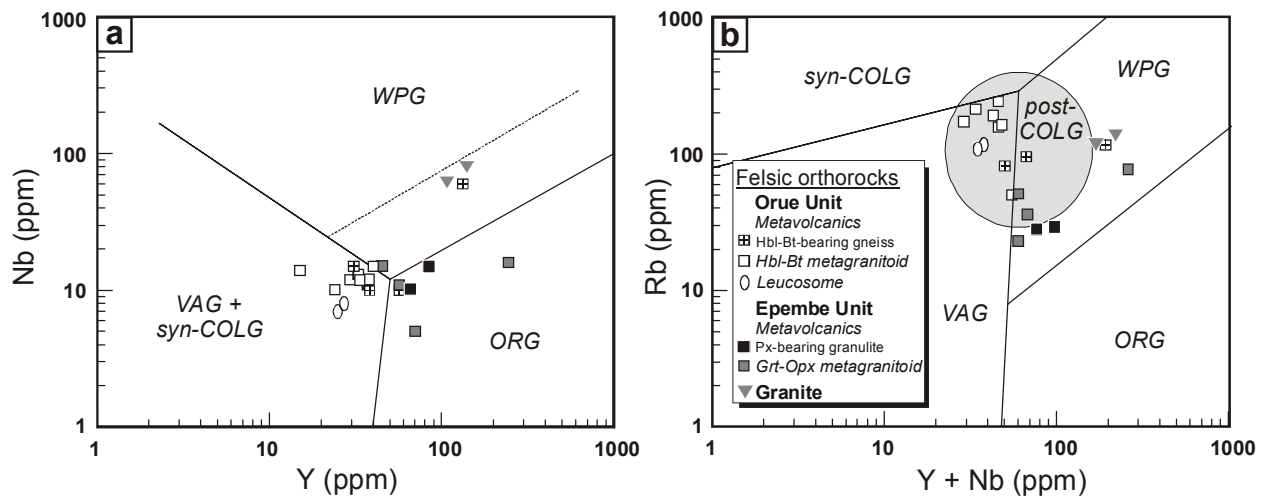


Fig. 3.9: Discrimination diagrams for the tectonic setting of granites. **a)** Nb vs. Y diagram and, **b)** Rb vs. Y + Nb diagram after Pearce et al. (1984) showing the fields of within-plate granites (WPG), volcanic arc granites (VAG), ocean ridge granites (ORG) and syn-collision granites (syn-COLG) with the field of post-collision granites (post-COLG) in Fig. 3.9b after Pearce (1996).

3.2.3 Paragneisses

According to the discrimination diagrams of Bhatia & Crook (1986) and Bhatia (1983) the protoliths of most analyzed paragneisses of the Orue Unit and the Epembe Unit were deposited in a basin situated in the vicinity of a continental island arc (Fig. 3.10a) or of an active continental margin (Fig. 3.10b), respectively.

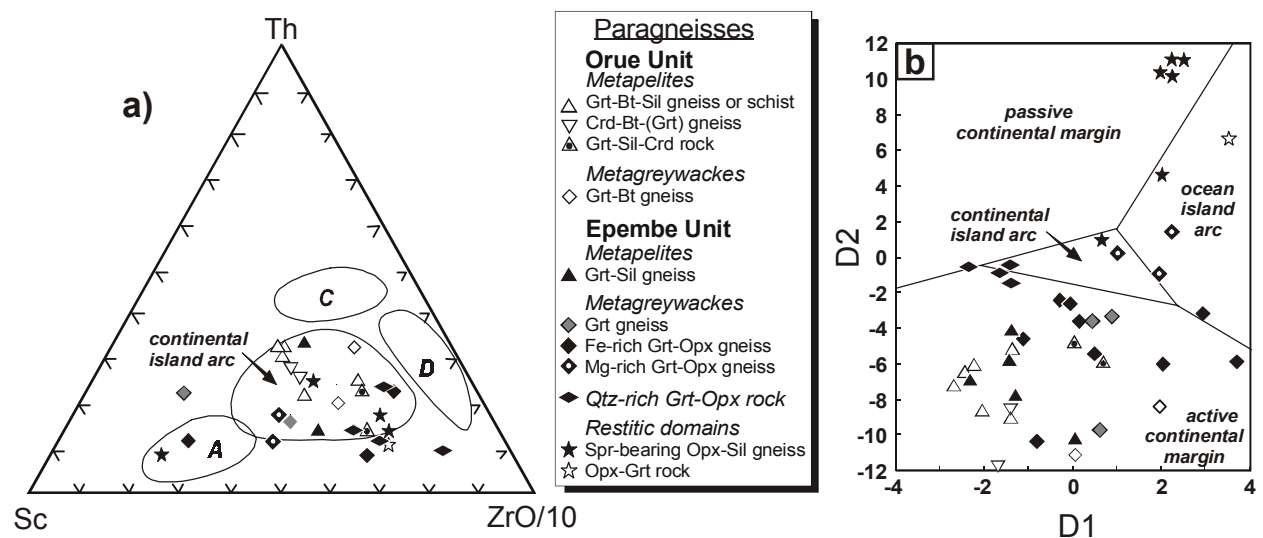


Fig. 3.10: Discrimination of the tectonic setting for the sedimentary protoliths of the paragneisses of the EC. **a)** Th-Sc-Zr/10 discrimination diagram for greywacken of Bhatia & Crook (1986) **A:** ocean island arc; **C:** active continental margin; **D:** passive continental margin; samples with Th contents below the detection limit have been excluded. **b)** D1–D2 diagram of Bhatia (1983). **D1:** $-0.0447 \text{ SiO}_2 - 0.972 \text{ TiO}_2 + 0.008 \text{ Al}_2\text{O}_3 - 0.267 \text{ Fe}_2\text{O}_3 + 0.208 \text{ FeO} - 3.082 \text{ MnO} + 0.140 \text{ MgO} + 0.195 \text{ CaO} + 0.719 \text{ Na}_2\text{O} - 0.032 \text{ K}_2\text{O} + 7.518 \text{ P}_2\text{O}_5 + 0.303$; **D2:** $-0.421 \text{ SiO}_2 + 1.988 \text{ TiO}_2 - 0.526 \text{ Al}_2\text{O}_3 - 0.551 \text{ Fe}_2\text{O}_3 - 1.610 \text{ FeO} + 2.720 \text{ MnO} + 0.881 \text{ MgO} - 0.907 \text{ CaO} - 0.177 \text{ Na}_2\text{O} - 1.840 \text{ K}_2\text{O} + 7.244 \text{ P}_2\text{O}_5 + 43.57$.

3.3 CHEMICAL VARIATIONS RELATED TO METAMORPHISM

A typical chemical characteristic of many granulite facies rocks is the variable depletion of the LIL elements, which is related to melt and fluid removal. On the other hand retrograde fluid influx might induce enrichment of LIL elements. High K/Rb ratios in rocks with $K_2O < 1$ wt.% are related to breakdown of biotite to orthopyroxene, K-feldspar and vapour under granulite facies condition (Rudnick et al., 1985); K/Rb ratios are considered to increase because biotite has proportionately more Rb than K-feldspar. In high-K rocks the K/Rb ratio is generally lower, although a slight increase in the ratio may be caused by the capture of Rb by fluid, that is equilibrated with K-Feldspar before removal (Rudnick et al., 1985).

By comparing the upper amphibolite facies rocks of the Orue Unit with the granulite facies rocks of the Epembe Unit minor but systematic variations are observed (Fig. 3.11). For rocks of comparable composition the commonly biotite-free granulite facies rocks generally exhibit slightly higher K/Rb ratios than the biotite-bearing upper amphibolite facies rocks (Fig. 3.11). However, high K/Rb ratios of > 500 , as typical of depleted granulites (Jahn, 1990), are observed for only few of the granulites, especially the Fe-rich Grt-Opx gneisses. The generally moderate K/Rb ratios of the granulites may be related to retrograde fluid influx. For the exceptionally low K/Rb ratios of the mafic Grt-Cpx granulites, which are exposed in a shear zone, high retrograde fluid activity seems to be very likely.

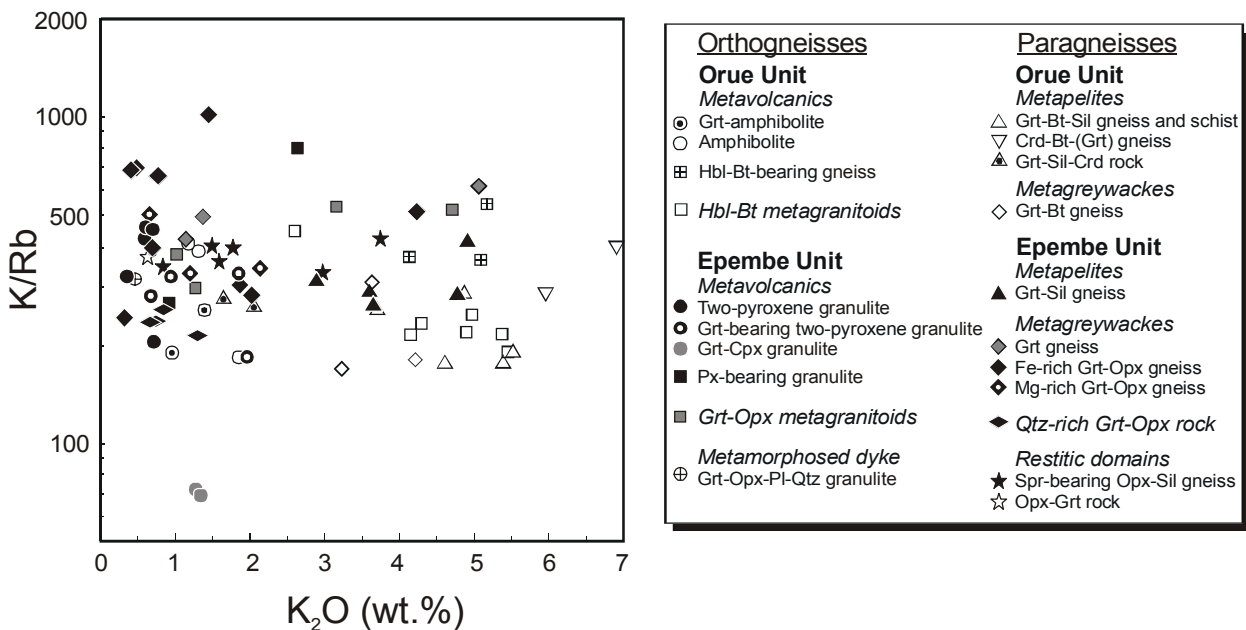


Fig. 3.11: K/Rb versus K diagram.

3.4 CONCLUSION

The geochemical data support the field observations that major parts of the Orue Unit and the Epembe Unit are constituted by volcano-sedimentary sequences. Remarkable compositional similarities between the sequences of both rock units point to their cogenetic evolution. In both units sub-alkaline tholeiitic metabasalts and dacitic to rhyolitic metavolcanites form a bimodal volcanic succession, which generally lacks volcanic rocks of intermediate composition. During the emplacement of the volcanics, sediments, predominantly of greywacke-composition, were deposited. The most possible tectonic setting for the formation of these sequences is a back-arc basin, situated between a continental margin and a volcanic or continental island arc of a collision zone. This interpretation is consistent with the palaeogeographic position of the EC at the south-western margin of the Congo Craton during Palaeoproterozoic times. The postulated collision event is probably related to the Eburnian orogenic event, that affected large parts of the northern Namibia and southern Angola, as is suggested by Palaeoproterozoic zircon core ages of the paragneisses and metavolcanites reported by Seth et al. (2003) and interpreted as ages of protolith formation. Subsequently, the volcano-sedimentary sequences were buried into deeper parts of the continental crust, whereby the volcano-sedimentary sequence of the Orue Unit was intruded by large volumes of I-type volcanic arc granitoids during the post-collisional stage. Granite plutonism is probably related to widespread post-tectonic granitoid emplacement in the late Eburnian in northern Namibia and south-western Angola (see chapter 1.2). The lack of comparable large volumes of granitoids in the Epembe Unit may suggest that the rocks were already situated in deeper crustal levels than the Orue Unit rocks during this time. Granitoid emplacement in the Orue Unit was followed by the intrusion of mafic dykes, probably synchronous with the emplacement of mafic dykes with subalkaline, tholeiitic basalt to andesite composition into the volcano-sedimentary sequence of the Epembe Unit.

4 METAMORPHIC EVOLUTION OF THE UPPER AMPHIBOLITE FACIES ROCKS OF THE ORUE UNIT

The studied part of the EC is mainly constituted by upper amphibolite facies rocks of the Orue Unit and subordinate granulite facies rock of the Epembe Unit. Since the upper amphibolite facies rocks of the Orue Unit lack granulite facies relics, it seems rather unlikely that they formed by retrogression of granulites like those exposed in the nearby Epembe Unit (Brandt et al., 2003). Following this interpretation, the rocks of the Orue Unit must have originated by an individual high-grade metamorphic event. Consequently, the P-T paths recorded by rocks of the Orue Unit may yield important implications on the tectonic evolution of the EC.

In the following, the metamorphic evolution of the Orue Unit rocks will be reconstructed by combining petrographic observations with mineral chemistry data, phase petrological considerations and conventional geothermobarometry. Individual rock samples of comparable composition from both the southern part and of the northern part of the Orue Unit display differing mineral assemblages, testifying to regional variations of the peak-metamorphic conditions, and were thus investigated in detail. In addition, the metamorphic evolution of contact metamorphic Grt-Sil-Crd rocks, exposed in a narrow reaction zone at the southern margin of the KIC, is investigated. The formation of these rocks is attributed to a contact thermal effect, induced by the intrusion of the anorthositic magmas of the KIC in the Mesoproterozoic (Brandt et al., 2003). The P-T paths recorded by these rocks, combined with petrogenetic investigations on the anorthosites (Drüppel et al., 2001; Drüppel, 2003), may hence yield important implications on possible interrelations between the magmatic and metamorphic rocks of NW Namibia during the Mesoproterozoic. Moreover, a comparison between the P-T paths recorded by the contact metamorphic rocks and those of the Orue Unit rocks exposed further south and lacking evidence for a contact metamorphic overprint, will elucidate possible genetic relationships between contact metamorphism and regional metamorphism.

4.1 PETROGRAPHY

Field observations and geochemical investigations indicate that the upper amphibolite facies Orue Unit is dominated by a metamorphosed volcano-sedimentary sequence, intruded by younger Hbl-Bt metagranitoids and mafic dykes. For simplicity, the Orue Unit has been subdivided into only three lithological subunits for the petrographic investigations:

- (1) Mafic metavolcanites of the volcano-sedimentary sequence and younger dykes.
- (2) Felsic metavolcanites of the volcano-sedimentary sequence and Hbl-Bt metagranitoids.
- (3) Paragneisses (predominantly metagreywackes and metapelites) of the volcano-sedimentary sequence.

Both, the rocks of the volcano-sedimentary sequence as well as the younger intrusives are exposed in the two major subzones of the Orue Unit: a) The northern part and b) the southern part, the latter of which is further subdivided into an eastern and a western region ('south-eastern region' and 'south-western region'; respectively), separated by late faults, and the contact zone at the anorthositic KIC (see Chapter 2.1).

In order to constrain the mineral assemblages and reaction textures, which constitute the basis for the reconstruction of the metamorphic evolution, a total of 145 thin sections, comprising samples of all lithological subunits and subzones of the Orue Unit, were investigated petrographically.

Prograde metamorphic mineral assemblages (*stage 1*) are preserved as inclusions in coarse-grained matrix minerals, which are in turn attributed to the peak of metamorphism (*stage 2*), whereas mineral reaction textures surrounding the peak-metamorphic minerals yield information about the retrograde history (*stage 3*) of the rocks.

4.1.1 Mafic rocks

The mafic rocks of the volcano-sedimentary sequence of the Orue Unit were broadly subdivided into amphibolites, Grt-amphibolites, garnet-bearing hornblende schists and (garnet-) hornblendites on the basis of field observations. However, based on the microscopic investigation of 58 thin sections, seven different mineral assemblages are recognized for the mafic rocks of the Orue Unit (Table 4.1):

Amphibolites (type 1), which may contain subordinate ilmenite, quartz and biotite, occur in the metavolcanic succession of both the northern part and the south-eastern region of the Orue Unit and of the metasedimentary succession of the northern part as well as metabasaltic xenoliths incorporated by Hbl-Bt metagranitoids. Locally, the amphibolites underwent partial melting, as is indicated by Pl-rich leucosomes. In contrast, clinopyroxene-bearing amphibolites (type 2) are

rare. These rocks mostly occur in the south-eastern region of the Orue Unit, where they are exposed as individual layers, presumably former dykes or sills, of both the metavolcanic and the paragneiss succession.

type	n	stage2						stage3
volcano-sedimentary sequence								
<i>South-eastern region</i>								
(1)	7		Hbl	Pl	± Qtz	Ilm	± Bt	Act, Chl, Ep
(2)	4	Cpx	Hbl	Pl	± Qtz	Ilm	± Bt	Hbl, Qtz, Act, Chl, Ep
(3)	4	Grt	Hbl	Pl	± Qtz	Ilm	± Bt	Hbl, Qtz, Act ± Czo, Cc, Qtz
(4)	2	Grt Cpx	Hbl	Pl	± Qtz	Ilm	± Bt	Hbl, Qtz, Act, Chl, Ep
(5)	15	Grt	Hbl	Pl	Qtz	Ilm	Bt	Hbl, Pl, Act, Chl, Ep
(6)	2	Grt	Hbl	± Pl				Act
<i>South-western region</i>								
(5)	2	Grt	Hbl	Pl	Qtz	Ilm	Bt	Hbl, Pl, Act, Chl, Ep
<i>Northern part</i>								
(1)	14		Hbl	Pl	± Qtz	Ilm		Act, Bt, Chl, Ep
(2)	1	Cpx	Hbl	Pl		Ilm		Hbl, Qtz
(5)	1	Grt	Hbl	Pl	Qtz	Ilm		Act, Chl
(7)	2		Hbl	± Pl				Act, Chl
mafic dykes								
(1)	3		Hbl	Pl		Ilm		Act, Chl, Ep

Table 4.1: Mineral assemblages in the mafic rocks of the Orue Unit (n.: number of investigated rock samples).

In contrast, only one clinopyroxene-bearing amphibolite has been observed in the northern part. Garnet-bearing amphibolites (type 3), two of them additionally containing Cpx (type 4), are restricted to the paragneiss succession of the south-eastern region. Comparable plagioclase-poor garnet-hornblende schists (type 5), generally bearing abundant biotite and quartz, occur as lenses and layers in the paragneisses of both the south-eastern and the south-western region, whereas they are rarely observed in the northern part. Hornblendites, containing minor garnet, occur as lenses in the paragneiss successions of the south-eastern region (type 6) whereas those exposed in the northern part are garnet-free (type 7). Mafic dykes, that intruded the Hbl-Bt metagranitoids of the Orue Unit are essentially quartz-free amphibolites (type 1). The local occurrence of migmatitic textures and the presence of Grt-Hbl-Pl assemblages in rocks of the southern part of

the Orue Unit indicate upper amphibolite facies peak-metamorphic conditions. The lack of orthopyroxene and/or its alteration products demonstrate that granulite facies conditions were not attained.

The observed differences in the mineralogy of the amphibolites in the south-eastern region of the Orue Unit are in good accordance with the respective bulk-rock composition of the investigated samples, as is demonstrated in A-C-F/M diagrams (Fig. 4.1):

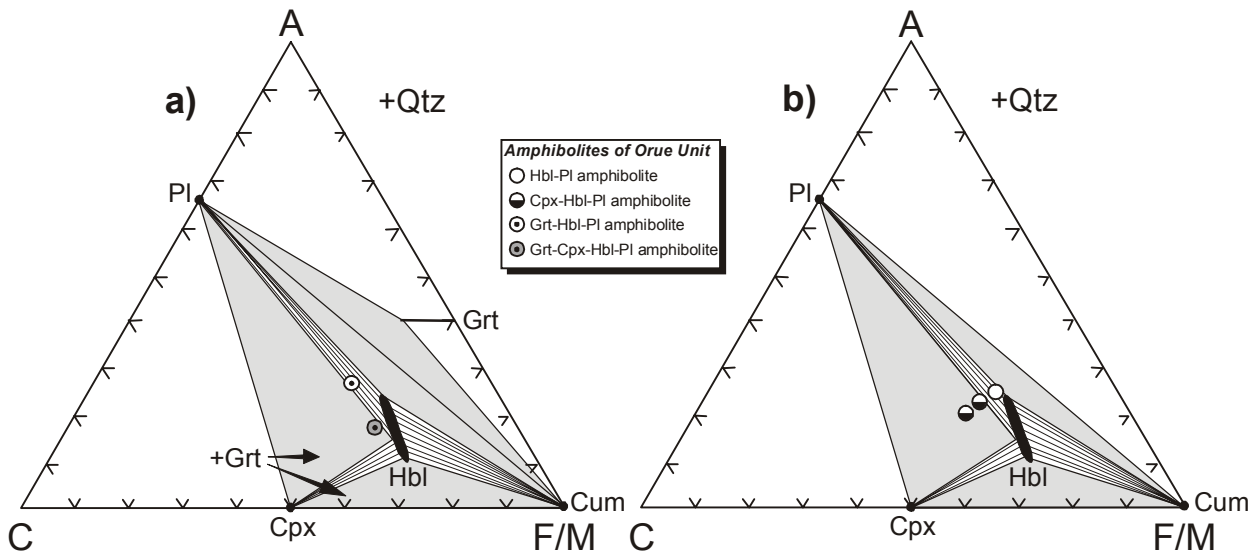


Fig. 4.1: Schematic A-C-F/M projections for **a)** Mg-rich mafic and **b)** Fe-rich mafic rocks of the upper amphibolite facies (after Spear, 1993), illustrating the consistent relationships between bulk-rock chemistry and observed mineral assemblages in the mafic rocks of the Orue Unit.

Garnet is generally restricted to Fe-rich amphibolites of the Orue Unit (bulk-rock X_{Mg} : 0.38-0.39), consistent with the observation of Spear (1993) that garnet is a typical phase in Fe-rich upper amphibolite facies metabasites. On the other hand, the presence of clinopyroxene in Grt-bearing amphibolites is related to a slightly higher bulk-rock Ca content when compared to clinopyroxene-free samples (Fig. 4.1a). Similar relationships explain the presence of clinopyroxene in magnesian, garnet-free amphibolites (bulk-rock X_{Mg} : 0.41-0.53; Fig. 4.1b).

4.1.1.1 Amphibolites

Due to textural and mineralogical similarities, amphibolites (type 1), Cpx-bearing amphibolites (type 2), Grt-bearing amphibolites (type 3) and Grt-Cpx-bearing amphibolites (type 4) were grouped together.

Amphibolites and Cpx-bearing amphibolites

south-eastern region

samples: B-172-A-98 (+Cpx), B-174-B-98, B-177-B-98, B-181-A-98, B-228-2-99, B-305-2-99 (+Cpx), B-311-5-99, B-386-99 (+Cpx), B-411-00, B-446-99, B-645-2-00 (+Cpx) and B-521-2-99, B-592-3-99, B-676-00 (mafic dykes)

northern part

samples: B-109-A-98, B-124-D-98, B-131-A-98, B-142-A-98, B-149-A-98, B-155-A-98, B-159-C-98, B-159-E-98, B-167-B-98, B-248-B-98, B-260-A-98, B-268-B-98, B-289-A-98 (+Cpx), B-294-A-98, B-396-2-99

Grt-bearing amphibolites and Grt-Cpx-bearing amphibolites

south-eastern region

samples: B-191-B-98 (+Cpx), B-197-B-98, B-345-3-99, B-401-3-99, B-405-1-99, B-591-1-99 (+Cpx)

Stage 1: Prograde evolution and Stage 2: Peak-metamorphic assemblages

All amphibolites are generally characterized by a medium-grained, equigranular texture, defined by nematoblastic, green and brown hornblende (Hbl₂; 35-65 vol.%), that form subhedral to euhedral prismatic crystals up to 3 mm in length, coexisting with fine- to medium-grained plagioclase (Pl₂; 31-61 vol.%). Hbl₂ and Pl₂ are weakly aligned, defining the S₁ foliation. Straight grain boundaries between Pl₂ and Hbl₂ indicate that they crystallized under equilibrium conditions, an interpretation, which is also constrained by their inclusion-relationship. Fine-grained ilmenite (Ilm₂) is a minor matrix phase (1-5 vol.%) but also occurs as inclusion (Ilm₁) in Hbl₂ and Pl₂. Minor amounts of fine-grained biotite (Bt₂; 0-5 vol.%), elongated subparallel to the S₁ foliation, and of fine-grained quartz (Qtz₂; 0-10 vol.%) may occur in the matrix, exhibiting straight grain boundaries against Hbl₂. In the Grt-bearing amphibolites garnet (Grt₂; 3-20 vol.%) forms anhedral to subhedral grains of up to 1 mm in diameter, displaying straight grain boundaries against Hbl₂ and Pl₂ (Fig. 4.2a) and hence indicating their contemporaneous formation at peak-metamorphic conditions. Grt₂ contains abundant inclusions of hornblende (Hbl₁), plagioclase (Pl₁) and ilmenite (Ilm₁; Fig. 4.2a). Pale green clinopyroxene (Cpx₂; 5-8 vol.%) occurs as anhedral grains of up to 1 cm in length embedded in the Hbl-Pl matrix and aligned parallel to the S₁ foliation. In the Cpx-bearing amphibolite of the northern part hornblende (Hbl₁) is preserved as corroded inclusions in Cpx₂ (Fig. 4.2b), suggesting Cpx₂ formation at the expense of Hbl₁, whereas in the Grt-Cpx-bearing amphibolites Hbl₁ occurs as inclusions in both Grt₂ and the coexisting Cpx₂, thus suggesting partial replacement of early hornblende by the peak-metamorphic Grt-Cpx assemblage.

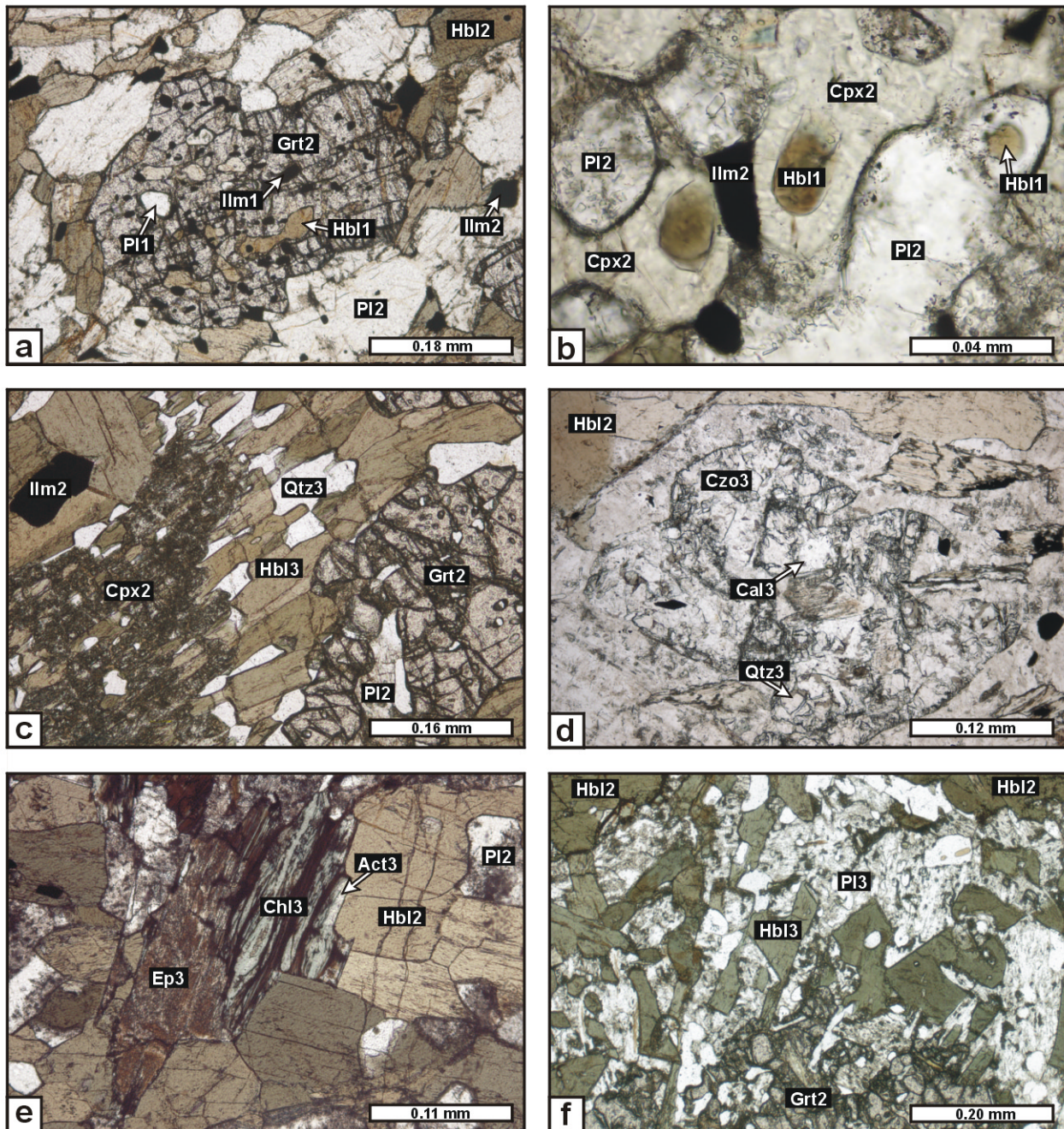


Fig. 4.2: Photomicrographs illustrating the metamorphic evolution of the mafic orthogneisses of the Orue Unit. **a)** Grt2 in a Hbl2-Pl2-Ilm2 matrix. Grt2 encloses Hbl1, Pl1 and Ilm1 (Grt-amphibolite B405-1-99). **b)** Cpx2 and P2 with corroded inclusions of Hbl1 (Cpx-bearing amphibolite B289-A-98). **c)** Intergrowth of Hbl3 and Qtz3 situated between Grt2 and altered Cpx2 and Hbl3 corona around Ilm2 (Grt-Cpx-bearing amphibolite B-191-B-98). **d)** Intergrowth of Czo3, Cal3 and Qtz3 pseudomorphing former Grt2 (Grt-amphibolite B-197-B-98). **e)** Intergrowth of Ep3, Chl3 and Act3 replacing Hbl2 and Pl2 (amphibolite B-311-5-99). **f)** Intergrowth of subhedral Hbl3 and Pl3 replacing Grt2 (Grt-Hbl schist B-679-3-00).

Stage 3: Retrograde evolution

During the retrograde evolution a third generation of hornblende (Hbl3) developed, occurring as reaction rims between Pl2 and Cpx2, where it is intimately intergrown with quartz (Qtz3). Similar Hbl3-Qtz3 intergrowths have been observed in the Grt-Cpx-bearing amphibolites, where they separate Grt2 from Cpx2 (Fig. 4.2c). In addition, Hbl3 may form monomineralic coronas around Ilm2 (Fig. 4.2c). The interpretation of late Hbl3 formation is supported by the presence of Grt2 inclusions in Hbl3. Thus, it can be concluded that even though garnet, clinopyroxene and quartz occur within single samples they do clearly not represent an equilibrium assemblage, hence proving that the high-pressure granulite facies assemblage of Grt-Cpx-Qtz was not developed in the metabasites of the Orue Unit.

The further retrograde evolution is characterized by the formation of greenschist facies mineral assemblages. In cases, Grt2 is partly or completely replaced by fine-grained intergrowths of pale yellow clinozoisite (Czo3), calcite (Cal3) and Qtz3 (Fig. 4.2d). Hbl2 is commonly rimmed by colourless to pale green actinolite (Act3) or is replaced by a post-tectonic intergrowth of yellowish epidote (Ep3), Act3, titanite (Ttn3) and pale green chlorite (Chl3; Fig. 4.2e), cross-cutting the S₁ foliation. Moreover, Ttn3 occurs as monomineralic corona around Ilm2. Relic Cpx2 is altered to Act3, Chl3 and Cal3.

Common accessories are apatite, zircon and hematite, the latter of which is rimmed by Ep3 as well as rutile, surrounded by Ilm2.

4.1.1.2 Garnet-hornblende schists and (garnet-bearing) hornblendites

The following garnet-hornblende schists and (garnet-bearing) hornblendites have been investigated:

Garnet-hornblende schists

south-eastern region

samples: B-184-2-99, B-197-99, B-220-B-98, B-308-1-99, B-310-2-00, B-342-10-00, B-342-11-00, B-407-3-99, B-407-4-99, B-588-2-99, B-590-99, B-679-2-00, B-679-3-00, B-680-2-00, B-681-5-00

south-western region

samples: B-246-D-98, B-246-F-98

northern part

samples: B-122-3-99, B-122-B-98

(Garnet-bearing) hornblendites

south-eastern region

samples: B-402-99, B-654-00

northern part

samples: B-122-A-98, B-126-A-98

Stage 1: Prograde evolution and Stage 2: Peak-metamorphic assemblages

Garnet-hornblende schists generally contain sub- to anhedral, rotated garnet porphyroblasts (Grt₂; 4-40 vol.%) of up to 1 cm in diameter, wrapped by a nematoblastic and well-foliated matrix mainly composed of green hornblende (Hbl₂; 20-65 vol.%). The poikiloblastic Grt₂ contains abundant inclusions of quartz, hornblende, biotite and ilmenite, forming a net-like texture. In all samples fine-grained biotite (Bt₂; 1-40 vol. %) and quartz (Qtz₂; 10-40 vol.%) are present in strongly varying proportions, whereas ilmenite (Ilm₂; 2-5 vol.%) is a minor phase. Aligned Hbl₂ and Bt₂ define the S₁ foliation. When compared to the plagioclase-rich amphibolites strongly sericitized plagioclase (Pl₂; 13-22 vol.%) forms an minor constituent of the garnet-hornblende schists.

In contrast, the massive Grt-hornblendites are dominated by green hornblende (Hbl₂; 75-95 vol.%), which forms euhedral to subhedral grains of up to 5 mm in length coexisting with garnet (Grt₂; 5-20 vol.%) and subordinately with plagioclase (Pl₂; 0-5 vol.%).

Apatite and zircon are common accessories of both the garnet-hornblende schists and the (garnet-) hornblendites.

Stage 3: Retrograde evolution

In places, Grt₂ of the garnet-hornblende schists is replaced by undeformed retrograde intergrowths of subhedral Hbl₃ and plagioclase (Pl₃; Fig. 4.2f). Furthermore, monomineralic coronas of late, granoblastic Pl₃ are developed around Grt₂, separating it from Hbl₂. Bt₂ is altered to chlorite (Chl₃)-titanite (Ttn₃) intergrowths, whereas Hbl₂ is replaced by fine-grained aggregates of Chl₃, actinolite (Act₃) and epidote (Ep₃).

4.1.2 Felsic gneisses and Hbl-Bt metagranitoids

The petrographic investigations concentrated on 31 selected samples of felsic orthogneisses of the Orue Unit. However, significant differences between the mineral assemblages of the metavolcanic felsic Hbl-Bt-bearing gneisses of the volcano-sedimentary sequence and those of

the Hbl-Bt metagranitoids are not observed, as both rock types are essentially hornblende- and biotite-bearing quartzofeldspathic gneisses (Table 4.2):

	n	stage2				stage3
<i>Felsic Hbl-Bt-bearing gneisses</i>						
(1)	16	Kfs	Pl	Qtz	± Bt ± Hbl	± Ep, Chl, Act
<i>Hbl-Bt metagranitoids</i>						
(2)	15	Kfs	Pl	Qtz	Bt Hbl	± Ep, Chl, Act

Table 4.2: Mineral assemblages in the felsic orthogneisses of the Orue Unit (n.: number of investigated rock samples).

4.1.2.1 Felsic Hbl-Bt-bearing gneisses

Felsic gneisses comprise rhyolitic to dacitic metavolcanites, sampled from both the northern part and the south-eastern region of the Orue Unit.

south-eastern region

samples: B-174-A-98, B-179-A-98, B-187-A-98, B-226-98, B-367-99, B-410-99, B-521-1-99, B-702-00

northern part

samples: B-106-B-98, B-112-B-98, B-114-A-98, B-114-C-98, B-133-A-98, B-152-A-98, B-159-A-98, B-159-D-98

Stage 1: Prograde evolution and Stage 2: Peak-metamorphic assemblages

All felsic gneisses are equigranular, homogeneous fine-grained rocks, which are generally dominated by perthitic K-feldspar (Kfs₂; 39-52 vol.%) and quartz (Qtz₂; 10-35 vol.%), whereas plagioclase (Pl₂) is generally less abundant (13-40 vol.%) than Kfs₂. Minor amounts of fine-grained ilmenite (Ilm₂; 0-5 vol.%), biotite (Bt₂; 1-10 vol.%) and green hornblende (Hbl₂; 0-4 vol.%) are present, the latter two being crudely aligned and defining a weak S₁ foliation (Fig. 4.3a).

Stage 3: Retrograde evolution

Hbl₂ and Bt₂ are partially or completely replaced by intergrowths of retrograde epidote (Ep₃), chlorite (Chl₃) and actinolite (Act₃). Common accessories are zircon, apatite, allanite and

titanite. Titanite either occurs as corona around Ilm2 or as euhedral grains dispersed in the matrix.

4.1.2.2 Hbl-Bt metagranitoids

The investigated Hbl-Bt metagranitoids comprise samples from the northern part and both the south-eastern and the south-western region of the Orue Unit:

South-western and southern-eastern region

samples: B-190-1-99, B-202-A-98, B-240-A-98, B-241-A-98, B-401-1-99, B-406-2-99, B-520-99, B-592-2-99, B-644-1-00, Ku97-46, Ku97-47

Northern part

samples: B-163-B-98, B-258-98, B-259-A-98, B-268-A-98

Stage 1: Prograde evolution and Stage 2: Peak-metamorphic assemblages

In clear contrast to the homogeneous metavolcanic Hbl-Bt-bearing gneisses, the Hbl-Bt metagranitoids comprise migmatitic textures with a separation into palaeosomes and leucosomes (Fig. 4.3b): The fine- to medium-grained palaeosomes contain variable amounts of biotite (Bt2; 1-20 vol.%), set in a granoblastic matrix composed of perthitic K-feldspar (Kfs2; 15-39 vol.%), plagioclase (Pl2; 29-37 vol.%) and quartz (Qtz2; 25-35 vol.%). In addition, minor amounts of

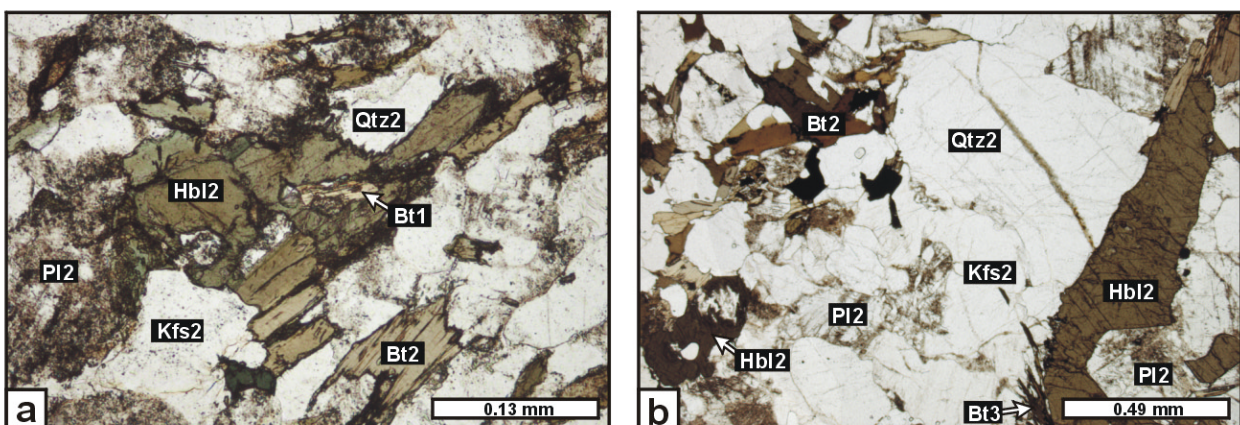


Fig. 4.3: Photomicrographs illustrating the metamorphic evolution of the felsic orthogneisses of the Orue Unit. **a)** Hbl2 and Bt2 of a felsic gneiss is set in a quartzofeldspathic matrix of Qtz2, Pl2 and Kfs2. Hbl2 encloses Bt1 (felsic Hbl-Bt-bearing gneiss B-159-A-98). **b)** Biotite- and hornblende-bearing palaeosome and hornblende-bearing leucosome of a Hbl-Bt metagranitoid. Hbl2 is partly replaced by late Bt3 (Hbl-Bt metagranitoid B-190-1-99).

anhedral green hornblende (Hbl₂; 1-5 vol.%) occur in the quartzofeldspathic matrix of the palaeosomes. Bt₂ and Hbl₂ are aligned and define a commonly well-developed S₁ foliation. The leucosomes, on the other hand, are rich in Kfs₂ (< 1 cm; ~ 40 vol.%), Qtz₂ (~ 40 vol.%) and Pl₂ (~ 15 vol.%) and contain only minor amounts of anhedral to subhedral, coarse-grained green Hbl₂ of up to 6 mm in diameter (~ 5 vol.%; Fig. 4.3b). Bt₂-Qtz₂ symplectites were observed at the contacts between the palaeosomes and leucosomes, suggesting that partial melting is related to dehydration melting of biotite, which is not preserved in the leucosomes.

Stage 3: Retrograde evolution

As observed in the metavolcanic felsic gneisses, Hbl₂ of both the leucosome and the palaeosome is locally replaced by fine-grained intergrowths of retrograde greenish chlorite (Chl₃) and pale yellow epidote (Ep₃) and/or rimmed by late biotite (Bt₃; Fig. 4.3b). Bt₂ is partly or completely altered to green Chl₃, associated by fine-grained titanite (Ttn₃). Moreover, titanite is present as subhedral grains in the matrix or forms rims around ilmenite. The most abundant accessory phase is euhedral apatite (up to 0.5 mm in diameter), whereas euhedral zircon and orange-brown subhedral allanite (< 0.5 mm in length), the latter of which being aligned parallel to the S₁ foliation, are comparably rare.

In late shear zones the Hbl-Bt metagranitoids are transformed during a late deformation event D₂ to mylonitic schists, which display a small-scaled mylonitic foliation S₂, defined by fine-grained chlorite and sericite alternating with layers of recrystallized fine-grained quartz and feldspar. Relic Pl₂, Qtz₂ and Kfs₂ are present as mm- to cm-sized porphyroblasts, which are wrapped by the fine-grained mylonitic matrix

4.1.3 Paragneisses

The aluminous paragneisses of the Orue Unit are broadly subdivided into sillimanite-free metagreywackes and sillimanite- or cordierite-bearing metapelites on the basis of field observations and their bulk-rock chemistry.

4.1.3.1 Metagreywackes

Based on the petrographic investigation of 30 metagreywacke samples only minor variations in the mineral assemblages are recognized. Significant petrological variations between samples from the south-eastern region and those from the northern part of the Orue Unit are not observed (Table 4.3).

south-eastern region

samples: B-171-A-98, B-177-A-98, B-178-A-98, B-184-A-98, B-186-A-98, B-191-A-98, B-197-A-9-8, B-220-A-98, B-310-1-99, B-342-2-99, B-345-99, B-401-4-99, B-404-1-99, B-404-2-99, B-406-1-99, B-407-2-99, B-511-2-99, B-592-1-99, B-593-99, B-600-99, B-601-99, B-605-99, B-640-00, B-645-1-00

northern part

samples: B-124-A-98, B-137-B-98, B-137-C-98, B-394-2-99, B-396-1-99, B-399-1-99

The metagreywackes are migmatitic Grt-Bt gneisses with or without K-feldspar (type 1 and type 2, respectively; Table 4.3). Few samples of the south-eastern region additionally contain green hornblende (type 3).

	n	stage2				stage3	
<i>South-eastern region</i>							
(1)	9	Grt	Bt	Kfs	Pl	Qtz	± Ms, Chl
(2)	12	Grt	Bt		Pl	Qtz	± Ms, Chl
(3)	3	Grt	Hbl	Bt		Pl	Qtz
<i>Northern part</i>							
(2)	6	Grt	Bt		Pl	Qtz	± Ms, Chl

Table 4.3: Mineral assemblages in the metagreywackes of the Orue Unit (n.: number of investigated rock samples).

Stage 1: Prograde evolution and Stage 2: Peak-metamorphic assemblages

The metagreywackes exhibit migmatitic textures: (1) Palaeosomes contain fine- to medium-grained, tabular (< 1.5 mm) biotite (Bt₂; Bt 6-27 vol.%), which is surrounded by a fine- to medium-grained granoblastic matrix composed of micropertitic K-feldspar (Kfs₂; 0-41 vol.%), plagioclase (Pl₂; 6-49 vol.%) and quartz (Qtz₂; 9-57 vol.%). Matrix Bt₂ is aligned and defines the planar S₁ foliation. Rare ilmenite (Ilm₂; 0-4 vol.%) and fine-grained green hornblende (Hbl₂; 0-3 vol.%; < 1 mm) are oriented sub-parallel to the S₁ foliation. Monomineralic coronas of Hbl₂ surrounding Bt₂ and separating it from Pl₂ (Fig. 4.4a), indicate Hbl₂ formation at the expense of Bt₂. Anhedral garnet (Grt₂; 1-30 vol.%) forms rotated porphyroblasts of up to 2.5 cm in diameter, that are wrapped by the S₁ foliation, suggesting pre- to syn-tectonic growth of Grt₂ with respect to D₁. Abundant inclusions of biotite (Bt₁), plagioclase (Pl₁) and quartz (Qtz₁) in

both Kfs2 and poikiloblastic Grt2 indicate that early Bt-Pl-Qtz assemblages were partially replaced by Grt2, Kfs2 and Hbl2 during prograde metamorphism. As the mineral inclusions show no preferred orientation, evidence for an early foliation pre-dating the external S_1 foliation is not recorded by the metagreywackes. (2) In contrast, coarse-grained leucosomes are rich in Kfs2 and Qtz2 whereas Pl2 is rare and Bt2 is absent. Net-like Grt2 (up to 2 cm in diameter) contains abundant inclusions of Pl1 and Qtz1. At the palaeosome-leucosome contacts skeletal Bt2 occurs, which is rimmed by a thin corona of Kfs2 and Grt2, separating Bt2 from Qtz2 (Fig. 4.4b). Like the inclusion patterns of Grt2 in the palaeosomes, the latter two textures indicate partial replacement of early Bt-Qtz by Grt2-Kfs2 assemblages. Common accessories are zircon and apatite.

Stage 3: Retrograde evolution

Evidence for the retrograde metamorphic evolution is poorly recorded by the metagreywackes: Grt2 is locally resorbed by late biotite (Bt3), that is locally intergrown with muscovite (Ms3). Due to a more intensive retrogression, Grt2 in metagreywackes of the northern part of the Orue Unit is mostly completely replaced by intergrowths of Ms3 and greenish chlorite (Chl3). Matrix Bt2 and late Bt3 are locally altered to Chl3 and titanite (Ttn3). The rocks were affected by a late mylonitic deformation D_2 , as is evident by subgrain formation and marginal recrystallization of Qtz2 and the development of flame perthite in Kfs2.

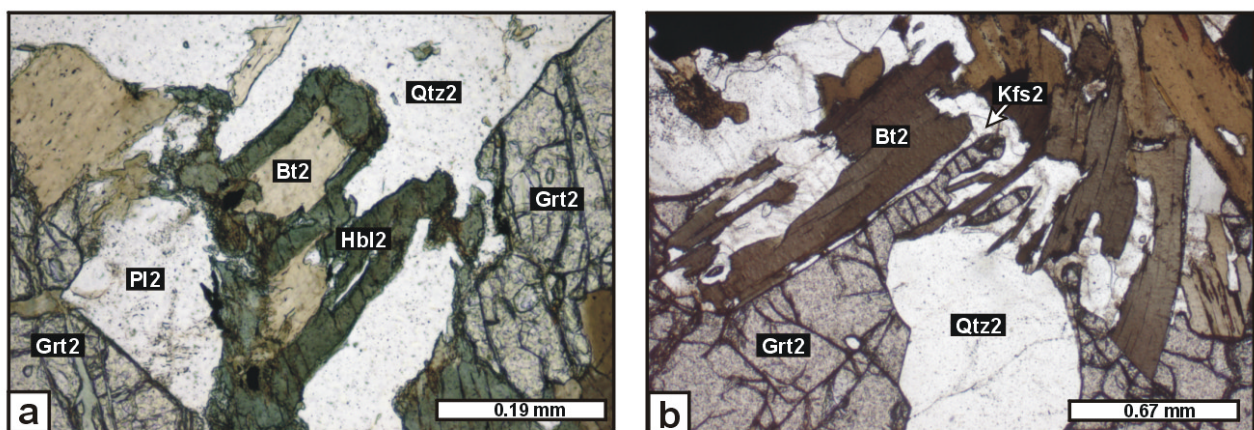


Fig. 4.4: Photomicrographs illustrating the metamorphic evolution of the metagreywacke-type Grt-Bt gneisses of the Orue Unit. **a)** Bt2 is rimmed by green Hbl2 (Grt-Bt-Hbl gneiss B-645-1-00). **b)** Bt2 rimmed by Kfs2 and Grt2 separating it from Qtz2 (Grt-Bt gneiss B-177-A-98).

4.1.3.2 Metapelites

Based on field observations and geochemical analyses the metapelites of the Orue Unit were subdivided into

- Grt-Bt-Sil gneisses and schists of the southern part
- Crd-Bt-(Grt) gneisses of the northern part
- Contact metamorphic Grt-Sil-Crd rocks of the southern part

This subdivision is supported by the microscopic investigation of 27 samples, whereby four mineral assemblages were recognized in the metapelites (Table 4.4): The metapelites of the eastern region and the western region of the southern part of the Orue Unit comprise the uniform, diagnostic peak-metamorphic mineral assemblage Grt + Bt + Sil + Kfs + Pl + Qtz (type 1). In contrast, most metapelites of the northern part of the Orue Unit are characterized by the peak-metamorphic garnet-free assemblage of Crd + Bt + Kfs + Pl + Qtz (type 2). One sample of the northern part additionally contains garnet (Grt + Crd + Bt + Kfs + Pl + Qtz; type 3). Remarkably,

	n	stage2							stage3
<i>South-eastern region</i>									
(1)	17	Grt	Sil	Bt	Kfs	Pl	Qtz	± Bt, Sil, Ms, Pl, Chl	
<i>South-western region</i>									
(1)	3	Grt	Sil	Bt	Kfs	Pl	Qtz	± Bt, Sil, Ms, Pl, Chl	
<i>Northern part</i>									
(2)	4		Crd	Bt	Kfs	Pl	Qtz	Ilm ± Spl	± Ms, Chl
(3)	1	Grt	Crd	Bt	Kfs	Pl	Qtz	Ilm ± Spl	± Ms, Chl
<i>Contact metamorphic rocks</i>									
(4)	2	Grt	Crd	Sil		Pl	Qtz	Ilm	Bt, Sil, Pl, St, Chl

Table 4.4: Mineral assemblages in the metapelites of the Orue Unit (n.: number of investigated rock samples).

Crd-bearing metapelites from the northern part (type 2 and 3) and Grt-Sil-bearing metapelites from the southern part (type 1) have broadly similar bulk-rock X_{Mg} ratios (0.28-0.36 and 0.33-0.44, respectively), hence suggesting that the different mineral assemblages reflect differences in the peak P-T conditions between the two major subzones of the Orue Unit. In clear contrast to the metapelitic gneisses and schists of the south-eastern region, the massive metapelitic rocks from the southern-eastern region, confined to narrow contact aureoles of the KIC, comprise a different peak-metamorphic assemblage of Grt + Sil + Crd + Pl + Qtz (type 4). The lack of K-

feldspar in these rocks is most probably related to the lower bulk-rock K₂O content of the Grt-Sil-Crd rocks when compared to the K-feldspar-bearing metapelites (K₂O: 1.6-2.1 wt.% and 3.7-6.9 wt.%, respectively).

Grt-Bt-Sil gneisses and schists

Grt-Bt-Sil gneisses and schists occur in both the eastern and the western region of the southern part of the Orue Unit.

south-eastern region

samples: B-307-2-99, B-307-3-99, B-341-1-99, B-342-3-99, B-345-1-99, B-345-2-99, B-401-2-99, B-440-2-99, B-588-1-99, B-589-1-99, B-612-99, B-679-1-00, B-681-1-00, B-681-2-00, B-681-3-00, B-685-00, B-703-00 and B-219-A-98, B-342-5-99 (leucosomes)

south-western region

samples: B-246-A-98, B-246-C-98, B-246-E-98

Stage 1: Prograde evolution and Stage 2: Peak-metamorphic assemblages

Both rock types display migmatitic textures, being composed of sharply restricted palaeosomes and quartzofeldspathic leucosomes:

Palaeosomes are generally rich in biotite (Bt₂; 11-30 vol.%) and fibrolitic to prismatic sillimanite (Sil₂; 2-35 vol.%). Furthermore, flame-perthitic K-feldspar (Kfs₂; 5-25 vol.%), quartz (Qtz₂; 12-50 vol.%) and plagioclase (Pl₂; 3-30 vol.%) constitute major phases of the palaeosomes. An accentuated S₁ foliation of the palaeosomes is defined by Bt₂, which was aligned during the main deformation phase D₁. A weak L₁ lineation is traced by prismatic and fibrolitic Sil₂ of up to 2 mm in length. The S₁ foliation is commonly straight; however, isoclinal folding on the millimetre scale is observed locally and attributed to a late deformation D₂. Subhedral to anhedral garnet (Grt₂; 2-13 vol.%) forms porphyroblasts of up to 10 mm in diameter, which are wrapped by the Bt₂-Sil₂ foliation (Fig. 4.5a). Straight grain boundaries between Grt, Sil₂, Bt₂ and Kfs₂ indicate that their crystallization took place under equilibrium conditions. Synchronous growth of Grt₂ and Kfs₂ is furthermore supported by the presence of euhedral Grt₂ inclusions in Kfs₂. In the cores of Grt₂ abundant inclusions of biotite (Bt₁), plagioclase (Pl₁), quartz (Qtz₁) and fibrolitic sillimanite (Sil₁) are preserved (Fig. 4.5a). In two samples inclusions of Bt₁ and Qtz₁ in Grt₂ cores and of Sil₁ in Grt₂ rims curve into the external S₁ foliation, thus defining a typical snow-ball texture (Fig. 4.5b & 4.5c, respectively), indicating syn-tectonic growth of Grt₂ with respect to the S₁ foliation. The inclusions of all other samples

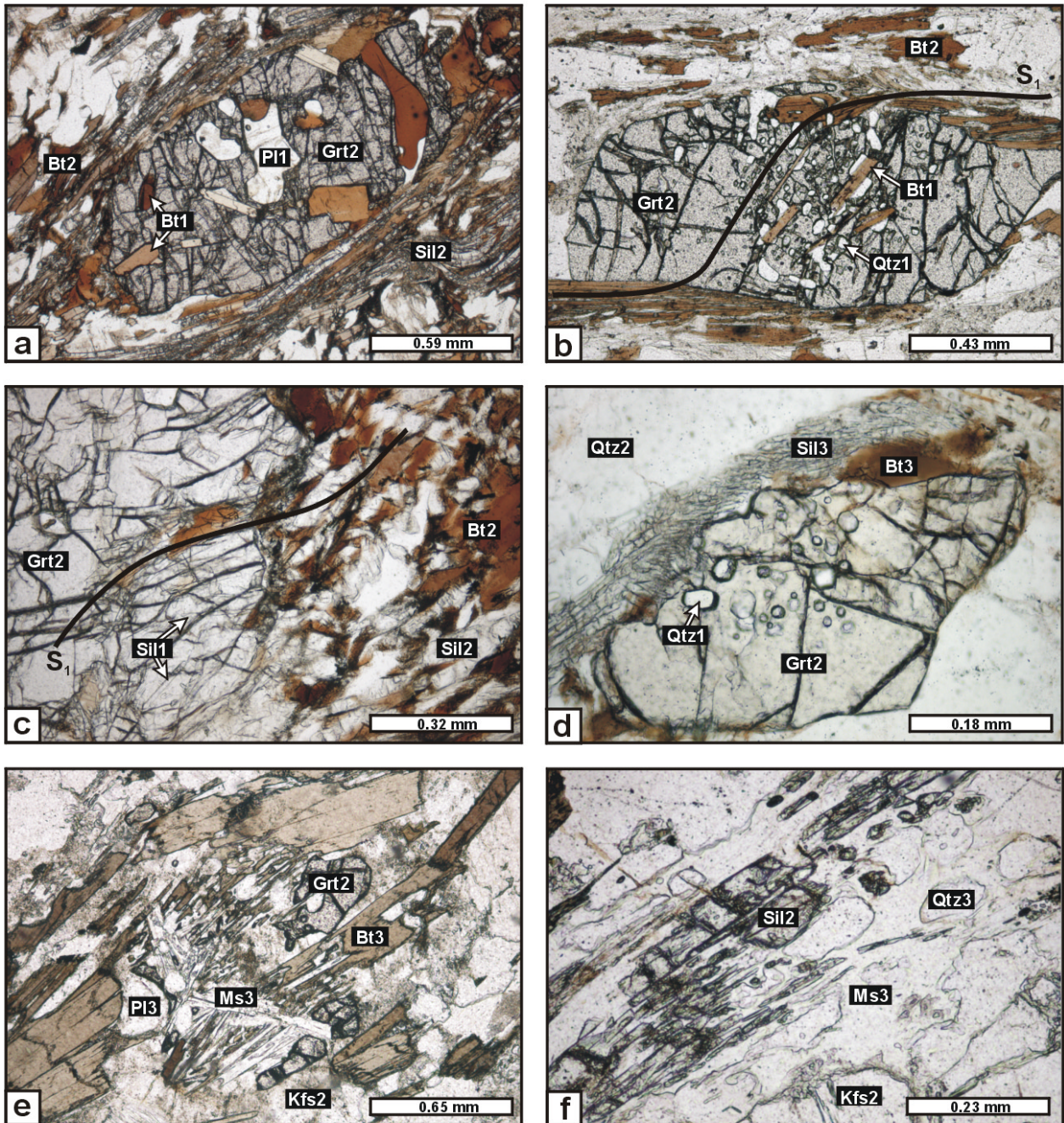


Fig. 4.5: Photomicrographs illustrating the metamorphic evolution of the metapelitic Grt-Bt-Sil gneisses and schists of the southern part of the Orue Unit. **a)** Grt2 porphyroblast with inclusions of Pl1 and Bt1 is wrapped by a Bt2-Sil2 foliation (Grt-Bt-Sil schist B-703-00). **b)** Oriented inclusions of Qtz1 and Bt1 in Grt2 curve into the external S_1 (Grt-Bt-Sil gneiss B-342-2-99). **c)** Sil1 and Bt1 inclusions in Grt2 rims curve into the external S_1 foliation (Grt-Bt-Sil schist B-703-00). **d)** Intergrowth of Bt3 and Sil3 partly replacing Grt2 (Grt-Bt-Sil gneiss B-679-1-00). **e)** Intergrowth of Bt3, Ms3 and Pl3 replacing Grt2 (Grt-Bt-Sil gneiss B-246-A-98). **f)** Intergrowth of Ms3 and Qtz3 replacing Kfs2 and Sil2 (Grt-Bt-Sil gneiss B-246-A-98).

show no preferred orientation, thus suggesting formation of these garnets under static conditions. Moreover, Bt1 and Sil1 are enclosed by Kfs2. Further inclusions in Grt2 are ilmenite (Ilm1) and rare rutile (Rt1), which are both not preserved in the matrix of the metapelites. The inclusion textures testify to the partial replacement of early Bt-Sil-Pl-Qtz-Rt-Ilm assemblages by coexisting Grt2 and Kfs2 under peak-metamorphic conditions.

Leucosomes are rich in medium- to coarse-grained Kfs2 and Qtz2. Coarse-grained Grt2 occurs as rare porphyroblasts (< 8 mm) in the granoblastic quartzofeldspathic matrix. Locally, rare Bt2 and Sil2 are preserved in the leucosomes. Zircon and apatite occur as accessory phases of the metapelites.

Stage 3: Retrograde evolution

Evidence for the retrograde metamorphic evolution is poorly recorded by the Grt-Bt-Sil gneisses and schists. Grt2 may be surrounded by texturally late biotite (Bt3), partly intergrown with sillimanite (Sil3; Fig. 4.5d), whereas Grt2-fissures are filled by Bt3. Grt2 of both the leucosomes and the palaeosomes is partially or completely replaced by undeformed intergrowths of muscovite (Ms3), Bt3 and Pl3 (Fig. 4.5e). Post-tectonic intergrowths of Ms3 and quartz (Qtz3), formed at the expense of Kfs2 and Sil2 (Fig. 4.5f), locally cross-cut the S₁ foliation. Monomineralic ilmenite coronas surround Bt2 and Bt3, which are partly altered to greenish chlorite (Chl3). Moreover, sagenite is developed in biotites of both generations, indicating that biotite exsolved Ti as both ilmenite and rutile during retrogression.

Crd-Bt gneisses (type 3) and Grt-Crd-Bt gneiss (type 4)

samples: B-122-C-98, B-143-C-98, B-145-A-98, B-148-A-98 (Crd-Bt gneisses) and B-103-A-98 (Grt-Crd-Bt gneiss)

Stage 1: Prograde evolution and Stage 2: Peak-metamorphic assemblages

The Crd-Bt gneisses and Grt-Crd-Bt gneiss display migmatitic structures with a well-developed separation into biotite-bearing palaeosomes and biotite-free leucosomes. The palaeosomes preserve an accentuated S₁ foliation, which is mainly defined by aligned, fine-grained biotite (Bt2; 20-25 vol.%; < 1 mm). Main constituents of the fine- to medium grained, granoblastic matrix are anhedral, flame-perthitic K-feldspar (Kfs2; 24-30 vol.%), plagioclase (Pl2; 7-13 vol.%) and quartz (Qtz2; 6-20 vol.%). In sillimanite-rich layers, polycrystalline aggregates of fine-grained, granoblastic cordierite (Crd2; 9-14 vol.%) occur, that show no evidence for

deformation, hence indicating a post-tectonic formation of Crd2. Fibrolitic sillimanite (Sil1; 4-8 vol.%) is only preserved in the cores of these Crd2 aggregates and is hence always separated from matrix Bt2 by inclusion-free Crd2 rims (Fig. 4.6a). Sil1 inclusion trails enclosed by Crd2 are always aligned parallel to the S_1 foliation. The presence of sillimanite-free cordierite rims indicates cordierite-growth at the expense of Sil1 and a first generation of biotite (Bt1), the latter of which being only preserved as rare corroded inclusion in Crd2 (Fig. 4.6a). Moreover, perthitic Kfs2 may be present in these textures, forming rims around Crd2, thus suggesting a contemporaneous formation of Kfs2 and Crd2. Locally, anhedral, dark green spinel (Spl2; < 1 vol.%) of up to 1 mm has been observed in the Crd2 aggregates (Fig. 4.6a). Fine-grained ilmenite (Ilm2; 1-2 vol.%) is generally restricted to cordierite-bearing domains, indicating its synchronous growth with Crd2 at the expense of biotite.

In the Grt-Crd-Bt gneiss the replacement of Bt1 and Sil1 by Crd2 (30-32 vol.%) and Kfs2 (37-40 vol.%) reached an almost pervasive extent. When compared to the Crd-Bt gneisses, matrix Ilm2 (2-4 vol.%) is slightly more abundant whereas matrix Bt2 (< 0.5 mm) is only rarely preserved (3-5 vol.%). Qtz2 (12-15 vol.%) and Pl2 (3-4 vol.%) are generally less frequent than in the Crd-Bt gneisses. Undeformed garnet (Grt2; 7-11 vol.%) occurs as euhedral to subhedral grains (< 2 mm), which generally display straight grain boundaries against both pinitized Crd2 and Kfs2 (Fig. 4.6b), suggesting their post-tectonic crystallization under equilibrium conditions, which is furthermore supported by the presence of euhedral inclusions of Crd2 in Grt2. Inclusions of Qtz1 and corroded Bt1 in Grt2 indicate growth of the peak-metamorphic Grt-Crd-Ilm-Kfs assemblage at the expense of early Bt-Sil-Qtz assemblages.

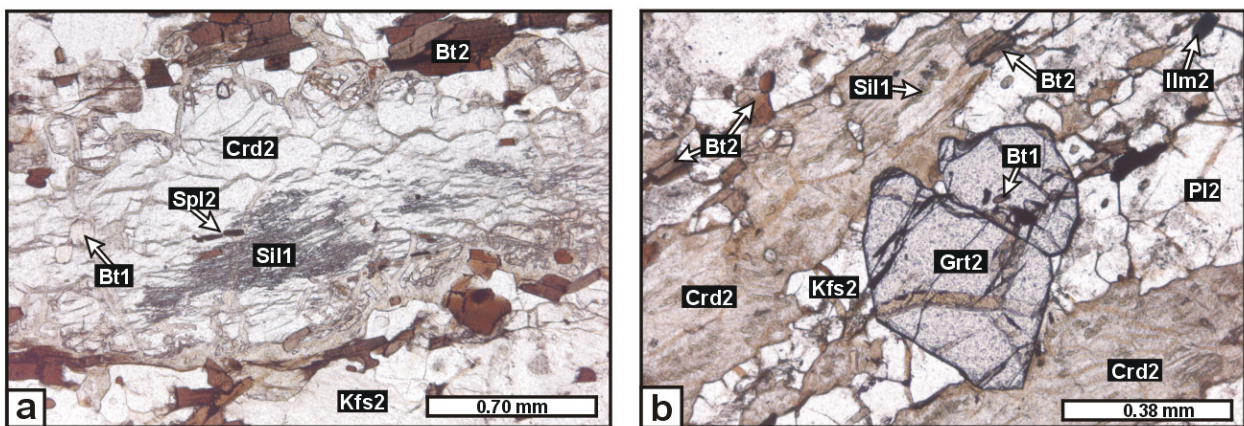


Fig. 4.6: Photomicrographs illustrating the metamorphic evolution of the metapelitic Crd-Bt-(Grt) gneisses of the Orue Unit. **a)** Polycrystalline Crd2-aggregate with sillimanite-free margin separating Sil1 from matrix Bt2. Crd2 encloses Bt1 and is intergrown with dark green Spl2 (Crd-Bt gneiss B-148-A-98). **b)** Subhedral Grt2, coexisting with Kfs2, displays straight boundaries against pinitized Crd2, which encloses Sil1. Grt2 encloses corroded Bt1. Matrix Bt2 is rare (Grt-Crd-Bt gneiss B-103-A-98).

Medium- to coarse-grained and concordant leucosomes of both rock types are mainly composed of Kfs₂, minor Qtz₂ and subordinate Pl₂. While the leucosomes contain minor Crd₂ and Grt₂; biotite is not preserved. At the margins of the leucosomes symplectitic intergrowths of skeletal Bt₂ and Qtz₂ occur, suggesting leucosome-formation through dehydration melting of matrix Bt₂. In both rock types retrograde reactions are not observed. Zircon is a common accessory phase.

Contact metamorphic Grt-Sil-Crd rocks (type 4)

samples: B-302-1-99, B-302-2-99

The rocks are characterized by an inhomogeneous texture, mainly consisting of massive, hornfels-like cordierite-plagioclase-quartz-biotite schlieren surrounded by a massive quartz-rich matrix. In the irregular bounded schlieren additional garnet and sillimanite may occur, forming coarse porphyroblasts, already visible on a macroscopic scale.

Stage 1: Prograde evolution and Stage 2: Peak-metamorphic assemblages

The quartz-rich zones are almost entirely composed of quartz (83 vol.%) and contain only minor plagioclase (17 vol.%).

In contrast, the main constituents of the hornfels-rich schlieren are fine-grained, anhedral cordierite (Crd₂; 10 vol.%; < 1 mm in diameter), fine- to medium-grained, anhedral plagioclase (Pl₂; 15 vol.%), fine-grained anhedral quartz (Qtz₂; 35 vol.%) and retrograde, fine-grained biotite (Bt₃; 13 vol. %), whereas ilmenite (Ilm₂), magnetite and zircon are common accessories. In addition, heterogeneously distributed, coarse-grained fibrolitic to prismatic sillimanite (Sil₂; 16 vol.%; up to 5 mm in length) and minor garnet (Grt₂; 7 vol.%) porphyroblasts of up to 5 mm in diameter may occur, the latter of which locally preserving straight grain boundaries against strongly pinitized Crd₂. Euhedral to subhedral Grt₂ comprises a color zonation, which can be correlated with a zonal distribution of mineral inclusions (Fig. 4.7a): Pink cores of 1-2 mm in diameter contain rare inclusions of rutile (Rt₁), ilmenite (Ilm₁) and quartz (Qtz₁). In the inner parts of broad colorless margins, corroded, fine-grained (< 0.1 mm) yellow staurolite (St₁) is enclosed, whereas Ilm₁ and irregular inclusions trails of prismatic sillimanite (Sil₁) occur in the outermost margins. Moreover, corroded St₁ is enclosed by Sil₂ (Fig. 4.7b), Crd₂ (Fig. 4.7c) and Pl₂. The lack of staurolite in the matrix, points to its replacement by Grt₂ and Sil₂ during the prograde evolution. Crd₂ furthermore contains rare corroded inclusions of biotite (Bt₁; Fig. 4.7c). Subhedral to euhedral magnetite (Mt₂) and zircon occur as accessory phases in the matrix.

Stage 3: Retrograde evolution

Retrograde formations include undeformed intergrowths of late Bt3 and sillimanite (Sil3) resorbing Crd2 (Fig. 4.7c). Sil3-Bt3 intergrowths also partly replace Grt2 (Fig. 4.7d). Locally, late fine-grained plagioclase (Pl3) is present in these textures. Matrix Sil2 is surrounded by fine-grained intergrowths of Bt3 and Pl3. In addition, a second generation of staurolite occurs (St3; 3 vol.%), which forms fine-grained (< 0.2 mm) subhedral crystals around Crd2 and Sil2 (Fig. 4.7b & d). In places, St3 is replaced by pale green chlorite (Chl3; Fig. 4.7b).

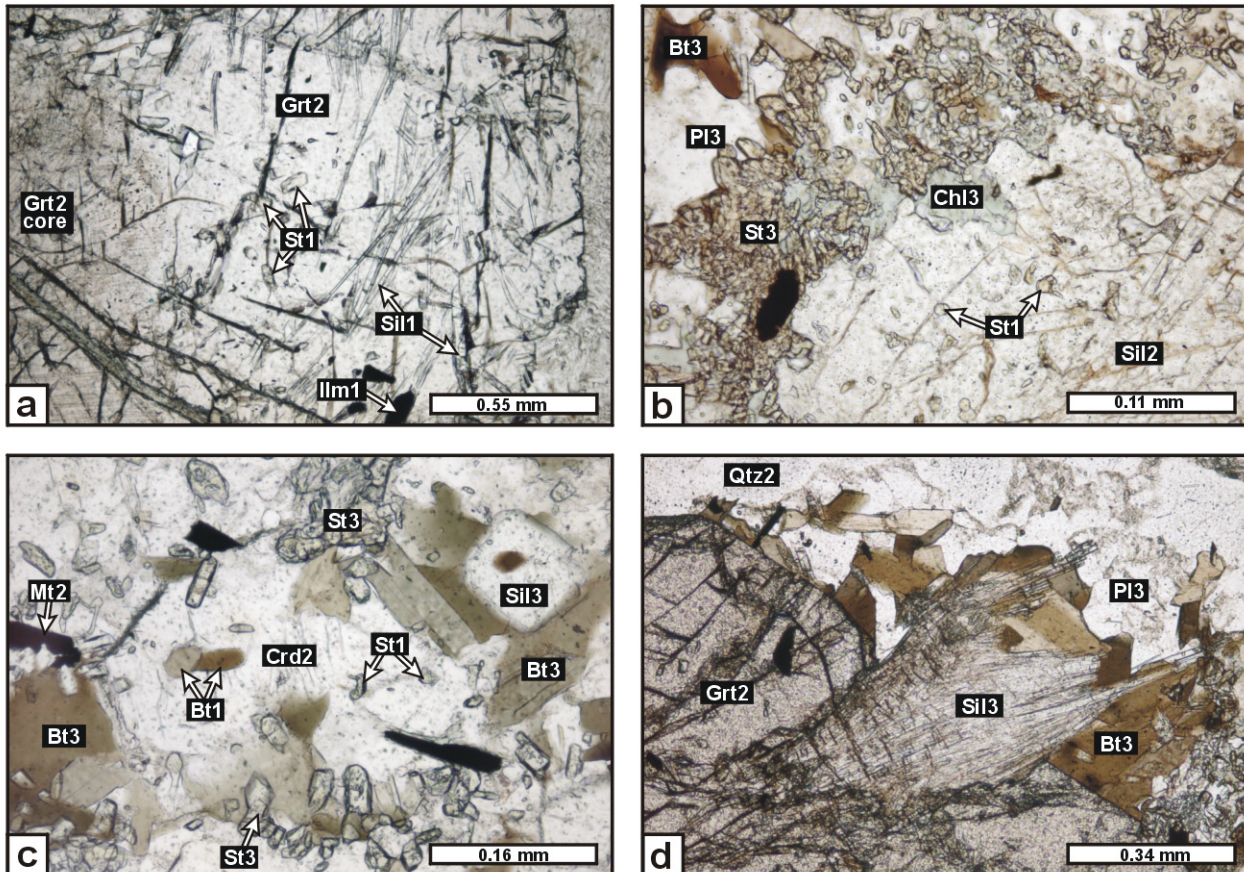


Fig. 4.7: Photomicrographs illustrating the metamorphic evolution of the contact metamorphic Grt-Sil-Crd rocks (sample B-302-2-99) of the Orue Unit. **a)** Grt2 porphyroblast with pink inclusion-poor core, corroded St1 inclusion in the inner margin and irregular Sil1 inclusions and Ilm1 inclusions in the outer margin. **b)** Inclusions of St1 in Sil2, which is rimmed by a corona of late St3. St3 is partly replaced by Chl3. **c)** Inclusions of Bt1 and St1 in matrix Crd2, which is rimmed by late St3, Sil3 and Bt3. **d)** Grt2 is partly replaced by Bt3-Sil3-Pl3 intergrowths.

4.2 MINERAL CHEMISTRY

Eleven selected samples of the Orue Unit have been investigated in detail with the help of electron microprobe (EMP) analysis. Sample locations as well as descriptions of the mineral formula calculation procedures and the analytical conditions are given in the Appendix (Figs. A.2.1 to A.2.5 and Chapter A.3.2, respectively). X_{Mg} ratios of garnet, clinopyroxene and amphibole were calculated as $Mg/(Mg+Fe^{2+})_{molar}$ whereas those of cordierite and biotite were calculated as $Mg/(Mg+Fe^{tot})_{molar}$. Microprobe analysis concentrated on the metapelites, since their mineral assemblages are highly suitable for phase petrological investigations and geothermobarometric calculations:

Metapelites

Grt-Bt-Sil gneisses and schist	B-246-A-98, B-342-3-99, B-401-2-99, B-679-1-00, B-703-00 and B-219-A-98 (Grt-Bt-Sil-bearing leucosome)
Grt-Sil-Crd rock	B-302-2-99
Grt-Crd-Bt gneiss	B-103-A-98

Metagreywackes

Grt-Bt gneisses	B-137-C-98, B-191-A-98
-----------------	------------------------

Amphibolites

Grt-Cpx-bearing amphibolite	B-191-B-98
-----------------------------	------------

The contact metamorphic Grt-Sil-Crd rock B-302-2-99 from the south-eastern region of the Orue Unit and the southward following Grt-Bt-Sil gneisses and schist B-219-A-98–B-342-3-99–B-703-00–B-401-2-99–B-679-1-00, crudely define a north-south-trending profile, continuously increasing in distance from the Kunene Intrusive Complex (KIC; Fig. 4.8a). The investigation of these samples aimed at the evaluation of a possible temperature gradient, induced by the emplacement of the KIC.

The metapelitic Grt-Bt-Sil gneiss B-246-A-98 of the south-western region of the Orue Unit and the metapelitic Grt-Crd-Bt gneiss B-103-A-98 of the northern part were investigated in order to study regional variations of the peak-metamorphic P-T conditions in the individual parts of the Orue Unit. Moreover, the Grt-Cpx-bearing amphibolite B-191-B-98 and the metagreywacke-type Grt-Bt gneiss B-191-A-98 of the south-eastern region were analyzed. The mylonitic Grt-Bt gneiss B-137-C-98 is sampled from a major shear zone exposed in the northern part and may, therefore, yield information about the P-T conditions during later tectonic activity.

4.2.1 Garnet

Garnet is present as peak-metamorphic phase (Grt2) in all investigated samples. Representative analyses are given in Table A.6.2.1 in the Appendix.

Metapelites

Grt2 of the metapelites of the Orue Unit is essentially an almandine-pyrope solid solution with generally low grossular and spessartine content.

Grt2 of the Grt-Bt-Sil gneisses and schists and the Grt-Sil-Bt-bearing leucosome B-219-A-98 of the investigated profile generally show uniform compositions with zoned, low to moderate X_{Mg} values (0.10-0.23) and similar zonation patterns (Fig. 4.8b & c). Following Spear (1993) such X_{Mg} values are characteristic for garnet occurring in Grt-Bt-Sil equilibrium assemblages formed under amphibolite facies conditions, thus ruling out the possibility, that Grt2 is a relic of a former granulite facies mineral assemblage. Most Grt2 display compositionally homogeneous core plateaus with the highest X_{Mg} values analyzed, pointing to intracrystalline, diffusional homogenization during high-grade metamorphism. In samples B-342-3-99, B-401-2-99 and B-703-00 the Grt2 core plateau compositions are in the range of $Alm_{73-75}Prp_{18-22}Grs_3Sps_3$ (X_{Mg} : 0.20-0.23). Rimward zoning to lower X_{Mg} (X_{Mg} : 0.12-0.15; $Alm_{79-81}Prp_{11-14}Grs_3Sps_{3-5}$) is interpreted to result from retrograde diffusive Fe-Mg re-equilibration with adjacent Bt3 during post-peak cooling.

Grt2 of the leucosome B-219-A-98 displays similar zonation patterns and generally exhibits similar compositions (X_{Mg} : 0.21; $Alm_{70}Prp_{18}Grs_2Sps_{10}$) but, in clear contrast to the above described Grt2, contains higher spessartine (Fig. 4.8c), most probably resulting from the comparably low modal amount of garnet in this sample. A marginal increase of spessartine, characteristic for retrograde garnet resorption, is significant (Fig. 4.8c) and in agreement with the occurrence of retrograde Bt3-Ms3 intergrowths replacing Grt2.

Grt2 of the garnet-poor sample B-679-1-00 has relatively high spessartine (X_{Mg} : 0.08-0.12; $Alm_{78-79}Prp_{7-10}Grs_3Sps_{9-11}$). The unusually low X_{Mg} of these garnets probably reflects the less magnesian bulk-rock composition of sample B-679-1-00 (bulk-rock X_{Mg} : 0.32) when compared to the other Grt-Bt-Sil gneisses and schists (bulk-rock X_{Mg} : 0.41-0.44).

Grt2 of the contact metamorphic Grt-Sil-Crd rock B-302-2-99 is exceptional in preserving a prograde growth zonation, that is mainly evident from the continuous decrease of spessartine from core towards the rim (Fig. 4.8d). This zonation pattern can be correlated with the observed color zonation and the zonal distribution of mineral inclusions (see Fig. 4.7a): Pink Grt2 cores, bearing inclusions of quartz, rutile and ilmenite, are rich in grossular and spessartine whereas

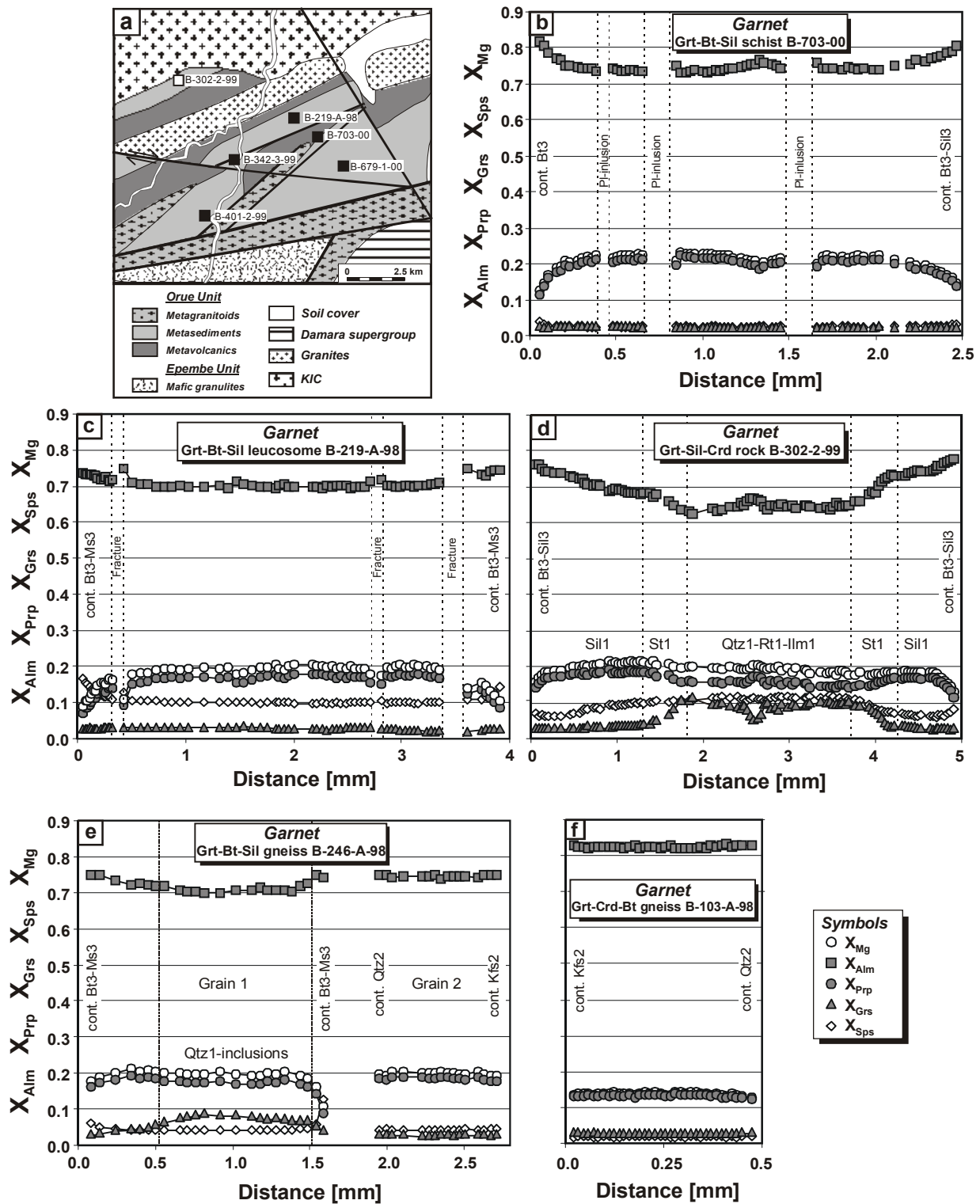


Fig. 4.8: a) Sample location map of south-eastern region, illustrating sampled profile and b-f) Garnet zoning profiles of the metapelites of the Orue Unit. Each profile extends from rim to rim through the core of the garnet grains. Note variable scale of each profile. b) Garnet of Grt-Bt-Sil schist B-703-00 of the south-eastern region. c) Garnet of Grt-Bt-Sil leucosome B-219-A-98 of the south-eastern region. d) Garnet of contact metamorphic Grt-Sil-Crd rock B-302-2-99. e) Garnet of Grt-Bt-Sil gneisses B-246-A-98 of the south-western region. f) Garnet of Grt-Crd-Bt gneiss B-103-A-98 of the northern part.

almandine and pyrope are relatively low (X_{Mg} : 0.18-0.20; Alm₆₃₋₆₇Prp₁₄₋₁₇Grs₅₋₁₁Sps₉₋₁₁). In a narrow zone of ~ 0.2 mm grossular abruptly decreases whereas almandine, pyrope and X_{Mg} increase. The broad colorless rim, containing inclusions of staurolite in the inner parts followed by inclusions of sillimanite in the outer part, is essentially unzoned with respect to grossular and has the most magnesian composition (X_{Mg} : 0.20-0.22; Alm₆₇₋₇₅Prp₁₇₋₁₉Grs₄₋₃Sps₉₋₅). These rims are interpreted to have formed simultaneously with matrix Crd2 under peak-metamorphic conditions. Increase of spessartine at the outermost margin (X_{Mg} : 0.16-0.13; Alm₇₆₋₇₈Prp₁₄₋₁₂Grs₃Sps₆₋₇) is presumably related to the resorption of Grt2 by Bt3-Sil3 intergrowths during post-peak cooling whereas a marked decrease in the X_{Mg} suggests retrograde intercrystalline diffusional Fe-Mg re-equilibration between Grt2 margins and adjacent Bt3.

Grt2 of the Grt-Bt-Sil gneiss B-246-A-98 from the south-western region of the Orue Unit is compositionally similar to Grt2 of the Grt-Bt-Sil gneisses and schists of the south-eastern region. However, larger Grt2 grains preserve a weak zonation in the grossular component, which decreases from quartz-inclusion-rich cores (X_{Mg} : 0.18-0.20; Alm₇₀₋₇₃Prp₁₈₋₁₆Grs₈₋₆Sps₄₋₅), towards inclusion-free rims (X_{Mg} : 0.20-0.21; Alm₇₂₋₇₃Prp₁₉₋₁₈Grs₃₋₅Sps₄₋₅; Fig. 4.8e). The latter are compositionally similar to smaller, unzoned Grt2 (X_{Mg} : 0.19-0.21; Alm₇₄₋₇₅Prp₁₈₋₁₉Grs₂₋₃Sps₄₋₅) and are interpreted to be in equilibrium with matrix Bt2 and Pl2. A marked increase of spessartine at the outermost margins (X_{Mg} : 0.11; Alm₇₄Prp₉Grs₄Sps₁₃) results from the replacement of Grt2 by Bt3-Ms3 intergrowths.

Grt2 of the Grt-Crd-Bt gneiss B-103-A-98 from the northern part of the Orue Unit is essentially unzoned (Alm₈₂₋₈₃Prp₁₃₋₁₄Grs₃₋₂Sps₂; Fig. 4.8f), pointing to either intracrystalline diffusional homogenization and/or to fast garnet growth. The X_{Mg} (0.13-0.14) is lower than that of Grt2 of the Grt-Bt-Sil gneisses and schists of the southern part. The lack of a marginal increase of spessartine is consistent with the unresorbed shape of Grt2, whereas constant X_{Mg} ratios indicate the lack of retrograde diffusional Fe-Mg exchange with adjacent Crd2.

Metagreywackes

Grt2 of the Grt-Bt gneiss B-191-A-98 of the south-eastern region of the Orue Unit strongly resembles Grt2 of the Grt-Bt-Sil gneisses in both its composition and its zoning patterns, even though it reveals slightly higher grossular contents (Fig. 4.9a). The highest X_{Mg} of Grt2 was analyzed in broad, unzoned core plateaus (X_{Mg} : 0.20; Alm₇₃Prp₁₈Grs₅Sps₃). Towards the rims X_{Mg} trends to lower values (X_{Mg} : 0.12; Alm₈₀Prp₁₁Grs₅Sps₅), resulting from retrograde diffusional Fe-Mg exchange with adjacent Bt3.

Grt2 of the mylonitic Grt-Bt gneiss B-137-C-98 of the northern part is characterized by a well-preserved prograde growth zonation, that is mainly evident from the bell-shaped spessartine

zonation pattern (Fig. 4.9b). Furthermore, Grt2 cores are rich in grossular (X_{Mg} : 0.10-0.12; $Alm_{58-62}Prp_{6-10}Grs_{23-20}Sps_{17-10}$). Towards the rims (X_{Mg} : 0.15-0.17; $Alm_{68-70}Prp_{11-13}Grs_{12-10}Sps_{6-5}$) both spessartine and grossular decrease whereas almandine, pyrope and X_{Mg} increase, indicating a rise of temperature during garnet growth. The outermost margin is enriched in spessartine and poor in pyrope (X_{Mg} : 0.10; $Alm_{71}Prp_8Grs_8Sps_{13}$), pointing to retrograde resorption by and/or retrograde Fe-Mg exchange with adjacent Bt3.

Amphibolites

Grt2 of the Grt-Cpx-bearing amphibolite B-191-B-98 from the south-eastern region of the Orue Unit is essentially pyrope-almandine solid solution with high grossular and low spessartine contents. Grt2 is either unzoned or displays a zonation in grossular, that decreases from core (X_{Mg} : 0.13-0.15; $Alm_{58-60}Prp_{10-11}Grs_{26-28}Sps_4$) towards the rim (X_{Mg} : 0.11-0.12; $Alm_{63-65}Prp_9_8Grs_{22}Sps_5$), whereas almandine increases in the same direction (Fig. 4.9c). A slight decrease of the X_{Mg} at the outermost rims suggests a weak retrograde Fe-Mg exchange with adjacent Hbl3.

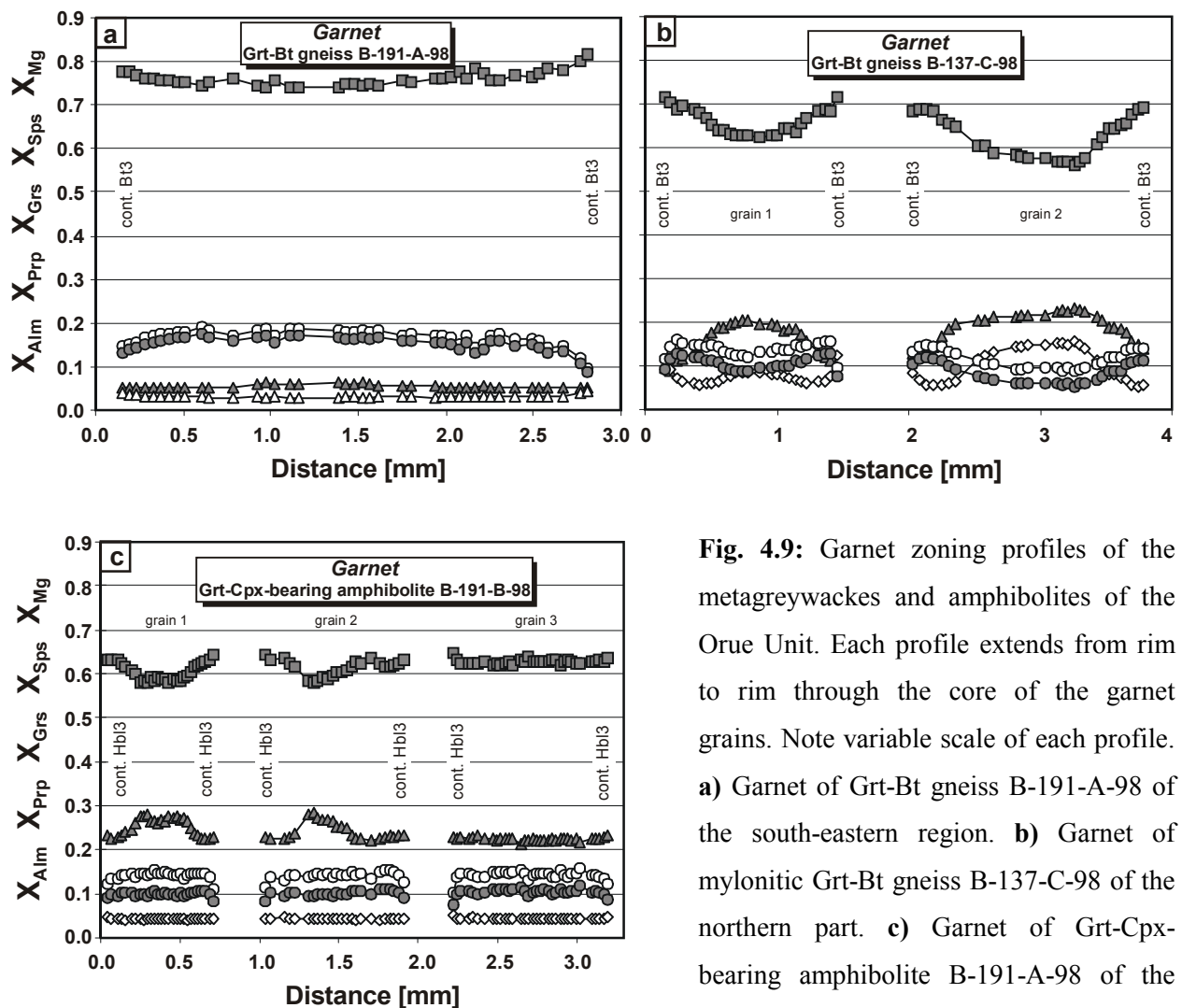


Fig. 4.9: Garnet zoning profiles of the metagreywackes and amphibolites of the Orue Unit. Each profile extends from rim to rim through the core of the garnet grains. Note variable scale of each profile. **a)** Garnet of Grt-Bt gneiss B-191-A-98 of the south-eastern region. **b)** Garnet of mylonitic Grt-Bt gneiss B-137-C-98 of the northern part. **c)** Garnet of Grt-Cpx-bearing amphibolite B-191-A-98 of the south-eastern region.

4.2.2 Biotite

Biotite occurs as prograde inclusion in the peak-metamorphic minerals (Bt1), as peak-metamorphic matrix phase (Bt2) and as retrograde breakdown product of Grt2 (Bt3) in the paragneisses of the Orue Unit. Biotite formulae have been calculated on an anhydrous 22 oxygen basis (Table A.6.2.2 in the Appendix).

Metapelites

For biotite of the Grt-Bt-Sil gneisses and schists of the south-eastern region of the Orue Unit systematic compositional variations are observed depending on its textural position:

Bt1 inclusions in Grt2 are more magnesian (X_{Mg} : 0.59-0.65) and have slightly lower Ti contents (Ti p.f.u.: 0.21-0.44) than matrix Bt2 (X_{Mg} : 0.39-0.53; Ti p.f.u.: 0.26-0.48) of the same samples, pointing to retrograde re-equilibration of Bt1 with the Grt2 host during post-peak cooling. Within individual samples the composition of matrix Bt2 varies in an even more restricted range (Fig. 4.10a). Regarding the muscovite-free equilibrium assemblage of Bt-Sil-Kfs

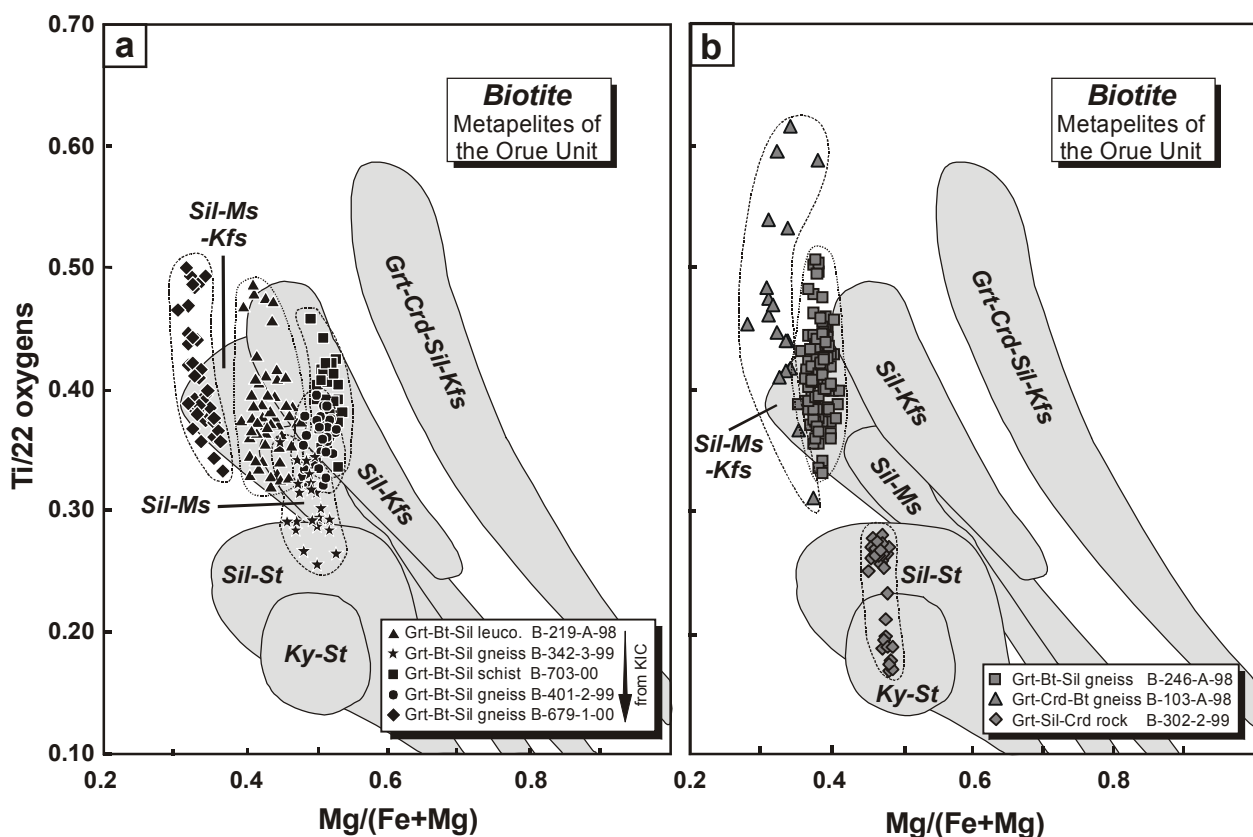


Fig. 4.10: Composition of biotite illustrated for Mg/(Fe+Mg) vs. Ti (per 22 oxygens) for (a) matrix biotite (Bt2) of the Grt-Bt-Sil gneisses sampled along the profile in the south-eastern region of the Orue Unit and (b) for matrix biotite (Bt2, samples B-246-A-98 & B-103-A-98) and late biotite (Bt3, sample B-302-2-99) of all other studied metapelites. The shaded fields indicate the compositional range of biotite from metamorphic zones in New England (Robinson et al., 1982).

displayed by the investigated samples, Bt2 of the metapelites should be expected to plot in the Sil-Kfs field in the X_{Mg} vs. Ti diagram of Robinson et al. (1982). This, however, holds only true for some of the matrix Bt2, whereas most analyses lie in the Sil-Ms-Kfs or Sil-Ms fields or even outside the fields illustrated by Robinson et al. (1982; Fig. 4.10a). This deviation probably reflects intensive retrograde re-equilibration of Bt2 during retrogression, an interpretation, that is supported by the abundance of exsolved ilmenite and rutile around and in matrix Bt2. The exceptionally low X_{Mg} of Bt2 of sample B-679-1-00 (X_M : 0.30-0.36; Fig. 4.10a) is interpreted to result from the low bulk-rock X_{Mg} of this sample when compared to the other Grt-Bt-Sil gneisses and schists (X_M : 0.32 and 0.36-0.44, respectively). Remarkably, a systematic increase of the X_{Mg} of Bt2, which would indicate an increase of the temperature with decreasing distance towards the KIC, is not observed for the samples of the profile.

Texturally late Bt3 of all samples investigated is generally slightly more magnesian (X_{Mg} : 0.45-0.54) than matrix Bt2 of the same sample, pointing to retrograde intercrystalline Fe-Mg re-equilibration of Bt3 with adjacent Grt2, which is in agreement with the rimward decreasing X_{Mg} in Grt2 (see Chapter 4.2.1). The fact, that late Bt3 displays only slightly higher X_{Mg} ratios than most of the peak-metamorphic matrix Bt2 is taken as evidence, that at least part of the matrix Bt2 underwent retrogression during post-peak cooling. In contrast, the Ti contents of Bt3 are significantly lower (Ti p.f.u.: 0.07-0.43) than those of matrix Bt2 whereas Al^{VI} behaves in an opposite way (Al^{VI} p.f.u.: 0.50-1.24 and 0.53-0.77, respectively).

Fluorine contents of biotite from the Grt-Bt-Sil gneisses and schists (Bt1, Bt2 and Bt3) generally range between 0.3 and 1.8 wt.% and show no systematic variations with respect to its textural position.

The X_{Mg} of late Bt3 (X_{Mg} : 0.45-0.50) of the contact metamorphic Grt-Sil-Crd rock (B-302-2-99) is similar to that of matrix Bt2 of the Grt-Bt-Sil gneisses and schists. However, due to its low Ti contents (Ti p.f.u.: 0.17-0.28), Bt3 plots in the Sil/Ky-St field (Fig. 4.10b), which is in agreement with the observation, that Bt3 coexists with late St3, formed at the expense of Grt2 and Sil2 during the retrograde evolution. In contrast to biotite of all other paragneisses, Bt3 of the Grt-Sil-Crd rock B-302-2-99 contains significant BaO (0.7-1.0 wt.%), whereas its fluorine contents (0.0-0.4 wt.%) are lower than those of the Grt-Bt-Sil gneiss and schist.

Matrix Bt2 (X_{Mg} : 0.35-0.44) of the Grt-Bt-Sil gneiss B-246-A-98 from the south-western region of the Orue Unit is generally slightly less magnesian than matrix Bt2 of Grt-Bt-Sil gneisses of the south-eastern region and reveals similar or even higher Ti contents (Ti p.f.u.: 0.28-0.51) than the latter (Fig. 4.10b). Late Bt3 (X_{Mg} : 0.38-0.42) displays a similar range of X_{Mg}

as Bt2, whereas its Ti contents are lower (Ti p.f.u.: 0.11-0.34).

Grt-Crd-Bt gneiss B-103-A-98 from the northern part of the Orue Unit contains the Ti-richest matrix Bt2 (Ti p.f.u.: 0.32-0.60) of all metapelites investigated (Fig. 4.10b). The large range of Ti contents presumably results from variable but generally intense chloritization. The exceptionally Fe-rich composition of Bt2 (X_{Mg} : 0.28-0.37) is probably related to the low bulk-rock X_{Mg} of sample B-103-A-98 (X_{Mg} : 0.28).

Metagreywackes

The composition of biotites of the Grt-Bt gneiss B-191-A-98 is similar to those of the metapelites: Prograde Bt1 inclusions (X_{Mg} : 0.46-0.57; Ti p.f.u.: 0.28-0.49) in Grt2 are more magnesian and have lower Ti contents than matrix Bt2 (X_{Mg} : 0.42-0.48; Ti p.f.u.: 0.39-0.53). Late Bt3 (X_{Mg} : 0.45-0.47; Ti p.f.u.: 0.20-0.33) in contact with Grt2 reveals lower Ti contents whereas its X_{Mg} is similar to that of matrix Bt2. Matrix Bt2 of the mylonitic Grt-Bt gneiss B-137-C-98 is slightly less magnesian and has lower Ti (X_{Mg} : 0.40-0.43; Ti p.f.u.: 0.22-0.31) than matrix Bt2 of Grt-Bt gneiss B-191-A-98.

4.2.3 Cordierite

Cordierite was analyzed in the metapelitic Grt-Crd-Bt gneiss (B-103-A-98) of the northern field area and the contact metamorphic metapelitic Grt-Sil-Crd rock (B-302-2-99) of the southern field area. Representative analyses are shown in Table A.6.2.3 in the Appendix.

In the Grt-Crd-Bt gneiss matrix Crd2 is always completely altered to pinite, hence revealing low Mg, Fe, Si and Al and high K. Assuming that the X_{Mg} ratios were not modified by the alteration, former Crd2 would have been more magnesian (X_{Mg} : 0.37-0.43) than coexisting Bt2 (X_{Mg} : 0.28-0.37), which is agreement with the general observation of higher X_{Mg} ratios of cordierite of metapelites when compared to coexisting biotite (e.g. Spear, 1993).

Fresh matrix Crd2 of Grt-Sil-Crd rock B-302-2-99 is more magnesian (X_{Mg} : 0.66-0.70) than that of the Grt-Crd-Bt gneiss. Individual Crd2 grains are essentially unzoned. The Na contents vary over a large range (Na p.f.u.: 0.02-0.16) but generally scatter around 0.04 Na p.f.u..

4.2.4 Staurolite

Staurolite has only been observed in the metapelitic Grt-Sil-Crd rock B-302-2-99, where it

occurs as prograde inclusions (St1) in Crd2, Sil2, Pl2, in broad Grt2 rims, and, moreover, as texturally late phase (St3) in corona textures surrounding Sil2 and Crd2. Representative staurolite analyses are listed in Table A.6.2.4 in the Appendix.

Prograde St1 inclusions and late St3 are chemically similar (see Table A.6.2.4), as they are Fe-rich and display significant Zn contents (X_{Mg} : 0.17-0.19; ZnO: 0.70-1.32 wt.% and X_{Mg} : 0.17-0.20; ZnO: 0.82-1.64 wt.%, respectively). Individual grains of both textures are essentially unzoned.

4.2.5 Clinopyroxene

Clinopyroxene compositions were determined in the Grt-Cpx amphibolite B-191-B-98; representative analyses are depicted in Table A.6.2.5 in the Appendix.

In the classification diagram of Morimoto (1988) matrix Cpx2 of the Grt-Cpx-bearing amphibolite B-191-B-98 in an intermediate diopside-hedenbergite solid solution and plots on or near the diopside-augite boundary (Fig. 4.11). Individual grains are almost unzoned with the X_{Mg} of Cpx2 varying in a restricted range of 0.51-0.56. The non-quadrilateral components are generally below 4.5 mol.%, with aegirine ranging between 0.6-1.8 mol.%, Ca-Tschermak's between 0.0-3.2, whereas the jadeite component is always zero (see Table A.6.2.5).

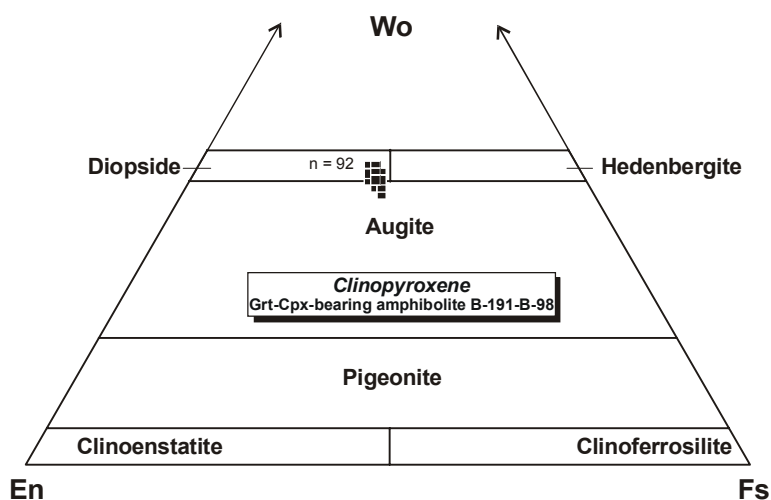


Fig. 4.11: Composition of matrix clinopyroxene of the Grt-Cpx-bearing amphibolite B-191-B-98 of the southern part of the Orue Unit.; classification after Morimoto (1988).

4.2.6 Amphibole

Amphibole occurs as prograde inclusion in Grt2 (Hbl1), as matrix phase (Hbl2) and as retrograde breakdown product of Grt2 (Hbl3) in the Grt-Cpx-bearing amphibolite B-191-B-98. Representative analyses are given in Table A.6.2.7 in the Appendix.

According to the classification of Leake et al. (1997) Hbl1, 2 and 3 of the Grt-Cpx-bearing amphibolite B-191-B-98 is ferro-hornblende to ferro-tschemakite (Fig. 4.12). Hbl1 inclusions in Grt2 are slightly more magnesian (X_{Mg} : 0.48-0.50) than matrix Hbl2 (X_{Mg} : 0.43-0.48), hence suggesting retrograde diffusional Fe-Mg re-equilibration between Hbl1 inclusions and the Grt2 host. The composition of Hbl3 (X_{Mg} : 0.43-0.47) is similar to that of matrix Hbl2, indicating lack of significant retrograde Fe-Mg exchange between Grt2 and adjacent Hbl3, which is in agreement with restricted marginal X_{Mg} zoning in Grt2. The Ti contents of Hbl1, 2 and 3 are generally low (Ti p.f.u.: 0.14-0.22) and lack systematic variations with respect to its textural positions.

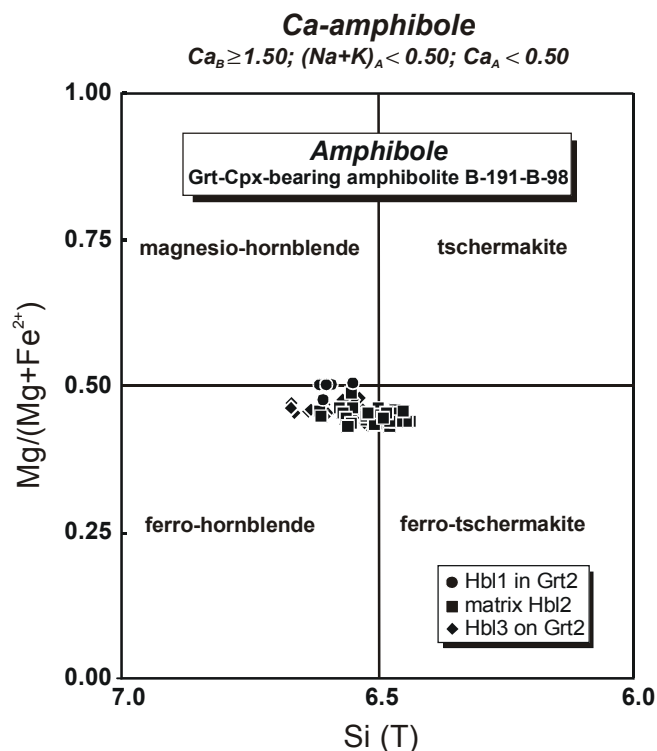


Fig. 4.12: Composition of amphibole in the Grt-Cpx-bearing amphibolite B-191-B-98 of the southern part of the Orue Unit; classification after Leake et al. (1997)

4.2.7 Ilmenite

Representative ilmenite compositions are listed in Table A.6.2.10 in the Appendix. Ilm1 inclusions in Grt2 of the contact metamorphic metapelitic Grt-Sil-Crd rock B-302-2-99 have

higher MnO contents than matrix Ilm2 (3.3-3.8 and 1.0-1.4 wt.%, respectively). The Fe₂O₃ contents of ilmenite from both textures are generally high (0.9-5.3 wt.%).

Matrix Ilm2 of the metapelitic Grt-Crd-Bt gneiss B-103-A-98 contains significant MnO (2.3-2.5 wt.%) and no Fe₂O₃.

Matrix ilmenite (Ilm2) of the Grt-Cpx-bearing amphibolite B-191-B-98 is the almost pure endmember with low MnO and low to moderate Fe₂O₃ contents (0.8-1.2 and 0.0-1.7 wt.%, respectively).

4.2.8 Rutile

Rt1 inclusions in Grt2 of the metapelitic Grt-Sil-Crd rocks contain minor amounts of Cr₂O₃ and FeO (0.4-0.5 wt.% and 0.4-0.9 wt.% respectively), whereas Rt1 inclusions in Grt2 of the metapelitic Grt-Bt-Sil gneiss are almost pure rutile, containing negligible Cr₂O₃ and FeO of < 0.1 wt.% and 0.3 wt.%, respectively (see Table A.6.2.10 in the Appendix).

4.2.9 Magnetite

Late magnetite of the Grt-Sil-Crd rock B-302-2-99 contains only traces of TiO₂ and Al₂O₃ of < 0.1 and < 0.2 wt.%, respectively (see Table A.6.2.10 in the Appendix).

4.2.10 Sillimanite

Matrix Sil2 of the metapelites is almost pure Al₂SiO₅. Traces of Fe₂O₃ (0.3-0.8 wt.%) have been detected (see Table A.6.2.10 in the Appendix).

4.2.11 Plagioclase

Plagioclase is present in all analyzed paragneisses of the Orue Unit. Representative analyses are listed in Table A.6.2.11 in the Appendix. Plagioclase of the investigated Grt-Cpx-bearing amphibolite B-191-A-98 is completely altered to sericite.

Metapelites

Selected zonation profiles of plagioclase of the metapelites are illustrated in Fig. 4.13. Plagioclase of the metapelites is essentially oligoclase (An₁₅₋₂₉) with low orthoclase and celsian

components ($Or_{0-2}Cs_{0-1}$). Early P11 inclusions in Grt2 of Grt-Bt-Sil schist B-703-00 display similar compositions and zonation patterns as matrix P12 of the same sample (Fig. 4.13). P11 inclusions are zoned with decreasing An from core (An_{29}) towards the rim (An_{23}). Matrix P12 of the same sample shows a zonation from An_{28} in cores to An_{22} at rims. Matrix P12 of the other Grt-Bt-Sil gneisses and schist and the Grt-Crd-Bt gneiss is essentially unzoned and rather uniform in composition (An_{15-29}). Matrix P12 of the Grt-Sil-Crd rock exhibits a weak zonation with An decreasing from cores (An_{29-27}) towards broad rims (An_{27-25}), which in turn are compositionally similar to late P13 intergrown with Bt3 (Fig. 4.13).

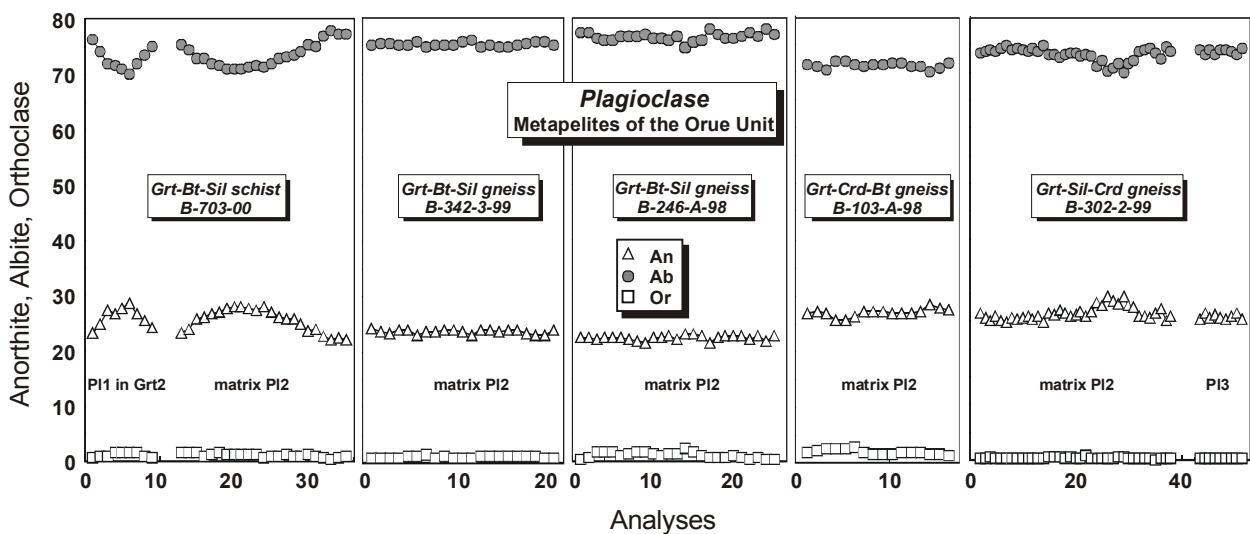


Fig. 4.13: Selected zoning profiles of plagioclase of the metapelites of the Orue Unit. Each profile extends from rim to rim through the core of the plagioclase grains.

Metagreywackes

Plagioclase of the Grt-Bt gneisses is slightly more calcic (andesine-oligoclase) than plagioclase of the metapelites. P11 inclusions (An_{25-31}) in Grt2 are compositionally similar to almost unzoned matrix P12 (An_{26-33}).

4.2.12 Alkalifeldspar

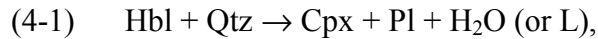
Matrix Kfs2 of the metapelitic Grt-Bt-Sil gneisses and schists contains significant albite, whereas its anorthite and celsian contents are negligible ($Or_{84-96}Ab_{15-3}An_{1-0}Cels_1$; see Table A.6.2.12 in the Appendix). Exsolutions are almost pure albite ($Or_{0-3}Ab_{97-98}An_{0-2}Cels_0$).

4.3 MINERAL REACTION HISTORY

4.3.1 Mafic and felsic orthogneisses

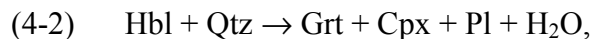
Stage 1: Prograde evolution and Stage 2: Peak-metamorphism

Due to the lack of suitable mineral inclusions, it was not possible to constrain hornblende-forming reactions for the amphibolites. However, Hbl1 inclusions in matrix Cpx2 (Fig. 4.2b) indicate progress of the generalized dehydration reaction



which is consistent with prograde heating (e.g. Spear, 1993). The melt-producing equivalent of reaction (4-1) explains the formation of partial melts in water-saturated metabasites, which are recorded in migmatitic amphibolites of the Orue Unit by plagioclase-rich leucosomes (see Chapter 2.1).

In Fe-rich amphibolites additional Grt2 was formed by the interrelated reaction



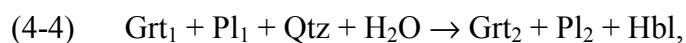
as is suggested by Hbl1 inclusions in Grt2.

Migmatitic textures are also displayed by the Hbl-Bt metagranitoids intruding the volcano-sedimentary sequence, thus indicating that both rock units were affected by the same upper amphibolite facies metamorphic event. The presence of biotite in the palaeosomes and the occurrence of hornblende in the biotite-free leucosomes (Fig. 4.3b) demonstrates dehydration-melting of biotite during the prograde metamorphic evolution, probably related to the reaction

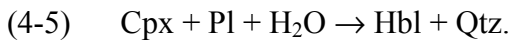


Stage 3: Retrograde evolution

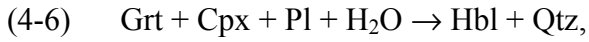
The early retrograde evolution of the mafic rocks of the Orue Unit is characterized by the formation of newly grown hornblende (Hbl3): Intergrowths of Hbl3 and Pl3 around Grt2 of the garnet-hornblende schists (Fig. 4.2f) are attributed to the reaction



with Grt₁/Pl₁ and Grt₂/Pl₂ representing the compositions of garnet and plagioclase cores and rims, respectively (Mengel & Rivers, 1991). In turn, Hbl3-Qtz3 intergrowths around matrix Cpx2 reflect reversal of reaction (4-1) during retrograde rehydration

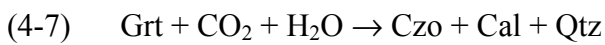


Intergrowths of Hbl₃ and Qtz₃ between Grt₂ and Cpx₂ of the Grt-Cpx-bearing amphibolites (Fig. 4.2c) are interpreted to be formed by



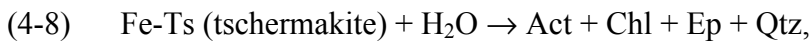
a reversal of reaction (4-2). Progress of the reactions (4-5) and (4-6) is consistent with post-peak cooling.

Intergrowths of Czo₃, Cal₃ and Qtz₃, partially or completely replacing peak-metamorphic Grt₂ of the amphibolites (Fig. 4.2d) indicate their formation after reaction



during rehydration and carbonatization.

Intergrowths of Chl₃, Act₃ and Ep₃, replacing matrix Hbl₂ of the amphibolites (Fig. 4.2e) and of the Hbl-Bt metagranitoids, are interpreted to result from the generalized reaction



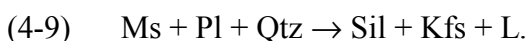
that marks the transition from amphibolite to greenschist facies conditions.

4.3.2 Metapelites and metagreywackes

Stage 1: Prograde evolution and Stage 2: Peak-metamorphism

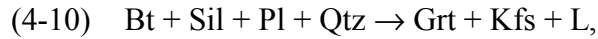
Inclusion of Sil₁ in peak-metamorphic Grt₂ (southern part) and Crd₂ (northern part) indicate that the prograde evolution proceeded through the sillimanite stability field. The migmatitic textures of the metapelites and the metagreywackes indicate that the paragneisses underwent partial melting, which can be expressed by various vapour-absent dehydration melting reactions:

The lack of Ms-Qtz assemblages and the presence of Kfs-Sil assemblages in most metapelites of the Orue Unit documents temperature conditions above the dehydration melting of muscovite, that is expressed by the reaction



Reaction (4-9) also explains the presence of abundant granitic leucosomes in the metapelites.

Inclusions of Bt₁, Pl₁ and Sil₁ in both Grt₂ and Kfs₂ of the Grt-Bt-Sil gneisses and schists (Fig. 4.5a-c) point to subsequent growth of garnet and K-feldspar according to the biotite-dehydration melting reaction

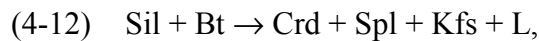


that also explains the formation of garnet-bearing leucosomes and the development of the peak-metamorphic Grt-Sil-Bt-Kfs-Qtz assemblages in the metapelites of the southern part.

In the cordierite-bearing metapelites of the northern part the presence of corroded Bt1 and Sil1 inclusions in Crd2, which are restricted to the cores of Crd2 and separate Sil1 from matrix Bt2 (Fig. 4.6a), as well as of cordierite-bearing leucosomes document progress of the biotite-dehydration melting reaction

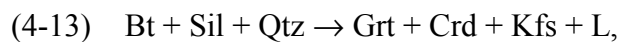


that accounts for the formation of the peak-metamorphic Crd-Bt-Kfs-Qtz assemblages in the metapelites of the northern part. The presence of Ilm2 in the cordierite-bearing domains suggests that the cordierite-formation was accompanied by ilmenite-formation, most probably due to the release of the Ti component of biotite. Consumption of the available SiO₂ and/or separation of Sil1 from SiO₂-rich matrix domains by Crd2 coronas resulted in the formation of localized, low-silica activity domains and thus triggered the growth of spinel in the Crd2-cores (Fig. 4.6a) according to the quartz-absent KFMASH reaction



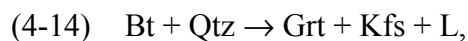
which has been proposed by Whittington et al. (1998) for low-pressure metapelites of the Nanga Parbat, northern Pakistan.

The presence of Crd2 coexisting with Grt2 and Kfs2 in the metapelitic Grt-Crd-Bt gneiss of the northern part (Fig. 4.6b) suggests crossing of the univariant KFMASH reaction



resulting in an almost complete consumption of early biotite and sillimanite.

In the sillimanite-free metagreywackes the formation of Grt2 and of garnet-bearing leucosomes is most probably related to progress of the biotite-dehydration melting reaction



as is evident from abundant corroded Bt1 inclusions in Grt2 and from Kfs2 rims surrounding Bt2 (Fig. 4.4b).

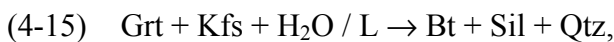
Corona textures of green Hbl2 around Bt2 of the metagreywackes (Fig. 4.4a) are interpreted to result from reaction (4-3).

The muscovite and biotite-dehydration melting reactions (4-9) to (4-14) are generally characterized by a steep slope in the P-T space and thus indicate, that the prograde evolution of the upper amphibolite facies paragneisses of the Orue Unit was mainly characterized by heating, as was also postulated for the mafic and felsic orthogneisses of the same unit.

Stage 3: Retrograde evolution

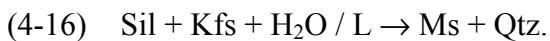
In the paragneisses of the Orue Unit retrograde reaction textures are rarely observed and are mainly related to rehydration reactions. The H₂O-rich fluids required were probably released during the crystallization of the leucosomes.

Fine-grained Bt₃-Sil₃ intergrowths replacing peak-metamorphic Grt₂ of the Grt-Bt-Sil gneisses and schists (Fig. 4.5d) are attributed to rehydration according to the reversal of reaction (4-10)

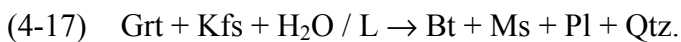


indicating initial retrogression still under amphibolite facies conditions, as demonstrated by the presence of sillimanite.

The formation of late, Ms₃-Qtz₃ intergrowths at the expense of Sil₂ and Kfs₂ (Fig. 4.5f) is interpreted to result from the reversal of reaction (4-9)



Ms₃-Bt₃-Pl₃ intergrowths replacing Grt₂ of the metapelites (Fig. 4.5e) and the metagreywackes are thought to be formed by reaction



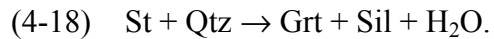
Progress of reactions (4-15) to (4-17) indicate that peak-metamorphism of the Orue Unit was followed by post-peak cooling.

4.3.3 Contact metamorphic Grt-Sil-Crd rocks

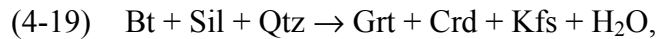
Stage 1: Prograde evolution and Stage 2: Peak-metamorphism

The presence of early St₁ inclusions in the inner margins of matrix Grt₂ (Fig. 4.7a) and in Sil₂ (Fig. 4.7b) and the presence of Sil₁ inclusions in the outermost margins of Grt₂ (Fig. 4.7a) indicate that early staurolite of the Grt-Sil-Crd rocks was replaced by Grt + Sil during prograde

heating. Following Bucher & Frey (1994), St-Qtz assemblages are finally decomposed to Grt + Sil at temperatures of around 670°C, according to the reaction



Corroded inclusions of Bt1 in Crd2 and of Sil1 in Grt2 suggest, that the subsequent growth of cordierite coexisting with garnet is related to progress of the melt-absent equivalent of reaction (4-13),



as the rocks show no clear evidence for partial melting. The lack of Kfs in the Grt-Sil-Crd rocks may be explained by low K contents of the rock samples investigated.

Stage 3: Retrograde evolution

Bt3-Sil3 intergrowths partly replacing Grt2 and Crd2 (Fig. 4.7c & d) were probably formed by the reversal of reaction (4-19). This rehydration may be due to infiltration of aqueous fluids from external sources. The formation of late St3 corona textures around Sil2 and Crd2 (Fig. 4.7b & c) is interpreted to result from progress of reaction (4-18) in the reverse direction, marking a re-entry into the St-Qtz stability field and thus indicating cooling to temperatures below 670°C.

4.4 PHASE RELATIONSHIPS

The mineral assemblage Grt + Bt + Sil + Kfs + Qtz of the metapelites of the profile sampled at the southern margin of the KIC, can be used to identify a possible thermal gradient related to the intrusion of the anorthositic magmas of the KIC. It can be expected that the composition of the ferromagnesian minerals will become more Mg-rich with increasing metamorphic grade (Thompson, 1976). This relationship is shown in Fig. 4.14, an AFM projection of the model KFMASH system, projected from quartz, K-feldspar and H₂O. As MnO and CaO contents in the studied garnet are low, their influence on the projected mineral compositions can be neglected.

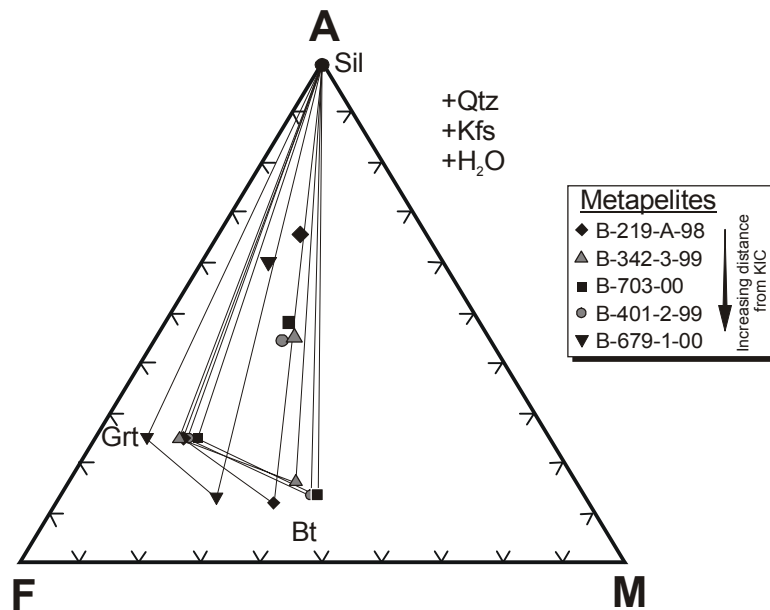


Fig. 4.14: Al₂O₃-FeO-MgO projection from quartz and K-feldspar of the assemblage Grt-Bt-Sil-Kfs-Qtz in the metapelites along the studied profile through the south-eastern region of the Orue Unit. Enlarged symbols mark the corresponding bulk-rock compositions.

A systematic shift of the three-phase field Grt-Bt-Sil towards less magnesian composition with increasing distance from the KIC is, however, not observed for the studied metapelites. A thermal gradient along the sampled profile can thus be excluded on the base of phase petrological considerations.

4.5 P-T CONDITIONS

Based on the investigation of specific peak-metamorphic mineral assemblages and the observation of widespread migmatitization, peak-metamorphic conditions of the upper amphibolite facies are constrained for the rocks of the Orue Unit. However, the systematic variations in the mineral assemblages between rocks of the northern and the southern part of the Orue Unit, which are of comparable bulk-rock composition, point to regional variations in the absolute peak P-T conditions. Therefore, conventional geothermobarometry was applied in order to constrain possible regional differences in the physical conditions during the metamorphic peak (stage 2) as well as during retrograde cooling (stage 3). A detailed description of the various geothermometer and geobarometer calibrations used is given in the Appendix (Chapter A.4). The P-T calculations were performed with mineral chemical data given in the Appendix A.6.2 (bold marked analyses of Tables A.6.2.1, A.6.2.2, A.6.2.3, A.6.2.5, A.6.2.7 and A.6.2.11).

4.5.1 Metapelites and metagreywackes

The results of the geothermobarometric calculations for the paragneisses of the Orue Unit are summarized in Table 4.5 and illustrated in Fig. 4.15. Temperatures for the paragneisses of the Orue Unit were calculated from Grt-Bt Fe-Mg exchange geothermometry (calibrations of Perchuk & Lavrent'eva, 1983; Bhattacharya et al., 1992; Kleemann & Reinhardt, 1994) and from Grt-Crd Fe-Mg exchange geothermometry (calibrations of Bhattacharya et al., 1988; Dwivedi et al. 1998). Pressures were mainly calculated by garnet-alumosilicate-quartz-plagioclase (GASP) barometry using the calibrations of Newton & Haselton (1981), Koziol & Newton (1988) and Powell & Holland (1988). The location of the Fe- and Mg-endmember reactions of the divariant reaction $\text{Grt} + \text{Sil} + \text{Qtz} \rightarrow \text{Crd}$ were calculated with the computer program THERMOCALC v.2.7 of Holland & Powell (1998a), using the updated internally consistent dataset of Holland & Powell (1998b), the garnet activity model of Berman (1990) and an ideal mixing model for hydrous cordierite. Due to the presence of cordierite, the location of the reactions strongly depend on the assumed water activity. Low totals of cordierite (~ 98 wt.%) suggest that either H₂O- or CO₂-rich fluids were present during cordierite formation. However, due to the lack of suitable fluid-inclusions, the water activity could not be calculated. Therefore, the results given in Table 4.5 and Fig. 4.15 were calculated for an assumed $a(\text{H}_2\text{O})$ of 1.0.

Zonation patterns of Grt₂ and the chemical composition of coexisting matrix Bt₂ indicate retrograde diffusional Fe-Mg exchange between the two phases. Therefore, peak-metamorphic conditions (stage 2) were generally calculated by combining the compositions of Grt₂ cores (with exception of samples B-302-2-99 and 137-A, that bear prograde zoned Grt₂) with that of

low X_{Mg} matrix Bt2 and low X_{Mg} Crd2. For GASP pressure calculations Grt2 core compositions were coupled with the core compositions of Pl2. Temperature calculations for the retrograde evolution (stage 3) were deduced by combining Grt2 rim compositions with the composition of adjacent late Bt3.

sample	assemblage	P(ref)	Temperature (°C)					Pressure (kbar)					
			Grt-Bt			Grt-Crd		T (ref)	GASP			Grt-Crd-Sil-Qtz	
			B1	PL	KR	B2	D		PH	NH	KN	HP1(Fe)	HP2(Mg)
stage 2: peak metamorphic conditions													
Metapelites													
<i>South-eastern region</i>													
B-219-A-98	Grt-Bt-Sil-Pl-Qtz	6.5	719	727	715	-	-	700	6.6	6.1	6.9	-	-
B-342-3-99	Grt-Bt-Sil-Pl-Qtz	6.5	713	701	685	-	-	700	6.6	6.2	7.0	-	-
B-703-00	Grt-Bt-Sil-Pl-Qtz	6.5	715	704	696	-	-	700	6.2	5.8	6.5	-	-
B-401-2-99	Grt-Bt-Sil-Pl-Qtz	6.5	699	686	681	-	-	700	6.3	5.9	6.7	-	-
B-679-1-00	Grt-Bt-Sil-Pl-Qtz	6.5	679	706	711	-	-	700	5.8	5.4	6.2	-	-
<i>Contact zone at KIC</i>													
B-302-2-99	Grt-Crd-Sil-Pl-Qtz	6.5	-	-	-	760	740	750	6.6	6.3	7.0	6.0	5.6
<i>South-western region</i>													
B-246-A-98	Grt-Bt-Sil-Pl-Qtz	8.0	836	810	818	-	-	800	7.9	7.7	8.4	-	-
<i>Northern Part</i>													
B-103-A-98	Grt-Crd-Bt-Sil-Pl-Qtz	6.5	827	785	807	789	894	800	6.2	6.4	7.1	4.9	6.3
Metagreywackes													
<i>South-eastern region</i>													
B-191-A-98	Grt-Bt-Pl-Qtz	6.5	722	705	723	-	-	-	-	-	-	-	-
<i>Northern Part</i>													
B-137-C-98	Grt-Bt-Pl-Qtz	6.5	666	660	696	-	-	-	-	-	-	-	-
stage 3: retrograde evolution													
<i>South-eastern region</i>													
B-401-2-99	Grt-Bt-Sil	5.0	584	565	557	-	-	-	-	-	-	-	-
B-703-00	Grt-Bt-Sil	5.0	598	577	564	-	-	-	-	-	-	-	-
<i>Contact metamorphism</i>													
B-302-2-99	Grt-Bt-Sil	5.0	636	629	626	-	-	-	-	-	-	-	-
<i>South-western region</i>													
B-246-A-98	Grt-Bt	5.0	560	609	594	-	-	-	-	-	-	-	-

Table 4.5: Representative results of conventional thermobarometry for the peak-metamorphic conditions (stage 2) and the retrograde evolution (stage 3) of the paragneisses of the Orue Unit; B1, Bhattacharya et al. (1992); PL, Perchuk & Lavrent'eva, (1983); KR, Kleemann & Reinhardt (1994); B2, Bhattacharya et al. (1988); D, Dwivedi et al. (1998); PH, Powell & Holland (1988); NH, Newton & Haselton (1981); KN, Koziol & Newton (1988); HP1, Holland & Powell (1998b); HP2, Holland & Powell (1998b).

Southern part

Regional metamorphic rocks of the south-eastern region: For the Grt-Bt-Sil gneisses and schists of the sampled profile of the south-eastern region remarkable uniform peak-metamorphic (stage 2) Grt-Bt temperatures of 727-681°C (for a P_{ref} of 6.5 kbar) were calculated (Fig. 4.15b-f), irrespective of their regional distribution. Thus it can be concluded, that the formation of the Grt-Bt-Sil gneisses and schists is clearly not related to a contact thermal effect induced by the intrusion of the KIC. Moreover, these uniform temperatures are consistent with the lack of systematic phase petrological variations (Fig. 4.14) and are in good agreement with Grt-Bt peak-temperature estimates for the metagreywacke-type Grt-Bt gneiss B-191-A-98 (722-705°C). Calculated temperatures for the retrograde evolution (stage 3) range between 598 to 557°C (for P_{ref} of 5 kbar).

Calculated GASP pressures for stage 2 vary in a restricted range of 7.0-5.4 kbar (for a T_{ref} of 700°C). However, these calculated pressures continuously decrease with increasing distance from the KIC (Fig. 4.15a & b-f), displaying average P values of ~ 7 kbar for metapelites sampled near the contact to the KIC (~ 2 km distance), whereas distinctly lower pressures of ~ 5.5 kbar were obtained for metapelites sampled in ~ 5 km distance from the contact. It hence seems most likely, that the south-eastern region of the Orue Unit represents a tilted mid-crustal section, with its deepest parts being exposed near the contacts to the KIC.

Contact zone: Grt-Crd temperatures of 760 to 740°C are obtained for the contact metamorphic Grt-Sil-Crd rock (Fig. 4.15g), using the compositions of Grt2 rims, that are interpreted to be in equilibrium with matrix Crd2, Sil2 and Pl2 (see chapter 4.2.1). These temperatures are only slightly higher than those calculated for Grt-Bt pairs of the southward following Grt-Bt-Sil gneisses and schist.

Calculated corresponding GASP pressures of 7.0 to 6.3 kbar are similar to that calculated for neighbouring Grt-Bt-Sil gneisses and schists, which, however, are unaffected by contact metamorphism s.s. (see above). In contrast, Grt-Crd-Sil-Qtz barometry yields slightly lower pressures of 6.0 to 5.6 (for T_{ref} of 750°C), which may be caused by late diffusional Fe-Mg exchange between Grt2 and Crd2. This, however, would imply, that the calculated peak-temperatures represent minimum values.

Temperature calculations indicate, that the formation of retrograde Bt3 at the expense of Grt2 (stage 3) proceeded in response to cooling down to temperatures of ~ 630°C (for P_{ref} of 5 kbar).

Regional metamorphic rocks of the south-western region: P-T calculations for the Grt-Bt-Sil gneisses of the south-western region of the Orue Unit were performed using the composition of

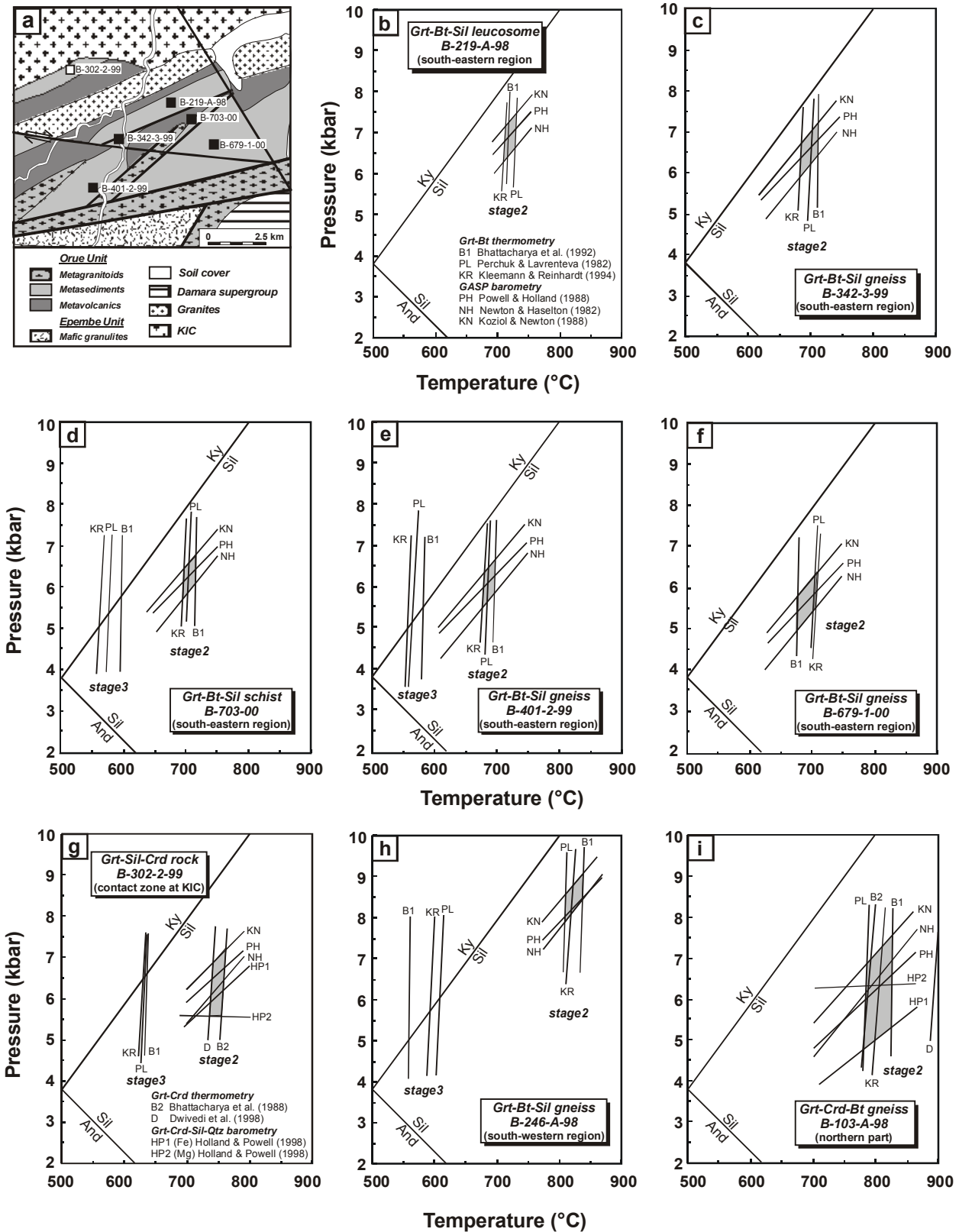


Fig. 4.15: a) Sample location map of the south-eastern region and b-i) P-T plots showing the results of geothermobarometric calculations for the peak-metamorphic conditions (stage 2) and the retrograde evolution (stage 3) of the metamorphic evolution applied to the metapelites of the Orue Unit. Source of data is Table 4.5.

unzoned Grt2, combined with the compositions of coexisting matrix Bt2, Sil2 and Pl2 (see chapter 4.2.1). Calculated peak-metamorphic Grt-Bt temperatures of 836-810°C (for P_{ref} of 8.0 kbar; Fig. 4.15h) are about 100°C higher than those revealed by the Grt-Bt-Sil gneisses of the south-eastern region of the Orue Unit.

Corresponding GASP pressures of 8.4 to 7.7 kbar (for T_{ref} of 800°C) are about 2 kbar higher than those of the south-eastern region.

Grt-Bt temperatures for the retrograde formation of Bt3-Ms3 (stage 3) range between 609 to 560°C (for P_{ref} of 5 kbar).

Northern Part

P-T calculations for the Grt-Crd-Bt gneiss of the northern part were performed by using the composition of unzoned Grt2, combined with the composition of coexisting pinitized Crd2, unzoned Pl2 and matrix Bt2. Peak-metamorphic temperatures of 827-785°C (for a P_{ref} of 6.5 kbar) are calculated using Grt-Bt thermometry (Fig. 4.15i). These high Grt-Bt temperatures are consistent with temperatures of $\sim 790^\circ\text{C}$ calculated with the Grt-Crd thermometer of Bhattacharya et al. (1988), whereas the Grt-Crd thermometer of Dwivedi et al. (1998) yields unrealistic high temperatures of $\sim 900^\circ\text{C}$. The calculated temperatures correspond to the granulite facies and are about 100°C higher than those obtained for the metapelitic Grt-Bt-Sil gneisses and schists of the south-eastern region.

Corresponding GASP and Grt-Crd-Sil-Qtz pressures of 7.1-6.2 kbar and of 6.3-4.9 kbar, respectively, are interpreted as maximum pressure ranges, since quartz and sillimanite are rare. The pressures are in the range of those calculated for the metapelitic Grt-Bt-Sil gneisses and schists of the south-eastern region.

Grt-Bt temperatures for the mylonitic Grt-Bt gneiss B-137-C-98 range between 696 to 660°C and are thus $\sim 150^\circ\text{C}$ lower than the temperatures calculated for the Grt-Crd-Bt gneiss. As the Grt-Bt gneiss is exposed in a major shear zone, the comparably low temperatures are presumably related to re-equilibration of the Grt-Bt gneiss during mylonitization.

4.5.2 Amphibolite

Grt-Cpx Fe-Mg geothermometry (Powell, 1985; Ai, 1994; Krogh Ravna, 2001) performed with grossular-rich Grt2 cores combined with the composition of matrix Cpx2 of the Grt-Cpx-bearing amphibolite B-191-B-98 (south-eastern region) yields peak-metamorphic (stage 2) temperatures of 753-715°C (Table 4.6). Lower temperatures of 700-600°C are calculated by Grt-Hbl Fe-Mg geothermometry (Graham & Powell, 1984; Perchuk et al., 1985), performed with Grt2 rims and

adjacent Hbl3. These temperature estimates are consistent with the interpretation of Hbl3 formation (stage 3) at the expense of Grt2 and Cpx2 during retrograde cooling. Since plagioclase is completely altered to sericite, it was impossible to calculate corresponding pressures.

The peak-metamorphic temperatures calculated for the Grt-Cpx-bearing amphibolite are in good accordance with those revealed by the Grt-Bt gneiss of the same outcrop (B-191-A-98) and those of the metapelitic Grt-Bt-Sil gneisses and schists of the south-eastern region of the Orue Unit.

sample	assemblage	P(ref)	Temperature (°C)				
			Grt-Cpx			Grt-Hbl	
			Po	A	K	GP	P
<i>South-eastern region</i>							
stage 2: peak metamorphic conditions							
B-191-B-98	Grt-Cpx	6.5	753	732	715	-	-
stage 3: retrograde evolution							
B-191-B-98	Grt-Hbl-Qtz	5.0	-	-	-	705	604

Table 4.6: Representative results of conventional thermobarometry for the peak-metamorphic conditions (stage 2) and the retrograde evolution (stage 3) of the Grt-Cpx-bearing amphibolite of the Orue Unit; Po, Powell, 1985; A, Ai (1994); K; Krogh Ravna (2001); GP, Graham & Powell, (1984); P, Perchuk et al. (1985).

4.6 DISCUSSION AND CONCLUSION

4.6.1 P-T path reconstruction

The recorded prograde metamorphic P-T paths of the Orue Unit rocks are characterized by significant heating as is evident from dehydration melting of amphibole, muscovite and biotite, i.e. reaction (4-1) in the amphibolites, reaction (4-3) in the Hbl-Bt metagranitoids and reactions (4-9) to (4-14) in the paragneisses. Heating proceeded throughout the stability field of sillimanite in all parts of the Orue Unit. The prograde dehydration melting reactions make it unlikely, that the Orue Unit rocks represent retrogressed former UHT granulites of the Epembe Unit. This interpretation is supported by the lack of relic orthopyroxene in all amphibolite facies rock types of the Orue Unit (Brandt et al., 2003).

Remarkable regional variations in the calculated peak-metamorphic P-T conditions correlate well with the stability fields of the observed peak-metamorphic mineral assemblages of the metapelites in the NaKFMASH system (Fig. 4.16). The univariant KFMASH reaction $\text{Grt} + \text{Bt} + \text{Qtz} \rightarrow \text{Opx} + \text{Crd} + \text{Kfs} + \text{L}$ was not crossed by the metapelites and therefore marks the upper thermal limit for the rocks of the Orue Unit. A lower thermal limit is given by reaction (4-9) $\text{Ms} + \text{Qtz} \rightarrow \text{Sil} + \text{Kfs} + \text{L}$, that was crossed by all metapelites investigated.

In the metapelites of the south-eastern region of the Orue Unit the peak-metamorphic conditions remained below the univariant KFMASH dehydration melting reaction (4-13) $\text{Bt} + \text{Sil} + \text{Qtz} \rightarrow \text{Grt} + \text{Crd} + \text{Kfs} + \text{L}$, which, at the pressure conditions realized for the Orue Unit (~ 5.5 - 8.0 kbar), is located between 750 and 850°C (Spear et al., 1999). In contrast, reaction (4-13) was overstepped by metapelitic samples of the northern part of the Orue Unit. These phase petrological variations are consistent with results of conventional geothermobarometry, that yielded peak-metamorphic temperatures of $\sim 700^\circ\text{C}$ for the Grt-Bt-Sil gneisses and schist of the south-eastern region and higher peak-metamorphic temperatures of $\sim 800^\circ\text{C}$ for the Grt-Crd-Bt gneisses of the northern part. Pre- to syn-tectonic formation of garnet in metapelites of the south-eastern region of the Orue Unit indicates that peak-temperatures were attained prior to or during the main deformation phase D_1 , whereas, in the northern part, the thermal peak was reached subsequently to D_1 , as is evident from post-tectonic garnet formation. For metapelites of both parts comparable peak-pressures (northern part: ~ 6.0 kbar; south-eastern region ~ 6.5 kbar) were calculated, corresponding to mid-crustal levels of ~ 20 km depth. For Grt-Bt-Sil gneisses of the south-western region of the Orue Unit peak-metamorphic temperatures of $\sim 820^\circ\text{C}$ and comparably high pressures of ~ 8 kbar ($\cong 24$ km depth) were obtained, that are consistent with P-T conditions realized below reaction (4-13).

Evidence for the pressure conditions during the prograde evolution is poorly recorded by the rocks of the Orue Unit. However, the unzoned grossular content of Grt2 and the generally unzoned anorthite content of coexisting Pl2 in the observed garnet-sillimanite-quartz-plagioclase assemblage of the metapelites of the south-eastern region of the Orue Unit part suggest nearly constant pressures during prograde heating. This interpretation requires that garnet and plagioclase have grown during the prograde evolution and that the grossular zonation was not modified at peak-metamorphic conditions. It can not be ruled out, however, that garnet has grown at peak-metamorphic conditions or that the grossular content was homogenized at peak-temperatures.

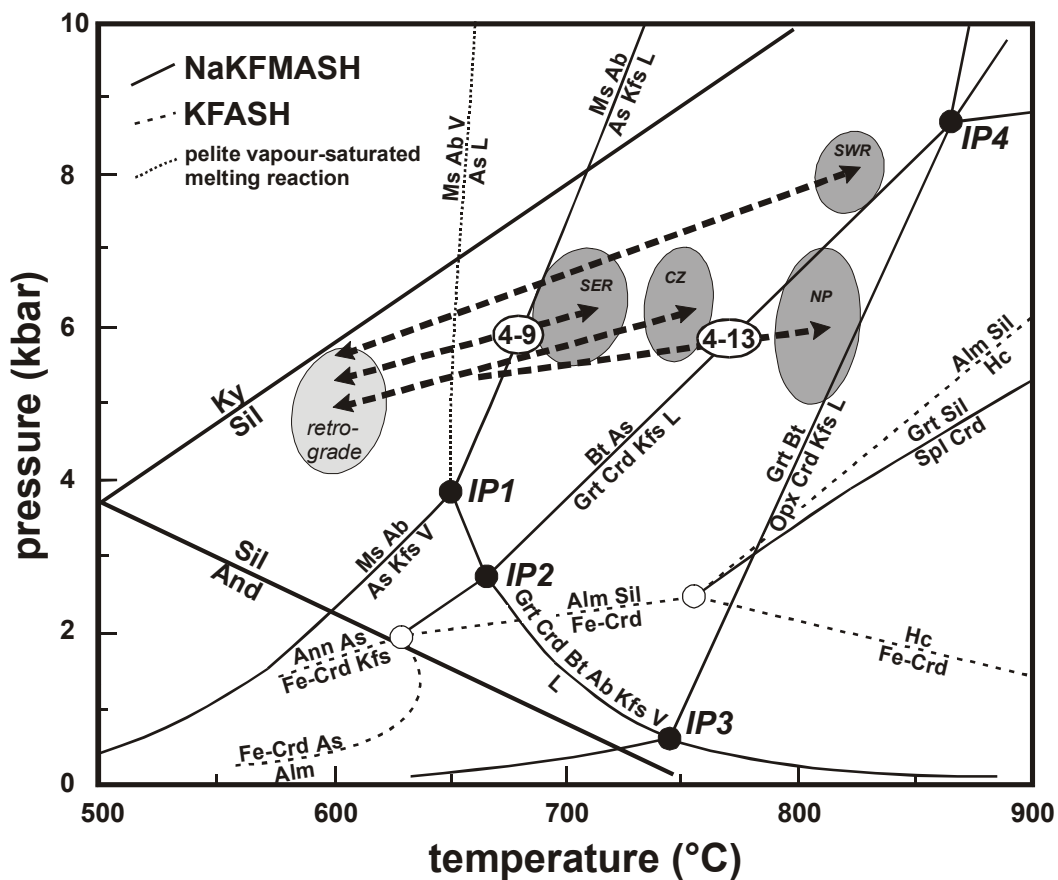


Fig. 4.16: P-T diagram of the NaKFMASH system with relevant reactions for metapelites of the Orue Unit (dashed lines: KFASH system; finely dotted line: pelite vapour-saturated melting reaction; KFMASH system reactions have been excluded for reasons of clarity). Melting and dehydration equilibria are from Spear et al. (1999) and references therein. Dark grey fields indicate peak-metamorphic P-T conditions for the individual parts of the Orue Unit (NP: northern part; SWR: south-western region; SER: south-eastern region) and for the contact metamorphic Grt-Sil-Crd rocks of the contact zone (CZ) at the KIC and light grey field indicates retrograde P-T conditions. Arrows show inferred P-T paths. Numbers refer to reactions discussed in the text. Aluminosilicate stability fields after Holdaway (1971).

The retrograde evolution of the Orue Unit rocks is characterized by cooling to middle amphibolite facies conditions of $\sim 600^{\circ}\text{C}$ in the sillimanite stability field, as is mainly evident from the progress of the dehydration melting reactions (4-9) and (4-10) in the reverse direction, following interaction with crystallizing melt. Cooling of the rocks is consistent with the rimward decrease of X_{Mg} of garnet of the metapelites of the southern part. In the metabasites cooling is mainly documented by the replacement of both garnet and clinopyroxene by late hornblende. The lack of post-peak reaction textures in the metapelites of the northern part prevents a reconstruction of their retrograde P-T evolution.

When comparing the data obtained for the three individual parts of the Orue Unit, their P-T evolution can be generally described as simple heating-cooling paths with probably minor pressure variations, suggesting that they were affected by the same metamorphic event. Due to the lack of suitable reaction textures, it remains uncertain, however, whether the P-T paths are clockwise or anti-clockwise. The different peak-metamorphic conditions indicate that the three parts of the Orue Unit represent individual crustal levels that were juxtaposed during later tectonic activity. Even though the temperatures obtained for the northern part and the southwestern region of the southern part ($\sim 800^{\circ}\text{C}$ and $\sim 820^{\circ}\text{C}$, respectively) lie at the amphibolite-granulite facies transition, the rocks are attributed to the upper amphibolite facies, since orthopyroxene and/or its alteration products are not observed. The absence of orthopyroxene is probably related to high H_2O activities of the Orue Unit rocks, that stabilized biotite and hornblende even under relative high temperatures.

The inferred P-T path of the contact metamorphic Grt-Sil-Crd rocks is remarkably similar to those deduced for the other metapelites of the Orue Unit and is characterized by prograde heating and retrograde cooling under near-isobaric conditions. Prograde consumption of staurolite and subsequent formation of cordierite indicates heating from middle amphibolite facies to upper amphibolite facies conditions. Rimward decreasing grossular content in prograde-zoned garnet suggests nearly constant or decreasing pressure conditions during heating. Re-growth of staurolite is taken as evidence for a re-entry into the middle amphibolite facies during retrograde cooling. Calculated peak-metamorphic minimum temperatures ($\sim 750^{\circ}\text{C}$) are only slightly higher than the temperature estimated for the southward following Grt-Bt-Sil gneisses and schist, whereas both rock units display similar peak-metamorphic pressures of ~ 6.5 kbar.

4.6.2 Geodynamic model

The petrological investigations demonstrate that all three individual parts of the Orue Unit and the contact metamorphic rocks underwent a similar P-T evolution. Taking into account the

overall regional geology, the structural data and the available age data, the inferred P-T evolution can be used to unravel the tectonic evolution of the Orue Unit:

Petrological investigations and P-T calculations demonstrate that the upper amphibolite facies rocks of all parts of the Orue Unit followed simple heating-cooling paths at pressures regionally varying between 6.0 ± 1.0 kbar (northern part), 6.5 ± 1.0 kbar (south-eastern region of the southern part), 8.0 ± 0.5 kbar (south-western region of the southern part) and 6.5 ± 1.0 kbar (contact zone). These pressures agree well with those determined for the emplacement of the anorthosites of the KIC, i.e. 7.0 ± 1.2 kbar (Drüppel et al., 2001, Drüppel, 2003), hence implying that contacts between the Orue Unit and the KIC represent original intrusion contacts, which underwent no major tectonic disturbance during or after the anorthosite intrusion. Moreover, the calculated mid-crustal peak-pressures for the Grt-Bt-Sil gneisses and schists (~ 6.5 kbar) are actually the same as those calculated for the nearby syenitic dykes and for the subsequent re-equilibration in the anorthosites at depths of ~ 20 km (6.5 ± 0.6 kbar; Drüppel, 2003). The interpretation of a cogenetic evolution of the anorthosites and the upper amphibolite facies metamorphism is in excellent agreement with the age relationships between anorthosite emplacement and high-grade metamorphism of the Orue Unit. U-Pb zircon and Pb-Pb garnet dating yielded ages of 1390-1318 Ma for the upper amphibolite facies metamorphism of the Orue Unit (Barbara Seth, pers. comm.), which broadly coincides with emplacement ages of 1387-1347 Ma obtained for both the Namibian and Angolan part of the KIC (Drüppel et al., 2000b; Mayer et al., 2000).

The simple heating-cooling path of and the lack of deformational textures in the Grt-Sil-Crd rocks, which were sampled in direct contact to the KIC, implies that these rocks underwent contact metamorphism under almost static conditions. The contact metamorphism was presumably induced by the intrusion of the anorthositic magmas of the KIC. As has been demonstrated by Drüppel et al. (2001) and Drüppel (2003) the late-magmatic crystallization of amphibole in the anorthosites occurred under temperatures of $\sim 970^\circ\text{C}$, a temperature, which was high enough to cause the heating constrained for the Grt-Sil-Crd rocks (up to $\sim 750^\circ\text{C}$).

For the Grt-Bt-Sil gneisses and schists, however, which were sampled in increasing distance from the KIC, the lack of a thermal gradient rules out a contact metamorphic origin *sensu stricto*. The uniform temperatures of 700 ± 30 °C rather point to a regional metamorphic event. However, an evolution related to a collisional event seems rather unlikely, since typical collisional structures, such as overthrusting tectonics, as well as a significant pressure increase during prograde metamorphism has not been observed. Moreover, the coinciding ages obtained for the anorthosites and the upper amphibolite facies rocks make an orogenic event at 1400-1300

Ma unlikely, which is in accordance with an anorogenic, extension-dominated emplacement of the huge massif-type anorthosite body of the KIC and of the associated granites and syenites favoured by Drüppel (2003). Therefore, prograde heating of the Grt-Bt-Sil gneisses and schists to upper amphibolite facies conditions is attributed to a regionally scaled perturbation of the geotherm related to the formation and emplacement of the anorthosites, which may be described as a 'regional contact metamorphism'. Upper amphibolite facies metamorphism was accompanied and followed by intense ductile deformation along dextral strike-slip faults. Post-peak cooling to middle amphibolite facies temperature is attributed to cooling and crystallization of the anorthosites and hence reaching of the stable geotherm.

Radiogenic age data for the higher grade rocks of the northern part of the Orue Unit do not exist. However, the striking similarities in the P-T evolution suggest that this part was affected by the same thermal event as the southern part of the Orue Unit, but, in clear contrast to the latter, was heated to higher temperatures.

In conclusion, the Mesoproterozoic metamorphism of the Orue Unit is interpreted to be related to the emplacement of the anorthositic magmas of the KIC and therefore to be anorogenic in nature. In contrast, burying of the Orue Unit rocks into mid-crustal levels of ~ 20 km depth must be related to an earlier orogenic tectonic event. Palaeoproterozoic zircon core ages (Barbara Seth, pers. comm.) suggest that the burial of the Orue Unit rocks into mid-crustal levels is related to the Eburnian orogeny.

5 METAMORPHIC EVOLUTION OF THE UHT GRANULITES OF THE EPEMBE UNIT

In the following section the petrology, mineral chemistry and reaction history of the mafic, felsic, metapelitic and metagreywacke-type ultrahigh-temperature (UHT) granulites of the Epembe Unit will be discussed. Furthermore, special attention is given to the metamorphic evolution of sapphirine-bearing Opx-Sil gneisses and Opx-Grt rocks, that has been preliminarily discussed by Brandt et al. (2000, 2001, 2002a). UHT conditions have been first reported for the recognized granulites by Brandt et al. (2000, 2001, 2002a, 2002b) and, in more detail for Mg-rich Grt-Opx gneisses and Qtz-rich Grt-Opx rocks by Brandt et al. (2003).

Based on textural relationships and published qualitative phase diagrams and supported by detailed mineral chemical data the relative P-T evolution of the individual granulite facies lithologies is reconstructed. The P-T paths are furthermore strengthened by conventional geothermobarometry, which was applied to elucidate absolute P-T data for the individual stages of the metamorphic evolution. In addition, a detailed phase petrological investigation of selected granulite samples was performed, using phase diagrams drawn for a specific bulk rock composition (i.e. P-T pseudosections) in the system FMAS, in order to reconstruct detailed P-T paths.

Taking into account the overall regional geology, the metamorphic evolution of the adjacent upper amphibolite facies rocks of the Orue Unit and the available geochronological data, the deduced P-T paths are used to constrain the tectonic scenario, that prevailed during the formation of the UHT granulites of the Epembe Unit at the south-western margin of the Congo Craton during the Mesoproterozoic.

5.1 PETROGRAPHY

Based on field observations (see Chapter 2.2) and geochemical investigations (see Chapter 3.1) the Epembe Unit is interpreted as a metamorphosed volcano-sedimentary sequence composed of

- 1) metavolcanic mafic granulites, interlayered with
- 2) metavolcanic felsic granulites, and
- 3) paragneisses, including metagreywackes, metapelites and Qtz-rich Grt-Opx rocks. In the metagreywackes, sapphirine-bearing Opx-Sil gneisses and Opx-Grt rocks occur as restitic domains.

This volcano-sedimentary sequence was intruded by intermediate dykes, which were metamorphosed to mafic granulites, as well as by rare granulite facies Grt-Opx metagranitoids.

In order to reveal the mineral assemblages and reaction textures, that constitute the basis for the further petrological investigations a total of 188 rock samples of all lithological sub-units, has been investigated. The sample localities are shown in Figs. A.2.2 to A.2.5 in the Appendix.

The granulites of the Epembe Unit preserve abundant and conspicuous reaction textures, which can be related to several specific stages of the metamorphic evolution. Therefore, the petrographic description of all lithologies investigated follows an uniform multistage scheme:

Stage 1: The prograde evolution is recorded by mineral inclusions in the peak-metamorphic phases.

Stage 2: During peak-metamorphic conditions granoblastic mineral assemblages were formed. Peak-metamorphism was accompanied by partial melting, leading to the formation of leucosomes.

Stage 3: The early stage of the retrograde evolution is characterized by the development of conspicuous corona and symplectite textures, formed at the expense of the peak-metamorphic phases.

Stage 4: Further retrogression predominantly led to the partial replacement of the early-stage retrograde and, less frequently, of peak-metamorphic phases.

Stage 5: The final stage of metamorphism is characterized by the consumption of stage 4 mineral phases.

While reaction textures, testifying to stages 1-4, are recorded by most of the samples investigated, stage 5 mineral phases are observed only in selected paragneiss samples. Minerals are abbreviated in terms of the specific metamorphic stage active during their formation.

5.1.1 Mafic granulites

Based on field relationships and geochemical data the metavolcanic mafic granulites of the Epembe Unit are subdivided into three subunits: 1) Basic (*garnet-bearing two-pyroxene granulites*) constitute major parts of the volcano-sedimentary sequence of the Epembe Unit. 2) Ultrabasic *Grt-Cpx granulites* occur in a tectonic lens, which is exposed in a marginal shear zone of the Epembe Unit. 3) (*Grt-bearing Opx-Pl-Qtz granulites*) are present in metamorphosed intermediate dykes, which cross-cut the compositional banding of the granulites of the volcano-sedimentary sequence.

The microscopic investigation of 71 selected rock samples of the three metabasite lithologies revealed systematic variations of the mineralogy and the modal abundance of minerals:

(1) The (*garnet-bearing two-pyroxene granulites*) are predominantly composed of orthopyroxene (11-30 vol.%), clinopyroxene (20-39 vol.%) and plagioclase (42-59 vol.%). 17 of 56 two-pyroxene granulite samples investigated contain garnet (5-20 vol.%). While all samples contain minor ilmenite (1-4 vol.%), green spinel (1 vol.%) only occurs in the garnet-bearing two-pyroxene granulite sample B-493-99. Pargasitic hornblende (0-40 vol.%), cummingtonite (0-7 vol.%) and quartz (0-5 vol. %) are present in highly variable amounts, depending on the degree of retrogression. Zircon, magnetite, rutile and apatite occur as accessory phases.

(2) The *Grt-Cpx granulites* contain abundant garnet (20-22 vol.%), clinopyroxene (12-21 vol.%), pargasitic hornblende (34-36 vol.%), plagioclase (17-20 vol.%) and subordinate ilmenite (2-4 vol.%). In contrast to the two-pyroxene granulites, orthopyroxene is absent or rare (0-5 vol.%) in the Grt-Cpx granulites. Accessories are rutile, clinozoisite, biotite, zircon and apatite.

(3) The (*Grt-bearing Opx-Pl-Qtz granulites*) contain abundant orthopyroxene (15-48 vol.%), plagioclase (32-53 vol.%), quartz (3-31 vol.%), ilmenite (6-10 vol.%) and garnet (0-15 vol.%). Accessories are biotite, zircon and apatite.

Mineral assemblages

Based on the microscopic investigation systematic variations of the peak-metamorphic (stage 2) and retrograde (stage 3 & 4) mineral assemblages are recognized (Table 5.1) between the three mafic granulite lithologies:

(1) The uniform quartz-free peak-metamorphic mineral assemblage (stage 2) of the *two-pyroxene granulites* consist of orthopyroxene (Opx₂), clinopyroxene (Cpx₂) and plagioclase (Pl₂). Two-pyroxene granulites containing peak-metamorphic garnet (Grt₂) are comparably rare (Table 5.1). Bulk-rock geochemical data suggest that the presence of garnet is related to the lower Si content of the garnet-bearing samples. A second generation of orthopyroxene (Opx₃)

and plagioclase (Pl3) was developed in the garnet-bearing two-pyroxene granulites during early retrogression (stage 3). In addition, green spinel (Spl3) may occur as early retrograde phase. Further retrogression (stage 4) led to the formation of pargasitic hornblende (Hbl4), plagioclase (Pl4), cummingtonite (Cum4), minor quartz (Qtz4) and to the re-growth of garnet (Grt4)

(2) The **Grt-Cpx granulites** contain the coarse-grained peak-metamorphic mineral assemblage (stage 2) of garnet (Grt2), clinopyroxene (Cpx2) and minor ilmenite (Ilm2). In contrast to the two-pyroxene granulites, orthopyroxene and plagioclase were not present at the peak-metamorphic pressures, but occur as prograde mineral inclusion in Grt2 and Cpx2. In addition, orthopyroxene (Opx3) and plagioclase (Pl3) are present in early retrograde corona textures (stage 3). The peak-metamorphic phases and the early stage retrograde phases are set in an amphibolitic matrix, which is predominantly composed of retrograde hornblende (Hbl4) and plagioclase (Pl4) with minor epidote (Ep4) formed during the late retrograde evolution (stage 4).

Their orthopyroxene- and plagioclase-free peak-metamorphic assemblage suggests that the Grt-Cpx granulites equilibrated at higher peak-metamorphic pressures than the two-pyroxene granulites. However, the differences in the peak-metamorphic assemblages could also be related to the respective bulk-rock composition of the ultrabasic Grt-Cpx granulites (olivine tholeiite to alkali-olivine basalt) and the basic two-pyroxene granulites (olivine tholeiite to quartz tholeiite). The reasons for the discrepancies in the peak-metamorphic mineral assemblages will be discussed later (see Chapter 5.3.1 & 5.4.1).

n	stage 2					stage 3			stage 4
<i>(Grt-bearing) two-pyroxene granulites</i>									
39	Opx	Cpx	Pl	Ilm				Grt, Hbl, Cum, Pl, Qtz	
17	Grt	Opx	Cpx	Pl	Ilm	Opx	Pl	Spl	Hbl, Pl, Cum, Qtz
<i>Grt-Cpx granulite</i>									
3	Grt		Cpx	Ilm		Opx	Pl		Hbl, Pl, Ep
<i>(Grt-bearing) Opx-Pl-Qtz granulites of metamorphosed dykes</i>									
10		Opx		Pl	Ilm	Qtz			Grt, Qtz
2	Grt	Opx		Pl	Ilm	Qtz	Opx	Pl	Grt, Qtz

Table 5.1: Mineral assemblages in the mafic granulites of the Epembe Unit (n: number of investigated rock samples).

(3) The **(Grt-bearing) Opx-Pl-Qtz granulites** of the metamorphosed dykes show a peak-metamorphic assemblage of granoblastic orthopyroxene (Opx2), plagioclase (Pl2), ilmenite (Ilm2) and quartz (Qtz2), hence suggesting that the dykes were affected by the same granulite

facies metamorphic event as the mafic granulites of the volcano-sedimentary sequence. Two samples contain additional peak-metamorphic garnet (Grt2), whereas clinopyroxene is not present. A second generation of orthopyroxene (Opx3) and plagioclase (Pl3) was formed in the Grt-bearing samples during the early retrograde evolution (stage 3), whereas a second generation of garnet (Grt4) and quartz (Qtz4) was developed during late stage retrogression (stage 4).

Texture

The *(Grt-bearing) two-pyroxene granulites* and the *(Grt-bearing) Opx-Pl-Qtz granulites* show a weak foliation (S_1), which is defined by aligned peak-metamorphic Opx2 and Cpx2, indicating growth of the pyroxenes prior to or during the main, ductile deformation phase (D_1). In contrast, the *Grt-Cpx granulites* display a massive texture. Mineral inclusions in the peak-metamorphic phases of all mafic granulites lack a preferred orientation, indicating the absence of an early deformation event prior to D_1 .

Mafic granulites sampled in the vicinity of shear zones surrounding the Epembe Unit are strongly retrogressed and display a late mylonitic fabric (S_2), defined by aligned Hbl4.

5.1.1.1 (Garnet-bearing) two-pyroxene granulites

Grt-free samples: B-206-E-98, B-207-B-98, B-208-99, B-230-B-98, B-317-1-99, B-317-2-99, B-321-99, B-326-2-99, B-327-99, B-336-99, B-358-6-99, B-373-2-99, B-379-2-99, B-423-99, B-427-1-99, B-427-2-99, B-447-1-99, B-459-99, B-465-4-99, B-468-1-99, B-485-99, B-486-4-99, B-513-99, B-545-3-99, B-557-3-99, B-573-99, B-615-4-99, B-629-00, B-647-00, B-663-1-00, B-663-2-00, B-664-00, B-666-2-00, B-666-4-00, B-698-00 and B-540-4-99, B-661-4-00, B-661-5-00, B-688-00 (xenoliths in Grt-Opx metagranitoid)

Grt-bearing samples: B-326-99, B-326-3-99, B-434-2-99, B-469-99, B-493-99, B-512-99, B-527-1-99, B-527-2-99, B-527-3-99, B-527-4-99, B-551-1-99, B-551-2-99, B-577-2-99, B-580-1-99, B-580-2-99, 660-00, B-666-1-00

Stage 1: Prograde evolution and stage 2: Peak-metamorphism

The texture of the two-pyroxene granulites is commonly equigranular and granoblastic. Straight grain boundaries are developed between fine- to medium-grained, anhedral to subhedral matrix orthopyroxene (Opx2) and clinopyroxene (Cpx2) as well as anhedral matrix plagioclase (Pl2; Fig. 5.1a), thus indicating crystallization of the peak-metamorphic mineral assemblage under equilibrium conditions. This interpretation is supported by the inclusion patterns of the peak-

metamorphic minerals, which all preserve their respective coexisting mineral phases as inclusions. Anhedraal garnet (Grt2) occurs as strongly resorbed porphyroblasts of up to 6 mm in diameter in the pyroxene-plagioclase matrix. Minor ilmenite (Ilm2) either occurs as an anhedraal matrix phase or as exsolved platelets in the pyroxenes.

Rare corroded inclusions of greenish or brownish hornblende (Hbl1) and quartz (Qtz1) in Opx2, Cpx2, Pl2 and Grt2 (Fig. 5.1a) are evidence for an early lower-grade assemblage, which was replaced by the 'dry' two-pyroxene assemblage (\pm garnet) during peak-metamorphism.

Stage 3: Corona and symplectite formation

Early stage retrograde reaction textures are only preserved in garnet-bearing two-pyroxene granulites, as their formation is closely related to the breakdown of peak-metamorphic Grt2. These textures include (1) broad, cm-sized, monomineralic coronas of Pl3 and (2) granoblastic corona textures of fine-grained orthopyroxene (Opx3) and plagioclase (Pl3), both of them partly or completely replacing Grt2 (Fig. 5.1b). In the core of former Grt2 additional fine-grained green spinel (Spl3) may occur in the Opx3-Pl3 intergrowths (Fig. 5.1c).

Stage 4: Re-growth of amphibole and garnet

The peak-metamorphic mineral assemblage as well as retrograde Opx3-Pl3 intergrowths of the two-pyroxene granulites may be replaced by texturally late greenish to brownish, paragonitic hornblende (Hbl4), cummingtonite (Cum4), plagioclase (Pl4), minor quartz (Qtz4), and/or garnet (Grt4). In two-pyroxene granulites, which are exposed in the vicinity of major shear zones this process of amphibolitization almost went to completion (Fig. 5.1d), hence suggesting that these major zones provided excellent pathways for large-scale retrograde fluid-flow. Moreover, these amphibolitized samples underwent extensive ductile deformation, as is indicated by the mylonitic foliation (S_2 ; Fig. 5.1d). In contrast, two-pyroxene granulites sampled at some distance from these shear zones mostly preserved their dry, peak-metamorphic two-pyroxene assemblage.

In the absence of early retrograde Opx3-Pl3 intergrowths, peak-metamorphic Grt2 is replaced by a symplectite of Hbl4 and Pl4 (Fig. 5.1e). Colorless Cum4 generally occurs as monomineralic rims around Opx2 of the (garnet-bearing) mafic granulites. Locally, this rim is followed by an outer corona of greenish to brownish Hbl4, intergrown with Qtz4. Where Cum4 is lacking, Opx2 is surrounded by a monomineralic seam of Hbl4 (Fig. 5.1a). Hbl4 was additionally observed as poikiloblastic grains intimately intergrown with Qtz4 and partially to completely replacing Cpx2. Hbl4 may be aligned, defining a S_2 foliation (Fig. 5.1d). Locally, retrograde Hbl4 and Qtz4 coexist with a second generation of garnet (Grt4), which occurs as subhedral to euhedral grains between Cpx2 and Pl2 (Fig. 5.1f). Hbl4 also forms coronas around Ilm2 (Fig. 5.1a & f).

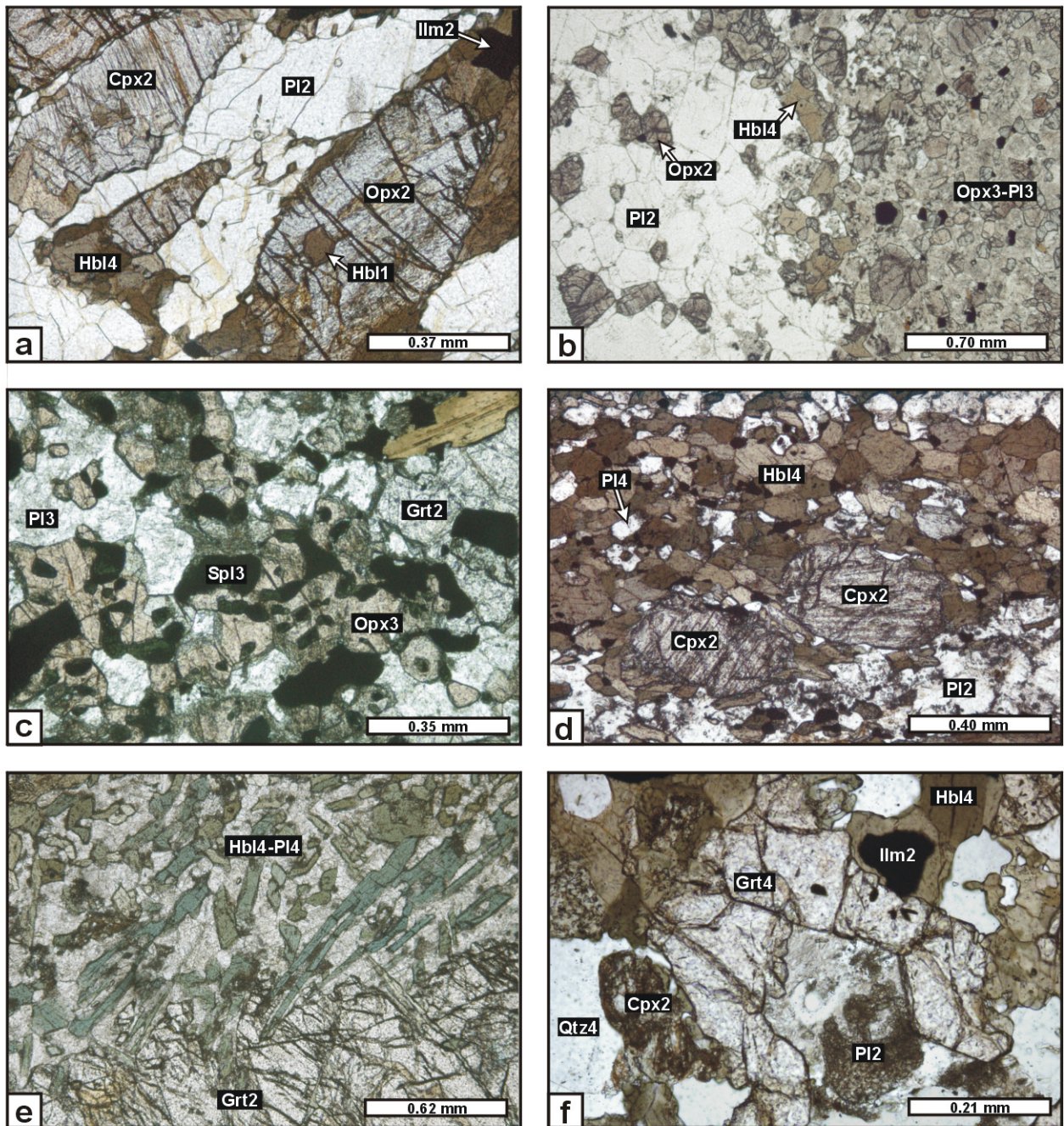


Fig. 5.1: Photomicrographs illustrating the metamorphic evolution of the mafic (Grt-bearing) two-pyroxene granulites of the Epembe Unit. **a)** Coexisting Opx₂, Cpx₂ and Pl₂. Early Hbl₁ is enclosed by Opx₂. Cpx₂, Opx₂ and Ilm₂ are marginally replaced by Hbl₄ (two-pyroxene granulite B-573-99). **b)** Fine-grained Opx₃-Pl₃ intergrowth, which pseudomorphs Grt₂ (Grt-bearing two-pyroxene granulite B-493-99). **c)** Opx₃-Pl₃-Spl₃ intergrowth, which replaces Grt₂ (Grt-bearing two-pyroxene granulite B-493-99). **d)** Relic Cpx₂ in a fine-grained, amphibolitic matrix of Hbl₄ and Pl₄. Hbl₄ defines a mylonitic foliation S₂ (retrogressed two-pyroxene granulite B-321-99). **e)** Hbl₄-Pl₄ symplectite, which partly replaces Grt₂ (Grt-bearing two-pyroxene granulite B-527-4-99). **f)** Re-grown Grt₄, which coexists with Hbl₄ and Qtz₄, separates altered Pl₂ from altered Cpx₂. Ilm₂ is rimmed by Hbl₄ (retrogressed two-pyroxene granulite B-427-1-99).

5.1.1.2 Grt-Cpx granulites

samples: B-311-1-99, B-311-3-00, B-311-4-00

Stage 1: Prograde evolution and stage 2: Peak-metamorphic assemblages

Peak-metamorphic coarse-grained garnet (Grt2) of the Grt-Cpx granulites occurs as anhedral grains of up to 3 cm in diameter, coexisting with coarse-grained, anhedral pale green clinopyroxene (Cpx2) of up to 1 cm in length (Fig. 5.2a). Fine grained peak-metamorphic ilmenite (Ilm2) displays hematite exsolution lamellae.

Grt2 contains abundant mineral inclusions, lacking a preferred orientation, which are interpreted as relics of the prograde evolution. Inclusions of subhedral to euhedral, pale greenish to brownish hornblende (Hbl1), optically zoned subhedral plagioclase (Pl1), ilmenite (Ilm1), rutile (Rt1), biotite (Bt1) and clinozoisite (Czo1; Fig. 5.2b) testify to the replacement of an early, amphibolite facies Bt-Czo-Hbl-Pl-Rt-Ilm assemblage during prograde metamorphism. Bt1 inclusions are separated from the Grt2 host by greenish Hbl1, whereas a corona of plagioclase is developed between Rt1 inclusions and the hosting Grt2. Poikiloblastic Cpx2 contains numerous corroded Pl1 and Opx1 inclusions in the core (Fig. 5.2c), whereas Cpx2 margins are virtually devoid of inclusions, thus suggesting that both Pl1 and Opx1 were consumed during the prograde evolution. The inclusion patterns moreover indicate the presence of a granulite facies Opx-Pl assemblages prior to the peak-metamorphic growth of coarse-grained Cpx2 and Grt2.

Stage 3: Corona and symplectite formation

During the early retrograde evolution fine-grained composite corona textures developed between Grt2 and Cpx2 (Fig. 5.2a): Block-like orthopyroxene (Opx3), locally intergrown with Pl3, forms rims around Cpx2 (Fig. 5.2a & d). Opx3-Pl3 intergrowths also occur around Grt2 in the absence of Cpx2 (Fig. 5.2e).

Stage 4: Re-growth of hornblende

Between retrograde Opx3-Pl3 intergrowth and Grt2 a corona of granoblastic, subhedral to euhedral greenish hornblende (Hbl4) and anhedral plagioclase (Pl4), followed by a radial coronitic Hbl4-Pl4 symplectite adjacent to the Grt2 margins, is developed (Fig. 5.2.a & e). Locally anhedral pale yellow epidote (Ep4) occurs in the Hbl4-Pl4 symplectites (Fig. 5.2f). Hbl4 furthermore forms monomineralic corona textures around Ilm2.

Extensive amphibolitization of the Grt-Cpx granulites is interpreted to result from high fluid flow within the hosting shear zone.

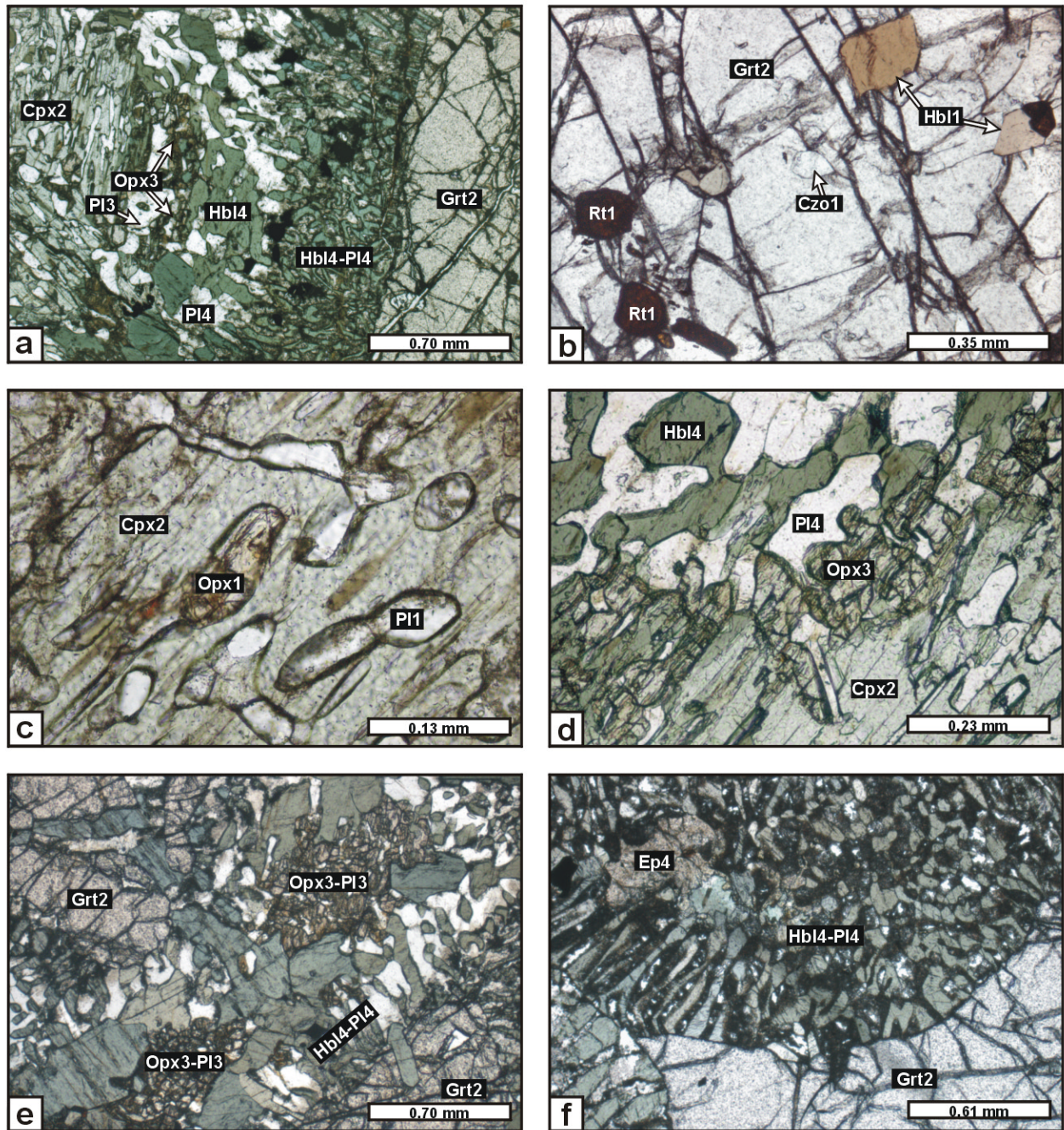


Fig. 5.2: Photomicrographs illustrating the metamorphic evolution of the mafic Grt-Cpx granulites of the Epembe Unit (sample B-311-3-00). **a)** Grt2 is separated by a composite corona of Opx3-Pi3, followed by a Hbl4-Pi intergrowth and a Hbl4-Pi4 symplectite adjacent to Grt2, from formerly coexisting Cpx2. **b)** Inclusions of brownish Hbl1, Rt1 and Czo1 in Grt2. **c)** Corroded inclusion of Opx1 and Pi1 in Cpx2. **d)** Monomineralic rim of Opx3, followed by a granoblastic Hbl4-Pi4 intergrowth, around Cpx2. **e)** Opx3-Pi3 intergrowth around Grt2, followed by a granoblastic Hbl4-Pi4 intergrowth and a Hbl4-Pi4 symplectite adjacent to Grt2. **f)** Hbl4-Pi4 symplectite with Ep4, formed at the expense of Grt2.

5.1.1.3 (Grt-bearing) Opx-Pl-Qtz granulites

samples: B-212-B-98, B-231-A-98, B-465-2-99, B-536-1-99, B-537-1-99, B-537-2-99, B-556-2-99, B-556-3-99, B-574-3-99, B-574-4-99, B-692-00 (Grt-bearing), B-700-3-00 (Grt-bearing)

Stage 1: Prograde evolution and stage 2: Peak-metamorphic assemblages

The (Grt-bearing) Opx-Pl-Qtz granulites of the metamorphosed dykes contain abundant fine-grained, anhedral to subhedral orthopyroxene (Opx₂), which is commonly aligned, defining a weak S₁ foliation. Opx₂ is part of a fine-grained, granoblastic matrix mainly consisting of Opx₂, plagioclase (Pl₂) and quartz (Qtz₂). Abundant fine-grained ilmenite (Ilm₂) is oriented parallel to the S₁ foliation. Rare garnet (Grt₂) is present as anhedral porphyroblast in the granoblastic Opx-Pl-Qtz-Ilm matrix.

Inclusions of biotite (Bt₁) in Grt₂ and in Opx₂ suggest the prograde replacement of an early biotite-bearing mineral assemblage.

Stage 3: Corona and symplectite formation

Peak-metamorphic Grt₂ is partially replaced by Opx₃-Pl₃ intergrowths, which form thin corona textures around Grt₂, separating it from matrix Qtz₂ (Fig. 5.3a).

Stage 4: Re-growth of garnet

Late Grt₄, coexisting with Qtz₄, forms thin continuous rims around peak-metamorphic Opx₂, separating it from Pl₂ (Fig. 5.3b).

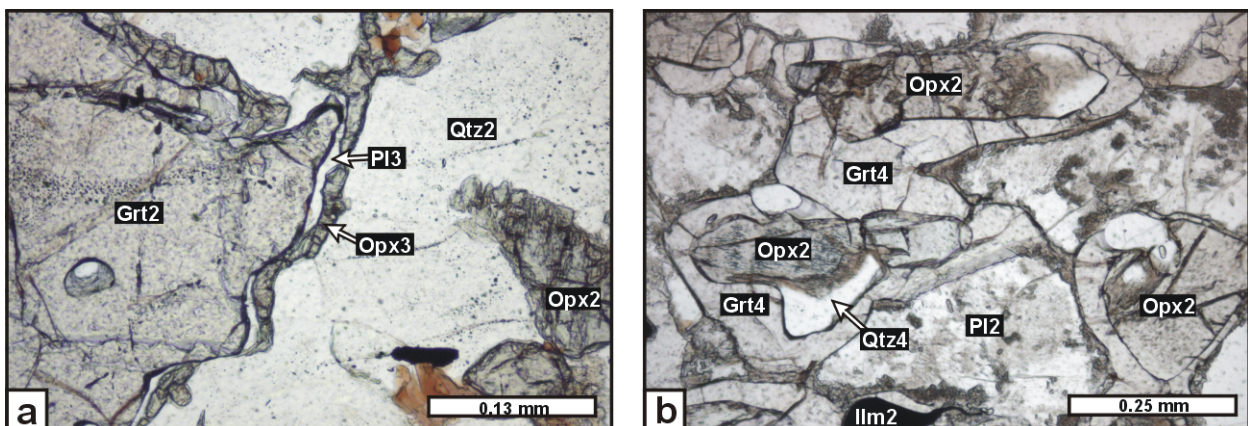


Fig. 5.3: Photomicrographs illustrating the metamorphic evolution of the mafic (Grt-bearing) Opx-Pl-Qtz granulites of the intermediate dykes of the Epembe Unit **a)** Corona of Opx₃ and Pl₃ around Grt₂, separating it from matrix Qtz₂ (Grt-bearing Opx-Pl-Qtz granulite B-700-3-00). **b)** Corona of Grt₄ coexisting with Qtz₄ around Opx₂, separating it from Pl₂ (Grt-bearing Opx-Pl-Qtz granulite B-465-2-99).

5.1.2 Felsic granulites and Grt-Opx metagranitoids

Metavolcanic felsic granulites of acid composition, termed as pyroxene-bearing granulites, are the most frequent rock type of the volcano-sedimentary sequence of the Epembe Unit, whereas Grt-Opx metagranitoids constitute rare and small bodies intrusive into the volcano-sedimentary sequence.

(1) The felsic ***Px-bearing granulites*** are garnet-free quartzofeldspathic rocks predominantly consisting of quartz (53-61 vol.%), K-feldspar (0-35 vol.%) and plagioclase (0-45 vol.%). Clinopyroxene (0-2 vol.%) and orthopyroxene (0-10 vol.%) may be present in minor amounts. Hornblende, biotite, epidote, actinolite, chlorite, zircon, apatite, magnetite, ilmenite and titanite are accessory phases.

(2) The ***Grt-Opx metagranitoids*** are quartzofeldspathic rocks, which are commonly dominated by quartz (13-45 vol.%). K-feldspar (0-45 vol.%) and plagioclase (2-52 vol.%) occur in highly variable amounts. While garnet is preserved in all samples (5-18 vol.%), orthopyroxene (0-21 vol.%) may be completely replaced during retrogression. Biotite (0-10 vol.%), pargasitic hornblende (0-1 vol.%), actinolite (0-5 vol.%) and chlorite (0-3 vol.%) occur as retrograde phases in most samples. Green spinel, ilmenite, zircon, hematite, monazite, apatite and rutile are common accessories.

Mineral assemblages

Based on the peak-metamorphic mineral assemblages four types of felsic Px-bearing granulites and two types of Grt-Opx metagranitoids are distinguished (Table 5.2). The presence of orthopyroxene, generally coexisting with K-feldspar and quartz, and the lack of biotite demonstrates granulite facies peak-metamorphic conditions for both the felsic Px-bearing granulites and the Grt-Opx metagranitoids:

(1) Most felsic ***Px-bearing granulites*** are composed of peak-metamorphic quartz (Qtz₂) and plagioclase (Pl₂), coexisting with minor orthopyroxene (Opx₂) and, in most samples, with abundant K-feldspar (Kfs₂). Two Opx₂-bearing felsic granulites contain peak-metamorphic clinopyroxene (Cpx₂). Furthermore one Cpx₂-bearing felsic granulite has been observed, which lacks Opx₂. The peak-metamorphic pyroxenes may be partly or completely replaced by hornblende (Hbl₄), biotite (Bt₄) and quartz (Qtz₄) during retrogression (stage 4).

(2) The inhomogeneous ***Grt-Opx metagranitoids*** compositionally range from charnockite to enderbite. Peak-metamorphic quartz (Qtz₂) and plagioclase (Pl₂) constitute a quartzofeldspathic matrix, with or without K-feldspar (Kfs₂; Table 5.2). Coexisting garnet (Grt₂) and orthopyroxene (Opx₂) are present as porphyroblasts. During retrogression (stage 4) Grt₂ and

Opx₂ were partly or completely replaced by fine-grained intergrowths composed of biotite (Bt₄), actinolite (Act₄), chlorite (Chl₄) and hornblende (Hbl₄). In addition, a second generation of garnet (Grt₄) was formed.

n	stage 2				stage 4
<i>Felsic Px-bearing granulites</i>					
4	Opx	Kfs	Pl	Qtz	Hbl, Bt, Qtz, Act, Chl, Ep
4	Opx		Pl	Qtz	Hbl, Bt, Qtz, Act, Chl, Ep
2	Opx	Cpx	Kfs	Pl Qtz	Hbl, Bt, Qtz, Act, Chl, Ep
1		Cpx	Kfs	Pl Qtz	Hbl, Bt, Qtz, Act, Chl, Ep
<i>Grt-Opx metagranitoids</i>					
5	Grt	Opx	Kfs	Pl Qtz	Grt, Bt, Chl
8	Grt	Opx		Pl Qtz	Grt, Hbl, Bt, Act, Chl

Table 5.2: Mineral assemblages of the metavolcanic felsic granulites and of the Grt-Opx metagranitoids of the Epembe Unit (n: number of investigated rock samples).

Texture

Both, the felsic *Px-bearing granulites* and the *Grt-Opx metagranitoids* show a massive texture, lacking a preferred orientation of both the peak-metamorphic and the retrograde phases.

5.1.2.1 Felsic pyroxene-bearing granulites

samples: B-206-C-98, B-207-C-98, B-208-B-98, B-229-A-98, B-230-C-98, B-380-99, B-382-99, B-434-1-99, B-531-99, B-614-2-99, B-671-1-00

Stage 1: Prograde evolution and Stage 2: Peak-metamorphic assemblages

The felsic Px-bearing granulites are dominated by fine-grained quartz (Qtz₂) coexisting with perthitic K-feldspar (Kfs₂) and antiperthitic plagioclase (Pl₂). These minerals constitute a granoblastic, equigranular and fine-grained matrix (average grain size: 0.5 mm), with generally straight grain boundaries being developed between Kfs₂, Pl₂ and Qtz₂. Fine-grained (< 0.3 mm), anhedral to subhedral orthopyroxene (Opx₂) and fine-grained (< 0.2 mm), anhedral clinopyroxene (Cpx₂) may occur in minor amounts in the quartzofeldspathic matrix (Fig. 5.4a).

Unfortunately, all the above mentioned peak-metamorphic phases are virtually devoid of mineral inclusions, thus making it impossible to infer a possible prograde mineral assemblage.

Stage 4: Re-growth of hornblende and biotite

Peak-metamorphic pyroxene, magnetite and ilmenite are surrounded by fine-grained retrograde intergrowths of green pargasitic hornblende (Hbl4) and quartz (Qtz4) or by a monomineralic seam of biotite (Bt4). Both ortho- and clinopyroxene are partially to completely altered to fine-grained intergrowths of epidote (Ep4), chlorite (Chl4) and actinolite (Act4).

5.1.2.2 Grt-Opx metagranitoids

samples: B-206-B1-98, B-206-B2-98, B-329-1-99, B-329-3-99, B-490-99, B-646-1-00, B-646-2-00, B-646-3-00, B-661-1-00, B-661-2-00, B-661-3-00, B-670-1-00, B-670-2-00

Stage 1: Prograde evolution and Stage 2: Peak-metamorphic assemblages

The Grt-Opx metagranitoids are generally characterized by a massive, granoblastic texture, lacking a preferred orientation of the mineral phases present. Anhedral to euhedral garnet porphyroblasts (Grt2) of up to 6 mm in diameter coexist with fine- to coarse-grained anhedral to subhedral orthopyroxene (Opx2) of up to 5 mm in diameter (Fig. 5.4b). Subhedral to euhedral inclusions of garnet (Grt1) in Opx2 and inclusions of orthopyroxene (Opx1) in Grt2 suggest contemporaneous growth of garnet and orthopyroxene. Grt2 and Opx2 are set in a fine- to medium-grained and partially recrystallized matrix predominantly composed of anhedral perthitic K-feldspar (Kfs2, microcline-microperthite; 0.1-3.0 mm), granoblastic quartz (Qtz2; 0.1-1.5 mm) and anhedral antiperthitic plagioclase (Pl2; 0.2-4 mm). Like Grt2 and Opx2, Pl2 contains inclusions of early formed Grt1 and Opx1. Kfs2 is partly replaced by myrmekitic plagioclase-quartz intergrowths. In quartz-free domains of the Kfs-free Grt-Opx metagranitoids Grt2 may additionally contain numerous inclusions of green spinel (Spl1; Fig. 5.4c). Fine to medium-grained ilmenite (Ilm2) and rutile (Rt2) are accessory matrix phases. Rutile also occurs as needle-like inclusions in Qtz2.

Early biotite (Bt1) is only preserved as rare corroded inclusions in Grt2, Pl2 and Opx2, indicating its replacement during prograde metamorphism. Further inclusions in the peak-metamorphic phases are quartz (Qtz1), plagioclase (Pl1) and ilmenite (Ilm1).

Stage 4: Re-growth of garnet and biotite and amphibole formation

Grt2 of the Kfs-bearing Grt-Opx metagranitoids is partially replaced by intergrowths of medium-grained green biotite (Bt4) and fine-grained, granular quartz (Qtz4, average grain sizes 0.1 mm). In addition, late Bt4 forms rims around Ilm2. Opx2 of the Kfs-bearing Grt-Opx metagranitoids is rimmed or pseudomorphosed by a lamellar intergrowth of Bt4 and Qtz4 (Fig. 5.4b). Along its

grain boundaries and along its cleavage Bt4 displays exsolution blebs of ilmenite. Opx2 of the Kfs-free Grt-Opx metagranulites is altered to fine-grained aggregates of pale green to colourless actinolite (Act4) with or without pale green chlorite (Chl4). The Act4(-Chl4) pseudomorphs are locally rimmed by fine-grained green pargasitic hornblende (Hbl4) and/or by Bt4, most probably formed prior to the alteration of Opx2 to Act4-Chl4 (Fig. 5.4d). As observed for the mafic granulites, a second generation of garnet (Grt4) is formed in the Grt-Opx metagranulites: In the Kfs-free Grt-Opx metagranulites Grt4 occurs as a corona around Opx2 separating it from Pl2. In the Kfs-bearing Grt-Opx metagranulites Grt2 is partially overgrown by late Grt4 (< 0.15 mm), the latter displaying euhedral shapes against neighbouring Qtz4 and Bt4 (Fig. 5.4b). Both Qtz4 and Bt4 were formed at the expense of Opx2 (Fig. 5.4b). Grt4 was also observed as a monomineralic corona around Ilm2. In the Kfs-free Grt-Opx metagranulites fine-grained (< 0.2 mm) subhedral Grt4 occurs in corona textures around Act4(-Chl4) pseudomorphs after Opx2 (Fig. 5.4d), where Grt4 is either associated by Bt4 and/or by Hbl4.

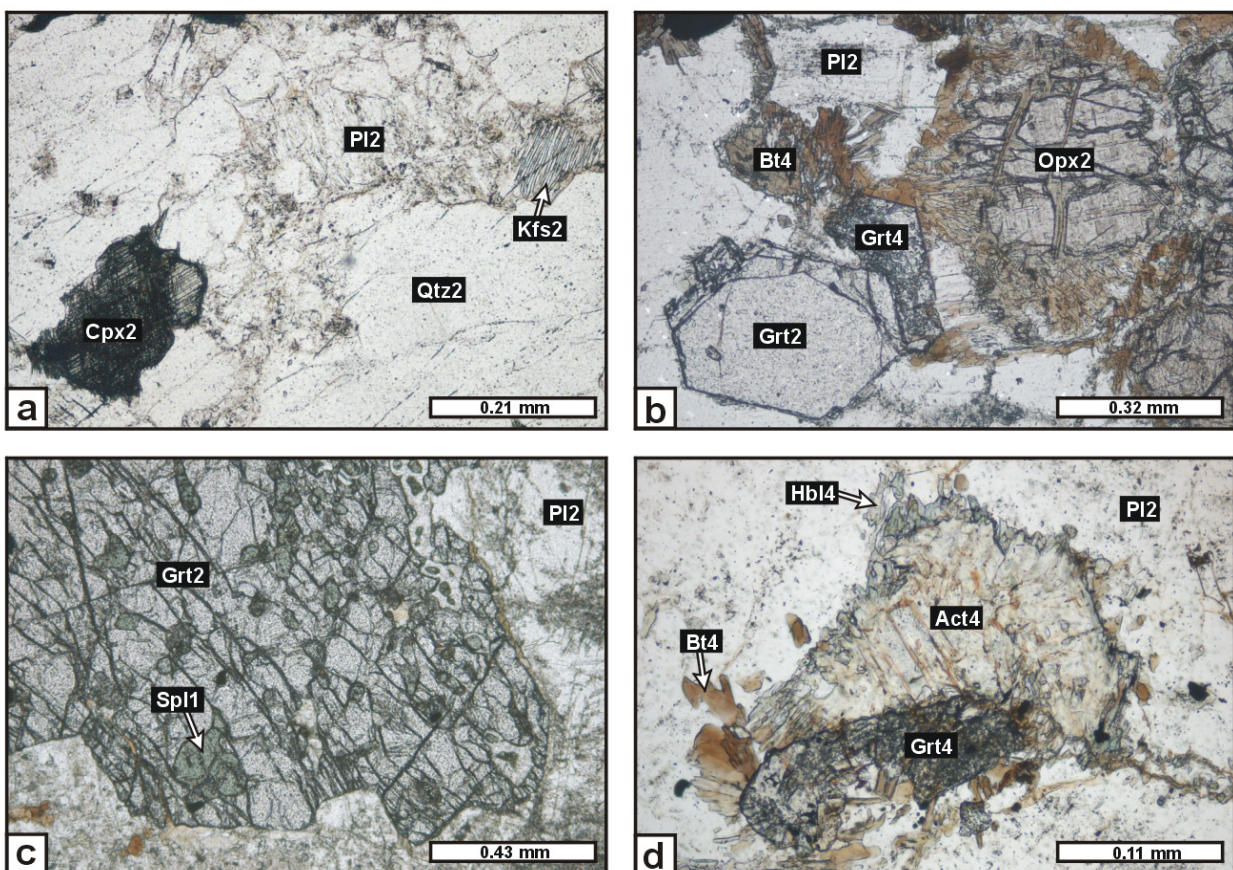


Fig. 5.4: Photomicrographs illustrating the metamorphic evolution of the metavolcanic felsic granulites and the Grt-Opx metagranulites of the Epembe Unit. **a)** Altered and corroded Cpx2 in a matrix of Kfs2, Pl2 and Qtz2 (Felsic Px-bearing granulite B-614-2-99). **b)** Coexisting Grt2 and Opx2. Opx2 is partly replaced by Bt4-Qtz4 intergrowths and Grt2 is partly rimmed by re-grown Grt4 (Grt-Opx metagranulite B-646-1-00). **c)** Grt2 with inclusions of Spl1 (Grt-Opx metagranulite B-329-3-99). **d)** Rim of green Hbl4 and Grt4 on former Opx2, which is altered to Act4 (Grt-Opx metagranulite B-661-1-00).

5.1.3 Paragneisses

Based on field observations and bulk-rock chemical data the paragneisses of the Epembe Unit are subdivided into:

Major formations

- Metagreywacke-type Fe-rich Grt-Opx gneisses
- Metagreywacke-type Mg-rich Grt-Opx gneisses
- Quartz-rich Grt-Opx rocks
- Metagreywacke-type Grt gneisses
- Metapelitic Grt-Sil gneisses

Restitic domains

- Sapphirine-bearing Opx-Sil gneisses
- Opx-Grt rocks

Due to similarities in composition, mineral assemblages and reaction textures, the following lithological units have been grouped together for the petrographic description: (1) Metagreywacke-type Mg-rich Grt-Opx gneisses and Qtz-rich Grt-Opx rocks, (2) metagreywacke-type Grt gneisses and metapelitic Grt-Sil gneisses and (3) restitic sapphirine-bearing Opx-Sil gneisses and Opx-Grt rocks.

5.1.3.1 Fe-rich Grt-Opx gneisses

Kfs-bearing samples: B-461-2-99, B-462-99, B-486-5-99, B-492-99, B-556-1-99, B-564-2-99, B-572-1-99, B-615-3-99, B-686-00, B-690-1-00

Kfs-free samples: B-447-4-99, B-461-1-99, B-466-3-99, B-509-3-99, B-564-3-99, B-572-3-99, B-690-2-00, B-691-2-00

The Fe-rich Grt-Opx gneisses are generally quartzofeldspathic rocks with high modal amount of quartz (22-51 vol.%) and plagioclase (15-39 vol.%). Ten of the 18 samples investigated contain K-feldspar (Table 5.3), which is present in highly variable amounts (3-32 vol.%). Orthopyroxene (6-25 vol.%), garnet (3-16 vol.%) and ilmenite (1-3 vol.%) occur in both Kfs-free and Kfs-bearing samples. Biotite (0-8 vol.%) and green spinel (0-1 vol.%) may be present in minor amounts. Zircon is a common accessory phase, whereas apatite has only been observed in two of 18 samples investigated.

Mineral assemblages

The Fe-rich Grt-Opx gneisses display quite uniform peak-metamorphic mineral assemblages and retrograde reaction textures (Table 5.3). The generally fine- to medium-grained rocks comprise a small-scaled compositional banding, which is defined by layers rich in orthopyroxene (Opx₂) with minor amounts of quartz (Qtz₂), K-feldspar (Kfs₂), plagioclase (Pl₂) and ilmenite (Ilm₂), alternating with Opx-poor quartzofeldspathic layers, which may contain minor amounts of biotite (Bt₂). Coarse-grained garnet porphyroblasts (Grt₂) occur in both the Opx-rich and Opx-poor layers and may locally coexist with minor green spinel (Spl₂).

A variety of retrograde reaction textures largely obliterate the peak-metamorphic assemblage: Between Grt₂ and Qtz₂ a broad plagioclase (Pl₃)-orthopyroxene (Opx₃) corona is developed, whereas orthopyroxene (Opx₂ and Opx₃) is replaced by a biotite(Bt₄)-quartz(Qtz₄) symplectite, with or without late garnet (Grt₄). Grt₄ is also present as re-growth rims on Grt₂, where it is intergrown with quartz (Qtz₄) or with the Bt₄-Qtz₄ symplectite.

n	stage 2								stage 3	stage 4
10	Grt	Opx	Kfs	Pl	Qtz	Ilm	±Bt	±Spl	Opx, Pl	Grt, Bt, Qtz
8	Grt	Opx		Pl	Qtz	Ilm	±Bt	±Spl	Opx, Pl	Grt, Bt, Qtz

Table 5.3: Mineral assemblages in the Fe-rich Grt-Opx gneisses of the Epembe Unit (n: number of investigated rock samples).

Texture

A weak foliation (S_1), oriented sub-parallel to the compositional banding, is defined by aligned peak-metamorphic Opx₂ and Bt₂, whereas mineral inclusions in the peak-metamorphic phases as well as minerals formed during retrogression of the rocks lack a preferred orientation.

Stage 1: Prograde evolution and Stage 2: Peak-metamorphic assemblages

The matrix of the Fe-rich Grt-Opx gneisses mainly consists of (1) layers rich in granoblastic to elongated, anhedral to subhedral orthopyroxene (Opx₂; up to 2.5 mm in diameter) and containing only minor amounts of granoblastic, fine-grained and anhedral quartz (Qtz₂), K-feldspar (Kfs₂) and plagioclase (Pl₂), alternating with (2) Opx-poor to Opx-free quartzofeldspathic layers (Fig. 5.5a). Kfs₂ commonly shows string and/or patch perthite exsolution whereas Pl₂ is antiperthitic. Straight grain boundary contacts are developed between peak-metamorphic Opx₂, Kfs₂, Pl₂ and Qtz₂, indicating their crystallization under equilibrium

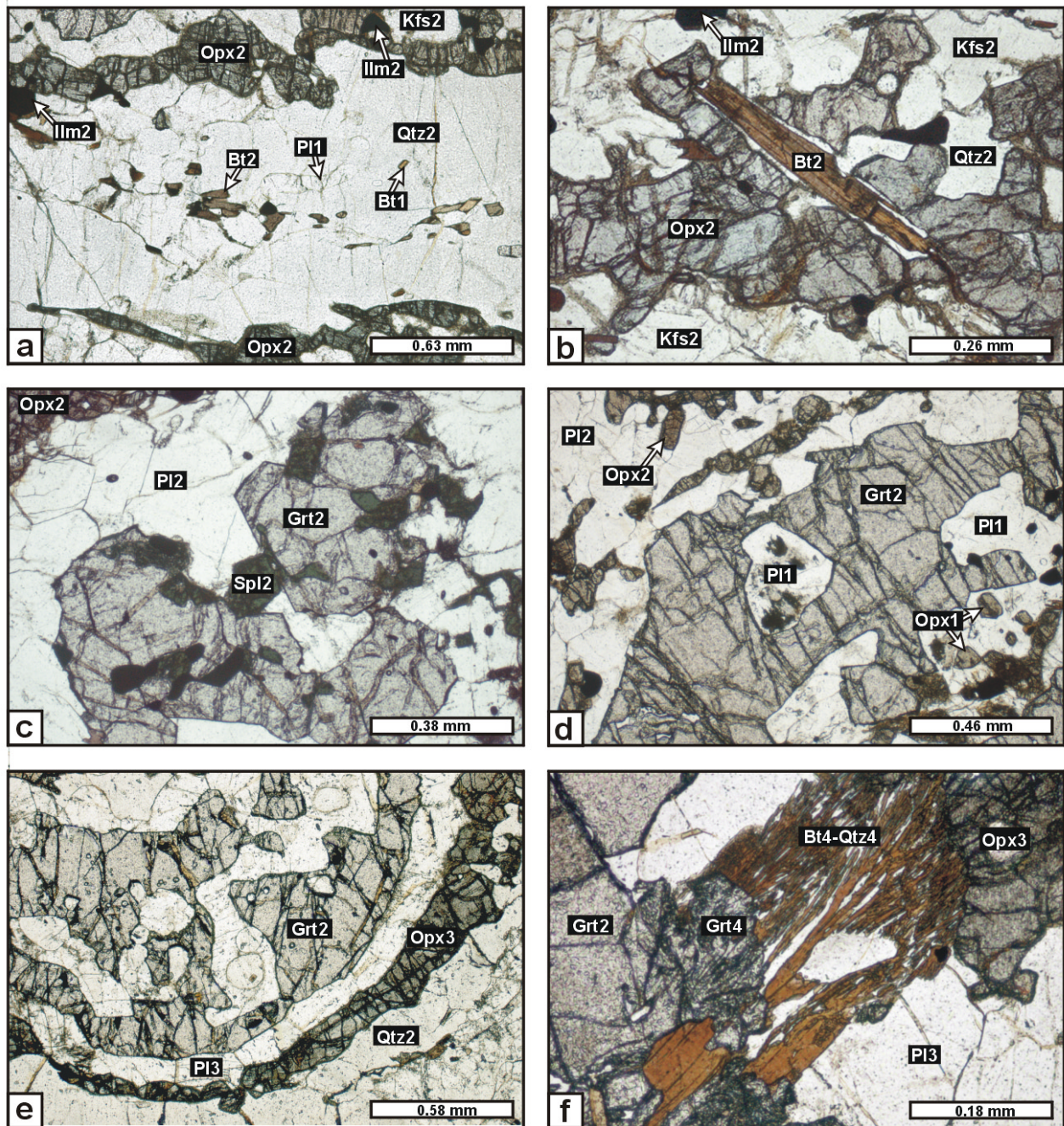


Fig. 5.5: Photomicrographs illustrating the metamorphic evolution of the Fe-rich Grt-Opx gneisses of the Epembe Unit. **a)** Opx2-free layer with matrix Bt2 and with inclusions of Bt1 and Pl1 in Qtz2. The biotite-bearing layer is surrounded by biotite-free layers, which consists of Kfs2, Opx2 and Ilm2 (Fe-rich Grt-Opx gneisses B-691-2-00). **b)** Corona of Opx2, coexisting with Kfs2, around Bt2 (Fe-rich Grt-Opx gneiss B-690-1-00) **c)** Intergrowth of Grt2 and Spl2 in a quartz-free layer (Fe-rich Grt-Opx gneiss B-690-2-00). **d)** Poikiloblastic Grt2 with inclusions of Opx1 and Pl1 (Fe-rich Grt-Opx gneiss B-691-2-00). **e)** Corona of Opx3 and Pl3 around Grt2, separating it from Qtz2 (Fe-rich Grt-Opx gneiss B-690-2-00). **f)** Rim of euhedral Grt4, which is intergrown with a symplectite of Bt4 and Qtz4, around peak-metamorphic Grt2. The Bt4-Qtz4 intergrowth partly replaces coronitic Opx3 and Pl3 (Fe-rich Grt-Opx gneiss B-690-2-00).

conditions. Resorbed, anhedral garnet (Grt2) occurs as porphyroblasts of up to 2.5 cm in diameter in the fine- to medium-grained matrix. Peak-metamorphic, fine-grained and red-brown biotite (Bt2) is only rarely preserved and is restricted to layers, that are devoid of Opx2 (Fig. 5.5a). In these zones Bt2 is commonly aligned parallel to the compositional banding and the S_1 foliation, indicating its syn-tectonic formation. In cases, Bt2 is surrounded by a monomineralic corona of Opx2, coexisting with matrix Kfs2 and separating Bt2 from Qtz2 (Fig. 5.5b). Opaque minerals include fine-grained anhedral ilmenite (Ilm2), that predominantly occurs in Opx2-rich layers (Fig. 5.5a), suggesting a cogenetic formation of Ilm2 and Opx2. In silica-deficient domains Grt2 is intergrown with fine-grained green spinel (Spl2; Fig. 5.5c).

Early biotite (Bt1) is preserved as corroded inclusion in matrix Grt2, Kfs2, Qtz2 and Opx2. Other mineral inclusions in these phases include plagioclase (Pl1), ilmenite (Ilm1) and quartz (Qtz1). Grt2 grains, lacking Bt1 inclusions, instead contain inclusions of orthopyroxene (Opx1; Fig. 5.5d), which indicate that anhydrous, granulite facies conditions were attained prior to garnet formation.

Stage 3: Corona formation

Between peak-metamorphic Grt2 and Qtz2 an undeformed, two-fold corona is developed (Fig. 5.5e). The corona consists of fine-grained, granular plagioclase (Pl3), adjacent to Grt2, followed by contemporaneously grown polygonal orthopyroxene (Opx3), adjacent to Qtz2 (Fig. 5.5e).

Stage 4: Re-growth of garnet and biotite

In presence of Kfs2, matrix Opx2 and late coronitic Opx3 are replaced by fine-grained symplectitic intergrowths of biotite (Bt 4) and quartz (Qtz4; Fig. 5.5f). Bt4 also forms monomineralic coronas around Ilm2. A second generation of garnet (Grt4), which is intergrown with the Bt4-Qtz4 symplectites, is commonly developed as re-growth rim on relic peak-metamorphic Grt2 (Fig. 5.5f), but also occurs as intergrowth with Bt4 in the absence of Grt2.

5.1.3.2 Qtz-rich Grt-Opx rocks and Mg-rich Grt-Opx gneisses

Qtz-rich Grt-Opx rocks

samples: B-447-5-00, B-536-2-99, B-548-1-99, B-548-2-99, B-574-2-99, B-574-5-99, B-577-1-99, B-587-1-99, B-614-1-99, B-614-3-00, B-614-4-00, B-614-10-00, B-615-1-99 and B-568-99, B-587-4-99 (Crd-bearing)

Metagreywacke-type Mg-rich Grt-Opx gneisses

samples: B-458-1-99, B-458-2-99, B-458-3-99, B-540-1-99, B-634-00

The Qtz-rich Grt-Opx rocks and the Mg-rich Grt-Opx gneisses display similar mineral assemblages, but differ in the modal abundance of the phases present:

(1) **Qtz-rich Grt-Opx rocks** contain abundant porphyroblastic garnet (25-32 vol.%), and subordinate orthopyroxene (1-4 vol.%). Garnet and orthopyroxene are set in a matrix, which is dominated by quartz (47-51 vol.%) with minor plagioclase (1-2 vol.%), K-feldspar (0-3 vol.%), ilmenite (1-3 vol.%) and biotite (3-7 vol.%). Cordierite (2-12 vol.%) and spinel (< 1 vol.%) generally occur in symplectite and corona textures. Sillimanite, rutile and zircon are present as accessories. Only two of 15 samples (B-568-99; B-587-4-99) contains porphyroblastic cordierite (15 vol.%).

(2) In contrast, the **metagreywacke-type Mg-rich Grt-Opx gneisses** are generally dominated by orthopyroxene (14-31 vol.%), coexisting with subordinate garnet (10-18 vol.%). Quartz (10-28 vol.%) is less abundant than in the Qtz-rich Grt-Opx rocks whereas plagioclase (11-26 vol.%) and biotite (10-18 vol.%) are more frequent. As in the Qtz-rich Grt-Opx rocks, K-feldspar (2-3 vol.%) is generally rare. Cordierite (1-12 vol.%) and spinel (0-1 vol.%) are present in symplectite and corona textures. Common accessory phases are sillimanite, rutile, ilmenite, zircon and apatite.

Mineral assemblages

While the Qtz-rich Grt-Opx rocks and the Mg-rich Grt-Opx gneisses display similar peak-metamorphic and retrograde mineral assemblages (Table 5.4), they exhibit differing structures:

(1) The homogeneous **Qtz-rich Grt-Opx rocks** are dominated by porphyroblasts of garnet (Grt₂), orthopyroxene (Opx₂) and, if present, cordierite (Crd₂), which are set in a fine-grained, massive to weakly foliated matrix of granoblastic quartz (Qtz₂), plagioclase (Pl₂) and K-feldspar (Kfs₂) with rare biotite (Bt₂), rutile (Rt₂) and ilmenite (Ilm₂).

(2) In contrast, the metagreywacke-type **Mg-rich Grt-Opx gneisses** display a migmatitic structure with the original compositional banding being modified by the development of frequent leucocratic layers and streaks, which are essentially composed of Grt₂, Opx₂, Pl₂, Qtz₂ and rare Kfs₂ and are interpreted as leucosomes. In general, two types of leucosomes can be distinguished: (i) The most abundant type of leucosome is concordant to the compositional banding and strongly deformed. These domains are interpreted to be derived from partial melting during the prograde metamorphism. (ii) In contrast, rare undeformed leucosomes cross-cut the compositional banding. Melanocratic layers and lenses comprise a restitic mineralogy, dominated by Opx₂ and subordinate Grt₂ coexisting with minor Pl₂, Qtz₂ and rare Kfs₂.

Peak-metamorphic Grt₂ and Opx₂ of both rock types are extensively replaced by conspicuous retrograde symplectite and corona textures consisting of cordierite (Crd₃), orthopyroxene

(Opx3), plagioclase (Pl3), spinel (Spl3) and ilmenite (Ilm3). Subsequently, the symplectite phases were partly replaced by biotite (Bt4) and garnet (Grt4). Bt4 is in turn surrounded by orthopyroxene (Opx5)-cordierite (Crd5) symplectites.

n	stage 2				stage 3				stage 4	stage 5	
<i>Qtz-rich Grt-Opx rocks</i>											
13	Grt	Opx	±Kfs	Pl	Qtz	±Bt	Ilm	Rt	Crd, Opx, Spl, Pl, Ilm	Grt, Bt	Opx, Crd
2	Grt	Opx	Crd	Pl	Qtz		Ilm	Rt		Grt, Bt, Sil	
<i>Mg-rich Grt-Opx gneisses</i>											
5	Grt	Opx	±Kfs	Pl	Qtz		Ilm	±Rt	Crd, Opx, Spl, Pl, Ilm	Bt	Opx, Crd

Table 5.4: Mineral assemblages in the Qtz-rich Grt-Opx rocks and the Mg-rich Grt-Opx gneisses of the Epembe Unit; (n: number of investigated rock samples).

Texture

In both rock types a weak S_1 foliation, oriented sub-parallel to the compositional banding is defined by aligned peak-metamorphic Opx2, Rt2 and Ilm2 and, if present, Bt2, indicating their growth prior to, or synchronous with, ductile D_1 deformation. In contrast, mineral inclusions in the peak-metamorphic phases (stage 1) show no preferred orientation; thus, evidence for an early foliation pre-dating the external S_1 foliation is not preserved in the rock samples investigated. This demonstrates the absence of an early deformation event pre-dating D_1 . Minerals formed during retrogression of the rocks (stage 3 to stage 5) lack a preferred orientation, indicating that the formation of the retrograde phases post-dated the development of the S_1 foliation.

Stage 1: Prograde evolution and Stage 2: Peak-metamorphic assemblages

The **Qtz-rich Grt-Opx rocks** are dominated by megacrystic anhedral garnet (Grt2) porphyroblasts of up to 5 cm in diameter, set in the quartz (Qtz2)-rich matrix. Fine-grained plagioclase (Pl2) and microperthitic K-feldspar (Kfs2), that locally show recrystallization to fine-grained neoblasts at grain boundaries, appear as isolated and anhedral grains in the quartzitic matrix. Grt2 coexists with porphyroblastic orthopyroxene (Opx2; up to 6 mm in diameter). Subhedral Opx2 exhibits exsolved platelets of ilmenite parallel (100). Kink bands and undulose extinction are evidence for strong deformation of Opx2. The dominant Ti-phase of the matrix is rutile (Rt2), whereas ilmenite (Ilm2) is rare. Biotite (Bt2) is a minor constituent of the quartzitic matrix where it is aligned parallel to the main S_1 foliation and occurs isolated from Grt2 and Opx2; therefore, its retrograde formation is rather unlikely and Bt2 is consequently attributed to

the peak-metamorphic assemblage. In the cordierite-bearing Qtz-rich Grt-Opx rock sample B-587-4-99 Grt2 and Opx2 coexist with subhedral cordierite (Crd2) of up to 1.2 mm in diameter as is indicated by locally preserved straight grain boundary contacts. Equilibrium conditions between the phases are furthermore supported by inclusions of Crd2 and Opx2 in Grt2, that, in turn, occurs as euhedral inclusion (< 0.2 mm) in Crd2. In contrast to the other Qtz-rich Grt-Opx rocks, euhedral to subhedral porphyroblastic Grt2 (< 1 cm) of sample B-587-4-99 is unresorbed.

As in the Qtz-rich Grt-Opx rocks, Grt2 (< 5 mm) and Opx2 (< 1 cm) of the *Mg-rich Grt-Opx gneisses* locally exhibit straight grain boundaries, suggesting their crystallization under equilibrium conditions.

The peak-metamorphic minerals of both rock types contain similar but rare mineral inclusions, that are ascribed to specific prograde metamorphic assemblages. Porphyroblastic Grt2 exhibits inclusions of corroded biotite (Bt1) and irregular inclusion trails of fibrolitic and prismatic sillimanite (Sil1; Fig. 5.6a), which is absent from the matrix. Further inclusions in Grt2 are rutile (Rt1), quartz (Qtz1), ilmenite (Ilm1) and plagioclase (Pl1). Porphyroblastic Opx2 encloses Bt1, Pl1 and Qtz1. In places, subhedral to euhedral grains of inclusion-free garnet (Grt1; < 0.25 mm) are enclosed in Opx2 cores (Fig. 5.6b), suggesting contemporaneous growth of both phases. These inclusion patterns testify to an early Bt-Sil-Pl-Qtz assemblage, that was replaced by the coarse-grained peak-metamorphic Grt-Opx assemblage.

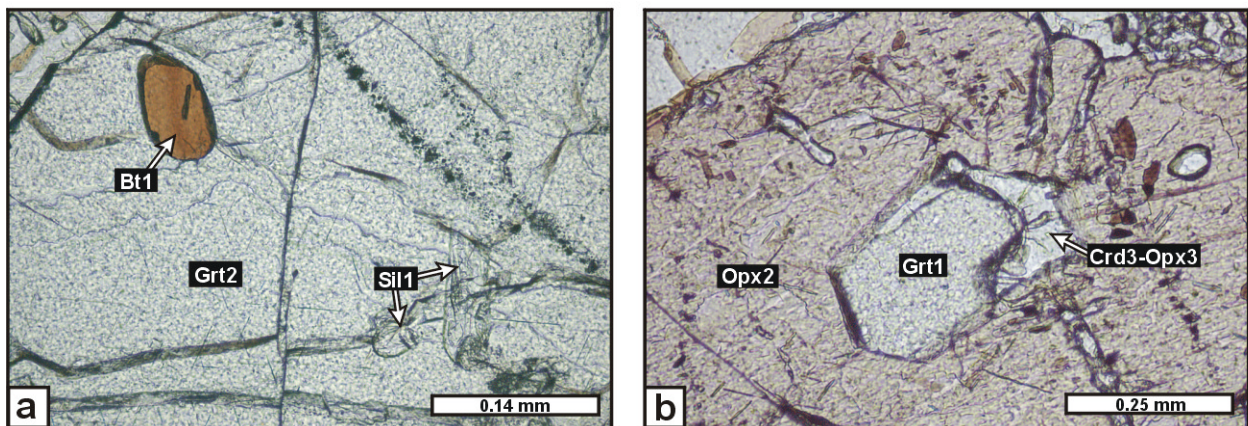


Fig. 5.6: Photomicrographs illustrating the prograde metamorphic evolution (stage 1) of the Mg-rich Grt-Opx gneisses and the Qtz-rich Grt-Opx rocks of the Epembe Unit. **a)** Inclusions of corroded Bt1 and Sil1 in porphyroblastic Grt2 (Mg-rich Grt-Opx gneiss B-634-00). **b)** Subhedral inclusion of Grt1 partly preserves straight grain boundaries against hosting porphyroblastic Opx2. Grt1 is locally replaced by a late Crd3-Opx3 symplectite (Qtz-rich Grt-Opx rock B-458-1-99).

Stage 3: Corona and symplectite formation

Between Grt2 and matrix Qtz2, complex corona textures are developed, that partly outline the shape of former euhedral Grt2 (Fig. 5.7a): An outer, relatively coarse-grained collar consists of Opx3 and granoblastic Pl3. The inner part of the corona in contact to Grt2 is composed of a double-layer symplectitic intergrowth of Opx3 and Crd3 (Fig. 5.7a & b). These Crd-Opx symplectites probably formed subsequently to the outer Opx-Pl collar since they are localized on individual garnet grains whereas the Opx-Pl symplectites form a continuous corona around several adjacent garnet grains or grain fragments (Fig. 5.7a). While the inner part of the Crd-Opx symplectite is formed by a dactylitic Crd-Opx intergrowth, which is dominated by Crd3, the outer part is predominantly or completely composed of Opx3 (Fig. 5.7b). The Crd-Opx symplectites may contain dispersed and fine-grained Pl3 and late Ilm3. In contrast to the scarce Opx-Pl collars, the Crd-Opx symplectites are present in all studied samples partially or completely replacing Grt2 and/or filling fissures in the outer margins of Grt2. In contrast, fissures in Grt2 cores contain a very fine-grained symplectitic intergrowth consisting of Opx3, Crd3 and green Spl3 (Fig. 5.7c), with symplectitic Opx3 and Spl3 commonly forming lamellar intergrowths. Similar Opx-Spl symplectites developed between porphyroblastic Opx2 and Grt2 (Fig. 5.7d). Symplectites composed of Crd3 and green Spl3, surrounded by a monomineralic Crd3 corona, are observed in Grt2 (Fig. 5.7e). These Crd-Spl symplectites are suggested to have formed through local replacement of former Sil1 inclusions, as is evidenced by preserved Sil1 inclusions in Grt2. A monomineralic corona of fine-grained Crd3 is developed between porphyroblastic Opx2 and matrix Qtz2, with cordierite locally displaying straight grain boundaries against Opx2 (Fig. 5.7f).

Stage 4: Re-growth of garnet, biotite and sillimanite

The Crd-Opx symplectites developed during stage 3 are, in turn, surrounded by broad rims of platy Bt4 (Fig. 5.8a). In addition, Bt4 appears as monomineralic rims or as Bt4-Qtz4 symplectites around porphyroblastic and coronitic orthopyroxene (Fig. 5.8b). In the latter texture Bt4 is locally intergrown with Pl4. Bt4 occurs throughout the restitic domains. It has to be mentioned, however, that Bt4 is most abundant along the leucosome margins, where it predominantly formed at the expense of Opx2. It can thus be concluded that biotite re-growth is related to an interaction between the crystallizing melt and minerals of the restitic layers.

In the Qtz-rich Grt-Opx rocks, the Crd3-Opx3 symplectites are partially replaced by a second generation of garnet (Grt4), which forms fine-grained euhedral crystals (< 0.3 mm) within symplectitic Crd3-Opx3 pseudomorphs after Grt2 (Fig. 5.8c). Re-grown Grt4 preserves

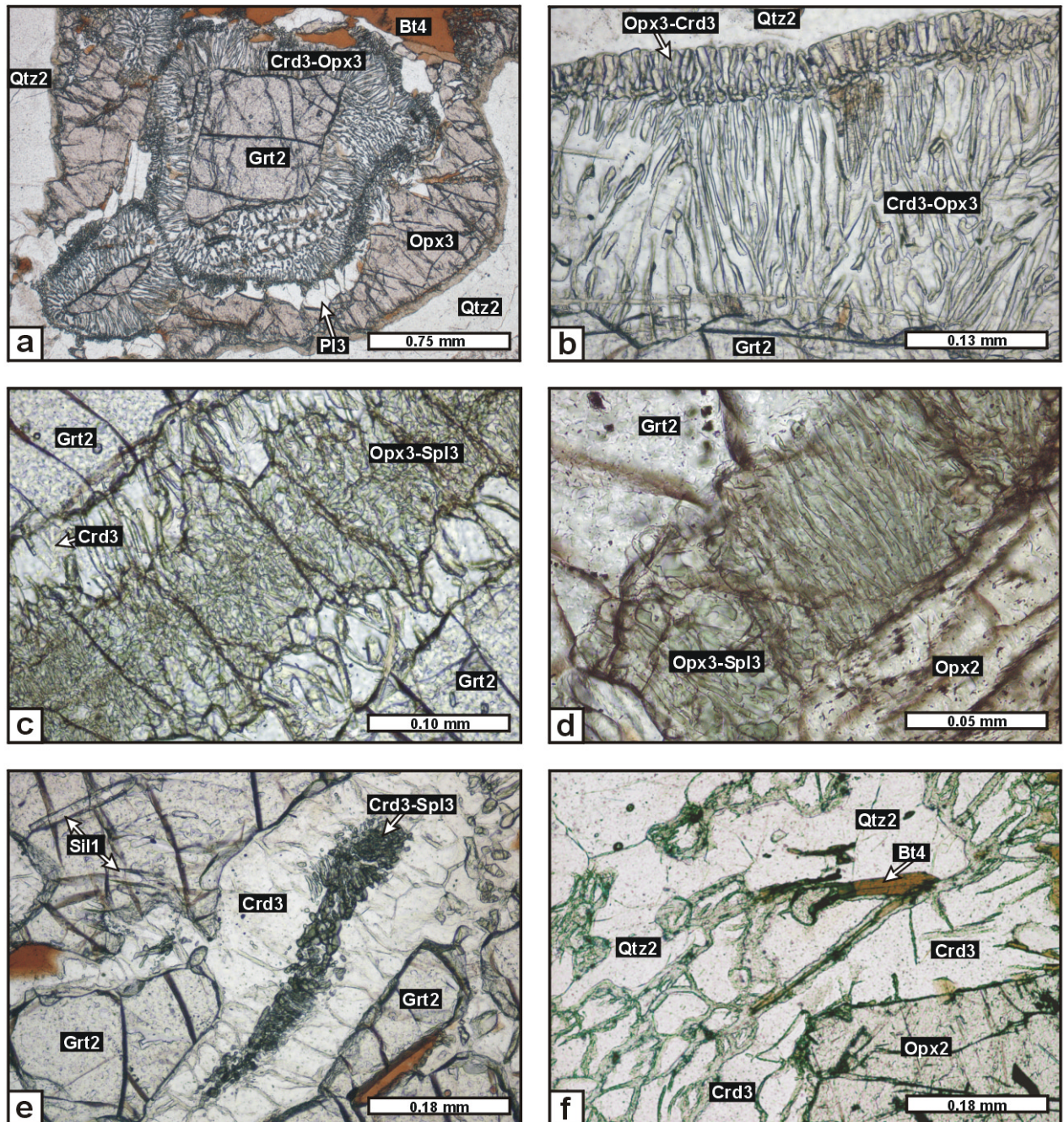


Fig. 5.7: Photomicrographs illustrating retrograde symplectite and corona textures (stage 3) of the Mg-rich Grt-Opx gneisses and the Qtz-rich Grt-Opx rocks of the Epembe Unit. **a)** Composite corona between Grt2 and Qtz2. The outer Opx3-Pl3 collar surrounds several Grt2 fragments. The inner Crd3-Opx3 symplectite is localized on individual garnet fragments (Mg-rich Grt-Opx gneiss B-634-00). **b)** Detail of the Crd3-Opx3 symplectite resorbing Grt2. The finger-like Crd3-Opx3 symplectite, dominated by Crd3, is rimmed by an Opx3-Crd3 intergrowth, which is dominated by Opx3 (Mg-rich Grt-Opx gneiss B-634-00). **c)** Crd3-Opx3-Spl3 symplectite, replacing Grt2 along fissures in Grt2 cores (Qtz-rich Grt-Opx rock B-614-3-00). **d)** Lamellar Opx3-Spl3 symplectite between Grt2 and Opx2 (Mg-rich Grt-Opx gneiss B-615-1-99). **e)** Spl3-Crd3 symplectite, rimmed by a monomineralic corona of Crd3, replacing former Sil1 inclusions in Grt2 (Mg-rich Grt-Opx gneiss B-634-00). **f)** Monomineralic Crd3 corona, separating Opx2 from Qtz2. Crd3 is partly replaced by late Bt4 (Mg-rich Grt-Opx gneiss B-634-00).

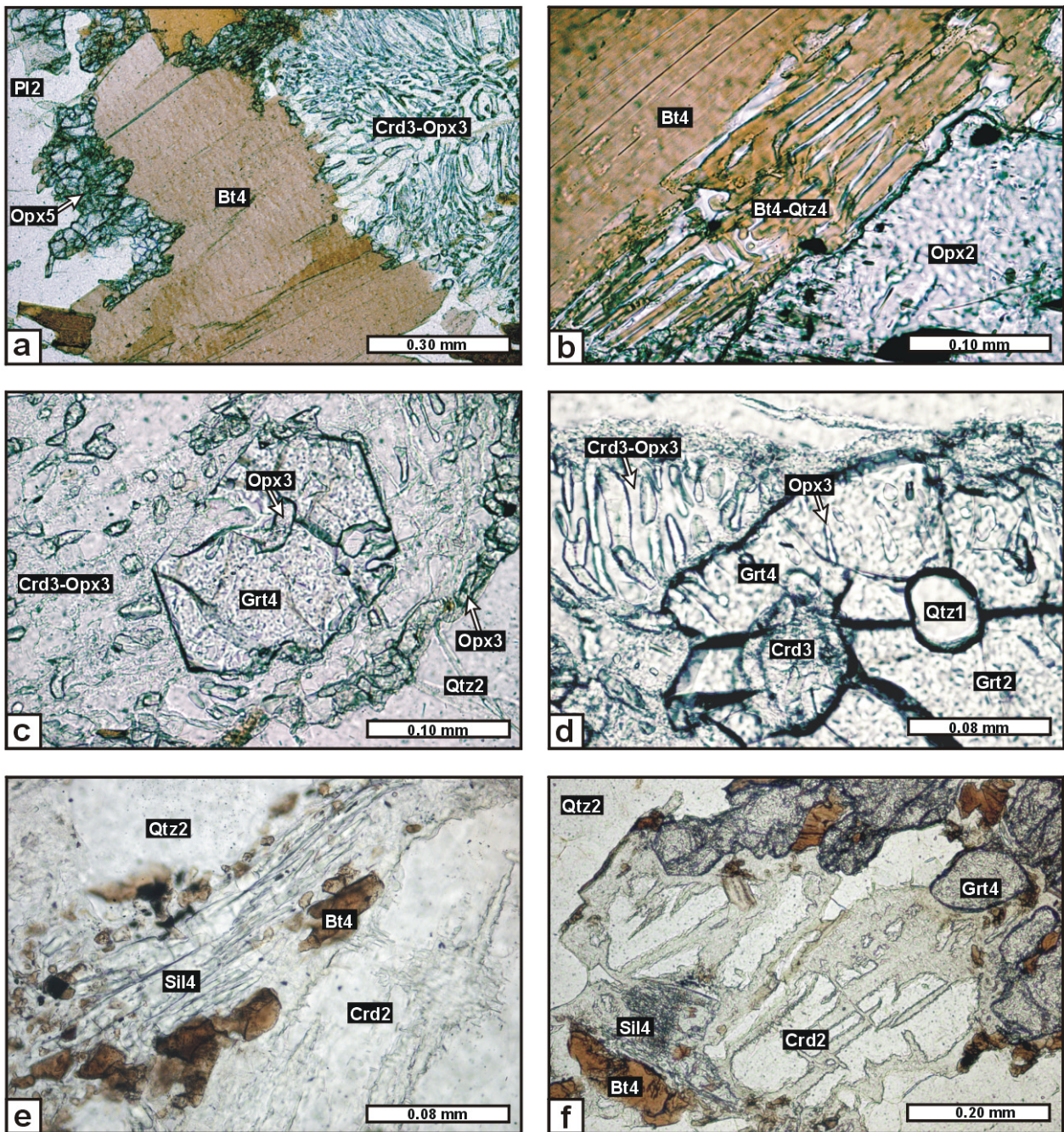


Fig. 5.8: Photomicrographs illustrating reaction textures resulting from the re-growth of garnet, biotite and sillimanite (stage 4) of the Mg-rich Grt-Opx gneisses and the Qtz-rich Grt-Opx rocks of the Epembe Unit. **a)** Rim of platy Bt4 around Crd3-Opx3 symplectite pseudomorphing former Grt2. Bt4, in turn, is partly rimmed by granoblastic Opx5 (Mg-rich Grt-Opx gneiss B-634-00). **b)** Bt4-Qtz4 symplectite, replacing Opx2 (Mg-rich Grt-Opx gneiss B-634-00). **c)** Euhedral Grt4 in Crd-Opx symplectites after former Grt2. Grt4 preserves inclusions of symplectitic Opx3. Zoning profile of Grt4 is given in Fig. 5.19a. (Qtz-rich Grt-Opx rock B-614-1-99). **d)** Grt4 re-growth rim on porphyroblastic Grt2. Grt4 encloses symplectitic Opx3 with the same orientation as Opx3 in the external Crd3-Opx3 symplectite (Qtz-rich Grt-Opx rock B-614-1-99). **e)** Intergrowth of Sil4 and Bt4, marginally replacing Crd2 (cordierite-bearing Qtz-rich Grt-Opx rock B-587-4-99). **f)** Pinitized Crd2, which is rimmed by Grt4, Sil4 and Bt4 (cordierite-bearing Qtz-rich Grt-Opx rock B-587-4-99).

inclusions of Opx3 (Fig. 5.8c) and/or Crd3, that indicate re-growth of garnet at the expense of the symplectitic phases. Grt4 furthermore appears as narrow re-grown rims on relict porphyroblastic Grt2, locally forming straight grain boundaries against Crd3-Opx3 symplectites or even enclosing elongated Crd3 and Opx3 grains, which preserved their original symplectite orientation (Fig. 5.8d). In the cordierite-bearing Qtz-rich Grt-Opx rock B-587-4-99 matrix Crd2 is replaced by late Bt4, which is intergrown with late sillimanite (Sil4; Fig. 5.8e). In places, Crd2 is rimmed by Grt4, which occurs as subhedral to euhedral grains (< 0.3 mm). In these textures Grt4 coexists with fibrolitic Sil4 and Bt4 (Fig. 5.8f). Sil4 furthermore occurs as inclusions, which lack a preferred orientation, in Grt4. Late Grt4, enclosing fibrolitic Sil4, also appears as thin re-growth rims of < 30 μm in width on porphyroblastic Grt2, separating it from adjacent Crd2).

Stage 5: Formation of late orthopyroxene and cordierite

In places, retrograde Bt4 is surrounded by a corona of fine-grained granoblastic orthopyroxene (Opx5; Figs. 5.8a & 5.9a), which is locally intergrown with very fine-grained cordierite (Crd5; Fig. 5.9b). These textures indicate that the development of Opx5 and Crd5 post-dated the re-appearance of biotite.

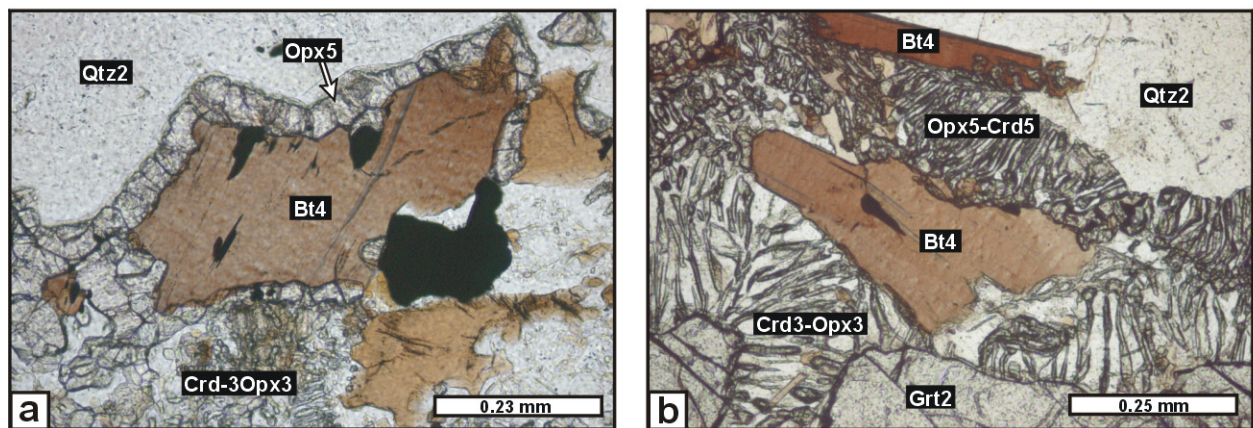


Fig. 5.9: Photomicrographs illustrating reaction textures resulting from the formation of late orthopyroxene and cordierite (stage 5) of the Mg-rich Grt-Opx gneisses and the Qtz-rich Grt-Opx rocks of the Epembe Unit. **a)** Bt4, formed at the expense of a Crd3-Opx3 symplectite, is rimmed by granoblastic Opx5 (Mg-rich Grt-Opx gneiss B-458-1-99). **b)** Platy Bt4 partly replaces a Crd3-Opx3 symplectite. Bt4, in turn, is resorbed and rimmed by an intergrowth of Opx5 and Crd5 (Mg-rich Grt-Opx gneiss B-634-00).

5.1.3.3 *Grt gneisses and Grt-Sil gneisses*

Metagreywacke-type Grt gneisses

samples: B-230-A-98, B-230-E-98, B-358-2-99, B-358-5-99, B-392-99, B-447-2-99, B-466-2-99, B-540-2-99, B-540-3-99, B-574-1-99, B-577-3-99, B-615-6-99, B-632-00, B-633-00, B-697-00

Metapelitic Grt-Sil gneisses

Qtz-bearing samples: Ku-97-85, B-206-F-98, B-212-C-98, B-230-F-98, B-426-99, B-447-3-99, B-447-6-00, B-457-99, B-465-1-99, B-466-1-99, B-486-1-99, B-486-6-99, B-488-99, B-509-2-99, B-545-1-99, B-557-2-99, B-564-1-99, B-569-99, B-570-99, B-572-2-99, B-576-99, B-587-2-99, B-615-5-99, B-625-00, B-689-00, B-699-00

Qtz-free samples: B-207-A-98, B-212-A-98, B-212-7-99, B-557-1-99

The microscopic investigation of 15 samples of Grt gneisses and 30 Grt-Sil gneiss samples revealed minor variations of the mineral phases present in the two rock types:

(1) Metagreywacke-type **Grt gneisses** contain highly variable amounts of garnet (5-30 vol.%), quartz (5-48 vol.%), plagioclase (3-45 vol.%) and K-feldspar (10-41 vol.%). In addition, spinel (0-1 vol.%), ilmenite (0-3 vol.%) and biotite (0-10 vol.%) may be present. Minor orthopyroxene (2-5 vol.%) and cordierite (2-10 vol.%) occur in symplectite textures in all samples. Accessories are sillimanite, rutile, zircon and apatite.

(2) The metapelitic **Grt-Sil gneisses** predominantly comprise quartz-bearing samples whereas quartz-free Grt-Sil gneisses are rare (Table 5.5): (i) The quartz-bearing metapelites are mainly composed of garnet (13-21 vol.%), sillimanite (5-18 vol.%), K-feldspar (25-32 vol.%) and quartz (15-30 vol.%). In addition, spinel (2-10 vol.%), orthopyroxene (2-5 vol.%), cordierite (5-12 vol.%), plagioclase (1-3 vol.%), biotite (0-3 vol.%) and ilmenite (1-2 vol.%) occur. (ii) Quartz-free metapelites contain slightly more garnet (25-28 vol.%), sillimanite (6-23 vol.%) and K-feldspar (34-50 vol.%) than Grt-Sil gneisses. Minor phases are spinel (2-3 vol.%), cordierite (3-5 vol.%), plagioclase (4-9 vol.%), biotite (1-2 vol.%) and ilmenite (1-2 vol.%). In both, Qtz-bearing and Qtz-free samples rutile, zircon and apatite are common accessories.

Mineral assemblages

As shown in Table 5.5, the metagreywacke-type Grt gneisses and the metapelitic Grt-Sil gneisses preserve similar peak-metamorphic mineral assemblages and retrograde mineral phases:

(1) The homogeneous metagreywacke-type **Grt gneisses** are dominated by porphyroblastic garnet (Grt₂), which is set in a massive or weakly foliated, medium- to coarse-grained

quartzofeldspathic matrix mainly composed of K-feldspar (Kfs2), quartz (Qtz2) and plagioclase (Pl2). Rutile (Rt2), ilmenite (Ilm2) and spinel (Spl2) are minor constituents of the matrix and in few samples biotite (Bt2) occurs as a matrix phase.

(2) The quartz-bearing and the quartz-free *Grt-Sil gneisses* show a characteristic migmatitic texture: Coarse-grained restitic domains are dominated by sillimanite (Sil2) coexisting with garnet (Grt2). Subordinate K-feldspar (Kfs2), spinel (Spl2), rutile (Rt2), ilmenite (Ilm2) and quartz (Qtz2) occur. The restitic layers alternate with concordant medium- to coarse-grained and granoblastic leucosomes, which are essentially composed of Kfs2 and Qtz2. Minor amounts of coarse-grained Grt2 are present in the leucosomes. In addition, minor Sil2, Spl2, Rt2 and Ilm2 may occur. In contrast to the Grt gneisses, peak-metamorphic plagioclase and biotite are not present in the Grt-Sil gneisses. A second generation of leucosomes occurs as discordant streaks cross-cutting the migmatitic banding (see Fig. 2.9a-c). Like the early concordant leucosomes, the discordant leucosomes are mainly composed of Kfs2, Qtz2 and minor Grt2.

The peak-metamorphic mineral assemblage of both the Grt gneisses and the Grt-Sil gneisses was extensively replaced by complex symplectite and corona textures during the early retrograde evolution (stage 3), mainly consisting of orthopyroxene (Opx3), cordierite (Crd3), plagioclase (Pl3), spinel (Spl3) and ilmenite (Ilm3; Table 5.5). The further retrograde evolution is characterized by the re-growth of biotite (Bt4), garnet (Grt4), sillimanite (Sil4) and rutile (Rt4), mainly formed at the expense of previously crystallized symplectitic and coronitic phases. Re-growth of garnet is restricted to quartz-bearing samples of both the Grt-Sil gneisses and the Grt gneisses. In the metapelite sample B-587-2-99, which was sampled close to the southern margin of the Epembe Unit, Grt4 coexists with retrograde Bt4 (~ 29 vol.%) and sillimanite (Sil4; ~ 9 vol.%), hence suggesting fluid-influx from the nearby shear zone.

n	stage2								stage3				stage4	
<i>metagreywacke-type Grt gneisses</i>														
15	Grt	Kfs	Qtz	± Spl	Rt	Ilm	Pl	± Bt	Crd, Spl, Pl, Opx, Ilm				Bt, Grt	
<i>metapelitic Grt-Sil gneisses</i>														
26	Grt	Sil	Kfs	Qtz	± Spl	Rt	Ilm	Crd, Spl, Pl, Opx, Ilm				Bt, Grt, Sil, Rt		
4	Grt	Sil	Kfs	± Spl		Rt	Ilm	Crd, Spl, Pl, Ilm				Bt		

Table 5.5: Mineral assemblages in the Grt-Sil gneisses and Grt gneisses of the Epembe Unit (n: number of investigated rock samples).

Texture

In the **Grt gneisses** a weak S_1 foliation is defined by aligned Rt2, Ilm2 and, if present, by Bt2. The **Grt-Sil gneisses** exhibit a weak S_1 foliation, oriented sub-parallel to the compositional banding, which is defined by aligned peak-metamorphic Sil2, Rt2 and Ilm2, indicating mineral growth prior to, or synchronous with, ductile D_1 deformation. Sil2 defines a weak stretching lineation L_1 . In contrast, mineral inclusions in the peak-metamorphic phases (stage 1) of both rock types do not display a preferred orientation, suggesting that an early foliation pre-dating the main S_1 foliation is lacking and hence indicating the absence of an early deformation event pre-dating D_1 . Early concordant leucosomes presumably crystallized pre- to syn-tectonically whereas the formation of the late, discordant leucosomes most probably post-dated the main deformation phase D_1 . Minerals formed during retrogression of both rock types (stage 3 and stage 4) lack a preferred orientation, indicating a static formation of the retrograde phases, which post-dated the development of the S_1 foliation.

Stage 1: Prograde evolution and Stage 2: Peak-metamorphic assemblages

The melanosome domains of the **Grt-Sil gneisses** are dominated by porphyroblastic garnet (Grt2) of up to 1 cm in diameter. Resorbed, anhedral Grt2 is wrapped by the straight external S_1 foliation, which is mainly defined by elongated coarse-grained sillimanite (Sil2), present as anhedral, prismatic grains of up to 4 mm in length. Subhedral rutile (Rt2; < 2 mm in length) and anhedral fine-grained ilmenite (Ilm2) are aligned parallel to S_1 . Rare, fine-grained green spinel (Spl2) appears as subhedral to anhedral grains of up to 1 mm in diameter in the melanosomes and locally preserves straight grain boundaries against quartz (Qtz2). Kfs2 and Qtz2 are rare in the melanosomes and appear as anhedral fine- to medium grained phases. Kfs2 exhibits string and/or patch perthite exsolution and is partially replaced by myrmekitic plagioclase-quartz or is marginally recrystallized to very fine-grained neoblasts (~ 0.05 mm in diameter). The concordant leucosomes are dominated by granoblastic medium- to coarse-grained perthitic K-feldspar (Kfs2), coexisting with quartz (Qtz2) in the quartz-bearing Grt-Sil gneisses. As Grt2 of the melanosomes, anhedral and coarse-grained Grt2 (< 5 mm in diameter) of the concordant leucosomes is strongly resorbed, indicating its crystallization prior to the corona and symplectite formation. Rt2, Ilm2, Spl2 and Sil2 are rare in the leucosomes.

In the **Grt gneisses** porphyroblastic Grt2 of up to 8 mm in diameter is set in a medium-grained, granoblastic matrix mainly composed of perthitic Kfs2 (up to 3 mm in diameter) and minor Qtz2, plagioclase (Pl2), Ilm2 and Rt2. Rare green Spl2 may be present as anhedral to subhedral grains in the quartzofeldspathic matrix. In places, fine-grained biotite (Bt2) is present in the quartzofeldspathic matrix. The mica is isolated from Grt2 and aligned parallel to the main

foliation S_1 ; therefore a retrograde formation of Bt2 seems rather unlikely.

The peak-metamorphic minerals of the Grt-Sil gneisses and Grt gneisses preserve similar mineral inclusions, which are interpreted as relics of the prograde metamorphic evolution: Early biotite (Bt1) is preserved as corroded inclusion in Grt2, Sil2 and Kfs2. Additionally, Grt2 contains rare inclusions of plagioclase (Pl1), quartz (Qtz1), rutile (Rt1) and ilmenite (Ilm1). Rt1 also occurs as abundant fine-grained needles in Qtz2. Fine-grained fibrolitic sillimanite (Sil1) forms irregular inclusion-trails in Grt2, which lack a preferred orientation (Fig. 5.10a). This indicates the absence of an early foliation pre-dating the external S_1 foliation and points to initial pre-tectonic garnet-growth with respect to S_1 . In both the sillimanite-free marginal zones of Grt2 and in matrix Sil2 fine-grained, subhedral to euhedral inclusions of cordierite (Crd1) may occur (Fig. 5.10b). At the outermost margins of Grt2, fine-grained green spinel (Spl1) and Qtz1 are enclosed, which are always separated from each other by Grt2 (Fig. 5.10b). The formation of Grt2 at the expense of Spl1 is supported by corona textures of Grt2 around Spl1, separating it from matrix Qtz2 (Fig. 5.10c). Isolated Spl1 and Qtz1 inclusions also occur in matrix Sil2. However, inclusions of euhedral Spl1 in Qtz2, which is in turn enclosed in Sil2 (Fig. 5.10d), testify to the presence of a stable Spl-Qtz assemblages during the prograde metamorphic evolution. In cases, matrix Spl2 is surrounded by a monomineralic corona of Sil2 (Fig. 5.10e), indicating that the formation of matrix Sil2 post-dates the development of the Spl-Qtz assemblage. Similar monomineralic Sil2 corona textures occur around matrix Ilm2. Sil2 coronas are furthermore developed around corundum (Crm1), separating it from matrix Qtz2 (Fig. 5.10f). Corundum and spinel are often altered to fine-grained, unspecified Al-hydroxides. In summary, the textural relationships suggest that an early Spl-Qtz assemblage was replaced by peak-metamorphic Grt and Sil during prograde metamorphism.

Stage 3: Corona and symplectite formation

Grt gneisses and Grt-Sil gneisses exhibit quite similar retrograde reaction textures:

Matrix Spl2 is separated from coexisting Qtz2 by a monomineralic rim of polygonal fine-grained Crd3 (Fig. 5.11a). Symplectites of Crd3, Opx3 and Spl3 are developed along fissures in the core of Grt2. In quartz-bearing samples of the Grt-Sil gneisses and the Grt gneisses, Grt2 in former contact with matrix Qtz2 is rimmed or completely replaced by a symplectitic intergrowth of Opx3 and Crd3 (Fig. 5.11b). These Crd3-Opx3 symplectites also occur in fissures transecting the margins of Grt2 and around Qtz1 inclusions in Grt2. In the absence of Crd3-Opx3 symplectites, monomineralic rims of late Pl3 are developed around Qtz1 inclusions in Grt2. The Crd3-Opx3 symplectite, in turn, is rimmed by polygonal Opx3 (Fig. 5.11b). In the Grt gneisses the Crd3-Opx3 symplectite is locally surrounded by a finger-like intergrowth of Opx3 and Pl3

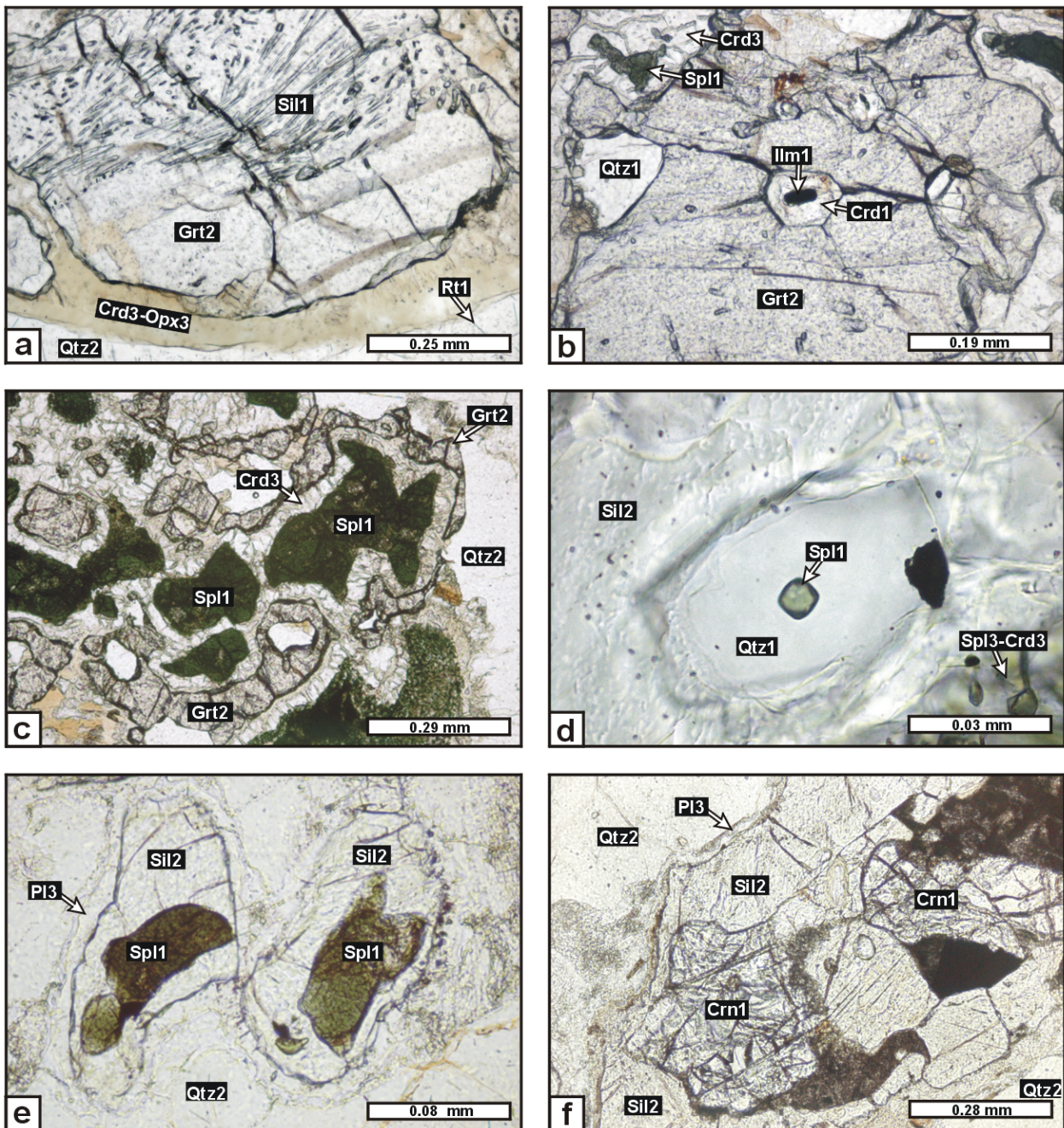


Fig. 5.10: Photomicrographs illustrating the prograde metamorphic evolution of the Grt-Sil gneisses and Grt gneisses of the Epembe Unit. **a)** Irregular inclusions trails of fibrolitic Sil1 in Grt2. Grt2 margins are sillimanite-free. Note fine-grained Rt1 needles in matrix Qtz2. Grt2 is surrounded by an altered Crd-Opx symplectite (Qtz-bearing Grt-Sil gneiss B-699-00). **b)** Euhedral Crd1 inclusion, enclosing Ilm1, in sillimanite-free Grt2 margin (Qtz-bearing Grt-Sil gneiss B-699-00). At the outermost Grt2 margin inclusions of Sp1 and Qtz1 occur, which are separated by Grt2. Sp1 is rimmed by late Crd3 (Qtz-bearing Grt-Sil gneiss B-699-00). **c)** Corona of Grt2 around Sp1, separating it from matrix Qtz2. Sp1 is rimmed by a late Crd3 corona (Qtz-bearing Grt-Sil gneiss B-699-00). **d)** Euhedral Sp1 inclusion in Qtz1, the latter of which is enclosed in matrix Sil2. Sil2 is rimmed by a late Sp3-Crd3 symplectite. (Grt-Sil gneiss B-699-00). **e)** Monomineralic corona of Sil2 around Sp1, separating it from matrix Qtz2. Sil2 is rimmed by late Pl3. (Qtz-bearing Grt-Sil gneiss B-699-00). **f)** Inclusion of Crn1, separated from matrix Qtz2 by a rim of Sil2, which, in turn, is surrounded by a thin rim of late Pl3 (Qtz-bearing Grt-Sil gneiss B-699-00).

(Fig. 5.11c). In presence of Qtz2 a double-layer corona is developed between Grt2 and Sil2 of the quartz-bearing Grt-Sil gneisses, which consists of a monomineralic rim of polygonal Crd3 adjacent to Grt2 and a symplectitic intergrowth of green Spl3 and minor Crd3 adjacent to Sil2 (Fig. 5.11d). The formation of these spinel-dominated symplectites also explains the distinct banding of the Grt-Sil gneisses (see Fig. 2.9a-c): Former restitic Sil2-rich layers are extensively or completely replaced by Spl3-Crd3 symplectites, which macroscopically appear as dark layers. In the Spl3-Crd3 symplectites minor dispersed late Ilm3 and Pl3 may occur. In the Grt gneisses former Sil1 inclusions in Grt2 are replaced by Spl3-Crd3 symplectites, which is surrounded by a monomineralic rim of Crd3, separating the symplectite from the Grt2 host. Spl3-Crd3 symplectites are also developed between Grt2 and Sil2 of the quartz-free Grt-Sil gneisses, whereas the monomineralic Crd3 corona is not developed in this texture. In the quartz-bearing Grt-Sil gneisses fine-grained, granoblastic Pl3 forms monomineralic rims around matrix Sil2 (Fig. 5.10e, 5.10f and 5.11e) and also surrounds matrix Rt2 (Fig. 5.11e). In the quartz-free Grt-Sil gneisses fine-grained Pl3 occurs as monomineralic reaction rims around Grt2, separating it from Kfs2 (Fig. 5.11f); Crd-Opx symplectites are not developed in these rock samples.

Many of the symplectite and corona textures observed in the Grt-Sil gneisses and Grt gneisses resemble stage 3 reaction textures described for the Mg-rich Grt-Opx gneisses and the Qtz-rich Grt-Opx rocks, indicating that the rocks experienced a similar retrograde evolution.

Stage 4: Re-growth of garnet, biotite and sillimanite

In the presence of Kfs2, Crd3-Opx3 symplectites are partly replaced by intergrowths of Bt4 and Qtz4 (Fig. 5.12a). In most samples fine-grained euhedral Grt4 (< 0.25 mm) appears in Crd3-Opx3 pseudomorphs after early porphyroblastic Grt2. Grt4 contains inclusions of symplectitic Opx3 and Crd3, evidencing that Grt4-growth post-dated symplectite formation (Fig. 5.12b). In the presence of Kfs2 re-grown Grt4 coexists with Bt4 as is evident from straight grain boundary contacts between the two phases (Fig. 5.12b) and abundant Bt4 inclusions in Grt4. Grt4 furthermore occurs as fine-grained re-grown rims on relic porphyroblastic Grt2, that is surrounded by Crd3-Opx3 symplectites. Moreover, Grt4, intergrown with fine-grained Sil4, is present as thin re-grown rims (< 0.05 mm) on relic Grt2, which is in turn surrounded by a monomineralic Crd3 corona (Fig. 5.12c). Re-grown Grt4 (< 0.7 mm), containing numerous very fine-grained inclusions of Sil4, also occur in the vicinity of rutile (Rt4), which forms skeletal corona textures around relic Ilm2 (Fig. 5.12d). In the presence of Kfs2, retrograde Crd3 is replaced by intergrowths of Bt4 and Sil4. In cases, euhedral Grt4 is present in the Bt4-Sil4 domains (Fig. 5.12e). Tabular Bt4 furthermore rims Spl3-Crd3 symplectites around Sil2, separating the symplectite from perthitic Kfs2 (Fig. 5.12f).

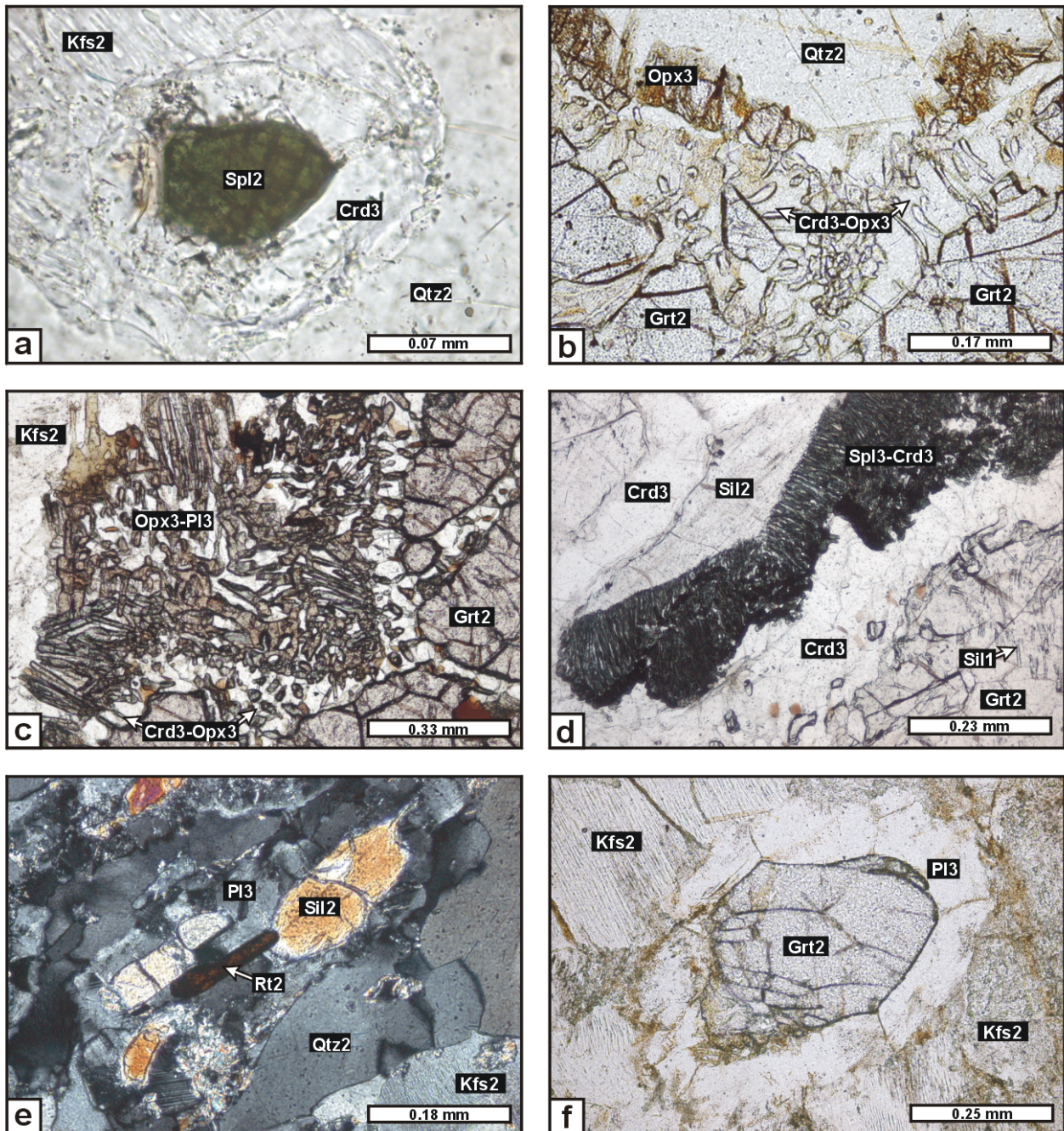


Fig. 5.11: Photomicrographs illustrating the retrograde symplectite and corona textures (stage 3) of the Grt-Sil gneisses and Grt gneisses of the Epembe Unit. **a)** Monomineralic Crd3 corona around Spl2, separating it from matrix Qtz2 and Kfs2 (Qtz-bearing Grt-Sil gneiss B-699-00). **b)** Crd3-Opx3 symplectite, rimmed by a monomineralic Opx3 corona, between Grt2 and Qtz2 (Qtz-bearing Grt-Sil gneiss Ku-97-85). **c)** Crd3-Opx3 symplectite adjacent to Grt2, followed by a finger-like Opx3-Pl3 intergrowth adjacent to Kfs2 (Grt gneiss B-633-00). **d)** Double layer corona between Grt2 and Sil2 with a monomineralic Crd3 rim adjacent to Grt2 and a Spl3-Crd3 symplectite adjacent to Sil2 (Qtz-bearing Grt-Sil gneiss B-699-00). **e)** Monomineralic Pl3 rim around matrix Sil2 and Rt2 (crossed polarized light; Qtz-bearing Grt-Sil gneiss B-230-F-98). **f)** Monomineralic Pl3 rim around Grt2 of the quartz-free Grt-Sil gneisses, separating Grt2 from Kfs2 (Qtz-free Grt-Sil gneiss B-212-A-98).

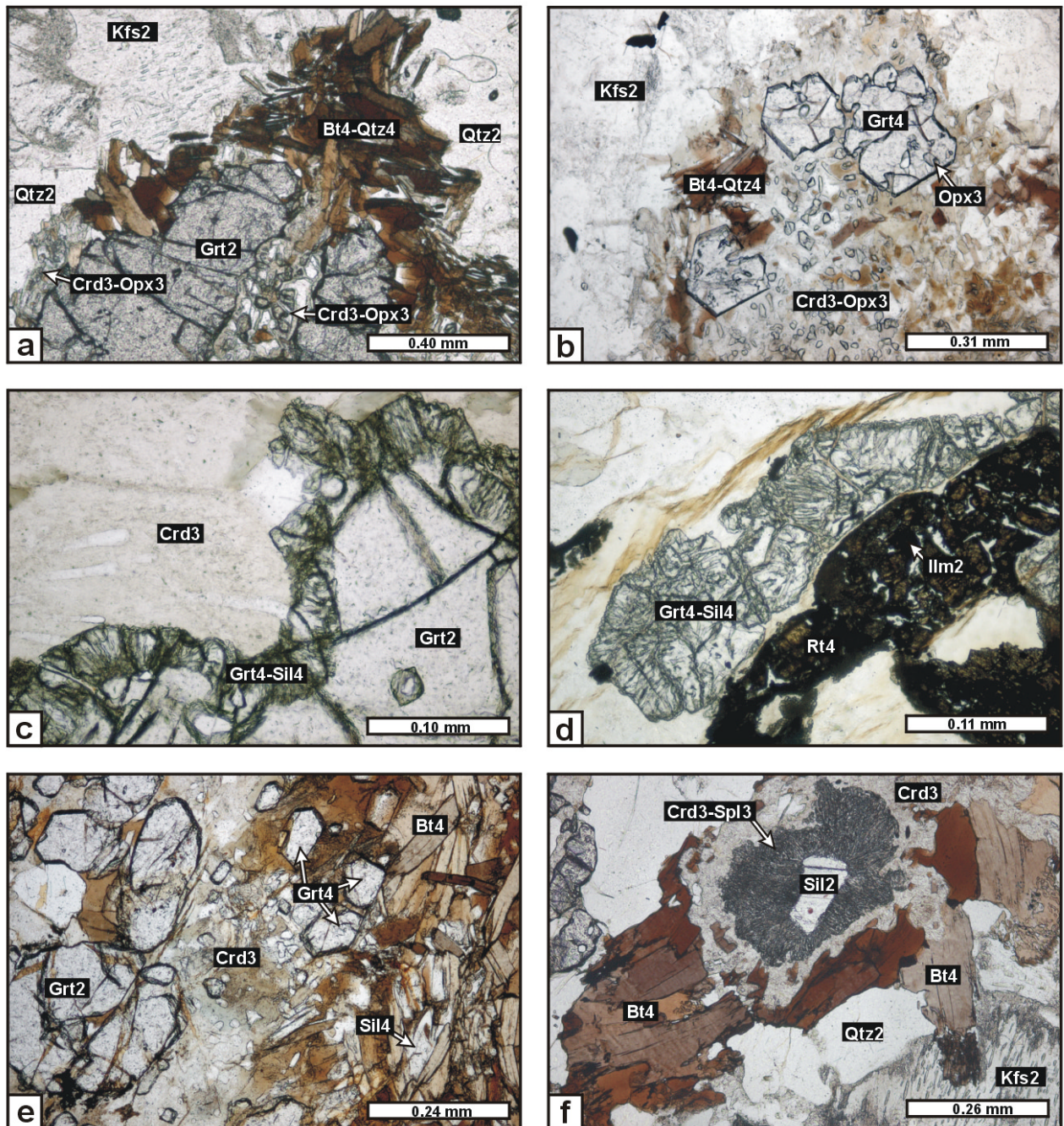


Fig. 5.12: Photomicrographs illustrating retrograde reaction textures resulting from the re-growth of garnet, biotite, sillimanite and rutile (stage 4) of the Grt-Sil gneisses and Grt gneisses of the Epembe Unit. **a)** Intergrowth of Bt4 and Qtz4, partly replacing Crd3-Opx3 symplectites on Grt2 in presence of Kfs2 (Grt gneiss B-633-00). **b)** Subhedral to euhedral Grt4, coexisting with Bt4-Qtz4 intergrowths, in a Crd3-Opx3 pseudomorph after Grt2. Grt4 contains inclusions of Opx3 (Qtz-bearing Grt-Sil gneiss B-230-F-98). **c)** Grt4 re-growth rim with inclusions of Sil4 on Grt2, which is surrounded by a retrograde monomineralic corona of pinitized Crd3 (Qtz-bearing Grt-Sil gneiss B-466-1-99). **d)** Grt4-Sil4 intergrowth, coexisting with Rt4, which forms a skeletal corona on Ilm2 (Qtz-bearing Grt-Sil gneiss B-689-00). **e)** Intergrowth of Bt4, Sil4 and Grt4, formed at the expense of retrograde Crd3 (Qtz-bearing Grt-Sil gneiss B-587-2-99). **f)** Bt4 rim around a Spl3-Crd3 symplectite on Sil2. Bt4 separates the symplectite from perthitic Kfs2 (Qtz-bearing Grt-Sil gneiss B-699-00).

5.1.3.4 Sapphirine-bearing Opx-Sil gneisses and Opx-Grt rocks

Sapphirine-bearing Opx-Sil gneisses

samples: B-458-4-99, B-458-5-00, B-458-6-00, B-458-7-00, B-458-8-00, B-458-9-00, B-693-00, B-700-2-00

Opx-Grt rocks

samples: B-700-1-00, B-700-4-00

Based on field relationships and geochemical data the sapphirine-bearing Opx-Sil gneisses and the Opx-Grt rocks are interpreted as restitic domains derived during partial melting of the hosting migmatitic Mg-rich Grt-Opx gneisses (see Chapter 2.2.2.2 and Chapter 3.1.2). The restitic nature of the rocks is also reflected by their quartz-feldspar-poor mineral assemblages:

(1) Most *sapphirine-bearing Opx-Sil gneisses* are dominated by orthopyroxene (51-62 vol.%). Sillimanite (1-10 vol.%), cordierite (9-25 vol.%), spinel (1-2 vol.%), biotite (5-15 vol.%), corundum (< 1 vol.%) and plagioclase (2-5 vol.%) are present in minor amounts. Few samples additionally contain garnet (0-6 vol.%) and quartz (0-11 vol.%). Corundum, zircon, monazite and, in rare cases, rutile occur as accessory phases. Two of 8 samples of the Spr-bearing Opx-Sil gneisses exhibit a slightly different mineral assemblage (Table 5.6), i.e.: (i) The highly aluminous and relatively Fe-rich Opx-Sil gneiss sample B-458-5-00 (bulk-rock X_{Mg} : 0.64) contains abundant garnet (27 vol.%) and sillimanite (22 vol.%) whereas orthopyroxene (7 vol.%) is a subordinate phase. Further constituents are plagioclase (5 vol.%), sapphirine (5 vol.%), spinel (2 vol.%), cordierite (19 vol.%) and biotite (13 vol.%). Quartz is absent. (ii) The highly aluminous and magnesian Opx-Sil gneiss sample 702-2 (bulk-rock X_{Mg} : 0.78) is characterized by a high modal amount of sapphirine (31-35 vol.%). In addition, orthopyroxene (22-23 vol.%), cordierite (17-20 vol.%), biotite (23-25 vol.%), spinel (0-1 vol.%), plagioclase (1-2 vol.%) and sillimanite (~ 1 vol.%) occur whereas garnet and quartz are absent.

(2) Like the Spr-bearing Opx-Sil gneisses, the *Opx-Grt rocks* predominantly consist of orthopyroxene (79 vol.%), which coexists with subordinate garnet (13 vol.%). Plagioclase (3 vol.%), cordierite (2 vol.%), biotite (2 vol.%), spinel (<1 vol.%) and quartz (2 vol.%) are minor phases, whereas rutile, ilmenite, apatite and zircon occur as accessory phases. Sillimanite and sapphirine have not been observed in the Opx-Grt rocks.

Mineral assemblages

(1) The *sapphirine-bearing Opx-Sil gneisses* are inhomogeneous rocks with complex coarse-grained peak-metamorphic mineral assemblages (stage 2; Table 5.6): The rocks exhibit a weak

compositional banding, which is defined by layers rich in orthopyroxene (Opx₂), alternating with thin layers or lenses rich in sillimanite (Sil₂). In cases, sapphirine (Spr₂) and/or garnet (Grt₂) occur as rare porphyroblasts in both textural domains, resulting in a variety of peak-metamorphic mineral assemblages. Minor amounts of plagioclase (Pl₂) and quartz (Qtz₂) are present throughout the rocks. Although peak-metamorphic Spr₂ and Qtz₂ may occur in the same thin section, they never occur in direct contact with each other.

Like Opx-Sil gneisses from other high-grade metamorphic terranes (e.g. Harley et al., 1990; Ouzegane & Boumaza, 1996; Raith et al., 1997, Harley, 1998b; Kriegsmann & Schumacher, 1999; Baba, 2003) the studied sapphirine-bearing Opx-Sil gneisses of the Epembe Unit preserve conspicuous fine-grained retrograde reaction textures consisting of orthopyroxene (Opx₃), cordierite (Crd₃), sapphirine (Spr₃), spinel (Spl₃), plagioclase (Pl₃), sillimanite (Sil₃) and corundum (Crn₃), formed at the expense of the peak-metamorphic mineral assemblages (stage 3). Further retrogression (stage 4) led to the limited formation of biotite (Bt₄), which in turn was partly replaced by late orthopyroxene (Opx₅) and cordierite (Crd₅) during stage 5.

(2) Uniform peak-metamorphic mineral assemblages (stage 2) are recognized for the homogeneous ***Opx-Grt rocks*** (Table 5.6). They exhibit a granoblastic texture, which is dominated by cm-sized orthopyroxene (Opx₂), coexisting with minor coarse-grained garnet (Grt₂). Fine-to medium grained plagioclase (Pl₂) and quartz (Qtz₂) are major constituents of the matrix. Green spinel (Spl₂) is present in interstices between individual Opx₂ grains.

The peak-metamorphic phases are surrounded by retrograde corona and symplectite textures (stage 3) consisting of orthopyroxene (Opx₃), plagioclase (Pl₃), cordierite (Crd₃) and spinel (Spl₃). Minor biotite is present as a late phase (Bt₄; stage 4) and is locally rimmed by symplectites of orthopyroxene (Opx₅) with or without cordierite (Crd₅) formed during stage 5.

n	stage 2					stage 3					stage 4	stage 5
<i>Sapphirine-bearing Opx-Sil gneisses</i>												
6	Opx	Sil	± Grt	± Spr	Pl ± Qtz	Spr, Crd, Opx, Spl, Pl, Sil, Crn					Bt	± Crd, Opx
1	Opx	Sil	Grt		Pl	Spr, Crd, Opx, Spl, Pl, Sil, Crn					Bt	± Crd, Opx
1	Opx	Sil		Spr	Pl	Spr, Crd, Opx, Spl, Pl					Bt	± Crd, Opx
<i>Opx-Grt rocks</i>												
2	Opx		Grt		Pl Qtz Spl	Crd, Opx, Spl, Pl					Bt	± Crd, Opx

Table 5.6: Mineral assemblages in the sapphirine-bearing Opx-Sil gneisses and the Opx-Grt rocks of the Epembe Unit (n: number of investigated rock samples).

Texture

The *sapphirine-bearing Opx-Sil gneisses* show a weak, straight S_1 foliation, which is defined by crudely aligned Opx2 and parallels the regional foliation trend. The S_1 foliation is accentuated by aligned Sil2, which is oriented sub-parallel to the orthopyroxene-foliation. Aligned Sil2 defines a weak stretching lineation (L_1). Prograde mineral inclusions in the peak-metamorphic phases and late Bt4 show no preferred orientation, indicating that the rocks were only affected by the main deformation event D_1 .

In contrast to the foliated Spr-bearing Opx-Sil gneisses, the *Opx-Grt rocks* are massive rocks. All minerals present, including prograde inclusions, peak-metamorphic minerals and retrograde phases, show no preferred orientation.

Both the sapphirine-bearing Opx-Sil gneisses and the Opx-Grt rocks show minor but systematic petrographical differences, and are therefore individually described in the following.

Sapphirine-bearing Opx-Sil gneisses

Stage 1: Prograde evolution and Stage 2: Peak-metamorphic assemblages

Most sapphirine-bearing Opx-Sil gneisses are dominated by cm-sized anhedral orthopyroxene porphyroblasts (Opx2a). Coexisting coarse-grained prismatic sillimanite (Sil2) is commonly enriched in layers and lenses, that are oriented sub-parallel to the orthopyroxene foliation. Locally cm-sized (< 5 cm) polycrystalline aggregates of Sil2 occur (Fig. 5.13a). As these Sil2 aggregates outline the shape of former kyanite, they testify to the polymorphic transformation of kyanite to sillimanite. Similar aggregates from other sapphirine-bearing Opx-Sil gneisses were interpreted in the same way (Droop & Bucher-Nurminen, 1984; Lal et al., 1984; Raith et al., 1997). Fine-grained anhedral and altered plagioclase (Pl2) and fine-grained quartz (Qtz2) are minor phases of the Opx-Sil gneisses.

Early biotite (Bt1) is present only as corroded inclusion in Opx2a and Sil2, suggesting its replacement at the expense of orthopyroxene during the prograde evolution. Further rare inclusions in Sil2 and Opx2a are plagioclase (Pl1), quartz (Qtz1) and rutile (Rt1). Rare inclusions of sillimanite (Sil1) in Opx2a indicate that the formation of orthopyroxene post-dates the transformation of kyanite to sillimanite. Rare inclusions of cordierite (Crd1) in Opx2a suggest that cordierite was already present during the prograde evolution.

Subhedral to anhedral peak-metamorphic sapphirine (Spr2a) appears as prismatic grains of up to 3 mm in length in quartz-absent domains of the Opx-Sil gneisses (Fig. 5.13b). Spr2a may be weakly aligned parallel to the S_1 foliation and is transected by several fissures along which it is

altered to very fine-grained spinel (Fig. 5.13b). The matrix Spr2a contains corroded inclusions of Opx1 and Sil1 (Fig. 5.13b), suggesting that the formation of sapphirine post-dates the development of the Opx-Sil assemblages. In cases Spr2a additionally contains resorbed inclusions of Bt1, which also occurs in Opx1 inclusions in Spr2a (Fig. 5.13b). In the Spr-rich Opx-Sil gneiss B-700-2-00 Spr2a forms pristine elongated porphyroblasts of up to 2.5 cm in length, that define a weak S_1 foliation. Spr2a of this sample encloses corroded sillimanite (Sil1) and spinel (Spl1; < 0.3 mm in diameter) or forms monomineralic coronas around Spl1 (Fig. 5.13c), suggesting its formation at the expense of spinel, which is not present as a matrix phase. In its central parts porphyroblastic Spr2a of Opx-Sil gneiss B-700-2-00 may consist of an oriented intergrowth with cordierite (Crd1); Spr2a margins are inclusion-free (Fig. 5.13d).

Porphyroblastic Opx2a of the Opx-Sil gneisses is partly or completely recrystallized to polygonal, fine-grained subgrains (Opx2b; 0.1-0.7 mm in diameter), which form granoblastic clusters predominantly in pressure shadows of porphyroblastic Opx2a (Fig. 5.13e). While Opx2a is kinked or fragmented and displays undulose extinction, recrystallized Opx2b is usually strain-free, indicating that the orthopyroxene recrystallisation post-dated the main deformation phase D_1 . Similar recrystallization of orthopyroxene has been described for a sapphirine-quartzite from the Napier Complex, Antarctica (Harley & Motoyoshi, 2000). Locally, anhedral sapphirine (Spr2b) is present in the recrystallized domains and fills interstices between the Opx2b neoblasts (Fig. 5.13f). At the margins of the recrystallized domains late cordierite (Crd3) occurs.

Garnet (Grt2) has been observed in various textural positions in the sapphirine-bearing Opx-Sil gneisses: (1) Locally, fine-grained Grt2 forms monomineralic corona textures around matrix Sil2 separating it from matrix Opx2 (Fig. 5.14a), indicating that Grt2 was formed subsequently to the Opx-Sil assemblages. (2) In rare cases, subhedral to euhedral Grt2 (0.1-0.3 mm) is present in the recrystallized Opx2b rims on porphyroblastic Opx2a (Fig. 5.14b). Partly preserved straight grain boundary contacts between Grt2 and adjacent Opx2b suggest their contemporaneous formation. (3) Strongly resorbed Grt2 of the matrix (up to 6 mm in diameter) is locally fragmented with the individual grains being elongated parallel to the S_1 foliation, indicating pre-tectonic garnet-growth. Locally, straight grain boundaries are preserved against recrystallized Opx2b and, in places, an intergrowth of matrix Grt2 and Opx2b is observed, supporting the interpretation of textural equilibrium between Grt2 and Opx2b. Inclusions of Spr2b (< 0.15 mm) and Opx2b (< 0.25 mm) in matrix Grt2 (Fig. 5.14c) indicate that the formation of Opx-Spr assemblages pre-date the growth of garnet. Matrix Grt2 of Spr2-free samples and domains encloses fine-grained corroded biotite (Bt1), quartz (Qtz1), plagioclase (Pl1) and sillimanite (Sil1), which probably represent prograde inclusions.

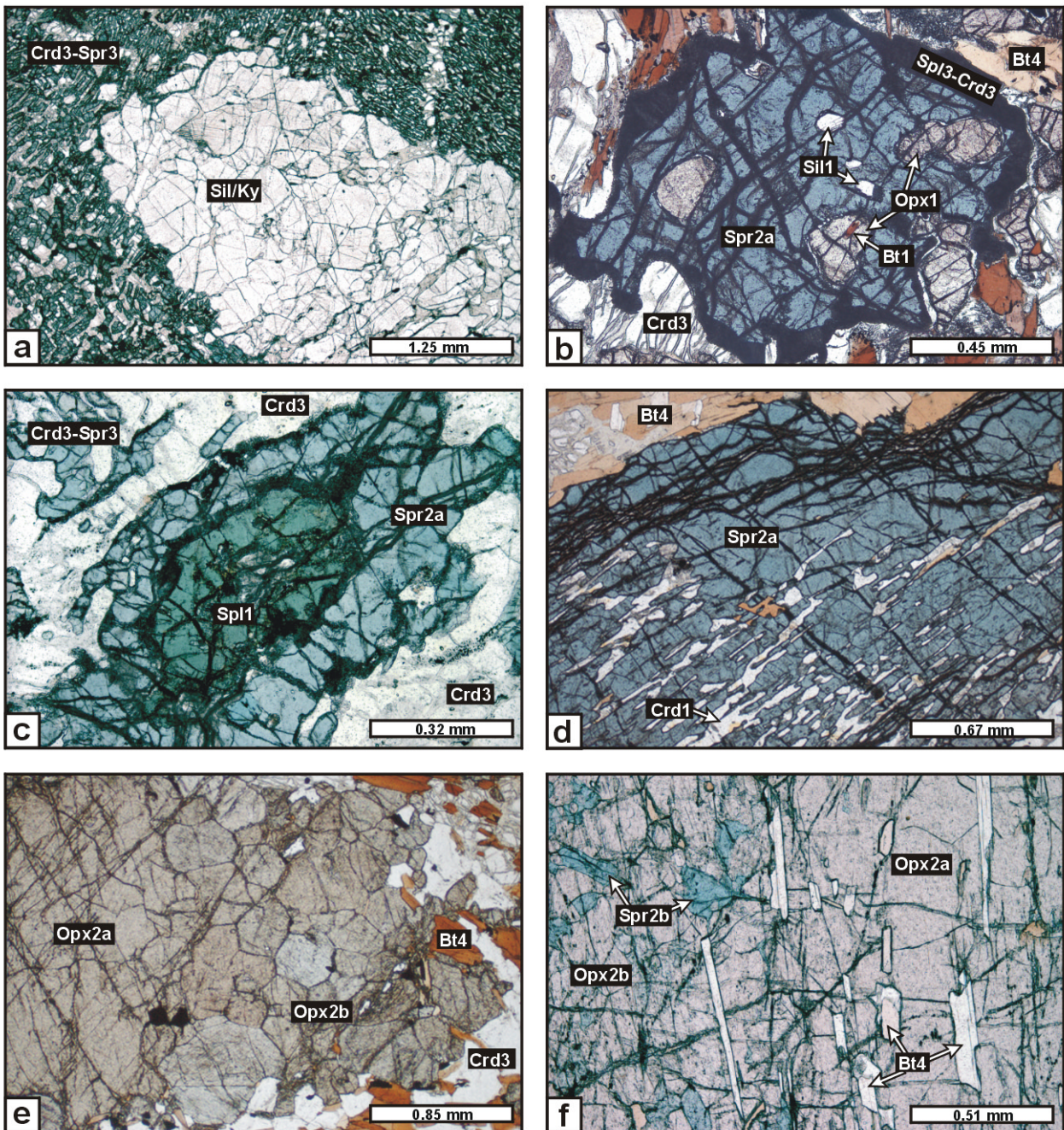


Fig. 5.13: Photomicrographs illustrating the prograde metamorphic evolution of the sapphirine-bearing Opx-Sil gneisses of the Epembe Unit. **a)** Polycrystalline sillimanite aggregate, which outlines the shape of former kyanite. Sillimanite is surrounded by a late Crd3-Spr3 symplectite (Grt-rich Opx-Sil gneiss B-458-5-00). **b)** Corroded Sil1 and Opx1 inclusions in matrix Spr2a, which is rimmed by a fine-grained Spl3-Crd3 symplectite. Opx1 encloses Bt1 (Opx-Sil gneiss B-458-7-00). **c)** Spl1, surrounded by a corona of Spr2a, that, in turn, is rimmed by late Crd3 and a late Crd3-Spr3 symplectite (Spr-rich Opx-Sil gneiss B-700-2-00). **d)** Oriented intergrowth of Spr2a and Crd1 in the core of sapphirine; the Spr2a margin is inclusion-free (Spr-rich Opx-Sil gneiss B-700-2-00). **e)** Porphyroblastic Opx2a, partly replaced by Opx2b, that forms granoblastic grain clusters in the pressure shadow of Opx2a (Opx-Sil gneiss B-693-00). **f)** Porphyroblastic Opx2a (right hand), rimmed by an Opx2b-Spr2b intergrowth (left hand). Opx2a is furthermore replaced by late Bt4 along fractures (Spr-rich Opx-Sil gneiss B-700-2-00).

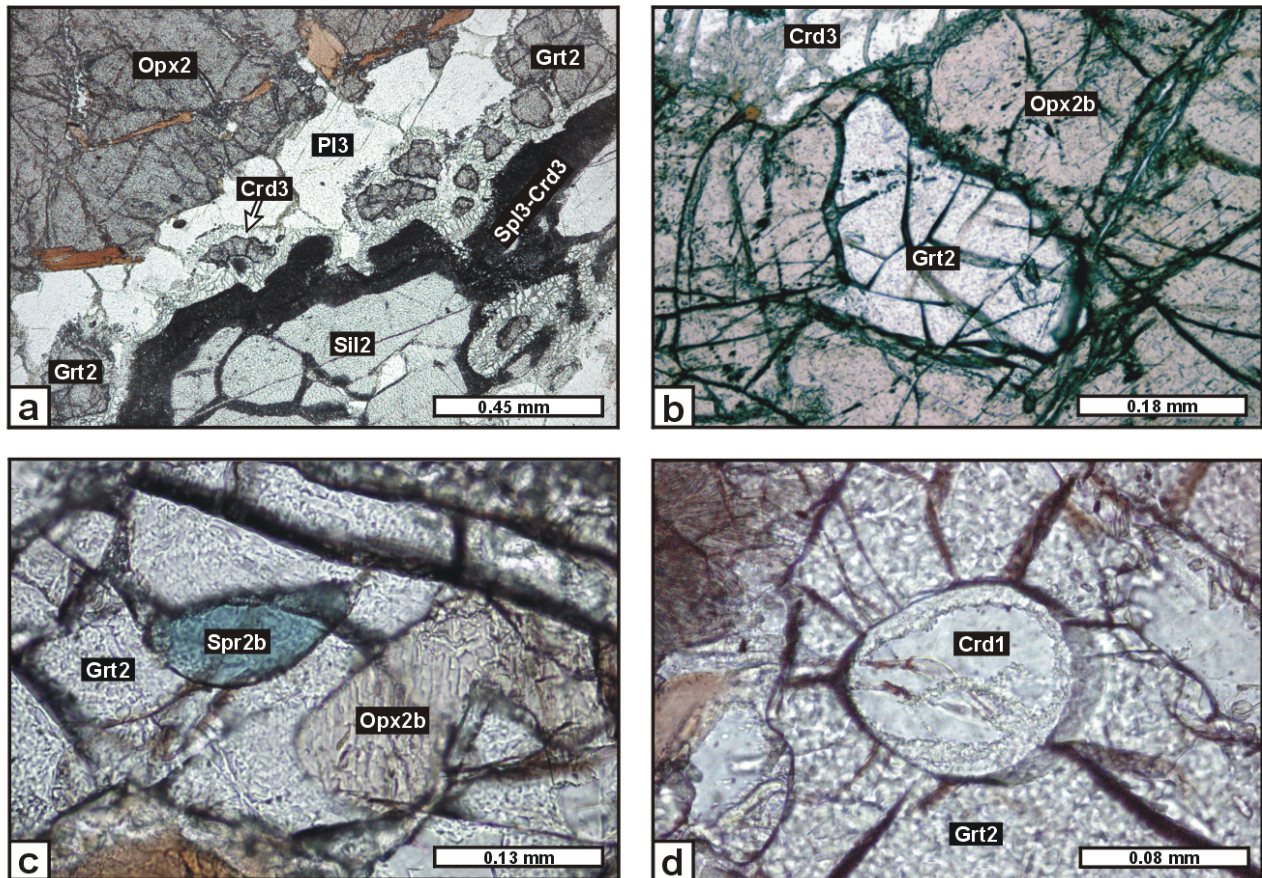


Fig. 5.14: Photomicrographs illustrating the prograde formation of garnet in the Opx-Sil gneisses of the Epembe Unit. **a)** A corona of Grt2 separates Opx2 from Sil2. Between Grt2 and Sil2 a retrograde double-layer corona, consisting of monomineralic Crd3 (adjacent to Grt2) and of a Spl3-Crd3 symplectite (adjacent to Sil2), is formed (Opx-Sil gneiss B-458-9-00). **b)** Subhedral Grt2 in a recrystallized Opx2b domain around porphyroblastic Opx2a. Grt2 shows partly preserved straight grain boundaries against recrystallized Opx2b. Zoning profile of the Grt2 inclusion is shown in Fig. 5.21b (Opx-Sil gneiss B-458-4-99). **c)** Corroded Spr1 and Opx1 inclusions in matrix Grt2 (Opx-Sil gneiss B-458-4-99). **d)** Marginally pinitized corroded Crd1 inclusion in matrix Grt2 (Opx-Sil gneiss B-693-00).

Furthermore, corroded inclusions of cordierite (Crd1; Fig. 5.14d) and spinel (Spl1) occur in Grt2 of Spr2-free samples, both of which are not preserved in the matrix of the Opx-Sil gneisses, indicating their replacement during the prograde metamorphic evolution.

Stage 3: Corona and symplectite formation

Porphyroblastic matrix Spr2a is surrounded by a monomineralic corona of fine-grained, polygonal Crd3, usually separating it from Opx2 or Pl2 (Fig. 5.15a). In the presence of Qtz2 a monomineralic corona composed of fine-grained, polygonal Crd3 is developed around Sil2 separating it from Opx2 (Fig. 5.15b). The most conspicuous reaction textures of the Opx-Sil

gneisses are delicate symplectites of Crd3 and Spr3, that separate Sil2 from Opx2 in silica-deficient domains (Fig. 5.15c). These symplectites are up to 4 mm in width and locally completely replace Sil2 (Fig. 5.15d). The symplectite is rimmed by a monomineralic moat of fine-grained, polygonal Crd3, which separates the symplectite from Opx2 (Fig. 5.15c). In places, the Crd3 moat, in turn, is followed by a narrow Pl3 rim adjacent to Opx2 (Fig. 5.15c). Identical reaction textures were described by Harley et al. (1990) for Spr-bearing granulites from Forefinger Point, Antarctica, and by Raith et al. (1997) from Palni Hills Range, Southern India. Crd-Spr symplectites occurring within Opx2 most likely replace former Sil1 inclusions. Similar Crd3-Spr3 symplectites also occur in the Spr-rich Opx-Sil gneiss B-700-2-00 (Fig. 5.13c), indicating the presence of former matrix Sil2 in these rocks, which is preserved only as inclusion in symplectitic Spr3. At the outer symplectite margins Spr3 of the Opx-Sil gneisses is surrounded by very fine-grained symplectites, which are dominated by green Spl3, intergrown with minor amounts of Crd3 (Fig. 5.15e). Similar Spl-Crd symplectites also occur around matrix Spr2a (Fig. 5.13b). Locally, anhedral to subhedral fine-grained corundum (Crn3) may occur in the Spl-Crd symplectite, resorbing Spr3 (Fig. 5.15e). In cases, a late generation of sillimanite (Sil3) is present in the Spl-Crd symplectites, forming corona textures around Spr3 (Fig. 5.15f). Sil3 also occurs as re-grown rims at the margins of the polycrystalline peak-metamorphic Sil2 aggregates, that are partly replaced by late Crd-Spr symplectites. As Sil3 encloses symplectite Spr3 in these textures, its formation clearly post-dates the symplectite development.

Like Opx2, Grt2 of the Opx-Sil gneisses is replaced by several symplectite and corona textures (Fig. 5.16a-f). In the marginal zones of matrix Opx2 fine-grained symplectite inclusions (0.1-0.3 mm) occur, that consist of Spr3, Crd3 and Opx3 and pseudomorph the outline of former garnet (Fig. 5.16a). Preserved inclusions of Grt2 in Opx2-margins (Fig. 5.14b) suggest that these symplectites result from the local breakdown of former Grt2 inclusions. Rare lamellar intergrowths of Opx3 and Spr3 with minor amounts of Crd3 occur in the matrix of the Opx-Sil gneisses (Fig. 5.16b) and are probably the replacement product of former matrix Grt2. In quartz-free domains relic Grt2 is surrounded by symplectitic intergrowths of Crd3, Opx3 and green Spl3, which also occur in fissures transsecting Grt2 (Fig. 5.16c). In sillimanite-bearing domains Grt2 is separated from Sil2 by lamellar symplectitic intergrowths of Crd3 and Spr3 (Fig. 5.16d), which resemble similar intergrowths formed between Opx2 and Sil2 (Fig. 5.15c). In places, fine-grained granoblastic Pl3 forms an additional phase in the Crd-Spr symplectite between Grt2 and Sil2 (Fig. 5.16d). As Spr3 formed from Opx2 and Sil2, Spr3 of the latter symplectite is largely replaced by a very fine-grained symplectite mainly composed of green Spl3 with minor amounts of Crd3 (Fig. 5.16d). Locally, Sil3 and Crn3 are present in the Spl-Crd symplectites. In cases, Grt2 and Sil2 are separated by a double-layer corona consisting of a lamellar symplectite of

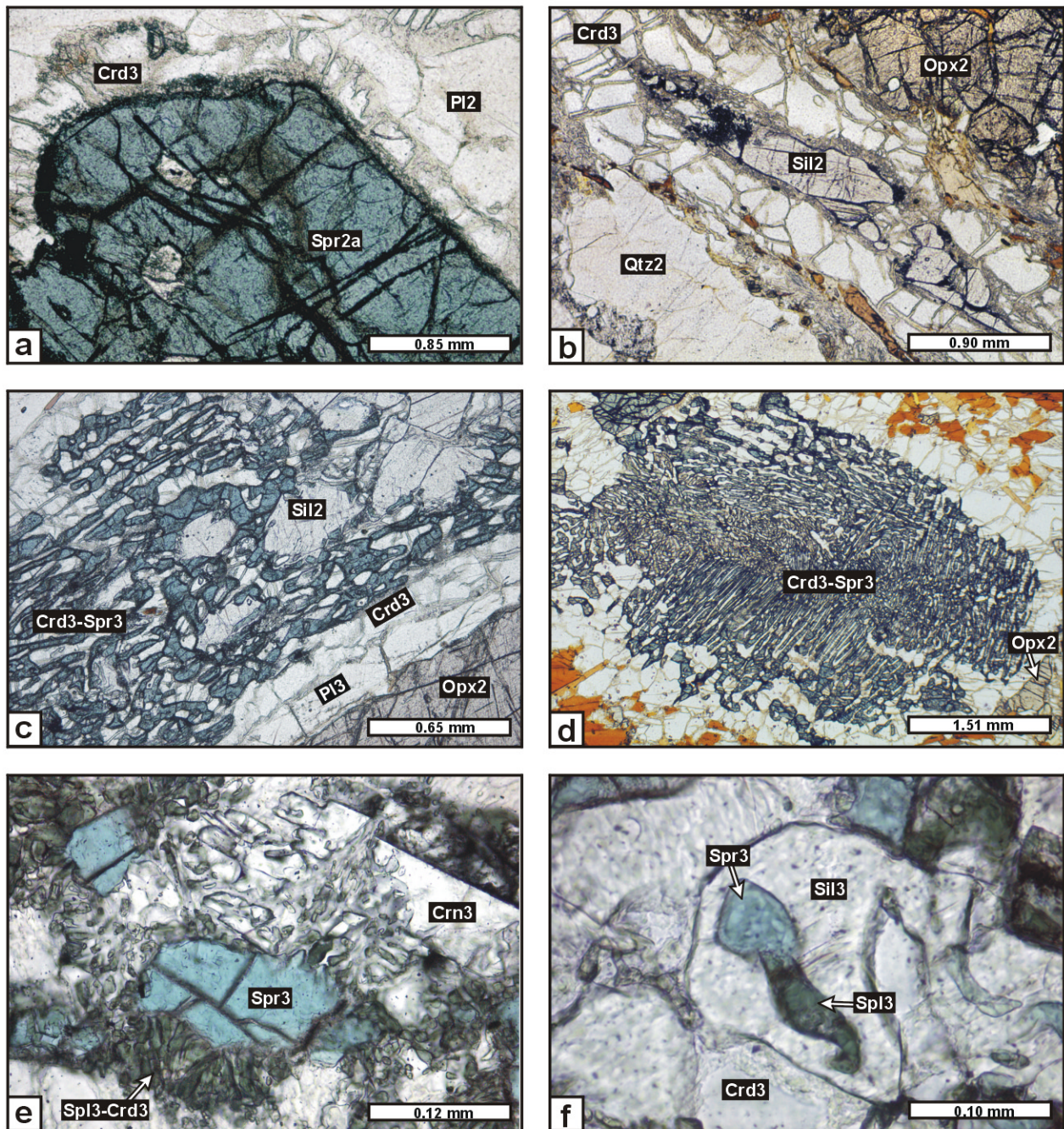


Fig. 5.15: Photomicrographs illustrating retrograde symplectite and corona textures resulting from the breakdown of peak-metamorphic sapphirine and orthopyroxene (stage 3) of the sapphirine-bearing Opx-Sil gneisses of the Epembe Unit. **a)** Porphyroblastic Spr2a, rimmed by a monomineralic corona of Crd3, separating Spr2a from matrix Pl2 (Opx-Sil gneiss B-458-9-00). **b)** Monomineralic corona of Crd3, separating Sil2 from Opx2 in the presence of Qtz2 (Opx-Sil gneiss B-458-7-00). **c)** Crd3-Spr3 symplectite between Sil2 and Opx2. The symplectite is rimmed by a monomineralic corona of Crd3, which is surrounded by a narrow rim of Pl3 (Opx-Sil gneiss B-458-7-00). **d)** Crd3-Spr3 symplectite, pseudomorphing former Sil2 in the presence of Opx2 (Opx-Sil gneiss B-458-7-00). **e)** Late Spr3, partly replaced by a Spl3-Crd3 symplectite. Locally, subhedral Crn3 is present in the Spl3-Crd3 symplectite (Opx-Sil gneiss B-458-5-00). **f)** Corona of Sil3 around Spr3 and Spl3 (Opx-Sil gneiss B-458-5-00).

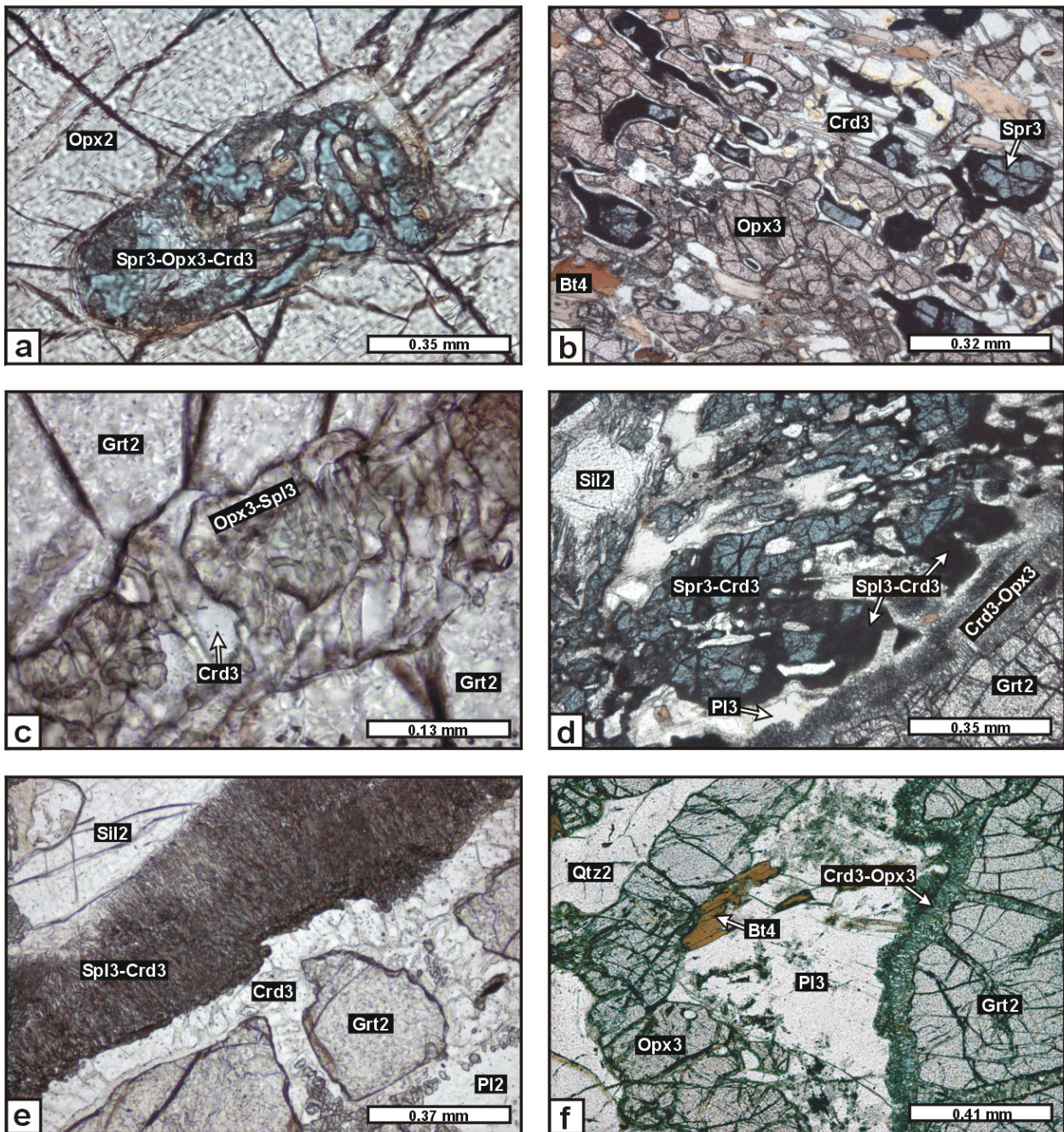


Fig. 5.16: Photomicrographs illustrating retrograde symplectite and corona textures resulting from the breakdown of peak-metamorphic Grt2 (stage 3) of the sapphirine-bearing Opx-Sil gneisses of the Epembe Unit. **a)** Crd3-Spr3-Opx3 symplectite, enclosed in the margin of porphyroblastic Opx2. The symplectite outlines the shape of former garnet (Opx-Sil gneiss B-458-4-99). **b)** Lamellar Crd3-Spr3-Opx3 intergrowth, probably replacing former matrix Grt2 (Opx-Sil gneiss B-458-7-00). **c)** Crd3-Spl3-Opx3 symplectite, present in a fissure of Grt2 (Opx-Sil gneiss B-458-4-99). **d)** Crd3-Spr3 symplectite between Grt2 and Sil2. Symplectitic Spr3 is rimmed by fine-grained Spl3-Crd3 symplectite and Grt2 is surrounded by a Crd3-Opx3 symplectite. Pl3 is present between the Spr3-Crd3 symplectite and Grt2 (Opx-Sil gneiss B-458-9-00). **e)** Spl3-Crd3 symplectite and monomineralic Crd3 corona between Grt2 and Sil2 (Opx-Sil gneiss B-458-6-00). **f)** Broad Opx3-Pl3 corona, separating Grt2 from matrix Qtz2. Between Grt2 and coronitic Pl3 a Crd3-Opx3 symplectite is developed (Opx-Sil gneiss B-458-4-99).

green Spl3 with minor amounts of Crd3 adjacent to Sil2 and a monomineralic corona of granoblastic Crd3 adjacent to Grt2 (Fig. 5.16e), resembling similar symplectites observed in the metapelitic Grt-Sil gneisses of the Epembe Unit (see Fig. 5.11d). As in most quartz-bearing paragneisses, Grt2 of the Opx-Sil gneisses is surrounded by a fine-grained symplectitic corona consisting of Crd3 and Opx3 (Fig. 5.16d & f). In the presence of quartz, the Crd-Opx symplectite, in turn, may be surrounded by a medium-grained, granoblastic intergrowth of Opx3 and Pl3, separating the symplectite from matrix Qtz2 (Fig. 5.16f).

Stage 4: Re-growth of biotite

The peak-metamorphic assemblages and the retrograde phases are further modified by the development of late biotite (Bt4). Re-growth of garnet, as recognized in many other paragneisses, is not observed in the sapphirine-bearing Opx-Sil gneisses.

Stage 5: Formation of late orthopyroxene and cordierite

As observed for the Mg-rich Grt-Opx gneisses, late Bt4 of the Opx-Sil gneisses is, in turn, rimmed by late, fine-grained orthopyroxene (Opx5), locally intergrown with cordierite (Crd5).

Opx-Grt rocks

Stage 1: Prograde evolution and Stage 2: Peak-metamorphic assemblages

The Opx-Grt rocks are dominated by anhedral cm-sized orthopyroxene (Opx2a). At the margins kinked Opx2a is locally recrystallized to polygonal neoblasts (Opx2b; 0.3-0.6 mm in diameter). Minor anhedral coarse-grained garnet (Grt2; < 6 mm) may exhibit straight grain boundary contacts against Opx2a, suggesting their contemporaneous formation. Minor portions of fine-grained anhedral green spinel (Spl2), quartz (Qtz2) and plagioclase (Pl2) occur in the orthopyroxene-matrix, but spinel-quartz associations are not observed. Zircon, rutile (Rt2), ilmenite (Ilm2) and apatite occur as accessory phases in the matrix.

Opx2a contains inclusions of biotite (Bt1), plagioclase (Pl1) and quartz (Qtz1), whereas Grt2 preserves inclusions of orthopyroxene (Opx1; < 0.3 mm), spinel (Spl1), biotite (Bt1), rutile (Rt1), ilmenite (Ilm1) and quartz (Qtz1). The presence of inclusions of subhedral to euhedral garnet (Grt1; < 0.2 mm) and orthopyroxene (Opx1; < 0.15 mm) in one single matrix Pl2 grain, suggests that both phases were formed early during the prograde metamorphic evolution.

Stage 3: Corona and symplectite formation

Grt2 of the Opx-Grt rocks is separated from matrix Qtz2 by broad coronas of orthopyroxene

(Opx3) and plagioclase (Pl3) and subsequently formed symplectites of cordierite (Crd3) and Opx3, the latter of which are present between the Opx-Pl coronas and Grt2. Crd-Opx symplectites furthermore occur in fissures in the outer margins of Grt2. In contrast, cracks in Grt2 cores are filled by fine-grained Crd3-Opx3-Spl3 symplectites.

Stage 4: Re-growth of biotite

Matrix Spl2 is rimmed by a corona of biotite (Bt4), which also appears as rims around Opx2.

5.1.3.5 Mineral assemblages in the light of the whole-rock geochemical data

The differing peak-metamorphic mineral assemblages of the paragneisses are consistent with the bulk-rock geochemistry, in terms of molar $\text{SiO}_2\text{-(FeO+MgO)-Al}_2\text{O}_3$ (S-FM-A) and $\text{Al}_2\text{O}_3\text{-FeO-MgO}$ (AFM) plots projected from feldspars (K-feldspar and plagioclase) and quartz (Fig. 5.17a & b):

The metagreywacke-type Fe-rich Grt-Opx gneisses (bulk-rock X_{Mg} : 0.37-0.46) and Mg-rich Grt-Opx gneisses (bulk-rock X_{Mg} 0.59-0.62) as well as the Qtz-rich Grt-Opx rocks (bulk-rock X_{Mg} : 0.52-0.56) plot in the Grt-Opx-Qtz field and, due to their low Al contents, generally close to the Opx-Qtz tieline (Fig. 5.17a). Differences in the modal amount of garnet and orthopyroxene between the Qtz-rich Grt-Opx rocks and the metagreywacke-type Mg-rich Grt-Opx gneisses are consistent with their respective bulk-rock chemistry: In the AFM projection (Fig. 5.17b) the garnet-rich Qtz-rich Grt-Opx rocks plot close to garnet whereas the less aluminous and slightly more magnesian Mg-rich Grt-Opx gneisses plot close to orthopyroxene.

The metagreywacke-type Grt gneisses (bulk-rock X_{Mg} : 0.39-0.44) plot close to the Grt-Qtz tieline in the S-FM-A diagram and close to the garnet composition in the AFM diagram. The metapelitic Grt-Sil gneisses have a bulk-rock X_{Mg} of 0.39-0.47, similar to that of the Grt gneisses, but are more aluminous and therefore fall into the Grt-Sil field in the AFM diagram. The quartz-bearing Grt-Sil gneisses plot above the Grt-Sil tieline whereas the one chemically investigated quartz-free Grt-Sil gneiss (sample B-212-A-98) plots below the Grt-Sil tieline in the S-FM-A projection (Fig. 5.17a).

The high X_{Mg} ratios of the sapphirine-bearing Opx-Sil gneisses (bulk-rock X_{Mg} : 0.64-0.78) are reflected by the occurrence of peak-metamorphic Opx + Sil \pm Qtz assemblages and of sapphirine (Fig. 5.17b). The recognized variations in the peak-metamorphic mineral assemblages of the sillimanite-bearing paragneisses (Opx-Sil gneisses and Grt-Sil gneisses) are consistent with calculated phase relationships for aluminous gneisses in the FMAS system, indicating that the

formation of Opx-Sil-Qtz assemblages is restricted to metapelites with relatively high bulk-rock X_{Mg} of > 0.50 (Aranovich & Berman, 1996). Minor variations in the modal composition of the investigated Opx-Sil gneisses correlate well with differences in the bulk-rock composition of the respective samples: In the S-FM-A projection the Opx-Sil gneisses plot slightly above or below the Opx-Sil tie-line; consistent with the rare presence of quartz in many samples. Exceptions are the both Si-poor and Al-rich samples B-458-5-00 and B-700-2-00, which plot below the Opx-Sil line, in agreement with the lack of quartz in the samples. Consistent with its high modal amount of garnet the relatively Fe-rich Opx-Sil gneiss B-458-5-00 (bulk-rock X_{Mg} : 0.64) plots close to the composition of garnet, whereas the highly magnesian sapphirine-rich Opx-Sil gneiss B-700-2-00 (bulk-rock X_{Mg} : 0.78) plots close to the Opx-Spr tie-line.

The Opx-Grt rocks have a similar highly magnesian composition (bulk-rock X_{Mg} : 0.67) as the sapphirine-bearing Opx-Sil gneisses but are less aluminous and therefore fall into the Grt-Opx stability field (Fig. 5.17b).

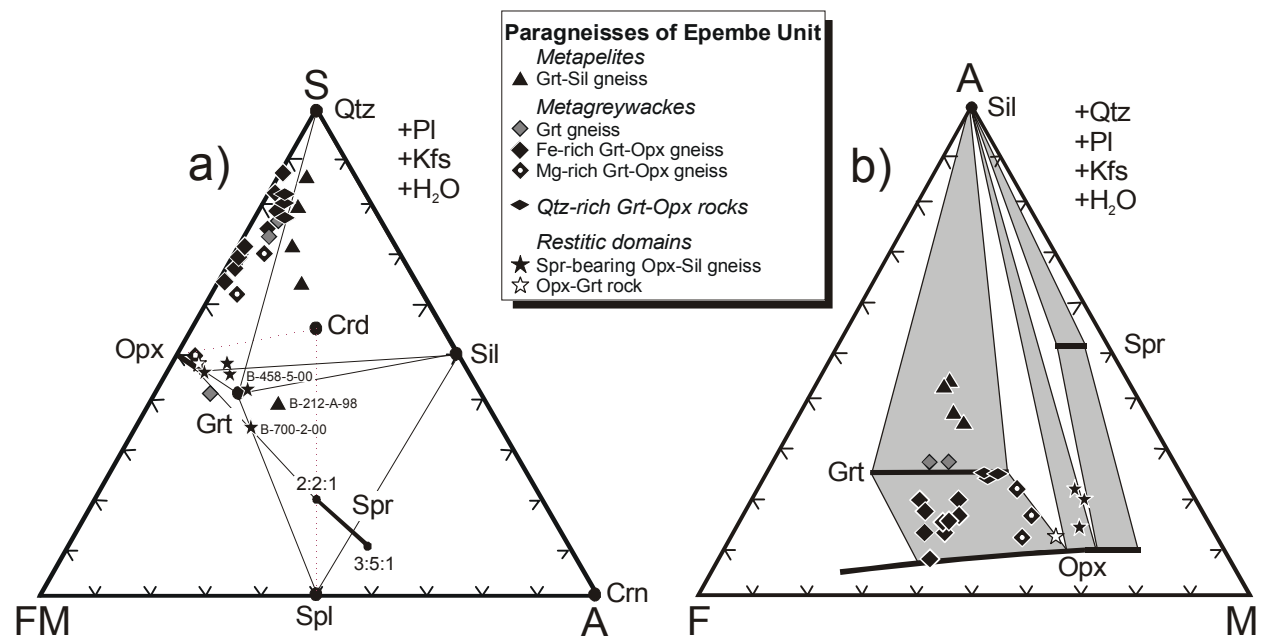


Fig. 5.17: Bulk-rock compositions (as molecular proportions) of the paragneisses of the Epembe Unit projected onto simplified compositional diagrams, illustrating consistent relationships between bulk-rock composition and observed peak-metamorphic mineral assemblages. **a)** S-FM-A projection from feldspars, illustrating the bulk-rock composition in terms of silica-saturation and reactions implied by textures in Qtz-bearing and Qtz-absent rocks discussed later in the text. **b)** Schematic AFM projection illustrating the bulk-rock composition in relation to the compositions of typical minerals of high-grade metamorphic paragneisses. Note that quartz-free samples are not illustrated in the AFM projection.

5.2 MINERAL CHEMISTRY

Sixteen selected granulite samples of the Epembe Unit have been investigated in detail with the help of electron microprobe (EMP) analysis. Descriptions of the mineral formula calculation procedures and the analytical conditions are given in the Appendix (Chapter A.3.2). X_{Mg} ratios of garnet, clinopyroxene, orthopyroxene, sapphirine, spinel and amphibole were calculated as $Mg/(Mg+Fe^{2+})_{molar}$ whereas those of cordierite and biotite were calculated as $Mg/(Mg+Fe^{tot})_{molar}$.

The investigated samples comprise representative samples of the major lithological subunits described in Chapter 5.1. Microprobe work, however, concentrated on metagreywacke-type Grt-Opx gneisses and Qtz-rich Grt-Opx rocks as their coarse-grained mineral assemblages are highly suitable for geothermobarometric calculations. In addition, special emphasis was given to the restitic sapphirine-bearing Opx-Sil gneisses.

Orthogneisses

Mafic two-pyroxene granulites	B-230-B-98, B-434-2-99 (Grt-bearing)
Mafic Grt-Cpx granulites	B-311-1-99
Grt-Opx metagranitoids	B-206-B1-98, B-646-1-00

Paragneisses

Fe-rich Grt-Opx gneisses	B-690-2-00
Mg-rich Grt-Opx gneisses	B-458-3-99, B-634-00
Qtz-rich Grt-Opx rocks	B-614-1-99, B-587-4-99 (Crd-bearing)
Grt gneisses	B-230-E-98
Grt-Sil gneisses	B-230-F-98
Sapphirine-bearing Opx-Sil gneisses	B-458-4-99, B-458-5-00, B-458-9-00
Opx-Grt rocks	B-700-1-00

Ten of 16 samples investigated were taken from a locally restricted area in the central part of the Epembe Unit (see Fig. 2.7a for the location of the Spr-bearing Opx-Sil gneisses and the Opx-Grt rock and the sample location maps A.2.2 to A.2.5 in the Appendix for the location of the other investigated samples). In addition, one mafic granulite sample (B-434-2-99) and one Grt-Opx metagranitoid sample (B-646-1-00) from the eastern part of the Epembe Unit as well as one cordierite-bearing Qtz-rich Grt-Opx rock sample (B-587-4-99) and one Fe-rich Grt-Opx gneiss

sample (B-690-2-00) from the south-western margin of the central part of the Epembe Unit were selected for microprobe studies in order to investigate possible regional variations in the metamorphic conditions. EMP analysis of one sample of a mafic Grt-Cpx granulite (B-311-1-99), taken from a major shear zone, yields information on the tectono-metamorphic evolution of the isolated granulite occurrence.

5.2.1 Garnet

In most granulite samples of the Epembe Unit peak-metamorphic garnet (Grt2) has been observed. Many of the samples investigated additionally contain a second generation of texturally late garnet (Grt4). Representative analyses of garnet are listed in Table A.6.2.1 in the Appendix.

Orthogneisses

Mafic granulites

Matrix Grt2 of the mafic two-pyroxene B-434-2-99 is grossular-rich and displays a weak zonation with the X_{Mg} decreasing from core towards rims and cracks (core: X_{Mg} : 0.23; Prp₁₈Alm₆₀Grs₂₁Sps₁; rim: X_{Mg} : 0.16; Prp₁₂Alm₆₂Grs₂₃Sps₃). This zonation pattern strongly suggests intensive retrograde Fe-Mg exchange between Grt2 and texturally late Hbl4, which occurs in cracks and along the margins of Grt2.

Grt2 of the mafic Grt-Cpx granulite B-311-1-99 differs from the analyzed peak-metamorphic Grt2 of all other granulite samples investigated, in preserving a prograde growth zonation, that is evident from a rimward increase of the X_{Mg} ratio (Fig. 5.18a), pointing to a temperature-increase during garnet growth. The generally high pyrope content of Grt2 continuously increases towards the rim by an average of about 6 mol.% (profile 1: Core: X_{Mg} : 0.42; Prp₃₃Alm₄₅Grs₂₀Sps₁; rim: X_{Mg} : 0.50; Prp₃₉Alm₃₉Grs₂₁Sps₁) whereas almandine concomitantly decreases. The low and essentially unzoned spessartine component was probably homogenized by intracrystalline diffusion during high-grade metamorphism. Grossular is generally high and variably zoned; grossular-rich cores may be preserved in selected garnets (profile 2), whereas others do not display systematic variations of grossular (profile 1). A weak spessartine increase at the outermost margin (X_{Mg} : 0.41; Prp₃₀Alm₄₅Grs₂₂Sps₃) is interpreted to result from the resorption of Grt2 by surrounding Hbl4-Pl4 symplectites whereas the abruptly decreasing X_{Mg} is suggested to reflect retrograde Fe-Mg re-equilibration of Grt2 rims and symplectitic Hbl4 during retrograde cooling.

Grt-Opx metagranitoids

Garnet of the Grt-Opx metagranitoids is essentially a pyrope-almandine solid solution with minor grossular and low spessartine contents. Significant chemical differences, however, are obtained for the two different textural types of garnet (Fig. 5.18b): Peak-metamorphic Grt2 of sample B-646-1-00 displays moderate rimward zoning to lower pyrope (core: X_{Mg} : 0.35; $Prp_{32}Alm_{60}Grs_6Sps_2$; rim: X_{Mg} : 0.29; $Prp_{26}Alm_{65}Grs_7Sps_2$), correlated with a slight increase of both almandine and grossular. Late euhedral Grt4, which occurs as re-grown rims on peak-metamorphic Grt2, is less magnesian than the latter. Grt4 displays a zonation pattern with rimward decreasing X_{Mg} (core: X_{Mg} : 0.27; $Prp_{23}Alm_{64}Grs_{11}Sps_2$; rim: X_{Mg} : 0.23; $Prp_{20}Alm_{69}Grs_9Sps_2$), most probably reflecting Fe-Mg re-equilibration with adjacent Bt4.

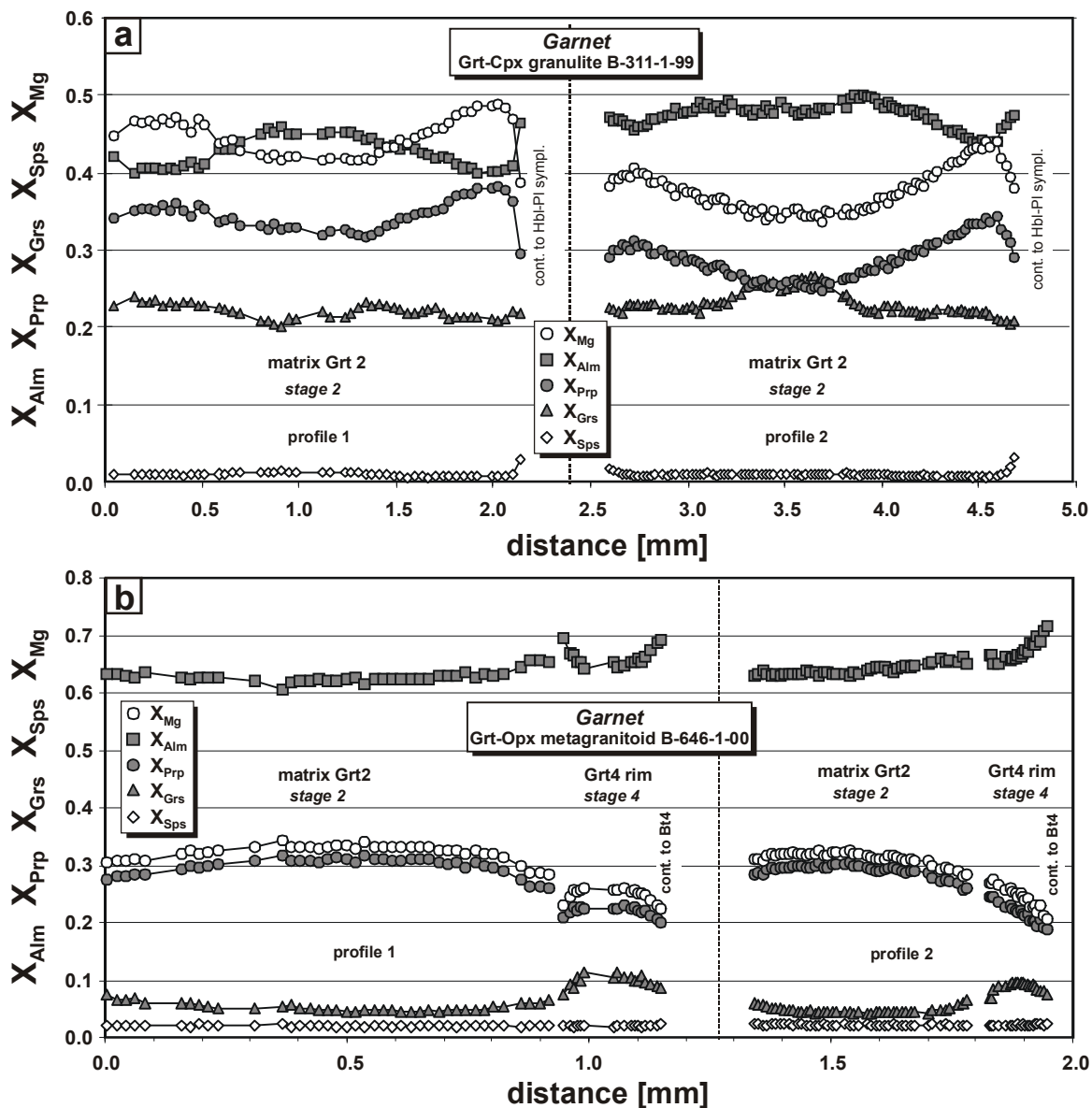


Fig. 5.18: Garnet zoning profiles of **a)** the mafic Grt-Cpx granulite B-311-1-99 and **b)** the Grt-Opx metagranitoid B-646-1-00 of the Epembe Unit, with respect to the textural position. Each profile extends from rim to rim through the core of the garnet grains. Note variable scale.

Paragneisses

Garnet of the paragneisses of the Epembe Unit is essentially a pyrope-almandine solid solution with low spessartine and grossular content (Fig. 5.19-5.21). Significant chemical variations, especially in the X_{Mg} , are observed between peak-metamorphic Grt2 and re-grown Grt4, hence supporting the observation of two texturally differing generations of garnet. Minor chemical differences are recognized for garnet of both generations occurring in different rock types.

Fe-rich and Mg-rich Grt-Opx gneisses and Qtz-rich Grt-Opx rocks

Prograde Grt1 inclusions preserved in cores of porphyroblastic Opx2 of the Qtz-rich Grt-Opx rock reveal minor chemical zoning (Fig. 5.19a), with pyrope decreasing from core (X_{Mg} : 0.35; Prp₃₃Alm₆₂Grs₂Sps₂) to rim (X_{Mg} : 0.33; Prp₃₁Alm₆₄Grs₃Sps₂). These inclusions are probably affected by significant Fe-Mg exchange with the hosting Opx2, as is evidenced by their relatively low X_{Mg} when compared to matrix Grt2 core composition. The highest pyrope contents for matrix Grt2 of the Qtz-rich Grt-Opx rock were obtained for core plateaus (X_{Mg} : 0.44-0.46; Prp₄₂₋₄₄Alm₅₂₋₅₄Grs₃₋₄Sps₁₋₂; Fig. 5.19a), which are interpreted to result from intracrystalline diffusional homogenization during the highest-grade metamorphic stage. Significant rimward zoning to lower pyrope content in Grt2 (X_{Mg} : 0.29-0.39) was presumably developed during the retrograde formation of the surrounding Crd-Opx symplectites, since Mg preferentially partitioned into symplectitic orthopyroxene (X_{Mg} : 0.52-0.66) and cordierite (X_{Mg} : 0.70-0.86). The preservation of core plateaus strongly depends on the grain size of Grt2, as they are only preserved in grains of > 4 mm in diameter. In contrast, smaller grains are completely modified (Fig. 5.19a). The grossular component shows minor but continuous zoning to lower Ca content from core (Grs₃₋₄) to rim (Grs₁₋₂). Re-grown euhedral Grt4, present in Crd-Opx symplectites (Fig. 5.8c), is significantly less magnesian (X_{Mg} 0.23-0.24; Prp₂₂Alm₇₁₋₇₂Grs₄Sps₃) than corresponding matrix Grt2 (X_{Mg} 0.46-0.29) and, in contrast to the latter, almost unzoned (Fig. 5.19a). The lower X_{Mg} suggests that Grt4 was formed at lower P-T conditions than peak-metamorphic Grt2. The grossular content is in the range of that of late Grt4 re-growth rims (X_{Mg} : 0.28-0.32; Prp₂₇₋₃₀Alm₆₅₋₆₈Grs₃₋₄Sps₂) on relic porphyroblastic Grt2 (Fig. 5.19a and Fig. 5.8d).

Matrix Grt2 of the Mg-rich Grt-Opx gneisses is chemically similar to Grt2 of the Qtz-rich Grt-Opx rock and shows the same zonation patterns (cores: X_{Mg} : 0.44-0.43; Prp₄₂Alm₅₅₋₅₄Grs₃₋₄Sps₁₋₂; rims: X_{Mg} : 0.39-0.32; Prp₃₇₋₃₀Alm₆₅₋₅₈Grs₂₋₃Sps₂).

Resorbed porphyroblastic Grt2 of the Fe-rich Grt-Opx gneiss B-690-2-00 is less magnesian than Grt2 of Mg-rich Grt-Opx gneisses and the Qtz-rich Grt-Opx rock and is essentially unzoned (X_{Mg} : 0.25-0.26 Prp₂₃₋₂₄Alm₆₆₋₆₈Grs₈₋₅Sps₃; Fig. 5.19b). Minor variations are only obtained for the Ca content. The lack of Fe-Mg exchange with surrounding coronitic Opx3 is explained by

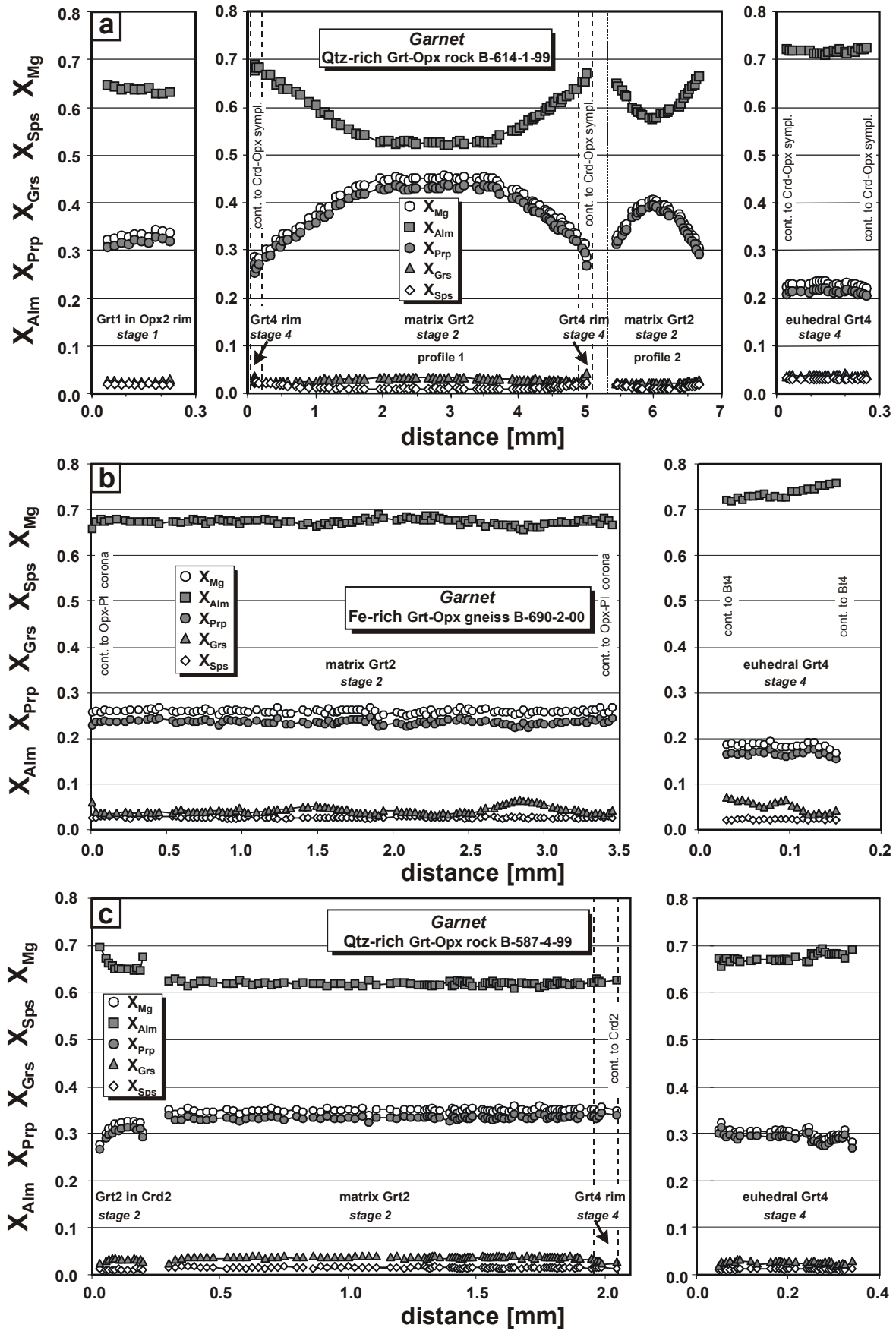


Fig. 5.19: Garnet zoning profiles of a) the Qtz-rich Grt-Opx rock B-614-1-99, b) the Fe-rich Grt-Opx gneiss B-690-2-00 and c) the cordierite-bearing Qtz-rich Grt-Opx rock B-587-4-99, with respect to textural position. Each profile extends from rim to rim through the core of the garnet grains.

the presence of a Pl3 corona, which is situated between Grt2 and Opx3 and hence prevents cation exchange between Grt2 and Opx3. Re-grown Grt4 of sample B-690-2-00, formed at the expense of Opx3, is less magnesian than the corresponding Grt2 and displays no systematic zonation (X_{Mg} : 0.17-0.19; Prp₁₇₋₁₅Alm₇₂₋₇₆Grs₉₋₆Sps₂₋₃).

Matrix Grt2 of the cordierite-bearing Qtz-rich Grt-Opx rock B-587-4-99 is almost unzoned (Fig. 5.19c) and less magnesian (X_{Mg} : 0.35; Prp₃₄Alm₆₁Grs₂Sps₁) than Grt2 of the Crd-free sample, presumably reflecting the presence of coexisting Crd2. Rimward zoning to lower X_{Mg} of Grt2 inclusions (core: X_{Mg} : 0.33; Prp₃₁Alm₆₅Grs₁Sps₁; rim: X_{Mg} : 0.28; Prp₂₇Alm₇₀Grs₀Sps₁) in Crd2 reflects retrograde Fe-Mg re-equilibration with the Crd2 host. Re-grown euhedral Grt4, formed at the expense of Crd2, is slightly less magnesian (X_{Mg} : 0.31-0.28; Prp₃₀₋₂₇Alm₆₇₋₆₉Grs₁Sps₁) than matrix Grt2. Re-grown rims of Grt4 on Grt2 display a significant decrease of the grossular content (X_{Mg} : 0.35; Prp₃₄Alm₆₃Grs₀Sps₁) whereas the X_{Mg} remains constant.

Grt-Sil gneisses and Grt gneisses

Garnet of the Grt-Sil gneisses and the Grt gneisses shows zonation patterns and compositional variations similar to that observed for garnet of the Qtz-rich Grt-Opx rocks and the Mg-rich Grt-Opx gneisses:

Porphyroblastic Grt2 of the Grt gneiss B-230-E-98 preserves compositionally homogeneous cores (Fig. 5.20a), that were probably flattened by intracrystalline diffusion during high-grade metamorphism. As a result of the lower bulk-rock X_{Mg} of this sample, core-plateau compositions (X_{Mg} : 0.42; Prp₄₀Alm₅₆Grs₃Sps₁) are slightly less magnesian than those of Grt2 of the Mg-rich Grt-Opx gneisses and the Qtz-rich Grt-Opx rock. Rimward zoning to lower X_{Mg} (X_{Mg} : 0.26; Prp₂₆Alm₆₈Grs₄Sps₂) presumably developed during the retrograde formation of the surrounding Crd-Opx symplectites since Mg preferentially fractionated in Crd3 and Opx3. Matrix Grt2 (Fig. 5.20b) of Grt-Sil gneiss B-230-F-98 is completely modified by intercrystalline diffusional Fe-Mg exchange with retrograde Crd-Opx symplectites, that surround and occur in fissures of Grt2.

In both samples re-grown Grt4 is present as euhedral grains in Crd-Opx symplectites. Grt4 is significantly less magnesian (X_{Mg} : 0.16-0.26) than the cores of corresponding Grt2 (Fig. 5.20a), suggesting that Grt4 was formed at lower P-T conditions than Grt2. Rimward zoning to lower X_{Mg} (sample B-230-E-98: core: X_{Mg} : 0.26; Prp₂₄Alm₇₀Grs₂Sps₂, rim: X_{Mg} : 0.19; Prp₁₇Alm₇₆Grs₂Sps₃) in Grt4 is interpreted to result from retrograde Fe-Mg exchange with adjacent Bt4. In the Grt-Sil gneiss B-230-F-98 Grt4 furthermore occurs as re-growth rim on Grt2. These re-growth rim is compositionally similar to Grt4 present in the Crd-Opx symplectites (Fig. 5.20b). Significant variations in the low spessartine and grossular content between Grt2 and Grt4 are not observed.

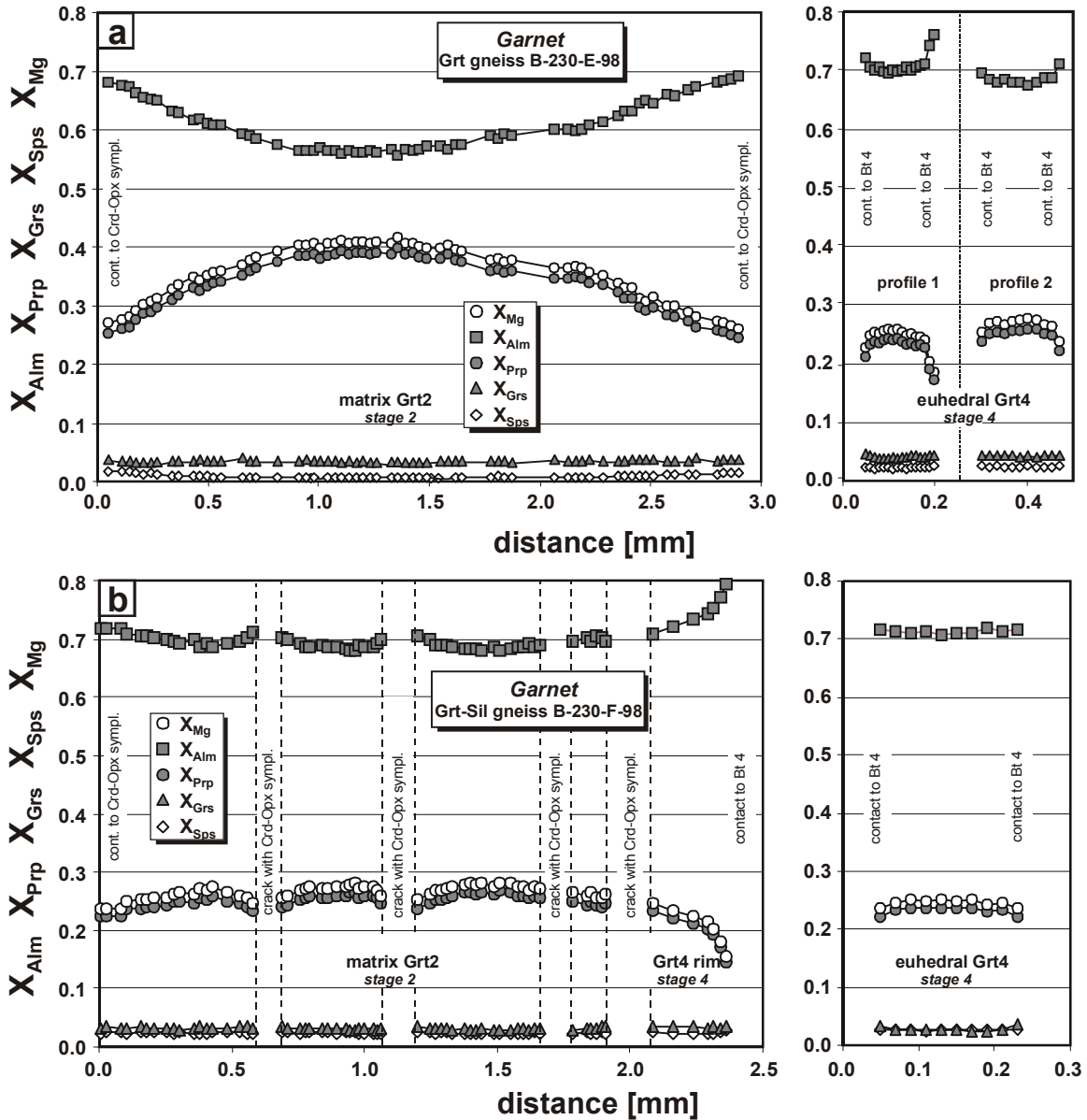


Fig. 5.20: Garnet zoning profiles of **a)** the metagreywacke-type Grt gneiss B-230-E-98 and **b)** the metapelitic Grt-Sil gneiss B-230-F-98 of the Epembe Unit with respect to the textural position. Each profile extends from rim to rim through the core of the garnet grains. Note variable scales.

Sapphirine-bearing Opx-Sil gneisses and Opx-Grt rocks

The garnet zonation patterns of garnet from both the Opx-Sil gneisses and the Opx-Grt rocks are similar to those of other paragneisses:

Early Grt1 inclusions in matrix P12 of the Opx-Grt rocks are moderately magnesian (X_{Mg} : 0.41-0.43; $Prp_{39-40}Alm_{56-54}Grs_4Sps_{1-2}$) and almost unzoned (Fig. 5.21a). Porphyroblastic matrix Grt2 of the same samples is significantly more magnesian (X_{Mg} : 0.54; $Prp_{52}Alm_{44}Grs_3Sps_1$), pointing to its growth at higher P-T conditions. In general, the highest X_{Mg} values of all investigated samples (X_{Mg} : 0.54) are revealed by peak-metamorphic Grt2 of the Opx-Grt rocks. Grt2 grains preserve up to 2 mm wide compositionally homogeneous cores, which were most

likely homogenized by intracrystalline diffusion during highest-grade metamorphism. Zoning to less magnesian compositions (X_{Mg} : 0.42; Prp₄₁Alm₅₅Grs₃Sps₁) towards rims and fissures reflects retrograde Fe-Mg re-equilibration with the surrounding and fissure-filling symplectitic phases.

Matrix Grt2 of the sapphirine-bearing Opx-Sil gneisses displays similar zonation patterns as Grt2 of the Opx-Grt rocks, but lacks compositionally homogeneous cores (Fig. 5.21b). Presumably as a result of its relatively small grain size the original composition of Grt2 was completely modified by intense retrograde Fe-Mg re-equilibration with surrounding symplectite phases, as is suggested by the decrease of X_{Mg} from the cores (X_{Mg} : 0.45-0.39; Prp₄₄₋₃₇Alm₅₃₋₅₉Grs₃₋₂Sps₁) towards rims and fissures (X_{Mg} : 0.38-0.35; Prp₃₇₋₃₄Alm₅₉₋₆₃Grs₃₋₂Sps₂). Grt2 (X_{Mg} : 0.46-0.44; Prp₄₂₋₄₄Alm₅₃₋₅₂Grs₄₋₃Sps₁) occurring together with recrystallized Opx2b along the margins of porphyroblastic Opx2a is compositionally similar to matrix Grt2 and weakly zoned.

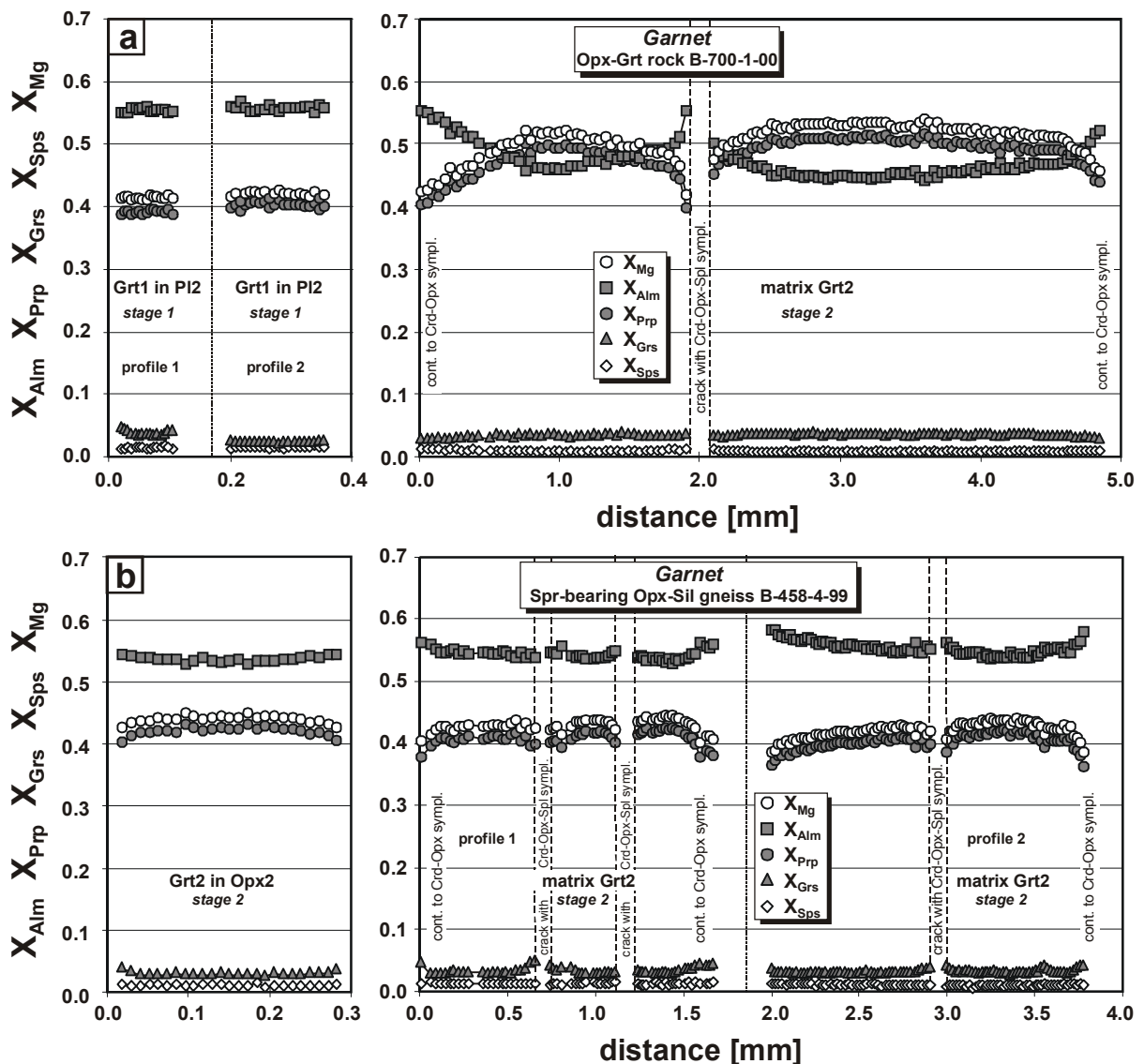


Fig.5.21: Zoning profiles of garnet of a) the Opx-Grt rocks B-700-1-00 and b) the sapphirine-bearing Opx-Sil gneiss B-458-4-99 with respect to the textural position. Profiles extend from rim to rim through the core of the grains. Note variable scales.

5.2.2 Biotite

Biotite is present in most granulites of the Epembe Unit either as prograde inclusion in peak-metamorphic minerals (Bt1), rarely as a peak-metamorphic phase (Bt2) or, more frequently, as a retrograde phase (Bt4), formed at the expense of the peak-metamorphic and symplectitic minerals. Biotite displays significant chemical variations with respect to its textural position (Table A.6.2.2 in the Appendix).

Orthogneisses

Mafic granulites

Rare Bt2 of the mafic granulite B-230-B-98 is the most ferroan biotite of all biotites analyzed (X_{Mg} : 0.48-0.55; Ti p.f.u.: 0.46-0.63).

Grt-Opx metagranitoids

Late Bt4, coexisting with Grt4, of the Grt-Opx metagranitoids has moderate Ti contents (X_{Mg} : 0.59-0.62; Ti p.f.u.: 0.25-0.35) and is affected by an intense retrogression, as is evident from its generally low K_2O contents (6.5-8.0 wt.%).

Paragneisses

Fe-rich and Mg-rich Grt-Opx gneisses and Qtz-rich Grt-Opx rocks

Matrix Bt2 (X_{Mg} : 0.63-0.72; Ti p.f.u.: 0.43-0.63) of the Qtz-rich Grt-Opx rock B-614-1-99 is slightly less magnesian and has higher Ti than late Bt4 (X_{Mg} : 0.65-0.74; Ti p.f.u.: 0.39-0.57; Fig. 5.22a), which was formed at the expense of the Crd-Opx symplectites of the Qtz-rich Grt-Opx rock and the Mg-rich Grt-Opx gneisses. This suggests that Bt2 was just weakly affected by retrograde Fe-Mg exchange. Bt4 in Bt-Qtz symplectites or Bt-Pl-Qtz intergrowths replacing Opx2 is even more magnesian (X_{Mg} : 0.71-0.78; Ti p.f.u.: 0.27-0.60). Bt4 generally has high fluorine contents (1.1-2.6 wt.%).

Biotite of the Fe-rich Grt-Opx gneisses slightly less magnesian than biotite of the Mg-rich Grt-Opx gneisses and the Qtz-rich Grt-Opx rock (Fig. 5.22a). Early Bt1 inclusions (X_{Mg} : 0.67-0.73; Ti p.f.u.: 0.48-0.55) in matrix Grt2 of the Fe-rich Grt-Opx gneisses are more magnesian and have lower Ti contents than matrix Bt2 (X_{Mg} : 0.54-0.58; Ti p.f.u.: 0.53-0.59). The inclusions were probably affected by retrograde Fe-Mg re-equilibration with the Grt2 host. Texturally late Bt4 (X_{Mg} : 0.61-0.66; Ti p.f.u.: 0.48-0.57) coexisting with Grt4 is more magnesian and has lower Ti contents than matrix Bt2. High fluorine contents of 1.4-2.3 wt.% display no systematic variations with respect to the textural position of biotite.

Late Bt4 (X_{Mg} : 0.62-0.63; Ti p.f.u.: 0.52-0.56) coexisting with Grt4 of the cordierite-bearing Qtz-rich Grt-Opx rock B-587-4-99 has a similar composition like late Bt4 (X_{Mg} : 0.59-0.74; Ti p.f.u.: 0.38-0.57) intergrown with Sil4 (Fig. 5.22a). Partly high fluorine contents of Bt4 vary over a large range (0.4-1.8 wt.%).

Grt-Sil gneisses and Grt gneisses

Biotite of the Grt-Sil gneisses and the Grt gneisses is generally less magnesian than that of the Grt-Opx gneisses and the Qtz-rich Grt-Opx rocks (Fig. 5.22a & b).

Early Bt1 inclusions (X_{Mg} : 0.64-0.80; Ti p.f.u.: 0.46-0.65) in matrix Grt2 of the Grt-Sil gneisses and Grt gneisses vary over a large compositional range but are generally more magnesian and have slightly lower Ti contents than matrix Bt2 (X_{Mg} : 0.52-0.60; Ti p.f.u.: 0.51-

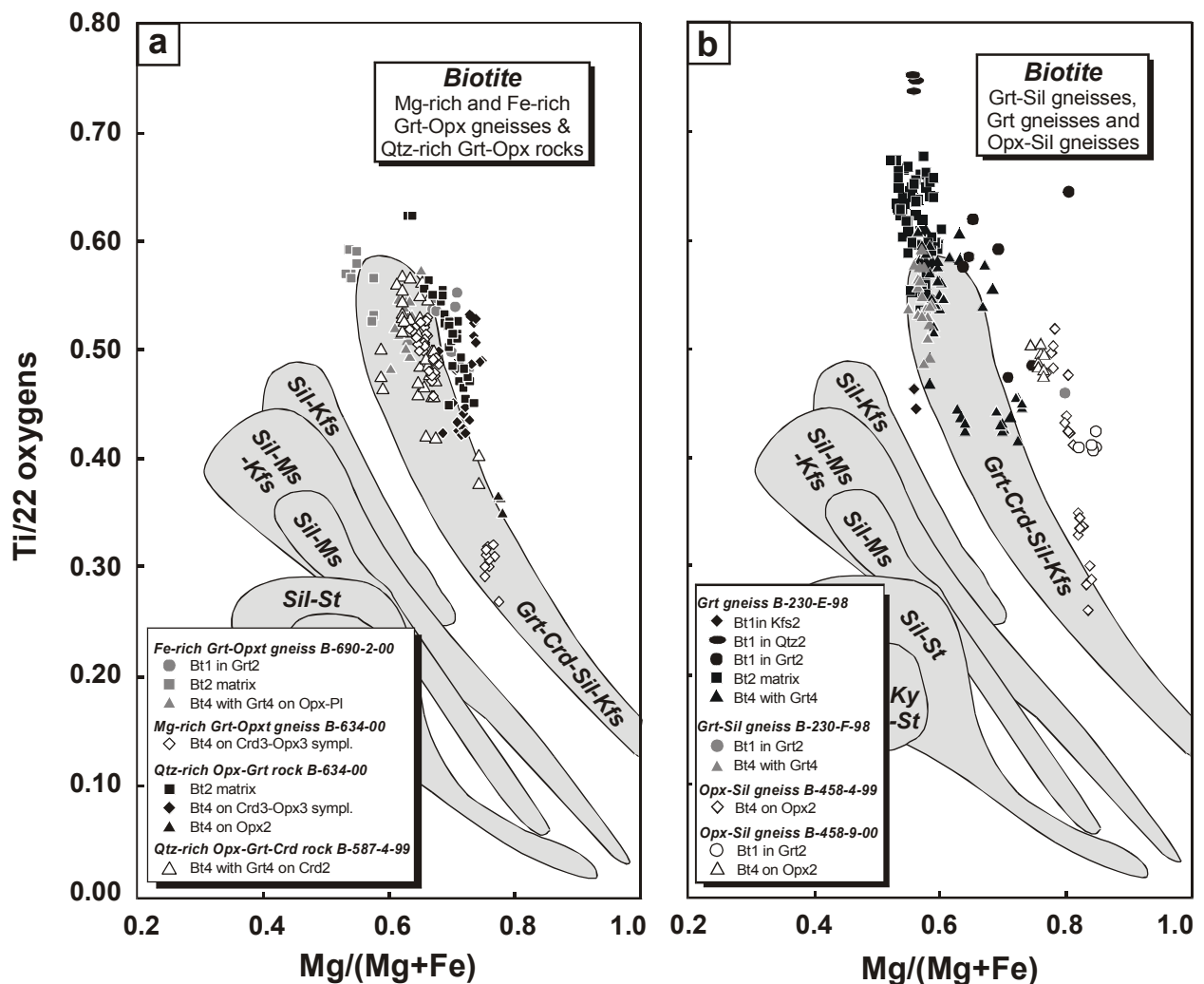


Fig. 5.22: Plot of Ti (per 22 oxygens) as a function of Mg/(Mg+Fe) for biotites of **a)** the Qtz-rich Grt-Opx rocks and the Fe-rich and Mg-rich Grt-Opx gneisses and **b)** the Grt-Sil gneisses, the Grt gneisses and the sapphirine-bearing Opx-Sil gneisses of the Epembe Unit. The shaded fields indicate the compositional range of biotite from metamorphic zones in New England (Robinson et al., 1982).

0.68) of the Grt gneisses (Fig. 5.22b), probably reflecting retrograde Fe-Mg re-equilibration of Bt1 with the Grt2 host during post-peak cooling. This interpretation is supported by the composition of early Bt1 inclusions (X_{Mg} : 0.56; Ti p.f.u.: 0.45-0.46) in Kfs2, that were shielded against retrograde Fe-Mg exchange and therefore yield higher Mg-values than Bt1 enclosed in Grt2. The high Ti contents of matrix Bt2 suggest extraordinarily high peak-metamorphic temperatures. The highest Ti contents of all biotites analyzed were determined for Bt1 (Ti p.f.u.: 0.74-0.75, \cong 6.5-6.7 wt.% TiO₂; X_{Mg} : 0.56) enclosed in matrix Qtz2.

Late Bt4 (Ti p.f.u.: 0.42-0.61) coexisting with Grt4 and formed at the expense of Crd-Opx symplectites of the Grt-Sil gneisses and Grt gneisses has lower Ti contents than matrix Bt2 but still has formed at high-grade metamorphic conditions since it plots in the Grt-Crd-Kfs-Sil field in the X_{Mg} vs. Ti diagram of Robinson et al. (1982; Fig. 5.22b). Bt4 is generally slightly more magnesian (X_{Mg} : 0.55-0.73) than matrix Bt2 and displays zoning with increasing X_{Mg} towards adjacent Grt4. Since Grt4 shows opposite zoning to lower X_{Mg} at Bt4 contacts (see Fig. 5.20 a & b) retrograde Fe-Mg re-equilibration between the two phases during late cooling is postulated. The fluorine contents (0.3-0.7 wt.% F) of the late Bt4 are low.

Sapphirine-bearing Opx-Sil gneisses and Opx-Grt rocks

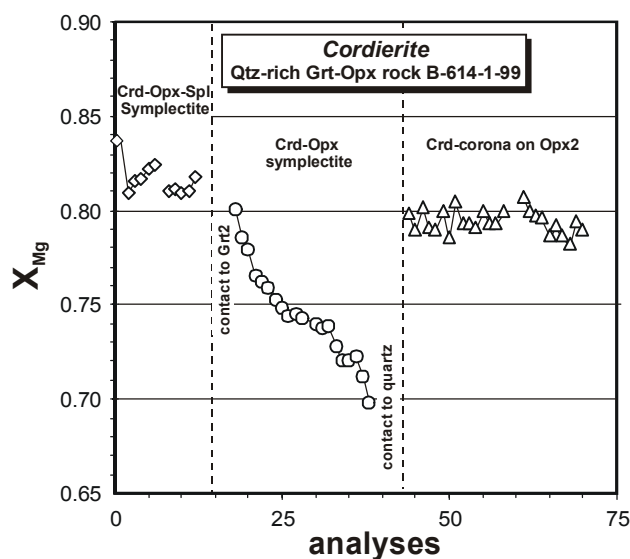
The Opx-Sil gneisses contain the most magnesian biotite (X_{Mg} : 0.80-0.85; Fig. 5.22b) of all studied granulites. Early Bt1 inclusions in Opx2 and Grt2 have the highest X_{Mg} and moderate Ti contents (X_{Mg} : 0.80-0.83; Ti p.f.u.: 0.33-0.48 and X_{Mg} : 0.82-0.85; Ti p.f.u.: 0.40-0.50, respectively). The high X_{Mg} values are probably due to a Fe-Mg re-equilibration with the hosting minerals during retrogression. Late Bt4 (X_{Mg} : 0.76-0.84; Ti p.f.u.: 0.40-0.52), rimming Opx2, is slightly less magnesian and has similar Ti content as Bt1. Late corona-forming Bt4 around Spl2 of the Opx-Grt rocks has a similar composition (X_{Mg} : 0.78-0.80; Ti p.f.u.: 0.40-0.42) like Bt4 of the Opx-Sil gneisses. The fluorine content of all biotites is high (2.0-3.0 wt.%).

5.2.3 Cordierite

Cordierite occurs in most paragneisses of the Epembe Unit as retrograde symplectitic and coronitic phase (Crd3) and only in the Qtz-rich Grt-Opx rock B-587-4-99 as a peak-metamorphic phase (Crd2). Representative analyses of cordierite are shown in Table A.6.2.3 in the Appendix. Partly low total sums (97-99 wt.%) generally point to the presence of fluid species (H₂O, CO₂) in the structural channels. Some cordierite analyses reveal significant amounts of Na₂O (up to 0.5 wt.%).

Mg-rich Grt-Opx gneisses and Qtz-rich Grt-Opx rocks

Crd3 in Crd-Opx-Spl symplectites (X_{Mg} : 0.81-0.87) is more magnesian than Crd3 in Crd-Opx symplectites (X_{Mg} : 0.70-0.86) since the former has grown from the relatively Mg-rich Grt2 cores. These chemical differences are consistent with variations obtained for symplectitic Opx3 (see above). Crd3 in the Crd-Opx symplectites may be strongly zoned to lower X_{Mg} with increasing distance from Grt2 (Fig. 5.23) as a result of retrograde Fe-Mg re-equilibration with Grt2. The preservation of such a retrograde zonation patterns strongly depends on the width of the Crd-Opx symplectite collar: Such a pattern is only preserved in Crd3 of sample B-614-1-99, which occurs in broad coronas of 0.5-1.1 mm in width, whereas Crd3 from the narrow coronas of all other



samples is homogenized. Crd3 (X_{Mg} : 0.80-0.81) in Spl-Crd symplectites, replacing former Sil1 inclusions in Grt2, and corona-forming Crd3 (X_{Mg} : 0.79-0.80) surrounding Opx2 are unzoned. Matrix Crd2 of the Qtz-rich Grt-Opx rock B-587-4-99 is unzoned (X_{Mg} : 0.75-0.81).

Fig. 5.23: Variations of the X_{Mg} of cordierite of the Qtz-rich Grt-Opx rock B-614-1-99 with respect to its textural position.

Grt-Sil gneisses and Grt gneisses

Crd3 of the Grt-Sil gneisses and the Grt gneisses is generally less magnesian (X_{Mg} : 0.70-0.79) than texturally similar Crd3 of the Mg-rich Grt-Opx gneisses and the Qtz-rich Grt-Opx rocks (X_{Mg} : 0.70-0.87). This relationship results from the less magnesian composition of the replaced Grt2 of the Grt-Sil gneisses and the Grt gneisses.

In the double-layer corona textures between Grt2 and matrix Sil2 of the Grt-Sil gneiss B-230-F-98 Crd3 (X_{Mg} : 0.70-0.74) in monomineralic Crd3 coronas is chemically similar to Crd3 (X_{Mg} : 0.71-0.72) in the adjacent Spl-Crd symplectites. Crd3 (X_{Mg} : 0.77-0.79) in Spl-Crd symplectites of Grt gneiss B-230-E-98, replacing Sil1 inclusions in Grt2 cores, is more magnesian than Crd3 in the Spl-Crd symplectites of the Grt-Sil gneiss B-230-F-98. In both samples Crd3 in Crd-Opx symplectites, replacing Grt2 and Qtz2, shows zoning to less magnesian compositions with increasing distance from Grt2 (X_{Mg} : 0.76-0.75 at Grt2 to 0.72-0.71 at Qtz2), suggesting retrograde re-equilibration with the Grt2 rim during late cooling. Crd3 (X_{Mg} : 0.70-0.76) in monomineralic Crd3 coronas around Spl1 inclusions in Grt2 and matrix Spl2 is chemically

similar to other Crd3.

Sapphirine-bearing Opx-Sil gneisses and Opx-Grt rocks

The Opx-Sil gneisses and Opx-Grt rocks contain the most magnesian symplectitic and coronitic Crd3 (X_{Mg} : 0.78-0.89) of all paragneiss samples investigated.

Crd3 in Crd-Opx-Spr symplectites (X_{Mg} : 0.86-0.88) and in Crd-Opx-Spl symplectites (X_{Mg} : 0.86-0.89), both formed at the expense of Grt2, and in monomineralic corona textures around matrix Spr2 (X_{Mg} : 0.83-0.85) has slightly higher X_{Mg} ratios than Crd3 in Crd-Spr symplectites (X_{Mg} : 0.83-0.88), the latter of which result from the breakdown of Grt2-Sil2 and Opx2-Sil2. Crd3 of Crd-Opx symplectites (X_{Mg} : 0.78-0.85), formed by the breakdown of Grt2 and Qtz2, is slightly less magnesian than in Crd-Spr symplectites. The X_{Mg} of late Crd3 (X_{Mg} : 0.83-0.85) from Spl-Crd symplectites replacing symplectitic Spr3, is in the range of Crd3 elsewhere.

5.2.4 Clinopyroxene

Clinopyroxene occurs as peak-metamorphic matrix phase (Cpx2) in the mafic granulites of the Epembe Unit. Representative analyses are depicted in Table A.6.2.5 in the Appendix.

Matrix Cpx2 of the garnet-bearing and the garnet-free two-pyroxene granulites is chemically similar and compositionally ranges from diopside to augite (Fig. 5.24a & b), according to the classification of Morimoto (1988). The analyzed X_{Mg} of Cpx2 generally varies over a large range (X_{Mg} : 0.57-0.69) even though individual grains are essentially unzoned. Non-quadrilateral components are generally below 6.3 mol.% (aegirine: 0.5-2.9 mol.%, Ca-Tschermak's: 0.0-3.8, jadeite: 0.0 mol.%; see Table A.6.2.5).

Matrix Cpx2 of the Grt-Cpx granulite B-311-1-99 is unzoned diopside (Fig. 5.24c), which is generally more magnesian (X_{Mg} : 0.73-0.80) than Cpx2 of the two-pyroxene granulites. The content of the non-quadrilateral components is between 3.1-10.3 mol.%, with aegirine ranging between: 2.2-5.3 mol.% and Ca-Tschermak's ranging between 0.0-7.6 mol.% whereas the jadeite component is always zero (see Table A.6.2.5).

5.2.5 Orthopyroxene

Orthopyroxene is present in the (Grt-bearing) mafic two-pyroxene granulites, in the Grt-Opx metagranitoids and in all investigated paragneisses. Representative analyses are given in Table A.6.2.6 in the Appendix.

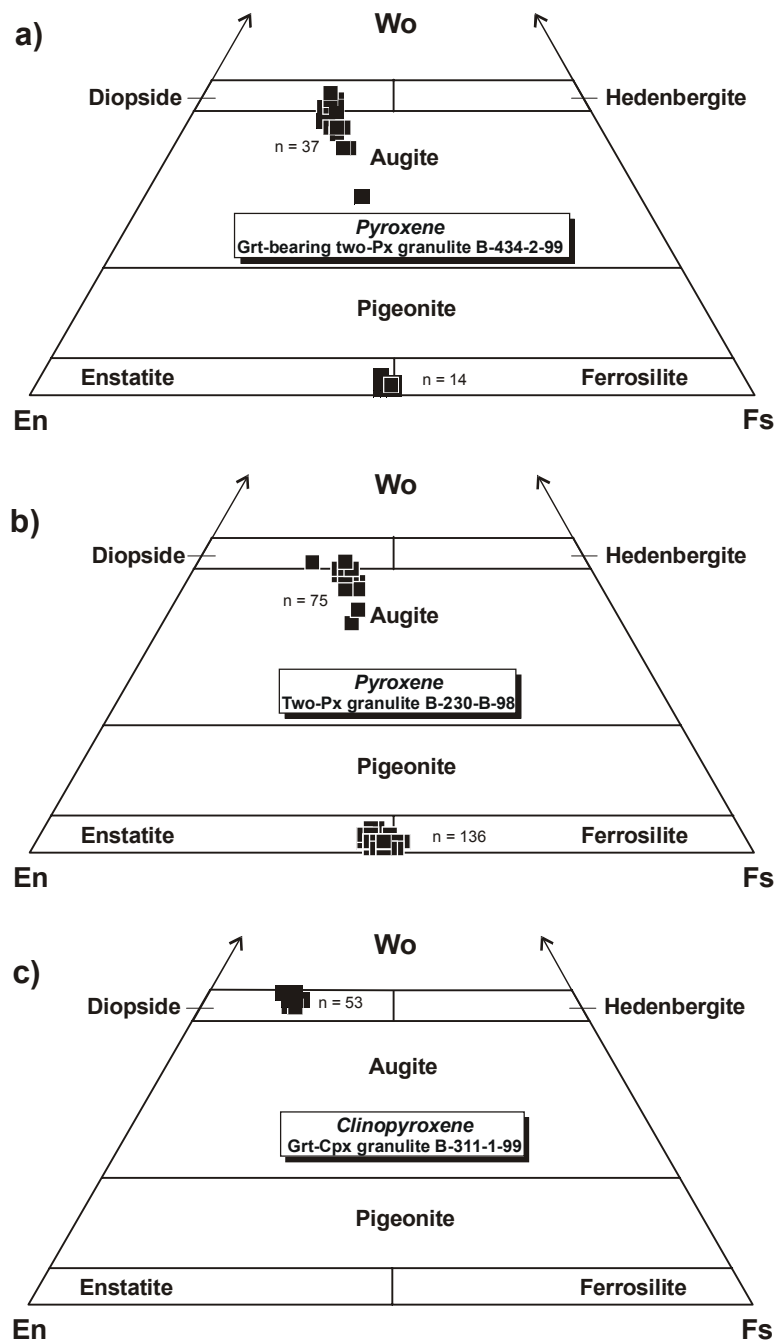


Fig. 5.24: Composition of clinopyroxene and orthopyroxene of **a & b**) the mafic (Grt-bearing) two-pyroxene granulites and **c**) the mafic Grt-Cpx granulite of the Epembe Unit; modified classification after Morimoto (1988).

Orthogneisses

Mafic granulites

Matrix orthopyroxene (Opx₂) of the (Grt-bearing) two-pyroxene granulites is essentially an enstatite-ferrosilite solid solution with only minor amounts of Al (Al^{tot} p.f.u.: 0.02-0.06) and Ca (Ca p.f.u.: 0.02-0.09). In the classification diagram of Morimoto (1988) Opx₂ plots on or near

the enstatite-ferrosilite boundary and is generally slightly less magnesian than the coexisting Cpx2 (Fig. 5.24a & b). Unzoned Opx2 of the garnet-bearing two-pyroxene granulite B-434-2-99 (X_{Mg} : 0.50-0.53) is chemically similar to unzoned Opx2 of the garnet-free two-pyroxene granulite B-230-B-98 (X_{Mg} : 0.49-0.54). In the latter sample Opx2 (X_{Mg} : 0.51-0.54) of Cpx2-free layers is slightly more magnesian than Opx2 (X_{Mg} : 0.49-0.51) of Cpx2-bearing zones.

Grt-Opx metagranitoids

Matrix orthopyroxene (Opx2) of the Grt-Opx metagranitoids is more aluminous and slightly more magnesian (X_{Mg} : 0.54-0.59) than Opx2 of the mafic granulites. Al slightly decreases from core (Al^{tot} p.f.u.: 0.27) towards the rims (Al^{tot} p.f.u.: 0.19), suggesting decreasing temperatures during orthopyroxene-growth.

Paragneisses

In the paragneisses of the Epembe Unit orthopyroxene is present in distinct textural domains and shows systematic compositional variations especially with respect to the partly high alumina content, which can be related to several stages of the metamorphic evolution (Fig. 5.25 & 5.26).

Fe-rich and Mg-rich Grt-Opx gneisses and Qtz-rich Grt-Opx rocks

Orthopyroxene of the Mg-rich Grt-Opx gneisses and the Qtz-rich Grt-Opx rocks shows comparable compositional variations and zonation patterns (Fig. 5.25a & b): The highest X_{Mg} and Al contents are preserved in the cores of porphyroblastic peak-metamorphic Opx2 (Al^{tot} p.f.u.: 0.52-0.42; X_{Mg} : 0.65-0.70) present in Grt2-absent domains of the Mg-rich Grt-Opx gneiss B-458-3-99. Opx2 coexisting with Grt2 is slightly less magnesian than Opx2 in Grt2-absent domains but preserves similar high Al contents in the core (Al^{tot} p.f.u.: 0.45-0.39; X_{Mg} : 0.61-0.65). Such high Al contents of orthopyroxene coexisting with garnet are a characteristic feature of ultrahigh-temperature (UHT) granulites (Harley, 1998a). In both textural domains Opx2 displays significant rimward zoning to less aluminous compositions and lower X_{Mg} (Al^{tot} p.f.u.: 0.30-0.12; X_{Mg} : 0.59-0.62; Fig. 5.25a & b), suggesting release of the Mg-Tschermak's component ($MgAl_2SiO_6$) towards the adjacent reaction domains. Opx3 in retrograde Opx-Pl corona textures around Grt2 is less magnesian (X_{Mg} : 0.54-0.56) than Opx2 (Fig. 5.25b), presumably as it was formed from the relatively Fe-rich Grt2 rims. Al in coronitic Opx3 is generally high (Al^{tot} p.f.u.: 0.38-0.26) but lower than in Opx2 cores, testifying to decreasing, but still very high temperatures during corona formation. Symplectitic Opx3 is less aluminous than coronitic Opx3 (Fig. 5.25a & b), which indicates that symplectite formation proceeded at lower temperatures, supporting the interpretation that the symplectites formed subsequently to the outer

Opx-Pl corona. The high X_{Mg} of Opx3 in Crd-Opx-Spl symplectites (X_{Mg} : 0.63-0.70; Al^{tot} p.f.u.: 0.24-0.15) probably reflects symplectite formation at the expense of the relatively Mg-rich Grt2 cores. Opx3 in Crd-Opx symplectites has similar Al contents but is significantly less magnesian (X_{Mg} : 0.52-0.66; Al^{tot} p.f.u.: 0.25-0.12) since it has grown from the relatively Fe-rich Grt2 rims. The highest X_{Mg} values are obtained for Opx3 in direct contact to Grt2 rims, suggesting Fe-Mg re-equilibration during later cooling. Late-stage, corona-forming Opx5 replacing retrograde Bt4 is characterized by the lowest Al contents (Al^{tot} p.f.u.: 0.16-0.09; X_{Mg} : 0.52-0.64) of all investigated orthopyroxenes.

In summary, orthopyroxene of the Mg-rich Grt-Opx gneisses and the Qtz-rich Grt-Opx rocks displays a systematic decrease in the Al content, that is correlated with its textural occurrence and indicates decreasing temperatures in the following temporal sequence: Matrix Opx2 (cores) > matrix Opx2 (rims) \cong Opx3-Pl3 > Crd3-Opx3 > late Opx5. Variations of the X_{Mg} are controlled by changing P-T conditions and the composition of coexisting garnet.

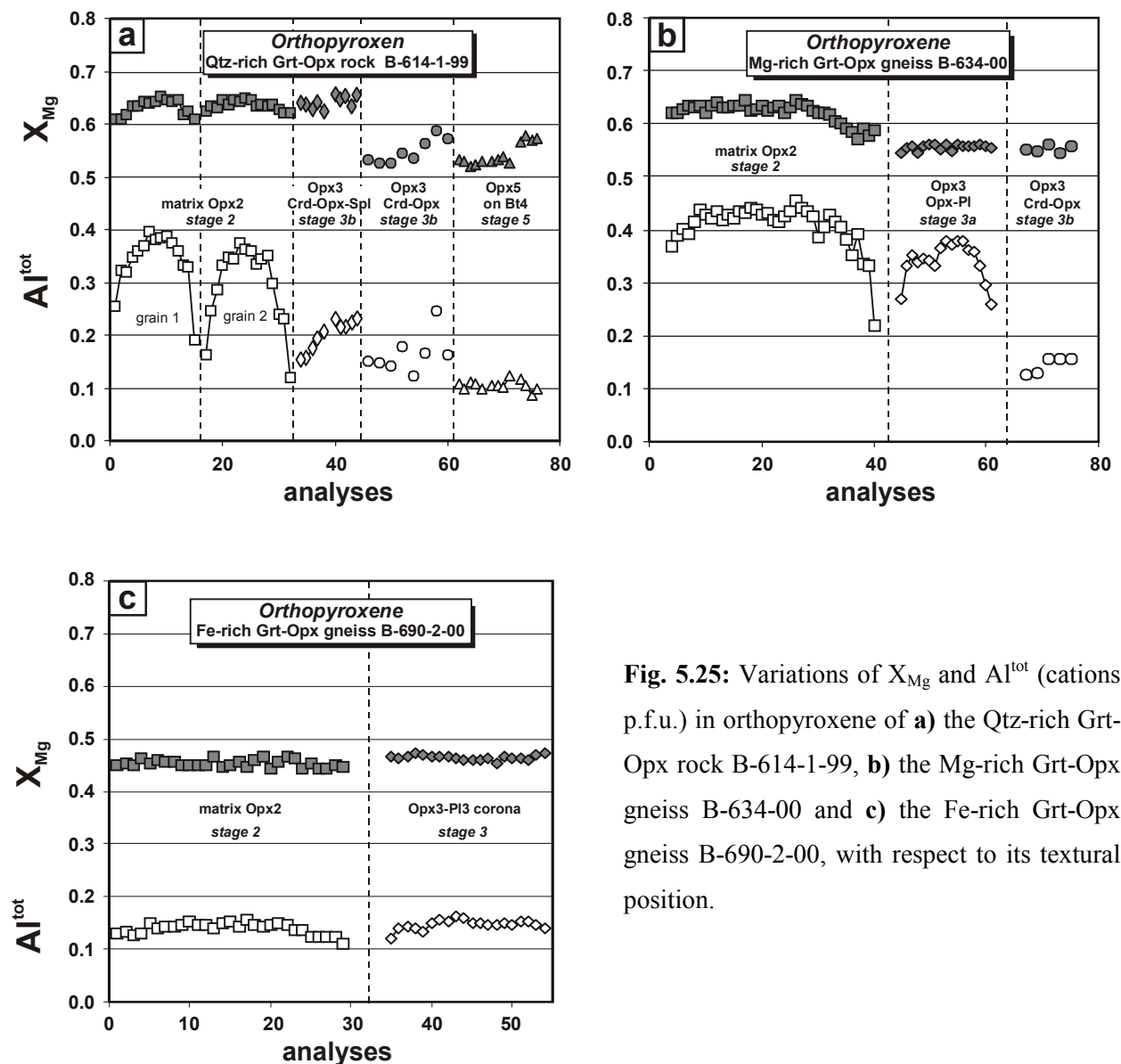


Fig. 5.25: Variations of X_{Mg} and Al^{tot} (cations p.f.u.) in orthopyroxene of **a)** the Qtz-rich Grt-Opx rock B-614-1-99, **b)** the Mg-rich Grt-Opx gneiss B-634-00 and **c)** the Fe-rich Grt-Opx gneiss B-690-2-00, with respect to its textural position.

Orthopyroxene of the Fe-rich Grt-Opx gneiss B-690-2-00 is the most ferroan Opx of all granulites analyzed. The two textural types of orthopyroxene reveal only minor chemical variations (Fig. 5.25c). The composition of matrix Opx2 varies in a restricted range (X_{Mg} : 0.44-0.46) with generally low Al contents (Al^{tot} p.f.u.: core: 0.15; rim: 0.11), that slightly decrease towards the rim, suggesting Opx2 growth under slightly decreasing temperatures. Opx3 in retrograde Opx-Pl coronas resorbing peak-metamorphic Grt2 is slightly more magnesian than Opx2 but has similar Al contents (X_{Mg} : 0.45-0.47; Al^{tot} p.f.u.: 0.12-0.16).

Prograde Opx1 inclusions in Grt2 of the cordierite-bearing Qtz-rich Grt-Opx rock sample B-587-4-99 are more magnesian and less aluminous (X_{Mg} : 0.66-0.68; Al^{tot} p.f.u.: 0.18-0.17) than matrix Opx2 (X_{Mg} : 0.55-0.64). The latter shows slight rimward zoning to lower Al contents (Al^{tot} p.f.u.: core: 0.33; rim: 0.30). Retrograde Opx3 is not present in the cordierite-bearing Qtz-rich Grt-Opx rock.

Grt-Sil gneisses and Grt gneisses

In the Grt-Sil gneisses and the Grt gneisses orthopyroxene occurs in retrograde Crd-Opx symplectites replacing Grt2. The Al content of Opx3 (X_{Mg} : 0.51-0.57; Al^{tot} p.f.u.: 0.23-0.16) in the inner Crd-Opx symplectites adjacent to Grt2 rims is slightly higher than that of Opx3 (X_{Mg} : 0.50-0.54; Al^{tot} p.f.u.: 0.18-0.10) in outer, block-like zones adjacent to Qtz2.

Sapphirine-bearing Opx-Sil gneisses and Opx-Grt rocks

Orthopyroxene of the sapphirine-bearing Opx-Sil gneisses and the Opx-Grt rocks display comparable compositional variations (Fig. 5.26a & b), that resemble those observed for the Mg-rich Grt-Opx gneisses and Qtz-rich Grt-Opx rocks (Fig. 5.25a & b). However, due to the more magnesian bulk-rock chemistry of the Opx-Sil gneisses and the Opx-Grt rocks, orthopyroxene is more magnesian when compared to Opx occurring in comparable textural positions in the Mg-rich Grt-Opx gneisses and Qtz-rich Grt-Opx rocks.

Prograde Opx1 inclusions in matrix Pl2 of the Opx-Grt rocks has high Al contents (X_{Mg} : 0.66-0.69; Al^{tot} p.f.u.: 0.44-0.38) and is essentially unzoned, as it is shielded against a retrograde overprint by the hosting Pl2. Matrix Opx2a of the Opx-Sil gneisses and the Opx-Grt rocks preserves extraordinary high Al contents in the core (Al^{tot} p.f.u.: 0.50-0.40; maximum: 11.7 wt.% Al_2O_3), clearly indicating their formation under UHT conditions. Rimward zoning to lower Al contents (Al^{tot} p.f.u.: 0.40-0.27) suggests decreasing temperatures during Opx2a growth. The X_{Mg} (0.64-0.73) of Opx2a is generally high and constant for individual grains. The Al content of recrystallized Opx2b (X_{Mg} : 0.71-0.73; Al^{tot} p.f.u.: 0.41-0.36) of the Opx-Sil gneisses, intergrown with Spr2b at Opx2a grain margins, is unzoned and chemically similar to Opx2a rim

compositions, suggesting continuously decreasing temperatures during orthopyroxene recrystallization. Opx2b of the Opx-Sil gneisses, which occurs in intergrowths with Grt2, is slightly less aluminous than that observed in intergrowths with Spr2b but displays similar zonation patterns with a rimward decreasing Al content (Al^{tot} p.f.u.: 0.38 (core) \rightarrow 0.32 (rim)). The X_{Mg} slightly increases towards the contact against Grt2 (X_{Mg} : 0.70 \rightarrow 0.72), suggesting retrograde Fe-Mg exchange. Opx2b inclusions in Grt2 of the Opx-Sil gneisses and the Opx-Grt rocks display similar rimward decreasing Al contents (Al^{tot} p.f.u.: 0.43-0.23), suggesting that Grt2 was formed during decreasing temperatures and is not in equilibrium with porphyroblastic Opx2a. The X_{Mg} ratios of the Opx2b inclusions generally vary between 0.61 and 0.76, however, a comparably narrow compositional range is revealed by individual grains and samples. The highest X_{Mg} values were measured for the outermost margin of Opx in contact to garnet, suggesting retrograde Fe-Mg exchange between Grt2 and Opx2b inclusions.

Post-peak Opx3 is generally characterized by lower Al contents than those of Opx2a and Opx2b (Fig. 5.26a & b): Opx3 in Opx-Pl coronas resorbing Grt2 is slightly zoned with Al^{tot} values decreasing from 0.36 in the core to 0.25 at the rim. The similar Al content of coronitic Opx3 when compared to recrystallized Opx2b suggests that the replacement of Grt2 and the recrystallization of Opx2 took place under similar temperatures. The X_{Mg} of coronitic Opx3 is unzoned and slightly lower (X_{Mg} : 0.66-0.70) than that of Opx2a and Opx2b. Opx3 in Crd-Opx-Spr symplectites has similar Al contents (Al^{tot} p.f.u.: 0.35-0.31) and X_{Mg} values (0.68-0.70) as coronitic Opx3. In the Opx-Sil gneisses Opx3 (Al^{tot} p.f.u.: 0.25-0.23; X_{Mg} : 0.68-0.76) in Crd-Opx-Spl symplectites and Opx3 (Al^{tot} p.f.u.: 0.19-0.15; X_{Mg} : 0.59-0.64) in Crd-Opx symplectites has the lowest Al contents (Fig. 5.26a). In the Opx-Grt rocks Opx3 of the Crd-Opx-Spl symplectites has partly high Al contents (Al^{tot} p.f.u.: 0.28-0.22; X_{Mg} : 0.74-0.76; Fig. 5.26b). Opx3 of the Crd-Opx symplectites has lower Al contents and is less magnesian (Al^{tot} p.f.u.: 0.23-0.20; X_{Mg} : 0.63-0.64) than that of the Crd-Opx-Spl symplectites since it has formed from the relatively Fe-rich Grt2 rims.

The systematic drop in the Al content of orthopyroxene (Opx2a (cores) > Opx2a (rims) > Opx2b-Spr2b > Opx2b-Grt2 > Opx3-Pl3 > Crd3-Opx3-Spr3 > Crd3-Opx3-Spl3 > Crd3-Opx3) suggests decreasing temperatures during the retrograde formation of the reaction sequence.

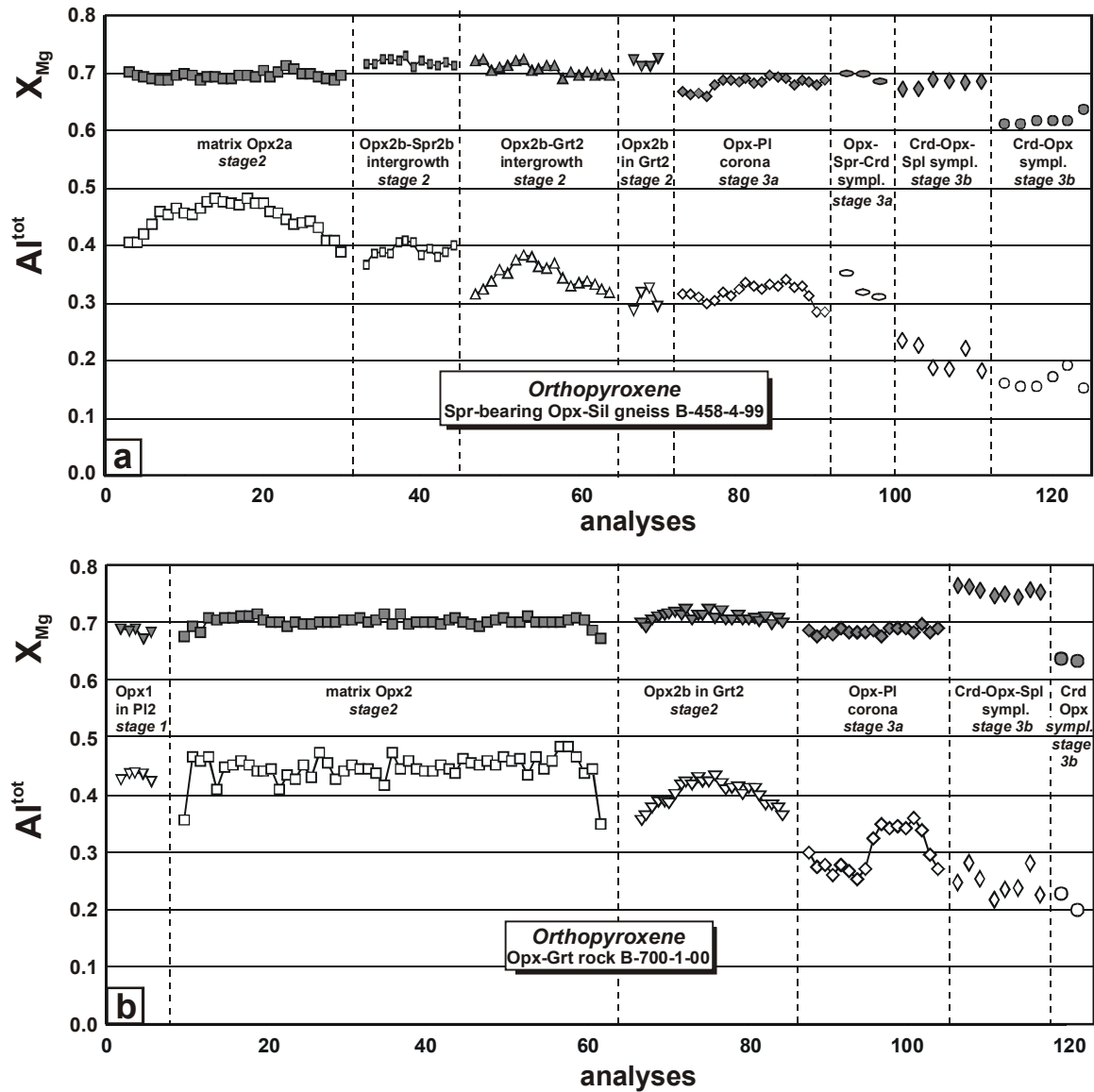


Fig. 5.26: Variations of X_{Mg} and Al^{tot} (cations p.f.u.) in orthopyroxene of **a)** the sapphirine-bearing Opx-Sil gneiss B-458-4-99 and **b)** the Opx-Grt rock B-700-1-00, with respect to its textural position.

5.2.6 Amphibole

In the mafic granulites and in the Grt-Opx metagranitoids amphibole occurs in various textural positions and shows variable compositions (Fig. 5.27; Table A.6.2.7 in the Appendix).

Mafic granulites

According to the classification of Leake et al. (1997), prograde (Hbl1) and retrograde amphibole (Hbl4) of the Grt-Cpx granulite is pargasite (Fig. 5.27a), that displays significant compositional variations with respect to its textural position: Inclusions of green pargasite (Hbl1; X_{Mg} : 0.74-0.81; Ti p.f.u.: 0.10-0.11) in Grt2 are magnesian and display a zoning pattern with the highest

X_{Mg} ratios being determined at hornblende-garnet contacts, hence indicating retrograde intercrystalline Fe-Mg re-equilibration. Inclusions of brown Hbl1 in Grt2 are less magnesian and have higher Ti contents (X_{Mg} : 0.61-0.64; Ti p.f.u.: 0.36-0.42) with the highest X_{Mg} being detected at the contacts to Grt2. As the incorporation of Ti in amphibole generally increases with the metamorphic grade (e.g. Raase, 1974; Spear, 1981) the higher Ti contents of brown Hbl1 when compared to green Hbl1 indicate higher temperatures during its consumption. Retrograde green pargasite in granoblastic Hbl4-P14 intergrowths (X_{Mg} : 0.64-0.72; Ti p.f.u.: 0.13-0.21) and in Hbl4-P14 symplectites (X_{Mg} : 0.69-0.74; Ti p.f.u.: 0.10-0.18), both replacing Grt2 and Cpx2, is more magnesian and has lower Ti contents than brown Hbl1 inclusions, therefore suggesting formation of Hbl4 at lower temperatures. In the Hbl-P1 symplectite Hbl4 is slightly zoned, with X_{Mg} continuously increasing and Ti continuously decreasing from the matrix contacts towards the Grt2 margin (X_{Mg} : 0.69; Ti p.f.u.: 0.18 and X_{Mg} : 0.74; Ti p.f.u.: 0.12, respectively). The Ti zonation suggests decreasing temperatures during Grt2 resorption. Taking into account the X_{Mg}

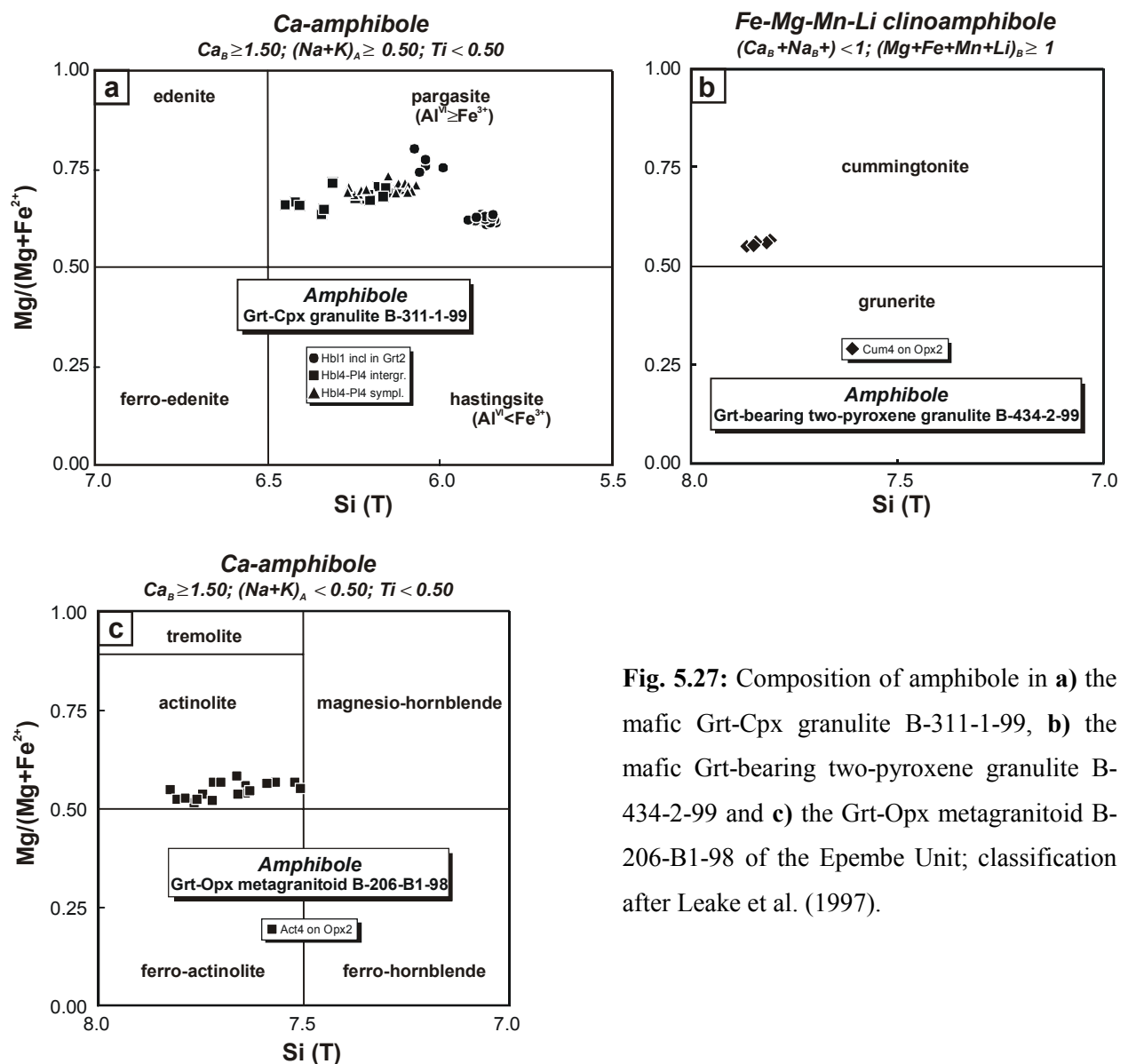


Fig. 5.27: Composition of amphibole in a) the mafic Grt-Cpx granulite B-311-1-99, b) the mafic Grt-bearing two-pyroxene granulite B-434-2-99 and c) the Grt-Opx metagranitoid B-206-B1-98 of the Epembe Unit; classification after Leake et al. (1997).

drop at the Grt2 rims (Fig. 5.18a) the opposite X_{Mg} zonation of Hbl4 points to retrograde Fe-Mg exchange between Grt2 rims and Hbl4 during cooling.

Retrograde corona-forming cummingtonite (Cum4; X_{Mg} : 0.55-0.57; Ti p.f.u.: 0.01; Fig. 5.27b) replacing Opx2 of the two-pyroxene granulites varies in a restricted compositional range, which is close to the X_{Mg} ratio of the resorbed Opx2 (X_{Mg} : 0.50-0.53).

Grt-Opx metagranitoids

In the Grt-Opx metagranitoid B-206-B1-98 matrix Opx2 is completely replaced by actinolite (Act4; X_{Mg} : 0.51-0.58; Fig. 5.27c).

5.2.7 Sapphirine

Sapphirine occurs as inclusion in Grt2 (Spr2b), as peak-metamorphic matrix phase (Spr2a & b) and as retrograde symplectitic phase (Spr3) in the Opx-Sil gneisses of the Epembe Unit. Representative analyses are listed in Table A.6.2.8 in the Appendix.

Sapphirine from all textural positions is magnesian (X_{Mg} : 0.72-0.79) and contains significant amounts of ferric iron (Fe^{3+} / Fe^{tot} : 0.10-0.23). The X_{Mg} of sapphirine is always higher than that of the coexisting orthopyroxene. Depending on its textural mode sapphirine displays systematic chemical variations in terms of extent of the Mg-Tschermak's substitution ($MgSi = Al^{VI}Al^{IV}$), with compositions ranging between the 7:9:3 endmember $Mg,Fe)_7Al_{18}Si_3O_{40}$ and 2:2:1 endmember $Mg,Fe)_8Al_{16}Si_4O_{40}$ (Fig. 5.28), thus supporting the observation of three stages of sapphirine-growth:

Porphyroblastic matrix Spr2a is the most Si-rich sapphirine and shows a slight zonation: The Al content increases from core (Al^{tot} p.f.u.: 8.37-8.42; X_{Mg} : 0.72-0.76) towards the rim (Al^{tot} p.f.u.: 8.46-8.72; X_{Mg} : 0.75). Spr2b, intergrown with recrystallized Opx2b, shows an opposite zonation pattern with the Al contents decreasing from core (Al^{tot} p.f.u.: 8.56; X_{Mg} : 0.80) to rim (Al^{tot} p.f.u.: 8.41; X_{Mg} : 0.77). Spr2b, which is enclosed by Grt2, is more aluminous (Al^{tot} p.f.u.: 8.63-8.75; X_{Mg} : 0.77-0.79). Retrograde Spr3 is generally more aluminous and more magnesian than Spr2. Spr3 in Crd-Opx-Spr symplectites is highly aluminous (Al^{tot} p.f.u.: 8.69-8.76; X_{Mg} : 0.77-0.79), whereas Spr3 in Crd-Spr symplectites has intermediate Al contents (Al^{tot} p.f.u.: 8.53-8.61). No significant differences of the X_{Mg} have been observed between Spr3 formed by Grt2 breakdown (X_{Mg} : 0.74-0.78) and Spr3, which replaces magnesian Opx2 (X_{Mg} : 0.74-0.79).

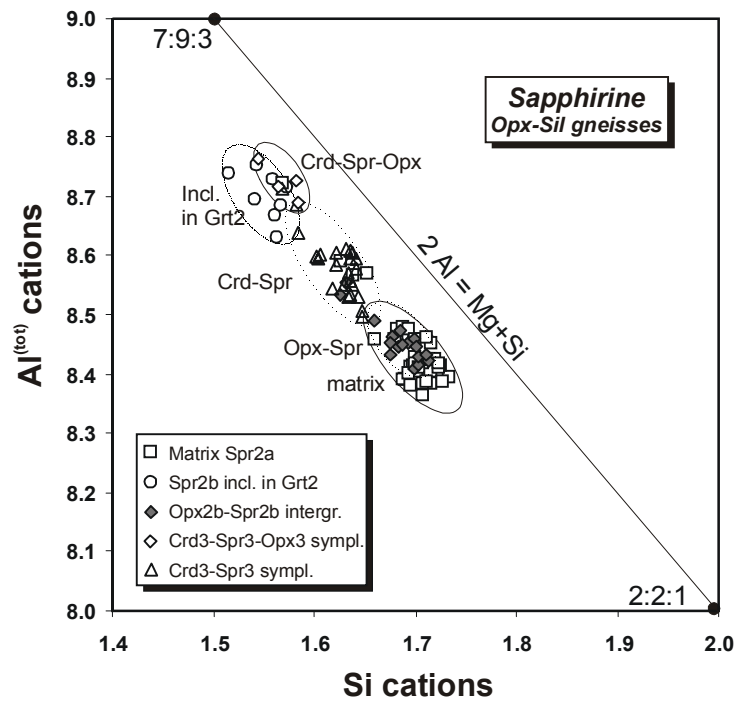


Fig. 5.28: Al^{tot} (cations p.f.u.) versus total Si (cations p.f.u.) diagram showing the compositional variations in sapphirine of the Opx-Sil gneisses with respect to the textural occurrence. Positions of the 7:9:3 and 2:2:1 end-members are indicated. Due to the significant amounts of Fe^{3+} the compositions plot below the ideal Tschermak's substitution line.

5.2.8 Spinel

Spinel is present in most paragneisses of the Epembe Unit and occurs as prograde inclusions (Spl1) in Grt2, as a rare matrix phase (Spl2) and in retrograde symplectites (Spl3), formed at the expense of Grt2, Sil2 or Spr3. In the symplectites Spl3 is always the most Fe-rich ferromagnesian phase. Spinel is essentially a hercynite-spinel solid solution with partly high gahnite (0.1-16.1 mol %), low chromite (0.1-1.5 mol %) and low magnetite (1.2-5.5 mol %) components, as calculated from ideal stoichiometry (Table A.6.2.9 in the Appendix).

Mg-rich Grt-Opx gneisses and Qtz-rich Grt-Opx rocks

Spl3 (X_{Mg} : 0.39-0.48) in Crd-Opx-Spl symplectites replacing Grt2 is more magnesian than Spl3 (X_{Mg} : 0.31-0.36) in Spl-Crd symplectites replacing Sil1 inclusions in Grt2. In both textures the gahnite component of Spl3 is < 3.5 mol.%.

Grt-Sil gneisses and Grt gneisses

Spl1 inclusions (X_{Mg} : 0.25-0.30; 6.6-9.6 mol.% gahnite) in Grt2 rims have similar composition like matrix Spl2 (X_{Mg} : 0.22-0.27; 6.8-13.8 mol.% gahnite). In contrast, retrograde Spl3 in Spl-

Crd symplectites has lower ZnO contents (3.1-5.2 mol.% gahnite). Since Spl3 (X_{Mg} : 0.32-0.33) in Spl-Crd symplectites of Grt gneiss B-230-E-98 has grown from Sil1 inclusions in relatively Mg-rich Grt2 cores it is more magnesian than Spl3 (X_{Mg} : 0.20) in similar Spl-Crd symplectites of the Grt-Sil gneiss B-230-F-98, that were formed from matrix Sil2 and adjacent and relatively Mg-poor Grt2 rims.

Sapphirine-bearing Opx-Sil gneisses and Opx-Grt rocks

Spl1 inclusions (X_{Mg} : 0.42-0.43; 15.1-15.5 mol.% gahnite) in Grt2 of the Opx-Grt rocks are more magnesian than matrix Spl2 (X_{Mg} : 0.33-0.36; 14.3-16.1 mol.% gahnite), but exhibit similar high ZnO contents. In contrast, retrograde Spl3 in Crd-Opx-Spl symplectites, replacing Grt2 of the Opx-Grt rocks, has low ZnO contents (X_{Mg} : 0.47-0.52; 1.0-1.2 mol.% gahnite). Spl3 (X_{Mg} : 0.30) from Crd-Opx-Spl symplectites replacing Grt2 of the Opx-Sil gneisses is less magnesian. Spl3 from Spl-Crd symplectites replacing symplectitic Spr3 varies over a large compositional range (X_{Mg} : 0.30-0.45; < 0.7 mol.% gahnite).

5.2.9 Ilmenite

Ilmenite is present in most granulites and occurs as prograde inclusions in the peak-metamorphic minerals (Ilm1), as peak-metamorphic matrix phase (Ilm2) and in the retrograde symplectites (Ilm3). Ilmenite displays minor chemical variations with respect to both its textural position and the rock type (Table A.6.2.10 in the Appendix).

Mafic granulites

Matrix Ilm2 of the two-pyroxene granulites and the Grt-Cpx granulites contains significant amounts of hematite (4.3-7.3 and 1.3-4.7 wt.% Fe_2O_3 , respectively) and pyrophanite (1.1-1.3 and 3.4-3.9 wt.% MnO, respectively).

Grt-Opx metagranitoids

Matrix Ilm2 is the almost pure ilmenite endmember with minor amounts of Fe_2O_3 and MnO (0.3-1.4 wt.% and 0.2-0.3 wt.%, respectively).

Fe-rich and Mg-rich Grt-Opx gneisses and Qtz-rich Grt-Opx rocks

Minor systematic variations depending on the textural position of ilmenite are observed with respect to its calculated Fe_2O_3 content: Since early Ilm1 inclusions in Grt2 of the Qtz-rich Grt-

Opx rocks and Fe-rich Grt-Opx gneisses generally contain minor Fe₂O₃ (0.0-1.2 wt.% Fe₂O₃) matrix Ilm2 of the both samples and of the Mg-rich Grt-Opx gneisses and the Qtz-rich Grt-Opx rocks are virtually devoid of Fe₂O₃ (0.0-0.8 wt.% Fe₂O₃). In contrast, late Ilm3 in retrograde Crd-Opx symplectites of the Qtz-rich Grt-Opx rocks contain considerable Fe₂O₃ (0.7-1.3 wt.% Fe₂O₃). The MnO content of ilmenite is generally low (0.3-2.2 wt.% MnO), irrespective of its textural position.

Grt-Sil gneisses and Grt gneisses

Ilmenite of the Grt-Sil gneisses and the Grt gneisses displays similar chemical variations like that of the other paragneisses: In contrast to matrix Ilm2 (0.0-1.6 wt.% Fe₂O₃), early Ilm1 inclusions (0.6-3.1 Fe₂O₃) in Spl2 and Grt2 as well as late Ilm3 (0.5-5.0 wt.% Fe₂O₃), which is present in retrograde Spl-Crd symplectites, contain significant amounts of Fe₂O₃. The low MnO content displays no systematic variation with respect to the textural position (0.4-2.0 wt.% MnO).

5.2.10 Rutile

Prograde rutile inclusions (Rt1) in Grt2 of the mafic Grt-Cpx granulite, in Grt2 of the Grt gneiss and in Grt2 of the Qtz-rich Grt-Opx rock as well as matrix rutile (Rt2) of the Grt-Sil gneiss, of the Qtz-rich Grt-Opx rocks and of the Opx-Sil gneisses display no significant chemical variations. In all textural position rutile is the almost pure endmember and contains only minor amounts of FeO (0.1-2.0 wt.% FeO; Table A.6.2.10 in the Appendix).

5.2.11 Sillimanite

Peak-metamorphic matrix sillimanite (Sil2) of the Opx-Sil gneisses and the Grt-Sil gneisses and late sillimanite (Sil4) of the cordierite-bearing Qtz-rich Grt-Opx rock B-587-4-99 contain traces of Fe₂O₃ (0.3-0.5 wt.%; Table A.6.2.10 in the Appendix).

5.2.12 Plagioclase

Plagioclase is present in all investigated granulite samples and occurs as prograde inclusions (P11), as peak-metamorphic phase (P12) or as retrograde coronitic or symplectitic phase (P13 & P14). Plagioclase of all granulite facies rock types contains minor orthoclase (Or₁₋₂), while the celsian component is < 0.5 mol % (Table A.6.2.11 in the Appendix).

Orthogneisses

Mafic granulites

Early P11 inclusions in matrix Cpx2 of the two-pyroxene granulite sample B-230-B-98 are more calcic (An₆₃₋₆₇) than matrix Pl2 (An₅₃₋₅₆) of the same sample. The latter rarely displays an inverse zonation with an abrupt increase of the An content at the outermost margins (An₆₅₋₆₉). In contrast, matrix Pl2 of the Grt-bearing two-pyroxene granulite sample B-434-2-99 is essentially unzoned (An₅₇₋₆₀).

P11 inclusions in Grt2 of the Grt-Cpx granulite are generally zoned with rimward increasing An contents (core: An₃₆₋₃₉; rim: An₄₃₋₄₅). P11 inclusions in matrix Cpx2 are always more calcic (An₅₃₋₅₈). Late Pl4 in retrograde Hbl4-Pl4 symplectites replacing Grt2 and in granoblastic Hbl4-Pl4 intergrowths are compositionally similar (An₅₂₋₆₀ and An₅₀₋₆₉, respectively) like the P11 inclusions in Cpx2. Matrix plagioclase is not present in the Grt-Cpx granulite.

Grt-Opx metagranitoids

Major chemical variations between early plagioclase inclusions (P11; An₄₄₋₄₆) in Grt2 and unzoned matrix plagioclase (Pl2; An₄₄₋₄₉) of the Grt-Opx metagranitoid sample B-206-B1-98 are not observed. Unzoned matrix Pl2 of Grt-Opx metagranitoid 646 is slightly less calcic (An₃₇₋₄₀).

Paragneisses

Fe-rich and Mg-rich Grt-Opx gneisses and Qtz-rich Grt-Opx rocks

Prograde plagioclase inclusions (P11) in matrix Grt2 of the Mg-rich Grt-Opx gneiss sample B-634-00 are relatively Ca-rich and slightly zoned with rimward decreasing An contents (core: An₅₆; rim: An₅₃; Fig. 5.29a). Peak-metamorphic matrix plagioclase (Pl2) of the same sample is significantly less calcic (An₂₇₋₃₂) than P11 and essentially unzoned. Matrix Pl2 of the Mg-rich Grt-Opx gneiss B-458-3-99 (An₃₆₋₄₁) and the Qtz-rich Grt-Opx rock B-614-1-99 (An₃₂₋₃₆) is slightly more calcic and shows a weak zonation with a rimward increase of the An content. Late plagioclase (Pl3) in retrograde Opx-Pl coronas (sample B-634-00: An₂₈₋₃₁) is slightly zoned with decreasing An content towards resorbed Grt2 (Fig. 5.29a), consistent with decreasing pressure during corona formation. Pl3 in Crd-Opx symplectites (sample B-458-3-99: An₄₀₋₄₄) resorbing Grt2 is essentially unzoned and has a similar composition like matrix Pl2 of the sample.

Plagioclase of the Fe-rich Grt-Opx gneiss B-690-2-00 displays similar compositional variations depending on its textural position like those observed for plagioclase of the Mg-rich Grt-Opx gneisses but is always more calcic (Fig. 5.29a & b). Early P11 enclosed in the cores of porphyroblastic Grt2 preserves higher anorthite contents (An₅₆₋₅₉) than P11, which is enclosed in the Grt2 margins (An₅₁₋₅₂). Matrix Pl2 is less calcic (An₃₉₋₄₉) and individual grains are essentially

unzoned. Exsolutions in antiperthitic Pl2 are orthoclase with significant albite component ($Ab_9Or_{89}An_0Cs_2$). Late Pl3 in Opx-Pl coronas resorbing Grt2 is compositionally similar (An_{37-48}) to matrix Pl2 and shows a zonation with moderately decreasing An content with increasing distance from the resorbed Grt2, pointing to a pressure decrease during the formation of the corona.

Matrix Pl2 of the cordierite-bearing Qtz-rich Grt-Opx rock B-587-4-99 is essentially unzoned (An_{35-39}) and compositionally similar to Pl2 of the Qtz-rich Grt-Opx rock B-614-1-99.

Grt-Sil gneisses and Grt gneisses

Significant compositional variations between unzoned matrix Pl2 (An_{35-42}) and late Pl3 (An_{35-43}), forming monomineralic coronas around Sil2 or present in Crd-Opx symplectites, are not obtained.

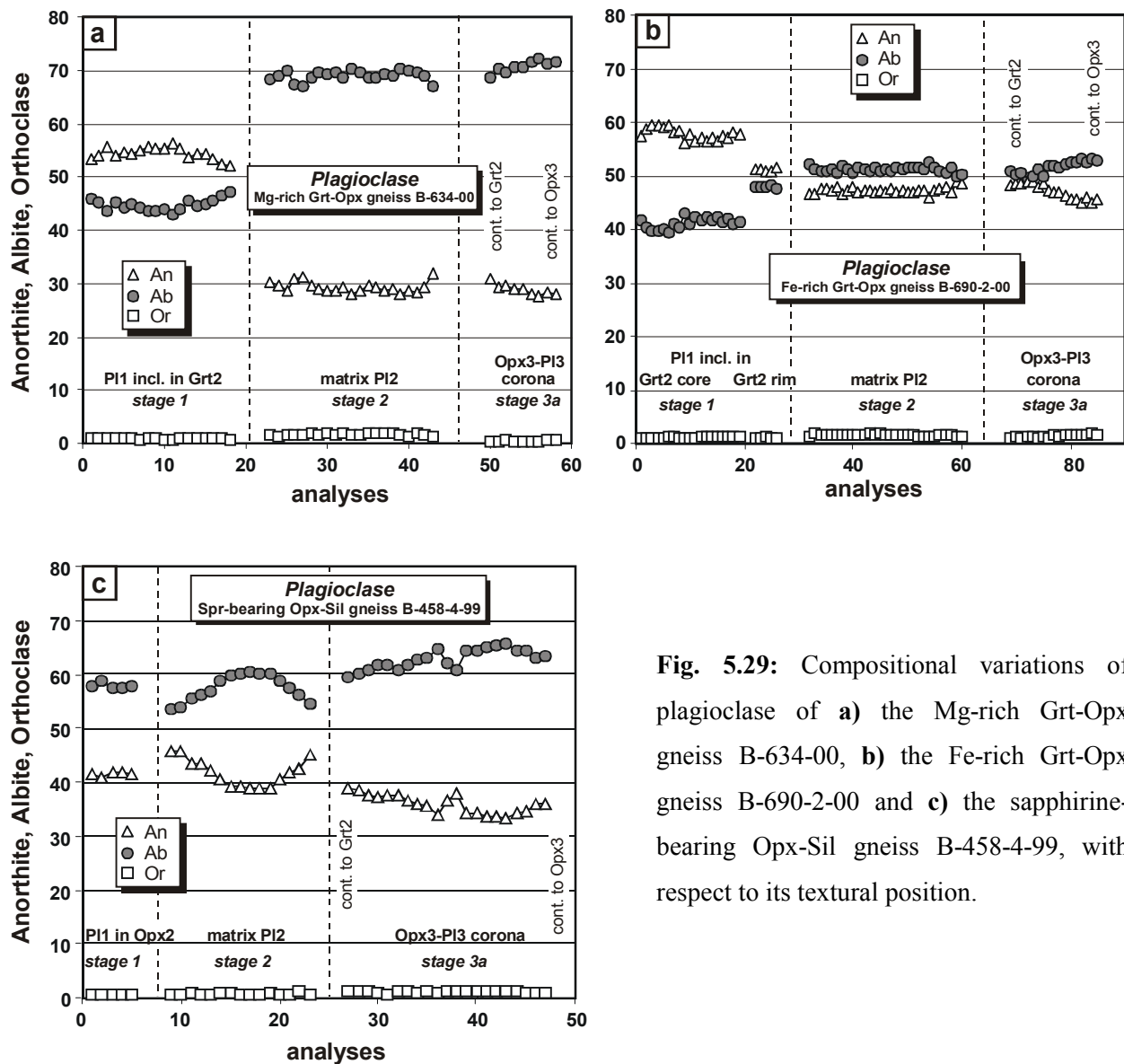


Fig. 5.29: Compositional variations of plagioclase of a) the Mg-rich Grt-Opx gneiss B-634-00, b) the Fe-rich Grt-Opx gneiss B-690-2-00 and c) the sapphire-bearing Opx-Sil gneiss B-458-4-99, with respect to its textural position.

Sapphirine-bearing Opx-Sil gneisses and Opx-Grt rocks

Early P11 inclusions (An_{41-42}) in Opx2 of the Opx-Sil gneisses are similar in composition to matrix P12 (An_{28-46} ; Fig. 5.29c). Individual P12 grains are slightly zoned and become more calcic towards the rim. Matrix P12 (core: An_{32} ; rims: An_{36}) of the Opx-Grt rock displays similar compositions and zonation patterns like P12 of the Opx-Sil gneisses. Retrograde P13 in Opx-Pl coronas resorbing Grt2 is slightly less calcic than P12 of the corresponding samples and smoothly zoned with increasing An content from coronitic Opx3 (An_{33}) towards the inner Crd-Opx symplectite (An_{39}), consistent with decreasing pressures during corona formation. P13 (An_{27-36}) occurring between Grt2 and Sil2 is unzoned and similar in composition to matrix P12 of the same sample.

5.2.13 Alkalifeldspar

Alkalifeldspar is a common matrix phase (Kfs2) of the Grt-Opx metagranitoids and most paragneisses. Representative analyses are given in Table A.6.2.12 in the Appendix.

Grt-Opx metagranitoids

Homogeneous matrix Kfs2 of Grt-Opx metagranitoid B-206-B1-98 has a composition ranging between $Or_{91-88}Ab_{7-9}An_0Cels_2$.

Grt-Sil gneisses and Grt gneisses

The composition of the host of perthitic matrix Kfs2 of Grt gneiss B-230-E-98 shows compositions of $Or_{89-80}Ab_{10-19}An_0Cels_1$, whereas the exsolved lamellae are albite-rich ($Or_{19}Ab_{79}An_2Cels_0$). The perthitic Kfs2 host of Grt-Sil gneiss B-230-F-98 ranges between $Or_{92-81}Ab_{7-17}An_{0-1}Cels_{0-1}$. Analyzed exsolved lamellae in Kfs2 of the Grt-Sil gneiss B-230-F-98 are mixture analyses of the host and the exsolution.

5.3 MINERAL REACTION HISTORY

The investigated granulites of the Epembe Unit preserve conspicuous reaction textures and mineral assemblages, that are attributed to a multistage P-T evolution. Information on the prograde metamorphic evolution is mainly revealed by mineral inclusions in the peak-metamorphic minerals and migmatitic textures as displayed by most of the granulite facies rock samples. Abundant and well-preserved reaction textures, replacing the peak-metamorphic phases, provide an excellent opportunity for the reconstruction of the retrograde evolution.

5.3.1 Mafic granulites

The P-T evolution of the metabasites of the Epembe Unit can be evaluated by interpreting the sequence of reaction textures in terms of phase equilibria in the model system CFMASH. This is illustrated for part of the reactions in Fig. 5.30 for the system CMASH.

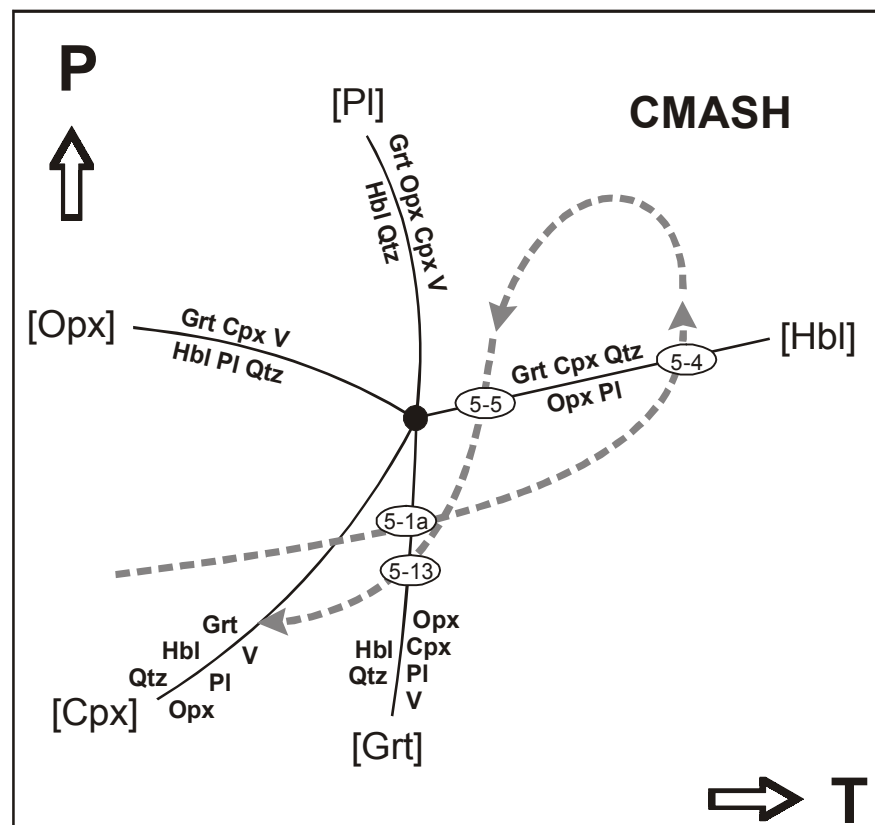
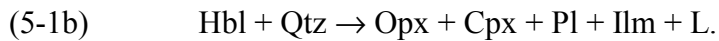


Fig. 5.30: P-T path most probably followed by the mafic granulites of the Epembe Unit, as deduced from the observed mineral assemblages and the sequence of reaction textures. The schematic P-T diagram shows the key phase relationships in metabasites in the system CMASH (after Wells, 1979), assuming the presence of quartz and water. The numbers in the P-T path refer to reactions discussed in the text.

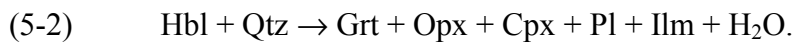
Stage 1: Prograde evolution and Stage 2: Peak-metamorphic assemblages

Corroded inclusions of greenish or brownish Hbl₁, Pl₁ and Qtz₁ in peak-metamorphic Cpx₂ and Opx₂ (Fig. 5.1a) of the basic two-pyroxene granulites indicate an almost complete replacement of an initial amphibolite facies mineral assemblage Hbl-Pl-Qtz by the anhydrous, granulite facies two-pyroxene assemblage during prograde metamorphism, according to the dehydration reactions



The related melt-producing reaction (5-1b) explains the local formation of plagioclase-rich leucosomes in the mafic granulites. Ilmenite is probably formed from released Ti of former Ti-bearing hornblende.

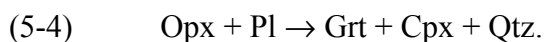
Garnet-bearing two-pyroxene granulites are probably formed by the related reaction



Inclusions of Czo₁, Bt₁, Hbl₁ and Pl₁ in cores of Grt₂ (Fig. 5.2b) testify to the replacement of a prograde amphibolite facies Bt-Czo-Hbl-Pl assemblage during prograde heating in the ultrabasic Grt-Cpx granulites. Inclusions of Pl₁ and Opx₁ in matrix Cpx₂ indicate that the formation of orthopyroxene pre-dates the formation of clinopyroxene and was probably related to the reaction



The occurrence of early Opx₁ and Pl₁ preserved as corroded inclusion in the cores of Cpx₂ (Fig. 5.2c), point to subsequent growth of the coarse-grained Grt₂-Cpx₂ assemblage at the expense of the earlier Opx₁-Pl₁ assemblage probably due the reaction

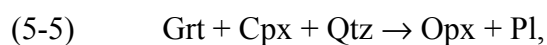


The lack of quartz is possibly related to the SiO₂-poor bulk-rock composition of the ultrabasic Grt-Cpx granulites.

Progress of reactions (5-1a) testifies to an initial temperature increase from amphibolite to granulite facies conditions (Fig. 5.30). Prograde heating is furthermore consistent with reactions (5-2) and (5-3). Progress of reaction (5-4) indicates a pressure increase following initial heating (Fig. 5.30).

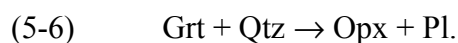
Stage 3: Corona and symplectite formation

The formation of Opx₃-Pl₃ intergrowths between Cpx₂ and Grt₂ (Fig. 5.2a) of the Grt-Cpx granulites point to post-peak progress of reaction (5-4) in a reverse direction



which also explains rims of Opx₃ around Cpx₂ (Fig. 5.2d).

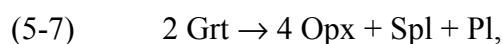
Opx₃-Pl₃ intergrowths around Grt₂ from clinopyroxene-free domains of the Grt-Cpx granulites (Fig. 5.2e) most probably reflect progress of the related reaction



Both reactions are consistent with near-isothermal decompression (near-ITD) still under granulite facies conditions (e.g. Harley, 1989; see Fig. 5.30). Fine-grained Opx₃-Pl₃ intergrowths, which outline the shape of former garnet, also occur in the two-pyroxene granulites (Fig. 5.1b). Rare relic Grt₂ in the intergrowths points to their formation according to reaction (5-5) and/or (5-6), that also explain broad monomineralic corona textures of Pl₃ around Grt₂.

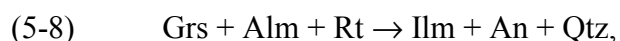
Both reactions necessitate the presence of quartz, which is generally absent in the metabasites of the Epembe Unit. Harley (1989) suggested that Opx-Pl coronas in quartz-free mafic rocks may be formed by an increase in the silica-activity through reaction with (1) adjacent felsic gneisses, (2) a melt phase or (3) fluids. As the mafic granulites of the Epembe Unit are interlayered with felsic granulites and various migmatitic paragneisses, options (1) and (2) are plausible to explain Opx-Pl corona formation. Reaction (5-6) also explains the formation of thin Opx₃-Pl₃ rims around Grt₂, separating it from matrix Qtz₂ (Fig. 5.3a), of the mafic Grt-Opx-Pl-Qtz granulites of the intermediate dykes.

Opx₃-Pl₃-Spl₃ intergrowths, present in the core region of former Grt₂ of the two-pyroxene granulites (Fig. 5.1c), suggest garnet-breakdown under silica-deficient conditions according to reaction



which was balanced for a pyrope-almandine with 16.5 mol % grossular component (Griffin, 1971) and is also consistent with decompression (e.g. Thost et al., 1990).

Pl₃ rims around Rt₁ inclusions in Grt₂ of the Grt-Cpx granulites are interpreted to result from progress of the GRIPS reaction



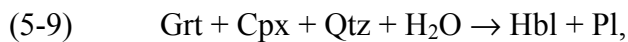
which is consistent with decompression.

In summary, progress of reactions (5-5) to (5-8) document that the early retrograde evolution of the mafic granulites is characterized by near-isothermal decompression (Fig. 5.30). The presence of orthopyroxene in the retrograde reaction textures testifies to granulite facies condition during decompression.

Stage 4: Re-growth of garnet and amphibole

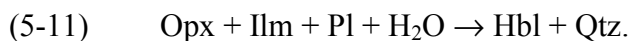
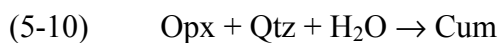
The further retrograde evolution is characterized by the widespread re-growth of amphibole, locally coexisting with a second generation of garnet, quartz and plagioclase, formed by various rehydration reactions:

In the Grt-Cpx granulites the decompressional Opx₃-Pl₃ intergrowths between Cpx₂ and Grt₂ are followed by a granoblastic pargasitic Hbl₄-Pl₄ intergrowth and a pargasitic Hbl₄-Pl₄ symplectite adjacent to Grt₂ (Fig. 5.2a & e) formed by progress of reaction

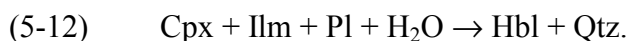


which also explains the formation of finger-like Hbl₄-Pl₄ intergrowths, replacing Grt₂ of the two-pyroxene granulites (Fig. 5.1e).

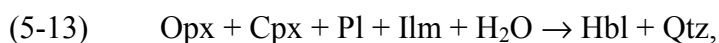
Monomineralic coronas of Cum₄, that are locally followed by a second, outer corona of green Hbl₄ intergrown with Qtz₄, around Opx₂ of the two-pyroxene granulites, indicate progress of reactions



The partial or complete replacement of Cpx₂ by brownish or greenish Hbl₄, intergrown with Qtz₄, is related to the reaction

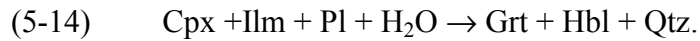


Reactions (5-11) and (5-12) also explain coronas of Hbl₄ around Ilm₂. Combination of reactions (5-11) and (5-12) results in reaction

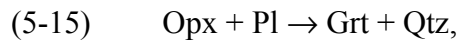


that accounts for the rehydration of the mafic (Grt-bearing) two-pyroxene granulites of the Epembe Unit.

The formation of subhedral Grt₄, coexisting with Hbl₄ and Qtz₄, at the expense of Cpx₂, Pl₂ and Ilm₂ (Fig. 5.1f) suggests progress of reaction



Rims of Grt₄, coexisting with Qtz₄, around peak-metamorphic Opx₂ and Pl₂ (Fig. 5.3b) of the Grt-Opx-Pl-Qtz granulites of the intermediate dykes document progress of reaction



the reversal of reaction (5-6).

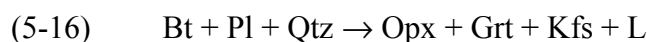
Rehydration reactions (5-9) to (5-14) are consistent with post-decompressional cooling (Fig. 5.30) and document the transition from granulite to amphibolite facies conditions. The re-growth of garnet testifies to crossing of the Grt-in curve, which has a shallow, positive slope in the P-T space (e.g. Green & Ringwood, 1967). Thus, progress of reaction (5-15) indicates, that cooling was near-isobaric.

5.3.2 Felsic granulites and Grt-Opx metagranitoids

Stage 1: Prograde evolution and Stage 2: Peak-metamorphic assemblages

Mineral inclusions are not preserved in the peak-metamorphic mineral assemblages of the metavolcanic felsic granulites of the Epembe Unit. However, the formation of the two-pyroxene assemblages is probably related to progress of the reaction (5-1), which has been postulated for the formation of the mafic two-pyroxene granulites.

Peak-metamorphic Grt₂ and Opx₂ of the metagranitoids preserve corroded inclusions of Bt₁, Pl₁ and Qtz₁, which suggest that the formation of the peak-metamorphic mineral assemblages is related to progress of the dehydration-melting reaction



postulated by Vielzeuf & Montel (1994) to explain biotite-dehydration melting of metagreywackes.

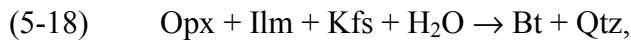
The growth of Grt₂ with inclusions of green spinel (Fig. 5.4c), present in quartz-absent domains of the Grt-Opx metagranitoids, is probably related to the dehydration-melting reaction



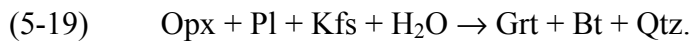
Stage 4: Re-growth of garnet, biotite and amphibole

Rims of amphibole (Hbl4) around pyroxene of the felsic granulites are attributed to progress of reaction (5-13) which has previously been formulated for the re-growth of amphibole in the mafic granulites.

The formation of Bt4-Qtz4 symplectites around matrix Opx2 of the Kfs-bearing Grt-Opx metagranitoids (Fig. 5.4b) indicates rehydration according to reaction



Re-growth of garnet (Grt4), biotite (Bt4) and Qtz4 at the expense of Opx2 (Fig. 5.4b) in the Grt-Opx metagranitoids is probably related to progress of the reaction



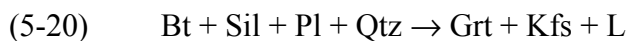
5.3.3 Paragneisses

The multistage P-T evolution of the paragneisses of the Epembe Unit can be evaluated and quantified by interpreting the sequence of conspicuous reaction textures of individual rock types and samples in terms of the ternary S-FM-A diagram (Fig. 5.17a) and in terms of phase equilibria in the model systems KFMASH and FMAS (Fig. 5.31; 5.33; 5.35). Furthermore, AFM diagrams were calculated using selected mineral chemical data (Fig. 5.32 & 5.34).

5.3.3.1 Fe-rich and Mg-rich Grt-Opx gneisses and Qtz-rich Grt-Opx rocks

Stage 1: Prograde evolution and Stage 2: Peak-metamorphic assemblages

Inclusions of Bt1, Pl1, Qtz1 and Sil1 in porphyroblastic Grt2 (Fig. 5.6a) of the Mg-rich Grt-Opx gneisses and the Qtz-rich Grt-Opx rocks suggest continuous progress of the fluid-absent dehydration-melting reaction



during prograde heating through the stability field of sillimanite. The unorientated appearance of the mineral inclusions indicates static conditions during heating. The lack of sillimanite inclusions in porphyroblastic Opx2 suggests that orthopyroxene formed subsequently to the complete consumption of matrix sillimanite, exhausted by reaction (5-20), and consequently after initial garnet growth. This interpretation is in agreement with the presence of Grt1 inclusions in Opx2 (Fig. 5.6b) and explains the lack of Opx-Sil-Qtz assemblages. Inclusions of Bt1, Pl1 and Qtz1 in Opx2 point to growth of orthopyroxene accompanied by continued garnet

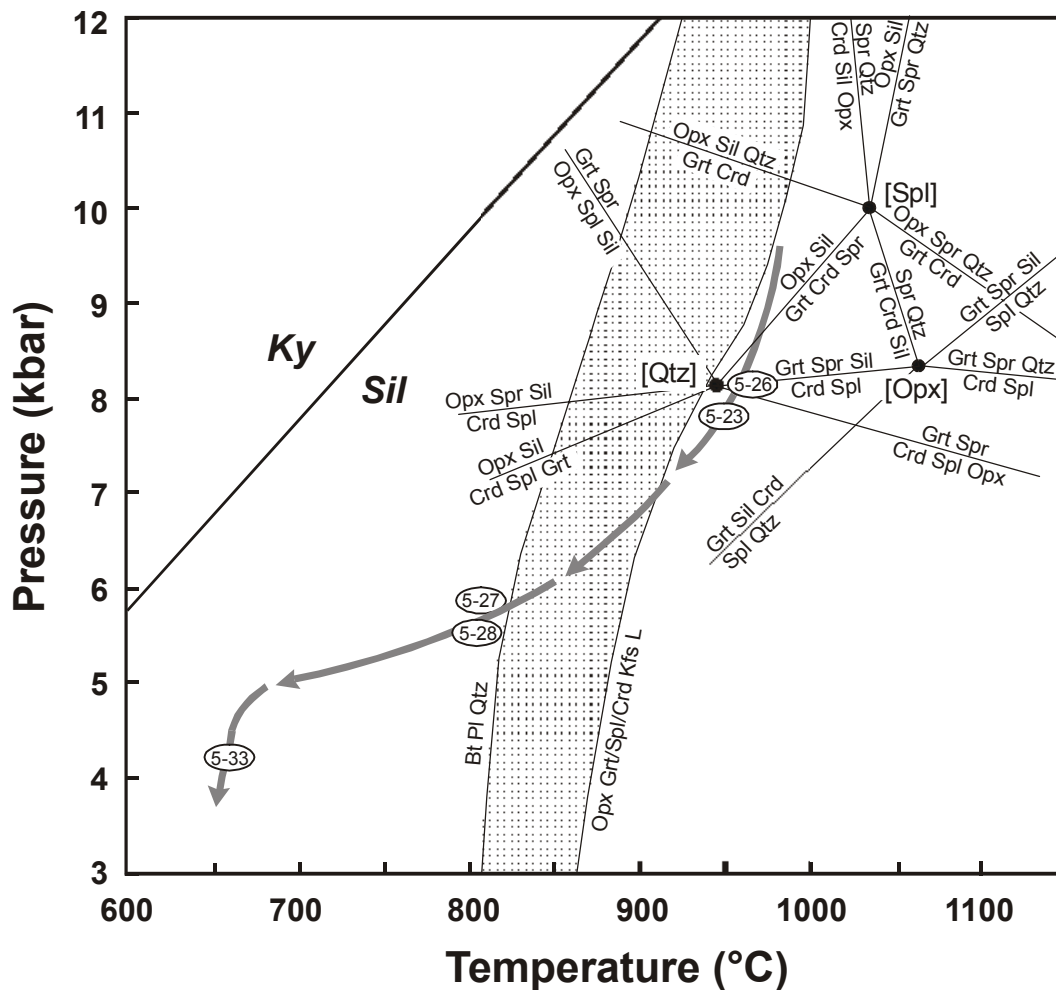
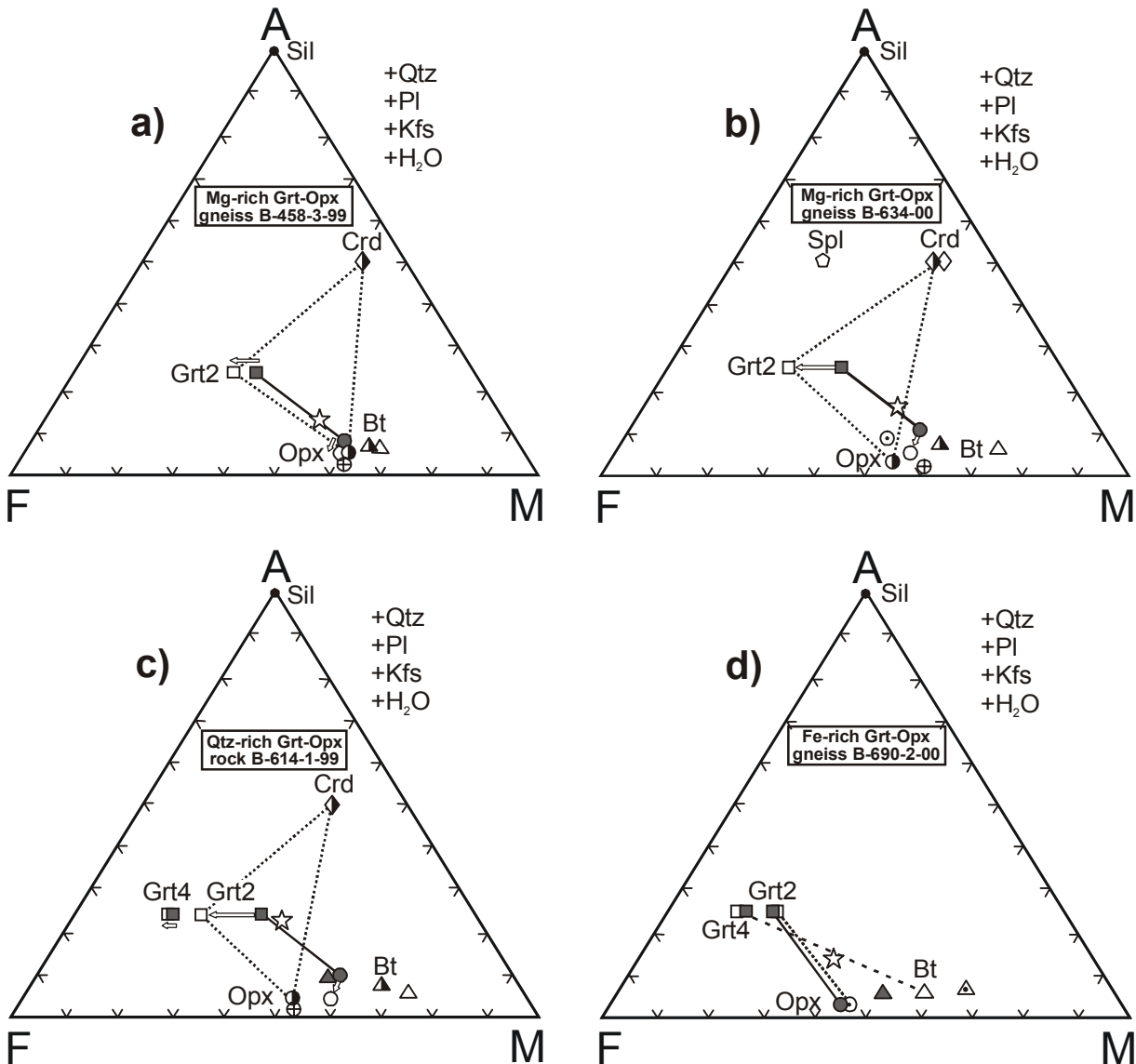


Fig. 5.31: P-T path most probably followed by the Grt-Opx gneisses and the Qtz-rich Grt-Opx rocks of the Epembe Unit, as deduced from the observed mineral assemblages and the sequence of reaction textures. The petrogenetic grid for high-grade, low $f(\text{O}_2)$ metapelites in the system FMAS is based on Hensen & Green (1973); Hensen (1987), Hensen & Harley (1990), Bertrand et al. (1991) and Harley (1998a). Also shown is the interval of the fluid-absent dehydration melting reaction $\text{Bt} + \text{Pl} + \text{Qtz} \rightarrow \text{Opx} + \text{Grt/Spl/Crd} + \text{Kfs} + \text{L}$ (stippled field) of Vielzeuf & Montel (1994). The numbers in the P-T path refer to reactions discussed in the text.

growth, according to the fluid-absent biotite dehydration-melting reaction (5-16) $\text{Bt} + \text{Pl} + \text{Qtz} \rightarrow \text{Opx} + \text{Grt} + \text{Kfs} + \text{L}$. The deduced reaction sequence with orthopyroxene formed subsequently to initial garnet growth is consistent with the observation of Montel & Vielzeuf (1997) that reaction (5-20) occurs at lower temperatures than reaction (5-16). Progress of reaction (5-16) and (5-20) resulted in the almost complete replacement of matrix biotite and furthermore explains the production of melt, that is recorded by the presence of garnet and/or orthopyroxene-bearing leucosomes. According to fluid-absent biotite-dehydration melting experiments for an aluminous and moderately magnesian metagreywacke (bulk-rock X_{Mg} : 0.49; Vielzeuf & Montel, 1994), similar in composition to the studied Mg-rich Grt-Opx gneisses and Qtz-rich Grt-Opx rocks

(bulk-rock X_{Mg} : 0.52-0.56), reaction (5-16) takes place at temperatures between 890°C and 990°C (at 10 kbar; Fig. 5.31) and produces garnet and highly aluminous orthopyroxene (Montel & Vielzeuf, 1997) similar in composition to high-Al Opx2 of the studied granulites. The

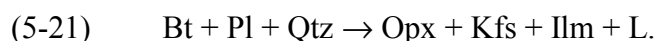


Symbols	
■	garnet core
□	garnet rim
●	matrix Opx2 core
○	matrix Opx2 rim
⊙	Opx3 in Opx-Pl corona
⊕	Opx3 in Crd-Opx sympl.
⊕	Opx5 on Bt4
▲	matrix Bt2
△	Bt4 on Opx2
▲	Bt4 on Crd-Opx sympl.
◆	Crd3 in Crd-Opx sympl.
◇	Crd3 in Crd-Spl sympl.
◇	Spl3 in Crd-Spl sympl.
☆	Bulk-rock composition

Fig. 5.32: AFM projections from quartz and feldspars for **a & b**) the Mg-rich Grt-Opx gneisses B-458-3-99 and B-634-00, **c**) the Qtz-rich Grt-Opx rock B-614-1-99 and **d**) the Fe-rich Grt-Opx gneiss B-690-2-00. Arrows indicate rimward zoning in garnet and orthopyroxene. Initial assemblages are joined by solid lines; Grt2(rims)-Crd-Opx-Qtz assemblages of Mg-rich Grt-Opx gneisses and the Qtz-rich Grt-Opx rock by dashed lines and the Grt4-Bt4 assemblage of the Fe-rich Grt-Opx gneiss by a stippled line. For reasons of clarity the composition of Crd-Opx-Spl symplectites has been excluded. Illustrated mineral compositions are given in the Appendix (bold marked analyses of Tables A.6.2.1, A.6.2.2, A.6.2.3, A.6.2.6 and A.6.2.9).

resulting peak-metamorphic Grt-Opx-Pl-Kfs-Qtz assemblages of the Mg-rich Grt-Opx gneisses and Qtz-rich Grt-Opx rocks correlate well with the bulk-rock compositions that plot on the Opx-Grt tie-line in the AFM projection (Fig. 5.32a-c). The presence of garnet in the studied samples indicates relatively high pressures since below 5 kbar cordierite instead of garnet would be formed (Vielzeuf & Montel, 1994). The occurrence of matrix biotite in only one of the studied Qtz-rich Grt-Opx rock samples (B-614-1-99) suggests peak-metamorphic temperatures close to the upper thermal stability limit of biotite. The preservation of this early biotite is probably related to its high Ti content (up to 5.5 wt.% TiO₂), which may extend the thermal stability of biotite (e.g. Patiño Douce, 1993; Stevens et al., 1997).

The slightly less aluminous Fe-rich Grt-Opx gneisses lack prograde sillimanite and therefore record a different prograde metamorphic evolution. Furthermore, inclusions of Opx1 in peak-metamorphic Grt2 indicate that the formation of orthopyroxene pre-dates the development of garnet in some of the Fe-rich Grt-Opx gneisses. Inclusions of Bt1, Pl1 and Qtz1 in porphyroblastic Opx2, corona textures of Opx2 around relic Bt2 (Fig. 5.5b) and biotite-bearing lenses, which are devoid of orthopyroxene (Fig. 5.5a), indicate that the replacement of biotite led to the formation of prograde Opx1 and peak-metamorphic Opx2, probably according to the fluid-absent biotite dehydration-melting reaction



This reaction furthermore explains the occurrence of orthopyroxene-bearing leucosomes in the Fe-rich Grt-Opx gneisses whereas the release of Ti of former biotite results in the formation of matrix Ilm2. The lower Al content of peak-metamorphic Opx2 of the Fe-rich Grt-Opx gneisses (Al^{tot} p.f.u.: 0.15-0.11) when compared to Opx2 of the Mg-rich Grt-Opx gneisses and the Qtz-rich Grt-Opx rocks (Al^{tot} p.f.u.: 0.52-0.39) is probably related to the high modal amount of plagioclase and K-feldspar, which fractionated the available Al. The lower X_{Mg} of Opx2 is related to the lower bulk-rock X_{Mg} of the Fe-rich Grt-Opx gneisses (Fig. 5.32d).

Corroded inclusions of Opx1 and Pl1 in Grt2 of the Fe-rich Grt-Opx gneisses (Fig. 5.5d) suggest the subsequent progress of the reaction (5-15) $\text{Opx} + \text{Pl} \rightarrow \text{Grt} + \text{Qtz}$, indicating that the formation of garnet outlasted orthopyroxene-formation and demonstrating that the initial prograde temperature increase was followed by a pressure increase, consistent with the prograde evolution postulated for the mafic Grt-Cpx granulites. Progress of reaction (5-15) is consistent with the continuous decrease of the An content of plagioclase in the following sequence: Pl1 inclusions in Grt2 cores > Pl1 inclusions in Grt2 margins > matrix Pl2 (see Fig. 5.29b).

Textural equilibrium between Grt2 and Opx2 suggests that both were formed through

progress of the reaction (5-16) $Bt + Pl + Qtz \rightarrow Opx + Grt + Kfs + L$, which has been postulated for the formation of the Grt-Opx metagranitoids and the Mg-rich Grt-Opx gneisses and also explains the development of orthopyroxene- and garnet-bearing leucosomes.

The formation of intergrowths of Grt2 with green Spl2 (Fig. 5.5c), present in quartz-absent domains of the Fe-rich Grt-Opx gneisses, is attributed to the reaction (5-17) $Bt + Pl \rightarrow Grt + Spl + Ilm + Kfs + L$.

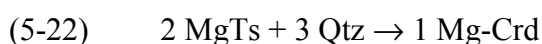
In summary, the prograde evolution of the Fe-rich and Mg-rich Grt-Opx gneisses and the Qtz-rich Grt-Opx rocks is characterized by a temperature increase, which is followed by a pressure increase.

Stage 3a: Corona formation

Retrograde corona textures in the Fe-rich and Mg-rich Grt-Opx gneisses and the Qtz-rich Grt-Opx rocks are diagnostic for decompression under ultrahigh temperatures:

Opx3-Pl3 coronas around peak-metamorphic Grt2 of the Fe-rich Grt-Opx gneisses, separating it from matrix Qtz2 (Fig. 5.5e), resemble similar Opx-Pl coronas observed in the mafic granulites and indicate garnet-breakdown via reaction (5-6) $Grt + Qtz \rightarrow Opx + Pl$, documenting post-peak decompression still under granulite facies conditions. The similar Al content of peak-metamorphic Opx2 and coronitic Opx3 (Fig. 5.25c) indicate that decompression took place close to the peak-metamorphic temperatures. Reaction (5-6) also explains the initial formation of Opx3-Pl3 coronas between Grt2 and Qtz2 (Fig. 5.7a) of the Mg-rich Grt-Opx gneisses. The high Al content of coronitic Opx3 (Al_2O_3 : up to 9 wt.%) suggests that the corona formed still under ultrahigh temperatures. Ca contents continuously increasing from the contact at Opx3 towards Grt2 of coronitic Pl3 (Fig. 5.29a & b) of both rock types demonstrate decreasing pressures during the formation of the Opx-Pl corona. Reaction (5-6) furthermore explains the formation of monomineralic corona textures around Qtz1 inclusions in Grt2 of the Fe-rich and Mg-rich Grt-Opx gneisses.

Monomineralic Crd3 coronas between porphyroblastic Opx2 and Qtz2 of the Mg-rich Grt-Opx gneisses and the Qtz-rich Grt-Opx rocks (Fig. 5.7f) may suggest progress of the divariant FMAS reaction $Opx + Sil + Qtz \rightarrow Crd$. However, since Opx-Sil-Qtz assemblages are not present in the Mg-rich Grt-Opx gneisses and the Qtz-rich Grt-Opx rocks (see above), cordierite formation is interpreted to result from the release of the Mg-Tschermak's component (MgTs) of orthopyroxene according to the model MAS reaction



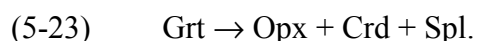
or $\text{high-Al Opx (cores)} + \text{Qtz} \rightarrow \text{low-Al Opx (rims)} + \text{Crd}$,

which is consistent with rimward zoning to lower Al and X_{Mg} in matrix Opx2 (Fig. 5.25a & b).

Stage 3b: Symplectite formation

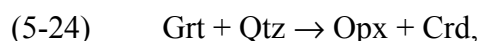
Subsequent symplectite formation in the Mg-rich Grt-Opx gneisses and the Qtz-rich Grt-Opx rocks proceeded under lower, but still granulite facies conditions as is suggested by the lower Al content of symplectitic Opx3 when compared to coronitic Opx3 (Fig. 5.25b).

Crd3-Opx3-Spl3 symplectites, which occur in fissures present in Grt2 cores (Fig. 5.7c), are interpreted to result from progress of the divariant FMAS reaction (Fig. 5.17a)



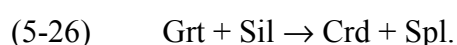
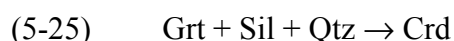
Reaction (5-23) requires the coexistence of Crd + Opx + Spl, which are stable on the low-pressure side of the univariant FMAS reaction $\text{Grt} + \text{Spr} \rightarrow \text{Opx} + \text{Crd} + \text{Spl}$ (Fig. 5.31). Furthermore, reaction (5-23) must occur at temperatures above and pressures below the univariant FMAS reaction $\text{Opx} + \text{Sil} \rightarrow \text{Grt} + \text{Crd} + \text{Spl}$, since it requires the coexistence of Grt + Crd + Spl. Therefore, progress of reaction (5-23) documents decompression to $P < 8$ kbar.

Crd3-Opx3 symplectites, which replace Grt2 coexisting with matrix Qtz2 (Fig. 5.7a & b), are interpreted to result from the divariant FMAS reaction (Fig. 5.17a)



which explains rimward zoning of Grt2 to lower X_{Mg} (Fig. 5.19a & 5.32a-c). The lack of Crd-Opx symplectites in the Fe-rich Grt-Opx gneisses is probably related to the relatively low X_{Mg} of Grt2 in these rocks (Fig. 5.32d).

Spl3-Crd3 symplectites enclosed in Grt2 of the Mg-rich Grt-Opx gneisses and the Qtz-rich Grt-Opx rocks, that are surrounded by monomineralic Crd3 coronas separating the symplectite from the Grt2 host (Fig. 5.7e), are interpreted to result from the breakdown of former Sil1 inclusions in Grt2 according to the following divariant FMAS reactions (Fig. 5.17a)



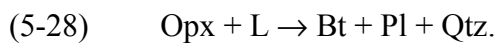
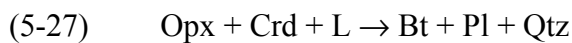
Influx of SiO_2 by ingressing melts or fluids along garnet fissures may have resulted in the formation of the outer cordierite coronas at initially high SiO_2 activity. Consumption of the available SiO_2 by reaction (5-25) and/or separation of sillimanite from the high- SiO_2 activity

domains by the cordierite coronas resulted in localized low-SiO₂ activity domains and thus initiated the growth of the Spl-Crd symplectites on the former sillimanite. Spl-Crd assemblages are stable on the low-pressure side of the univariant FMAS reaction $\text{Grt} + \text{Sil} + \text{Spr} \rightarrow \text{Crd} + \text{Spl}$ (Fig. 5.31) and therefore progress of reaction (5-26) documents decompression to $P < 8$ kbar.

Like reaction (5-6) of stage 3a, reactions (5-23) to (5-26) of stage 3b have a shallow positive dP/dT slope and are therefore consistent with continued decompression or heating. However, the latter process is ruled out by the lowered Al₂O₃ content of symplectitic Opx₃ when compared to coronitic Opx₃.

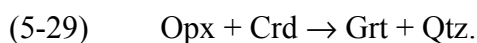
Stage 4: Re-growth of biotite and garnet

The formation of Bt₄ at the expense of the Crd₃-Opx₃ symplectites of the Mg-rich Grt-Opx gneisses and the Qtz-rich Grt-Opx rocks (Fig. 5.8a) and of Bt₄-Qtz₄ symplectites surrounding Opx₂ (Fig. 5.8b) is in agreement with progress of the melt-present hydration reactions



The extensive formation of Bt₄ at leucosome-melanosome contacts suggests that biotite re-growth is related to reactions of the crystallizing anatectic melt with the minerals of the restitic layers. This interpretation is supported by the presence of plagioclase, that is locally intergrown with Bt₄. Crystallization of the melt may have resulted in the release of H₂O-rich fluids, which reacted with orthopyroxene and/or cordierite to produce biotite. Progress of the reactions (5-27) and (5-28) is consistent with cooling to temperatures below 800°C (Vielzeuf & Montel, 1994; Fig. 5.31).

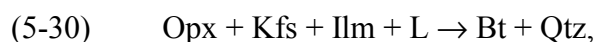
Texturally late Grt₄, present in Crd₃-Opx₃ symplectites (Fig. 5.8c) and as rims on relic porphyroblastic Grt₂ of the Qtz-rich Grt-Opx rocks (Fig. 5.8d), encloses the symplectitic phases, which points to garnet re-growth according to reaction (5-24) in a reverse direction



The lack of re-growth of garnet in the Mg-rich Grt-Opx gneisses is interpreted to result from their slightly more magnesian bulk-rock composition (bulk-rock X_{Mg} : 0.59-0.62) when compared to the Qtz-rich Grt-Opx rocks (bulk-rock X_{Mg} : 0.52-0.56).

Matrix Opx₂ and coronitic Opx₃, which occur in former contact with Kfs₂ or in the vicinity of leucosomes of the Fe-rich Grt-Opx gneisses, are replaced by symplectites of Bt₄, Pl₄ and

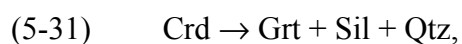
Qtz4, indicating rehydration according to the melt-present reaction



that also explains Bt4 rims on Ilm2. Coexisting re-grown Grt4, Bt4 and Qtz4, formed at the expense of Opx3-Pl3 corona textures (Fig. 5.5f), are attributed to the reaction (5-19) $\text{Opx} + \text{Pl} + \text{Kfs} + \text{H}_2\text{O} \rightarrow \text{Grt} + \text{Bt} + \text{Qtz}$.

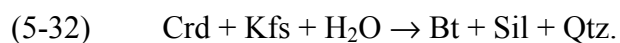
Re-grown rims of Grt4 and Qtz4 around relic Grt2 of the Fe-rich Grt-Opx gneisses, that was previously resorbed by Opx-Pl coronas, suggest garnet-growth through the reversal of reaction (5-6), i.e. reaction (5-15) $\text{Opx} + \text{Pl} \rightarrow \text{Grt} + \text{Qtz}$.

In the cordierite-bearing Qtz-rich Grt-Opx rock B-587-4-99 late Grt4, coexisting with Sil4, occurs around Crd2 (Fig. 5.8f) and as rims on Grt2 in former contact with Crd2. Grt4 of both textures contains non-oriented Sil4 inclusions, suggesting garnet-growth according to the divariant FMAS reaction



the reversal of reaction (5-25).

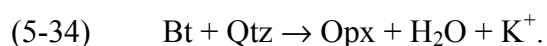
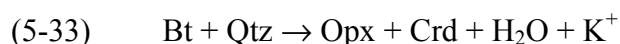
Intergrowths of Bt4 and Sil4 replacing Crd2 of the cordierite-bearing Qtz-rich Grt-Opx rock B-587-4-99 (Fig. 5.8e) are attributed to the hydration reaction



Progress of the reactions (5-15), (5-19) and (5-27) to (5-32) are consistent with a cooling-dominated P-T path at this stage.

Stage 5: Formation of late orthopyroxene and cordierite

Rims of low-Al Opx5, locally intergrown with Crd5, around retrograde Bt4 of the Mg-rich Grt-Opx gneisses and the Qtz-rich Grt-Opx rocks (Fig. 5.8a and 5.9a & b) indicate late-stage, melt-absent biotite dehydration according to the KFMASH reactions



Orthopyroxene re-growth may result from (1) renewed heating or (2) continued decompression under melt-absent and fluid-absent conditions, as H₂O-rich fluids were exhausted by the biotite-forming reactions (5-27) and (5-28). Possibility (1) seems rather unlikely since Opx5 has lower Al contents than symplectitic Opx3.

5.3.3.2 Grt-Sil gneisses and Grt gneisses

The retrograde reaction textures of the Grt gneisses and the Grt-Sil gneisses are similar to those described for the Mg-rich Grt-Opx gneisses and Qtz-rich Grt-Opx rocks. However, prograde mineral inclusions in the peak-metamorphic phases of the Grt-Sil gneisses and the Grt gneisses additionally allow to reconstruct the prograde metamorphic evolution; thus a more complete P-T path can be constrained (Fig. 5.33). Due to the less magnesian bulk-rock composition of the Grt gneisses and the Grt-Sil gneisses, all mineral compositions are shifted towards the Fe-side of the AFM diagram (Fig. 5.34) when compared to the mineral compositions of the Mg-rich Grt-Opx gneisses and Qtz-rich Grt-Opx rocks (Fig. 5.32).

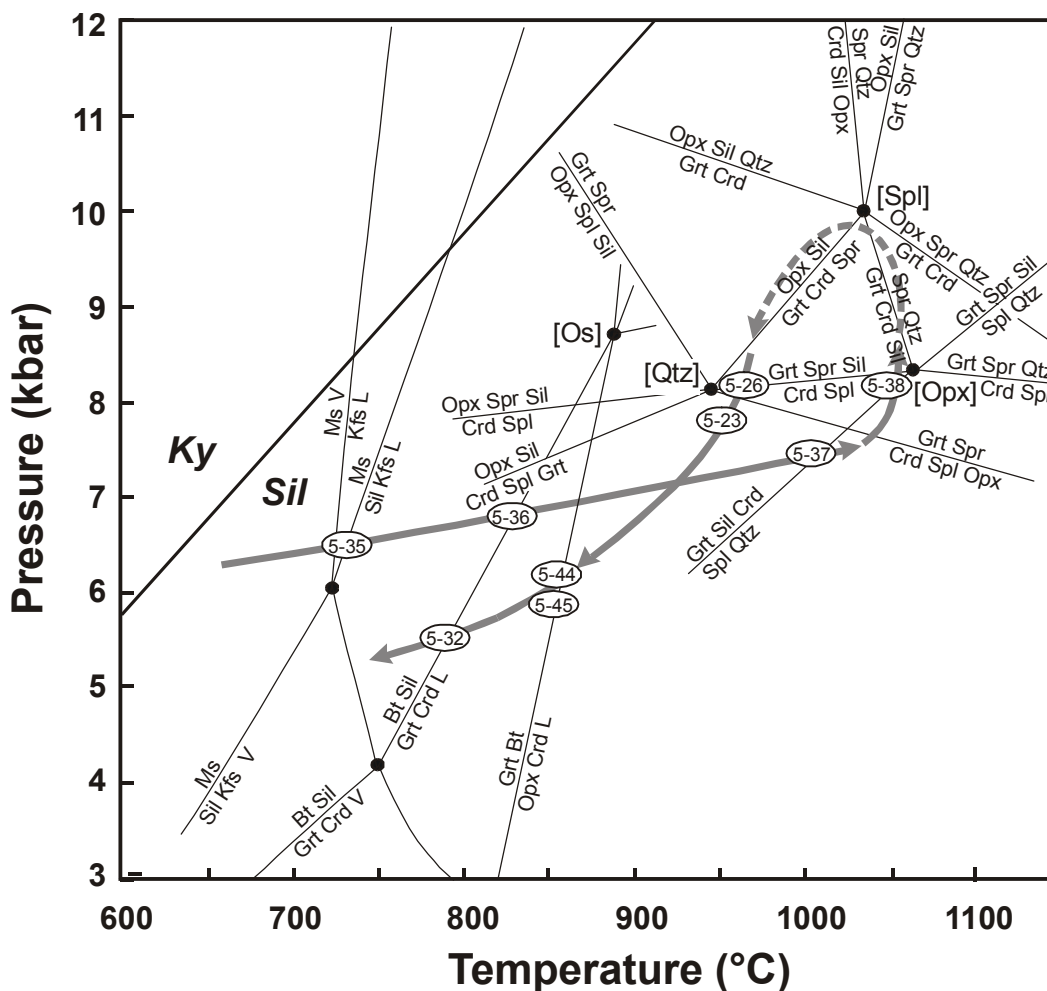


Fig. 5.33: P-T path most probably followed by the Grt gneisses and the Grt-Sil gneisses of the Epembe Unit, as deduced from the observed mineral assemblages and the sequence of reaction textures. The petrogenetic grid for high-grade low $f(\text{O}_2)$ metapelites in the system FMAS is based on Hensen & Green (1973); Hensen (1987), Hensen & Harley (1990), Bertrand et al. (1991) and Harley (1998a). Also shown are the locations of relevant KFMASH melting and dehydration reactions (Spear et al. 1999) with the location of the invariant point [Os(umelite)] after Carrington & Harley (1995). The numbers in the P-T path refer to reactions discussed in the text.

Stage 1: Prograde evolution and Stage 2: Peak-metamorphic assemblages

Inclusion trails of fibrolitic Sil1 in peak-metamorphic Grt2 of the Grt-Sil gneisses and Grt gneisses indicate that the prograde evolution proceeded through the sillimanite stability field. The absence of muscovite and the presence of the Sil-Kfs assemblages demonstrates temperatures above the dehydration melting of muscovite (Fig. 5.33) as expressed by the vapour-absent KFMASH reaction



which moreover explains the formation of quartzofeldspathic leucosomes. Early Bt1 and fibrolitic Sil1, together with Qtz1 and rare Pl1, are only preserved as corroded inclusions in cores of Grt2 of the Grt-Sil gneisses and the Grt gneisses. Grt2 coexists with Kfs2, that preserves the same mineral inclusions as Grt2. These textural relationships point to contemporaneous garnet and K-feldspar growth during dehydration-melting of biotite as described by the KFMASH reaction (5-20) $\text{Bt} + \text{Sil} + \text{Pl} + \text{Qtz} \rightarrow \text{Grt} + \text{Kfs} + \text{L}$, which resulted in the consumption of biotite in the Grt-Sil gneisses and of sillimanite in the Grt gneisses. Since the inclusion trails of fibrolitic Sil1 generally display no preferred orientation, prograde heating presumably proceeded under static conditions. Progress of the melt-producing reaction (5-20) is furthermore consistent with

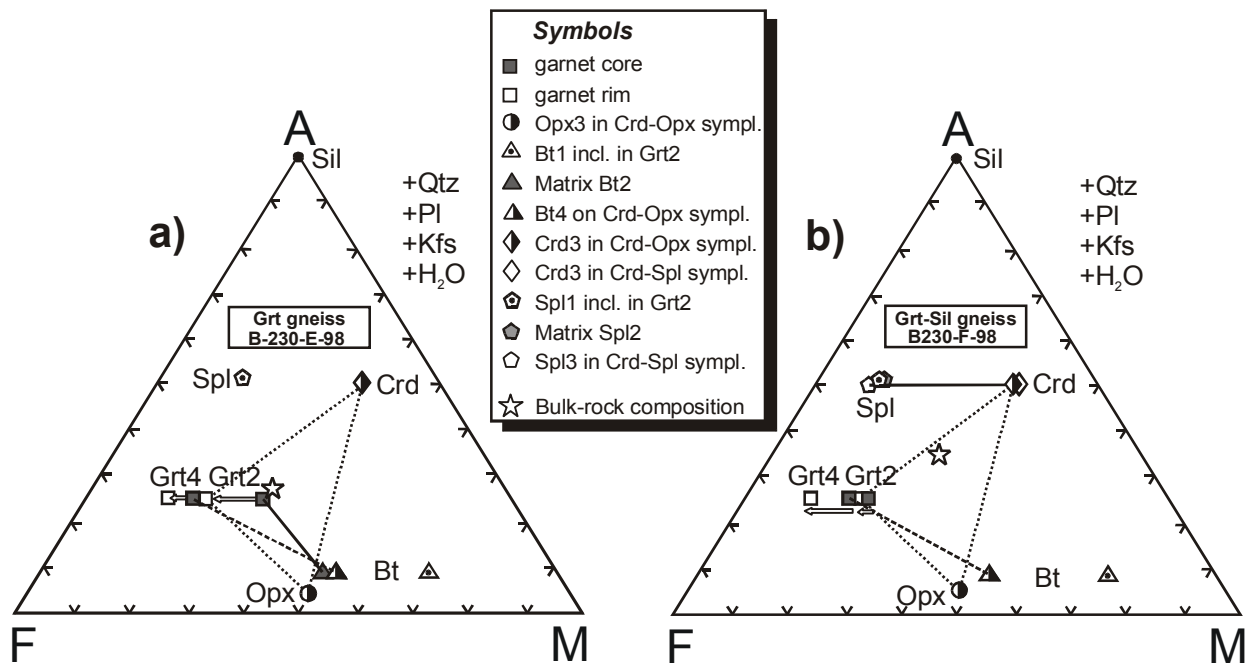
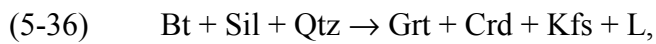


Fig. 5.34: AFM projections from quartz and feldspars for the **a)** Grt gneisses and **b)** the Grt-Sil gneisses of the Epembe Unit. Arrows indicate rimward zoning in garnet. Initial assemblages are joined by solid lines; Grt2(rims)-Crd-Opx-Qtz assemblages and late Grt-Bt assemblages by dashed lines. Illustrated mineral compositions are given in the Appendix A.6.2 (bold marked analyses of Tables A.6.2.1, A.6.2.2, A.6.2.3, A.6.2.6 and A.6.2.9).

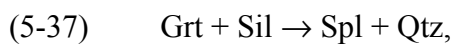
the presence of abundant garnet-bearing quartzofeldspathic leucosomes in the Grt-Sil gneisses and the Grt gneisses.

Rare Crd1 inclusions in both, Grt2 rims (Fig. 5.10b) and in prismatic matrix Sil2, demonstrate that cordierite was present during the prograde evolution. The occurrence of partly euhedral Crd1 inclusions in sillimanite-free Grt2 margins points to cordierite growth accompanied by continued garnet growth according to the univariant melt-producing KFMASH reaction



which is consistent with further heating (Fig. 5.33).

Coexisting Qtz1 and Spl1 inclusions in prismatic matrix Sil2 (Fig. 5.10d) indicate the presence of Spl-Qtz assemblages prior to the growth of aligned Sil2. Inclusions of Spl1 associated with Qtz1 in the sillimanite-free Grt2 rims (Fig. 5.10b) suggest that these Spl-Qtz associations were formed by progress of the divariant FMAS reaction (Fig. 5.17a)



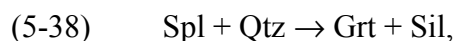
which indicates crossing of the univariant FMAS reaction $\text{Grt} + \text{Sil} + \text{Crd} \rightarrow \text{Spl} + \text{Qtz}$ through continued heating and is thus diagnostic of UHT conditions of $> 900^\circ\text{C}$ in the FMAS system under the assumed low $f\text{O}_2$ (Fig. 5.33). However, additional components in spinel, particularly high contents of Fe^{3+} and Zn, may extend the stability field of Spl-Qtz assemblages (e.g. Harley, 1986; Hensen, 1986; Powell & Sandiford, 1988; Shulters & Bohlen, 1989). In addition, decomposition of spinel into polyphase aggregates of spinel + magnetite + corundum + hemoilmenite, which is reported for several Spl-Qtz metapelites (e.g. Waters, 1991; Dasgupta et al., 1995), complicates the reconstruction of the original spinel composition. Therefore, it is ambiguous to infer UHT metamorphic conditions solely on the basis of Spl-Qtz assemblages in oxidized rocks (e.g. Harley, 1998a). In the studied Grt-Sil gneisses and Grt gneisses decomposition of spinel is absent and therefore the analyzed spinel compositions are interpreted to represent the original composition. Consequently, the low contents of Fe_2O_3 and ZnO in the investigated spinel solid solutions exclude a stabilizing effect on the Spl-Qtz assemblage and therefore, they are diagnostic of UHT conditions in the investigated granulites.

Sil2 corona textures around Crn1, separating it from matrix Qtz2 (Fig. 5.10f), might suggest progress of the reaction $\text{Crn} + \text{Qtz} \rightarrow \text{Sil}$, implying the presence of former Crn-Qtz assemblages. Natural Crn-Qtz occurrences with direct grain contacts or separated by sillimanite are reported from few high-grade metamorphic terranes (e.g. Motoyoshi et al., 1990; Guiraud et al., 1996; Shaw & Arima, 1998). Although textures in some of the reported occurrences suggest that Crn +

Qtz may form a stable assemblage (Guiraud et al., 1996; Shaw & Arima, 1998) current thermodynamic (e.g. Holland & Powell, 1998b) and experimental data (Harlov & Milke, 2002) demonstrate that Crn + Qtz do not coexist at P-T conditions realized in the crust and upper mantle. Consequently, the observed Crn + Qtz assemblages of the Grt-Sil gneisses are interpreted to have formed in distinct disequilibrium domains only. Taking into account the migmatitic structure of the Grt-Sil gneisses it seems likely that corundum was formed as one of the phases of the restitic mineral assemblages and came in arbitrary contact with matrix quartz from associated leucosomes.

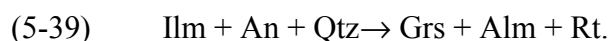
The absence of peak-metamorphic matrix cordierite and its occurrence as prograde inclusion in Grt2 and Sil2 point to its replacement and the growth of the matrix Grt-Sil-Qtz assemblages according to the divariant FMAS reaction (5-31) $\text{Crd} \rightarrow \text{Grt} + \text{Sil} + \text{Qtz}$, which is diagnostic of a pressure increase.

Spl-Qtz associations commonly only occur as inclusions in Grt2 rims and in prismatic matrix Sil2, separated by hosting Grt2 and Sil2, respectively. These relationship and the monomineralic corona textures of Grt2 and of Sil2 around Spl1 (Fig. 5.10c & 5.10e, respectively) suggest that the replacement of the Spl-Qtz associations and the growth of the Grt-Sil assemblages is related to the FMAS reaction (Fig. 5.17a)

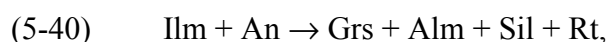


the reversal of reaction (5-37). Progress of reaction (5-38) suggests crossing of the univariant FMAS reaction $\text{Grt} + \text{Sil} + \text{Crd} \rightarrow \text{Spl} + \text{Qtz}$ or the univariant FMAS reaction $\text{Grt} + \text{Sil} + \text{Spr} \rightarrow \text{Spl} + \text{Qtz}$, due to either cooling or compression (Fig. 5.33).

The lack of matrix plagioclase and the presence of early plagioclase (P11) preserved as rare inclusion in Grt2 together with Qtz1 suggest consumption of plagioclase of the Grt-Sil gneisses during the prograde metamorphic evolution. Rutile is the dominant Ti-phase in the quartz-rich matrix of most Grt-Sil gneisses and Grt gneisses whereas early ilmenite forms abundant inclusions in Grt2 and Sil2. These textural relationships are consistent with progress of the GRIPS reaction



Monomineralic rims of Sil2 around relic matrix Ilm2 point to an accompanied progress of the GRIPA reaction

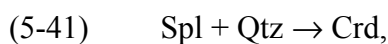


which also explains the formation of the peak-metamorphic Grt-Sil-Rt assemblages of the quartz-free Grt-Sil gneisses.

In summary, progress of the melt-producing reactions (5-35), (5-20) and (5-36) indicate prograde heating. Therefore, the subsequent progress of reaction (5-37) is interpreted to be related to continued heating during the prograde evolution and resulted in the formation of Spl-Qtz assemblages, which are diagnostic of UHT conditions. Replacement of cordierite and the Spl-Qtz assemblages through progress of the reactions (5-31) and (5-38) is interpreted to result from a subsequent pressure increase, possibly associated by slight cooling, that led to the formation of the peak-metamorphic assemblages Grt-Sil-Kfs-Qtz, Grt-Kfs-Sil and Grt-Kfs-Qtz. The postulated pressure increase is consistent with progress of the garnet- and rutile-forming reactions (5-39) and (5-40). As the peak-assemblages are stable over a large P-T range, the P-T evolution at peak-metamorphic conditions is not well constrained by the Grt-Sil gneisses and Grt gneisses (Fig. 5.33) and therefore it remains uncertain whether the Grt-bearing peak-pressure assemblages were formed at higher, similar or lower temperatures than the Spl-Qtz assemblages.

Stage 3: Corona and symplectite formation

Monomineralic rims of polygonal Crd₃ separating coexisting relic matrix Spl₂ from Qtz₂ (Fig. 5.11a) indicate progress of the FMAS reaction (Fig. 5.17a)



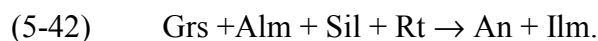
which proceeded with decompression and/or cooling (e.g. Fitzsimons, 1996) and also accounts for monomineralic rims of Crd₃ around Spl₁ inclusions in Grt₂ (Fig. 5.10b) and between Grt₂ and Spl₂ (Fig. 5.10c).

Crd₃-Opx₃-Spl₃ symplectites, present in fissures of Grt₂ cores, are interpreted to result from the divariant FMAS reaction (5-23) $\text{Grt} \rightarrow \text{Opx} + \text{Crd} + \text{Spl}$. Conspicuous Crd₃-Opx₃ symplectites separate Grt₂ from matrix Qtz₂ (Fig. 5.11b) and are also present in fissures, which occur in Grt₂ margins (Fig. 5.11c). Their formation indicate breakdown of garnet via the divariant FMAS reaction (5-24) $\text{Grt} + \text{Qtz} \rightarrow \text{Opx} + \text{Crd}$. In the Grt gneisses the Crd₃-Opx₃ symplectites are locally surrounded by finger-like Opx₃-Pl₃ intergrowths (Fig. 5.11c), which are interpreted to result from progress of reaction (5-6) $\text{Grt} + \text{Qtz} \rightarrow \text{Opx} + \text{Pl}$. This reaction also explains the occurrence of late Pl₃ in the Crd₃-Opx₃ symplectites.

Broad monomineralic moats of polygonal Crd₃ between Grt₂ and Sil₂ (Fig. 5.11d) in the

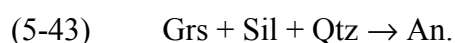
quartz-bearing Grt-Sil gneisses were formed through the continuous FMAS reaction (5-25) $\text{Grt} + \text{Sil} + \text{Qtz} \rightarrow \text{Crd}$. After consumption of quartz Spl3-Crd3 symplectites were formed adjacent to Sil2 (Fig. 5.11d) according to the continuous FMAS reaction (5-26) $\text{Grt} + \text{Sil} \rightarrow \text{Crd} + \text{Spl}$ (Fig. 5.17a). Such Spl3-Crd3 symplectites also occur in the quartz-free Grt-Sil gneisses and in the Grt gneisses. In the latter they replace former Sil1 inclusions in Grt2.

Locally, late Ilm3 and Pl3 occur in the Spl3-Crd3 symplectites. Rarely preserved inclusions of Rt2 in Ilm3 suggest progress of the GRIPA reaction (5-40) in the reverse direction



The reaction also explains the formation of late monomineralic Pl3 rims around Grt2 of the quartz-free Grt-Sil gneisses (Fig. 5.11f).

In the quartz-bearing Grt-Sil gneisses late monomineralic rims of polygonal Pl3 around matrix Sil2 (Fig. 5.11e) in silica-saturated domains and Pl3 rims around Qtz1 inclusions in Grt2 indicate progress of the GASP reaction



This reaction also accounts for the occurrence of Pl3 in the monomineralic Crd3 corona around Grt2 formed after the reaction (5-25).

Progress of reactions (5-6) and (5-23) to (5-26) has also been postulated for the formation of similar reaction textures in the Mg-rich Grt-Opx gneisses and the Qtz-rich Grt-Opx rocks, thus indicating that the rocks experienced the same metamorphic evolution. However, due to the less magnesian composition of resorbed Grt2 of the Grt-Sil gneisses and the Grt gneisses, the symplectitic phases of these rock samples are less magnesian than the symplectitic phases of the Mg-rich Grt-Opx gneisses and the Qtz-rich Grt-Opx rocks, which contain more magnesian Grt2 (Fig. 5.32 & 5.34). These reactions as well as reactions (5-42) and (5-43) have a shallow dP/dT slope in the P-T space and are therefore diagnostic for decompression. As described for the Mg-rich Grt-Opx gneisses and the Qtz-rich Grt-Opx rocks, progress of reactions (5-26) and (5-23) is related to crossing of the univariant FMAS reactions $\text{Grt} + \text{Sil} + \text{Spr} \rightarrow \text{Crd} + \text{Spl}$ and $\text{Grt} + \text{Spr} \rightarrow \text{Crd} + \text{Opx} + \text{Spl}$, respectively, through decompression to $P < 8$ kbar (Fig. 5.33).

The presence of symplectitic orthopyroxene indicates that decompression proceeded under granulite facies conditions. Petrological evidence for initially UHT conditions of decompression is not recorded by the Grt-Sil gneisses or the Grt gneisses. However, the lack of retrograde Spl-Qtz assemblages indicates that decompression proceeded at temperatures below the Spl-Qtz stability (Fig. 5.33).

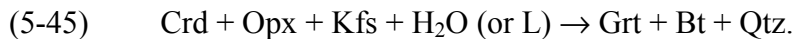
Stage 4: Re-growth of garnet and biotite

Intergrowths of Bt4 and Qtz4, partly replacing the Crd3-Opx3 symplectites in the presence of Kfs2 (Fig. 5.12a), demonstrate progress of the reaction



In the quartz-bearing samples of both the Grt-Sil gneisses and the Grt gneisses re-grown Grt4 occurs in Crd3-Opx3 pseudomorphs after former Grt2 (Fig. 5.12b). Grt4 contains inclusions of the symplectitic phases, indicating post-decompressional garnet re-growth at the expense of Crd3 and Opx3 according to the reversal of the divariant FMAS reaction (5-24), i.e. reaction (5-29) $\text{Opx} + \text{Crd} \rightarrow \text{Grt} + \text{Qtz}$. This reaction also explains narrow rims of re-grown Grt4 around porphyroblastic Grt2.

In the presence of Kfs2 garnet re-growth was accompanied by the re-occurrence of biotite (Fig. 5.12b). Straight grain boundary contacts between the two phases and the occurrence of Bt4 inclusions in Grt4 suggest contemporaneous growth of the two phases resulting from the discontinuous KFMASH reaction (Fig. 5.33)



Grt4 also occurs in monomineralic Crd3 corona textures around Grt2 and forms re-growth rims on relic Grt2 (Fig. 5.12c). Fine needles of fibrolitic Sil4 enclosed in Grt4 indicate progress of the divariant FMAS reaction (5-25) in a reverse direction (5-31) $\text{Crd} \rightarrow \text{Grt} + \text{Sil} + \text{Qtz}$. Locally, Crd3 is replaced by irregular intergrowths of Bt4 and Sil4 (Fig. 5.12e) indicating progress of the reaction (5-32) $\text{Crd} + \text{Kfs} + \text{H}_2\text{O} \rightarrow \text{Bt} + \text{Sil} + \text{Qtz}$. The localized formation of euhedral Grt4 in the Bt4-Sil4 domains (Fig. 5.12e) is probably related to progress of the reaction (5-31).

Skeletal rutile (Rt4), coexisting with intergrowths of subhedral Grt4 and fibrolitic Sil4, preserves corroded inclusions of Ilm2 (Fig. 5.12d), hence suggesting progress of the GRIPA reaction (5-40) $\text{Ilm} + \text{An} \rightarrow \text{Grs} + \text{Alm} + \text{Sil} + \text{Rt}$.

Reactions (5-29), (5-31) and (5-23) have a shallow positive dT/dT slope in the P-T space and may therefore be diagnostic of either cooling or compression. However, progress of the reactions (5-32), (5-44) and (5-45), which have a steep dT/dT slope (Fig. 5.33), indicates cooling. The presence of sillimanite-bearing reaction textures evidences that cooling proceeded in the stability field of sillimanite.

5.3.3.3 Sapphirine-bearing Opx-Sil gneisses and Opx-Grt rocks

Due to their highly magnesian and aluminous bulk-rock composition, the sapphirine-bearing Opx-Sil gneisses and the Opx-Grt rocks preserve unusual mineral assemblages and several conspicuous retrograde reaction textures, which are absent in the previously described paragneisses of the Epembe Unit. These reaction textures provide an excellent opportunity for a detailed P-T path reconstruction on the basis of phase relationships in the model system FMAS (Fig. 5.35).

Stage 1: Prograde evolution and Stage 2: Peak-metamorphic assemblages

Sil2 pseudomorphing former kyanite (Fig. 5.13a) testifies to the polymorphic transformation



indicating either prograde heating or decompression. Sil2 preserves rare inclusions of Bt1, Pl1, Rt1 and Qtz1, that point to initial Bt + Ky/Sil + Pl + Qtz + Rt assemblages.

Prograde biotite-dehydration melting reactions

The further metamorphic evolution is characterized by the replacement of early Bt1, probably through dehydration melting reactions as indicated by the migmatitic appearance of the Mg-rich Grt-Opx gneiss host rocks. Inclusions of sillimanite in Opx2 prove that the transformation (5-46) pre-dates the growth of orthopyroxene. The biotite dehydration reactions can be correlated with experimental data of Stevens et al. (1997) on the fluid-absent biotite-dehydration of magnesian metagreywackes and metapelites.

Matrix Opx2 of the Opx-Sil gneisses and Opx-Grt rocks encloses corroded Bt1, Pl1 and Qtz1. Since biotite is absent in the matrix, plagioclase and quartz may occur with minor proportions. These textural relationships point to the complete biotite and partial plagioclase and quartz replacement by orthopyroxene, formed during prograde heating via the melt-producing reaction



The reaction was postulated by Stevens et al. (1997) to explain biotite dehydration melting of magnesian metagreywackes. Individual matrix Pl2 of the studied Opx-Sil gneisses become more calcic towards the rim (Fig. 5.29c). This zoning is consistent with increasing temperatures during biotite-dehydration melting (Stevens et al., 1997). Applying the experimental results to the observed biotite-, cordierite- K-feldspar and generally garnet-free peak-metamorphic mineral

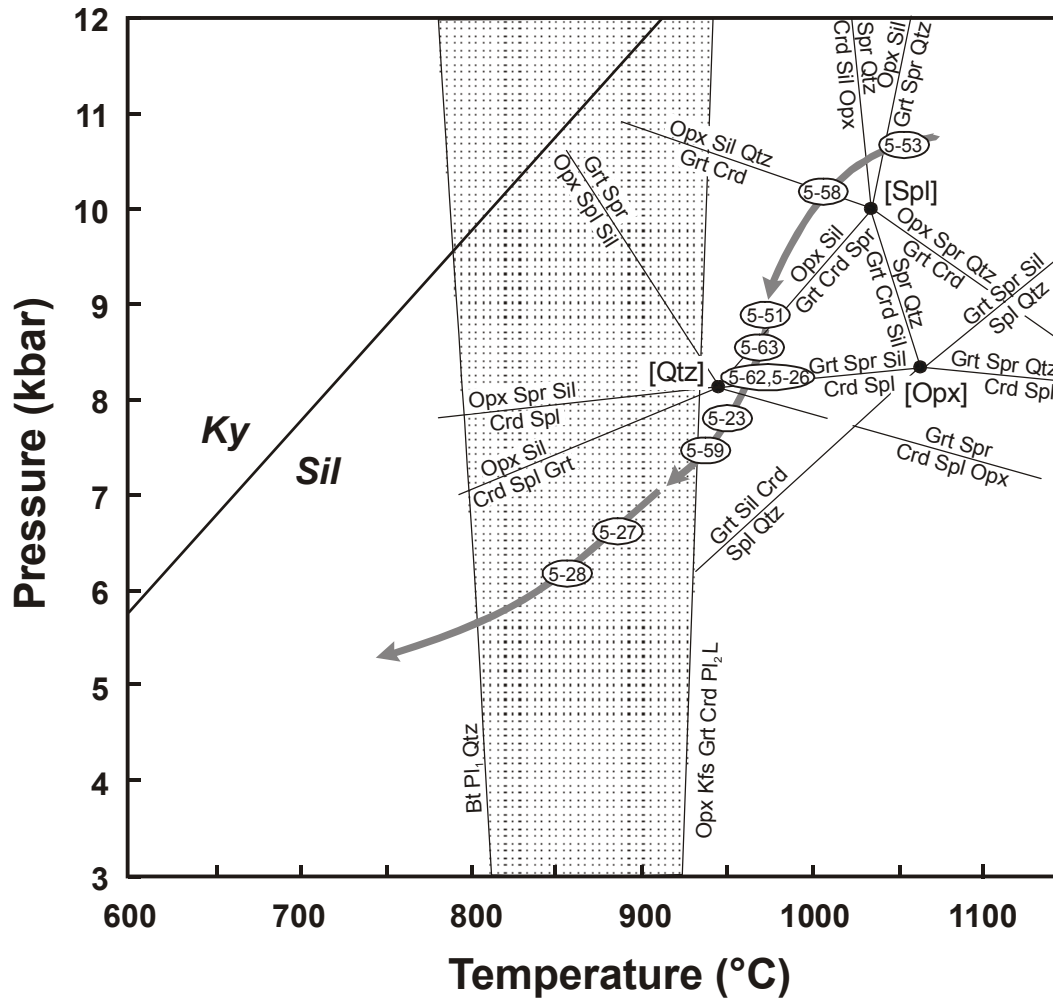
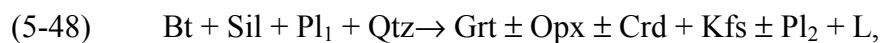


Fig. 5.35: P-T path most probably followed by the sapphirine-bearing Opx-Sil gneisses and the Opx-Grt rocks of the Epembe Unit, as deduced from the observed mineral assemblages and the sequence of reaction textures. The petrogenetic grid for high-grade, low $f(O_2)$ metapelites in the system FMAS is based on Hensen & Green (1973); Hensen (1987), Hensen & Harley (1990), Bertrand et al. (1991) and Harley (1998a). Also shown is the interval of the fluid-absent dehydration melting reaction $Bt + Pl_1 + Qtz \rightarrow Opx + Kfs \pm Grt \pm Crd + Pl_2 + L$ (stippled field) of Stevens et al. (1997). The numbers in the P-T path refer to reactions discussed in the text.

assemblages of the Opx-Sil gneisses, suggests that dehydration melting of Ti-bearing biotite must have occurred at $T > 940^\circ\text{C}$ (Fig. 5.35) and resulted in the growth of highly aluminous orthopyroxene, with a similar composition as those derived in the experiments, coexisting with sillimanite, plagioclase and locally quartz. In the Opx-Grt rocks the growth of Al-rich orthopyroxene was accompanied by the formation of garnet.

The exceptionally Al-rich Opx-Sil gneiss sample B-458-5-00 has a metapelitic composition and is dominated by Sil₂ and Grt₂ coexisting with minor amounts of Opx₂. Corroded inclusions of Bt₁, Pl₁, quartz and rarely Sil₁ in Grt₂ point to garnet growth via reaction

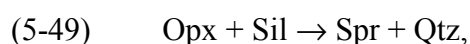


which was postulated by Stevens et al. (1997) for biotite-dehydration melting of magnesian metapelites. The observed peak-metamorphic mineral assemblage in sample B-458-5-00 comprises garnet with minor amounts of aluminous orthopyroxene; cordierite and biotite are absent. Judging from the experimental results of Stevens et al. (1997) this indicates dehydration melting of biotite at $T > 970^\circ\text{C}$.

In summary, the biotite dehydration reactions (5-47) & (5-48) indicate early prograde heating to UHT conditions (Fig. 5.35), which is consistent with the transformation of kyanite to sillimanite through reaction (5-46).

Sapphirine growth

Corroded inclusions of Opx1 and Sil1 (Fig. 5.13b) in porphyroblastic matrix Spr2a of the Opx-Sil gneisses point to early sapphirine-formation resulting from progress of the continuous FMAS reaction (Fig. 5.17a)



that explains the presence of the peak-metamorphic Opx-Sil \pm Spr \pm Qtz assemblages of the Opx-Sil gneisses. The lack of stable Spr-Qtz assemblages may be related to the following two processes: (i) Post-peak monomineralic coronas of cordierite around Spr2a (see Fig. 5.15a), separating Spr2a from Pl2 or Opx2, suggest that formerly present quartz was exhausted by the cordierite-forming reaction (see below; reaction 5-57). (ii) Quartz, formed from progress of reaction (5-49), has entered the melt phase, which is represented by the leucosomes of the migmatitic Mg-rich Grt-Opx gneiss host rock.

The postulated former presence of the Spr-Qtz assemblages indicates peak-temperatures of $> 1050^\circ\text{C}$, while the presence of Opx-Sil-Qtz assemblages testifies to peak pressures of > 10 kbar (e.g. Bertrand et al., 1991; Harley, 1998a; Fig. 5.35). The stability of the Opx-Sil-Qtz assemblage relative to the lower pressure assemblage Grt-Crd is related to the univariant FMAS reaction $\text{Grt} + \text{Crd} \rightarrow \text{Opx} + \text{Sil} + \text{Qtz}$. The location of this reaction is controlled by the position of the invariant [Spl]-absent point, which based on experimental studies, is placed between 9.5 ± 1 kbar (Hensen & Green, 1973) and 10.8 ± 1 kbar (Bertrand et al., 1991) under H_2O -bearing conditions. Consistently, Aranovich & Berman (1996) place the invariant reaction between 10.2 and 10.5 kbar at temperatures close the invariant [Spl]-absent point, based on calculations with fully hydrated cordierite and using an internally consistent dataset (Berman & Aranovich, 1996) As the stability of cordierite is maximized under hydrous conditions (e.g. Newton, 1972) these P-

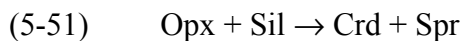
T data provide the maximum pressure limit of cordierite-bearing assemblages. The postulated presence of Spr-Qtz assemblages is supported by the high temperatures, as derived from the very high Al content of porphyroblastic Opx2a (up to 11.7 wt.%) coexisting with sapphirine.

The presence of corroded Spl1 inclusions in Spr2a of the silica-deficient Spr-rich Opx-Sil gneiss B-700-2-00 and the lack of matrix spinel suggests that early spinel was consumed during the prograde evolution by the sapphirine-producing (7:9:3 end-member) FMAS reaction

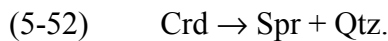


which also explains the growth of Spr2a rims around early Spl1 (Fig. 5.13c).

The central parts of porphyroblastic Spr2a of the Spr-rich Opx-Sil gneiss B-700-2-00 consist of an oriented intergrowth between Crd1 and Spr2a (Fig. 5.13d). The formation of these early Crd-Spr intergrowths is probably related to the progress of the continuous FMAS reaction (Fig. 5.17a)

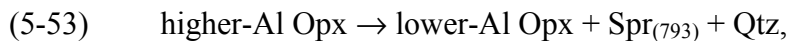


The lack of cordierite in Spr2a rims (Fig. 5.13d) suggests that early Crd1 was replaced during the continued growth of sapphirine probably via reaction (Fig. 5.17a)



As postulated for reaction (5-49), the lack of quartz in these textures may be related to either (a) its retrograde replacement through cordierite-producing coronas around Spr2a or (b) by the entry of quartz into a melt phase.

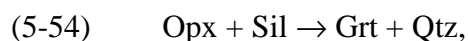
Intergrowths of Opx2b and Spr2b partly replacing porphyroblastic Opx2a (Fig. 5.13f) of the Opx-Sil gneisses suggest progress of the continuous FMAS reaction (Fig. 5.17a)



which was formulated by Harley (1998a) and may also be written as the MAS reaction $\text{MgTs} \rightarrow \text{En} + \text{Qtz} + \text{Spr}_{(793)}$, developed by Harley & Motoyoshi (2000) for sapphirine quartzites of the Napier Complex, Antarctica. Progress of reaction (5-53) is consistent with the lowered Al_2O_3 content of recrystallized Opx2b (10.0-7.6 wt.% Al_2O_3) when compared to porphyroblastic Opx2a (11.7-9.1 wt.% Al_2O_3): This lower Al content indicates that Opx-Spr intergrowth have been formed in response to cooling. As quartz is absent in the observed texture, the Spr-Opx intergrowths may have formed as a result of the addition of MgO or the release of SiO_2 , as suggested by Rickers et al. (2001) for similar textures in sapphirine granulites from India.

Garnet growth

In sillimanite-bearing domains of the Opx-Sil gneisses Grt2 forms rims around Sil2 separating it from Opx2 (Fig. 5.14a). This texture points to progress of the divariant FMAS reaction (Fig. 5.17a)



which is in agreement with the presence of Opx1 and Sil1 inclusions in Grt2 and is consistent with a pressure increase or a temperature decrease during the prograde evolution. As postulated for the Spr-Qtz forming reactions (5-49) and (5-52), the lack of quartz in the reaction texture might be (a) related to the formation of late cordierite coronas around Grt2 (see below; reaction 5-25) or (b) to the entry of SiO₂ into the melt phase.

Subhedral to euhedral inclusions of Grt2 enclosed in recrystallized Opx2b margins (Fig. 5.14b) are interpreted to result from the generalized reaction (Fig. 5.17a)



(Harley, 1989), which is also consistent with either cooling or a pressure increase. Reaction (5-55) is furthermore consistent with locally preserved straight grain boundary contacts between Grt2 and recrystallized Opx2b, indicating their synchronous growth, and also explains intergrowths of matrix Grt2 and Opx2b.

Corroded inclusions of Opx2b and Spr2b (Fig. 5.14c) preserved in matrix Grt2 indicate that the growth of garnet *post-dates* the formation of the sapphirine and orthopyroxene. The lower Al content of the Opx2b-inclusions in Grt2 and of Opx2b in intergrowths with Grt2 when compared to porphyroblastic Opx2a point to decreasing temperatures during garnet-growth.

One Opx-Sil gneiss contains matrix Grt2 with corroded inclusions of Crd1 (Fig. 5.14d) and Spl1, indicating the presence of these phases during the prograde evolution.

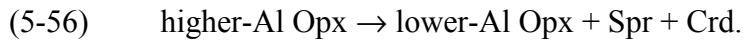
The postulated progress of reactions (5-49) indicates heating to UHT temperatures of > 1050°C at pressures of > 10 kbar (for fully hydrated cordierite) resulting in assemblages consisting of high-Al Opx + Spr ± Qtz ± Sil. Reaction (5-53) proceeded in response to cooling into the stability field of Spr-Qtz. Therefore, progress of the garnet-forming reactions (5-54) and (5-55) is interpreted to result from further continued cooling possibly accompanied by slightly increasing pressures.

Stage 3: Corona and symplectite formation

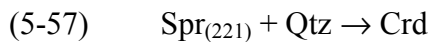
The peak-metamorphic Opx2 + Sil2 ± Grt2 ± Spr2 ± Qtz2 mineral assemblages were extensively

replaced by corona and symplectite textures composed of Opx₃, Crd₃, Spr₃, Spl₃, Pl₃, Sil₃ and Crn₃, that were formed at UHT conditions in the early stage.

Formation of Crd₃ at the margins of the recrystallized Spr-Opx intergrowth domains suggests progress of the FMAS reaction (Fig. 5.17a)



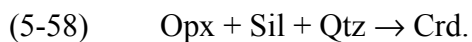
Monomineralic rims of Crd₃ around porphyroblastic Spr_{2a} (Fig. 5.15a) are attributed to the breakdown of sapphirine (2:2:1 endmember) according to the FMAS reaction (Fig. 5.17a)



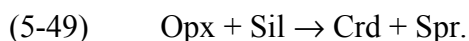
However, as mentioned earlier, Spr-Qtz assemblages were never observed. Possible explanations for the lack of quartz are (a) formerly present quartz was completely replaced during retrograde cordierite formation or (b) quartz was absent and cordierite formed instead by a reaction between Spr_{2a} and residual melt.

Reactions involving orthopyroxene

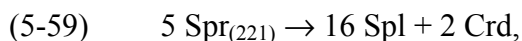
Monomineralic rims of polygonal Crd₃, separating Opx₂ and Sil₂ in the presence of Qtz₂ (Fig. 5.15b), are interpreted to result from the quartz-present continuous FMAS reaction



The formation of Crd₃-Spr₃ symplectites between Opx₂ and Sil₂ in silica-deficient domains (Fig. 5.15c & 5.15d) is attributed to progress of the quartz-absent continuous FMAS reaction

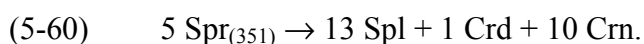


Spl₃-Crd₃ symplectites replacing matrix Spr₂ (Fig. 5.13b) and symplectitic Spr₃ (Fig. 5.15e) are interpreted to result from breakdown of sapphirine (2:2:1 endmember) according to the FMAS reaction

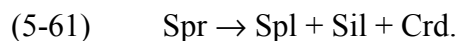


which is consistent with the observed low modal abundance of cordierite in the symplectite.

The formation of corundum (Crd₃) in the Spl-Crd symplectites resorbing Spr₃ (Fig. 5.15e) can be explained by the breakdown of the less siliceous sapphirine 3:5:1 endmember,

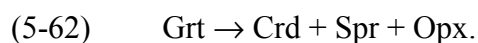


Furthermore, late sillimanite (Sil₃), coexisting with Spl₃ and Crd₃ may occur as corona around retrograde Spr₃ (Fig. 5.15f). Sil₃ also occurs along the margins of the polycrystalline Sil₂ aggregates, which are partly replaced by Crd₃-Spr₃ symplectites. Sil₃ encloses the symplectitic phases, clearly indicating its post-decompressional formation, which can be exemplified by the breakdown of sapphirine following the generalized reaction



Reactions involving garnet

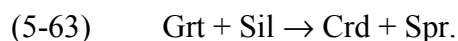
Symplectites of Spr₃, Crd₃, and Opx₃, replacing garnet inclusions in matrix Opx₂ (Fig. 5.16a), suggest localized garnet breakdown according to the quartz-absent FMAS reaction



Similar Spr-Opx-Crd pseudomorphs after garnet enclosed in orthopyroxene were reported from sapphirine-bearing granulites from the Palni Hills, South India and interpreted in the same way (Raith et al., 1997). Reaction (5-62) may also explain lamellar intergrowths of Opx₃, Spr₃ and minor Crd₃, that are present in the orthopyroxene-matrix (Fig. 5.16b).

Symplectites of Crd₃, Opx₃ and Spl₃ present around Grt₂ in quartz-free domains and in cracks of Grt₂ (Fig. 5.16c) are interpreted to result from the quartz-absent FMAS reaction (5-23) $\text{Grt} \rightarrow \text{Opx} + \text{Crd} + \text{Spl}$. This reaction also explains the formation of Crd-Opx-Spl symplectites in cracks of matrix Grt₂ of the Opx-Grt rocks, indicating a similar retrograde metamorphic evolution of both rock types. Crd-Spl-Opx symplectites formed via reaction (5-23) have been described for other paragneiss lithologies of the Epembe Unit (see Chapter 5.3.3.1 & 5.3.3.2).

Lamellar symplectitic intergrowths of Crd₃ and Spr₃, which are developed between Grt₂ and Sil₂ in quartz-absent domains (Fig. 5.16d), are attributed to the quartz-absent continuous FMAS reaction



Like symplectitic Spr₃ formed by reaction (5-49), Spr₃ resulting from reaction (5-61) is surrounded by fine-grained Spl₃-Crd₃ (Fig. 5.16d), Spl₃-Crd₃-Cm₃ or Spl₃-Crd₃-Sil₃ symplectites formed by reactions (5-59), (5-60) and (5-61).

Double layer corona textures between Grt₂ and Sil₂ consisting of a Spl-Crd symplectite (adjacent to Sil₂) followed by a monomineralic Crd₃ rim (adjacent to Grt₂; Fig. 5.16e) are interpreted to result from progress of the continuous FMAS reactions (5-25) $\text{Grt} + \text{Sil} \rightarrow \text{Crd} + \text{Spl}$ and (5-26) $\text{Grt} + \text{Sil} + \text{Qtz} \rightarrow \text{Crd}$, which have been described in Chapter 5.3.3.1 and 5.3.3.2

for the formation of similar corona textures in the other Sil-bearing paragneiss lithologies of the Epembe Unit. In sapphirine-bearing granulites from the Rauer Group, East Antarctica, Harley (1998b) recognized, that the formation of Crd-Spl symplectites instead of Crd-Spr symplectites (reaction 5-63) is related to the composition of the resorbed garnet: In these rocks Spl-Crd symplectites are formed from less magnesian garnet (X_{Mg} : 0.52-0.48) when compared to garnet (X_{Mg} : 0.61-0.56), which was resorbed by Crd-Spr symplectites.

Crd3-Opx3 symplectites replacing Grt2 in quartz-bearing domains of the Opx-Sil (Fig. 5.16d & 5.16f) and in the Opx-Grt rocks are formed through the continuous FMAS reaction (5-24) $Grt + Qtz \rightarrow Opx + Crd$. Opx3-Pl3 corona textures around the Crd3-Opx3 symplectite (Fig. 5.16f) of the Opx-Sil gneisses and the Opx-Grt rocks suggest initial garnet breakdown according to the reaction (5-6) $Grt + Qtz \rightarrow Opx + Pl$. As observed for similar double-layer corona textures around Grt2 of the Mg-rich Grt-Opx gneisses, coronitic Opx3 of the Opx-Sil gneisses and of the Opx-Grt rocks has higher Al contents than symplectitic Opx3 (Al^{tot} p.f.u.: 0.36-0.25 and 0.19-0.15, respectively), indicating initial Grt2 growth according to reaction (5-6) under ultrahigh temperatures.

Monomineralic Pl3 corona textures around Sil2 close to resorbed Grt2 are interpreted to result from the release of the grossular component of garnet following the GASP reaction (5-43) $Grs + Sil + Qtz \rightarrow An$, which also explains the formation of Pl3 in Crd3-Spr3 symplectites, resorbing Grt2 and Sil2 (Fig. 5.16d).

The sequence of symplectitic and coronitic reaction textures demonstrates decompression from peak-metamorphic P-T conditions above the [Spl]-absent invariant point to pressures below the [Qtz]-absent invariant point, i.e. a pressure interval of 2-3 kbar, by crossing several univariant FMAS reactions (Fig. 5.35): Initial decompression is recorded by the replacement of Opx-Sil assemblages in quartz-bearing (reaction 5-58) and quartz-absent (reaction 5-51) domains. At slightly lower pressures Grt2 and Grt2-Sil2 were replaced in quartz-absent domains through the sapphirine-producing reactions (5-62) and (5-63), respectively, and by reaction (5-6) in quartz-bearing domains. During continued decompression sapphirine became unstable and was replaced by spinel (reaction 5-59). In addition, spinel-bearing symplectites were formed by progress of reactions (5-26) and (5-23), the spinel-producing equivalents of reactions (5-62) and (5-63). Progress of reactions (5-62), (5-63) and (5-51) constrain the P-T decompressional path to have passed towards the high-temperature side of the [Qtz]-absent invariant point, which is located at $\sim 950^\circ\text{C}$ and 8-9 kbar (Hensen, 1987; Hensen & Harley, 1990). It is thus concluded that initial decompression proceeded under UHT conditions of $> 950^\circ\text{C}$, consistent with the high

Al content of symplectitic Opx3 coexisting with sapphirine (7.1-7.9 wt.% Al₂O₃). The reduced Al content of symplectitic Opx3 coexisting with spinel (4.1-5.5 wt.% Al₂O₃) indicates that further decompression took place under lower but still granulite facies conditions.

Stage 4: Re-growth of biotite

The relic peak-metamorphic assemblages and the post-peak reaction textures were overprinted by extensive development of late Bt4. Since K-feldspar is never observed in the Opx-Sil gneisses two possible formations of biotite are to be considered: (i) Former present K-feldspar was completely replaced by biotite or, (ii) back-reaction of the restitic domains with crystallizing melts (e.g. Raith et al., 1997) as represented by the leucosomes in the migmatitic Mg-rich Grt-Opx gneiss host rock. The observed occurrence of plagioclase in biotite re-growth textures rather points to model (2) as also postulated for the re-growth of biotite in the Mg-rich Grt-Opx gneisses and the Qtz-rich Grt-Opx rocks.

Monomineralic retrograde Crd3 and Crd3-Opx3 symplectites are surrounded by broad rims of Bt4. Qtz4 and Pl4 are commonly present in the biotite re-growth textures, suggesting progress of reaction (5-27) $\text{Opx} + \text{Crd} + \text{L} \rightarrow \text{Bt} + \text{Pl} + \text{Qtz}$. Bt4-Pl4 intergrowths and Bt4-Qtz4 symplectites around matrix Opx2 are probably formed by reaction (5-28) $\text{Opx} + \text{L} \rightarrow \text{Bt} + \text{Pl} + \text{Qtz}$.

In summary, the re-appearance of biotite is probably related to back-reactions between the relic peak-metamorphic phases and the crystallizing melt during cooling to temperatures below 800°C subsequent to decompression (Fig. 5.35). Following this, fluids, released during the crystallization of the melt, may have reacted with residual peak-metamorphic and symplectitic phases. Regarding the interpretation that the re-growth of garnet in the paragneisses of the Epembe Unit is restricted to rocks with bulk-rock $X_{\text{Mg}} < 0.59$, i.e. the Fe-rich Grt-Opx gneisses, the Qtz-rich Grt-Opx rocks, the Grt-Sil gneisses and the Grt gneisses, the lack of re-grown garnet in the Opx-Sil gneisses and the Opx-Grt rocks is most probably a consequence of their highly magnesian bulk-rock composition (bulk-rock X_{Mg} : 0.64-0.78).

Stage 5: Formation of late orthopyroxene and cordierite

Locally, late Bt4, in turn, is rimmed by a corona of granoblastic Opx5. Similar reaction textures were also observed in the Mg-rich Grt-Opx gneisses and interpreted to result from continued decompression subsequently to cooling under melt- and fluid-absent condition with formerly

present fluids exhausted by the biotite-forming reactions (5-27) and (5-28).

The similarities in the metamorphic evolution between the sapphirine-bearing Opx-Sil gneisses and the metagreywacke-type Mg-rich Grt-Opx gneisses point to a cogenetic evolution of both rock types and thus support the interpretation that the Opx-Sil gneisses represent restitic domains formed during partial melting of the Mg-rich Grt-Opx gneiss host rocks.

5.3.4 Summary and conclusions

The various granulite facies lithologies of the Epembe Unit record a similar multistage metamorphic evolution, clearly indicating that they were affected by the same metamorphic event:

Stage 1: Prograde evolution

Prograde heating resulted in the replacement of hydrous mineral assemblages, involving amphibole (mafic granulites and felsic granulites) and biotite (paragneisses and Grt-Opx metagranitoids), by anhydrous mineral assemblages. During early prograde heating kyanite was transformed to sillimanite in the sapphirine-bearing Opx-Sil gneisses. The further metamorphic evolution proceeded through the sillimanite stability field. Mineral inclusions of orthopyroxene in peak-metamorphic clinopyroxene of the mafic Grt-Cpx granulites and in peak-metamorphic garnet of the Fe-rich Grt-Opx gneisses indicate that granulite facies P-T conditions were attained during the prograde metamorphic evolution prior to the growth of garnet. Furthermore, Spl-Qtz associations in peak-metamorphic garnet and sillimanite of the metapelites demonstrate that already during prograde heating UHT conditions were reached. These textural relationships suggest that prograde heating was near-isobaric.

Stage 2: Peak-metamorphic conditions

The commonly garnet-bearing peak-metamorphic mineral assemblages were formed in response to a pressure increase. The extraordinary high Al content of peak-metamorphic orthopyroxene of the Mg-rich Grt-Opx gneisses, the Qtz-rich Grt-Opx rocks, the Spr-bearing Opx-Sil gneisses and the Opx-Grt rocks indicates ultrahigh temperatures of $> 900^{\circ}\text{C}$, consistent with the presence of Opx-Sil-Qtz assemblages in the sapphirine-bearing Opx-Sil gneisses. The postulated occurrence of Spr-Qtz associations in the Opx-Sil gneisses suggest even higher temperatures of $> 1050^{\circ}\text{C}$.

The main deformation phase D_1 took place during the latest stage of peak-metamorphism,

subsequently to the formation of the peak-metamorphic mineral assemblages but prior to the formation of the decompressional reaction textures.

Stage 3: Corona and symplectite formation

Subsequent near-isothermal decompression is recorded by conspicuous undeformed corona and symplectite textures present in all granulite facies lithologies (Table 5.7), except of the garnet-free felsic granulites and the Grt-Opx metagranitoids. Stage 3 is subdivided into initial UHT decompression (stage 3a) followed by HT decompression (stage 3b):

Sapphirine-bearing symplectites of the Opx-Sil gneisses demonstrate that early decompression proceeded still under ultrahigh temperatures (stage 3a). Early UHT decompression is furthermore supported by the partly high Al content of orthopyroxene in decompressional Opx-Pl corona textures replacing garnet, which are present in the mafic granulites and in most paragneisses (Table 5.7).

Further decompression (stage 3b) is mainly recorded by the growth of Crd-Opx symplectites formed at the expense of Grt-Qtz in most paragneisses (Table 5.7). The lower Al content of symplectitic orthopyroxene compared to coronitic orthopyroxene in the earlier Opx-Pl coronas testifies to decreasing temperatures during decompression. In addition, the formation of Spl-Crd symplectites and Crd corona textures in sillimanite-bearing paragneisses (Table 5.7), which were

	Opx-Pl c.	Crd-Opx-Spl s.	Crd-Opx s.	Spl-Crd s.	Crd c.
Mafic granulites					
Grt-bearing two-Px granulites	x	-	-	-	-
Grt-Cpx granulites	x	-	-	-	-
Grt-Opx-Pl-Qtz granulites	x	-	-	-	-
Paragneisses					
Fe-rich Grt-Opx gneisses	x	-	-	-	-
Mg-rich Grt-Opx gneisses	x	x	x	x	x
Qtz-rich Grt-Opx rocks	-	x	x	x	x
Grt gneisses	x	x	x	x	x
Grt-Sil gneisses	-	-	x	x	x
Spr-bearing Opx-Sil gneisses	x	x	x	x	x
Opx-Grt rocks	x	x	x	-	-

Table 5.7: Summary of selected decompression reaction textures (stage 3) in the granulites of the Epembe Unit (c.: corona; s.: symplectite; x: texture is present; -: texture is absent)

formed at the expense of Grt-Sil and Grt-Sil-Qtz, respectively, testify to HT decompression. In addition, the presence of Crd-Opx-Spl symplectites, formed at the expense of garnet in silica-deficient domains of most paragneisses (Table 5.7), demonstrates decompression to $P < 8$ kbar.

Stage 4: Re-growth of garnet, biotite, sillimanite and amphibole

The subsequent re-growth of biotite, formed by an interaction between the crystallizing melt with the restitic minerals, and of amphibole in the mafic granulites and the felsic granulites, indicates post-decompressional cooling. The re-growth of garnet, which is less magnesian than peak-metamorphic Grt₂, demonstrates that cooling was near-isobaric. While biotite was formed in all paragneisses and in the Grt-Opx metagranitoids, re-growth of garnet is restricted to the Grt-Opx metagranitoids, the mafic granulite and the mafic dykes and to paragneisses with a bulk-rock $X_{Mg} < 0.59$ (Qtz-rich Grt-Opx rocks, Grt-Sil gneisses, Grt gneisses and Fe-rich Grt-Opx gneisses). The presence of late sillimanite in the Grt-Sil gneisses and in the cordierite-bearing Qtz-rich Grt-Opx rocks demonstrates at least amphibolite facies condition during late cooling.

By integrating the obtained data, an anti-clockwise P-T paths is constrained for the UHT granulites of the Epembe Unit, which is characterized by prograde near-isobaric heating to UHT conditions at moderate pressures, followed by a pressure increase at UHT conditions to the peak-metamorphic pressures. Subsequent decompression initially still under UHT conditions was followed by continued decompression under granulite facies conditions. Late stage cooling led to the re-growth of garnet, biotite, sillimanite and amphibole.

5.4 P-T CONDITIONS

The phase-petrological interpretation of the observed reaction textures and mineral assemblages has demonstrated that the granulites of the Epembe Unit followed a multistage anti-clockwise P-T path. Based on the microscopic observations conventional thermobarometry was applied to specific mineral assemblages of the various rock types of the Epembe Unit in order to confirm the P-T conditions attained during the multiple stages of the metamorphic evolution. Special emphasis is given to the documentation of ultrahigh-temperature (UHT) conditions during peak-metamorphism on the basis of conventional geothermobarometry.

Rare mineral inclusions in the peak-metamorphic minerals are used to elucidate the P-T conditions attained during the prograde evolution (stage 1). The mineral chemistry and the mineral zonation pattern suggest that in several of the studied granulites of the Epembe Unit the peak-metamorphic mineral composition is preserved in core plateaus of Grt₂ and in the cores of coexisting phases such as Opx₂, Cpx₂, Bt₂, and Pl₂. It is hence possible to calculate the peak-metamorphic P-T conditions (stage 2) from conventional geothermobarometry. The abundant and well-preserved decompressional reaction textures (stage 3) provide an excellent possibility to calculate the P-T conditions attained during the early retrograde evolution. The P-T conditions during late near-isobaric cooling (stage 4) were estimated by combining the core composition of re-grown Grt₄ with the composition of coexisting re-grown phases. Consequently, the granulites of the Epembe Unit are highly suitable for the application of a variety of widely used geothermobarometers and hence allow a detailed documentation of the physical conditions attained during the metamorphic evolution.

Temperatures were calculated from Grt-Opx Fe-Mg exchange geothermometry (calibrations of Lee & Ganguly, 1988; Carswell & Harley, 1990; Bhattacharya et al., 1991) and Grt-Opx Al-geothermometry (Harley & Green, 1982; Aranovich & Berman, 1997), from Grt-Bt Fe-Mg exchange geothermometry (calibrations of Perchuk & Lavrent'eva, 1983; Bhattacharya et al., 1992; Kleemann & Reinhardt, 1994) and from Grt-Crd Fe-Mg exchange geothermometry (calibrations of Bhattacharya et al. 1988; Dwivedi et al. 1998). For the mafic Grt-Cpx granulite sample temperatures were calculated from Grt-Hbl Fe-Mg exchange geothermometry (calibrations of Graham & Powell, 1984; Perchuk et al., 1985) and from Grt-Cpx Fe-Mg exchange geothermometry (calibrations of Powell, 1985; Ai, 1994; Krogh Ravna, 2001). Two-pyroxene thermometry (calibrations of Bertrand & Mercier, 1985; Brey & Köhler, 1990) was applied to calculate the peak-temperatures for the mafic two-pyroxene granulites.

Corresponding pressures were calculated with the Grt-Opx-Pl-Qtz geobarometer, using the calibrations of Newton & Perkins (1982) and Eckert et al. (1991) for the Mg-endmember

reaction and of Bohlen et al. (1983a) and Moecher et al. (1988) for the Fe-endmember reaction. In the sillimanite-bearing paragneisses additional pressures were calculated by application of the garnet-alumosilicate-quartz-plagioclase (GASP) equilibrium with the calibrations of Newton & Haselton (1981), Powell & Holland (1988) and Koziol & Newton (1988). Pressure calculations for the mafic Grt-Cpx granulite were performed with the Grt-Hbl-Pl-Qtz geobarometer (Kohn & Spear, 1990) and with the Grt-Cpx-Pl-Qtz geobarometer in the calibrations of Newton & Perkins (1982), Eckert et al. (1991) and Moecher et al. (1988) for the Mg-endmember reaction and of Moecher et al. (1988) for the Fe-endmember reaction. A more detailed description of the applied geothermometers and geobarometers is given in the Appendix (Chapter A.4).

The location of the Fe- and Mg-endmember reactions of the divariant retrograde decompression reactions $\text{Grt} + \text{Sil} + \text{Qtz} \rightarrow \text{Crd}$, $\text{Grt} + \text{Sil} \rightarrow \text{Crd} + \text{Spl}$ and $\text{Grt} + \text{Qtz} \rightarrow \text{Crd} + \text{Opx}$ was calculated with the computer program THERMOCALC v.2.7 of Holland & Powell (1998a), using the updated internally consistent dataset of Holland & Powell (1990, 1998a & b) and the activity model of Berman (1990) for garnet, of Wood & Banno (1973) for orthopyroxene, of Holland & Powell (1998b) for spinel and an ideal mixing model for anhydrous cordierite. Endmember activities were calculated with the computer program AX of Holland & Powell (2000). Due to the presence of cordierite, the location of the reactions strongly depends on the water activity. The presence of fluid species (H_2O , CO_2) in the structural channels of cordierite point to fluid-infiltration during retrogression, but due to the lack of suitable fluid-inclusions, the water activity was not estimated. Therefore, the results given in Tables 5.9-11 and in Fig. 5.36 were calculated for an intermediate $a(\text{H}_2\text{O}) = 0.5$. Calculations for fluid-absent conditions lower the pressures by the order of 0.5-1.0 kbar whereas calculations with pure H_2O -fluids would increase the pressures by the order of 0.5-1.0 kbar.

For most paragneisses the P-T results calculated from conventional geothermobarometry will be compared for the individual stages with P-T estimates obtained for the application of isopleth diagrams, that were contoured for the composition of garnet and orthopyroxene in the assemblage Grt-Opx-Sil-Qtz at higher pressures and the assemblage Grt-Opx-Crd-Qtz at lower pressures. The isopleth diagrams of Hensen & Harley (1990) and of Harley (1998a), the latter based on the experiments of Carrington & Harley (1995), have been contoured for X_{Al} and X_{Mg} in orthopyroxene and X_{Mg} in coexisting garnet. The diagram of Aranovich & Berman (1996) has been contoured for X_{Prp} in garnet and for Al_2O_3 in orthopyroxene. In all diagrams X_{Mg} in garnet is an excellent pressure indicator since the X_{Mg} isopleths are very shallow in the P-T space. In contrast, the Al content of orthopyroxene is an excellent temperature indicator since the Al-isopleths are very steep in the P-T space. Thus, the systematic decrease in the Al content of

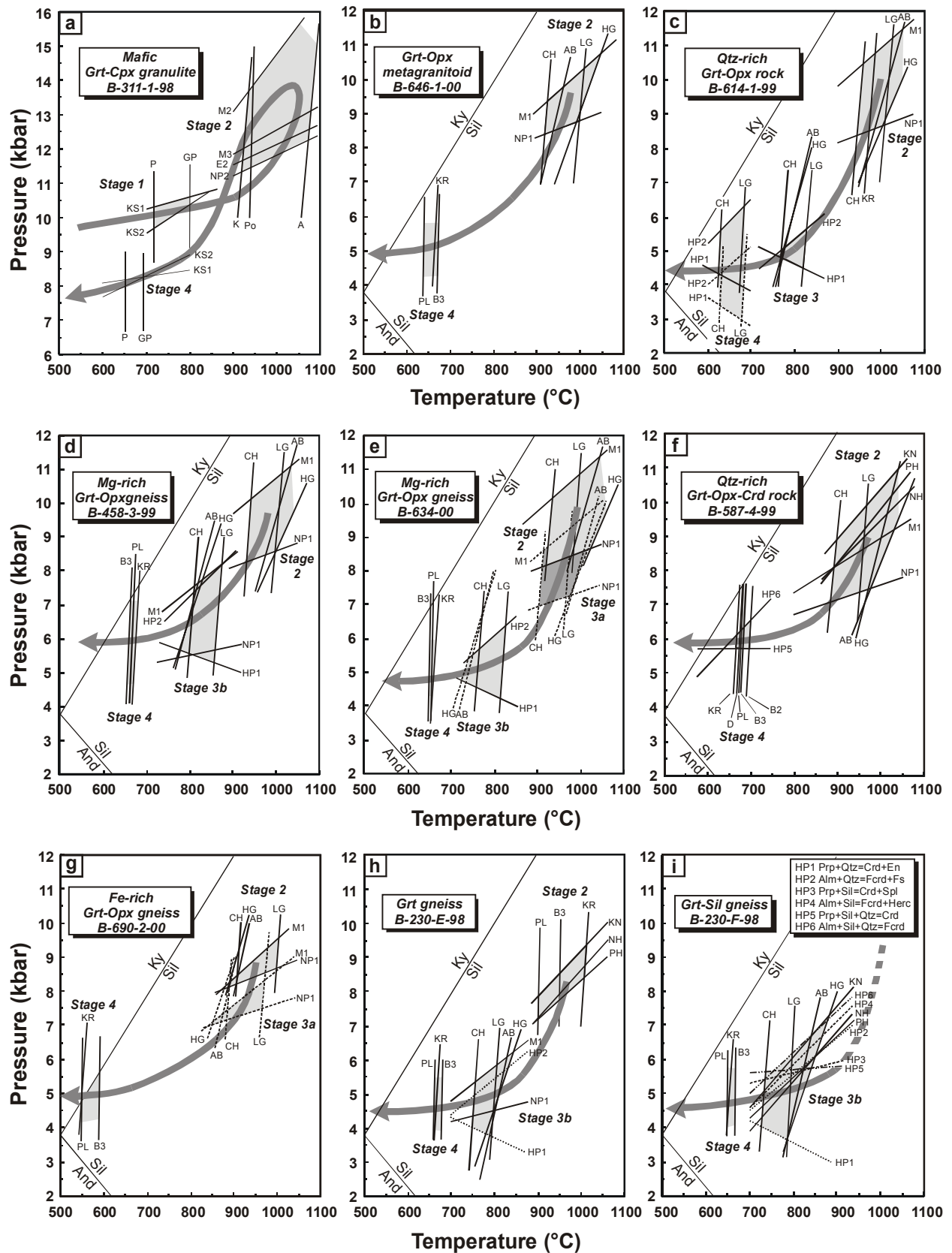


Fig. 5.36: P-T plots showing the results of geothermobarometric calculations for the prograde evolution (stage 1), the peak-metamorphic conditions (stage 2) and the retrograde evolution (stage 3 & 4) of the granulites of the Epembe Unit. The P-T path most probably followed by the rock is indicated as heavy line. Note differing pressure scale in Fig. 5.36a. Abbreviations are explained on the next page.

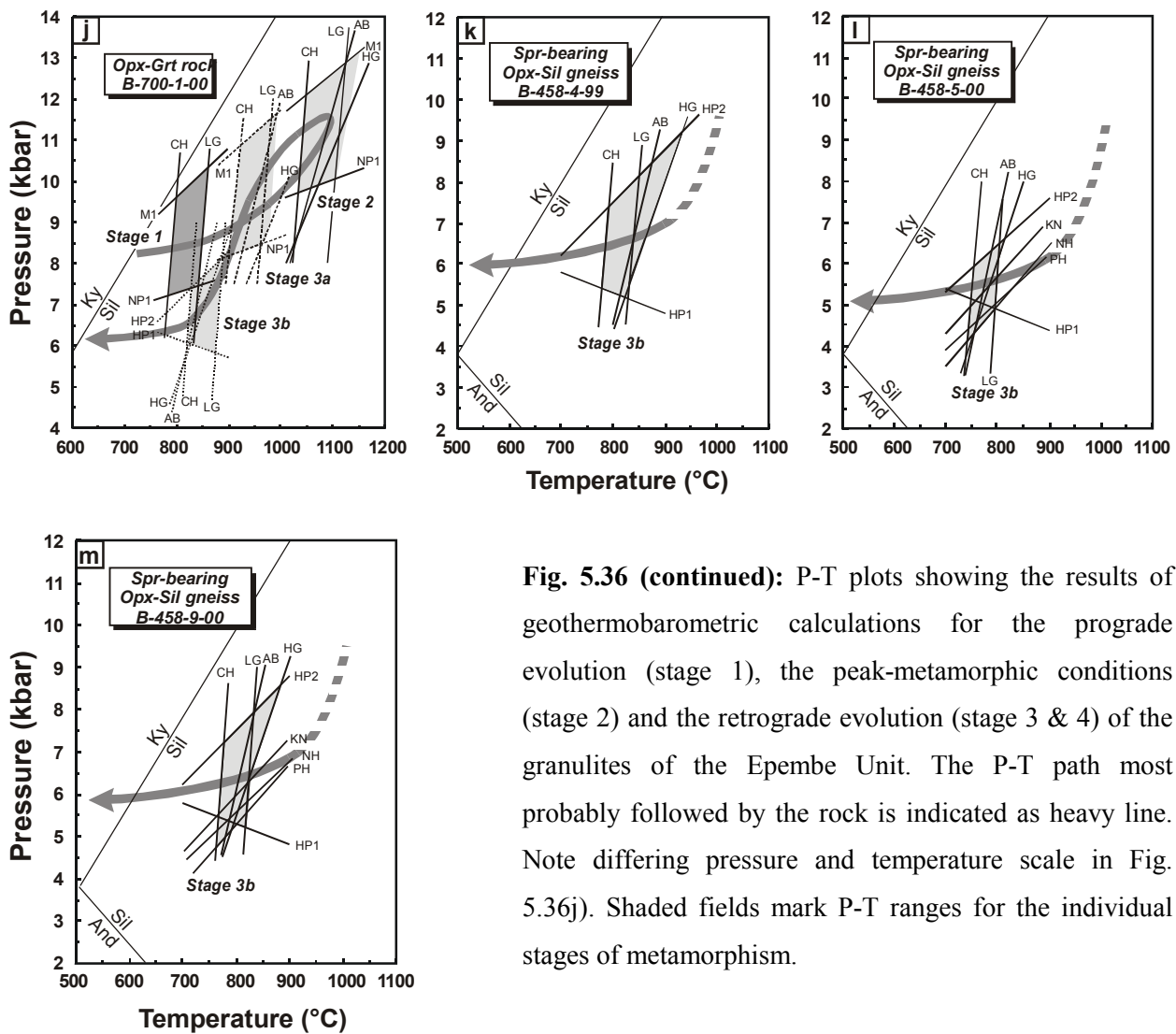


Fig. 5.36 (continued): P-T plots showing the results of geothermobarometric calculations for the prograde evolution (stage 1), the peak-metamorphic conditions (stage 2) and the retrograde evolution (stage 3 & 4) of the granulites of the Epembe Unit. The P-T path most probably followed by the rock is indicated as heavy line. Note differing pressure and temperature scale in Fig. 5.36j). Shaded fields mark P-T ranges for the individual stages of metamorphism.

Abbreviations in Fig. 5.36: Geothermometers: Po, Powell (1985); A, Ai (1994); K, Krogh Ravn (2001); CH, Carswell & Harley (1990); LG, Lee & Ganguly (1988); HG, Harley & Green (1982); AB, Aranovich & Berman (1997); GP, Graham & Powell (1984); P, Perchuk et al. (1985); PL, Perchuk & Lavrent'eva (1983); B3, Bhattacharya et al. (1992); KR, Kleemann & Reinhardt (1994); D, Dwivedi et al. (1998); B2, Bhattacharya et al. (1988). **Geobarometers:** NP1-2, Newton & Perkins (1982); M1-3, Moecher et al. (1988); E2, Eckert et al. (1991); PH, Powell & Holland (1988); KN, Koziol & Newton (1988); NH, Newton & Haselton (1981); HP1-6, Holland & Powell (1998b)

orthopyroxene in the various textural domains of the studied Mg-rich Grt-Opx gneisses, the Qtz-rich Grt-Opx rocks, the sapphirine-bearing Opx-Sil gneisses and the Opx-Grt rocks (Fig. 5.25 & 5.26) provides a first-order indication that post-peak decompression was accompanied by a significant temperature decrease.

Based on P-T estimates for the Mg-rich Grt-Opx gneisses and the Qtz-rich Grt-Opx rocks (Brandt et al., 2003) the temperatures calculations were generally performed with the following

reference pressures: 9.5 kbar for stage 2; 6 kbar for stage 3 and 5 kbar for stage 4 (with exception of the mafic Grt-Cpx granulite sample B-311-1-99). Pressures were estimated with the following reference temperatures: 970°C for stage 2; 800°C for stage 3 and 660°C for stage 4. The P-T calculations were performed with mineral chemical data given in the Appendix A.6.2 (bold marked analyses of Tables A.6.2.1, A.6.2.2, A.6.2.3, A.6.2.5, A.6.2.6, A.6.2.7, A.6.2.9 and A.6.2.11).

5.4.1 Mafic granulites

The widespread occurrence of two-pyroxene assemblages and the lack of the high-pressure granulite facies mineral assemblage Grt-Cpx-Qtz indicate that the mafic granulites of the Epembe Unit equilibrated in the medium pressure granulite field (Opx-Pl) of Green & Ringwood (1967). The transition to the high pressure granulite field (Grt-Cpx-Qtz) is related to the reaction (5-4), $\text{Opx} + \text{Pl} \rightarrow \text{Grt} + \text{Cpx} + \text{Qtz}$, and is sensitive to the bulk-rock composition; low bulk X_{Mg} , low Na/Ca ratios and SiO_2 under-saturation cause the Grt-Cpx-Qtz association to appear at lower pressures (Green & Ringwood, 1967). Although the basic two-pyroxene granulites are generally SiO_2 -poor olivine-tholeiites, garnet is very rare and never occurs in the high-pressure granulite assemblage Grt-Cpx-Qtz. These relationships suggest that the mafic granulites equilibrated at pressures close to the Grt-in curve for olivine-tholeiites, hence for a reference temperature of 970°C at pressures of ~ 9 kbar.

In contrast, the mafic Grt-Cpx granulite, which occurs in an isolated tectonic lens within a major shear zone, has ultrabasic olivine-tholeiite to alkali-olivine tholeiite compositions with low Na/Ca ratios and a low SiO_2 content. Therefore the postulated crossing of reaction (5-4) in this rock is either related to its bulk-rock composition or to its equilibration under higher pressures.

The lack of peak-metamorphic hornblende in the mafic granulites of the Epembe Unit is characteristic for metabasites, that equilibrated at very high metamorphic temperatures of > 900°C (Spear, 1981).

Results of the P-T calculations for the mafic granulites are summarized in Table 5.8. and illustrated for the mafic Grt-Cpx granulite in Fig. 5.36a.

Stage 1: Prograde evolution

Upper amphibolite facies to granulite facies P-T conditions of 717 to 801°C at a pressure of ~ 10 kbar were calculated from Grt-Hbl-Pl-Qtz geothermobarometry for the Grt-Cpx granulite B-311-1-99, using Hbl1 and Pl1 inclusions in Grt2 coupled with the core composition of the hosting

prograde zoned Grt₂. Inclusions of orthopyroxene and plagioclase in matrix Cpx₂ suggest further prograde heating into the granulite facies. However, the investigated thin section lacks orthopyroxene-inclusions and therefore P-T data were not calculated.

Stage 2: Peak-metamorphic conditions

Ultrahigh P-T conditions of ~ 1000°C and 12-15 bar were calculated for the Grt-Cpx granulite B-311-1-99 from Grt-Cpx-Pl-Qtz geothermobarometry by using the composition of high X_{Mg} rims of prograde zoned Grt₂ coupled with the composition of unzoned matrix Cpx₂ and of Pl₁ inclusions in Cpx₂. The highest pressures were calculated for the Fe-endmember reaction whereas the Mg-endmember reaction defines a lower pressure limit. While the calculated temperatures are in the range of those of the other granulites, the calculated pressures are significantly higher than those of the other granulites.

Two-pyroxene thermometry performed for the garnet-bearing two-pyroxene granulite B-434-2-99 and the garnet-free two-pyroxene granulite B-230-B-98 yields temperatures of 944-885°C (for $P_{(ref.)}$ of 9.5 kbar). Grt-Opx Fe-Mg thermometry and Grt-Cpx Fe-Mg thermometry for the garnet-bearing mafic granulite B-434-2-99 yields significantly lower temperatures of ~ 800°C, which point to extensive Fe-Mg re-equilibration of Grt₂ and retrograde Hbl₄, present in Grt₂ cracks and around Grt₂. Consequently, geobarometry on this sample yields meaningless results.

Stage 3: Corona and symplectite formation

Breakdown of Grt₂ is documented by Opx₃-Pl₃-Spl₃ intergrowths and by Opx₃-Pl₃ corona textures in the mafic granulites, both of which are indicative of post-peak decompression. However, the analyzed samples lack high-temperature decompression textures and therefore absolute P-T conditions were not estimated.

Stage 4: Re-growth of hornblende

Upper amphibolite facies P-T conditions of 693-651°C and ~ 8 kbar were calculated from Grt-Hbl-Pl geothermobarometry for the development of the Hbl₄-Pl₄ symplectites replacing Grt₂ of the Grt-Cpx granulites, by using the composition of the outermost Grt₂ rim coupled with the compositions of the adjacent symplectitic Hbl₄ and Pl₄. The calculations indicate decompression accompanied by significant cooling from the peak-metamorphic conditions. The relatively high pressure during decompression, when compared to the other granulites, indicates that the uplift of the mafic Grt-Cpx granulites proceeded in a deeper crustal level.

5.4.2 Grt-Opx metagranitoids

Results of the P-T calculations for the Grt-Opx metagranitoid B-646-1-00 are summarized in Fig. 5.36b and in Table 5.8.

Stage 2: Peak-metamorphic conditions

Grt-Opx Fe-Mg exchange geothermometry yields ultrahigh temperatures between 1002°C and 925°C (for $P_{(ref.)}$ of 9.5 kbar) for the formation of the peak-metamorphic Opx2-Grt2 assemblages (Fig. 5.36b). The Grt-Opx Fe-Mg temperatures are consistent with the T-results of Grt-Opx Al-geothermometry, that range between 1014°C and 956°C. Corresponding pressures, calculated with the Grt-Opx-Pl-Qtz geobarometer, range between 10.8 kbar and 8.1 kbar (for $T_{(ref.)}$ of 970°C) with the lower values being obtained for the Mg-endmember reaction.

sample	rock type	texture	Temperature (°C)														
			P (ref.)	Grt-Opx					Opx-Cpx		Grt-Bt			Grt-Hbl		Grt-Cpx	
	B1 Fe-Mg	LG Fe-Mg		CH Fe-Mg	HG Al	AB Al	BK	BM	KR Fe-Mg	B3 Fe-Mg	PL Fe-Mg	GP Fe-Mg	P Fe-Mg	A Fe-Mg	K Fe-Mg	Po Fe-Mg	
stage 1 (prograde)																	
B-311-1-99	Grt-Cpx granulite	Hbl1-Pl1-Grt2 (core)	10.0	-	-	-	-	-	-	-	-	801	717	-	-	-	
stage 2 (peak)																	
B-230-B-98	mafic granulite	Opx2-Cpx2 (cores)	9.5	-	-	-	-	-	885	919	-	-	-	-	-	-	
B-434-A-98	Grt-bearing mafic granulite	Opx2-Cpx2 (cores)	9.5	-	-	-	-	-	893	944	-	-	-	-	-	-	
B-311-1-99	Grt-Cpx granulite	Grt2(rim)-Cpx2-Pl1	12.0	-	-	-	-	-	-	-	-	-	-	1071	923	942	
B-646-1-00	Grt-Opx metagranitoid	Grt2-Opx2-Pl2-Qtz2	9.5	955	1002	925	1014	956	-	-	-	-	-	-	-	-	
stage 4 (Grt, Hbl and Bt re-growth)																	
B-311-1-99	Grt-Cpx granulite	Grt2(rim)-Hbl4-Pl4	8.0	-	-	-	-	-	-	-	-	693	651	-	-	-	
B-646-1-00	Grt-Opx metagranitoid	Grt4 (rim on Grt2)-Bt4	5.0	-	-	-	-	-	-	-	665	673	638	-	-	-	

sample	rock type	texture	Pressure (kbar)										
			T (ref.)	Grt-Opx-Pl-Qtz				Grt-Cpx-Pl-Qtz				Grt-Hbl-Pl-Qtz	
	NP1 Mg	E1 Mg		M1 Fe	Bo Fe	NP2 Mg	M2 Mg	E2 Mg	M3 Fe	KS1 Mg	KS2 Fe		
stage 1 (prograde)													
B-311-1-99	ultramafic granulite	Hbl1-Pl1-Grt2 (core)	750	-	-	-	-	-	-	-	-	10.4	10.0
stage 2 (peak)													
B-311-1-99	ultramafic granulite	Grt2(rim)-Cpx2-Pl1	970	-	-	-	-	11.6	12.3	12.0	14.3	-	-
B-646-1-00	Grt-Opx metagranitoid	Grt2-Opx2-Pl2-Qtz2	970	8.7	8.1	9.9	10.8	-	-	-	-	-	-
stage 4 (Grt, Hbl and Bt re-growth)													
B-311-1-99	ultramafic granulite	Grt2(outer rim)-Hbl4-Pl4	660	-	-	-	-	-	-	-	-	7.8	7.7

Table 5.8: Results of conventional geothermobarometry for the mafic granulites and the Grt-Opx metagranitoids of the Epembe Unit. B1, Bhattacharya et al. (1991); LG, Lee & Ganguly (1988); CH, Carswell & Harley (1990); HG, Harley & Green (1982); AB, Aranovich & Berman (1997); BK, Brey & Köhler (1990); BM, Bertrand & Mercier (1985); KR, Kleemann & Reinhardt (1994); B3, Bhattacharya et al. (1992); PL, Perchuk & Lavrent'eva (1983); GP, Graham & Powell (1984); P, Perchuk et al. (1985); A, Ai (1994); K, Krogh Ravn (2001); Po, Powell (1985); NP1-2, Newton & Perkins (1982); Bo, Bohlen et al. (1983a); M1-3, Moecher et al. (1988); E2, Eckert et al. (1991); KS, Kohn & Spear (1990)

Stage 4: Re-growth of garnet and biotite

Grt-Bt thermometry yields amphibolite facies temperatures of 673-638°C (for $P_{(\text{ref.})}$ of 5.0 kbar) for the re-growth of coexisting Grt4 and Bt4 during late-stage near-isobaric cooling.

5.4.3 Paragneisses

5.4.3.1 Fe-rich and Mg-rich Grt-Opx gneisses and Qtz-rich Grt-Opx rocks

The first evidence with regard to the P-T conditions attained during the metamorphic evolution of the Mg-rich Grt-Opx gneisses and the Qtz-rich Grt-Opx rocks is given by the observed mineral assemblages, reaction textures and mineral compositions: The high Al contents of peak-metamorphic Opx2 (10.6-7.8 wt.% Al_2O_3) indicate UHT metamorphism with temperatures > 900°C. UHT conditions are furthermore supported by the prograde biotite-dehydration reactions and the rare preservation of prograde biotite, that point to peak-temperatures ranging between 990°C and 890°C (Fig. 5.31). The formation of Crd-Opx-Spl and Spl-Crd symplectites, replacing peak-metamorphic garnet, indicate post-peak decompression to $P < 8$ kbar (Fig. 5.31). Results of the P-T calculations are summarized in Figs. 5.36c-g and in Table 5.9.

Stage 2: Peak-metamorphic conditions

Grt-Opx Fe-Mg exchange geothermometry yields ultrahigh temperatures between 1013°C and 931°C (for $P_{(\text{ref.})}$ of 9.5 kbar) for the formation of the peak-metamorphic Al-rich Opx2-Grt2 assemblages of the Mg-rich Grt-Opx gneisses B-458-3-99 and B-634-00 and the Qtz-rich Grt-Opx rock B-614-1-99 (Fig. 5.36c-e). The estimates for sample B-634-00 are minimum temperatures, since Grt2 core plateaus are not preserved. The ultrahigh Grt-Opx Fe-Mg temperatures are supported by results of Grt-Opx Al-geothermometry, that range between 1068°C and 1003°C. Furthermore, Grt-Bt Fe-Mg exchange geothermometry, performed with matrix Bt2 of the Qtz-rich Grt-Opx rock combined with Grt2 cores, yields extreme temperatures of 978-863°C. The calculated ultrahigh temperatures are consistent with the very high Al contents of porphyroblastic Opx2 (Al_2O_3 : 10.6-7.8 wt.%; Al/2 p.f.u.: 0.23-0.20) coexisting with Grt2. Application of the isopleth diagrams of Hensen & Harley (1990) and Aranovich & Berman (1996) yields ultrahigh temperatures of 1050-980°C, whereas slightly lower temperatures of 950-920°C are obtained for the isopleth diagram of Harley (1998a). Corresponding pressures, calculated with the Grt-Opx-Pl-Qtz geobarometer, range between 11.5 and 7.7 kbar (for $T_{(\text{ref.})}$ of 970°C) with the lower estimates being obtained for the Mg-endmember reaction.

UHT peak-metamorphic conditions of 1043-904°C at 9.5-6.6 kbar are also calculated for the

cordierite-bearing Qtz-rich Grt-Opx rock B-587-4-99 (Fig. 5.36f).

Ultrahigh temperatures of 1005-916 °C and 927-920°C (for $P_{(ref.)}$ of 9.5 kbar) are furthermore calculated by Grt-Opx Fe-Mg exchange geothermometry and Grt-Opx Al-geothermometry, respectively, for the formation of the peak-metamorphic Grt₂-Opx₂ assemblages of the Fe-rich Grt-Opx gneiss B-690-2-00 (Fig. 5.36g). Corresponding pressures, calculated from Grt-Opx-Pl-Qtz geobarometry, are between 10.1 and 8.0 kbar (for $T_{(ref.)}$ of 970°C). Grt-Bt Fe-Mg exchange geothermometry performed with matrix Bt₂ and Grt₂ yields relatively low temperatures of 841-712°C, suggesting that the composition of Bt₂ was affected by retrogression.

Best-fit peak-metamorphic P-T conditions of 970 ± 40 °C and 9.5 ± 2 kbar encompass most of the calculated P-T data for the peak-metamorphic conditions of the Fe-rich and Mg-rich Grt-Opx gneisses and the Qtz-rich Grt-Opx rocks and are in agreement with the lack of Opx-Sil-Qtz assemblages and with the temperature range (990-890°C) obtained for the biotite-dehydration melting reactions (Fig. 5.31).

Stage 3a: Corona formation

Initial breakdown of garnet of both the Mg-rich and the Fe-rich Grt-Opx gneisses is documented by the formation of decompressional Opx-Pl coronas around Grt₂. Grt-Opx Fe-Mg geothermometry performed with coronitic Opx₃ of the Grt-Opx Mg-rich gneiss B-634-00 coupled with Grt₂ rim composition yields ultrahigh temperatures of 970-911°C (for $P_{(ref.)}$ of 8.0 kbar), close to the peak-metamorphic conditions (Fig. 5.36e) and in agreement with the high Al content of coronitic Opx₃ (Al₂O₃: 9-6 wt.%). UHT conditions are consistent with Grt-Opx Al-geothermometry, which yields temperatures of ~ 1000°C. Corresponding Grt-Opx-Pl-Qtz pressures of 10.0-6.5 kbar (for $T_{(ref.)}$ of 940°C) are 1.2-1.7 kbar lower than peak-metamorphic pressures.

Grt-Opx Fe-Mg and Grt-Opx Al-geothermometry performed with coronitic Opx₃ in Opx-Pl coronas at Grt₂ of the Fe-rich Grt-Opx gneiss sample B-690-2-00 rims yields temperatures of 966-874 °C (for $P_{(ref.)}$ of 8.0 kbar; Fig. 5.36g), close to the estimates for the Mg-rich Grt-Opx gneiss. Corresponding Grt-Opx-Pl-Qtz pressures of 8.5-6.7 kbar (for $T_{(ref.)}$ of 940°C) are again 1.2-1.6 kbar lower than the peak-metamorphic pressures.

The P-T calculations indicate that initial garnet breakdown in both the Mg-rich and Fe-rich Grt-Opx gneisses proceeded in response to near-isothermal decompression to 8.0 ± 2 kbar still under ultrahigh temperatures of 940 ± 60 °C.

Stage 3b: Symplectite formation

P-T conditions for subsequent symplectite development in the Mg-rich Grt-Opx gneisses and in the Qtz-rich Grt-Opx rocks were estimated using Grt2 rim composition and the composition of symplectitic orthopyroxene, cordierite, spinel and plagioclase. Calculations for the formation of Crd-Opx-Spl symplectites, that replace Grt2 along fissures, were performed by combining the composition of the symplectitic phases with the composition of the adjacent Grt2. Temperatures calculated from Grt-Opx Fe-Mg and Al-geothermometry mainly cluster around 800°C (for $P_{(ref.)}$ of 6.0 kbar) for both the Crd-Opx-Spl and the Crd-Opx symplectites. Partly lower temperatures (828-658°C) were calculated from Grt-Crd Fe-Mg geothermometry and probably reflect intense retrograde Fe-Mg re-equilibration of Crd3 with Grt2, that is evident from the garnet and cordierite zonation (Fig. 5.19 & 5.23). Consequently, even Grt-Opx Fe-Mg geothermometry provides minimum temperatures for the symplectite formation since they were calculated with the modified Grt2 rim composition. Grt-Opx-Pl-Qtz pressures are highly variable, ranging between 8.0 kbar and 4.8 kbar (for $T_{(ref.)}$ of 800°C). With values of 7.3-4.3 kbar pressures calculated for the formation of Crd-Opx symplectites (reaction 5-24) at Grt2 rims and of Spl-Crd symplectites (reaction 5-26) in Grt2 cores are consistent with those derived by Grt-Opx-Pl-Qtz barometry.

The P-T results calculated from conventional geothermobarometry are consistent with P-T estimates obtained for the application of the isopleth diagrams of Hensen & Harley (1990) and Aranovich & Berman (1996) contoured for the Grt-Opx-Crd-Qtz assemblage, that yields P-T conditions of 850-750°C at 6-5 kbar and of 920-770°C at 7-6 kbar, respectively. Best-fit P-T conditions of 800 ± 60 °C at 6 ± 2 kbar for the formation of the symplectites indicate subsequent decompression accompanied by cooling from stage 3a.

Stage 4: Re-growth of garnet, biotite and sillimanite

P-T conditions for the re-growth of garnet in the Qtz-rich Grt-Opx rock B-614-1-99 were calculated using core composition of re-grown Grt4 combined with the composition of adjacent Crd3-Opx3 symplectites. Temperatures calculated from Grt-Opx Fe-Mg and Grt-Crd Fe-Mg geothermometry are between 701°C and 628°C (for $P_{(ref.)}$ of 5.0 kbar). Grt-Opx Al-geothermometry yields higher temperatures (831-718°C), suggesting that the Al₂O₃ content of orthopyroxene did not re-equilibrate during cooling. Another possible explanation for the lower Fe-Mg temperatures is provided by retrograde Fe-Mg exchange, that affected the garnet-orthopyroxene pairs. However, since re-grown Grt4 is almost unzoned (see Fig. 5.19a) the latter possibility seems rather unlikely and the Fe-Mg exchange temperatures are interpreted to be more realistic. Pressures of 5.9-3.1 kbar, calculated from the Grt-Opx-Crd-Qtz barometer, are

consistent with estimates obtained for the isopleth diagrams of Hensen & Harley (1990) and Aranovich & Berman (1996) for the present Grt-Opx-Crd-Qtz assemblage: Based on the X_{Mg} of re-grown Grt4 pressures of < 5 kbar and 5.5-4.5 kbar, respectively, are estimated. Grt-Bt geothermometry, using Grt2 rim composition coupled with Bt4 present in the Crd-Opx symplectites of the Mg-rich Grt-Opx gneisses, yields temperatures of 672-650°C, that are broadly consistent with the results of Grt-Opx and Grt-Crd Fe-Mg geothermometry.

Grt-Bt and Grt-Crd thermometry yields temperatures of 694-667°C during the re-growth of Grt4 and Bt4 at the expense of Crd2 in the cordierite-bearing Qtz-rich Grt-Opx rock sample B-587-4-99. Corresponding pressures of 5.9-5.7 kbar are calculated for the formation of Grt4, Sil4 and Qtz4 at the expense of Crd2 (reaction 5-31) and are consistent with the pressure estimates for garnet re-growth in the Qtz-rich Grt-Opx rock sample B-614-1-99.

Low temperatures of 589-549°C (for $P_{(ref.)}$ of 5.0 kbar) are calculated by Grt-Bt thermometry for the re-growth of Grt4 and Bt4 in the Fe-rich Grt-Opx gneisses.

Best-fit P-T conditions of 660 ± 40 °C at 5 ± 2 kbar, corresponding to the upper amphibolite facies, indicate that garnet and biotite re-growth proceeded in response to near-isobaric cooling of about ~ 140 °C from stage 3b.

sample	rock type	texture	Temperature (°C)										
			P (ref.)	Grt-Opx					Grt-Crd		Grt-Bt		
				B1 Fe-Mg	LG Fe-	CH Fe-Mg	AB Al	HG Al	B2 Fe-Mg	D Fe-	KR Fe-Mg	B3 Fe-	PL Fe-Mg
stage 2 (peak)													
B-458-3-99	Mg-rich Grt-Opx gneiss	Grt2-Opx2-Pl2-Qtz2 (cores)	9.5	956	1005	941	1003	1031	-	-	-	-	-
B-634-00	Mg-rich Grt-Opx gneiss	Grt2-Opx2-Pl2-Qtz2 (cores)	9.5	943	990	931	1004	1068	-	-	-	-	-
B-614-1-99	Qtz-rich Grt-Opx rock	Grt2-Opx2-Bt2-Pl2-Qtz2 (cores)	9.5	965	1013	954	1009	1031	-	-	978	867	863
B-690-2-00	Fe-rich Grt-Opx gneiss	Grt2-Opx2-Pl2-Qtz2 (cores)	9.5	963	1005	916	927	920	-	-	841	735	712
B-587-4-99	Qtz-rich Grt-Opx-Crd rock	Grt2-Opx2-Pl2-Qtz2 (cores)	9.5	933	967	904	1013	1043	-	-	-	-	-
stage 3a (corona formation)													
B-634-00	Mg-rich Grt-Opx gneiss	Opx3-Pl3 corona - Grt2 (rim)	8.0	925	970	911	994	1004	-	-	-	-	-
B-690-2-00	Fe-rich Grt-Opx gneiss	Opx3-Pl3 corona - Grt2 (rim)	8.0	923	966	887	887	874	-	-	-	-	-
stage 3b (symplectite formation)													
B-458-3-99	Mg-rich Grt-Opx gneiss	Crd-Opx sympl. - Grt2 (rim)	6.0	809	861	802	785	787	696	704	-	-	-
B-458-3-99	Mg-rich Grt-Opx gneiss	Crd-Opx-Spl sympl. - Grt2 (at crack)	6.0	733	771	720	757	795	658	678	-	-	-
B-634-00	Mg-rich Grt-Opx gneiss	Crd-Opx sympl. - Grt2 (rim)	6.0	788	822	767	763	757	742	737	-	-	-
B-634-00	Mg-rich Grt-Opx gneiss	Crd-Spl sympl. - Grt2 (at cont.)	6.0	-	-	-	-	-	721	719	-	-	-
B-614-1-99	Qtz-rich Grt-Opx rock	Crd-Opx sympl. - Grt2 (rim)	6.0	801	832	778	797	794	805	828	-	-	-
B-614-1-99	Qtz-rich Grt-Opx rock	Crd-Opx-Spl sympl. - Grt2 (at crack)	6.0	806	851	799	799	812	734	761	-	-	-
stage 4 (Grt and Bt re-growth)													
B-458-3-99	Mg-rich Grt-Opx gneiss	Grt2 (rim) - Bt4 (in sympl.)	5.0	-	-	-	-	-	-	-	672	665	669
B-634-00	Mg-rich Grt-Opx gneiss	Grt2 (rim) - Bt4 (in sympl.)	5.0	-	-	-	-	-	-	-	659	650	652
B-614-1-99	Qtz-rich Grt-Opx rock	Grt4 (core) - Crd-Opx sympl.	5.0	676	684	630	718	730	701	676	-	-	-
B-614-1-99	Qtz-rich Grt-Opx rock	Grt4 (rim on Grt2) - Crd-Opx sympl.	5.0	671	679	628	781	831	675	649	-	-	-
B-690-2-00	Fe-rich Grt-Opx gneiss	Grt4 (rim on Grt2) - Bt4	5.0	-	-	-	-	-	-	-	549	589	549
B-587-4-99	Qtz-rich Grt-Opx-Crd rock	Crd2 - Grt4 (core)-Bt4-Sil4-Qtz4	5.0	-	-	-	-	-	694	671	667	676	677

sample	rock type	texture	Pressure (kbar)											
			T (ref.)	Grt-Opx-Pl-Qtz				Grt-Crd-Opx-Qtz		Grt-Sil-Crd-Spl		Grt-Sil-Qtz-Crd		
				E1	NP1	Bo	M1	HP1	HP2	HP3	HP4	HP5	HP6	
				Mg	Mg	Fe	Fe	Mg	Fe	Mg	Fe	Mg	Fe	
stage 2 (peak)														
B-458-3-99	Mg-rich Grt-Opx gneiss	Grt2-Opx2-Pl2-Qtz2 (cores)	970	7.7	8.4	11.0	10.4	-	-	-	-	-	-	
B-634-00	Mg-rich Grt-Opx gneiss	Grt2-Opx2-Pl2-Qtz2 (cores)	970	7.7	8.4	11.4	10.5	-	-	-	-	-	-	
B-614-1-99	Qtz-rich Grt-Opx rock	Grt2-Opx2-Bt2-Pl2-Qtz2 (cores)	970	7.9	8.5	11.5	10.6	-	-	-	-	-	-	
B-690-2-00	Fe-rich Grt-Opx gneiss	Grt2-Opx2-Pl2-Qtz2 (cores)	970	8.0	8.6	10.1	9.2	-	-	-	-	-	-	
B-587-4-99	Qtz-rich Grt-Opx-Crd rock	Grt2-Opx2-Pl2-Qtz2 (cores)	970	6.6	7.4	9.5	8.6	-	-	-	-	-	-	
stage 3a (corona formation)														
B-634-00	Mg-rich Grt-Opx gneiss	Opx3-Pl3 corona - Grt2 (rim)	940	6.5	7.2	10.0	8.8	-	-	-	-	-	-	
B-690-2-00	Fe-rich Grt-Opx gneiss	Opx3-Pl3 corona - Grt2 (rim)	940	6.7	7.4	8.5	8.0	-	-	-	-	-	-	
stage 3b (symplectite formation)														
B-458-3-99	Mg-rich Grt-Opx gneiss	Crd-Opx sympl. - Grt2 (rim)	800	4.8	5.5	8.0	7.4	5.6	7.3	-	-	-	-	
B-458-3-99	Mg-rich Grt-Opx gneiss	Crd-Opx-Spl sympl. - Grt2 (at crack)	800	-	-	-	-	-	-	-	-	-	-	
B-634-00	Mg-rich Grt-Opx gneiss	Crd-Opx sympl. - Grt2 (rim)	800	-	-	-	-	4.3	6.1	-	-	-	-	
B-634-00	Mg-rich Grt-Opx gneiss	Crd-Spl sympl. - Grt2 (at cont.)	800	-	-	-	-	-	-	5.5	7.1	-	-	
B-614-1-99	Qtz-rich Grt-Opx rock	Crd-Opx sympl. - Grt2 (rim)	800	-	-	-	-	4.6	5.3	-	-	-	-	
B-614-1-99	Qtz-rich Grt-Opx rock	Crd-Opx-Spl sympl. - Grt2 (at crack)	800	-	-	-	-	-	-	-	-	-	-	
stage 4 (Grt and Bt re-growth)														
B-458-3-99	Mg-rich Grt-Opx gneiss	Grt2 (rim) - Bt4 (in sympl.)	660	-	-	-	-	-	-	-	-	-	-	
B-634-00	Mg-rich Grt-Opx gneiss	Grt2 (rim) - Bt4 (in sympl.)	660	-	-	-	-	-	-	-	-	-	-	
B-614-1-99	Qtz-rich Grt-Opx rock	Grt4 (core) - Crd-Opx sympl.	660	-	-	-	-	3.1	4.7	-	-	-	-	
B-614-1-99	Qtz-rich Grt-Opx rock	Grt4 (rim on Grt2) - Crd-Opx sympl.	660	-	-	-	-	4.1	5.9	-	-	-	-	
B-690-2-00	Fe-rich Grt-Opx gneiss	Grt4 (rim on Grt2) - Bt4	660	-	-	-	-	-	-	-	-	-	-	
B-587-4-99	Qtz-rich Grt-Opx-Crd rock	Crd2 - Grt4 (core)-Bt4-Sil4-Qtz4	660	-	-	-	-	-	-	-	-	5.7	5.9	

Table 5.9: Results of conventional geothermobarometry for the Mg-rich and Fe-rich Grt-Opx gneisses and the Qtz-rich Grt-Opx rocks of the Epembe Unit. B1, Bhattacharya et al. (1991); LG, Lee & Ganguly (1988); CH, Carswell & Harley (1990); HG; Harley & Green (1982); AB, Aranovich & Berman (1997); B2, Bhattacharya et al. (1988); D, Dwivedi et al. (1998); PL, Perchuk & Lavrent'eva, (1983); B3, Bhattacharya et al. (1992); KR, Kleemann & Reinhardt (1994); NP, Newton & Perkins (1982); E, Eckert et al. (1991), M, Moecher et al. (1988); Bo, Bohlen et al. (1983a); HP1-4, Holland & Powell (1998b).

Stage 5: Formation of late orthopyroxene and cordierite

Application of the isopleth diagrams of Hensen & Harley (1990) and Aranovich & Berman (1996) yields temperatures of < 700°C for the growth of late low-Al Opx5 (3-2 wt.% Al₂O₃). The temperatures are in the range of those calculated for stage 4 and support the interpretation that the growth of late orthopyroxene is related to continued decompression at a low water activity rather than to renewed heating.

5.4.3.2 Grt-Sil gneisses and Grt gneisses

Phase petrology demonstrated that the Grt-Sil gneisses and the Grt gneisses were heated to UHT

condition during the prograde heating (Fig. 5.33). A subsequent pressure increase led to the growth of peak-metamorphic Grt-Kfs, Grt-Sil-Kfs-Qtz and Grt-Sil-Kfs assemblages. As described for the Mg-rich Grt-Opx gneisses and the Qtz-rich Grt-Opx rocks, the retrograde evolution is characterized by decompression to $P < 8$ kbar as demonstrated by the formation of Crd-Opx-Spl and Spl-Crd symplectites formed at the expense of garnet.

The calculated P-T conditions for the Grt gneisses B-230-E-98 and the Grt-Sil gneiss B-230-F-98 are summarized in Fig. 5.36h and 5.34i, respectively, and in Table 5.10.

Stage 2: Peak-metamorphic conditions

Grt-Bt thermometry yields UHT peak-metamorphic conditions of 1014-903°C (for $P_{(\text{ref.})}$ of 9.5 kbar) for the composition of the Grt2 core plateaus combined with the composition of coexisting matrix Bt2 of the Grt gneiss sample B-230-E-98. The preservation of early biotite under such extreme conditions is probably related to its high Ti content (up to 6.7 wt.% TiO_2), which extends the thermal stability of biotite (e.g. Patiño Douce, 1993; Stevens et al., 1997). Corresponding peak-pressures of 9.3 to 8.4 kbar are calculated from the GASP reaction (for $T_{(\text{ref.})}$ of 970°C) for the composition of Grt2 core plateaus combined with the composition of matrix Pl2. The presence of sillimanite during peak-metamorphic conditions is indicated by Sil1 inclusions in the Grt2 cores.

Stage 3: Corona and symplectite formation

Grt-Opx Fe-Mg exchange thermometry applied to Crd3-Opx3 symplectites replacing Grt2 yields temperatures of 817-740°C (for $P_{(\text{ref.})}$ of 6.0 kbar), that are slightly lower than the temperatures of 849-829°C calculated from Grt-Opx Al-thermometry, thus suggesting retrograde Fe-Mg exchange between Grt2 and Opx3 during cooling. Retrograde Fe-Mg exchange between Grt2 rims and the symplectitic phases is furthermore supported by relatively low temperatures of ~ 760°C as calculated from Grt-Crd Fe-Mg exchange thermometry.

GASP barometry, performed for coronitic Pl3 around matrix Sil2 combined with the composition of Grt2 rims, and Grt-Opx-Pl-Qtz barometry yields pressures of 6.1-5.4 and of 7.0-3.7 kbar, respectively (for $T_{(\text{ref.})}$ of 800°C). Similar pressures of 6.2-5.6 kbar are calculated for monomineralic Crd coronas (reaction 5-25) and Spl-Crd symplectites (reaction 5-26) at Grt2 rims in the presence of Sil2 whereas for Crd-Opx symplectites at Grt2 rims in the presence of Qtz2 (reaction 5-24) slightly lower pressures of 5.5-3.5 kbar are calculated.

The P-T results calculated from conventional geothermobarometry are consistent with P-T estimates obtained by application of isopleth diagrams: P-T conditions of 890-770°C at pressures of ~ 5.5 kbar are obtained for the present Grt-Opx-Crd-Qtz assemblage using the diagram of

Aranovich & Berman (1996) whereas the diagram of Hensen & Harley (1990) yields slightly lower P-T conditions of 850-750 °C at ~ 4.5 kbar.

Stage 4: Re-growth of garnet, biotite and sillimanite

Grt-Bt thermometry indicates that the re-growth of Grt4 and Bt4 at the expense of the Crd-Opx symplectites proceeded in response to cooling to amphibolite facies temperatures of 680-651°C (for $P_{(ref.)}$ of 5.0 kbar).

			Temperature (°C)										
sample	rock type	texture		Grt-Opx					Grt-Crd		Grt-Bt		
stage 2 (peak)			P (ref.)	B1 Fe-Mg	LG Fe-Mg	CH Fe-Mg	AB Al	HG Al	B2 Fe-Mg	D Fe-Mg	KR Fe-Mg	B3 Fe-Mg	PL Fe-Mg
B-230-E-98	Grt gneiss	Grt2-Bt2-Pl2-Qtz2-(cores)	9.5	-	-	-	-	-	-	-	1014	951	903
stage 3b (symplectite formation)													
B-230-E-98	Grt gneiss	Crd-Opx-Pl sympl. - Grt2	6.0	792	817	759	829	838	757	759	-	-	-
B-230-F-98	Grt-Sil gneiss	Crd-Opx sympl. - Grt2	6.0	773	795	740	830	849	760	758	-	-	-
B-230-F-98	Grt-Sil gneiss	Crd(-Spl) sympl. - Grt2	6.0	-	-	-	-	-	765	766	-	-	-
stage 4 (Grt and Bt re-growth)													
B-230-E-98	Grt gneiss	Grt4 (core) - Bt4	5.0	-	-	-	-	-	-	-	672	680	667
B-230-F-98	Grt-Sil gneiss	Grt4 (core) - Bt4	5.0	-	-	-	-	-	-	-	654	667	651

			Pressure (kbar)													
sample	rock type	texture		Grt-Opx-Pl-Qtz				GASP			Grt-Crd-Opx-Qtz		Grt-Sil-Crd-Spl		Grt-Sil-Qtz-Crd	
stage 2 (peak)			T (ref.)	E1 Mg	NP1 Mg	Bo Fe	M1 Fe	PH	NH	KN	HP1 Mg	HP2 Fe	HP3 Mg	HP4 Fe	HP5 Mg	HP6 Fe
B-230-E-98	Grt gneiss	Grt2-Bt2-Pl2-Qtz2-(cores)	970	-	-	-	-	8.4	8.7	9.3	-	-	-	-	-	-
stage 3b (symplectite formation)																
B-230-E-98	Grt gneiss	Crd-Opx-Pl sympl. - Grt2	800	3.8	4.5	7.0	5.8	-	-	-	3.7	5.4	-	-	-	-
B-230-F-98	Grt-Sil gneiss	Crd-Opx sympl. - Grt2	800	-	-	-	-	-	-	-	3.5	5.5	-	-	-	-
B-230-F-98	Grt-Sil gneiss	Crd(-Spl) sympl. - Grt2	800	-	-	-	-	5.5	5.4	6.1	-	-	5.6	5.8	5.7	6.2

Table 5.10 Results of conventional geothermobarometry for the Grt gneisses and the Grt-Sil gneisses of the Epembe Unit. NH, Newton & Haselton (1981), PH, Powell & Holland (1988), KN, Koziol & Newton (1988). Other abbreviations as in Table 5.9.

5.4.3.3 Sapphirine-bearing Opx-Sil gneisses and Opx-Grt rocks

Phase petrological considerations suggest that the peak-metamorphic Opx + Sil ± Spr ± Qtz ± Grt assemblages of the Opx-Sil gneisses were formed under UHT conditions ($T > 1050^{\circ}\text{C}$; $P > 10$ kbar; Fig. 5.35), which are furthermore supported by the very high Al content of peak-metamorphic orthopyroxene (up to 11.9 wt.% Al_2O_3). Post-peak decompression in the order of 2-3 kbar proceeded still under UHT conditions ($T > 950^{\circ}\text{C}$) in the first stage and under granulite

facies conditions in the later stage.

Results of the conventional geothermobarometry are summarized in Table 5.11 and illustrated for the Opx-Grt rock B-700-1-00 in Fig. 5.36j and for the sapphirine-bearing Opx-Sil gneisses B-458-4-99, B-458-5-00 and B-458-9-00 in Figs. 5.34k-5.34m.

Stage 1: Prograde Evolution

Opx-Grt rock B-700-1-00 contains inclusions of Grt1 and Opx1 in matrix Pl2, which are suitable to deduce the physical conditions during the prograde evolution. Grt-Opx Fe-Mg thermometry yields temperatures of 844-785°C (at $P_{(\text{ref.})}$ of 7 kbar), whereas higher temperatures of 961-898°C were retrieved from Grt-Opx Al-thermometry. Corresponding pressures of 6.8-10.5 kbar were calculated from Grt-Opx-Pl-Qtz barometer by using Opx1 and Grt1 combined with the composition of the hosting Pl2 (at $T_{(\text{ref.})}$ of 800°C). These pressures are interpreted as maximum pressures, since quartz is not present in the textures.

The mineral inclusions reveal P-T conditions of about 800°C at ~ 8 kbar during the prograde evolution.

Stage 2: Peak-metamorphic conditions

Peak-metamorphic P-T conditions were calculated using the core composition of coexisting Al-rich Opx2, Pl2 and Grt2 in sample B-700-1-00. Application of Grt-Opx Fe-Mg thermometry yields ultrahigh temperatures of 1102-1034 °C (at $P_{(\text{ref.})}$ of 9.5 kbar), which represent the highest temperatures of all investigated granulites. These extreme temperatures are supported by results of the Grt-Opx Al-thermometry (1061-1051°C). Corresponding Grt-Opx-Pl-Qtz pressures range between 11.9 kbar and 8.8 kbar (for $T_{(\text{ref.})}$ of 970°C). Again, these pressures are interpreted as maximum values, since quartz is not present.

By applying the Grt-Opx Fe-Mg exchange thermometer and Grt-Opx Al-thermometer to the Spr-bearing Opx-Sil gneisses inconsistent temperatures of 850-650°C and of 980-900°C, respectively, are obtained. This discrepancy is most likely due to an intensive retrograde diffusional Fe-Mg exchange between Grt2 and surrounding symplectitic phases, as is also suggested by the Grt2 zonation patterns (Fig. 5.21b).

The calculated extreme temperatures for the Opx-Grt rock are supported by the very high Al content of porphyroblastic Opx2a (11.7-9.5 wt%Al₂O₃; Al/2 p.f.u.: 0.24-0.18) of both, the Opx-Grt rocks and the Opx-Sil gneisses. Using the isopleth diagrams (Hensen & Harley, 1990; Aranovich & Berman, 1996; Harley, 1998a) ultrahigh temperatures of 1100-950°C are obtained.

Peak-metamorphic conditions of 1050 ± 50°C at 10.5 ± 1.5 kbar encompass most of the calculated data for the Opx-Grt rock and indicate that prograde heating from stage 1 was

accompanied by a pressure-increase of about 2.5 kbar. The calculated P-T conditions are in good accordance with the P-T estimates suggested by phase petrological considerations.

Stage 3a: Corona formation

The initial breakdown of garnet of the Opx-Grt rocks is documented by the formation of decompressional Opx-Pl coronas around Grt2. Grt-Opx Fe-Mg thermometry and Grt-Opx Al-thermometry performed on coronitic Opx3 and Grt2 rims yield consistent ultrahigh temperatures of 958-897°C (for $P_{(ref.)}$ of 8.0 kbar). These high temperatures are consistent with the high alumina contents of coronitic Opx3 (Al^{tot} p.f.u.: 0.36-0.25). Pressures of 11.8-7.8 kbar (at $T_{(ref.)}$ 940°C) are calculated with the Grt-Opx-Pl-Qtz barometer and are about 2 kbar lower than the peak-pressures. As quartz is rare, these are, however, maximum pressures.

The P-T calculations support the petrological observation that initial post-peak decompression of about 2 kbar proceeded still under UHT conditions.

Stage 3b: Symplectite formation

P-T conditions for the subsequent symplectite development in the Opx-Sil gneisses and the Opx-Grt rocks were estimated using Grt2 rim composition and compositions of symplectitic Opx3 and Crd3 (reaction 5-24) and of coronitic Pl3 between Grt2 and Sil2 (GASP reaction 5-43). Calculated Grt-Opx Fe-Mg temperatures of 875-755°C are consistent with temperatures of 846-782°C (at $P_{(ref.)}$ 6 kbar) calculated from Grt-Opx Al-thermometry. Lower temperatures (752-691°C), calculated from the Grt-Crd Fe-Mg thermometers, are interpreted to reflect continued Fe-Mg re-equilibration with the Grt2 rims. For the divariant reaction (5-24) $Grt + Qtz \rightarrow Opx + Crd$ pressures of 7.5 kbar to 4.9 kbar (at $T_{(ref.)}$ 800°C) were obtained, which are consistent with estimates of 6.0-5.0 kbar calculated from GASP barometry.

The calculated physical conditions confirm to with P-T estimates of 900-740°C at 7.0-5.5 kbar, that were obtained by applying the isopleth diagrams for the assemblage Grt-Opx-Crd-Qtz (Hensen & Harley, 1990; Aranovich & Berman 1996) with symplectitic Opx3 (Al^{tot} p.f.u.: 0.23-0.15; X_{Mg} : 0.64-0.59) coexisting with Grt2 rim (X_{Mg} : 0.42-0.35).

P-T conditions of some 800 ± 60 °C at 6 ± 2 kbar encompass most of the estimates for the formation of the symplectites in the Opx-Sil gneisses and the Opx-Grt rocks, indicating that the subsequent decompression from stage 3a was accompanied by cooling.

sample	rock type	texture	Temperature (°C)							
			P (ref.)	Grt-Opx				Grt-Crd		
				B1	LG	CH	AB	HG	B2	D
				Fe-Mg	Fe-Mg	Fe-Mg	Al	Al	Fe-Mg	Fe-Mg
stage 1 (prograde)										
B-700-1-00	Opx-Grt rock	Grt1-Opx1 (incl. in Pl2)	7.0	801	844	785	898	961	-	-
stage 2 (peak)										
B-700-1-00	Opx-Grt rock	Grt2-Opx2-Pl2-Qtz2 (cores)	9.5	1046	1102	1034	1051	1061	-	-
stage 3a (corona formation)										
B-700-1-00	Opx-Grt rock	Opx3-Pl3 corona - Grt2 (rim)	8.0	903	958	897	921	951	-	-
stage 3b (symplectite formation)										
B-458-4-99	Opx-Sil gneiss	Crd-Opx sympl. - Grt2 (rim)	6.0	797	836	784	828	846	691	692
B-458-5-00	Opx-Sil gneiss	Crd-Opx sympl. - Grt2 (rim)	6.0	772	802	755	782	799	737	743
B-458-9-00	Opx-Sil gneiss	Crd-Opx sympl. - Grt2 (rim)	6.0	782	823	771	798	814	695	700
B-700-1-00	Opx-Grt rock	Crd-Opx sympl. - Grt2 (rim)	6.0	822	875	819	821	826	722	752

sample	rock type	texture	Pressure (kbar)									
			T (ref.)	Grt-Opx-Pl-Qtz				GASP			Grt-Crd-Opx-Qtz	
				NP	E	M	B	HP	KN	NH	HP1	HP2
				Mg	Mg	Fe	Fe				Mg	Fe
stage 1 (prograde)												
B-700-1-00	Opx-Grt rock	Grt1-Opx1 (incl. in Pl2)	800	7.3	6.8	9.6	10.5	-	-	-	-	-
stage 2 (peak)												
B-700-1-00	Opx-Grt rock	Grt2-Opx2-Pl2-Qtz2 (cores)	970	9.4	8.8	11.3	11.9	-	-	-	-	-
stage 3a (corona formation)												
B-700-1-00	Opx-Grt rock	Opx3-Pl3 corona - Grt2 (rim)	940	8.4	7.8	11.0	11.8	-	-	-	-	-
stage 3b (symplectite formation)												
B-458-4-99	Opx-Sil gneiss	Crd-Opx sympl. - Grt2 (rim)	800	-	-	-	-	-	-	-	5.2	7.4
B-458-5-00	Opx-Sil gneiss	Crd-Opx sympl. - Grt2 (rim)	800	-	-	-	-	5.1	5.7	5.0	4.9	6.4
B-458-9-00	Opx-Sil gneiss	Crd-Opx sympl. - Grt2 (rim)	800	-	-	-	-	5.5	6.0	5.3	5.3	7.5
B-700-1-00	Opx-Grt rock	Crd-Opx sympl. - Grt2 (rim)	800	-	-	-	-	-	-	-	6.1	7.0

Table 5.11: Results of conventional geothermobarometry for the sapphirine-bearing Opx-Sil gneisses and the Opx-Grt rocks of the Epembe Unit. Abbreviations as in Table 5.9 & 5.10.

5.4.4 Summary and conclusions

With the exception of the mafic Grt-Cpx granulite, remarkably uniform P-T conditions were calculated from conventional geothermobarometry for the respective stages of the metamorphic evolution in the various granulite facies lithologies (Table 5.12), which support the phase petrology-based interpretation, that the granulites of the Epembe Unit follow an anti-clockwise P-T path (Fig. 5.36):

Stage 1: Prograde evolution

Prograde near-isobaric heating to granulite facies conditions of $\sim 800^{\circ}\text{C}$ proceeded at moderate pressures of ~ 8 kbar as is indicated by P-T calculations for garnet and orthopyroxene inclusions in matrix plagioclase of Opx-Grt rock B-700-1-00.

Stage 2: Peak-metamorphic conditions

For the peak-metamorphic mineral assemblage of the most samples UHT conditions of $970 \pm 70^{\circ}\text{C}$ at 9.5 ± 2.5 kbar were calculated (Table 5.12). However, the extreme temperatures calculated for the Opx-Grt rock ($1030\text{--}1100^{\circ}\text{C}$) might suggest that even higher temperatures of $\sim 1050^{\circ}\text{C}$ were attained in the Epembe Unit and the mineral compositions of the other samples were affected by minor retrograde Fe-Mg exchange.

No systematic regional variations are observed for the peak-metamorphic P-T conditions of samples of the central part of the Epembe Unit (mafic two-pyroxene granulite B-230-B-98, Mg-rich Grt-Opx gneisses B-458-3-99 and B-634-00, Qtz-rich Grt-Opx rock B-614-1-99, Grt gneiss B-230-E-98, Opx-Grt rock B-700-1-00), of the south-western margin of the central (Crd-bearing Qtz-rich Grt-Opx rock B-587-4-99 and Fe-rich Grt-Opx gneiss B-690-2-00) and eastern part of the Epembe Unit (mafic Grt-bearing two-pyroxene granulite B-434-2-99 and Grt-Opx metagranitoid B-646-1-00; Fig. 5.36). These uniform P-T conditions demonstrate the lack of a pressure or temperature gradient in the Epembe Unit, consistent with the regional uniformity of the observed peak-metamorphic mineral assemblages of the respective lithologies.

The similar peak-metamorphic P-T conditions suggest that the Grt-Opx metagranitoids were emplaced into the granulites of the volcano-sedimentary sequence (paragneisses and metavolcanic (Grt-bearing) mafic granulites) prior to or during UHT metamorphism.

Stage 3: Corona and symplectite formation

Calculated P-T conditions of $940 \pm 70^{\circ}\text{C}$ at 8 ± 2 kbar for the formation of Opx-Pl coronas indicate that the initial decompression of ~ 1.5 kbar was near-isothermal and proceeded at UHT conditions (stage 3a), consistent with the high Al content of coronitic Opx₃ and the formation of sapphirine-bearing symplectites in the Opx-Sil gneisses.

The subsequent formation of various symplectite and corona textures in the paragneisses (stage 3b) proceeded in response to decompression of ~ 2 kbar to 6 ± 2 kbar at lower but still granulite facies temperatures of $800 \pm 60^{\circ}\text{C}$, consistent with the lowered Al content of Opx₃ in the symplectites when compared to coronitic Opx₃.

Stage 4: Re-growth of garnet, biotite, sillimanite and amphibole

Subsequent near-isobaric cooling to upper amphibolite facies P-T conditions of $660 \pm 30^\circ\text{C}$ at 5 ± 1.5 kbar led to the re-growth of garnet, biotite, sillimanite and amphibole.

	Stage1		Stage 2		Stage3a		Stage3b		Stage4	
	T(°C)	P(kbar)	T(°C)	P(kbar)	T(°C)	P(kbar)	T(°C)	P(kbar)	T(°C)	P(kbar)
Orthogneisses										
Mafic granulites	-	-	885-944	-	-	-	-	-	-	-
Grt-Cpx granulite	717-801	11.1-11.7	942-1007	12.0-14.9	-	-	-	-	693-651	7.7-7.8
Grt-Opx metagranitoid	-	-	925-1014	8.1-10.8	-	-	-	-	673-638	-
Paragneisses										
Fe-rich Grt-Opx gneiss	-	-	916-1005	8.6-10.1	874-966	6.7-8.5	-	-	549-589	-
Mg-rich Grt-Opx gneisses	-	-	931-1068	8.4-11.4	911-1004	6.5-10.0	757-861	4.3-8.0	650-672	-
Qtz-rich Grt-Opx rocks	-	-	904-1043	6.6-11.5	-	-	778-851	4.6-5.3	628-694	3.1-5.9
Grt gneiss	-	-	903-1014	8.4-9.3	-	-	759-838	3.8-7.0	667-680	-
Grt-Sil gneiss	-	-	-	-	-	-	740-849	3.5-6.2	651-667	-
Opx-Sil gneisses	-	-	-	-	-	-	755-846	4.9-6.0	-	-
Opx-Grt rock	785-961	6.8-10.5	1034-1102	8.8-11.9	897-958	7.8-11.8	819-875	6.1-7.0	-	-

Table 5.12: Summary of P-T calculation for the granulites of the Epembe Unit with respect to the multiple stages of the metamorphic evolution. For stage 3b the results of Grt-Crd thermometry have been excluded.

While the relative metamorphic evolution and the temperature estimates for the mafic Grt-Cpx granulite are consistent with the P-T path and temperatures calculated for the other granulites investigated (see Fig. 5.36), the pressure estimates for the several stages of the metamorphic evolution are always ~ 4 kbar higher than those of the other granulite samples (Table 5.12), indicating that the mafic Grt-Cpx granulite was heated to UHT conditions in a deeper crustal level. Although the calculated pressures were interpreted as maximum values, since quartz is absent in the sample, this discrepancy is too high to be explained by this fact alone. Taking into account the exceptional structural position of the mafic Grt-Cpx granulite, which is exposed as a discordant lens within a major shear zone, it is interpreted as a tectonic slab, which was sheared off in the lower crust and subsequently uplifted along the hosting shear zone.

5.5 P-T PSEUDOSECTIONS

P-T pseudosections in the system FeO-MgO-Al₂O₃-SiO₂-H₂O (FMASH) were calculated in order to reconstruct the metamorphic evolution of the sapphirine-bearing Opx-Sil gneisses and the metapelitic Grt-Sil gneisses in some more detail and to investigate the influence of the bulk-rock geochemistry on the mineral assemblages. In general, the sapphirine-bearing Opx-Sil gneisses are characterized by low CaO, Na₂O, K₂O and MnO contents and, consequently, their chemistry can be approximated by the FMASH system. Due to their significant K₂O content, the composition of the Grt-Sil gneisses was recalculated as a projection from K-feldspar. The P-T pseudosections are based on a petrogenetic grid in the system FMASH, designed by Dr. Thomas Will. This grid was calculated by using the computer program THERMOCALC v.2.7 of Holland & Powell (1998a) and the internally consistent thermodynamic dataset of Holland & Powell (1990; 1998a & b), including the phases orthopyroxene, sillimanite, kyanite, garnet, spinel, sapphirine, cordierite and quartz, and assuming ideal ionic mixing and a low water activity of $a(\text{H}_2\text{O})$ of 0.01 (Thomas Will, pers. comm). The FeMg₋₁ exchange vector was taken into account for all ferromagnesian minerals, and the Tschermak's exchange, $(\text{Fe,Mg})_{-1}\text{Si}_{-1}\text{Al}^{\text{VI}}\text{Al}^{\text{IV}}$, for orthopyroxene and sapphirine.

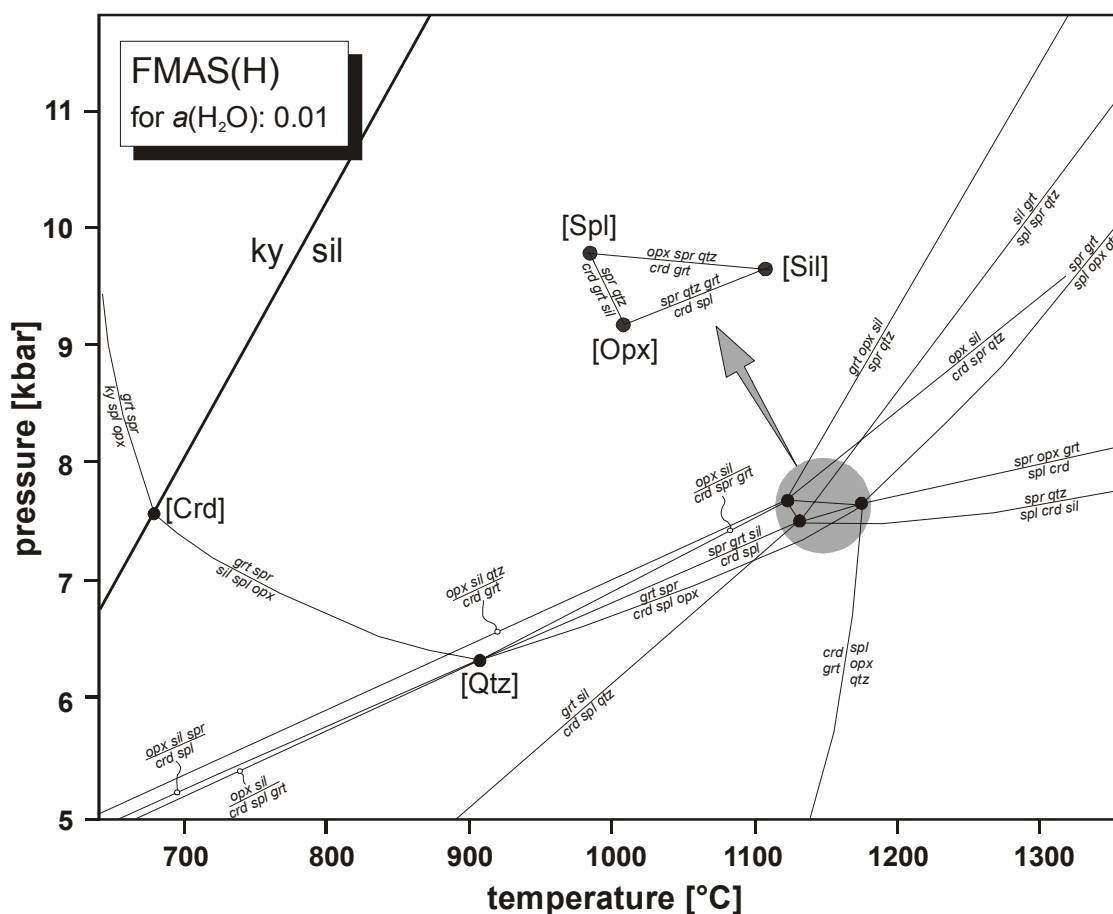


Fig. 5.37: P-T projection for the system FeO-MgO-Al₂O₃-SiO₂-H₂O (FMASH) with a low fixed water activity of 0.01 for granulite facies metapelites. Invariant points are marked as filled circles.

5.5.1 Comparison with previously published FMASH grids

The overall topology of the calculated grid (Fig. 5.37) is similar to those of previously published experimentally derived FMAS(H) grids for high-grade metamorphic metapelites (Hensen & Green, 1973; Hensen, 1987; Hensen & Harley, 1990; Bertrand et al., 1991; Harley, 1998a; see Fig. 5.31), however the absolute P-T values are somewhat different: As noticed by Harley (1998a) the location of the Spl-absent invariant point [Spl] is the key to the FMAS(H) grid, as it limits the stability of Grt + Crd relative to the higher pressure assemblage Opx + Sil + Qtz. In the calculated grid the [Spl] point is located at 7.8 kbar, 1120°C. Experimental studies, using hydrated cordierite, place the [Spl] point at significantly higher pressures and lower temperatures of 9.5 ± 1 at 1030°C (Hensen & Green, 1973) and 10.8 ± 1 at 1040°C (Bertrand et al., 1991). As the stability of cordierite is maximized under fully hydrated conditions (e.g. Newton, 1972), the lower pressure limit of the Grt + Crd assemblage in the grid is a function of the low water activity used in the calculations. A second major effect of the slightly differing position of the [Spl] point is a shift of the lower thermal limit of Spr-Qtz assemblages: While in the calculated grid Spr-Qtz assemblages are stable at temperatures of $> 1120^\circ\text{C}$, they occur at lower temperatures of $> 1050^\circ\text{C}$ in the experimentally derived FMAS(H) grids.

Based on the petrogenetic FMASH grid, P-T pseudosections were calculated for two sapphirine-bearing Opx-Sil gneisses (B-458-4-99, B-702-00) and two Grt-Sil gneisses (B-230-F-98, B-699-00). By combining the observed textural relationships (prograde mineral inclusion, peak assemblages, retrograde reaction textures) with the calculated P-T pseudosections, it is possible to constrain detailed P-T paths most probably followed by these rocks. A detailed description of the construction of P-T pseudosections is given in the Appendix A.5.

5.5.2 Sapphirine-bearing Opx-Sil gneisses

Sapphirine-bearing Opx-Sil gneiss B-458-4-99

The Opx-Sil gneiss B-458-4-99 contains most of the reaction textures described previously for the sapphirine-bearing Opx-Sil gneisses (see Chapter 5.3.3.3). The calculated P-T pseudosection (Fig. 5.38a) is dominated by large trivariant fields, which are separated by narrow divariant fields acting as almost univariant equilibria. Remarkably, orthopyroxene is stable over the whole investigated P-T range. Therefore, isopleths for the Al content and the X_{Mg} of orthopyroxene and, in addition, for the X_{Mg} of garnet have been calculated (Fig. 5.38b) to compare the theoretical mineral compositions with those analyzed. The calculated isopleths for the Al content of orthopyroxene have a very steep slope in the P-T diagram with the Al content increasing with increasing temperature, which is consistent with calculations in the FMAS system of Hensen &

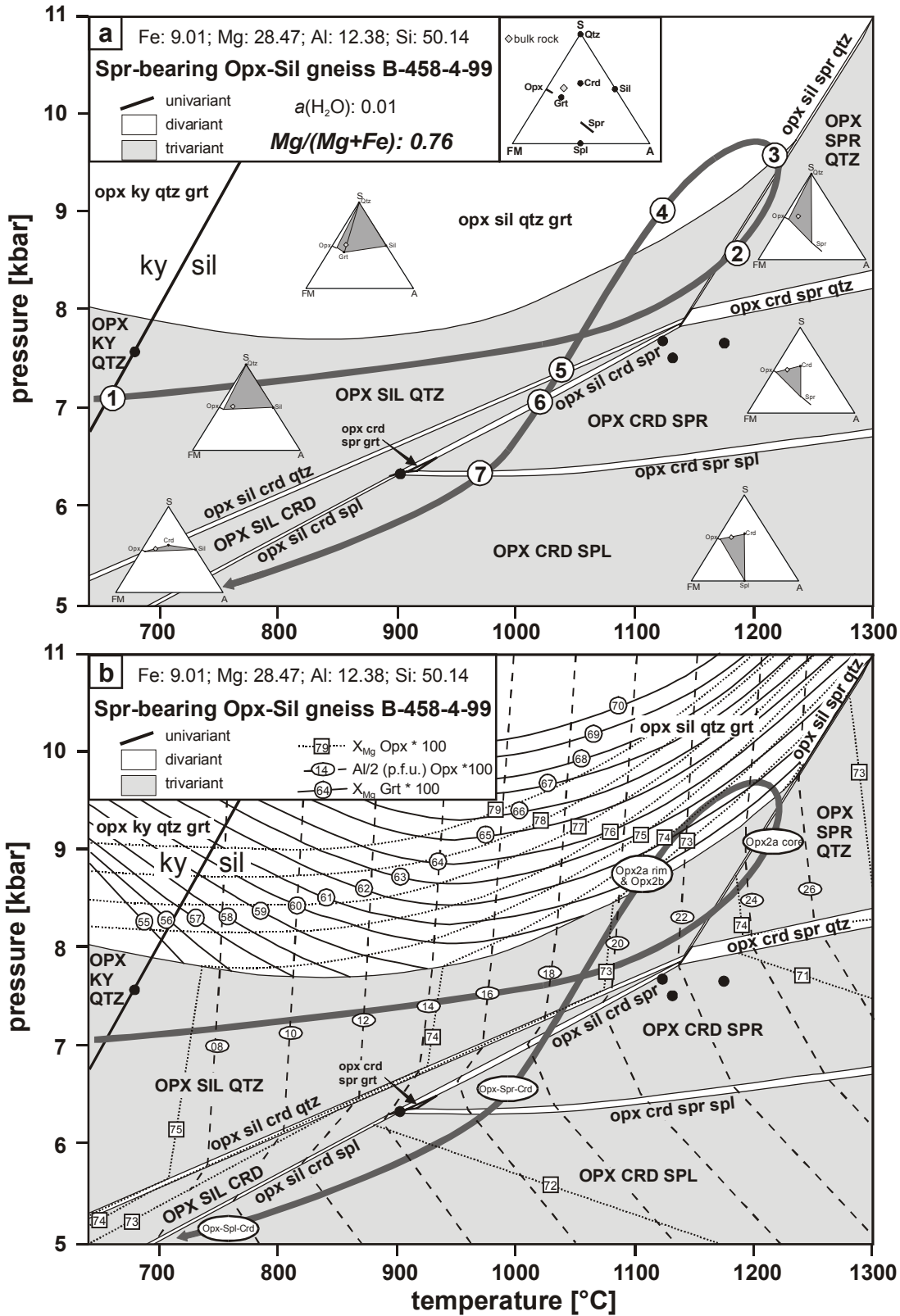


Fig. 5.38: a) P-T-pseudosection for the sapphirine-bearing Opx-Sil gneiss B-458-4-99 in the system FMASH. The bulk-rock composition is given as the normalized mole-proportions of the FMAS-components at the top of the diagram. Trivariant equilibria are marked in upper case; divariant equilibria in lower case. The P-T path most probably followed by the rock is indicated as heavy line and the numbers on the P-T-path correspond to those given in the text. For comparison with Fig. 5.37 the invariant points are shown as black points. b) Calculated isopleths for orthopyroxene and garnet. The ellipses indicate the Al content of orthopyroxene in the respective textural position.

Harley (1990), Aranovich & Berman (1996) and Harley (1998a). In contrast to the Al content, the X_{Mg} of orthopyroxene shows only minor variations (Fig. 5.38b) and is therefore not diagnostic for the P-T evolution of the rocks. The P-T path indicated on Figs. 5.38a & b is based on the following textural relationships and constraints from the mineral composition of orthopyroxene:

1. Sillimanite pseudomorphs after kyanite indicate exit of the trivariant Opx-Ky-Qtz field and entry into the Opx-Sil-Qtz field at a pressure of ~ 7 kbar and temperatures below 700°C . The lack of cordierite and garnet inclusions in the cores of porphyroblastic Opx2 demonstrates that the further evolution proceeded through the Opx-Sil-Qtz field.
2. Inclusions of Opx1 and Sil1 in matrix Spr2a suggest entry into the trivariant Opx-Spr-Qtz field by crossing the divariant Opx-Spr-Qtz-Sil field at temperatures of $\sim 1200^\circ\text{C}$, which is consistent with the very high Al content of Opx2a ($\text{Al}/2^{\text{tot}}$ p.f.u.: 0.25-0.20; X_{Mg} : 0.71-0.68) coexisting with Spr2a.
3. Coronas of Grt2 between Opx2 and Sil2 suggest entry into the divariant Grt-Opx-Sil-Qtz field by compression probably accompanied by minor continued heating. Inclusions of sapphirine and orthopyroxene in Grt2 demonstrate that the growth of Grt2 occurred *subsequently* to crossing of the Spr-Opx-Qtz field. Due to intensive retrograde Fe-Mg exchange with the surrounding symplectites, the composition of garnet (X_{Mg} : 0.45-0.40) varies from the calculated composition (X_{Mg} : 0.65-0.60) at the postulated P-T conditions.
4. Formation of lower-Al Opx2b ($\text{Al}/2^{\text{tot}}$ p.f.u.: 0.22-0.18; X_{Mg} : 0.74-0.71) at the expense of Opx2a and rimward zoning to lower Al content in Opx2a (rims: $\text{Al}/2^{\text{tot}}$ p.f.u.: 0.22-0.17; X_{Mg} : 0.70-0.66) testifies to post-peak cooling.
5. The occurrence of cordierite in the divariant field Opx-Sil-Qtz-Crd indicates subsequent decompression. After entry into the narrow field Opx-Sil-Crd cordierite-growth is accompanied by the disappearance of quartz.
6. Under quartz-absent conditions, relic sillimanite subsequently disappears in the trivariant field Opx-Crd-Spr at slightly lower pressures but still ultrahigh temperatures of $> 900^\circ\text{C}$. Entry into this field is supported by Crd-Opx-Spr symplectites replacing garnet. The Al contents of Opx3 in the latter symplectite ($\text{Al}/2^{\text{tot}}$ p.f.u.: 0.18-0.16; X_{Mg} : 0.70-0.69) suggest its formation at temperatures between 950°C and 1000°C (Fig. 5.38b).
7. Finally, retrograde sapphirine reacts out and late spinel appears instead of sapphirine by crossing the divariant field Crd-Opx-Spr-Spl and entry into the Crd-Opx-Spl field at even lower pressures. Entry into this field is consistent with growth of Crd-Opx-Spl at the expense of garnet and the low Al content of symplectitic Opx3 ($\text{Al}/2^{\text{tot}}$ p.f.u.: 0.10-0.08; X_{Mg} : 0.69-

0.68) points to its formation at $T < 800^{\circ}\text{C}$ (Fig. 5.38b).

The resulting P-T path is anti-clockwise with a characteristic loop: Prograde heating, accompanied or followed by minor compression, from 700°C at ~ 7 kbar to temperatures of $\sim 1200^{\circ}\text{C}$ at ~ 8.5 kbar resulted in the growth of Spr-Qtz assemblages coexisting with very Al-rich orthopyroxene. Subsequent compression led to the formation of Grt-Opx-Sil-Qtz assemblages at the peak-pressure conditions of ~ 9.5 kbar. Post-peak initial decompression of about 2-3 kbar at UHT conditions of $> 950^{\circ}\text{C}$ was followed by further decompression to $P < 6$ kbar accompanied by cooling.

Sapphirine-rich Opx-Sil gneiss B-700-2-00

Due to its higher Al and lower Si content, the calculated P-T pseudosection for the sapphirine-rich Opx-Sil gneiss B-700-2-00 (Fig. 5.39) shows some significant differences to the pseudosection for sample B-458-4-99 (Fig. 5.38). Most significant is the lack of garnet stability fields, which is in agreement with the observed garnet-free mineral assemblage. Furthermore, sapphirine, coexisting with Opx-Sil, is already present at moderate temperatures of $\sim 750^{\circ}\text{C}$. In addition, quartz is only stable in Spr-Qtz assemblages at very high temperatures. Opx-Sil-Qtz assemblages, as present in the pseudosection for Opx-Sil gneiss B-458-4-99, are not stable in the pseudosection for the Opx-Sil gneiss sample B-700-2-00.

The indicated P-T path for the sapphirine-rich Opx-Sil gneiss B-700-2-00 in Figure 5.37 is based on the following textural relationships:

1. Inclusions of spinel and sillimanite within porphyroblastic Spr2a suggest an initial Opx-Sil-Spl assemblage.
2. Rims of Spr2a around Spl1, which is not preserved in the matrix, indicate formation of sapphirine at the expense of spinel by crossing the divariant field Opx-Spl-Sil-Spr and entry into the trivariant field Opx-Sil-Spr during prograde heating.
3. Oriented Spr-Crd intergrowths in the central part of Spr2a point to entry into the trivariant Opx-Crd-Spr field at higher temperatures after crossing the divariant Opx-Sil-Crd-Spr field.
4. Cordierite-free Spr2a rims and the absence of matrix cordierite points to cordierite-replacement via crossing the divariant field Crd-Qtz-Spr-Opx and entry into the trivariant field Spr-Opx-Qtz, indicating a pressure increase.
5. Spr-Opx intergrowths replacing peak-metamorphic Opx suggest subsequent cooling, which probably proceeded into the Opx-Sil-Spr field.
6. Replacement of relic Sil2 by Crd-Spr symplectites indicates post-peak decompression by crossing the divariant field Crd-Sil-Spr-Opx and re-entry into the trivariant field Crd-Spr-

Opx.

- Finally, development of late spinel at the expense of prograde and retrograde sapphirine points to exit of the Crd-Spr-Opx field and entry into the trivariant field Crd-Spl-Opx field via crossing the divariant field Crd-Spr-Spl-Opx, indicating continued decompression accompanied by cooling.

The resulting anti-clockwise P-T path for sapphirine-rich Opx-Sil gneiss B-700-2-00 shows a characteristic loop and is similar to the path deduced for Opx-Sil gneiss sample B-458-4-99, but not as accurately defined as the latter as it contains less reaction textures, that could be used to determine the path more precisely.

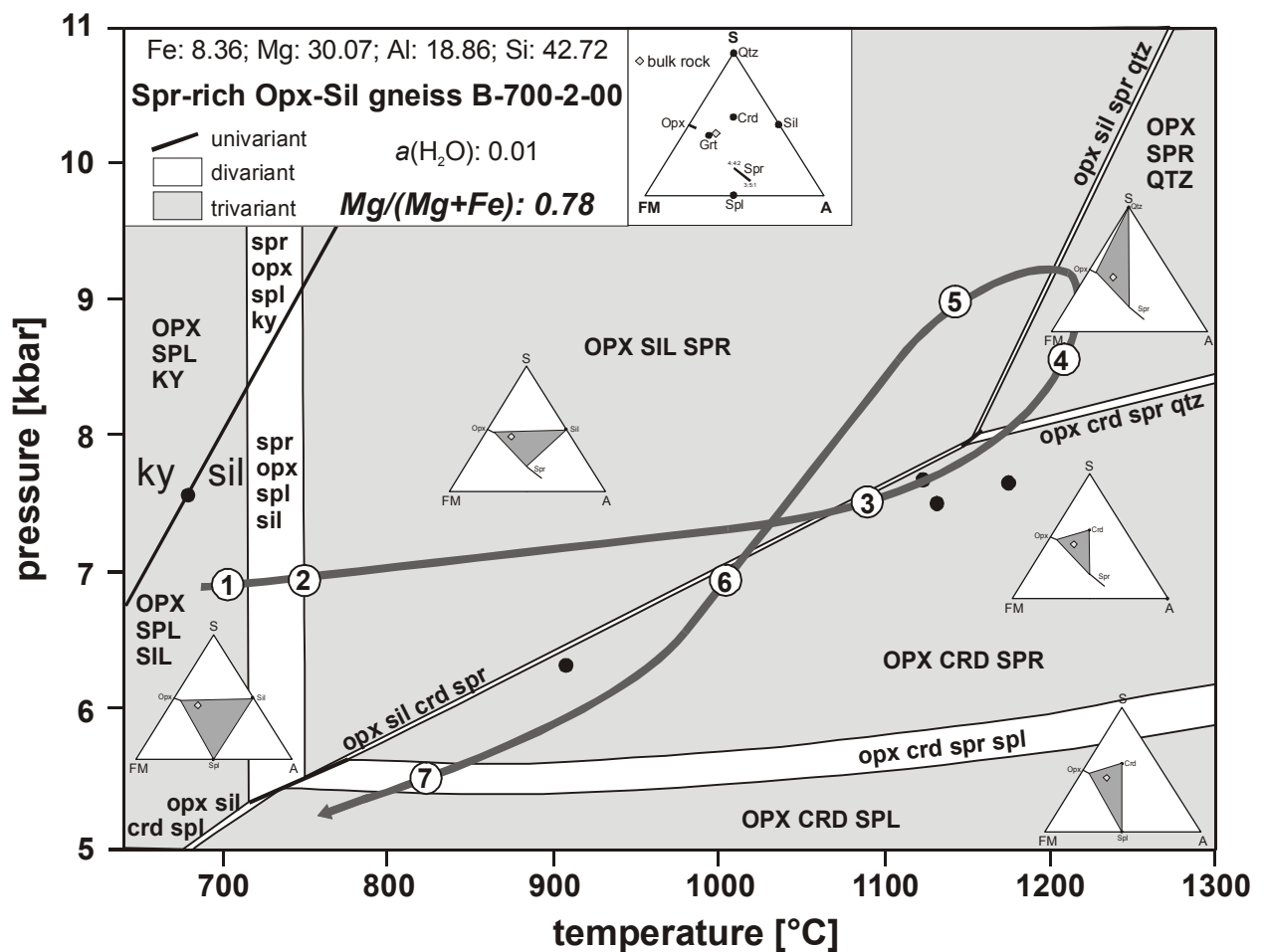


Fig. 5.39: P-T-pseudosection for the sapphirine-rich Opx-Sil B-700-2-00 in the system FMASH. The bulk-rock composition is given as the normalized mole-proportions of the FMAS-components at the top of the diagram. Trivariant equilibria are marked in upper case; divariant equilibria in lower case. The P-T path most probably followed by the rock is indicated as heavy line and the numbers on the P-T-path correspond to those given in the text. For comparison with Fig. 5.37 the invariant points are shown.

5.5.3 Grt-Sil gneisses

The P-T pseudosections calculated for two samples of metapelitic Grt-Sil gneisses are remarkably similar (Fig. 5.40 & 5.41) and will therefore be discussed together. The only significant difference is the presence of a sapphirine-stability field at very high temperatures in the slightly more magnesian Grt-Sil gneiss sample B-230-F-98 (Fig. 5.40), which does not occur in the Grt-Sil gneiss sample B-699-00 over the whole investigated P-T range (Fig. 5.41). The pseudosections of the Grt-Sil gneisses differ significantly from the pseudosections calculated for the sapphirine-bearing Opx-Sil gneisses: In contrast to the Opx-Sil gneisses orthopyroxene in the Grt-Sil gneisses is stable only at very high temperatures and/or moderate to low pressures. Thus, Opx-Sil-Qtz assemblages are not stable in the investigated P-T space of the Grt-Sil gneisses. In addition, sapphirine is only stable at very high temperatures in the Grt-Sil gneiss B-230-F-98 whereas it is stable in several di- and trivariant fields in the Opx-Sil gneisses.

The P-T paths of the Grt-Sil gneisses indicated in Figure 5.40 and 5.41 are based on the following textural relationships:

1. Inclusions of Sil1 in Grt2 indicate testify to initial Grt-Sil-Qtz assemblages.
2. Euhedral Crd1 inclusions in Grt2 indicate entry into to divariant Grt-Crd-Sil-Qtz field through prograde heating.
3. Inclusions of coexisting Spl1 and Qtz1 in the margins of Grt2 demonstrate entry into the divariant Grt-Crd-Spl-Qtz field by further heating, consistent with the lack of Sil1 inclusions in Grt2 margins.
4. The absence of matrix cordierite indicates exit from the cordierite-stability field through entry into the divariant Grt-Sil-Spl-Qtz field in sample B-230-F-98 and into the trivariant field Grt-Spl-Qtz in sample B-699-00 by compression. The lack of peak-metamorphic orthopyroxene in both samples and the lack of sapphirine in sample B-230-F-98 provide an upper temperature limit.
5. Subsequently, the Spl-Qtz associations were replaced by the coarse-grained Grt2-Sil2 assemblages, indicating entry into the Grt-Sil-Qtz field through continued compression to peak-pressures of ~ 9.5 kbar as calculated by conventional geothermobarometry. Due to strong retrogression, the peak-metamorphic composition of Grt2 is not preserved.
6. Replacement of Grt-Sil-Qtz assemblages by monomineralic Crd3 corona textures indicates post-peak decompression into the divariant Grt-Crd-Sil-Qtz field at $P < 7$ kbar.
7. Continued decompression resulted in the formation of Crd-Spl symplectites, indicating entry into the Grt-Crd-Spl-Qtz field. As the isopleths for X_{Mg} in garnet are near-horizontal in the

- Grt-Crd-Spl-Qtz field, decompression is consistent with rimward decreasing X_{Mg} in Grt2 from 0.28 in the core to 0.24 at the rims.
8. Cordierite-coronas around relic Spl-Qtz associations indicate further decompression to the trivariant Grt-Crd-Qtz field.
 9. Formation of Crd-Opx symplectites demonstrates entry into the divariant Grt-Opx-Crd-Qtz field through continued decompression to $P < 5$ kbar. The Al content of symplectitic Opx3 ($Al/2^{tot}$ p.f.u.: 0.12-0.08) indicates still high temperatures $< 1000^{\circ}C$ during decompression.
 10. Re-growth of garnet at the expense of the Crd-Opx symplectites demonstrates exit of the Grt-Opx-Crd-Qtz field and re-entry into the Grt-Crd-Qtz field through subsequent cooling. Rimward zonation of the X_{Mg} of re-grown Grt4 from 0.25 in the core to 0.15 at the rims demonstrates further cooling.

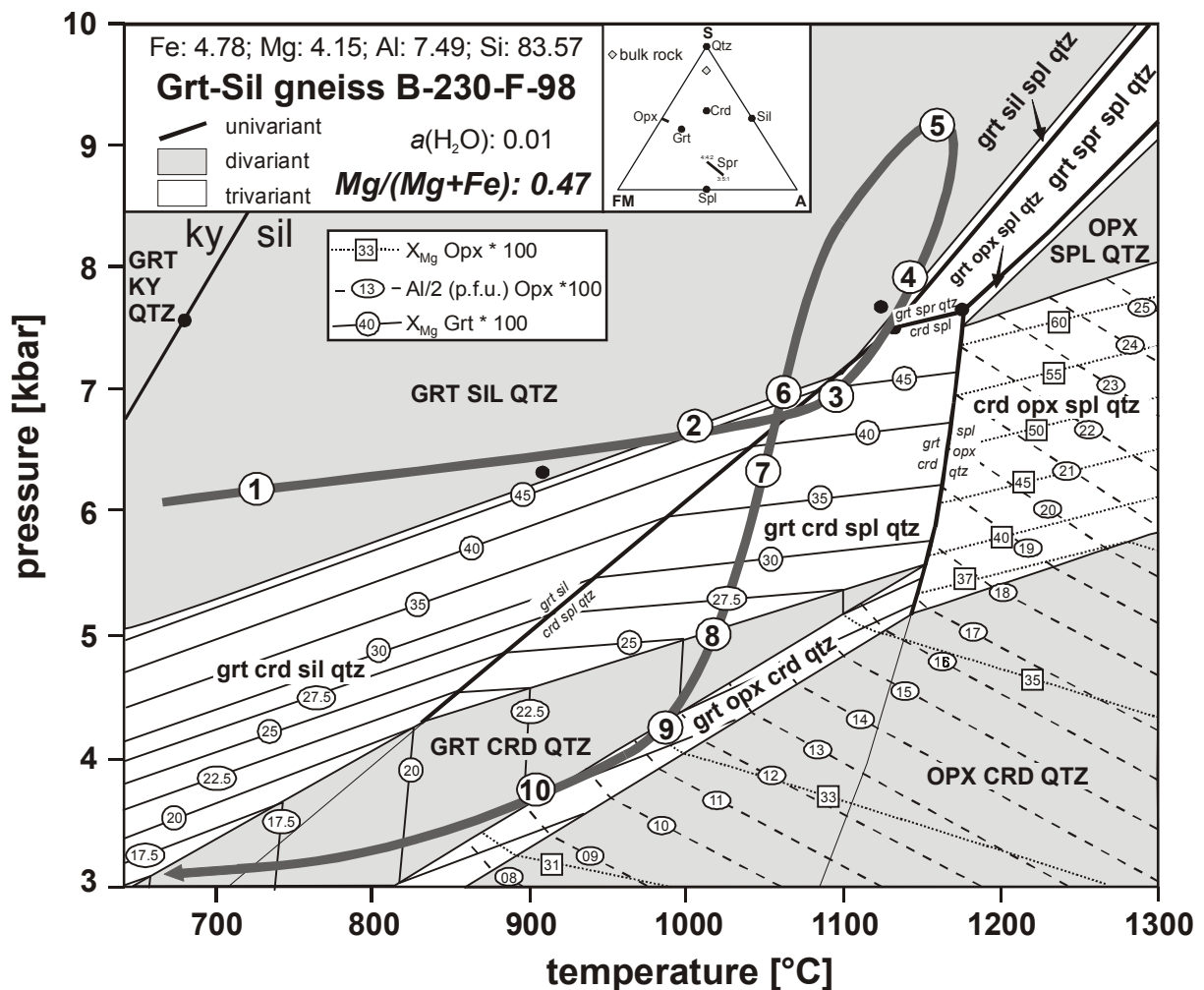


Fig. 5.40: P-T-pseudosection for the Grt-Sil gneiss B-230-F-98 in the system FMASH. The bulk-rock composition is given as the normalized mole-proportions of the FMAS-components at the top of the diagram. Trivariant equilibria are marked in upper case; divariant equilibria in lower case. Calculated isopleths for orthopyroxene and garnet are delineated. The P-T-path most probably followed by the rock is indicated as heavy lines and the numbers on the P-T-path correspond to those given in the text. For comparison with Fig. 5.37 the invariant points are shown as black points.

The resulting anti-clockwise P-T paths show a similar loop as those deduced for the sapphirine-bearing Opx-Sil gneisses and are a combination of prograde near-isobaric heating to UHT conditions at moderate pressures of 6-7 kbar resulting in the formation of Spl-Qtz assemblages. Due to subsequent pressure increase of about 2-3 kbar, peak-metamorphic Grt-Sil assemblages were developed. It remains uncertain, however, whether compression proceeded with slightly increasing temperatures (as shown in Fig. 5.40 & 5.41), at constant temperatures or with slightly decreasing temperatures. Significant post-peak decompression was near-isobaric and was followed by cooling.

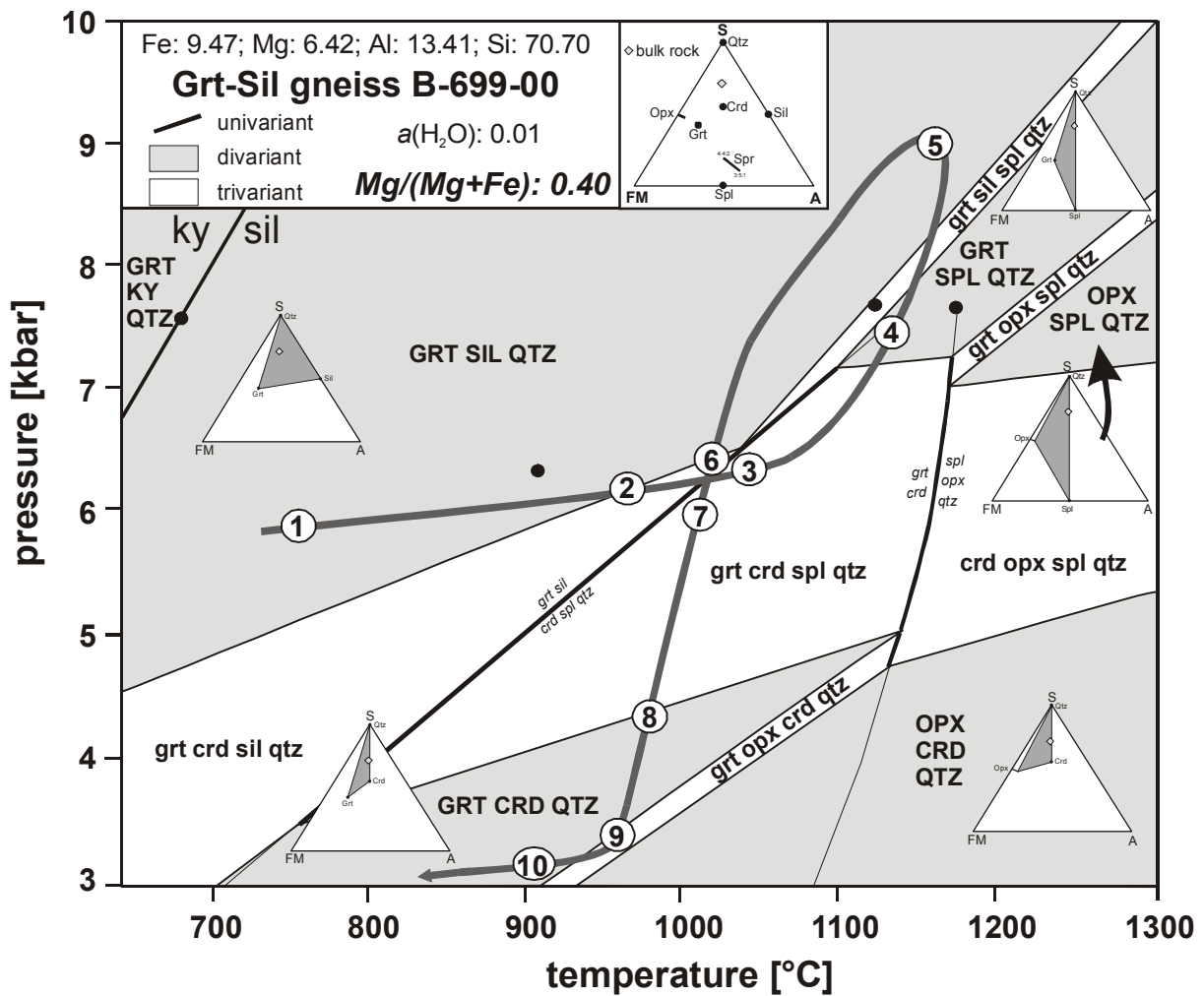


Fig. 5.41: P-T-pseudosection for the Grt-Sil gneiss B-699-00 in the system FMASH. The bulk-rock composition is given as the normalized mole-proportions of the FMAS-components at the top of the diagrams. Trivariant equilibria are marked in upper case; divariant equilibria in lower case. The P-T-path most probably followed by the rock is indicated as heavy lines and the numbers on the P-T-path correspond to those given in the text. For comparison with Fig. 5.37 the invariant points are shown as black points.

The very high temperatures and low pressures of decompression and cooling, as deduced from the pseudosections, are a result of the low applied water activity, i.e. an $a(\text{H}_2\text{O})$ of 0.01. As a consequence, cordierite-bearing textures are stable at lower pressures and higher temperatures in the pseudosections than the P-T ranges calculated for the respective textures from conventional geothermobarometry, which, however, was performed for an intermediate water activity of $a(\text{H}_2\text{O}) = 0.5$. The postulated increase of the water activity during the retrograde evolution is mainly evident from the formation of biotite at temperatures of $< 700^\circ\text{C}$, due to reactions with the crystallizing melts.

5.5.4 Discussion

The calculated P-T pseudosections for the sapphirine-bearing Opx-Sil gneisses and the Grt-Sil gneisses support the interpretation that the granulites of the Epembe Unit followed an multistage anti-clockwise P-T path with a characteristic loop at UHT conditions so far not described in the literature. Unfortunately, the absolute P-T data, as deduced from the P-T pseudosections, have to be treated with caution: The extreme peak-temperatures of $\sim 1200^\circ\text{C}$ for the formation of Spr-Qtz assemblages are geologically not reasonable. This overestimation is most probably a result of uncertainties concerning the thermodynamic data of sapphirine. As noted by Harley (1998a) more reliable experimental data on sapphirine are needed to upgrade the internally consistent thermodynamic dataset.

5.6 DISCUSSION AND CONCLUSIONS

5.6.1 P-T path reconstruction

Based on textural relationships, mineral chemistry and conventional geothermobarometry *clockwise retrograde* P-T paths have been constructed for the Mg-rich Grt-Opx gneisses and the Qtz-rich Grt-Opx rocks of the Epembe Unit, as evidence for the prograde evolution is only poorly recorded by these rocks (Brandt et al., 2003). However, integration of the more detailed textural relationships, mineral chemistry and conventional geothermobarometry of all investigated granulite facies lithologies demonstrates that the P-T path as a whole is *anti-clockwise*, as is also supported by the interpretation of P-T pseudosections for the sapphirine-bearing Opx-Sil gneisses and the metapelitic Grt-Sil gneisses. This anti-clockwise P-T path can be subdivided into several stages (Fig. 5.42):

Stage 1: Prograde evolution

The early prograde evolution of all granulite-facies rock types investigated is characterized by the almost complete replacement of biotite- or hornblende-bearing mineral assemblages by anhydrous mineral assemblages through various dehydration melting reaction. Removal of a granitoid melt in the metagreywacke-type Mg-rich Grt-Opx gneisses resulted in the formation of restitic sapphirine-bearing Opx-Sil gneisses and of restitic Opx-Grt rocks. In the Opx-Sil gneisses kyanite was transformed into sillimanite during an early stage of prograde heating. The further metamorphic evolution proceeded in the sillimanite stability-field. Inclusions of orthopyroxene in peak-metamorphic clinopyroxene of the mafic Grt-Cpx granulite and in peak-metamorphic garnet of the Fe-rich Grt-Opx gneisses demonstrate that granulite facies P-T conditions were attained during the prograde evolution prior to the growth of the peak-metamorphic mineral assemblages. Cordierite-inclusions in garnet of the Opx-Sil gneisses and of the Grt-Sil gneisses provide evidence that prograde heating was near-isobaric and proceeded at moderate pressures of ~ 7 kbar, which is supported by results of conventional geothermobarometry on prograde mineral inclusions of the Opx-Grt rocks (~ 8 kbar at $\sim 800^\circ\text{C}$). Spl-Qtz assemblages in peak-metamorphic garnet and sillimanite of the Grt-Sil gneisses demonstrate that UHT conditions were already reached during prograde heating.

Stage 2: Peak-metamorphism

During a subsequent pressure increase of about 2-3 kbar the coarse-grained peak-metamorphic mineral assemblages were formed at ultrahigh temperatures of at least $970 \pm 70^\circ\text{C}$ and moderate pressures of 9.5 ± 2.5 kbar. The extreme temperatures calculated for the Opx-Grt rock (1030-

1100°C) suggest that even higher temperatures of $\sim 1050^\circ\text{C}$ were attained throughout the Epembe Unit. Such extreme temperatures would be supported by the very high Al content of porphyroblastic orthopyroxene in many paragneisses and by the postulated presence of Spr-Qtz assemblages in the Opx-Sil gneisses. The moderate calculated peak-pressure of ~ 9.5 kbar is consistent with (1) the presence of Opx-Sil-Qtz assemblages in the Opx-Sil gneisses, (2) the occurrence of sillimanite as the stable peak-metamorphic aluminosilicate and (3) the predominance of garnet-free two-pyroxene assemblages in the mafic granulites. Due to the lack of unambiguous textural data, it remains uncertain whether the pressure increase was accompanied by continued minor heating or by minor cooling and, consequently, whether the thermal peak pre-dates or coincides with the pressure-peak

During the latest stage of peak-metamorphism the mineral assemblages were affected by the main deformation phase D_1 . Subsequent cooling is mainly evident from Spr-Opx intergrowths on and Al-zonation pattern in peak-metamorphic orthopyroxene.

Stage 3: Corona and symplectite formation

Post-peak decompression is recorded by undeformed corona and symplectite textures present in all granulite facies lithologies and is furthermore evident from rimward decreasing X_{Mg} in peak-metamorphic garnet. Decompression proceeded still under UHT decompression in the early evolution (stage 3a) and under granulite facies conditions in the later evolution (stage 3b):

Initial near-isothermal UHT decompression of about ~ 2 kbar is texturally demonstrated by the formation of sapphirine-bearing symplectites in the Opx-Sil gneisses at pressures of ~ 7 kbar at $T > 950^\circ\text{C}$. In addition, the formation of Al-rich Opx-Pl coronas at the expense of peak-metamorphic garnet and quartz in the Fe-rich and Mg-rich Grt-Opx gneisses and in the Opx-Grt rocks occurred at UHT conditions of $940 \pm 60^\circ\text{C}$ at 8 ± 2 kbar.

Further decompression (stage 3b) to 6 ± 2 kbar was accompanied by significant cooling to $800 \pm 60^\circ\text{C}$ and is mainly recorded by the development of delicate Crd-Opx symplectites, Crd-Opx-Spl symplectites and Spl-Crd-symplectites, formed at the expense of peak-metamorphic garnet-quartz, garnet and garnet-sillimanite, present in the paragneisses. Low Al contents of symplectitic orthopyroxene when compared to those recorded by coronitic orthopyroxene support the lower temperatures during stage 3b. In the Opx-Sil gneisses sapphirine was replaced by spinel during high-temperature decompression.

Uplift from peak-metamorphic lower crustal depths (~ 29 km) into mid-crustal levels (~ 18 km) probably proceeded along the subvertical shear zones, that surround the UHT granulites.

Stage 4: Re-growth of garnet, biotite, sillimanite and amphibole

Subsequent near-isobaric cooling to upper amphibolite conditions (660 ± 30 °C at 5 ± 1.5 kbar) is evident from the re-growth of biotite, hornblende and garnet, formed at the expense of the symplectitic phases or of relic peak-metamorphic phases by interaction with the crystallizing anatectic melts. The calculated P-T range is consistent with the re-growth of sillimanite in the metapelitic Grt-Sil gneisses and the cordierite-bearing Qtz-rich Grt-Opx rocks.

Stage 5: Formation of late orthopyroxene and cordierite

During a second stage of decompression low-alumina orthopyroxene, intergrown with cordierite, was formed at temperatures of < 700 °C at the expense of retrograde biotite in the Mg-rich Grt-Opx gneisses, in the sapphirine-bearing Opx-Sil gneisses and in the Opx-Grt rocks.

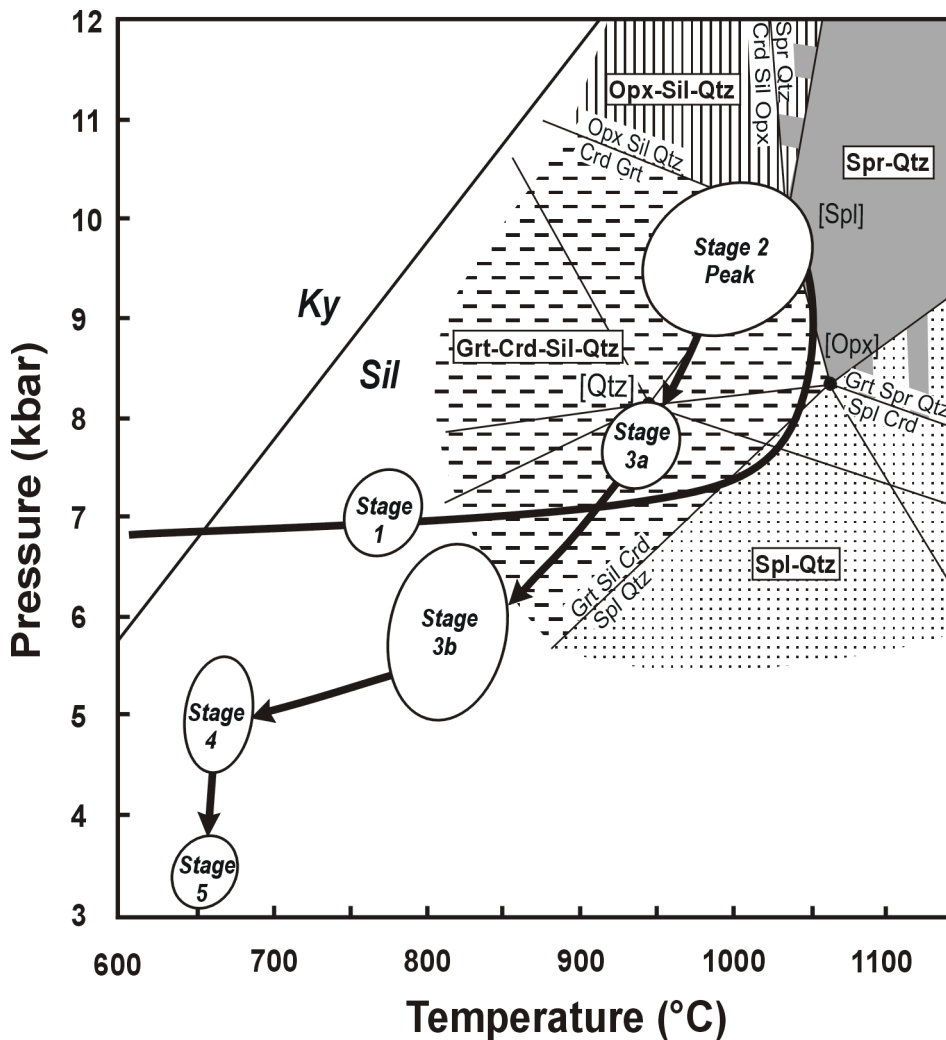


Fig. 5.42. Multistage P-T path of the UHT granulites of the Epembe Unit, as deduced from mineral assemblages, reaction textures, geothermobarometric calculations and interpretation of P-T pseudosections. Also shown is the petrogenetic grid for high-grade metapelites in the system FMAS (for references see Fig. 5.31) and the fields of the key FMAS assemblages (Spr+Qtz, Opx+Sil+Qtz, Grt+Crd+Sil+Qtz, Spl+Qtz). For reasons of clarity only the key univariant FMAS reactions are shown.

The continuity of the deduced reaction sequence and the corresponding P-T data suggests that the inferred P-T path from stage 1 to stage 5 is the result of one single Mesoproterozoic, rather than of two or more tectono-metamorphic events. This interpretation is consistent with the lack of Pan-African tectonism in the study area. However more detailed geochronological data, mainly on the mineral phases formed during retrogression, is needed to support this interpretation. The retrograde P-T path, recorded by the paragneisses of the Epembe Unit is remarkably similar to those documented for sapphirine-bearing UHT granulites from Mather Peninsula (Harley, 1998b) and Forefinger Point (Harley et al., 1990) of Antarctica and from the Palni Hills, southern India (Raith et al., 1997).

5.6.2 Evidence for UHT metamorphism in the granulites of the Epembe Unit

UHT crustal metamorphism with temperatures in the range of 900–1050°C at moderate pressures of 7-13 kbar, as documented for the granulites of the Epembe Unit, has been reported for a small number of 15-20 high-grade metamorphic terranes worldwide (reviewed in Harley, 1998a) and thus yields important implications for crust-forming processes. Based on well-constrained theoretical and experimental data (reviewed in Hensen & Harley, 1990; Bertrand, et al., 1991; Harley, 1998a) mineral assemblages in sapphirine-bearing rocks of highly aluminous and magnesian bulk composition (MgAl-rich granulites) and the occurrence of highly aluminous orthopyroxene ($\text{Al}_2\text{O}_3 > 8 \text{ wt.}\%$), coexisting with garnet and/or sillimanite, are the key indicators of UHT metamorphism (e.g. Harley, 1998a). In contrast, conventional geothermobarometry commonly yields erroneously low temperatures (reviewed in Harley, 1998a).

The newly recognized UHT granulites of the Epembe Unit investigated in this study are exceptional from the other known UHT terranes worldwide in providing phase petrological, mineral chemical and geothermobarometric evidence of UHT conditions:

- Unusual mineral assemblages (Opx-Sil-Qtz and Spr-Qtz) and spectacular retrograde reaction textures (symplectites of Crd-Spr and Crd-Spr-Opx) of the sapphirine-bearing Opx-Sil gneisses document UHT condition on the basis of phase petrological constraints. UHT conditions are furthermore supported on the phase petrological basis by prograde Spl-Qtz assemblages in the metapelitic Grt-Sil gneisses.
- In addition, UHT conditions are documented by the occurrence of highly aluminous orthopyroxene coexisting with garnet and/or sillimanite in several granulite facies paragneisses (up to 10.6 wt.% Al_2O_3 in the Mg-rich Grt-Opx gneisses, up to 9.1 wt.% Al_2O_3 in the Qtz-rich Grt-Opx rocks, up to 11.9 wt.% Al_2O_3 sapphirine-bearing Opx-Sil gneisses and up to 11.3 wt.% Al_2O_3 in the Opx-Grt rocks).

- UHT conditions are furthermore retrieved for most investigated samples from conventional geothermobarometry.

The present study is therefore an important contribution to the increasing recognition of UHT crustal-forming processes.

5.6.3 The preservation of UHT conditions in the granulites of the Epembe Unit

With rare exceptions, such as in Grt-Opx gneisses from Mather Peninsula, Antarctica (Harley, 1998b), UHT conditions at moderate pressures of 7-13 kbar were not recovered by conventional geothermometry, which is mainly based on Fe-Mg exchange reactions. The mineral compositions were commonly affected and modified by post-peak diffusional cation exchange (e.g. Harley, 1989; Frost & Chacko, 1989; Fitzsimons & Harley, 1994; Harley, 1998a) and, consequently, conventional geothermobarometry generally yielded erroneously low temperatures.

Due to the preservation of their highest-grade mineral compositions, UHT conditions are retrieved from conventional geothermobarometry for several paragneisses (Mg-rich and Fe-rich Grt-Opx gneisses, Qtz-rich Grt-Opx rocks, Grt gneiss and Opx-Grt rock) and for several orthogneisses (mafic Grt-Cpx granulite and Grt-Opx metagranitoid) of the Epembe Unit without the necessity of back-calculation of mineral compositions to account for post-peak Fe-Mg exchange (methods of Fitzsimons & Harley, 1994; Harley, 1998a). According to Harley (1998a) the retrieval of UHT conditions by Fe-Mg geothermometry is mainly favored by (1) Mg-rich garnet compositions, (2) the lack of Fe-Mg phases adjacent to garnet, (3) large garnet grain sizes and (4) a rapid cooling rate. Moreover, the preservation of the original peak-metamorphic mineral compositions is supported by a low water-activity, as is realized in the investigated granulite facies rock samples.

Peak-metamorphic garnet of the Mg-rich Grt-Opx gneisses (X_{Mg} : 0.44-0.32; ~ 5 mm in diameter), of the Grt gneiss (X_{Mg} : 0.42-0.62; ~ 3 mm in diameter), of the Qtz-rich Grt-Opx rocks (X_{Mg} : 0.46-0.29; ~ 5 mm in diameter) and of the Opx-Grt rocks (X_{Mg} : 0.54-0.42; ~ 5 mm in diameter) is surrounded by Crd-Opx symplectites whereas peak-metamorphic garnet of the mafic Grt-Cpx granulite (X_{Mg} : 0.50-0.41; ~ 2 mm in diameter) is rimmed by Hbl-Pl symplectites. In addition, garnet of these rocks is of intermediate rather than of magnesian composition. Therefore, the first two options are not very likely to explain the preservation of the highest-grade mineral compositions in these rocks. Presumably the large grain size of analyzed garnet (up to 5 mm) selected for EMP studies is the main factor to account for the preservation of the

peak-metamorphic mineral compositions. Furthermore, a rapid cooling rate, that may be inferred from the rather unusual preservation of significant cordierite zoning (Fig. 5.23), could explain the limited retrograde diffusional Fe-Mg exchange between garnet and the surrounding Fe-Mg symplectite phases, that resulted in the preservation of the highest-grade compositions in core plateaus in the largest garnet grains.

A large grain size and a rapid cooling rate also accounts for the preservation of the peak-metamorphic composition of garnet (X_{Mg} : 0.26-0.25; ~ 3.5 mm in diameter) of the Fe-rich Grt-Opx gneiss, which is furthermore supported by the Pl3 corona around garnet, shielding it against Fe-Mg exchange with following Opx3.

In contrast, peak-metamorphic garnet of the Grt-Opx metagranitoids is fine-grained (X_{Mg} : 0.35-0.29; ~ 1 mm in diameter) and therefore the peak-metamorphic composition is interpreted to be preserved as a result of (1) rapid cooling and (2) the lack of Fe-Mg phases adjacent to garnet in these rock samples.

5.6.4 Geodynamic model

The general tectonic settings, necessary for the formation of UHT granulites, are still under discussion (e.g. Harley, 1998a), although it is generally accepted that UHT metamorphism requires an anomalous thermal input into the lower crust (e.g. Raith et al., 1997). Only in a few cases, possible heat sources were constrained: UHT metamorphism in the Palni Hills, southern India, is interpreted to result from the emplacement of voluminous enderbite intrusives (Raith et al., 1997) whereas UHT metamorphism in the South Harris granulite belt of the Lewisian of Scotland is correlated with the emplacement of anorthosites and related magmatic rocks (Baba, 1999). In addition, Sengupta et al. (1999) documented UHT granulites from the Eastern Ghats Belt, southern India, which they interpret to result from the accretion of voluminous basic melts.

Due to the lack of clear evidence of their prograde evolution, UHT metamorphism and the *clockwise retrograde* decompression-cooling P-T path observed for the Mg-rich Grt-Opx gneisses and the Qtz-rich Grt-Opx rocks was previously discussed in the light of two possible tectonic models (Brandt et al., 2003) by taking into the account the regional geology and the available geochronological data of Seth et al. (2003), i.e:

(1) UHT metamorphism is related to crustal thickening during a collision event between 1520 and 1447 Ma. Post-collisional collapse of the tectonically thickened crust resulted in post-peak decompression followed by late cooling of the rapidly uplifted crust to the stable geotherm. This

model was also postulated by Seth et al. (2003) on the basis of age relationships. It has to be mentioned, however, that typical collision structures, such as thrusting or large scale folding, as well as feasible heat sources for UHT metamorphism, like syn-collisional intrusives, have not been observed in the studied area.

(2) Regarding the close spatial relationship between the Mesoproterozoic anorthosites of the Kunene Intrusive Complex (KIC) and the Mesoproterozoic UHT granulites of the Epupa Complex (EC), a genetic connection between the two units has been considered by Drüppel et al. (2000a, 2001) and Brandt et al. (2003). Thermal release of mantle-derived basic melts, parental to the anorthosites and emplaced at the mantle-crust boundary, could have caused UHT metamorphism and partial melting of lower crustal rocks, whereas the subsequent uplift and near-isothermal decompression may be caused by crustal extension. In this case, late cooling would result from thermal relaxation of the rapidly uplifted crust to the former stable geotherm. Following this model, crustal thickening has to be related to an earlier, presumably Palaeoproterozoic orogenic event at ~ 2.0 -1.8 Ga, as is suggested by the Palaeoproterozoic zircon core ages obtained by Seth et al. (2003) for the granulite facies rocks of the Epembe Unit.

The more complete and precisely defined P-T path presented in this study enlightens the prograde evolution and hence demonstrates that the P-T path of the UHT granulites of the Epembe Unit as a whole is anti-clockwise (Fig. 5.42). The recorded prograde evolution, with near-isobaric heating and a *subsequent* pressure increase, clearly contradicts a collision-related evolution but supports the tectonic model 2. The multistage anti-clockwise P-T path can be correlated with the formation of the anorthositic rocks of the KIC: Prograde near-isobaric heating to UHT conditions at middle to lower crustal levels (some 20 km depth; stage 1) is probably related to the emplacement of large volumes of mantle-derived basic melts at the mantle-crust boundary. The subsequent pressure increase of about 2-3 kbar at still UHT conditions, which led to the formation of the peak-metamorphic mineral assemblages of the Epembe Unit (stage 2), is interpreted to result from magmatic loading, which is probably related to the emplacement of anorthositic crystal mushes of the KIC. Remarkably, the pressures calculated for the emplacement of the anorthosites (8 ± 1 kbar; Drüppel et al., 2001; Drüppel, 2003) correlate fairly well with the initial crustal position of the granulites (7-8 kbar). Subsequent uplift and near-isothermal decompression still under UHT granulite facies conditions in the first stage (stage 3) could be related to extensional relaxation of the thickened crust whereas late cooling (stage 4) marks the final stages of magmatism. This model would imply that UHT metamorphism of the Epembe Unit of the EC occurred contemporaneous with the formation of the anorthositic rocks of the KIC. Unfortunately, the age for the initial formation of the magma-chamber, which acted

as source for the anorthosites, is uncertain, so far. The emplacement age of 1385 ± 25 Ma obtained for the youngest anorthosite generation (Drüppel et al., 2000b) provides a minimum age, as they intrude older, but yet undated, anorthosite lithologies (Drüppel et al., 2001).

As the rocks of the Epembe Unit were already situated in middle to lower crustal depths of ~ 24 km (7-8 kbar) during prograde metamorphism at 1520-1510 Ma, burial of the Epembe Unit rocks into middle to lower crustal levels must be related to the Eburnian Orogeny (2100-1660 Ma), which is indeed documented for the UHT granulites by their Palaeoproterozoic zircon core ages of 1810-1635 Ma (Seth et al., 2003). This interpretation is consistent with the recognition of Palaeoproterozoic ages for different lithologies of other parts of the Epupa Complex, indicating that the Epupa Complex as a whole was affected by the Eburnian Orogeny (Tegtmeier & Kröner, 1985; Seth et al. 1998; Franz et al., 1999). The postulated model for Mesoproterozoic anorogenic UHT metamorphism of the Epembe Unit is furthermore in excellent agreement with the observation of Cahen et al. (1984) and Olson (2000) that the time span between 1660 Ma and 1400 Ma is a period of tectonic stability in southern Africa, followed by a period of large-scaled anorogenic magmatism.

Due to the limited geochronological and structural data for the UHT granulites, a more precise geodynamic model of their evolution cannot be constrained. Additional geochronological data, mainly on the formation of the retrograde reaction textures, and structural data are required.

5.6.5 Other UHT occurrences of southern Africa

UHT granulite facies metamorphism in southern Africa is only reported from one other locality: Sapphirine-bearing UHT granulites, which record an isothermal decompression (ITD) P-T path similar to that reconstructed for the UHT granulites of the Epembe Unit, are reported from the Central Zone of the Limpopo Belt of Botswana and South Africa (Harris & Holland, 1984; Droop, 1989; Hisada & Miyano, 1996). Single zircon U-Pb dating on pelitic gneisses yielded early Proterozoic ages of ~ 2027 Ma for high-grade metamorphism in the Central Zone of the Limpopo Belt (Jaekel et al., 1997), consistent with an U-Pb single zircon age of ~ 2022 Ma obtained for the emplacement of an anatectic granite by Kröner et al. (1999).

Sapphirine-bearing granulites, associated with hercynite-quartz granulites, are furthermore reported from the Namaqualand of South Africa (Waters, 1986; 1991). However, as the peak-metamorphic temperatures range between 750-850°C (Waters, 1986; 1991), these high-temperature/low-pressure granulites are not ascribed to the yet known UHT occurrences as

reviewed by Harley (1998a). Moreover, peak-metamorphism has been dated at 1060-1030 Ma by Robb et al. (1999) and is thus significantly younger than that of the Epembe Unit.

Following this, it can be concluded, that this study represents the first recognition of early Mesoproterozoic UHT metamorphism of southern Africa.

6 COMPARISON BETWEEN THE ORUE UNIT AND THE EPEMBE UNIT

The aim of the present study was a reconstruction of the tectono-metamorphic evolution of the Epupa Complex.

Based on field observations and petrological constraints two distinct high-grade metamorphic units were recognized in the study area, which are separated by sub-vertical ductile shear zones: (1) the upper amphibolite facies Orue Unit and (2) the UHT granulite facies Epembe Unit. In both metamorphic units rocks of broadly similar bulk-rock composition occur, which, however, display different peak-metamorphic mineral assemblages, diagnostic of upper amphibolite facies in the Orue Unit and of granulite facies conditions in the Epembe Unit (Table 6.1). Systematic variations are observed between rocks of the southern and of the northern part of the Orue Unit (Table 6.1).

		Epembe Unit	Orue Unit	
	Rock Type		Southern part	Northern Part
Orthogneisses	Mafic rocks	Opx + Cpx + Pl ± Grt	Hbl + Pl ± Grt ± Cpx ± Qtz	Hbl + Pl ± Cpx ± Qtz
		Grt + Cpx		
	Mafic dykes	Opx + Pl + Qtz ± Grt	Hbl + Pl	
	Felsic rocks	Opx + Pl ± Kfs + Qtz ± Cpx	Hbl + Pl ± Kfs + Qtz ± Bt	Hbl + Pl + Qtz ± Kfs ± Bt
	Metagranitoids	Grt + Opx + Pl + Qtz ± Kfs	Hbl ± Bt + Kfs + Pl + Qtz	Hbl ± Bt + Kfs + Pl + Qtz
Paragneisses	Metapelites	Grt + Sil + Kfs + Qtz ± Spl	Grt + Bt + Sil + Kfs + Pl + Qtz	Crd ± Grt + Bt ± Sil + Kfs + Qtz ± Pl
	Metagreywackes	Grt + Opx + Pl + Qtz ± Kfs	Grt + Bt + Pl + Qtz ± Kfs ± Hbl	Grt + Bt + Pl + Qtz +
		Grt + Kfs + Pl + Qtz ± Spl		
	Opx-Sil gneisses	Opx + Sil + Pl ± Grt ± Spr ± Qtz		

Table 6.1: Comparison between peak-metamorphic mineral assemblages in rock of similar bulk-rock composition of the Orue Unit and of the Epembe Unit of the Epupa Complex.

Nature of the protoliths

Major parts of the Orue Unit and the Epembe Unit are constituted by high-grade metamorphic volcano-sedimentary sequences: In both units sub-alkaline tholeiitic metabasalts and dacitic to rhyolitic metavolcanites form a bimodal volcanic succession, which generally lacks volcanic rocks of intermediate composition. During the emplacement of the volcanics, sediments, predominantly greywackes and less frequently pelites and arkoses, were deposited.

While the volcano-sedimentary sequence of the Orue Unit was intruded by large volumes of I-type volcanic arc granitoids, similar granitoids are absent in the Epembe Unit; S-type Grt-Opx metagranitoids are rare and constitute small bodies. Granitoid emplacement within the Orue Unit was

followed by the intrusion of mafic dykes, probably synchronous with the emplacement of mafic dykes of subalkaline, tholeiitic basalt to andesite composition into the volcano-sedimentary sequence of the Epembe Unit.

Metamorphic evolution

The Orue Unit and the Epembe Unit were affected by two distinct metamorphic events, as evident from their respective P-T paths, differences between their peak-metamorphic conditions and different ages of peak-metamorphism:

(1) The granulites of the Epembe Unit underwent UHT metamorphism during the early Mesoproterozoic (1520-1447 Ma) and record a multistage anti-clockwise P-T path:

Stage 1: Prograde near-isobaric heating to UHT conditions proceeded at middle to lower crustal depths (7-8 kbar). **Stage 2:** The peak-metamorphic mineral assemblages were formed in response to a pressure increase of 2-3 kbar at lower crustal UHT conditions ($970 \pm 70^\circ\text{C}$; 9.5 ± 2.5 kbar). Most probably even higher temperatures of $\sim 1050^\circ\text{C}$ were attained throughout the Epembe Unit. During the latest stage of peak-metamorphism the UHT granulites were affected by ductile deformation. **Stage 3:** Subsequent UHT decompression of about ~ 1.5 kbar ($940 \pm 60^\circ\text{C}$; 8 ± 2 kbar) was followed by continued HT decompression of ~ 2 kbar still under granulite facies conditions, which was accompanied by cooling ($800 \pm 60^\circ\text{C}$; 6 ± 2 kbar). **Stage 4:** Subsequent cooling to upper amphibolite conditions ($660 \pm 30^\circ\text{C}$ at 5 ± 1.5 kbar) was near-isobaric. **Stage 5:** A second stage of decompression proceeded at temperatures of $< 700^\circ\text{C}$.

The multistage anti-clockwise P-T path is interpreted to result from the initial, but yet undated, formation of the anorthositic rocks of the KIC.

(2) In contrast, the rocks of the Orue Unit were affected by an upper amphibolite facies metamorphic event at 1390-1318 Ma, about ~ 100 Ma later than UHT metamorphism of the Epembe Unit. While the UHT granulites of the Epembe Unit follow a multistage anti-clockwise P-T path, the upper amphibolite facies rocks of the Orue Unit follow a simple heating-cooling P-T path with presumably only minor pressure variations:

Stage 1: Prograde heating was probably near-isobaric. **Stage 2:** The peak-metamorphic mineral assemblages were formed at mid-crustal upper amphibolite facies condition. While the peak-metamorphic P-T condition and the mineral assemblages in the UHT granulites are similar throughout the Epembe Unit, systematic variations are recognized for three individual parts the Orue Unit (\sim

700°C at 6.5 ± 1.0 kbar in the south-eastern region; $\sim 820^\circ\text{C}$ at 8 ± 0.5 kbar in the south-western region and $\sim 800^\circ\text{C}$ at 6.0 ± 1.0 kbar in the northern part of the Orue Unit). The three parts represent individual crustal levels, that were juxtaposed during later tectonic activity. The formation of the peak-metamorphic mineral assemblages occurred syn- to post-tectonically with respect to the main deformation phase. **Stage 3:** Retrograde cooling to middle amphibolite facies conditions of $\sim 600^\circ\text{C}$ was probably near-isobaric. A heating-cooling P-T path at near-isobaric conditions is also inferred for contact metamorphic metapelitic Grt-Sil-Crd rocks, which occur in the vicinity to the KIC: Heating from middle amphibolite facies to peak-metamorphic upper amphibolite facies conditions ($\sim 750^\circ\text{C}$, ~ 6.5 kbar) was followed by cooling into the middle amphibolite facies.

Upper amphibolite facies metamorphism is attributed to a ‘regional contact metamorphism’ event induced by the emplacement of large volumes of anorthositic magma into the middle crust, which furthermore resulted in contact metamorphism *senso stricto* affecting rocks which are situated at the direct contact to the KIC.

The lack of radiogenic evidence for a 1520-1447 Ma UHT granulite facies event in the rocks of the Orue Unit, either suggests that a) the radiogenic ages were reset during later upper amphibolite facies metamorphism or b) they were not affected by the UHT granulite facies. The prograde vapour-absent dehydration melting reactions and the lack of granulite facies relics make it unlikely that the Orue Unit rocks represent retrogressed UHT granulites of the Epembe Unit and, therefore, rather support the latter assumption. Following the interpretation that UHT metamorphism resulted from the magmatic accretion of basic melts at the base of the crust, the lack of this event in the Orue Unit might be explained by their position in a higher crustal level during the UHT event, far away from the accretion front. The lack of evidence of an UHT event in the Orue Unit rocks furthermore supports the interpretation that UHT metamorphism did not result from a collisional event, as this most probably would have affected the crust as a whole.

7 A GEODYNAMIC MODEL FOR THE EPUPA COMPLEX

By integrating the data obtained by this study the following geodynamic model was evaluated for the tectono-metamorphic evolution of the Epupa Complex:

Palaeoproterozoic evolution

The volcano-sedimentary sequences of the Orue Unit and of the Epembe Unit were most probably formed during the Palaeoproterozoic in a back-arc basin, which was situated along the south-western margin of the Congo Craton. During the Palaeoproterozoic Eburnian Orogeny, which affected large parts of present-day northern Namibia and southern Angola, the volcano-sedimentary sequences were buried into mid-crustal levels, whereby the volcano-sedimentary sequence of the Orue Unit was intruded by large volumes of I-type granitoids during the post-collisional stage. Granite plutonism is most probably related to widespread post-tectonic granitoid emplacement in the late Eburnian in northern Namibia and south-western Angola (see chapter 1.2).

Mesoproterozoic evolution

During the Mesoproterozoic the tectonically thickened crust became unstable and extensional tectonics commenced, which led to the anorogenic emplacement of the huge massif-type anorthosite body of the KIC and of associated granites and syenites at 1400-1300 Ma (Drüppel, 2003). Mesoproterozoic high-grade metamorphism in the Epembe Unit and in the Orue Unit of the Epupa Complex is interpreted to be related to the formation of the anorthositic KIC:

During an early phase of extension the granulites of the Epembe Unit were heated to UHT conditions (1520-1447 Ma) at moderate crustal levels (some 20 km depth), most probably due to the accretion of a mantle-derived magma chamber at the base of the crust, which acted as source for the anorthosites. Subsequent emplacement of a first generation of anorthositic crystal mushes led to the burial of the Epembe Unit rocks into lower crustal levels (~ 29 km depth), due to magmatic loading. Subsequent uplift into mid-crustal levels (~ 18 km depth) of the granulites is related to continued extension, that affected the thickened crust and probably proceeded along the subvertical shear zones, that surround the UHT granulites. Late cooling of the granulites may have been related to cooling of the anorthosite body.

About 100 Ma years later (1390-1318 Ma; Barbara Seth, pers. comm.) the rocks of the Orue Unit were heated to upper amphibolite facies conditions in mid-crustal levels (~ 20 km depth) as a result of 'regional contact metamorphism' presumably related to the emplacement of a second generation of anorthositic rocks of the KIC at about 1385-1347 Ma (Drüppel et al., 2000b; Mayer et al., 2000), which were emplaced into mid-crustal levels (~ 21 km depth; Drüppel et al., 2001, Drüppel, 2003).

Rocks in the vicinity to the KIC were affected by contact metamorphism *sensu stricto* in mid-crustal levels (~ 20 km depth; Grt-Sil-Crd rocks of the Orue Unit).

The investigated EC rocks are overlain by un-metamorphosed Neoproterozoic sediments, which indicate that the studied area was not affected by the Pan-African orogeny, but was a stable part of the Congo Craton during the Neoproterozoic.

8 REFERENCES

- Ai, Y.** (1994). A revision of the garnet-clinopyroxene Fe^{2+} -Mg exchange geothermometer. *Contributions to Mineralogy and Petrology*, **115**, 467-473.
- Alkmim, F. F. & Marshak, S.** (1998). Transamazonian Orogeny in the Region, Minas Gerais: evidence for a Palaeoproterozoic collision and collapse in the Quadrilatero Ferrifero. *Precambrian Research*, **90**, 29-58.
- Allsopp, H. L.** (1975). Summary of age determinations on the Kunene Complex. Unpublished report, University of the Witwatersrand, Johannesburg, 4 pp.
- Aranovich, L. Y. & Berman, R. G.** (1996). Optimized standard state and solution properties of minerals. II. Comparisons, predictions, and applications. *Contributions to Mineralogy and Petrology*, **126**, 25-37.
- Aranovich, L. Y. & Berman, R. G.** (1997). A new garnet-orthopyroxene thermometer based on reversed Al_2O_3 solubility in $\text{FeO-Al}_2\text{O}_3\text{-SiO}_2$ orthopyroxene. *American Mineralogist*, **82**, 345-353.
- Ashwal, L. D.** (1993). *Anorthosites. Minerals and Rocks Series 21*. Springer-Verlag, Berlin, 422 pp.
- Baba, S.** (1999). Sapphirine-bearing orthopyroxene-kyanite/sillimanite granulites from South Harris, NW Scotland: evidence for Proterozoic UHT metamorphism in the Lewisian. *Contributions to Mineralogy and Petrology*, **136**, 33-47.
- Baba, S.** (2003). Two stages of sapphirine formation during prograde and retrograde metamorphism in the Palaeoproterozoic Lewisian Complex in South Harris, NW Scotland. *Journal of Petrology*, **44**, 329-354.
- Barker, F.** (1979). Trondhjemite: definition, environment and hypothesis of origin. In: **Barker F.** (ed.), *Trondhjemites, Dacites and Related Rocks*. Elsevier, Amsterdam, pp. 1-12.
- Beetz, P. F. W.** (1933). Geology of South West Angola, between Cunene and Lunda Axis. *Transactions of the Geological Society of South Africa*, **36**, 137-176.
- Berman, R. G.** (1990). Mixing properties of Ca-Mg-Fe-Mn garnets. *American Mineralogist*, **75**, 328-344.
- Berman, R. G. & Aranovich, L. Y.** (1996). Optimized standard state and solution properties of minerals I. Model calibrations for olivine, orthopyroxene, cordierite, garnet and ilmenite in the system $\text{MnO-FeO-MgO-CaO-Al}_2\text{O}_3\text{-TiO}_2\text{-SiO}_2$. *Contributions to Mineralogy and Petrology*, **126**, 1-24.
- Bertrand, P., Ellis, D. J. & Green, D. H.** (1991). The stability of sapphirine-quartz and hypersthene-sillimanite-quartz assemblages: an experimental investigation in the system $\text{FeO-MgO-Al}_2\text{O}_3\text{-SiO}_2$ under H_2O and CO_2 conditions. *Contributions to Mineralogy and Petrology*, **108**, 55-71.
- Bertrand, P. & Mercier, J. C. C.** (1985). The mutual solubility of coexisting ortho- and

- clinopyroxene: towards an absolute geothermometer for the natural system? *Earth and Planetary Science Letters*, **76**, 109-122.
- Bhatia, M. R.** (1983). Plate tectonics and geochemical composition of sandstones. *Journal of Geology*, **91**, 611-627.
- Bhatia, M. R. & Crook, K. A. W.** (1986). Trace element characteristics of greywackes and tectonic discrimination of sedimentary basins. *Contributions to Mineralogy and Petrology*, **92**, 181-193.
- Bhattacharya, A.** (1986). Some geobarometers involving cordierite in the FeO-Al₂O₃-SiO₂-(±H₂O) system: refinements, thermodynamic calibration, and applicability in granulite facies rocks: *Contributions to Mineralogy and Petrology*, **94**, 387-394.
- Bhattacharya, S. & Kar, R.** (2002). High temperature dehydration melting and decompressive P-T path in a granulite complex from the Eastern Ghats, India. *Contributions to Mineralogy and Petrology*, **143**, 175-191.
- Bhattacharya, A., Krishnapur, K. R., Raith, M. & Sen, S. K.** (1991). An improved set of *a-X* parameters for Fe-Mg-Ca garnets and refinements of the orthopyroxene-garnet-thermometer and the orthopyroxene-garnet-plagioclase-quartz barometer. *Journal of Petrology*, **32**, 629-656.
- Bhattacharya, A., Mazumdar, A. C. & Sen, S. K.** (1988). Fe-Mg mixing in cordierite: constraints from natural data and implications for cordierite-garnet thermometry in granulites. *American Mineralogist*, **3**, 338-344.
- Bhattacharya, A., Mohanty, L., Maji, A., Sen, S. K. & Raith, M.** (1992). Non-ideal mixing in the phlogopite-annite binary: Constraints from experimental data on Mg-Fe partitioning and a reformulation of the biotite-garnet geothermometer. *Contributions to Mineralogy and Petrology*, **111**, 87-93.
- Biswal, T. K., Gyani, K. C., Partasarathy, R. & Pant, D. R.** (1998). Implications of the geochemistry of the pelitic granulites of the Delhi Supergroup, Aravalli Mountain Belt, northwestern India. *Precambrian Research*, **87**, 75-85.
- Bohlen, S. R., Wall, V. J. & Boettcher, A. L.** (1983a). Geobarometry in granulites. In: **Saxena, S. K.** (ed.) *Kinetics and Equilibrium in Mineral Reactions*. Advances in Physical Geochemistry, Volume 3, Springer-Verlag, New York, pp. 141-172.
- Bohlen, S. R., Wall, V. J. & Boettcher, A. L.** (1983b). Experimental investigation of model garnet granulite equilibria. *Contributions to Mineralogy and Petrology*, **83**, 52-61.
- Brandt, S., Klemd, R. & Okrusch, M.** (1999). Metamorphic evolution of the pre-Pan-African Epupa Complex, Namibia. *31th International Geological Congress Rio de Janeiro, Abstract Volume*, 23.
- Brandt, S., Klemd, R. & Okrusch, M.** (2000). Evidence for ultrahigh-temperature metamorphism in the pre-Pan-African Epupa Complex, NW Namibia. *GEOLUANDA 2000, Abstract Volume*, 33-34.
- Brandt, S., Klemd, R. & Okrusch, M.** (2002b). A garnet-clinopyroxene metabasite in medium

- pressure, ultrahigh temperature granulites of the Proterozoic Epupa Complex, NW Namibia: Evidence for a high pressure event? *IMA 2002 Edinburgh, Abstract Volume*, 233.
- Brandt, S., Klemd, R., & Okrusch, M.** (2003). Ultrahigh-temperature metamorphism and multistage evolution of garnet-orthopyroxene granulites from the Proterozoic Epupa Complex, NW Namibia. *Journal of Petrology*, **44**, 1121-1144.
- Brandt, S., Will, T. M. & Klemd, R.** (2001). Metamorphic evolution of sapphirine-bearing orthopyroxene-sillimanite gneisses and associated felsic granulites from the Proterozoic Epupa Complex, NW Namibia. *EUG XI, Strasbourg, Abstract Volume*, 571.
- Brandt, S., Will, T. M., Klemd, R. & Okrusch, M.** (2002a). A calculated petrogenetic grid in the system FeO-MgO-Al₂O₃-SiO₂-H₂O (FMASH) for high grade metapelites with application to sapphirine granulites from the meso-Proterozoic Epupa Complex, NW Namibia. *Berichte der Deutschen Mineralogischen Gesellschaft, Beihefte zum European Journal of Mineralogy*, **14**, 27.
- Brey, G. P. & Köhler, T.** (1990). Geothermobarometry in four-phase lherzolites II. New thermobarometers, and practical assessment of thermobarometers. *Journal of Petrology*, **31**, 1353-1378.
- Bucher, K. & Frey, M.** (1994). *Petrogenesis of metamorphic rocks*. Springer-Verlag, Berlin-Heidelberg-New York, 318 pp.
- Burger, A. J., Clifford, T. N. & Miller, R. Mc G.** (1976). Zircon U-Pb ages of the Fransfontein granitic suite, northern South West Africa. *Precambrian Research*, **3**, 405-431.
- Burger, A. J., & Coertze, F. J.** (1975). Age determinations – April 1972 to March 1974. *Annual of the Geological Survey of South Africa*, **10**, 135-141.
- Cahen, L., Snelling, N. J., Delhal, J. & Yail, J. R.** (1984). *The geochronology and evolution of Africa*. Clarendon Press, Oxford, 512 pp.
- Carrington, D. P. & Harley, S. L.** (1995). Partial melting and phase relations in high-grade metapelites: an experimental petrogenetic grid in the KFMASH system. *Contributions to Mineralogy and Petrology*, **120**, 270-291.
- Carswell D. A. & Harley, S. L.** (1990). Mineral thermometry and barometry. In: **Carswell, D. A. (ed.)** *Eclogite facies rocks*. Blackie and Sons, Glasgow, pp. 83-110.
- Carvalho, H. de** (1984). Estratigrafia do Precambrien de Angola. Garcia de Orta, Serie Geologia, *Instituto de Investigacao Tropical*, **7 (1-2)**, 1-66.
- Carvalho, H. de & Alves, P.** (1990). Gabbro-Anorthosite Complex of SW Angola/ NW Namibia. Garcia de Orta, *Série de Ciências da Terra, Comunicações*, **2**, 1-66.
- Carvalho, H. de & Alves, P.** (1993). The Precambrian of SW Angola and NW Namibia. Garcia de Orta, *Série de Ciências da Terra, Comunicações*, **4**, 1-38.
- Carvalho, H., Crasto, J., Silva, Z. C. & Vialette, Y.** (1987). The Kibarian cycle in Angola: a

- discussion. *Geological Journal*, **22**, 85-102.
- Carvalho, H. de, Fernandes, F.C. & Vialette, Y.** (1979). Chronologie absolue du Précambrien du Sud-Ouest de l'Angola. *Comptes Rendus Académie Sciences Paris*, **288**, 1647-1650.
- Carvalho, H. de, Tassinari, C., Alves, P., Guimaraes, F. & Simoes, M. C.** (2000). Geochronological review of the Precambrian in western Angola: links with Brazil. *Journal of African Earth Science*, **31**, 383-402.
- Dasgupta, S., Sengupta, P., Ehl, J., Raith, M & Bardhan, S.** (1995). Reaction textures in a suite of spinel granulites from the Eastern Ghats Belt, India: evidence for polymetamorphism, a partial petrogenetic grid in the system KFMASH and the roles of ZnO and Fe₂O₃. *Journal of Petrology*, **36**, 435-461.
- Dingeldey, D. P.** (1997). *Tectono-metamorphic evolution of the Pan-African Kaoko belt, NW Namibia*. PhD thesis, University of Würzburg, 247 pp.
- Dingeldey, D. P., Dürr, S. B., Charlesworth, E. G., Franz, L., Okrusch, M. & Stanistreet, I. G.** (1994). A traverse through the northern coastal branch of the Damara Orogen west of Sesfontein, Namibia. *Journal of African Earth Science*, **19**, 315-329.
- Droop, G. T. R.** (1989). Reaction history of garnet-sapphirine granulites and conditions of Archean high-pressure granulite facies metamorphism in the Central Limpopo Mobile Belt. *Journal of Metamorphic Geology*, **7**, 383-403.
- Droop, G. T. R. & Bucher-Nurminen, K.** (1984). Reaction textures and metamorphic evolution of sapphirine-bearing granulites from the Gruf Complex, Italian Central Alps. *Journal of Petrology*, **25**, 766-803.
- Drüppel, K.** (1999). *Petrologie und Geochemie von Anorthositen des Kunene-Intrusiv-Komplexes, NW Namibia*. Diploma (M.Sc.) thesis, University of Würzburg, 217 pp.
- Drüppel, K.** (2003). *Petrogenesis of the Mesoproterozoic anorthosite, syenite and carbonatite suites of NW Namibia and their contribution to the metasomatic formation of the Swartbooisdrif sodalite deposits*. PhD thesis, University of Würzburg, 345 + 199 pp.
- Drüppel, K., Brandt, S. & Okrusch, M.** (2000a). Evolution of the anorthositic Kunene Intrusive Complex and the metamorphic rocks of the Epupa Complex, NW Namibia: Evidence for cogenetic formation during Proterozoic crustal extension? *GEOLUANDA 2000, Abstract Volume*, 47-48.
- Drüppel, K., Littmann, S. & Okrusch, M.** (2000b). Geo- und isopenchemische Untersuchungen der Anorthosite des Kunene-Intrusiv-Komplexes (KIC) in NW Namibia. *Berichte der deutschen Mineralogischen Gesellschaft, Beihefte zum European Journal of Mineralogy*, **12**, 37.
- Drüppel, K., von Seckendorff, V. & Okrusch, M.** (2001). Subsolidus reaction textures in the anorthositic rocks of the southern part of the Kunene Intrusive Complex, NW Namibia. *European Journal of Mineralogy*, **13**, 289-309.

- Dwivedi, S. B., Mohan, A. & Lal, R. K.** (1998). Recalibration of the Fe-Mg exchange reaction between garnet and cordierite as a thermometer. *European Journal of Mineralogy*, **10**, 281-289.
- Eckert, J. O., Newton, R. C. & Kleppa, O. J.** (1991). The ΔH of reaction and recalibration of garnet-pyroxene-plagioclase-quartz geobarometer in the CMAS system by solution calorimetry. *American Mineralogist*, **76**, 148-160.
- Essene, E. J.** (1989). The current status of thermobarometry in metamorphic rocks. In: **Daly J. S., Cliff, R. A. & Yardley, B. W. D. (eds.)** *Evolution of Metamorphic Belts*. Geological Society, London, Special Publications, **43**, 1-44.
- Ellis, D. J. & Green, D. H.** (1979). An experimental study of the effect of Ca upon garnet-clinopyroxene Fe-Mg exchange equilibria. *Contributions to Mineralogy and Petrology*, **71**, 13-22.
- Ferguson, J., McIver, J. R. & Danchlin, R. V.** (1975). Fenitisation associated with the alkaline-carbonatite complex of Epembe, South West Africa. *Transactions of the Geological Society of South Africa*, **78**, 111-121.
- Ferry J. M. & Spear F. S.** (1978). Experimental calibration of the partitioning of Fe and Mg between biotite and garnet. *Contributions to Mineralogy and Petrology*, **66**, 113-117.
- Fitzsimons, I. C. W.** (1996). Metapelitic migmatites from Brattstrand Bluffs, East Antarctica: metamorphism, melting and exhumation of the mid crust. *Journal of Petrology*, **37**, 395-414.
- Fitzsimons, I. C. W. & Harley, S. L.** (1994). The influence of retrograde cation exchange on granulite *P-T* estimates and a convergence technique for the recovery of peak metamorphic conditions. *Journal of Petrology*, **35**, 543-576.
- Franz, L. & Häussinger, H.** (1990). Die Anwendung interaktiver Programme in der Mineralogie am Beispiel des Programms "Amphibol". *Beiheft zum European Journal of Mineralogy*, **2**, 68.
- Franz, L., Romer, R. L. & Dingeldey, D. P.** (1999). Diachronous Pan-African granulite-facies metamorphism (650 Ma and 550 Ma) in the Kaoko Belt, NW Namibia. *European Journal of Mineralogy*, **11**, 167-180.
- Frets, D. C.** (1969). *Geology and structure of the Huab-Welwitschia area, South West Africa*. University of Cape Town Bulletin, **5**, 235 pp.
- Frost B. R. & Chacko T.** (1989). The granulite uncertainty principle; limitations on thermobarometry in granulites. *Journal of Geology*, **97**, 435-450.
- Ganguly, J. & Saxena, S. K.** (1984). Mixing properties of aluminosilicate garnets: constraints from natural and experimental data, and applications to geothermo-barometry. *American Mineralogist*, **69**, 88-97.
- Geiger, C. A., Newton, R. C. & Kleppa, O. J.** (1987). Enthalpy of mixing of synthetic almandine-grossular and almandine-pyrope garnets from high temperature solution calorimetry. *Geochimica et Cosmochimica Acta*, **51**, 1755-1763.

- Graham, C. M. & Powell, R.** (1984). A garnet-hornblende geothermometer: Calibration, testing and application to the Pelona Schists, Southern California. *Journal of Metamorphic Geology*, **2**, 13-21.
- Green, D. H. & Ringwood, A. E.** (1967). An experimental investigation of the gabbro to eclogite transformation and its petrological applications. *Geochimica et Cosmochimica Acta*, **31**, 767-833.
- Green, T. H. & Adam, J.** (1991). Assessment of the garnet-clinopyroxene Fe-Mg exchange using new experimental data. *Journal of Metamorphic Geology*, **9**, 341-347.
- Griffin, W. L.** (1971). Genesis of coronas in anorthosites of the Upper Jotun Nappe, Indre Sogn, Norway. *Journal of Petrology*, **12**, 219-243.
- Guiraud, M., Kienast, J.-R. & Ouzegane, K.** (1996). Corundum-quartz-bearing assemblage in the Ihouhaouene area (In Ouzzal, Algeria). *Journal of Metamorphic Geology*, **14**, 755-761.
- Harley, S. L.** (1984). An experimental study of the partitioning of Fe and Mg between garnet and orthopyroxene. *Contributions to Mineralogy and Petrology*, **86**, 359-373.
- Harley, S. L.** (1986). A sapphirine-cordierite-garnet-sillimanite granulite from Enderby Land, Antarctica: implications for FMAS petrogenetic grids in the granulite facies. *Contributions to Mineralogy and Petrology*, **94**, 452-460.
- Harley, S. L.** (1989). The origins of granulites: a metamorphic perspective. *Geological Magazine*, **126**, 215-247.
- Harley, S. L.** (1998a). On the occurrence and characterization of ultrahigh-temperature crustal metamorphism. In: **Treloar, P. J. & O'Brien, P. J. (eds.)** *What Drives Metamorphism and Metamorphic Reactions?* Geological Society, London, Special Publication, **138**, pp. 81-107.
- Harley, S. L.** (1998b). Ultrahigh-temperature granulites metamorphism (1050°C, 12 kbar) and decompression in garnet (Mg70)-orthopyroxene-sillimanite gneisses from the Rauer Group, East Antarctica. *Journal of Metamorphic Geology*, **16**, 541-562.
- Harley, S. L. & Green, D. H.** (1982). Garnet-orthopyroxene barometry for granulites and peridotites. *Nature*, **300**, 697-701.
- Harley S. L., Hensen, B. J. & Sheraton, J. W.** (1990). Two-stage decompression in orthopyroxene-sillimanite granulites from Forefinger Point, Enderby Land, Antarctica: implications for the evolution of the Archean Napier Complex. *Journal of Metamorphic Geology*, **8**, 591-613.
- Harley, S. L. & Motoyoshi, Y.** (2000). Al zoning in orthopyroxene in a sapphirine quartzite: evidence for 1120°C UHT metamorphism in the Napier Complex, Antarctica, and implications for the entropy of sapphirine. *Contributions to Mineralogy and Petrology*, **138**, 293-307.
- Harlov, D. E. & Milke, R.** (2002). The stability of corundum + quartz relative to kyanite and sillimanite at high temperature and pressure. *American Mineralogist*, **87**, 424-432.
- Harris, N. B. W.** (1981). The application of spinel bearing metapelites to P/T determinations: an example from South India. *Contributions to Mineralogy and Petrology*, **76**, 229-233.

- Harris, N. B. W. & Holland, T. J. B.** (1984). The significance of cordierite-hypersthene assemblages from the Beitbridge region of the Central Limpopo Belt; evidence for rapid decompression in the Archean? *American Mineralogist*, **69**, 1036-1049.
- Hartnady, C. J. H., Joubert, P. & Stowe, C.** (1985). Proterozoic crustal evolution in South-western Africa. *Episodes*, **8**, 236-244.
- Hensen, B. J.** (1986). Theoretical phase relations involving garnet and cordierite revisited: the influence of oxygen fugacity on the stability of sapphirine and spinel in the system Mg-Fe-Al-Si-O. *Contributions to Mineralogy and Petrology*, **92**, 191-214.
- Hensen, B. J.** (1987). *P-T* grids for silica-undersaturated granulites in the system MAS (n+4) and FMAS (n+3) - tools for the derivation of *P-T* paths of metamorphism. *Journal of Metamorphic Geology*, **5**, 255-271.
- Hensen, B. J. & Green, D. H.** (1973). Experimental study of the stability of cordierite and garnet in pelitic compositions at high pressures and temperatures. III. Synthesis of experimental data and geological applications. *Contributions to Mineralogy and Petrology*, **38**, 151-166.
- Hensen, B. J. & Harley, S. L.** (1990). Graphical analysis of *P-T-X* relations in granulite facies metapelites. In: **Brown, M. & Ashworth, J. R. (eds.)** *High-grade Metamorphism and Crustal Anatexis*. Unwin Hyman, London, pp. 19-55.
- Hisada, K. & Miyano, T.** (1996). Petrology and microthermometry of aluminous rocks in the Botswanan Limpopo Central Zone: evidence for isothermal decompression and isobaric cooling. *Journal of Metamorphic Geology*, **14**, 183-197.
- Hoffmann, P.F., Hawkins, D. P. Isachsen, C. E. & Bowring, S. A.** (1996). Precise U-Pb zircon ages for early Damara magmatism in the Summas Mountains and Welwitschia Inlier, northern Damara Belt, SWA/Namibia. *Communications of the Geological Survey of Namibia*, **11**, 47-52.
- Holdaway, M. J.** (1971). The stability of andalusite and the aluminium silicate phase diagram. *American Journal of Science*, **271**, 97-131.
- Holland, T. J. B. & Powell, R.** (1990). An enlarged and updated internally consistent data-set with uncertainties and correlations: the system K₂O-Na₂O-CaO-MgO-MnO-Fe₂O₃-Al₂O₃-TiO₂-SiO₂-C-H₂-O₂. *Journal of Metamorphic Geology*, **8**, 89-124.
- Holland, T. J. B. & Powell, R.** (1998a). THERMOCALC v.2.7. <http://www.esc.cam.uk/astaff/holland/thermocalc.html>.
- Holland, T. J. B. & Powell, R.** (1998b). An internally consistent data set for phases of petrological interest. *Journal of Metamorphic Geology*, **16**, 309-343.
- Holland, T. J. B. & Powell, R.** (2000). AX. <http://www.esc.cam.uk/astaff/holland/ax.html>.
- Irvine, J. N. & Baragar, W. R. A.** (1971). A guide to the chemical classification of common volcanic rocks. *Canadian Journal of Earth Science*, **8**, 523-548.

- Jacob, R. E., Kröner, A. & Burger, A. J.** (1978). Areal extent and first U-Pb age of the pre-Damara Abbabis complex in the central Damara belt of South West Africa (Namibia). *Geologische Rundschau*, **67**, 706-718.
- Jaeckel, P., Kröner, A., Kamo, S. L., Brandl, G. & Wendt, J. I.** (1997). Late Archaean to early Proterozoic granitoid magmatism and high-grade metamorphism in the central Limpopo belt. *Journal of the Geological Society of London*, **154**, 25-44.
- Jahn, B. M.** (1990). The origin of granulites: geochemical constraints from Archean granulite facies rocks of the Sino-Korean craton, China. In: **Vielzeuf, D. & Vidal, Ph.** (eds.) *Granulites and Crustal Evolution*. Kluwer Academic, Dordrecht, pp. 471-492.
- Janardhan, A. S., Newton, R. C. & Hansen, E. C.** (1982). The transformation of amphibolite facies gneiss to charnockite in Southern Karnataka and Northern Tamil Nadu, India. *Contributions to Mineralogy and Petrology*, **79**, 130-149.
- Kleemann, U. & Reinhardt, J.** (1994). Garnet-biotite thermometry revisited: The effect of Al^{VI} and Ti in biotite. *European Journal of Mineralogy*, **6**, 925-941.
- Kataria, P., Chaudhari, M. W. & Althause, E.** (1988). Petrochemistry of amphibolites from the Banded Gneiss Complex of Amet, Rajasthan, Northwestern India. *Chemie der Erde*, **48**, 89-111.
- Kohn, M. J. & Spear, F. S.** (1990). Two new barometers for garnet amphibolites with applications to southeastern Vermont. *American Mineralogist*, **75**, 89-96.
- Kohn, M. J. & Spear, F. S.** (1996). Program GTB (GeoThermoBarometry) v. 2.0. http://ees.geo.rpi.edu/MetaPetaRen/GTB_Prog/GTB.html
- Koziol, A. M. & Newton, R. C.** (1988). Redetermination of the anorthite breakdown reaction and improvement of the plagioclase-garnet-Al₂SiO₅-quartz geobarometer. *American Mineralogist*, **73**, 216-233.
- Köstlin, E. C.** (1967). *The geology of part of the Kunene basic complex, Kaokoveld, South West Africa*. M.Sc. thesis, University of Cape Town, Cape Town, 92 pp.
- Köstlin, E. C.** (1974). The Kunene basic complex, northern South West Africa. In: **Kröner, A.** (ed.) *Contributions to the Precambrian geology of southern Africa*. University of Cape Town Bulletin, **15**, pp. 123-135.
- Kretz, R.** (1983). Symbols for rock-forming minerals. *American Mineralogist*, **68**, 277-279.
- Kriegsmann, L. M. & Schumacher J. C.** (1999). Petrology of sapphirine-bearing and associated granulites from central Sri Lanka. *Journal of Petrology*, **40**, 1211-1239.
- Krogh Ravna E.** (2001). The garnet-clinopyroxene Fe²⁺-Mg exchange geothermometer: an updated calibration. *Journal of Metamorphic Geology*, **18**, 211-219.
- Kröner, A., Jaeckel, P., Brandl, G., Nemchin, A. A. & Pidgeon, R. T.** (1999). Single zircon ages for granitoid gneisses in the Central Zone of the Limpopo Belt, Southern Africa and geodynamic

- significance. *Precambrian Research*, **93**, 299-337.
- Kröner, S., Kröner, A., Konopasek, J., Poller, U. & Hoffmann, K.-H.** (2002). Geochronological and geochemical studies of crustal rocks in NW Namibia (Kaokobelt). *Berichte der Deutschen Mineralogischen Gesellschaft, Beihefte zum European Journal of Mineralogy*, **14**, 93.
- Lal, R. K., Ackermann, D., Raith, M., Raase, P. & Seifert, F.** (1984). Sapphirine-bearing assemblages from Kiranur, Southern India: a study of chemographic relationships in the $\text{Na}_2\text{O}-\text{FeO}-\text{MgO}-\text{Al}_2\text{O}_3-\text{SiO}_2-\text{H}_2\text{O}$ system. *Neues Jahrbuch für Mineralogie*, **150**, 121-152.
- Leake, B. E., Schumacher, J. C., Smith, D. C., Stephenson, N. C. N., Ungaretti, L., Whittaker, E. J. W., Youzhi, G.** (1997). Nomenclature of Amphiboles. *European Journal of Mineralogy*, **9**, 623-642.
- Lee, H. Y. & Ganguly, J.** (1988). Equilibrium compositions of coexisting garnet and orthopyroxene: experimental determinations in the system $\text{FeO}-\text{MgO}-\text{Al}_2\text{O}_3-\text{SiO}_2$, and applications. *Journal of Petrology*, **29**, 93-113.
- Le Maitre, R. W.** (ed.) (1989). *A Classification of Igneous Rocks and Glossary of Terms*. Blackwell, Oxford, 193 pp.
- Leyreloup, A., Dupuy, C. & Andriambololona R.** (1977). Catazonal xenoliths in French Neogene volcanic rocks: 2. Chemical composition and consequences of the evolution of the French Massif Central Precambrian crust. *Contributions to Mineralogy and Petrology*, **62**, 283-300.
- Littmann, S., Romer, R.L. & Okrusch, M.** (2000). Nephelinsyenite der Epembe-Swartbooisdrif- Alkali-Provinz (ESAP)/ NW Namibia. *Berichte der deutschen Mineralogischen Gesellschaft, Beihefte zum European Journal of Mineralogy*, **12**, 115.
- Martin, H.** (1965). The Precambrian geology of South West Africa and Namaqualand. Precambrian Research Unit, University of Cape Town, 159 pp.
- Mayer, A., Sinigoi, S., Miguel, L. G., Morais, E. & Petrini, R.** (2000). Kibarian ages in the Kunene Intrusive Complex. *GEOLUANDA 2000, Abstract Volume*, 106.
- Menge, G. F. W.** (1996). *The eastern portion of the Kunene complex, its satellite intrusions and the alkaline suite between Epembe and Swartbooisdrif*. Unpublished Report, 128 pp.
- Menge, G. F. W.** (1998). The antiformal structure and general aspects of the Kunene Complex. *Zeitschrift der Deutschen Geologischen Gesellschaft*, **149**, 431-448.
- Mengel, F. & Rivers, T.** (1991). Decompression reactions and P-T conditions in high-grade rocks, Northern Labrador: P-T-t paths from individual samples and implications for Early Proterozoic tectonic evolution. *Journal of Petrology*, **32**, 139-167.
- Miyashiro, A.** (1974). Volcanic arc rock series in island arcs and active continental margins. *American Journal of Science*, **274**, 321-355.
- Miyashiro, A.** (1978). Nature of alkalic volcanic rock series. *Contributions to Mineralogy and Petrology*, **66**, 91-104.

- Miller, R. Mc G.** (1983). The Pan-African Damara Orogen of South West Africa/Namibia. In: **Miller, R. Mc. G.** (ed.) *Evolution of the Damara Orogen of South West Africa/Namibia. Geological Society of South Africa, Special Publication*, **11**, pp. 431-515.
- Moecher, D. P., Essene, E. J. & Anovitz, L. M.** (1988). Calculation and application of clinopyroxene-garnet-plagioclase-quartz geobarometers. *Contributions to Mineralogy and Petrology*, **100**, 92-106.
- Montel, J. M. & Vielzeuf, D.** (1997). Partial melting of metagreywackes, Part II. Compositions of minerals and melts. *Contributions to Mineralogy and Petrology*, **128**, 176-196.
- Morais, E., Sinigoi, S., Mayer, A., Mucana, A., Miguel, L.G. & Rufino Neto, J.** (1998). The Kunene gabbro-anorthosite Complex: preliminary results based on new field and chemical data. *African Geoscience Review*, **5**, 485-498.
- Morimoto, N.** (1988): Nomenclature of pyroxenes. *Mineralogical Magazine*, **52**, 535-550.
- Motoyoshi, Y, Hensen, B. J. & Matsueda, H.** (1990). Metastable growth of corundum adjacent to quartz in a spinel-bearing quartzite from the Archean Napier Complex, Antarctica. *Journal of Metamorphic Geology*, **8**, 125-130..
- Mullen, E. D.** (1983). MnO/TiO₂/P₂O₅: A minor element discrimination for basaltic rocks of oceanic environments and its implications for petrogenesis. *Earth and Planetary Science Letters*, **62**, 53-62.
- Newton, R. C.** (1972). An experimental determination of the high-pressure stability limits of magnesian cordierite under wet and dry conditions. *Journal of Geology*, **80**, 398-420.
- Newton, R. C.** (1983). Geobarometry of high-grade metamorphic rocks. *American Journal of Science*, **283**, 1-28.
- Newton, R. C. & Haselton, H. T.** (1981). Thermodynamics of the garnet-plagioclase-Al₂SiO₅-quartz geobarometer. In: **Newton, R. C., Navrotsky, A. & Wood, B.J.** (eds.) *Thermodynamics of minerals and melts*, Springer-Verlag, New York, pp. 131-147.
- Newton, R. C. & Perkins, D.** (1982). Thermodynamic calibration of geobarometers based on the assemblages garnet-plagioclase-orthopyroxene (clinopyroxene)-quartz. *American Mineralogist*, **67**, 203-222.
- Nichols, G. T, Berry, R. F. & Green, D. H.** (1992). Internally consistent gahnitic spinel-cordierite-garnet equilibria in the FMASHZn system: geothermobarometry and applications. *Contributions to Mineralogy and Petrology*, **111**, 362-377.
- Olson, S. F.** (2000). The Proterozoic evolution of Africa. *University of the Witwatersrand, Johannesburg, Economic Geology Research Unit, Information Circular*, **343**, 1-61.
- Ouzegane, K. & Boumaza, S.** (1996). An example of ultrahigh-temperature metamorphism: - orthopyroxene-sillimanite-garnet, sapphirine-quartz and spinel-quartz parageneses in Al-Mg granulites from In Hihaou, In Ouzzal, Hoggar. *Journal of Metamorphic Geology*, **14**, 693-708.
- Papike, J. J., Cameron, K. L. & Baldwin, K.** (1974). Amphiboles and pyroxenes: Characterization of

- other than quadrilateral components and estimates of ferric iron from microprobe data. *Geological Society of America, Abstracts with Program*, **6**, 1053-1054.
- Patiño Douce, A. E.** (1993). Titanium substitution in biotite – an empirical model with applications to thermometry; O₂ and H₂O barometers, and consequence for biotite stability. *Chemical Geology*, **108**, 133-162.
- Pearce, J. A.** (1982). Trace element characteristics of lavas from plate boundaries. In: **Thorpe, R. S.** (ed.) *Andesites*. Wiley & Sons, New York, pp. 525-548.
- Pearce, J. A.** (1996). Sources and settings of granitic rocks. *Episodes*, **19**, 120-125.
- Pearce, J. A. & Cann, J. R.** (1973). Tectonic setting of volcanic rocks determined using trace element analyses. *Earth and Planetary Science Letters*, **19**, 290-300.
- Pearce, J. A. & Gale, G. H.** (1977). Identification of ore deposition environments from trace-element geochemistry of associated igneous rocks. *Geological Society of London, Special Publication*, **7**, 14-24.
- Pearce, J. A., Harris, N. B. W. & Tindle, A. G.** (1984). Trace element discrimination diagrams for the tectonic interpretation of granitic rocks. *Journal of Petrology*, **25**, 956-983.
- Perchuk, L. L. & Lavrent'eva, I. V.** (1983). Experimental investigation of the exchange equilibria in the system cordierite-garnet-biotite. In: **Saxena, S. K.** (ed.) *Kinetics and equilibrium in mineral reactions*. Springer-Verlag, New York, pp. 199-239.
- Perchuk, L. L., Aranovich, L. Y., Podlesskii, K. K., Lavrent'eva, I. V., Gerasimov, V. Y., Fed'kin, V. V., Kitsul, V. I., Karsakov, L. P. & Berdnikov, N. V.** (1985). Precambrian Granulites of the Aldan Shield, Eastern Siberia, USSR. *Journal of Metamorphic Geology*, **3**, 265-310.
- Powell, R.** (1985). Regression diagnostics and robust regression in geothermometer/geobarometer calibration: the garnet-clinopyroxene geothermometer revisited. *Journal of Metamorphic Geology*, **3**, 231-243.
- Powell, R. & Holland, T. J. B.** (1988). An internally consistent dataset with uncertainties and correlations: 3. Applications to geobarometry, worked examples and a computer program. *Journal of Metamorphic Geology*, **6**, 173-204.
- Powell, R. & Sandiford, M.** (1988). Sapphirine and spinel phase relationships in the system FeO-MgO-Al₂O₃-SiO₂-TiO₂-O₂ in the presence of quartz and hypersthene. *Contributions to Mineralogy and Petrology*, **98**, 64-71.
- Raase, P.** (1974). Al and Ti contents of hornblende, indicators of pressure and temperature of regional metamorphism. *Contributions to Mineralogy and Petrology*, **45**, 231-236.
- Raith, M., Karmakar, S. & Brown, M.** (1997). Ultra-high-temperature metamorphism and multistage decompressional evolution of sapphirine granulites from the Palni Hills Range, southern India. *Journal of Metamorphic Geology*, **15**, 379-399.

- Raith, M., Srikantappa, C., Buhl, D. & Koehler, H.** (1999). The Nilgiri enderbites, South India: nature and age constraints on protolith formation, high grade metamorphism and cooling history. *Precambrian Research*, **98**, 129-150.
- Rickers, K., Raith, M. & Dasgupta, S.** (2001). Multistage reaction textures in xenolithic high-MgAl granulites at Anakapalle, Eastern Ghats, India: examples of contact polymetamorphism and infiltration-driven metasomatism. *Journal of Metamorphic Geology*, **19**, 561-580.
- Robb, L. J., Armstrong, R. A. & Waters, D. J.** (1999). The history of granulite-facies metamorphism and crustal growth from single zircon U-Pb geochronology, Namaqualand, South Africa. *Journal of Petrology*, **40**, 1747-1770.
- Robinson, P. R., Hollocher, K. T., Tracy, R. J. & Dietsch, C. W.** (1982). High grade Arcadian regional metamorphism in south-central Massachusetts. In: **Josten, R. Q. S.** (ed.) *Guidebook for Fieldtrips in Connecticut and South-Central Massachusetts*. NEIGC 74th Annual Meeting of the State Geological and Natural History Survey of Connecticut, Storrs, University of Connecticut, pp. 289-340.
- Rollinson, H. R.** (1983). The geochemistry of mafic and ultramafic rocks from the Archean greenstone belts of Sierra Leone. *Mineralogical Magazine*, **47**, 267-280.
- Rudnick, R.L., McLennan, S. M. & Taylor, S. R.** (1985). Large ion lithophile elements of rocks from high-pressure granulite facies terrains. *Geochimica et Cosmochimica Acta*, **49**, 1645-1655.
- SACS** (South African Committee for Stratigraphy) (1980). Stratigraphy of South Africa, Part I (comp. **Kent, L.E.**), *Geological Survey of South Africa, Handbook*, **8**, 690 pp.
- Sen, S. K. & Bhattacharya, A.** (1984). An orthopyroxene-garnet thermometer and its application to the Madras charnockites. *Contributions to Mineralogy and Petrology*, **88**, 64-71.
- Sengupta, P., Sen, J., Dasgupta, S., Raith, M., Bhui, U. K. & Ehl, J.** (1999). Ultra-high-temperature metamorphism of metapelitic granulites from Kondapalle, Eastern Ghats Belt: Implications for the Indo-Antarctic Correlation. *Journal of Petrology*, **40**, 1065-1087.
- Seth, B., Armstrong, R. A., Brandt, S., Villa, I. M. & Kramers, J. D.** (2003). Mesoproterozoic U-Pb and Pb-Pb ages of granulites in NW Namibia: reconstructing a complete orogenic cycle. *Precambrian Research*, **126**, 147-168.
- Seth, B., Brandt, S. & Kramers, J. D.** (2001). First isotopic age determinations of mid-Proterozoic granulite facies metamorphism in the Epupa Complex. *EUG XI, Strasbourg Abstract Volume*, 597.
- Seth, B., Kröner, A., Mezger, K., Nemchin, A. A., Pidgeon, R. T. & Okrusch, M.** (1998). Archean to Neoproterozoic magmatic events in the Kaoko Belt of NW Namibia and their geodynamic significance. *Precambrian Research*, **92**, 341-363.
- Shaw, D. M.** (1972). The origin of the Apsley gneiss, Ontario. *Canadian Journal of Earth Science*, **9**, 13-48.

- Shaw, R. K. & Arima, M.** (1998). A corundum-quartz assemblage from the Eastern Ghats Granulite Belt, India: evidence for high P-T metamorphism?. *Journal of Metamorphic Geology*, **16**, 189-196.
- Shervais, J. W.** (1982). Ti-V plots and the petrogenesis of modern and ophiolitic lavas. *Earth and Planetary Science Letters*, **59**, 101-118.
- Shulters, J. C. & Bohlen, S. R.** (1989). The stability of hercynite and hercynite-gahnite spinel in corundum- or quartz-bearing assemblages. *Journal of Petrology*, **30**, 1017-1031
- Spear, F. S.** (1981). An experimental study on hornblende stability and compositional variability in amphibolite. *American Journal of Science*, **281**, 697-734.
- Spear, F. S.** (1989). Relative geothermobarometry and metamorphic P-T paths. In: **Daly J. S., Cliff, R. A. & Yardley, B. W. D.** (eds.) *Evolution of Metamorphic Belts*. Geological Society, London, Special Publications, **43**, 63-81.
- Spear, F. S.** (1993). *Metamorphic phase equilibria and pressure-temperature-time paths*. Mineralogical Society of America, Washington D.C., 799 pp.
- Spear, F. S. & Kimball, K. L.** (1984). RECAMP-A FORTRAN IV program for estimating Fe³⁺ contents in amphiboles. *Computers in Geology*, **10**, 317-325.
- Spear, F. S., Kohn, J & Cheney, J. T.** (1999). P-T paths from anatexitic pelites. *Contributions to Mineralogy and Petrology*, **134**, 17-32.
- Stevens, G., Clemens, J. D. & Droop, G. T. R.** (1997). Melt production during granulite-facies anatexis: experimental data from “primitive” metasedimentary protoliths. *Contributions to Mineralogy and Petrology*, **128**, 352-370.
- Talarico, F., Borsi, L. & Lombardo, B.** (1995). Relict granulites in the Ross Orogen of northern Victoria Land (Antarctica), II. Geochemistry and palaeo-tectonic implications. *Precambrian Research*, **75**, 157-174.
- Tegtmeyer, A. & Kröner, A.** (1985). U-Pb zircon ages for granitoid gneisses in northern Namibia and their significance for Proterozoic crustal evolution of south-western Africa. *Precambrian Research*, **28**, 321-326.
- Thompson, A. B.** (1976). Mineral reactions in pelitic rocks: II. calculation of some P-T-X (Fe-Mg) phase relations. *American Journal of Science*, **276**, 425-454.
- Thompson, R. N.** (1984). Dispatches from the basalt front. 1. Experiments. *Proceedings of the Geological Association*, **95**, 249-262.
- Thost, D. E., Hensen, B. J. & Motoyoshi, Y.** (1990). Two-stage decompression in garnet-bearing granulites from Sostrene Island, Prydz Bay, East Antarctica. *Journal of Metamorphic Geology*, **9**, 245-256.
- Torquato, J. R. & Carvalho, J. A. R.** (1992). Idade Rb-Sr do granito do Carculo, uma nova evidência para a existência do evento Namib no Sudoeste de Angola. *Revista Geologia*, **50**, 157-167.

- Torquato, J. R. & Oliviera, J. T.** (1977). Sobre a idade dos granitos e do grupo vulcano-sedimentar da região de Chipindo, Angola. *Comunicações Serviços Geológicos Portugal*, **61**, 223-238.
- Torquato, J. R., Silva, A. T. S. F. da, Cordani, U. G. & Kawashita, K.** (1979). A evolução geológica do Cinturão Móvel do Quipungo no Ocidente de Angola. *Anais Academia Brasileira Ciências*, **51**, 133-143.
- Trompette, R.** (1994). *Geology of Western Gondwana (2000-500 Ma). Pan-African-Brasiliano aggregation of South America and Africa*. Balkema, Rotterdam, 350 pp.
- Vielzeuf, D. & Montel, J. M.** (1994). Partial melting of metagreywackes. Part I. Fluid-absent experiments and phase relationships. *Contributions to Mineralogy and Petrology*, **117**, 375-393.
- Walker, K. R., Joplin, G. A. Lovering, J. F. & Green, R.** (1960). Metamorphic convergence of basic igneous rocks and lime-magnesia sediments of the Precambrium of northwestern Queensland. *Journal of the Geological Society of Australia*, **6**, 149-178.
- Waters, D. J.** (1986). Metamorphic history of sapphirine-bearing and related magnesian gneisses from Namaqualand, South Africa. *Journal of Petrology*, **27**, 541-565.
- Waters, D. J.** (1991). Hercynite-quartz granulites: phase relations, and implications for crustal processes. *European Journal of Mineralogy*, **3**, 367-386.
- Wells, P. R. A.** (1979). Chemical and thermal evolution of Archaean sialic crust, southern West Greenland. *Journal of Petrology*, **20**, 187-226.
- Werner, C. D.** (1987). Saxonian granulites-igneous or lithogenous. A contribution to the geochemical diagnosis of the original rocks in high-metamorphic complexes. *ZFS-Mitteilungen*, **133**, 221-250.
- Whalen, J. B., Currie, K. L. & Chappell, B. W.** (1987). A-type granites: geochemical characteristics, discrimination and petrogenesis. *Contributions to Mineralogy and Petrology*, **95**, 407-419.
- Whittington, A., Harris, N. & Baker, J.** (1988). Low-pressure anatexis: the significance of spinel and cordierite from metapelitic assemblages at Nanga Parbat, northern Pakistan. In: **Treloar, P. J. & O'Brien, P. J.** (eds.) *What Drives Metamorphism and Metamorphic Reactions?* Geological Society, London, Special Publication, **138**, pp. 183-198.
- Will, T. M.** (1998a). *Phase equilibria in metamorphic rocks: thermodynamic properties and petrological background*. Lecture notes in earth science, **71**, Springer-Verlag, Berlin-Heidelberg, 315 pp.
- Will, T. M.** (1998b). Phase diagrams and their application to determine pressure-temperature paths of metamorphic rocks. *Neues Jahrbuch für Mineralogie, Abhandlungen*, **174**, 103-130.
- Wilson, M.** (1989). *Igneous Petrogenesis*. Harper Collins Academic, London, 466 pp.
- Wimmenauer, W.** (1984). Das prävariskische Kristallin im Schwarzwald. *Fortschritte der Mineralogie, Beihefte*, **62**, 69-86.
- Winchester, J. A. & Floyd, P. A.** (1976). Geochemical magma type discrimination: Application to

- altered and metamorphosed basic igneous rocks. *Earth and Planetary Science Letters*, **28**, 459-469.
- Winchester, J. A. & Floyd, P. A.** (1977). Geochemical discrimination of different magma series and their differentiation products using immobile elements. *Chemical Geology*, **20**, 325-343.
- Winchester, J. A., Park, G. R. & Holland, J. G.** (1980). The geochemistry of Lewisian semipelitic schists from the Gairloch District, Wester Ross, *Scottish Journal of Geology*, **16**, 165-179.
- Wood, B. J. & Banno, S.** (1973). Garnet-orthopyroxene and orthopyroxene-clinopyroxene relationships in simple and complex systems. *Contributions to Mineralogy and Petrology*, **42**, 109-124.

Lebenslauf

Sönke Brandt
Virchowstr. 18
97072 Würzburg

Geburtsdatum: 10.07.1970
Geburtsort: Kiel
Familienstand: ledig

Schulischer Werdegang

08/1981-05/1990 Gymnasium Kronshagen
05/1990 Abitur

Wehrdienst

07/1990–07/1991 Goslar und Eckernförde

Studium

10/1991-04/1998 Studium der Geologie-Paläontologie an der Christian-Albrechts-Universität zu Kiel
05/1994 Diplomvorprüfung im Studiengang Geologie-Paläontologie
10/1995–02/1996 Studienaufenthalt an der Fakultät für Geologie der Universität Barcelona im Rahmen des Erasmus-Programmes
07/1996-10/1997 Diplomkartierung im Studiengang Geologie-Paläontologie über das Thema “Die Geologie am Nordrand der Serre in Kalabrien, Süd-Italien”
Diplomarbeit im Studiengang Geologie-Paläontologie über das Thema “Polymetamorphose in Metapeliten der ‘Castagna-Einheit’ und Quarzphylliten der ‘Bagni-Einheit’ in Kalabrien, Süd-Italien”
10/1997 Kompaktkurs Geochemie am Max-Planck-Institut für Chemie, Mainz
04/1998 Diplomhauptprüfung im Studiengang Geologie-Paläontologie
04/1998 Diplom
seit 05/1998 Promotionsstudium am Mineralogischen Institut der Universität Würzburg

Tätigkeiten als wissenschaftliche Hilfskraft

09/1996–03/1998 Wissenschaftliche Hilfskraft am Mineralogisch-Petrographischen Institut der Universität Kiel; Fachbereich: Petrologie

Tätigkeiten als wissenschaftlicher Angestellter

05/2001–05/2003 Wissenschaftlicher Angestellter am Mineralogischen Institut der Universität Würzburg; Betreuung der Übungen zur Lehrveranstaltung “Mikroskopie der gesteinsbildenden Minerale”.